DOCTORAL THESIS

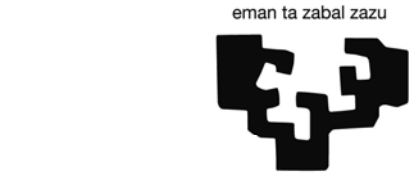

DEVELOPMENT OF FUNCTIONALISED BIOMATERIAL-BASED SOLUTIONS FOR THE TREATMENT OF OCULAR SURFACE PATHOLOGIES

BIOMATERIAL FUNTZIONALIZATUETAN OINARRITUTAKO TRATAMENDUEN GARAPENA BEGI-GAINAZALEKO GAIXOTASUNETARAKO

Author / Egilea:
Cristina Romo Valera

Supervisors / Zuzendariak:
Dr. Mª Noelia Andollo Victoriano
Dr. Jon Arluzea de Jauregizar

April, 2024/ Apirila, 2024

Summary

The human cornea is the outermost tissue of the eye and possesses unique properties such as transparency, avascularity and a specific structure that enables vision and acts as the first barrier against external insults. It consists of five different cellular and acellular layers with distinct composition and function that operate in coordination.

Persistent epithelial defects (PED) and chronic corneal ulcers are common ocular lesions that do not heal even after two weeks of treatment. The corneal surface becomes less sensitive and heals inadequately over time, which can result in corneal lysis and perforation. Although not challeging to diagnose, PEDs are challenging to treat, with management and follow-up associated with high social and healthcare costs. They may also arise in the context of limbal stem cell deficiency (LSCD) due to impaired re-epithelialisation caused by limbal progenitor cell involvement. LSCD is a chronic ocular surface pathology caused by the dysfunction or destruction of the limbal niche or the limbal epithelial progenitor cells (LEPC), which are responsible for the normal corneal epithelial homeostasis. It clinically presents corneal neovascularisation, occasional corneal opacity and can lead to vision loss or blindness. The most common treatments for PEDs are conventional eye drops and topical antibiotics. However, when the stroma is affected and the eyeball's structural integrity may be compromised, surgical interventions such as tissue grafts or stem cell transplants may be necessary. The only current effective treatment for LSCD is the transplantation of *in vitro* expanded LEPCs obtained from small limbal fragments. However, the success rates of this therapy have significant room for improvement, as it often needs to be repeated. Considering the actual clinical needs, the objective of this thesis was to develop biomaterial-based solutions for the restoration of visual function in cases of LSCD, PEDs and corneal ulcers.

A biocompatible hydrogel was developed to act as a filler for the damaged corneal stroma, functionalised with bioactive molecules to support biological tissue repair mechanisms and restore ocular health and visual properties in PED- or stromal ulcer-affected patients. Firstly, the physicochemical characterisation, biocompatibility and suitability for use in cell cultures of four protein-based biomaterials in the form of biofilms was carried out. Based on the results obtained from this characterisation, gelatine was selected as the main material for the development of the defect-filling

solution. Chemical crosslinking using riboflavin phosphate (RFP) was chosen to enhance the stability and mechanical properties of the gelatine, resulting in the formation of a gelatine-RFP hydrogel. The decision to use RFP as the crosslinking agent was based on its widespread use in ophthalmology.

In vitro evaluations were conducted to assess the physicochemical properties, biocompatibility and release kinetics of four gelatine-RFP based hydrogels. The initial hydrogel was composed solely of gelatine and RFP, the other three hydrogels contained dextran, hyaluronic acid, or methyl cellulose, respectively. The *in vitro* evaluation revealed that the gelatine-RFP hydrogel was the simplest and most functional composition. Following the selection of this hydrogel's biomaterials, it was enriched with components that reduce inflammation and accelerate the wound healing process. Haemoderivatives and human amniotic membrane extracts (HAMe) were chosen as sources rich in growth factors to functionalise the hydrogel and Infliximab was selected as an anti-inflammatory agent. The therapeutic effect of the added compounds was assessed through *in vitro*, *ex vivo*, and *in vivo* evaluations in bovine and rabbit animal models. Corneal defects were reproduced *in vivo* through anterior superficial stromal keratectomies in rabbit models, the clinical aspects of wound closure were evaluated during the study period and finally, processed samples were evaluated using immunohistochemistry and gene expression analysis. The use of hydrogel, whether functionalised or not, enhanced the wound healing response by reducing inflammation, promoting re-epithelialisation and decreasing the fibrotic response.

Regarding LSCD cases, corneal substitutes that promote the oligopotent growth of LEPCs and resemble the native cornea in composition and anatomy could be a viable therapeutic alternative for transplantation. Thus, primary cultures of LEPC and their interactions with other cells present in the sclerocorneal limbus, such as melanocytes were characterised. The comparable expression of stemness and melanocyte markers showed a strong correlation between primary LEPC cultures and melanocytes in the limbal niche. This correlation provided a new approach to optimise the culture conditions needed for future corneal constructs that would be generated to offer an alternative to the donor transplants currently used to treat LSCD.

Laburpena

Giza kornea begiaren kanpoaldean aurkitzen den ehuna da eta gardentasuna, abaskulartasuna eta egitura espezifiko bat izatea ditu ezaugarri. Osaera eta funtzio ezberdina betetzen duten bost geruzaz osatuta dago eta modu koordinatuan jarduten dute ikusmena bermatu eta kanpoaldeko erasoen aurrean begia babesteko.

Epitelio-akats iraunkorrak (EAI) eta korneako ultzera kronikoak begietako lesio ohikoak dira. 2 asteko tratamenduaren ondoren ere, akats hauetan begia ez da gai epitelioan sortutako zauria berrepitelizatzeko. Denborak aurrea egin ahala, gainazalaren sentikortasuna gutxitu, kornea modu desegokian orbaintzen hasten da eta horrek kornea lisia eta zulaketa eragin ditzake. Diagnostikatzen zailak ez diren arren, EAI-k tratatzeko zailak dira eta horien tratamenduak eta jarraipenak gizarte- eta osasun-kostu handiak dakartza. Era berean, linboko zelula amen gutxitasunaren (LZAG) testuinguruan ere sor daitezke, linboko zelula progenitoreak kaltetzearen ondorioz berrepitelizazio gaitasuna galdu delako. LZAG-a linboko nitxoaren edo epitelioko homeostasi normalaren erantzule diren linboko epitelio zelula amen (LEZA) disfuntzioak edo suntsipenak eragindako begi-gainazalaren patologia kronikoa da. Klinikoki, neobaskularizazio korneala, kornea-opakutasuna, ikusmen galera edo itsutasuna eragin ditzake. EAI-en tratamendurik ohikoenak kolirio konbentzionalak eta antibiotiko topikoak dira. Hala ere, estroma kaltetuta dagoenean eta begi-globoaren osotasuna arriskuan egon daitekeenean, beharrezkoa izan daiteke ebakuntza kirurgikoak egitea, hala nola ehun-mentuak edo zelula amen transplanteak. LZAG-erako egungo tratamendu eraginkor bakarra linbo-zati txikietatik lortutako *in vitro* kultibatutako LEZA-en transplantea da. Hala ere, terapia honen arrakasta-tasak asko hobetu daitezke, askotan errepikatu egin behar izaten baita. Egungo behar klinikoak kontuan hartuta, tesi honen helburua biomaterialetan oinarritutako soluzioak garatzea izan da, LZAG, EAI eta kornea-ultzeren kasuetan ikusmen-funtzioa berrezartzeko.

Hondatutako estromaren betegarri gisa jardungo duen hidrogel biobateragarri bat garatu dugu, EAI-k edo ultzera estromalak dituzten pazienteen ikusmen funtzioa berrezartzen lagunduko duten molekula bioaktiboekin funtzionalizatutakoa. Lehenik eta behin, proteinetan oinarritutako 4 biofilmen karakterizazio fisiko-kimikoa, biobateragarritasuna eta zelula-hazkuntzetan erabiltzeko egokitasuna ebaluatu ditugu.

Emaitza horietatik abiatuta, gelatina hautatu dugu hidrogela garatzeko material nagusi gisa. Gelatina erriboflabina fosfato (RFP) bidez kimikoki erretikulatuz, gelatina-RFP hidrogela sortu dugu. RFP oftalmologian duen erabileragatik agente saregile gisa hautatu dugu.

Gelatina-RFP-n oinarritutako lau hidrogelen propietate fisiko-kimikoak, biobateragarritasuna eta askapen zinetika *in vitro* ebaluatu ditugu ondoren. Hasierako gelatina-RFP hidrogeletik abiatuta, beste 3 bertsio sortu ditugu, dextranoa, azido hialuronika edo metilzelulosa gehituz, hurrenez hurren. Hala, *in vitro* ebaluazioak gelatina-RFP hidrogela konposizio erraz eta funtzionalena dela erakutsi digu. Hidrogel horren osaera hautatu ondoren, hantura murriztu eta zauriak orbaintzeko prozesua bizkortzen duten osagaiekin aberastu dugu. Odol-eratorriak eta giza mintz amniotikoaren estraktuak (GMAe) hautatu ditugu hidrogela funtzionalizatzeko hazkuntza-faktoreetan aberatsak diren iturri gisa eta Infliximab-a hautatu dugu hanturaren aurkako eragile bezala. Funtzionalizazio-konposatu erantsien efektu terapeutikoa *in vitro*, *ex vivo* eta *in vivo* ebaluatu ditugu behi- eta untxi-korneen ereduetan.

Kornea-akatsak aurreko estromako keratektomien bitartez *in vivo* erreproduzitu ditugu, zauriaren itxieraren alderdi klinikoak ebaluatu ditugu finkatutako azterketa denboran, eta, azkenik, immunohistokimika eta adierazpen genikoaren analisi bidez prozesatutako laginak ebaluatu ditugu. Hidrogela erabiltzeak, funtzionalizatuta egon ala ez, hobetu egin du zauriaren orbaintze-erantzuna, hantura murriztu, berrepitelizazioa sustatu eta erantzun fibrotikoa hobetu baitu.

LZAG kasuei dagokienez, LEZA-en hazkuntza oligopotentea sustatzen duten eta konposizioan eta anatomian kornea imitatzen duten kornea-ordezkoak transplanteen aukera terapeutiko bideragarria izan daitezke. Hala, LEZA hazkuntza primarioak karakterizatu ditugu, baita linbo esklerokornealean dauden melanozitoekin dituzten interakzioak ere. Zelula amen eta melanozitoen markatzaileen adierazpenek korrelazio handia erakutsi dute LEZA hazkuntza primarioen eta linboko nitxoko melanozitoen artean. Korrelazio horrek ikuspegi berri bat eskaintzen du etorkizunean sortuko diren kornea-ordezkoetarako beharrezkoak diren hazkuntza-baldintzak optimizatzeko, gaur egun LZAG tratatzeko erabiltzen diren emaileen transplanteei alternatiba bat eskainiz.

Contents

I. INTRODUCTION **1**

1. The ocular surface . . . 3
   - 1.1. The tear film . . . 3
   - 1.2. Conjunctiva . . . 5
   - 1.3. The human cornea . . . 5
     - 1.3.1. Anatomy, histology and function . . . 5
   - 1.4. The sclerocorneal limbus . . . 10
     - 1.4.1. The limbal niche . . . 10
     - 1.4.2. Stem cells in the limbus . . . 12
   - 1.5. Corneal epithelium homeostasis . . . 13
   - 1.6. Limbal stem cell deficiency (LSCD) . . . 15
     - 1.6.1. Epidemiology and pathology . . . 15
     - 1.6.2. Diagnosis and treatments . . . 15
   - 1.7. Overview of corneal regeneration . . . 20
     - 1.7.1. Epithelial wound healing . . . 20
     - 1.7.2. Basement membrane wound healing . . . 20
     - 1.7.3. Stromal wound healing . . . 21
     - 1.7.4. Corneal endothelial wound healing . . . 23
   - 1.8. Corneal defects . . . 24
     - 1.8.1. Epithelial defects . . . 24
     - 1.8.2. Persistent epithelial defects and neurotrophic ulcers . . . 24
2. Regenerative medicine and Tissue engineering . . . 27
   - 2.1. Classification of biomaterials based on their origin . . . 28
     - 2.1.1. Natural Biomaterials . . . 28
     - 2.1.2. Synthetic biomaterials . . . 35
   - 2.2. Hydrogels . . . 36
     - 2.2.1. Main physicochemical properties of hydrogels . . . 36

2.2.2. Classification of hydrogels based on their crosslinking . 41
3. Regenerative medicine approaches for corneal regeneration 47
3.1. Cell sheet engineering (CSE) 47
3.2. Scaffold-based approaches: Use of biomaterials 48
3.2.1. Development of therapeutic contact lenses 49
3.2.2. Application of hydrogels for different corneal injuries . 50

II. HYPOTHESIS AND OBJECTIVES **63**
1. Hypothesis 65
2. Objectives 66

III. MATERIALS AND METHODS **69**
1. Biomaterial characterisation 71
1.1. Film synthesis 71
1.2. Hydrogel synthesis 72
1.3. Fourier Transform Infrared (FTIR) Spectroscopy 73
1.4. X-Ray Diffraction (XRD) 74
1.5. Rheological measurements 74
1.6. Swelling and expansion tests 75
1.7. Light transmittance and transparency tests 76
1.8. Biodegradability assay 76
1.9. *In vitro* release studies 77
1.9.1. FITC Labelling 78
1.10. Hydrogel functionalisation 78
1.10.1. Procurement of human amniotic membrane (HAM) . . 78
1.10.2. Human amniotic membrane extract (HAMe) preparation 80
1.10.3. Extraction of blood derivatives 80
1.10.4. Quantification of growth factors 82
1.10.5. Synthesis of functionalised hydrogels 84
2. Cell culture 85
2.1. Established cell line culture 86
2.1.1. Thawing cryopreserved cells 86
2.1.2. Cell subculture 87
2.1.3. Freezing cells 87
2.1.4. Cell counting 87

3. Cell isolation from human corneas . . . 88
3.1. Dissection of donor corneoscleral tissues and sclerocorneal rims . 88
3.2. Tissue digestion and cell isolation . . . 89
4. *In vitro* citocompatibility and biocompatibility assays . . . 89
4.1. MTT assay . . . 89
4.2. Live/Dead citotoxicity assay . . . 91
4.3. Cell cycle analysis . . . 91
4.4. Migration assay . . . 92
5. *In vitro* inflammation model . . . 92
5.1. Establishment of the *in vitro* inflammation model . . . 92
5.2. *In vitro* inflammation assay . . . 93
6. *Ex vivo* eye model . . . 95
6.1. *Ex vivo* surgical procedure . . . 95
7. Adhesion study . . . 97
8. *In vivo* eye model . . . 98
8.1. *In vivo* surgical procedure . . . 99
8.2. Clinical evaluation of eye injuries . . . 100
9. Acquisition and analysis of tear samples . . . 103
9.1. Collection and quantification of tear using Schirmer strips . . . 103
9.2. Protein elution from Schirmer strips . . . 104
9.3. Protein quantification-BCA assay . . . 104
9.4. Evaluation of the expression of inflammatory molecules in tear samples by immunodetection-Antibody arrays . . . 105
10. Gene expression analysis . . . 106
10.1. RNA extraction from *in vitro* samples . . . 107
10.2. RNA extraction from *in vivo* samples . . . 107
10.3. RNA quantification . . . 108
10.4. Retrotransciption . . . 109
10.5. cDNA preamplification of *in vivo* samples . . . 109
10.6. Real time RT-qPCR . . . 110
10.6.1. Analysis of RT-qPCR results . . . 111
11. Histological analysis . . . 112
11.1. Haematoxylin-Eosin (H-E) staining . . . 112
11.2. Impression cytology . . . 112

11.3. PAS staining of impression cytology samples . . . 113
12. Inmunofluorescence . . . 113
12.1. Immunocytochemistry . . . 115
12.1.1. Cytospin . . . 116
12.2. Immunohistochemistry . . . 116
13. Microscopy techniques . . . 117
13.1. Phase contrast microscopy . . . 117
13.2. Bright-field microscopy . . . 117
13.3. Fluorescence/confocal microscopy . . . 117
13.4. Scanning electron microscopy (SEM) . . . 118
14. Analysis and Statistics . . . 119

IV. RESULTS **123**

1. *In vitro* assessment of protein-based biofilms . . . 125
1.1. Physicochemical and morphological analysis . . . 125
1.2. Light transmittance and transparency . . . 127
1.3. Biodegradability . . . 130
1.4. Cell proliferation and viability . . . 131
1.5. Cell adhesion . . . 133
1.6. Cell migration . . . 135
2. *In vitro* assessment of gelatine hydrogel . . . 137
2.1. Rheological measurements . . . 137
2.2. Swelling and expansion measurements . . . 140
2.3. Light transmittance and transparency . . . 141
2.4. *In vitro* release assays . . . 143
2.5. Cytocompatibility assesment . . . 147
2.6. Culture of corneal cells embedded in the hydrogel . . . 148
3. Quantification of growth factors . . . 149
3.1. Quantification of blood-derived products . . . 150
3.2. Quantification of HAMe samples . . . 150
4. *In vitro* inflammation assessment . . . 154
4.1. *In vitro* inflammation model . . . 154
4.2. *In vitro* inflammation assay . . . 155
5. *Ex vivo* assays . . . 157

6. *Ex vivo* adhesion test . . . 159
7. *In vivo* assays . . . 161
7.1. Pilot study to fine-tune the experimental procedure conditions . 161
7.1.1. Re-epithelialisation . . . 162
7.1.2. Clinical assesment . . . 163
7.1.3. Evaluation of the expression of inflammatory cytokines in tear samples . . . 164
7.2. *In vivo* re-epithelialisation in a rabbit animal model . . . 166
7.3. Clinical assessment . . . 169
7.4. Quantification of tear volume and protein concentration . . . 170
7.5. Gene expression analysis of rabbit corneal samples . . . 172
7.6. Histological analysis . . . 176
7.6.1. Haematoxylin-Periodic Acid-Schiff (PAS) staining of impression cytology samples . . . 176
7.6.2. Haematoxylin-Eosin staining of rabbit corneal tissues . 178
7.7. Immunofluorescence analysis of rabbit corneal tissues . . . 181
8. Primary limbal cell cultures . . . 189
8.1. ΔNp63α and melan A cell markers' expression in human sclerocorneal tissue . . . 189
8.2. Isolation and culture of limbal epithelial cells . . . 190
8.3. Presence of melanocytes in the epithelial cell culture . . . 192

V. DISCUSSION **197**

1. Evaluation of the films that could be used for corneal wound healing . . 199
2. Hydrogel solution for the treatment of corneal ulcers . . . 202
2.1. Hydrogel's composition and crosslinking mechanism . . . 203
2.2. Hydrogel's functionalisation . . . 208
2.2.1. Quantification of growth fators . . . 210
2.2.2. Anti-inflammatory agent: Infliximab . . . 213
3. Application and effect of functionalised hydrogels on wound healing in *in vivo* experiments . . . 214
3.1. Establishment of *in vivo* surgical conditions . . . 215
3.2. Re-epithelialisation and healing . . . 216
3.3. Adhesion . . . 220

3.4. Fibrosis 221
3.5. Eye irritation and inflammation 225
3.6. Overall *in vivo* response of the treatments 228
4. Characterisation of primary limbal cell cultures 229

VI. CONCLUSIONS **235**

REFERENCES **487**

A. PUBLISHED ARTICLES **533**

Gaien Aurkibidea

I. SARRERA **241**

1. Begiaren gainazala 243
   - 1.1. Malko-geruza 243
   - 1.2. Konjuntiba 245
   - 1.3. Kornea 245
     - 1.3.1. Anatomia eta funtzioa 245
   - 1.4. Linbo esklerokorneala 250
     - 1.4.1. Linbo esklerokornealeko zelula amen nitxoa 251
     - 1.4.2. Linboko zelula ama motak 253
   - 1.5. Korneako epitelioaren homeostasia 254
   - 1.6. Linboko zelula amen gutxitasuna 256
     - 1.6.1. Epidemiologia eta patologia 256
     - 1.6.2. Diagnosia eta tratamenduak 257
   - 1.7. Kornearen birsortze prozesua 261
     - 1.7.1. Epitelioaren birsortze prozesua 261
     - 1.7.2. Mintz basalaren birsortze prozesua 261
     - 1.7.3. Estromaren birsortze prozesua 262
     - 1.7.4. Endotelioaren birsortze prozesua 265
   - 1.8. Korneako akatsak 265
     - 1.8.1. Epitelio akatsak 265
     - 1.8.2. Epitelio akats iraunkorrak eta ultzera neurotrofikoak . . 266
2. Medikuntza birsortzailea eta Ehun-ingeniaritza 268
   - 2.1. Jatorriaren araberako biomaterialen sailkapena 269
     - 2.1.1. Biomaterial naturalak 269
     - 2.1.2. Biomaterial sintetikoak 276
   - 2.2. Hidrogelak 277
     - 2.2.1. Hidrogelen propietate fisiko-kimiko nagusiak 277

2.2.2. Gurutzaketa edo erretikulazio metodoaren araberako hidrogelen sailkapena . . . 282
3. Medikuntza birsortzaileari lotutako kornea birsortzeko konponbideak . 288
3.1. Zelula-xaflen ingeniaritza . . . 288
3.2. 3 dimentsiotako euskarriak: biomaterialen erabilera . . . 289
3.2.1. Ukipen-lente terapeutikoen garapena . . . 290
3.2.2. Hidrogelen erabilera korneako zauri ezberdinetan . . . 291

II. HIPOTESIA ETA HELBURUAK 305
1. Hipotesia . . . 307
2. Helburuak . . . 308

III. MATERIALAK ETA METODOLOGIA 311
1. Biomaterialen karakterizazioa . . . 313
1.1. Biofilmen sintesia . . . 313
1.2. Hidrogelen sintesia . . . 314
1.3. Fourierren transformatuaren bidezko espektroskopia infragorria (FTIR) . . . 316
1.4. X izpien difrakzioa (XRD) . . . 316
1.5. Erreologia neurketak . . . 317
1.6. Puzte- eta hedatze-saiakuntzak . . . 317
1.7. Transmitantzia eta gardentasun saiakuntzak . . . 318
1.8. Biodegradazio saiakuntza . . . 319
1.9. *In vitro* askapen saiakuntzak . . . 319
1.9.1. FITC markaketa . . . 320
1.10. Hidrogelen funtzionalizazioa . . . 321
1.10.1. Giza mintz amniotikoa (GMA)-ren erauzpena . . . 321
1.10.2. Giza mintz amniotikoko estraktuen (GMAe) prestakuntza . . . 322
1.10.3. Odol-eratorrien prestakuntza . . . 322
1.10.4. Hazkuntza faktoreen kuantifikazioa . . . 324
1.10.5. Funtzionalizatutako hidrogelen sintesia . . . 326
2. Hazkuntza zelularrak . . . 327
2.1. Zelula lerroak . . . 327
2.1.1. Kriokontserbatutako zelulak desizoztea . . . 328

2.1.2. Zelulen hazkuntza 328
2.1.3. Zelulak izoztea 329
2.1.4. Zelula-zenbaketa 329
3. Giza korneetako zelulen erauzketa 330
3.1. Emaileen ehun eta eraztun esklerokornealen disekzioa 330
3.2. Ehunen digestioa eta zelulen erauzketa 330
4. *In vitro* zitobateragarritasun eta biobateragarritasun saiakuntzak 331
4.1. MTT saiakuntza 331
4.2. Zitotoxikotasun saiakuntza 332
4.3. Ziklo zelularraren analisia 333
4.4. Migrazio-saiakuntza 334
5. *In vitro* inflamazio saiakuntza 334
5.1. *In vitro* inflamazio ereduaren ezarpena 334
5.2. *In vitro* inflamazio saiakuntza 335
6. *Ex vivo* begi eredua 337
6.1. *Ex vivo* prozedura kirurgikoa 337
7. Atxikidura proba 339
8. *In vivo* begi eredua 340
8.1. *In vivo* prozedura kirurgikoa 341
8.2. Korneako zaurien ebaluazio klinikoa 343
9. Malko-laginak eskuratzea eta aztertzea 345
9.1. Schirmer-en tiren bidez malkoa biltzea eta kuantifikatzea 345
9.2. Schirmer-en tiretatik lortutako laginetako proteinen eluzioa . . . 346
9.3. Proteina edukiaren kuantifikazioa-BCA saiakuntza 346
9.4. Immunodetekzioaren eta antigorputz-array bidezko malko-laginetako hantura-molekulen adierazpenaren ebaluazioa 347
10. Gene-adierazpenaren analisia 348
10.1. RNA-ren erauzketa *in vitro* lortutako laginetatik 349
10.2. RNA-ren erauzketa *in vivo* lortutako laginetatik 349
10.3. RNA-ren kuantifikazioa 350
10.4. Erretrotranskripzioa 351
10.5. *In vivo* laginetatik lortutako cDNA-ren preanplifikazioa 351
10.6. Polimerasaren kate-erreakzio kuantitatiboa denbora errealean (RT-qPCR) 352

10.6.1. RT-qPCR emaitzen analisia . . . 353
11. Analisi histologikoa . . . 354
11.1. Hematoxilina-Eosina (H-E) tindaketa . . . 354
11.2. Inprimatze zitologia . . . 354
11.3. Inprimatze zitologia bidez lortutako laginen PAS tindaketa . . . 355
12. Immunofluoreszentzia . . . 355
12.1. Immunozitokimika . . . 357
12.1.1. Zitospina . . . 357
12.2. Immunohistokimika . . . 358
13. Mikroskopia teknikak . . . 359
13.1. Fase-kontraste mikroskopia . . . 359
13.2. Eremu argiko mikroskopia . . . 359
13.3. Fluoreszentziazko mikroskopia eta mikroskopia konfokala . . . 359
13.4. Ekorkuntz mikroskopia elektronikoa (SEM) . . . 360
14. Analisia eta estatistika . . . 360

IV. EMAITZAK **365**

1. Izaera proteikoko biofilmen *in vitro* ebaluazioa . . . 367
1.1. Analisi fisiko-kimikoa eta morfologikoa . . . 367
1.2. Transmitantzia eta gardentasuna . . . 369
1.3. Biodegradazioa . . . 372
1.4. Zelulen proliferazioa eta bideragarritasuna . . . 373
1.5. Zelulen atxikidura . . . 376
1.6. Zelulen migrazioa . . . 378
2. Gelatinazko hidrogelen *in vitro* ebaluazioa . . . 379
2.1. Erreologia neurketak . . . 379
2.2. Puzte- eta hedatze-neurketak . . . 382
2.3. Transmitantzia eta gardentasuna . . . 383
2.4. *In vitro* askapen saiakuntzak . . . 385
2.5. Zitobateragarritasunaren ebaluazioa . . . 389
2.6. Hidrogelean txertatutako korneako zelulen hazkuntza . . . 390
3. Hazkuntza faktoreen kuantifikazioa . . . 391
3.1. Odol-eratorrien kuantifikazioa . . . 392
3.2. GMAe laginen kuantifikazioa . . . 392

4. *In vitro* inflamazio saiakuntza 396
4.1. *In vitro* inflamazio ereduaren ezarpena 396
4.2. *In vitro* inflamazio saiakuntza 397
5. *Ex vivo* saiakuntzak 399
6. *Ex vivo* atxikidura proba 401
7. *In vivo* saiakuntza 403
7.1. Prozedura esperimentalaren baldintzak doitzeko azterketa pilotua 403
7.1.1. Berrepitelizazioa 404
7.1.2. Ebaluazio klinikoa 405
7.1.3. Malko-laginetako hantura-zitokinen adierazpenaren ebaluazioa 406
7.2. Korneetako *in vivo* berrepitelizazioa untxietan 408
7.3. Ebaluazio klinikoa 411
7.4. Malko-bolumen eta proteina edukiaren kuantifikazioa 412
7.5. Gene-adierazpenaren analisia untxi-korneetako laginetan 414
7.6. Analisi histologikoa 418
7.6.1. Inprimatze zitologiaren bidez lortutako laginen Hematoxilina-PAS tindaketa 418
7.6.2. Untxi-korneetako laginen Hematoxilina-Eosina (H-E) tindaketa 420
7.7. Immunofluoreszentzia analisia untxi-korneetako laginetan 423
8. Linboko zelula primarioen hazkuntza 431
8.1. ΔNp63α eta melan A markatzaile zelularren adierazpena giza ehun esklerokornealetan 431
8.2. Linboko epitelio-zelulen erauzketa eta hazkuntza 432
8.3. Melanozitoen presentzia zelula epitelialen hazkuntzetan 435

V. EZTABAIDA **441**

1. Korneako zauriak orbaintzeko erabil litezkeen biofilmen ebaluazioa . . . 443
2. Korneako ultzerak tratatzeko hidrogela 446
2.1. Hidrogelaren konposizioa eta erretikulazioa mekanismoa 447
2.2. Hidrogelaren funtzionalizazioa 453
2.2.1. Hazkuntza-faktoreen kuantifikazioa 455
2.2.2. Infliximab: hanturaren aurkako eragilea 457

3. Funtzionalizatutako hidrogelen aplikazioa eta eragina *in vivo* 458
3.1. *In vivo* prozedura kurgikoaren baldintzen ezarpena 459
3.2. Berrepitelizazioa eta sendatzea 460
3.3. Atxikidura 464
3.4. Fibrosia 466
3.5. Begiaren narritadura eta hantura 470
3.6. Tratamenduen *in vivo* erantzun orokorra 473
4. Linboko zelula primarioen karakterizazioa 474

VI. ONDORIOAK **481**

List of Figures

I.1. Schematic illustration showing 3 of the ocular surface components. **a**) Diagram illustrating the various layers present in the tear film. **b**) Illustration showing the location of the different parts of the conjunctiva; the palpebral conjunctiva, the bulbar conjunctiva and the conjunctival fornix. **c**) Main anatomical components of the ocular globle and detailed illustration of the different layers of the cornea. 4

I.2. Detailed illustration of the corneal components. The epithelium is a 5-6 layered stratified epithelium with a complex network of junctions between the different heterogeneous cell layers. The stroma's anterior third comprises of diagonally positioned lamellae that facilitate significant alterations in the z-axis. In contrast, the stroma's posterior two thirds comprise of parallelly positioned lamellae that offer longitudinal strength in the x and y axes. The arrangement of collagen fibrils within each lamella plays a significant role in preventing fibril waviness and thereby, enhancing the initial axial tensile strength of each individual fibril. Finally, the corneal barrier and the metabolic pump sites are detailed in the corneal endothelium. Image modified from [10]. 7

I.3. Detailed illustration of the limbal niche. 11

I.4. Schematic representation of LESC hypothesis. **a**) The stem cells located in the basal epithelium of the limbus divide asymmetrically to produce transient amplifying cells (TAC). These TACs migrate towards the central corneal epithelium, gradually transforming into post-mitotic cells (PMC) and then into terminally differentiated cells (TDC). LECr, SP, LESC, TAC, PMC and TDC refer to the limbal epithelial crypts, stromal projections, limbal epithelial stem cells, transient amplifying cells, post-mitotic cells and terminally differentiated cells, respectively. **b**) LESCs possess the ability to self-renew and differentiate into more specialised cells within the cornea. 14
I.5. Schematic representation and description of the stages during LSCD. . . 16

I.6. Overview of the corneal regeneration process. Following epithelial damage, growth factors including EGF, PDGF, IGF, insulin and other cytokines are released due to an intense biochemical activity triggered by damaged epithelial cells. Subsequently, healthy corneal epithelial cells undergo cell reorganisation, resulting in a series of morphological and functional changes. After this process begins, the epithelium closes as a result of the activation of LEPCs residing in the limbus, which proliferate and differentiate into increasingly differentiated epithelial cells, creating the stratification of the normal epithelium. In the corneal stroma, IL-1 and TNFα secreted by epithelial cells initiate keratocyte apoptosis. Within a few hours, the keratocytes neighbouring the acellular area begin to activate. Likewise, the initial apoptosis of subepithelial keratocytes is followed by the migration and proliferation of the neighbouring keratocytes, triggered by PDGF. This migration is then followed by the differentiation into myofibroblasts, a process mediated by TGF-β released by the epithelial cells. These myofibroblasts trigger the production of growth factors, namely HGF and KGF, which activate genes encoding extracellular matrix components and deactivate genes encoding molecules that preserve corneal transparency. Subsequently, there is an increased production of collagenases and other matrix MMPs, ultimately leading to stromal remodelling. The aforementioned processes lead to a significant increase in extracellular matrix production, stromal hypercellularity, and tissue contraction, resulting in tissue opacity or haze. Finally, stromal repair is completed through apoptotic mechanisms of the cells involved in stromal healing and by the restoration of keratocytes to their normal state. Concerning the endothelium, its regeneration is achieved through migration, expansion or thinning of cells to cover the maximum surface area. Epithelial cells secrete growth factors indicated in blue, while stromal cells secrete those indicated in red. 22

I.7. Overview of the strategies, components, and interactions used in RM. Regenerative medicine therapies involve delivering cells, biomaterials, or biomolecules, such as injecting regenerative cells or implanting acellular biomaterial scaffolds to stimulate endogenous tissue repair. Interdependent interactions can also be harnessed for tissue engineering, drug delivery, and immunomodulation. Although the solutions developed in this field are complex, these strategies offer the opportunity to target the most effective solutions for tissue regeneration and repair. Modified from [122]. 27

I.8. Photographs of the synthesis process of silk fibroin-methacryloyl (Sil-MA) bioink and hydrogel. **a**) After measuring the weight of cocoons, the silk is degummed with 1 l of 0.05 M sodium carbonate for 1 h, rinsed twice with distilled water and dehydrated in the oven overnight. Then the silk is disolved in LiBr salt solution and filtered. Glycidyl methacrylate (GMA) is added dropwise to regenerated SF (RSF) and RSF-GMA solution is stirred on a hot plate (60 °C) at 800 rpm for 6 h to allow SF and GMA to react. The solution is then dyalised in distilled water during 7 days and lyophilised for another 5-7 days. The lyophilised Sil-MA sponge is disolved in 0.2% (wt/vol) LAP containing PBS and homogeneously mixed. Finally, the solution is centrifuged to remove air bubbles. **b**) A tracheal shape hidrogel printed with PKH67-labeled cells (green) and PKH26 labeled cells (red). From left to right, CAD design of a tracheal construct, images of the hydrogels that have been printed, fluorescence (FL) image using confocal or single plane illumination microscopy and merged image of fluorescent hydrogel and CAD design. Images taken from [164]. 33

I.9. Schematic illustration of the main hydrogel properties related to hydrogel design guidance. **a**) Mesh size, **b**) swelling behaviour, **c**) viscoelastic behaviour, **d**) degradation profile, **e**) biocompatibility and **f**) properties related to application specificity. 37

I.10. Schematic illustration of the different physical and chemical crosslinking strategies for hydrogel synthesis. 42

I.11. **a**) Structure of riboflavin; **b**) Oxidation states of riboflavin (**a** and **b** modified from [218]); **c**) Collagen and riboflavin crosslinking chemistry (modified from [219]); **d**) Possible crosslinking reaction between gelatine and riboflavin phosphate after UV irradiation. 45
I.12. Cell sheet engineering (CSE) principle. **a**) Confluent cells are harvested individually using enzymatic digestion. **b**) Temperature-responsive culture dishes demonstrate the attachment and detachment of cell sheets. The dishes are composed of a thermoresponsive polymer that alters its hydrophilicity at specific temperatures, allowing for the formation and removal of cohesive cell sheets and providing an effective and non-invasive method for their creation and manipulation. . 48
I.13. Hydrogel solutions for different corneal injuries. **a**) Therapeutic dressings for superficial corneal epithelial wounds. **b**) Ocular adhesives as suture replacement for small corneal incisions. **c**) Hydrogels as filling agents for corneal defects affecting the stroma and corneal perforations. **d**) The use of full corneal substitutes. 51
I.14. *In vivo* application of GelCORE bioadhesives into corneal defects in rabbits. **a**) and **b**), Creation of a stormal defect in rabbit corneas. **c**) *in situ* application of gelCORE solution, **d**) crossslinking process, **e**) formation of a transparent gelCORE adhesive on corneal stromal defect. Anterior segment optical coherence tomography images **f**) before and **g**) after treatment with GelCORE. Images reproduced from [306]. 57
I.15. **a**) Illustration of human cornea and *in vitro* 3D corneal tissue model. Scale bar corresponds to 3 mm. **b**) Porcine cornea, co-culture of hCECs, hCSSCs and DRG explants in liquid and co-culture at air-liquid interface at day 28. Both co-cultures are soaked in glycerol. Scale bar corresponds to 3 mm. hCEC: human corneal epithelial cells; hCSSC: human corneal stromal stem cells; DRG: chicken dorsal root ganglion neurons; ESD-LC: tri-culture of all cell types in liquid interface; ESD-ALIC: tri-culture of all cell types in air-liquid interface. Image reproduced from [327]. 60

III.1. Chemical structures of the compounds used for the synthesis of the hydrogels. **a**) Gelatin, **b**) riboflavin phosphate (RFP), **c**) dextran (D), **d**) hyaluronic acid (HA) and **e**) methyl cellulose (MC). 73
III.2. **a, b**) Injection and crosslinking process of gelatine-RFP hydrogel. **c, d**) Handling of the gelatine and RFP hydrogel after blue light crosslinking. 74
III.3. Schematic representation of the subregions of the human amniotic membrane (HAM) inside and outside the uterus. The placental amnion (blue, covering the placenta), the reflected amnion (orange, lining the uterine wall), and the umbilical amnion (gray, covering the umbilical cord). The reflected amnion can be divided into proximal amnion, the area that is closest to the placental disk, the medial amnion, and the distal amnion, the area farthest from the placental disk. Figure created based on [332]. 79
III.4. Schematic representation of **a**), sandwich ELISA and **b**), Luminex assay working principles. 83
III.5. **a**) NIH-3T3 fibroblast cell line and **b**) HCE cell line. Images taken with 10× magnification lens. Scale bars correspond to 100 μm. 86
III.6. Scheme of treatments used in the *in vitro* inflammation assay. 94
III.7. Extraction and processing procedure for the *ex vivo* bovine corneal model. 96
III.8. Extraction and processing procedure for the *ex vivo* rabbit corneal model. 96
III.9. Representation of the vertical displacement of the cylindrical probe into the corneal wound in the adhesion test. 97
III.10Steps followed for the *in vivo* surgical procedure. 100
III.11Tear adquisition procedure from Schirmer strip. 103
III.12Cytokine array working procedure. **a**) The glass slide containing the capture antibody is completely air dried before starting any incubation. **b**) Samples are added and inmobilized to the antibodies present in the solid support. **c**) The immobilized samples are then complexed with a biotinylated antibody. **d**) The enzyme complexes are incubated with Cy3 Equivalent Dye-Streptavidin to produce a detectable signal. **e**) The array is scanned and the data is analysed. 106

IV.1. FTIR spectra of the films **a**) from 4000 to 850 cm^{-1} and **b**) from 1750 to 850 cm^{-1}. X-ray diffraction patterns of films (**c**). SEM image sections of the films obtained with 3000 (**d**), 180 (**e**), 1100 (**f**), and 450× magnification (**g**). COL, collagen; SPI, soy protein isolate; GEL-LAC, lactose-crosslinked gelatine; GEL-CA, citric acid-crosslinked gelatine. . . 126

IV.2. Light transmittance spectra and transparency differences of dried and hydrated films. The graphs show the percentage of light transmitted by each film in the visible spectrum (**a-d**). Data are presented as the mean percentage of transmittance ± standard deviation (SD). Statistically significant differences indicate variations between the dried and hydrated states of each film (∗ $p < 0.05$, ∗∗ $p < 0.01$, ∗∗∗ $p < 0.001$; $n = 9$). The figures **e-l** illustrate the transparency level of each film when placed at a distance of 12 cm from a specific pattern for both dried (**e-h**) and hydrated (**i-l**) films. All the images were taken of the same pattern and with the same conditions. 129

IV.3. *In vitro* degradation profiles of the films immersed in 200 μg/ml collagenase A solution or PBS at 37 °C over time. Films immersed in deionised water at 37 °C were used as control. **a**) Represents the degradation profiles of COL films, **b**) the degradation profiles of SPI films, **c**) the degradation profiles of GEL-LAC films and **d**) the degradation profiles of GEL-CA films. Data are reported as means ± SD, and statistically significant differences of films in collagenase A (∗) and PBS (#) are reported with respect to those in deionised water. ∗, # $p < 0.05$, ∗∗, ## $p < 0.01$, ∗∗∗, ### $p < 0.001$; $n = 3$. 130

IV.4. Effects of film composition on the **a**) proliferation and **b-d**) viability of NIH-3T3 cells. Cells seeded in p96-well plates were exposed to each film for 24, 48, and 72 h. Cells seeded on wells without any biomaterial were used as controls. Proliferation results are represented as the proliferation rate mean ± SD of viable cells compared with viable cells at t = 0 h. Viability results are expressed as percentages of viable cells in relation to control wells (100% viability). The lines drawn inside each box represent the medians of viability values of each film. Statistically significant differences showed differences with respect to control (∗ $p < 0.05$, ∗∗ $p < 0.01$, ∗∗∗ $p < 0.001$; $n = 9$). 132

IV.5. Effects of film composition on the **a**) proliferation and **b-d**) viability of human corneal epithelial (HCE) cells. Cells seeded in p96-well plates were exposed to each film for 24, 48, and 72 h. Cells seeded on wells without any biomaterial were used as controls. Proliferation results are represented as the proliferation rate mean ± SD of viable cells compared with viable cells at t = 0 h. Viability results are expressed as percentages of viable cells in relation to control wells (100% viability). The lines drawn inside each box represent the medians of viability values of each film. Statistically significant differences showed differences with respect to control (∗ $p < 0.05$, ∗∗ $p < 0.01$, ∗∗∗ $p < 0.001$; n = 9). 133

IV.6. Culture of 3T3 cells above the films. Contrast phase microscopic images of 3T3 cells on tissue culture well plate (control) and the films after 24 h of cell seeding (**a-d**). Representative Calcein AM-EthD1 live/dead assay images (**e-h**) and SEM images (**i-l**). **a-h**) Images taken with 10× magnification; scale bars correspond to 100 μm. **i-l**) Images taken with 450× magnification. 134

IV.7. Culture of HCE cells above the films. Contrast phase microscopic images of HCE cells on tissue culture well plate (control) and the films after 24 h of cell seeding (**a-d**). Representative Calcein AM-EthD1 live/dead assay images (**e-h**) and SEM images (**i-l**). **a-h**) Images taken with 10× magnification; scale bars correspond to 100 μm. **i-l**) Images taken with 450× magnification. 135

IV.8. Migration assay of HCE and 3T3 cells seeded above GEL-LAC after 24, 48, and 72 h. Images taken with 10 × magnification; scale bars correspond to 50 μm. Data in **a**) and **b**) represent the evolution of the gap closure by 3T3 (**a**) and HCE (**b**) cells in each film. No significant differences were recorded. 136

IV.9. **a**) Strain-dependent (angular frequency (ω) = 10 rad/s, 25 °C) and **b**) frequency-dependent (strain (ε) = 1%, 25 °C) oscillatory shear rheology of G, G-D, G-HA and G-MC hydrogel formulations. 138

IV.10 **a**) Steady-shear reology of G, G-D, G-HA and G-MC hydrogels demonstrating highly shear-thinning behavior. **b**) Step-shear measurements of G, G-D, G-HA and G-MC hydrogels over four cycles of alternating low shear (gray; 0.1 s^{-1}) and high shear (white; 10 s^{-1}) rates. 139

IV.11 Stress-controlled yield stress measurements of **a**) G, **b**) G-D, **c**) G-HA and **d**) G-MC hydrogels were performed from low to high stress with steady-state sensing. Static yield stress values are indicated on the corresponding graphs. 140

IV.12 **a**) Swelling and **b**) expansion measurements performed in G, G-D, G-HA and G-MC hydrogels 24 h after their immersion in PBS. Results are indicated as average fold-changes $\pm$ SD with respect to G hydrogel. Statistical significance is defined as p-value $*$ $p < 0.05$, $**$ $p < 0.01$, $***$ $p < 0.001$, $****$ $p < 0.0001$. 141

IV.13 Light transmittance spectra and transparency differences of G, G-D, G-HA and G-MC hydrogels before and after crosslinking. **a-d**) Graphs show the percentage of light transmitted by the crosslinked and non-crosslinked version of each film in the 400-800 nm range. Data are presented as the mean percentage of transmittance $\pm$ SD. Statistically significant differences indicate variations between the crosslinked and non-crosslinked states of each film ($*$ $p < 0.05$, $**$ $p < 0.01$, $***$ $p < 0.001$, $****$ $p < 0.0001$). The figures in **e**) illustrate the transparency level of each hydrogels before and after their irradiation with blue light. The same pattern and the same conditions were used to take all the images. . 142

IV.14 **a**) FITC-labelled IgG, **b**) FITC-labelled Albumin and **c**) Vigamox release profiles of G, G-D, G-HA and G-MC hydrogels. The cumulative release was expressed as the normalised percentage of the total amount released over 15-day duration of the experiment. 146

IV.15 Cytocompatibility results of NIH-3T3 and HCE cell cultures exposed to G, G-D, G-HA and G-MC hydrogels compared to cells seeded in a normal tissue culture plate (TCP). **a**) Representative Calcein AM-EthD1 live/dead assay images of NIH-3T3 and HCE cell cultures exposed to the different hydrogel versions. **b**) Cell counts after 72 h of culture. **c**) Percentage of viable cells registered in each group. **d, e**) Percentage of cells registered in each of the cell cycle phases for (**d**) NIH-3T3 and (**e**) HCE cultures. 148

IV.16 Human stromal primary cells seeded by embedding them in G hydrogel. **a**) Phase-contrast microscopy image taken after 48 hours in culture. **b**) Calcein AM-EthD1 live/dead assay image conducted after 48 hours in culture. Scale bars correspond to 100 μm. 149

IV.17 Relative normalised gene expression ($\Delta\Delta$Cq) of **a**) IL-6 and **b**) IL-1β genes in inflamed and non-inflamed HCE cultures. Cells cultured with HCE medium and no inflammation stimuli were used as control (C-M.HCE). Statistical significance is defined as p-value $*$ p < 0.05, $**$ p < 0.01, $***$ p < 0.001, $****$ p < 0.0001 with respect to control (C-M.HCE). 154

IV.18 Relative normalised gene expression ($\Delta\Delta$Cq) of IL-1β in HCE cultures seeded in the presence of different functionalised hydrogel versions. Statistically significant differences showed differences with respect to the cells cultured with HCE medium and no inflammation stimuli (M-M). Statistical significance is defined as p-value $*$ p < 0.05, $**$ p < 0.01, $***$ p < 0.001, $****$ p < 0.0001. 156

IV.19 Evolution of epithelial wound closure in the central cornea of an *ex vivo* bovine corneal model treated with the hydrogel over an 8-day period. . 157

IV.20 Haematoxylin-Eosin staining of the histological section of the central cornea of the *ex vivo* bovine corneal model after re-epithelialisation and treatment with hydrogel H. The cornea was processed 8 days after wound reproduction. The large and small images were taken with 10$\times$ and 40$\times$ magnification lenses, respectively. The scale bars correspond to 50 μm. Complete epithelial repair was observed as well as maintenance of the applied hydrogel. Abundant adhesion points were observed for the hydrogel with the basal epithelium and with the anterior stroma at 400$\times$ magnification. 158

IV.21 Haematoxylin-Eosin staining of the histological section of the central cornea of the *ex vivo* rabbit corneal model after re-epithelialisation and treatment with hydrogel H. The cornea was processed 6 days after wound reproduction. Image was taken with 10× magnification lens and the scale bar corresponds to 100 μm. Complete epithelial repair was observed as well as maintenance of the applied hydrogel (marked with yellow arrows). A part of the applied hydrogel was noticeable above the new epithelium, indicating the long-lasting effect of the hydrogel throughout the wound healing process. 159

IV.22 Haematoxylin-Eosin staining of the histological sections of the limbal region from *ex vivo* models of **a**) bovine and **b**) rabbit corneas. The melanin concentration in the basal layer of the bovine limbus was significantly higher compared to that of the rabbit model. Images were taken with 20× magnification lens and the scale bars correspond to 50 μm. 159

IV.23 Characteristic force displacement curve for H hydrogel in the mucoadhesion analysis. The maximum force required to separate the hydrogel-containing probe from the cornea is represented by the peak value of F_{max}. The area shaded in grey indicates the work of adhesion (W_{adh}) needed to detach the hydrogel from the cornea. 160

IV.24 Mucoadhesive properties of H hydrogel in terms of **a**) the detachment force (F_{max}) and **b**) the work of adhesion (W_{adh}). Measurements were performed in 3 biological replicates. Statistical significance is defined as p-value $*$ $p < 0.05$, $**$ $p < 0.01$, $***$ $p < 0.001$, $****$ $p < 0.0001$. 160

IV.25 Evolution of the epithelial defect *in vivo* in rabbit eyes of the pilot study treated with artificial tears (Control) or the different hydrogel versions (H, H-Ab, H-AS and H-HAMe) from day 3 (D3) to day 5 (D5). The epithelial injury was assessed using fluorescein staining. 162

IV.26 Evolution of the epithelial defect *in vivo* in rabbit eyes of the pilot study. **a**) The percentage of the initial area of the surgical epithelial wound remaining open from the day of surgery (D0) to day 10 (D10). **b**) The percentage of wounds closed per day from day 4 (D4) to day 10 (D10). Statistically significant differences are defined as p-value $*$, + $p < 0.05$, $**$, ++ $p < 0.01$, $***$, +++ $p < 0.001$, $****$, ++++ $p < 0.0001$. "$*$" and "+" show significant differences of H and H-AS hydrogels with respect to the control treatment. 163

IV.27 Draize test score of the pilot study from day 2 (D2) to day 9 (D9). The range of scores on the Draize scale based on Kay and Calandra's classification from 2.5 to 15 represents the minimally irritative toxicity range. (Dotted line at y = 15). Any values exceeding 15 points would be classified as mildly irritative or higher. No statistically significant differences were found among the samples. 164

IV.28 The normalised amounts (pg/mg) of **a**) MIP-1β, **b**) MMP-9, **c**) NCAM-1, and **d**) IL-8 in the tear samples collected during the pilot study. The expression of each cytokine per study day is shown without distinguishing between treatments. 165

IV.29 The normalised amounts (pg/mg) of **a**) MIP-1β, **b**) MMP-9, **c**) NCAM-1, and **d**) IL-8 in the tear samples collected during the pilot study per day and per study group. 166

IV.30 Evolution of the epithelial defect *in vivo* in rabbit eyes treated with artificial tears (Control) or the different hydrogel versions (H, H-Ab, H-AS and H-HAMe) from the day of surgery (D0) to day 5 (D5). The epithelial injury was assessed using fluorescein staining. 167

IV.31 Evolution of the epithelial defect *in vivo* in rabbit eyes. **a**) The percentage of the initial area of the surgical epithelial wound remaining open from the day of surgery (D0) to day 7 (D7). **b**) The percentage of wounds closed per day from day 4 (D4) to day 7 (D7). **c**) The percentage of the initial area of the surgical epithelial wound remaining open from the day 3 (D3) to day 7 (D7). No statistically significant differences were found between the samples. 168

IV.32. Draize test score from day 3 (D3) to day 7 (D7). The range of scores on the Draize scale based on Kay and Calandra's classification from 2.5 to 15 represents the minimally irritative toxicity range. (Dotted line at y = 15). Any values exceeding 15 points will be classified as mildly irritative or higher. No statistically significant differences were found among the samples. 170
IV.33. Collected tear volume via Schirmer strips for each treatment on days 0, 1, 4, and 7 of the study. No statistically significant differences were found among the samples. 171
IV.34. Amount of protein quantified from the elution of tear samples collected by Schirmer strips for each treatment on days 0, 1, 4 and 7 of the study. Statistical significance is defined as p-value $*$, +, # $p < 0.05$, $**$, ++, ## $p < 0.01$, $***$, +++, ### $p < 0.001$, $****$, ++++, #### $p < 0.0001$."$*$", "+" and "#" show significant differences with respect to control, H-AS and H-HAMe hydrogels, respectively. 171
IV.35. Relative normalised gene expression ($\Delta\Delta$Cq) of IL-1β and α-SMA genes in rabbit corneal samples extracted 7 days (**a, c**) or 21 days (**b, d**) post surgery. Statistically significant differences defined as p-value $* p < 0.05$, $** p < 0.01$, $*** p < 0.001$, $**** p < 0.0001$ are shown with respect to the control of each time point. 173
IV.36. Relative normalised gene expression ($\Delta\Delta$Cq) of p63, PAX6 and CK3 genes in rabbit corneal samples extracted 7 days (**a, c, e**) or 21 days (**b, d, f**) post surgery. Statistically significant differences defined as p-value $* p < 0.05$, $** p < 0.01$, $*** p < 0.001$, $**** p < 0.0001$ are shown with respect to the control of each time point. 174
IV.37. Relative normalised gene expression ($\Delta\Delta$Cq) of Ki67 and CD44 genes in rabbit corneal samples extracted 7 days (**a, c**) or 21 days (**b, d**) post surgery. Statistically significant differences defined as p-value $* p < 0.05$, $** p < 0.01$, $*** p < 0.001$, $**** p < 0.0001$ are shown with respect to the control of each time point. 175
IV.38. Haematoxylin and PAS staining of impression cytology samples obtained before surgery (D0) from the bulbar conjunctivas of rabbit eyes of the *in vivo* assay. Images were taken with 20$\times$ magnification and the scale bars correspond to 50 μm. 176

IV.39 Haematoxylin and PAS staining of impression cytology samples obtained from bulbar conjunctivas 7 (**a-e**) and 21 days (**f-j**) after surgery. Rabbit corneas were treated with artificial tears (Control) or with H, H-Ab, H-AS or H-HAMe hydrogels. Images were taken with 20× magnification and the scale bars correspond to 50 μm. 177

IV.40 Haematoxylin-Eosin staining of the histological sections of the central cornea of rabbit corneal samples obtained from the *in vivo* assay after re-epithelialisation. Rabbit corneas were treated with artificial tears (Control) or with H, H-Ab, H-AS or H-HAMe hydrogels, and processed 7 (**a, c, e, g, i**) and 21 days (**b, d, f, h, j**) after surgery. Images were taken with 20× magnification lens and the scale bars correspond to 50 μm. . . 180

IV.41 Percentaje of Ki67 positive cells detected in rabbit corneal samples obtained from the *in vivo* assay. The corneas were treated with artificial tears (Control) or with H, H-Ab, H-AS or H-HAMe hydrogels and processed 7 and 21 days after surgery. 183

IV.42 Fluorescent immunostaining for α-SMA marker in the central cornea of rabbit corneal samples obtained from the *in vivo* assay. Rabbit corneas were treated with artificial tears (Control) or with H, H-Ab, H-AS or H-HAMe hydrogels and processed 7 (**a-e**) and 21 (**f-j**) days after surgery. The yellow arrows in images **c** and **h** indicated the real α-SMA labelling in the tissue. The green staining of the stroma in **c** and **h** mostly belonged to the autofluorescence acquired by the tissue itself. Images were taken with 20× magnification lens and the scale bars correspond to 100 μm. 184

IV.43 Fluorescent immunostaining for Integrin-β4 marker in the central cornea of rabbit corneal samples obtained from the *in vivo* assay. Rabbit corneas were treated with artificial tears (Control) or with H, H-Ab, H-AS or H-HAMe hydrogels and processed 7 (**a-e**) and 21 (**f-j**) days after surgery. Images were taken with 20× magnification lens and the scale bars correspond to 100 μm. 185

IV.44.Inmunofluoresce staining of PanCK marker in the central cornea of rabbit corneal samples obtained from the *in vivo* assay Rabbit corneas were treated with artificial tears (Control) or with H, H-Ab, H-AS or H-HAMe hydrogels and processed 7 (**a-e**) and 21 (**f-j**) days after surgery. Images were taken with 20× magnification lens and the scale bars correspond to 100 μm. 186
IV.45.Expression of CK3 (red) and CK15 (green) markers in the limbus of rabbit corneal samples obtained from the *in vivo* assay. Rabbit corneas were treated with artificial tears (Control) or with H, H-Ab, H-AS or H-HAMe hydrogels and processed 7 (**a-e**) and 21 (**f-j**) days after surgery. Images were taken with 20× magnification lens and the scale bars correspond to 100 μm. 187
IV.46.Expression of ZO-1 (red) and Ki67 (green) markers in the central cornea of rabbit corneal samples obtained from the *in vivo* assay. Rabbit corneas were treated with artificial tears (Control) or with H, H-Ab, H-AS or H-HAMe hydrogels and processed 7 (**a-e**) and 21 (**f-j**) days after surgery. Images were taken with 20× magnification lens and the scale bars correspond to 100 μm. 188
IV.47.Expressions of ΔNp63α and melan A-positive cells in a histological section of the limbal area of a human sclerocorneal tissue. The image was taken with a 20× magnification lens and scale bar corresponds to 50 μm. The image shows the specific localisation of ΔNp63α and melan A-positive cells in the limbal crypts. 189

IV.48 Expressions of CK15, vimentin and ΔNp63α markers in human limbal epithelial cells directly isolated after tissue enzymatic digestion (**a** and **e**, p0 Cytospin) or cultured during several cell passages p0 (**b, f**) and p1-p2 (**c, g**). The images **a** and **e** show that the cells extracted directly after tissue digestion highly expressed the non-differentiation markers CK15 and ΔNp63α. An exponential decrease in the undifferentiation markers and a predominant vimentin staining were registered throughout the passages (Images **b, c, f, g**). The graphs show the evolution of the percentage of CK15- and vimentin-positive cells (graph **d**) and ΔNp63α bright cells (graph **h**) from several sclerocorneal tissues throughout the passages. Statistical significance is defined as p-value $*$ p < 0.05, $**$ p < 0.01, $***$ p < 0.001, $****$ p < 0.0001. Images were taken with 20$\times$ magnification and the scale bars correspond to 25 μm. 191

IV.49 Expression of the vimentin marker in human limbal epithelial (**a**) and stromal (**b**) cell cultures. Both cultures corresponded to p0 passage. Both images were taken with a 20$\times$ magnification lens and the scale bars correspond to 25 μm. 192

IV.50 Human limbal epithelial cell culture of passage p0 and passage p1. The phase-contrast microscopy image on the left (**a**) shows epithelial cells of passages p0 seeded above a *feeder layer* of 3T3 cells. Cells marked with yellow arrowheads correspond to the melanocytes that enclosed the forming epithelial stem cell colony. **b**) and **c**) fluorescence microscopy images show the expression of the melan A marker in epithelial cells of passages p0 and p1. All the images were taken with 20$\times$ magnification lens and all the scale bars correspond to 50 μm. 193

IV.51 Different confocal planes (**a-c**) of a holoclon of CK15-labelled epithelial stem/progenitor cells embraced by Melan A positive melanocytes. Figure **d** shows the reconstruction of all the acquired planes of the colony. The image was taken with a super-resolution microscope with 40$\times$ magnfication lens. The scale bar corresponds to 25 μm. 194

III.1. *In vitro* inflamazio saiakuntzan erabilitako tratamenduen eskema. 336

Irudien zerrenda

I.1. Begiaren gainazalaren 3 osagai erakusten dituen eskema. **a**) Malko-geruzako 4 atalen diagrama. **b**) Konjuntibaren atalen kokapena; betazaleko konjuntiba, konjuntiba bulbarra eta konjuntiba-fornixa. **c**) Begi-globoaren osagai anatomiko nagusiak eta korneako geruzen ilustrazio xehatua. 244

I.2. Korneako osagaien ilustrazio xehatua. Epitelioa 5-6 geruzako epitelio estratifikatua da eta geruza zelular heterogeneoen arteko lotura-sare konplexua du. Estromaren aurreko herena diagonalean orientatutako xaflek osatzen dute, eta horiek z ardatzean aldaketa esanguratsuak eragiten dituzte. Aitzitik, estromaren atzeko bi herenak x eta y ardatzetan luzetarako erresistentzia eskaintzen duten xafla paraleloz osatuta daude. Kolageno-zuntzexkek lamela bakoitzaren barruan duten kokapenak zeregin garrantzitsua du zuntzexken ondulazioaren prebentzioan eta, beraz, banakako zuntxezka bakoitzaren trakzioarekiko erresistentziaren hobekuntzan. Azkenik, kornea-hesia eta ponpaketa metabolikoko lekuak korneako endotelioan zehazten dira. [10]-tik moldatutako irudia. 247

I.3. Linbo esklerokornealeko zelulen nitxoa. 251

I.4. LEZA bidezko kornearen birsortze hipotesiaren azalpen grafikoa. **a**) Linbo eremuko epitelio basalean kokatutako zelula amak asimetrikoki banatzen dira ZDZI-k sortzeko. ZDZI horiek kornea zentraleko eremura migratzen dute, pixkanaka ZPM eta, ondoren, DEZ bilakatuz. LKrE, EP, LEZA, ZDZI, ZPM eta DEZ linboko kripta epitelialei, estromako proiekzioei, linboko epitelio zelula amei, zatitzen doazen zelula igarokorrei, zelula post mitotikoei eta desberdindutako epitelio zelulei dagokie, hurrenez hurren. **b**) LEZA-ek autoberritzeko eta zelula espezializatuagoetan desberdintzeko gaitasuna dute. 255

I.5. LZAG-k izan ditzakeen aldi ezberdinen azalpen grafikoa. 258
I.6. Kornea birsortzeko prozesuaren ikuspegi orokorra. Kalte epitelial baten ondoren, hazkuntza faktoreak askatzen dira, hala nola EGF, PDGF, IGF, intsulina eta beste zitokina batzuk, kaltetutako zelula epitelialek eragindako jarduera biokimiko handi baten ondorioz. Ondoren, korneako zelula epitelial osasuntsuek berrantolaketa zelularra izaten dute, eta horrek aldaketa morfologiko eta funtzional batzuk eragiten ditu. Prozesu hori hasi ondoren, epitelioa itxi egiten da linboko eremuan kokatuta dauden LEZA/P-k aktibatzearen ondorioz, gero eta zelula epitelial desberdinduagoetan ugaldu eta bereizten baitira, epitelio arruntaren estratifikazioa sortuz. Korneako estroman, zelula epitelialek jariatutako IL-1 eta TNFα delakoek keratozitoen apoptosia eragiten dute. Ordu batzuen buruan, zelularik gabeko eremuaren ondoko keratozitoak aktibatzen hasten dira. Era berean, epitelioaren azpiko keratozitoen hasierako apoptosiaren ondoren, PDGF-k eragindako inguruko keratozitoen migrazioa eta ugaltzea ematen da. Migrazio horren ostean, aktibatutako keratozitoak miofibroblastoetara desberdintzen dira, zelula epitelialek askatutako TGF-β-ren eraginaren bitartez. Miofibroblasto horiek HGF eta KGF hazkuntza faktoreen ekoizpena eragiten dute. Faktore hauek zelulaz kanpoko matrizearen osagaiak kodetzen dituzten geneak aktibatu eta kornearen gardentasuna babesten duten molekulak kodetzen dituzten geneak desaktibatzen dituzte. Ondoren, kolagenasen eta matrizearen beste metaloproteinasa batzuen ekoizpena handitu egiten da, eta horrek estroma birmoldatzea dakar. Aipatutako prozesuek zelulaz kanpoko matrizearen, estromako zelula kantitatearen eta ehun-uzkurduraren ekoizpena nabarmen handitzea eragiten dute, eta horrek ehunaren opakutasuna eragiten du. Azkenik, estromaren konponketa estroma orbaintzean inplikatutako zelulen mekanismo apoptotikoen bidez eta keratozitoak egoera normalera berrezartzearen bidez osatzen da. Endotelioa, honen zelulak migratuz, hedatuz edo argalduz birsortzen da, ahalik eta azalera handiena estaltzeko. Zelula epitelialek urdinez adierazitako hazkuntza faktoreak jariatzen dituzte, eta estromako zelulek, berriz, gorriz adierazitakoak. 263

I.7. Medikuntza birsortzailean erabilitako estrategien, osagaien eta interakzioen ikuspegi orokorra. Medikuntza birsortzaileko terapietan zelulak, biomaterialak eta biomolekulak sartzen dira jokoan, hala nola zelula birsortzaileak injektatzea edo ehun endogenoen konponketa sustatzeko biomaterial azelularren euskarriak sortzea. Arlo honetan garatutako soluzioak konplexuak badira ere, estrategia horiek ehunak birsortzeko eta konpontzeko erantzun eraginkorrenak bideratzeko aukera ematen dute. [122]-tik moldatutako irudia. 268

I.8. Metakriloil-zeta fibroinazko (Sil-MA) biotinta eta hidrogela prestatzeko prozesua. **a**) Kapuluak pisatu ondoren, zeta 1 l 0,05 M sodio karbonatoarekin nahastu, ur destilatuarekin bi aldiz garbitu eta gau osoan zehar berogailuan deshidratatzen da. Ondoren, zeta LiBr gatz-disoluzio batean disolbatu eta iragazi egiten da. Glizilato metakrilatoa (GMA) tantaz tanta gehitzen zaio zeta fibroinari (RZF), eta RZF-GMA soluzioa plaka bero baten gainean (60 °C) nahasten da 6 orduz 800 b/min-tara, zeta fibroinak eta GMA-k erreakziona dezaten. Ondoren, disoluzioa ur destilatuan diluitzen da 7 egunez, eta beste 5-7 egunez liofilizatzen da. Sil-MA liofilizatuaren belakia LAP konposatua % 0,2-ko kontzentrazioa duen PBS soluzio baten disolbatu eta homogeneoki nahasten da. Azkenik, soluzioa zentrifugatu egiten da aire-burbuilak ezabatzeko. **b**) PKH67 (berdea) markatutako zelulekin eta PKH26 (gorria) markatutako zelulekin inprimatutako trakea forma duen hidrogela. Ezkerretik eskuinera: trakea baten CAD diseinua, inprimatu diren hidrogelen irudiak, fluoreszentzia-irudia (FL) mikroskopia konfokala edo plano bakarreko argiztapen-mikroskopia erabiliz, eta hidrogel fluoreszentearen eta CAD diseinuaren irudi bateratua. [164]-tik hartutako irudiak. 274

I.9. Hidrogelen diseinuan kontuan izan beharreko propietate nagusiak. **a**) Sarearen tamaina, **b**) puzteko jokaera, **c**) biskoelastikotasuna, **d**) biodegradagarritasuna, **e**) biobateragarritasuna eta **f**) aplikazioaren espezifikotasunari lotutako propietateak. 278

I.10. Hidrogelen sintesirako erretikulazio estrategia fisiko eta kimikoen sailkapena. 283

I.11. **a**) Erriboflabinaren egitura; **b**) Erriboflabinaren oxidazio egoerak (**a** eta **b** [218]-tik moldatuta); **c**) Kolageno eta erriboflabinaren arteko gurutzaketa prozesua ([219]-tik moldatuta); **d**) UV izpiekin irradiatu ondoren, gelatina eta erriboflabina fosfatoaren arteko erretikulazio prozesuaren erreakzio posiblea. 286

I.12. Zelula-xaflen ingeniaritza. **a**) Konfluentzian dauden zelulak banaka askatzen dira digestio entzimatikoaren bidez. **b**) Zelula-xaflen atxikipena eta askatzea termoiraunkorrak diren hazkuntza plaketan. Plakak polimero termoiraunkor batez estalita daude, eta horrek bere hidrofilia tenperatura espezifikoetan aldatzea baimentzen du. Metodo eraginkor eta ez-inbaditzailea izanik, xafla zelularrak eratu, zelulak elkarri lotuta mantendu eta xafla osoa aska daiteke. 289

I.13. Korneako akats ezberdinetarako hidrogelen aplikazioak. **a**) Korneako sakonera txikiko epitelio-zaurietarako apositu terapeutikoak. **b**) Ebakidura txikietarako josturen ordezko gisa erabiliko diren begietako itsasgarriak. **c**) Korneako akats sakonak eta zulaketak betetzeko hidrogelak. **d**) Kornea bere osotasunean ordeztuko duten konstruktuen erabilera. 292

I.14. GelCORE itsasgarriaren *in vivo* aplikazioa untxien korneako zaurietan **a**) eta **b**) Untxien korneetan sortutako akats estromalak. **c**) GelCORE itsasgarriaren zuzeneko aplikazioa, **d**) erretikulazio prozesua, **e**) akats estromalaren gaineko gelCORE itsasgarri gardenaren eraketa. GelCORE tratamenduaren **f**) aurretik **g**) ostean ateratako aurreko segmentuaren koherentziazko tomografia bidez lortutako irudiak. [306]-tik hartutako irudiak. 298

I.15. **a**) Giza kornearen eta *in vitro* 3D kornea-ehunaren eredua. 3 mm-tako eskala lerroa. **b**) Txerri kornea, interfaze likido eta aire-likido interfazean hCEC, hCSSC eta DRG zelulen hazkuntza bateratua 28. egunean. Hazkuntza biak glizerolez busti dira. 3 mm-tako eskala lerroa. hCEC: giza korneako zelula epitelialak; hCSSC: giza korneako zelula ama estromalak; DRG: oilasko-erro dortsaleko neurona ganglionarrak; ESD-LC: interfaze likidoko mota zelular guztietako hazkuntza bateratua; ESD-ALIC: aire-likido interfazeko zelula-mota guztietako hazkuntza bateratua. [327]-tik hartutako irudia. 301

III.1. Hidrogelen sintesirako erabilitako konposatuen egitura kimikoa. **a**) Gelatina, **b**) erriboflabina fosfatoa (RFP), **c**) dextranoa (D), **d**) azido hialuronikoa (AH) eta **e**) metilzelulosa (MZ). 315
III.2. Gelatina eta RFP hidrogelaren injekzio eta erretikulazio prozesua. 316
III.3. Giza mintz amniotikoaren eskualdeen irudikapen eskematikoa umetokiaren barruan eta kanpoan. Kareneko amniosa (urdinez markatuta, karena estaltzen du), zaku-amniotikoko amniosa edo islatutako amniosa (laranjez markatuta, umetoki-pareta estaltzen du) eta zilbor-amniosa (grisez markatuta, zilbor-hestea estaltzen du). Zaku-amniotikoko amniosa 3 gunetan bana daiteke, disko karendunetik hurbilen dagoen gunea, erdiko gunea eta urruneko amniosa, disko karendunetik urrunen dagoen gunea. [332]-tik abiatuta moldatutako irudia. 321
III.4. **a**) Sandwich motako ELISA eta **b**) Luminex teknologiaren funtzionamenduaren irudikapen eskematikoa. 326
III.5. **a**) NIH-3T3 fibroblastoen zelula lerroa eta **b**) KZE zelula lerroa. $10\times$ handipen objektiboarekin ateratako irudiak. Eskala lerroek 100μm-ko neurriak adierazten dituzte. 328
III.6. *Ex vivo* eredurako behi-kornearen prozesamendua. 338
III.7. *Ex vivo* eredurako untxi-kornearen prozesamendua. 338
III.8. Zunda zilindrikoaren korneako zauriarekiko desplazamendu bertikala. 339
III.9. *In vivo* prozedura kirurgikoa egiteko jarraitutako pausuak. 342
III.10Schirmer tiratik malkoa jasotzeko prozedura. 345
III.11Zitokinen arrayaren lan-prozedura. **a**) Atzemate-antigorputzak dituen beirazko euskarria erabat lehortzen da edozein inkubazio hasi aurretik. **b**) Laginak gehitu eta euskarrian dauden antigorputzekin lotzen dira. **c**) Ondoren, biotinarekin markatutako bigarren detekzio-antigorputz bat gehitzen da, zitokinaren beste epitopo bat ezagutzeko gai dena. **d**) Estreptabidinarekin konjugatutako Cy3 tindaketa gehitzen da seinale detektagarri bat sortzeko. **e**) Array-a irakurri eta datuak aztertzen dira. . 348

IV.1. Filmen **a**) 4000-850 cm^{-1} eta **b**) 1750-850 cm^{-1} bitarteko FITR espektroak. **c**) Filmetako X izpien difrakzio-analisia. 3000 (**d**), 180 (**e**), 1100 (**f**) eta 450× (**g**) handipenekin lortutako filmen SEM irudiak. KOL: Kolagenoa; SPI: Soja-proteina isolatua; GEL-LAK: Laktosarekin erretikulatutako gelatina; GEL-AZ: Azido zitrikoarekin erretikulatutako gelatina. 368

IV.2. Film hidratatuen eta lehorren transmitantzia eta gardentasuna. **a-d**) Grafikoek film bakoitzak espektro ikusgaian transmititutako argiaren ehunekoa erakusten dute. Datuek transmitantzia-ehunekoaren batez bestekoa ± desbideratze estandarra (DE) adierazten dute. Ezberdintasun estatistikoki esanguratsuek film bakoitzaren egoera lehor eta hidratatuen arteko aldaketak adierazten dituzte (∗ $p < 0,05$, ∗∗ $p < 0,01$, ∗∗∗ $p < 0,001$; $n = 9$). **e-l**) irudiek film bakoitzaren gardentasun-maila erakusten dute, bai film lehorretan (**e-h**), bai hidratatuetan (**i-l**). Irudi guztiak baldintza berdinekin atera genituen. . . 371

IV.3. 24 orduz 37 °C-tan 200 μg/ml-ko kolagenasa A soluzioan edo PBS-tan mantendutako filmen *in vitro* degradazio-profilak. Ur desionizatuan murgildutako filmak kontrol gisa erabili genituen. **a**) KOL filmen degradazio-profilak, **b**) SPI filmen degradazio-profilak, **c**) GEL-LAK filmen degradazio-profilak eta **d**) GEL-AZ filmen degradazio-profilak. Datuek batez bestekoa ± DE adierazten dute, eta kolagenasa A-n (∗) eta PBS-n (#) sartutako filmen eta ur desionizatuan sartutako filmen arteko alde estatistikoki esanguratsuak adierazten dituzte. ∗, # $p < 0,05$, ∗∗, ## $p < 0,01$, ∗∗∗, ### $p < 0,001$; $n = 3$. 372

IV.4. Filmen eragina NIH-3T3 zelulen **a**) proliferazioan eta **b-d**) bideragarritasunean. 3T3 zelulak film bakoitzarekin kontaktuan jarri genituen 24, 48 eta 72 orduz. Inolako biomaterialik gabe ereindako zelulak kontrol gisa erabili genituen. Proliferazio-emaitzek zelula bideragarrien ugaltze-tasaren batez bestekoa ± DE adierazten dute, t = 0 h-ko zelula bideragarriekin alderatuta. Bideragarritasun-emaitzek zelula bideragarrien ehunekoa adierazten dute, kontrolarekin alderatuta (% 100-eko bideragarritasuna). Grafikoen kutxa bakoitzaren barruan marraztutako lerroek film bakoitzaren bideragarritasun-balioen medianak adierazten dituzte. Kontrolarekiko desberdintasun estatistikoki esanguratsuak ikusi daitezke (∗ $p < 0,05$, ∗∗ $p < 0,01$, ∗∗∗ $p < 0,001$; $n = 9$). 374

IV.5. Filmen eragina KZE zelulen **a**) proliferazioan eta **b-d**) bideragarritasunean. KZE zelulak film bakoitzarekin kontaktuan jarri genituen 24, 48 eta 72 orduz. Inolako biomaterialik gabe ereindako zelulak kontrol gisa erabili genituen. Proliferazio-emaitzek zelula bideragarrien ugaltze-tasaren batez bestekoa ± DE adierazten dute, t = 0 h-ko zelula bideragarriekin alderatuta. Bideragarritasun-emaitzek zelula bideragarrien ehunekoa adierazten dute, kontrolarekin alderatuta (% 100-eko bideragarritasuna). Grafikoen kutxa bakoitzaren barruan marraztutako lerroek film bakoitzaren bideragarritasun-balioen medianak adierazten dituzte. Kontrolarekiko desberdintasun estatistikoki esanguratsuak ikusi daitezke (∗ $p < 0,05$, ∗∗ $p < 0,01$, ∗∗∗ $p < 0,001$; $n = 9$). 375

IV.6. 3T3 zelulen hazkuntza filmen gainean. **a-d**) Fase-kontrasteko mikrospioaren bidez, 3T3 zelulen hazkuntza-plakaren (Kontrola) edo filmen gaineko hazkuntzen irudiak 24 orduz kultibatu ondoren. **e-h**) AM-Kaltzeina-EthD1 saiakuntzaren irudiak eta **i-l**) SEM bidez ateratako irudiak. **a-h**) Irudiak 10× handipen objektiboarekin atera genituen eta eskala lerroek 100 μm-ko neurriak adierazten dituzte. **i-l**) Irudiak 450× handipenarekin atera genituen. 376

IV.7. KZE zelulen hazkuntza filmen gainean. **a-d**) Fase-kontrasteko mikrospioaren bidez, KZE zelulen hazkuntza-plakaren (Kontrola) edo filmen gaineko hazkuntzen irudiak 24 orduz kultibatu ondoren. **e-h**) AM-Kaltzeina-EthD1 saiakuntzaren irudiak eta **i-l**) SEM bidez ateratako irudiak. **a-h**) Irudiak 10× handipen objektiboarekin atera genituen eta eskala lerroek 100 μm-ko neurriak adierazten dituzte. **i-l**) Irudiak 450× handipenarekin atera genituen. 377

IV.8. GEL-LAK-en gainean ereindako KZE eta 3T3 zelulen migrazio-saiakuntza, 24, 48 eta 72 orduz kultibatu ondoren. Irudiak 10× handipen objektiboarekin atera genituen; eskala lerroek 50 μm-ko neurriak adierazten dituzte. **a,b**) grafikek film bakoitzean 3T3 (**a**) eta KZE (**b**) zelulen hutsune-itxieraren bilakaera adierazten dute. 378

IV.9. **a**) G, G-D, G-AH eta G-MZ hidrogelen anplitude-ekorketak (frekuentzia angeluarra (ω) = 10 rad/s, 25 °C) eta **b**) G, G-D, G-AH eta G-MZ hidrogelen maiztasun oszilazio-ekorketak (tentsioa (ε) = % 1, 25 °C). 380

IV.10 **a**) G, G-D, G-AH eta G-MZ hidrogeletako fluxu-ekorketak. **b**) G, G-D, G-HA eta G-MZ hidrogeletako tartekatutako ebakidura neurketak, lau ziklotan txandakatutako ebakidura-indar baxuan (grisa; 0.1 s^{-1}) eta altuan (zuria; 10 s^{-1}). 381

IV.11 G (**a**), G-D (**b**), G-AH (**c**) eta G-MZ (**d**) hidrogelen muga elastikoaren neurketak. Muga elastiko estatikoaren balioak dagozkien grafikoetan adierazita daude. 382

IV.12 G, G-D, G-AH eta G-MZ hidrogeletan egindako puzte (**a**) eta hedatze (**b**) neurketak, PBS-tan murgildu eta 24 ordura. Emaitzek G hidrogelarekiko aldaketa ± DE adierazten dute. Alde estatistikoki esanguratsuak $*$ p < 0,05, $**$ p < 0,01, $***$ p < 0,001, $****$ p < 0,0001 bezala definitu ditugu. 383

IV.13.G, G-D, G-AH eta G-MZ hidrogelen transmitantzia eta gardentasun ezberdintasunak, erretikulazioaren aurretik eta ondoren. **a-d**) Grafikoek erretikulatu eta erretikulatu gabeko hidrogelek transmititutako argiaren ehunekoa erakusten dute, 400-800 nm tartean. Datuek transmisioaren batez besteko ehunekoa $\pm$ DE adierazten dute. Ezberdintasun estatistikoki esanguratsuek film bakoitzaren erretikulatutako eta erretikulatu gabeko egoeren arteko aldaketak adierazten dituzte ($*$ p < 0,05, $**$ p < 0,01, $***$ p < 0,001, $****$ p < 0,0001). **e**) Irudiek hidrogel bakoitzaren gardentasun-maila erakusten dute, argi urdinarekin irradiatu aurretik eta ondoren. Irudi guztiak baldintza berberak erabiliz atera genituen. 384

IV.14.Hidrogeletan pilatutako FITC-IgG (**a**), FITC-Albumina (**b**) eta Vigamox (**c**) konposatuen askapen zinetika. Datuek 15 egunetan askatutako guztizko kopuruaren ehuneko normalizatua adierazten dute. 388

IV.15.G, G-D, G-AH eta G-MZ hidrogelekin ereindako NIH-3T3 eta KZE zelula-hazkuntzen zitobateragarritasunaren ebaluazioa, hazkuntza-plaka (HP) arrunt batean ereindako zelulekin alderatuta. **a**) AM-Kaltzeina-EthD1 saiakuntzaren NIH-3T3 eta KZE zelula-hazkuntzen irudiak, hidrogel ezberdinen eraginpean. **b**) Zelulen kontaketa 72 orduz kultibatu ondoren. **c**) Talde bakoitzean erregistratutako zelula bideragarrien ehunekoa. **d, e**) Ziklo zelularraren fase bakoitzean erregistratutako NIH-3T3 (**d**) eta KZE (**e**) zelulen ehunekoa. 390

IV.16.G hidrogelean txertatutako giza estromako zelula primarioen hazkuntzak. **a**) Fase-kontraste mikroskopioaren bitartez, zelulak 48 orduz kultiboan egon ondoren lortutako irudia. **b**) AM Kaltzeina-EthD1 saiakuntzaren bitartez, zelulak 48 orduz kultiboan egon ondoren lortutako irudia. Eskala lerroek 100 μm-ko neurriak adierazten dituzte. 391

IV.17 **a**) IL-6 eta **b**) IL-1β geneen adierazpen erlatibo normalizatua ($\Delta\Delta$Cq) KZE hazkuntza inflamatu eta inflamatu gabeetan. KZE medioarekin eta hantura-estimulurik gabe kultibatutako zelulak kontrol gisa erabili genituen (K-M.KZE). Kontrolarekin alderatutako (K-M.KZE) alde estatistikoki esanguratsuak $*$ p < 0,05, $**$ p < 0,01, $***$ p < 0,001, $****$ p < 0,0001 bezala definitu ditugu. 396

IV.18 IL-1β genearen adierazpen erlatibo normalizatua ($\Delta\Delta$Cq) hidrogel funtzionalizatuaren bertsio desberdinekin kultibatutako KZE hazkuntzetan. Estatistikoki esanguratsuak diren desberdintasunak KZE medioarekin eta hantura-estimulurik gabe (M-M) kultibatutako zelulekiko adierazi ditugu, $*$ p < 0,05, $**$ p < 0,01, $***$ p < 0,001, $****$ p < 0,0001. 398

IV.19 Zauri epitelialaren itxieraren bilakaera *ex vivo* behi-korneako ereduan hidrogelarekin tratatutako 8 eguneko aldian. 399

IV.20 Hematoxilina-Eosina tindaketa *ex vivo* kultibatutako behi-kornearen ereduan. Irudiak H hidrogelarekin tratatu osteko berrepitelizazioa adierazten du. Zauria egin eta 8 egunetara prozesatu genuen kornea. Irudiak 10$\times$ eta 40$\times$ objektiboekin atera genituen, hurrenez hurren. Eskala lerroek 50 μm-ko neurria adierazten dute. Berrepitelizazio osoa ikusi genuen, baita aplikatutako hidrogelaren mantenua ere. 400$\times$ handipenarekin, hidrogelak epitelioarekin eta aurreko estromarekin sortutako atxikimendu puntuak ikus daitezke. 400

IV.21 Hematoxilina-Eosina tindaketa *ex vivo* kultibatutako untxi-kornearen ereduan. Irudiak H hidrogelarekin tratatu osteko berrepitelizazioa adierazten du. Zauria egin eta 6 egunetara prozesatu genuen kornea. Irudia 10$\times$ objektiboarekin atera genuen eta eskala lerroak 100 μm-ko neurria adierazten du. Berrepitelizazio osoa ikusi genuen, baita aplikatutako hidrogelaren mantenua ere (gezi horiekin adierazita). Aplikatutako hidrogelaren zati bat epitelio berriaren gainetik ikus zitekeen, hidrogelak zauria orbaintzeko prozesuan zehar duen eragin iraunkorra adieraziz. 401

IV.22. Hematoxilina-Eosina tindaketa *ex vivo* kultibatutako behi- (**a**) eta untxi-kornea (**b**) ereduen linboko eremuan. Behi-kornearen linbo eremuko geruza basalean melanina-kontzentrazioa untxi-kornean baino nabarmenagoa izan zen. Irudiak 20× handipen objektiboarekin atera genituen eta eskala lerroek 50 μm-ko neurriak adierazten dituzte. . 401

IV.23. Atxikidura-proban, H hidrogelarentzako indar-desplazamendu kurba bereizgarria. Hidrogela duen zunda korneatik bereizteko behar den gehieneko indarra, F_{max} balioak adierazten du. Grisez itzaldutako eremuak hidrogela eta kornea bereizteko beharrezkoa den atxikitze-lana adierazten du (W_{adh}). 402

IV.24. H hidrogelaren propietate itsaskorrak, **a**) gehieneko askatze-indarrari (F_{max}) eta **b**) atxikitze-lanari (W_{adh}) dagokienez. Neurketak 3 erreplika biologikotan egin genituen. Alde estatistikoki esanguratsuak honela definitu ditugu: $*$ p < 0,05, $**$ p < 0,01, $***$ p < 0,001, $****$ p < 0,0001. . 402

IV.25. Malko artifizialekin (Kontrola) edo hidrogelaren bertsio desberdinekin (H, H-Ag, H-SA eta H-GMAe) tratatutako proba pilotuko untxi-korneen akats epitelialen *in vivo* bilakaera, 3. egunetik (3 e.) 5. eguneraino (5 e.). Akats epiteliala fluoreszeinarekin tindatuta ebaluatu genuen. 404

IV.26. Proba pilotuko untxi-korneetako akats epitelialen *in vivo* bilakaera. **a**) Irekitako zauri epitelialaren eremuaren ehunekoa kirurgiaren egunetik (0 e.) 10. egunera (10 e.). *b*) Itxitako zaurien ehunekoa, 4. egunetik (4 e.) 10. egunera (10 e.). Alde estatistikoki esanguratsuak honela definitu ditugu: $*$, + p < 0,05, $**$, ++ p < 0,01, $***$, +++ p < 0,001, $****$, ++++ p < 0,0001. "$*$" eta "+", H eta H-AS hidrogelek kontrol-tratamenduarekiko dituzten desberdintasunak adierazten dituzte. 405

IV.27. Proba pilotuaren Draize testaren puntuazioa azterketaren 2. egunetik (2 e.) 9. egunera (9 e.). Draize eskalaren Kay eta Kalandraren sailkapenean, 2,5-etik 15-era bitarteko puntuazio-tarteak gutxieneko narritadura tartea adierazten du (y = 15). 15 puntutik gorako edozein balio apur bat narritagarri edo oso narritagarri gisa sailkatuko litzateke. Laginen artean ez genuen alde estatistikoki esanguratsurik ikusi. 406

IV.28 Proba pilotuan bildutako malko-laginetako **a**) MIP-1β, **b**) MMP-9, **c**) NCAM-1 eta **d**) IL-8 zitokinen balio normalizatuak. Grafikak aztertutako egun bakoitzeko zitokina bakoitzaren adierazpena erakusten du, tratamenduak bereizi gabe. 407
IV.29 Proba pilotuan bildutako malko-laginetako **a**) MIP-1β, **b**) MMP-9, **c**) NCAM-1 eta **d**) IL-8 zitokinen balio normalizatuak, eguneko eta azterketa-taldeko. 408
IV.30 Malko artifizialekin (Kontrola) edo hidrogelaren bertsio desberdinekin (H, H-Ag, H-SA eta H-GMAe) tratatutako untxi-korneetako akats epitelialen *in vivo* bilakaera kirurgiaren egunetik (0 e.) 5. eguneraino (5 e.). Akats epiteliala fluoreszeinarekin tindatuta ebaluatu genuen. . . . 409
IV.31 Untxi-korneetako akats epitelialen *in vivo* bilakaera. **a**) Irekitako zauri-eremuaren ehunekoa kirurgiaren egunetik (0 e.) 7. egunera (7 e.). **b**) Itxitako zaurien ehunekoa eguneko, 4. egunetik (4 e.) 7. egunera (7 e.). **c**) Irekitako zauri-eremuaren ehunekoa 3. egunetik (3 e.) 7. egunera (7 e.). Laginen artean ez genuen alde estatistikoki esanguratsurik aurkitu. 410
IV.32 Draize testaren puntuazioa azterketaren 3. egunetik (3 e.) 7. egunera (7 e.). Draize eskalaren Kay eta Kalandraren sailkapenean, 2,5-etik 15-era bitarteko puntuazio-tarteak gutxieneko narritadura tartea adierazten du (y = 15). 15 puntutik gorako edozein balio apur bat narritagarri edo oso narritagarri gisa sailkatuko litzateke. Laginen artean ez genuen alde estatistikoki esanguratsurik hauteman. 412
IV.33 Azterketaren 0., 1., 4. eta 7. egunetan, Schirmer-en tiren bidez bildutako malkoen bolumena tratamendu bakoitzerako. Laginen artean ez genuen alde estatistikoki esanguratsurik aurkitu. 413
IV.34 Azterketaren 0., 1., 4. eta 7. egunetan Schirmer-en tiren bidez jasotako malko-laginen eluziotik abiatuta kuantifikatutako proteina kantitatea tratamendu bakoitzerako. Alde estatistikoki esanguratsuak honela definitu ditugu: $*$, +, # $p < 0{,}05$, $**$, ++, ## $p < 0{,}01$, $***$, +++, ### $p < 0{,}001$, $****$, ++++, #### $p < 0{,}0001$. "$*$", "+" eta "#" ikurrek kontrol, H-SA eta H-GMAe tratamenduekiko desberdintasunak adierazten dituzte, hurrenez hurren. 413

IV.35.IL-1β eta α-SMA geneen adierazpen erlatibo normalizatua ($\Delta\Delta$Cq) 7 egunez (**a, c**) edo 21 egunez (**b, d**) prozesatutako untxi-korneen laginetan. p $*$ p < 0,05, $**$ p < 0,01, $***$ p < 0,001, $****$ p < 0,0001 balioek denbora-puntu bakoitzeko kontrol-tratamenduarekiko alde estatistikoki esanguratsuak erakusten dituzte. 415

IV.36.p63, PAX6 eta CK3 geneen adierazpen erlatibo normalizatua ($\Delta\Delta$Cq) 7 egunez (**a, c, e**) edo 21 egunez (**b, d, f**) prozesatutako untxi-korneen laginetan. p $*$ p < 0,05, $**$ p < 0,01, $***$ p < 0,001, $****$ p < 0,0001 balioek denbora-puntu bakoitzeko kontrol-tratamenduarekiko alde estatistikoki esanguratsuak erakusten dituzte. 416

IV.37.Ki67 eta CD44 geneen adierazpen erlatibo normalizatua ($\Delta\Delta$Cq) 7 egunez (**a, c**) edo 21 egunez (**b, d**) prozesatutako untxi-korneen laginetan. p $*$ p < 0,05, $**$ p < 0,01, $***$ p < 0,001, $****$ p < 0,0001 balioek denbora-puntu bakoitzeko kontrol-tratamenduarekiko alde estatistikoki esanguratsuak erakusten dituzte. 417

IV.38.Untxi-begien konjuntibetatik, inprimatze zitologia bidez lortutako *in vivo* laginen Hematoxilina-PAS tindaketa kirurgia egin aurreko unean (0 e.). Irudiak 20$\times$ handipen objetiboarekin egin genituen eta eskala lerroek 50 μm-ko neurriak adierazten dituzte. 418

IV.39.Untxi-begien konjuntibetatik, inprimatze zitologia bidez lortutako *in vivo* laginen Hematoxilina-PAS tindaketa kirurgia osteko 7. (**a-e**) eta 21. egunetan (**f-j**). Untxi-korneak malko artifizialekin (Kontrola) edo H, H-Ag, H-SA edo H-GMAe hidrogelekin tratatu genituen. Irudiak 20$\times$ handipen objetiboarekin egin genituen eta eskala lerroek 50 μm-ko neurriak adierazten dituzte. 419

IV.40.Hematoxilina-Eosina tindaketak *in vivo* saiakuntzatik lortutako berrepitelizatutako untxi-korneen laginetan. Untxi-korneak malko artifizialekin (Kontrola) edo H, H-Ag, H-SA edo H-GMAe hidrogelekin tratatu eta 7 (**a-e**) eta 21 egunetara (**f-j**) prozesatu genituen. Irudiak 20$\times$ handipen objektiboarekin atera genituen eta eskala lerroek 50 μm-ko neurriak adierazten dituzte. 422

IV.41 *In vivo* saiakuntzako untxi-korneako laginetan detektatutako Ki67 zelula positiboen ehunekoa. Korneak malko artifizialekin (Kontrola) edo H, H-Ag, H-SA edo H-GMAe hidrogelekin tratatu eta kirurgia egin eta 7 eta 21 egunetara prozesatu genituen. 425

IV.42 α-SMA markatzailearen immunofluoreszentzia tindaketa *in vivo* saiakuntzatik lortutako untxi-korneako laginetan. Untxi-korneak malko artifizialekin (Kontrola) edo H, H-Ag, H-SA edo H-GMAe hidrogelekin tratatu eta kirurgia egin eta 7 (**a-e**) eta 21 (**f-j**) egunetara prozesatu genituen. **c** eta **h** irudietako gezi horiek α-SMA tindaketa erreala adierazten dute. Estromaren tindaketa berdea **c** eta **h** irudietan ehunaren beraren autofluoreszentziatik eratorria da batez ere. Irudiak 20$\times$ handipen objektiboarekin egin genituen eta eskala lerroek 100 μm-ko neurriak adierazten dituzte. 426

IV.43 Integrina-β4 markatzailearen immunofluoreszentzia tindaketa *in vivo* saiakuntzatik lortutako untxi-korneako laginetan. Untxi-korneak malko artifizialekin (Kontrola) edo H, H-Ag, H-SA edo H-GMAe hidrogelekin tratatu eta kirurgia egin eta 7 (**a-e**) eta 21 (**f-j**) egunetara prozesatu genituen. Irudiak 20$\times$ handipen objektiboarekin egin genituen eta eskala lerroek 100 μm-ko neurriak adierazten dituzte. . . . 427

IV.44 PanCK markatzailearen immunofluoreszentzia tindaketa *in vivo* saiakuntzatik lortutako untxi-korneako laginetan. Untxi-korneak malko artifizialekin (Kontrola) edo H, H-Ag, H-SA edo H-GMAe hidrogelekin tratatu eta kirurgia egin eta 7 (**a-e**) eta 21 (**f-j**) egunetara prozesatu genituen. Irudiak 20$\times$ handipen objektiboarekin egin genituen eta eskala lerroek 100 μm-ko neurriak adierazten dituzte. . . . 428

IV.45 CK3 (gorria) eta CK15 (berdea) markatzaileen immunofluoreszentzia tindaketa *in vivo* saiakuntzatik lortutako untxi-korneako laginetan. Untxi-korneak malko artifizialekin (Kontrola) edo H, H-Ag, H-SA edo H-GMAe hidrogelekin tratatu eta kirurgia egin eta 7 (**a-e**) eta 21 (**f-j**) egunetara prozesatu genituen. Irudiak 20$\times$ handipen objektiboarekin egin genituen eta eskala lerroek 100 μm-ko neurriak adierazten dituzte. 429

IV.46 ZO-1 (gorria) eta Ki67 (berdea) markatzaileen immunofluoreszentzia tindaketa *in vivo* saiakuntzatik lortutako untxi-korneako laginetan. Untxi-korneak malko artifizialekin (Kontrola) edo H, H-Ag, H-SA edo H-GMAe hidrogelekin tratatu eta kirurgia egin eta 7 (**a-e**) eta 21 (**f-j**) egunetara prozesatu genituen. Irudiak 20× handipen objektiboarekin egin genituen eta eskala lerroek 100 μm-ko neurriak adierazten dituzte. 430

IV.47 ΔNp63α eta melan A zelula-positiboen adierazpena ehun korneoskleralaren linboko eremuan. Irudia 20× handipen objektiboarekin atera genuen eta eskala lerroak 50 μm-ko neurria adierazten du. Irudiak kripta linbarretan ΔNp63α eta melan A zelula-positiboen kokapen zehatza erakusten du. 431

IV.48 CK15, bimentina eta ΔNp63α markatzaileen adierazpena ehunetik zuzenean isolatutako zelula epitelialetan (**a** eta**e**, p0 pasea, zitospinarekin isolatuta) edo kultibatutako p0 (**b, f**) eta p1-2 (**c, g**) paseetako zeluletan. **a** eta **e** irudiek erakusten dutenez, ehunaren digestioaren ondoren zuzenean erauzitako zelulek CK15 eta ΔNp63α markatzaileen adierazpen altua erakusten dute. Paseetan zehar, desberdintze-markatzaileen murrizketa esponentziala eta bimentinaren markaketaren nagusitzea erregistratu genituen (**b, c, f, g** irudiak). Grafikoek ehun esklerokornealeko CK15-bimentina (**d** grafikoa) eta ΔNp63α (**h** grafikoa) zelula-positiboen ehunekoaren bilakaera adierazten dute. Esanahi estatistikoa honela definitu genuen: p $*$ p < 0,05, $**$ p < 0,01, $***$ p < 0,001, $****$ p < 0,0001. Irudiak 20× handipen objektiboarekin atera genituen eta eskala lerroek 25 μm-ko neurriak adierazten dituzte. 434

IV.49 Bimentina markatzailearen adierazpena linboko zelula epitelial (**a**) eta zelula estromalen (**b**) hazkuntzetan. Bi hazkuntzak p0 paseari dagozkie. Bi irudiak 20× handipen objektiboarekin atera genituen eta eskala lerroek 25 μm-ko neurriak adierazten dituzte. 435

IV.50 p0 eta p1 paseetako linboko zelula epitelialen hazkuntzak. Ezkerreko irudiak (**a**), inaktibatutako 3T3 zelula-geruza baten gainean ereindako p0 paseko zelula epitelialak erakusten ditu. Gezi horiz markatutako zelulak sortzen ari ziren zelula ama epitelialen kolonia inguratzen zuten melanozitoei dagozkie. **b**) eta **c**) irudiek p0 eta p1 paseetako zelula epitelialetan melan A markatzailearen adierazpena erakusten dute. Irudi guztiak 20× handipen objektiboarekin atera genituen eta eskala lerroek 50 μm-ko neurriak adierazten dituzte. 435

IV.51 CK15-z markatutako zelula ama/progenitore epitelialez osatutako holokloi baten plano konfokal desberdinak (**a-c**), melanozito Melan A positiboz inguratuta. **d** irudiak koloniako plano guztien muntaia erakusten du. Irudia bereizmen handiko mikroskopio batekin atera genuen 40× handipeneko objektiboarekin. Eskala lerroak 25 μm-ko neurria adierazten du. 437

List of Tables

I.1. Principal causes of LSCD. 15
I.2. List of active clinical trials related to LSCD. 19
I.3. Characteristics of the polymers used as contact lenses' substrates. Table reproduced from [263]. 50

III.1. List of the ELISA assays used for the quantification of growth factors. . . 83
III.2. Detailed description of the used cell lines, culture medium and culture conditions. 86
III.3. Composition of the hydrogels tested in the *in vitro* inflammation assay. . 93
III.4. Composition of the 4 hydrogel treatments used in the *in vivo* assay. . . . 98
III.5. Draize scale's weighted scores for classifying the severity of eye injuries. Reproduced from [337]. 102
III.6. Eye irritation index values reported by Kay and Calandra [338]. 103
III.7. Sequences and properties of the primers used in *in vitro* and *in vivo* assays.111
III.8. List of primary and secondary antibodies used for IF assays. 117

IV.1. Mean $\pm$ SD percentage values of the released amounts for each of the analysed cargoes in G, G-D, G-HA and G-MC hydrogels. Statistical significance is expressed with respect to G ($*$ $p < 0.05$, $**$ $p < 0.01$, $***$ $p < 0.001$, $****$ $p < 0.0001$). 145
IV.2. Concentration of the growth factors measured in the extracted blood-derived products. The results are expressed as quantification mean $\pm$ SD. Statistically significant differences between AS and sPRGF samples are defined as p-value $*$ $p < 0.05$, $**$ $p < 0.01$, $***$ $p < 0.001$, $****$ $p < 0.0001$ for each patient. 151

IV.3. Concentration of the growth factors measured in HAMe samples. The results are expressed as quantification mean ± SD. Statistically significant differences defined as p-value ∗, +, † $p < 0.05$, ∗∗, ++, †† $p < 0.01$, ∗∗∗, +++, † † † $p < 0.001$, ∗∗∗∗, ++++, † † †† $p < 0.0001$ are shown with respect to "∗" HAMe-D, "+" HAMe-P and "†" HAMe-Pool. 152

IV.4. Concentration of the growth factors measured in HAMe pool samples. The results are expressed as quantification mean ± SD. Statistically significant differences defined as p-value ∗, † $p < 0.05$, ∗∗, †† $p < 0.01$, ∗∗∗, † † † $p < 0.001$, ∗∗∗∗, † † †† $p < 0.0001$ are shown with respect to "∗" patient 1 (p1) and "†" patient 3 (p3). 153

IV.5. Progression of re-epithelialisation in rabbit eyes of the pilot experiment treated with the different hydrogels or the control treatment. Results are expressed as the mean of the percentage of opened wound area ± SD. Statistically significant differences are defined as p-value ∗, + $p < 0.05$, ∗∗, ++ $p < 0.01$, ∗∗∗, +++ $p < 0.001$, ∗∗∗∗, ++++ $p < 0.0001$. "∗" and "+" show significant differences with respect to the control treatment and H-Ab hydrogel, respectively. 163

IV.6. Differences in the mean percentage of opened wound area ± SD for each experimental day between the pilot study (E01) and the remaining 5 experiments (E02-E06). Statistically significant differences are defined as p-value ∗ $p < 0.05$, ∗∗ $p < 0.01$, ∗∗∗ $p < 0.001$, ∗∗∗∗ $p < 0.0001$. 167

IV.7. Progression of re-epithelialisation in rabbit eyes treated with the different treatments or control. Results are expressed as the mean of the percentage of opened wound area ± SD. No statistically significant differences were found between the different treatments on different time points. 168

Taulen zerrenda

I.1. LZAG-ren kausa nagusiak. 256

I.2. LZAG tratatzeko abian dauden saiakera klinikoen zerrenda. 260

I.3. Ukipen-lenteetan erabilitako polimeroen ezaugarriak. [263]-tik hartutako taula. 291

III.1. Hazkuntza faktoreak kuantifikatzeko erabilitako ELISA saiakuntzen zerrenda. 325

III.2. Erabilitako lerro zelularren, hazkuntza-medioen eta hazkuntza-baldintzen deskribapena. 328

III.3. *In vitro* inflamazio-saiakuntzan erabilitako hidrogelen konposizioa. . . . 335

III.4. *In vivo* saiakuntzan erabilitako tratamenduen konposizioa. 340

III.5. Begiko zaurien larritasuna sailkatzeko Draize eskalaren puntuazio sistema. [337]-tik hartuta. 344

III.6. Kay eta Calandrak ezarritako begiko narritaduraren indizearen balioak [338]. 345

III.7. *In vitro* eta *in vivo* saiakuntzetan erabilitako abiarazleen sekuentziak eta propietateak. 353

III.8. IF saiakuntzetan erabilitako antigorputz primario eta sekundarioen zerrenda. 358

IV.1. G, G-D, G-AH eta G-MZ hidrogeletan pilatutako karga bakoitzaren askapen profilen ehunekoen batez bestekoa $\pm$ DE. Alde estatistikoki esanguratsuak G-rekiko adierazi ditugu ($*$ p < 0,05, $**$ p < 0,01, $***$ p < 0,001, $****$ p < 0,0001). 387

IV.2. Hazkuntza-faktoreen kontzentrazioa odol-eratorrien laginetan. Emaitzek kuantifikazioaren batez bestekoa $\pm$ DE adierazten dute. Paziente bakoitzaren SA eta sPRGF-en arteko alde estatistikoki esanguratsuak honela definitu ditugu: $*$ p < 0,05, $**$ p < 0,01, $***$ p < 0,001, $****$ p < 0,0001. 393

IV.3. Hazkuntza-faktoreen kontzentrazioa GMAe laginetan. Emaitzek kuantifikazioaren batez bestekoa ± DE adierazten dute. Alde estatistikoki esanguratsuak honela definitu ditugu: ∗, +, † $p < 0,05$, ∗∗, ++, †† $p < 0,01$, ∗∗∗, +++, ††† $p < 0,001$, ∗∗∗∗, ++++, †††† $p < 0,0001$. "∗", "+" eta "†" ikurrek GMAe-D, GMAe-P eta GMAe-Nahasketarekiko aldeak erakusten dituzte, hurrenez hurren. 394
IV.4. Hazkuntza-faktoreen kontzentrazioa GMAe-Nahasketako-laginetan. Emaitzek kuantifikazioaren batez bestekoa ± DE adierazten dute. Alde estatistikoki esanguratsuak honela definitu ditugu: ∗, † $p < 0,05$, ∗∗, †† $p < 0,01$, ∗∗∗, ††† $p < 0,001$, ∗∗∗∗, †††† $p < 0,0001$. "∗" eta "†" ikurrek p1 pazientearekiko eta p3 pazientearekiko aldeak erakusten dituzte, hurrenez hurren. 395
IV.5. Proba pilotuko untxi-korneen berrepitelizazioaren bilakaera, hidrogelekin edo kontrol-tratamenduarekin tratatutako begietan. Emaitzak irekitako zauri-eremuaren ehunekoaren batez besteko ± DE gisa adierazi ditugu. Alde estatistikoki esanguratsuak honela definitu ditugu: ∗, + $p < 0,05$, ∗∗, ++ $p < 0,01$, ∗ ∗ ∗, +++ $p < 0,001$, ∗ ∗ ∗∗, ++++ $p < 0,0001$. "∗" eta "+" ikurrek, kontrol eta H-Ag tratamenduekiko desberdintasun esanguratsuak erakusten dituzte, hurrenez hurren. . . . 405
IV.6. Azterketa pilotuaren (E01) eta gainerako 5 esperimentuen (E02-E06) arteko aldeak irekitako zauri-eremuaren batez besteko ± DE ehunekoan esperimentuko egun bakoitzerako. Alde estatistikoki esanguratsuak honela definitu ditugu: ∗ $p < 0,05$, ∗∗ $p < 0,01$, ∗∗∗ $p < 0,001$, ∗∗∗∗ $p < 0,0001$. 409
IV.7. Hidrogel- edo kontrol-tratamenduekin tratatutako untxi-korneen berrepitelizazioaren bilakaera. Emaitzak irekitako zauri-eremuaren ehunekoaren batez besteko ± DE gisa adierazi ditugu. Ez genuen desberdintasun estatistikoki esanguratsurik aurkitu tratamenduen artean une desberdinetan. 410

Abbreviations

Ab	Antibody	**IgG**	Immunoglobulin
ALDH	Aldehyde dehydrogenase	**IHC**	Immunohistochemistry
AM	Amniotic membrane	**IL**	Interleukin
AMEED	Amniotic membrane extract eye drop	**KGF**	Keratinocyte growth factor
ARPE	Human retinal pigment epithelial cell line	**LC**	Limbal crypt
AS	Autologous serum	**LEPC**	Limbal epithelial progenitor cell
ATR-FTIR	Attenuated total reflectance Fourier transform infrared spectroscopy	**LES/PC**	Limbal epithelial stem/progenitor cell
AUC	Area under the curve	**LESC**	Limbal epithelial stem cell
BAC	Benzalkonium chloride	**LNC**	Limbal niche cell
BCA	Bicinchoninic acid	**LPS**	Lipopolysaccharide
BDNF	Brain derived neurotrophic factor	**LSCD**	Limbal stem cell deficiency
BM	Basement membrane	**LVR**	Linear viscoelastic regime
BSA	Bovine serum albumin	**MAPK**	Mitogen-activated protein kinase
Calcein-AM	Calcein acetoxymethyl ester	**MC**	Methyl cellulose
CESC	Corneal epithelial stem cell	**MIP-1β**	Macrophage inflammatory protein 1β
CK	Cytokeratin	**MMP**	Metalloproteinase
COL	Collagen	**MSC**	Mesenchymal stem cell
CSE	Cell sheet engineering	**MTA**	Material Transfer Agreement
CSSC	Corneal stromal stem cell	**MTT**	3-(4,5-dimethylthiazol-2-yl)-2-5-diphenyltetrazolium bromide
CTA	Cyanoacrylate	**NCAM-1**	Neural cell adhesion molecule 1
CV	Collagen vitrigel	**NF-$\kappa\beta$**	Nuclear factor kappa light chain enhancer

D	Dextran	**NGF**	Nerve growth factor
dECM	Decellularised extracellular matrix	**NGS**	Normal goat serum
DED	Dry eye disease	**NIH-3T3**	NIH-3T3 murine fibroblasts cell line
DMEM	Dulbecco's Modified Eagle Medium	**NK**	Natural killer cell
DMEM:F12	Dulbecco's Modified Eagle Medium/Nutrient mixture F-12	**NP**	Nanoparticle
DMSO	Dimethyl sulfoxide	**OCT**	Optimal cutting temperature compound
DPX	Dibutylphthalate polystyrene xylene	**OEG**	Oligoethylene glycol
DRG	Dorsal root ganglion neuron	**PAS**	Periodic acid Schiff stainig
dT	Deoxythymidine	**PBMNC**	Peripheral blood-derived mononuclear cell
ECM	Extracellular matrix	**PBS**	Phosphate buffered saline
EDTA	Ethylenediaminetetraacetic acid	**PBST**	TX-100 in phosphate buffered saline
EGF	Epidermal growth factor	**PCL**	Poly(ϵ-caprolactone)
ELISA	Enzyme-linked immunosorbent assay	**PDGF**	Platelet-derived growth factor
ELP	Elastin-like polypeptide	**PDMS**	Polydimethylsiloxane
EMA	European Medicines Agency	**PE**	Phycoerythrin
EMT	Endothelial Mesenchymal Transition	**PED**	Persistent epithelial defect
EthD1	Ethidium homodimer-1	**PEDF**	Pigment epithelium derived factor
EU	European union	**PEG**	Polyethylene glycol
FBS	Fetal bovine serum	**PES**	Polyethersulfone
FDA	Food and Drug Administration	**PFA**	Paraformaldehyde
FGF	Fibroblast growth factor	**PI**	Propidium iodide
FGF2	Fibroblast growth factor 2	**PIPAAm**	Poly(N-isopropylacrylamide)
FITC	Fluorescein isothiocyanate isomer I	**PMC**	Post-mitotic cell
G	Gelatine	**POV**	Palisades of Vogt

G″	Loss modulus	**PTX3**	Pentraxin 3
G′	Storage modulus	**PU**	Polycarbonate urethane
GAG	glycosaminoglycan	**RFP**	Riboflavin phosphate
G-AS	Gelatine hydrogel functionalised with autologous serum	**RM**	Regenerative medicine
G-D	Gelatine-Dextran hydrogel	**RT-qPCR**	Real time quantitative polymerase chain reaction
GDNF	Glial derived neurotrophic factor	**SAOS**	Small amplitude oscillatory shear
GEL-CA	Citric acid-crosslinked gelatine	**SD**	Standard deviation
GEL-LAC	Lactose-crosslinked gelatine	**SEM**	Scanning Electron Microscopy
GelMA	Gelatine methacrylate	**SF**	Silk fibroin
G-HA	Gelatine-Hyaluronic acid hydrogel	**SP**	Stromal projection
G-HAMe	Gelatine hydrogel functionalised with human amniotic membrane extract	**S-P**	Substance P
GMA	Glycidyl methacrylate	**SPI**	Soy protein isolate
G-MC	Gelatine-Methyl cellulose hydrogel	**sPRGF**	Serum derived from plasma rich in growth factors
H	Hydrogel	**Tβ4**	Thymosin-β4
HA	Hyaluronic Acid	**Ta**	Annealing temperature
H-Ab	Antibody-functionalised hydrogel	**TAC**	Transient amplifying cell
HAM	Human amniotic membrane	**TCP**	Tissue culture plate
HAMe	Human amniotic membrane extract	**TDC**	Terminally differentiated cell
HAMe D	Distal part of the human amniotic membrane	**TE**	Tissue engineering
HAMe M	Medial part of the human amniotic membrane	**TGFα**	Transforming growth factor α
HAMe P	Proximal part of the human amniotic membrane	**TGFβ**	Transforming growth factor β
H-AS	Autologous serum-functionalised hydrogel	**THS**	Therapeutic hydrogel sheet
HCE	Human corneal epithelial cell line	**TIMP**	Inhibitor of metalloproteinase
H-E	Hematoxylin-Eosin staining	**Tm**	Melting temperature

HGF	Hepatocyte growth factor	**TNFα**	Tumour necrosis factor α
H-HAMe	Human amniotic membrane extract-functionalised hydrogel	**UV**	Ultraviolet
HIV	Human immunodeficiency virus	**VEGF**	Vascular endothelial growth factor
HRP	Horseradish peroxidase	**XRD**	X-ray diffraction
ICC	Immunocytochemistry	**ZO**	Zonula ocluddens
IF	Immunofluorescence	**α-SMA**	α-smooth muscle actin
IGF-1	Insulin-like growth factor 1		

Laburdurak

AEEB	Animaliekin egiten den Esperimentaziorako Etika Batzordea
Ag	Antigorputza
AH	Azido hialuronikoa
ALDH	Aldehido deshidrogenasa
AM-Kaltzeina	Azeto-metoxilo kaltzeina
ARPE	Giza betsareako zelula epitelial pigmentarioen lerroa
BAK	Benzalkonio kloruroa
BCA	Azido bizinkoninikoa
BDNF	Garunetik eratorritako faktore neurotrofikoa
BL	Begi lehorra
BSA	Behi-seroalbumina
CK	Zitokeratina
D	Dextranoa
DE	Desbideratze estandarra
DEZ	Desberdindutako epitelio zelula
DMSO	Dimetilsulfoxidoa
DRG	Erro dortsaleko neurona ganglionarra
dT	Desoxitimidina
EAI	Epitelio akats iraunkorra
EAP	Elastinaren antzeko polipeptidoa
EB	Europar Batasuna
IgG	Immunoglobulina
IL	Interleukina
KEZA	Korneako epitelio zelula ama
KGF	Keratinozitoen hazkuntza faktorea
KOL	Kolagenoa
KSZA	Korneako estroma zelula ama
KZE	Korneako zelula epitelialak
LEZA	Linboko epitelio zelula ama
LEZA/P	Linboko epitelio zelula ama/progenitorea
LEZP	Linboko epitelio zelula progenitorea
LKrE	Linboko kripta epiteliala
LPS	Lipopolisakaridoa
LZAG	Linboko zelula amen gutxitasuna
MA	Mintz amniotikoa
MAPK	Mitogenoek aktibatutako kinasa proteina
MB	Medikuntza birsortzailea
MIP-1β	1β makrofagoetako proteina inflamatorioa
MMP	Metaloproteinasa
MTT	(3-(4,5-dimetilthazol-2-il)-2,5-difenil tetrazolio bromuroa
MZ	Metilzelulosa
NCAM-1	Nerbio zelulei atxikitzeko 1 motako molekula

EBL	Eremu biskoelastiko lineala
EDTA	Azido etilendiaminotetraazetikoa
EGF	Hazkuntza faktore epidermikoa
EI	Ehun-ingeniaritza
EMT	Trantsizio-prozesu endotelial-mesenkimala
EP	Estromako proiekzioa
EthD1	Etidio-1 homodimeroa
EZ	Etilzelulosa
FBS	Behi-serum fetala
FDA	Elikagai eta Sendagaien Administrazioa
FGF	Fibroblastoen hazkuntza faktorea
FGF2	Fibroblastoen hazkuntza faktorea 2
FITC	Fluoreszeina isotiozianato I isomeroa
FITR	Fourierren transformatuaren bidezko espektroskopia infragorria
G	Gelatina
G′	Biltegiratze modulua
G″	Galera modulua
GAG	Glikosaminoglikanoa
G-AH	Gelatina-azido hialuroniko hidrogela
G-D	Gelatina-dextrano hidrogela
GDNF	Glia-lerro zelularretik eratorritako faktore neurotrofikoa
GEL-AZ	Azido zitrikoarekin erretikulatutako gelatina
GEL-LAK	Laktosarekin erretikulatutako gelatina
GelMA	Metakrilatutako gelatina
NF-$\kappa\beta$	Aktibatutako β zelulen kappa kate arinak indartzen dituen faktore nuklearra
NGF	Nerbio hazkuntza faktorea
NIH-3T3	NIH-3T3 fibroblastoen zelula lerro komertziala
NK	Zelula hiltzailea
NP	Nanopartikula
OCT	Ebaketa tenperatura optimoko konposatua
PAS	Azido periodiko-Schiff-en tindaketa
PDGF	Plaketetatik eratorritako hazkuntza faktorea
PDMS	Polidimetilsiloxanoa
PE	Fikoeritrina
PEDF	Epitelio pigmentariotik eratorritako faktorea
PEG	Polietilenglikola
PES	Polietersulfona
PFA	Paraformaldehidoa
PGT	Propoxilatutako glizerilo-triakrilatoa
PI	Propidio ioduroa
PIPAAm	Poli(N-isopropilakrilamida)
PKL	Polikaprolaktona
PLGA	Poli-(azido laktiko -koglikolikoa)
PTX3	Pentraxina 3
PU	Polikarbonato uretanoa
RFP	Erriboflabina fosfatoa
RT-qPCR	Polimerasaren kate-erreakzio kuantitatiboa denbora errealean
SA	Serum autologoa

G-GMAe	Giza mintz amniotikoaren estraktuekin funtzionalizatutako gelatina	**SEA**	Sendagaien Europako Agentzia
GIB	Giza immunoeskasiaren birusa	**SEM**	Ekorkuntz mikroskopia elektronikoa
GIEB	Gizakiekin lotutako Ikerketetarako Etika Batzordea	**S-P**	P Substantzia
GMA	Giza mintz amniotikoa	**SPI**	Soja-proteina isolatua
GMAe	Giza mintz amniotikoaren estraktua	**sPRGF**	Hazkuntza faktoreetan aberatsa den plasmatik eratorritako seruma
GMAe D	Urruneko eremutik ateratako giza mintz amniotikoaren estraktua	**Tβ4**	Timosina-β4
GMAe M	Erdiko eremutik ateratako giza mintz amniotikoaren estraktua	**Ta**	Hibridazio tenperatura
GMAe P	Hurbileko eremutik ateratako giza mintz amniotikoaren estraktua	**TGFα**	α motako hazkuntza faktore eraldatzailea
G-MZ	Gelatina-metilzelulosa hidrogela	**TGFβ**	β motako hazkuntza faktore eraldatzailea
G-SA	Serum autologoarekin funtzionalizatutako gelatina	**TIMP**	Metaloproteinasen inhibitzailea
H	Hidrogela	**Tm**	Fusio tenperatura
H-Ag	Antigorputzarekin funtzionalizatutako hidrogela	**TNFα**	Tumore nekrosi faktorea α
H-E	Hematoxilina-Eosina tindaketa	**UV**	Ultramorea
HEMA	Poli-hidroxietilmetakrilatoa	**VEGF**	Hazkuntza faktore endotelial baskularra
HGF	Hepatozitoen hazkuntza faktorea	**XRD**	X izpien difrakzioa
H-GMAe	Giza mintz amniotikoaren estraktuekin funtzionalizatutako hidrogela	**ZDZI**	Zatitzen doan zelula igarokorra
HMDS	Hexametildisilazanoa	**ZF**	Zeta fibroina
HP	Hazkuntza plaka	**ZKM**	Zelulaz kanpoko matrizea
H-SA	Seru autologoarekin funtzionalizatutako hidrogela	**ZPM**	Zelula post mitotikoa
IF	Immunofluoreszentzia	**ZXI**	Zelula-xaflen ingeniaritza
IGF-1	Intsulina antzeko hazkuntza faktorea 1	**α-SMA**	Muskulu leuneko α-aktina

I. INTRODUCTION

1. The ocular surface

The ocular surface is the functional anatomical unit that includes the tear film, the conjunctiva, the cornea, the sclerocorneal limbus and associated palpebral structures (Figure I.1). All components are functionally linked by the continuity of the epithelia, innervation and endocrine, vascular and immune systems [1]. All these components comprise the outermost part of the eye, protect it from external threats and help to maintain proper corneal transparency, which implies the maintenance of an adequate ocular surface homeostasis, stability of the immune barrier and repair capacity.

1.1. The tear film

The tear film provides the liquid interface between the corneal and conjunctival epithelia and the external environment and plays an essential role in eye optics, as it is the first refractive surface of the eye [2]. It is necessary for the oxygenation, hydration and metabolism of the corneal and conjunctival epithelia and it acts as a lubricating agent of the ocular surface by reducing friction during blinking and eye movements [2].

The tear film consists of four layers of a mixture of secretions from multiple tissues and epithelia. The glycocalyx of the microvilli of the superficial corneal cells is the innermost layer and is composed of a network of mucins produced by the stratified squamous cells of the corneal and conjunctival epithelium. It keeps the tear film attached to the corneal epithelium and acts as a barrier against bacterial invasion and inflammatory cells.

The second layer is a mucous layer consisting of MUC5AC mucin, proteins, electrolytes and water secreted by conjunctival goblet cells that are part of the glycocalyx. The third layer is an aqueous layer containing electrolytes, water, proteins and small soluble mucins produced by the lacrimal glands and conjunctival epithelium. This layer may mix with the previous mucous layer. The outermost layer contains lipids, it is secreted by the meibomian glands and acts as a barrier to prevent evaporation, protecting the eyes from dryness [3]. Like the mucous and aqueous layers, the aqueous and lipid layers may mix.

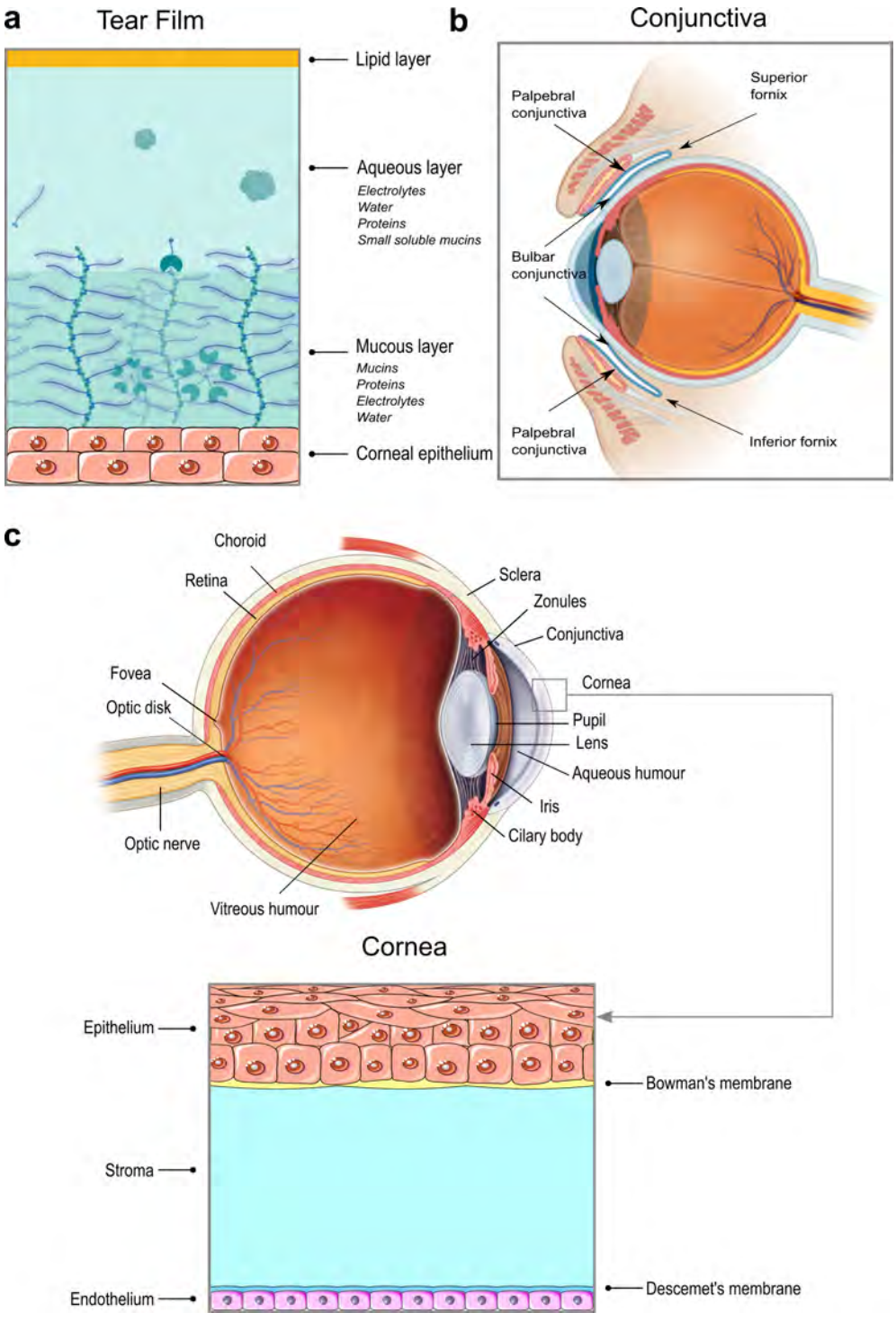

I.1. FIGURE: Schematic illustration showing 3 of the ocular surface components. **a**) Diagram illustrating the various layers present in the tear film. **b**) Illustration showing the location of the different parts of the conjunctiva; the palpebral conjunctiva, the bulbar conjunctiva and the conjunctival fornix. **c**) Main anatomical components of the ocular globle and detailed illustration of the different layers of the cornea.

Mechanical, chemical or thermal stimuli activate the corneal and conjunctival sensory nerves, which in turn activate the parasympathetic and sympathetic efferent nerves that innervate the lacrimal gland and conjunctival goblet cells. The activation

of these nerves causes secretion of the mucous and aqueous layers. Finally, blinking is responsible for regulating the release of lipids pre-secreted from the meibomian gland and stored in the meibomian duct to form the lipid layer.

1.2. Conjunctiva

The conjunctiva is a mucous membrane consisting of a non-keratinised stratified epithelium with distributed mucin-producing goblet cells essential for tear stability and corneal transparency. This non-keratinised stratified epithelium rests on a fibrovascular connective tissue known as the substantia propia, which is divided into a superficial layer containing lymphocytes and a deeper layer containing blood vessels, lymphatic vessels and nerve endings [4].

It has enormous potential to respond to infections due to its high vascularisation, large numbers of immune cells and secretion of immunoglobulins and bactericidal enzymes. The conjunctival epithelium is capable of absorbing substances diluted in the tear film by endocytosis or by diffusion through intercellular junctions. This property facilitates the therapeutic effect of instilling eye drops into the fornices.

1.3. The human cornea

The cornea is the outermost tissue of the eye surface, a highly differentiated avascular transparent (refractive index 1.33) tissue of ectodermal (epithelium) and neuroectodermal (estroma and endothelium) embryonic origin. It acts as the first protective barrier against external harmful stimuli and allows most of the refraction of the eye [5].

1.3.1. Anatomy, histology and function

The human adult cornea is naturally prolate in shape (around 12 mm of horizontal diameter and 11 mm of vertical diameter) and thickens gradually from 0.55 mm at the center to 0.65 mm at the periphery. Its anterior radius of curvature measures 7.8 mm and the posterior radius is about 6.5 mm, all of them subjected to slight variations among individuals [5, 6].

It is a two-face structure comprised between the tear film and the aqueous humour consisting of 5 different layers that, together with sensory nerves, form the light transduction system in charge of focusing light into the retina. The epithelium,

Bowman's membrane and the stroma forms what is called the anterior cornea; while the posterior cornea is made up of Descemet's membrane and the endothelium (Figure I.2).

1.3.1.1. Corneal epithelium

It is a 5-6 layered non-keratinised, stratified squamous epithelium of approximately 50 μm thick that is covered with the tear film. The basal layer is composed of columnar basal cells that are attached to the basement membrane and underlying Bowman's membrane by hemidesmosomes and a complex network of collagen unions. This basement membrane is secreted by the basal cells themselves, it is composed of type IV collagen, laminin, heparan sulfate, fibronectin and collagen VII and its function is to support epithelial cells' movement and migration [7–9]. The basal cells differentiate to form 2-3 central layers of wing cells and eventually ends up forming the remaining upper layers consisting of tightly attached squamous cells. These cells are enclosed by a continuous band of apical zonula occludens tight junctions [10].

The complex network of junctions among cells and the basal membrane allow the epithelium to perform its main function: provide a protective barrier against external harmful stimuli and prevent the entrance of fluid from the tears into the stroma. It is also highly innervated to detect and prevent damage to the cornea [10].

1.3.1.2. Bowman's membrane

Bowman's layer is the first acellular membrane of the cornea. It is an 8-12 μm thick layer composed of a network of collagen fibrils (mainly type I collagen, but also type III, V and VII) randomly organised [11]. This layer is found in humans but not in all animal species and it is located between the epithelial basement membrane and the anterior stroma [12].

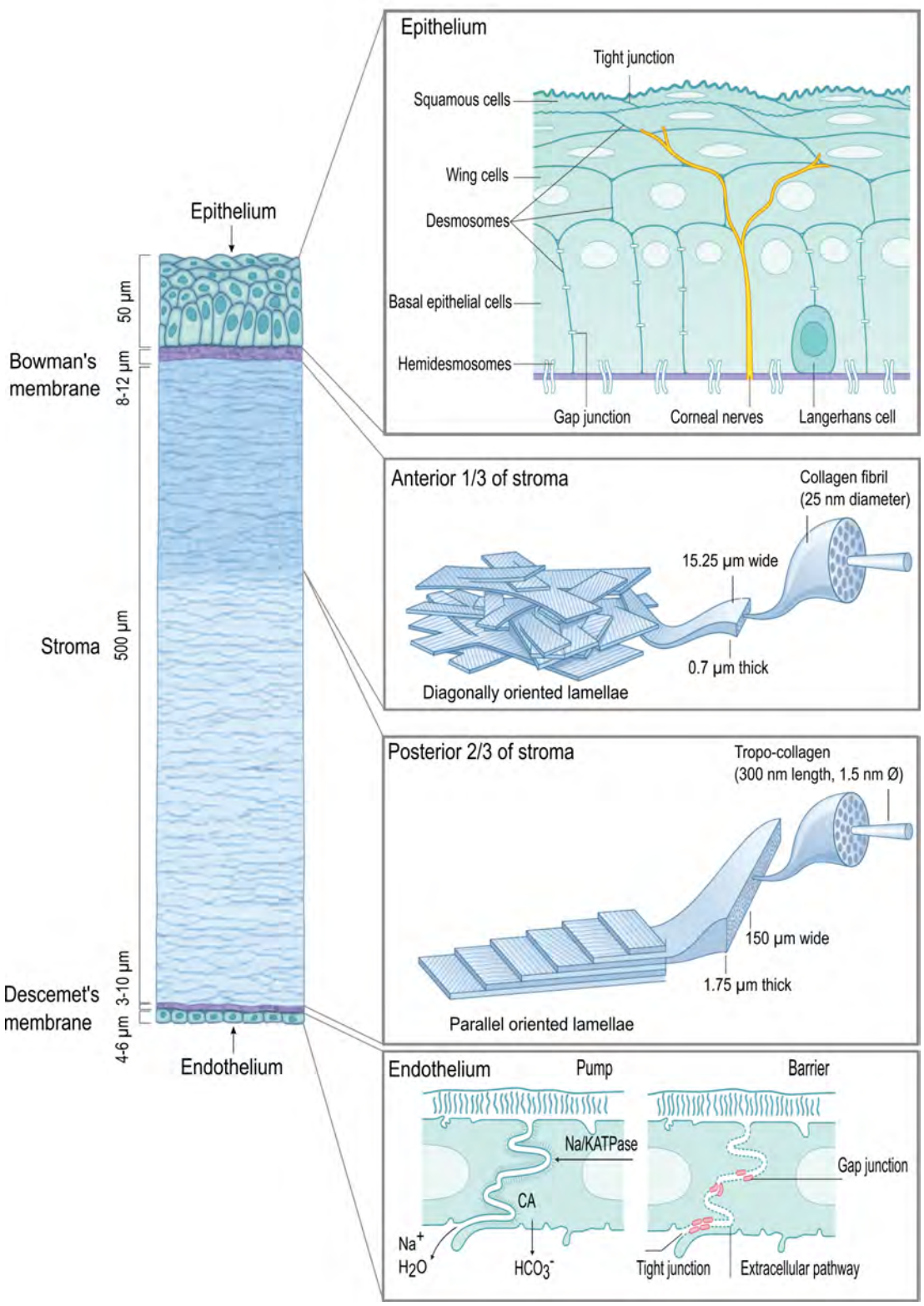

I.2. FIGURE: Detailed illustration of the corneal components. The epithelium is a 5-6 layered stratified epithelium with a complex network of junctions between the different heterogeneous cell layers. The stroma's anterior third comprises of diagonally positioned lamellae that facilitate significant alterations in the z-axis. In contrast, the stroma's posterior two thirds comprise of parallelly positioned lamellae that offer longitudinal strength in the x and y axes. The arrangement of collagen fibrils within each lamella plays a significant role in preventing fibril waviness and thereby, enhancing the initial axial tensile strength of each individual fibril. Finally, the corneal barrier and the metabolic pump sites are detailed in the corneal endothelium. Image modified from [10].

1.3.1.3. Corneal stroma

The stroma constitutes approximately 90% of the corneal thickness (around 500 μm). It is mainly composed of extracellular matrix (ECM), keratocytes and corneal nerves. The ECM is made up of collagen fibrils (composed of type I and V collagen molecules), proteoglycans and glycosaminoglycans (GAG) such as keratan sulfate, chondroitin sulfate and dermatan sulfate that retain water to hydrate and assist in corneal transparency [10, 13].

This characteristic nanoscale organisation of the stroma provides good corneal transparency and adequate mechanical properties [13].

Collagen fibrils in the stroma are organised in approximately 300 lamellae in the center and 500 lamellae in the periphery, with differences in size, directionality, and the amount of entanglement in the different stromal regions. The anterior third of the stroma closest to Bowman's membrane is thin and narrow, and consist of diagonally oriented lamellae. The posterior two thirds of the stroma are thicker and wider than the anterior third and maintain a parallel orientation. Except for the ones in contact with Bowman's layer, the remaining sheets are distributed from side to side forming a circumferential ring responsible for maintaining the curvature of the cornea [14].

Intercalated between collagen lamellae, keratocytes represent 3-10% of the stroma and they are the main responsible for maintaining the precise organisation and order of the ECM. They secrete the main components of the ECM like collagen or glycosaminoglycans to maintain the normal corneal structure [15]. They act as modified fibroblasts and form most of the stromal ECM during neonatal life but remain in a quiescent state in the adult stroma. However, they become metabolically active when the cornea is injured, they transform into myofibroblasts that apply contractile forces to repair the damaged tissue and produce metalloproteinases (MMP) capable of digesting collagen. They also mediate the inmmune response when needed [16, 17]. In addition to keratocytes, monocyte/macrophages, neutrophils, Langerhans cells or natural killer (NK) cells have also been observed as part of the stromal immune activity and repair [18].

Besides collagen and keratocytes, proteoglycans are the third most abundant component of the stroma. They are perpendicularly arranged to collagen fibrils

and provide tissue volume, resistance to forces and viscoelastic properties whereas maintaining the organisation of collagen fibrils in the stroma [10].

Another important aspect of the stroma is the innervation that presents. Nerve fibers from the ophthalmic branch of the trigeminal nerve enter the mid stroma and divide into smaller branches that penetrate Bowman's membrane first and the epithelial basement membrane then. Underneath the corneal epithelium the sub-basal plexus in formed, which responds to mechanical, chemical, and temperature stimuli, permits the basal epithelial layer innervation and releases trophic factors to maintain a healthy ocular surface [10, 19].

The last update in the cornea's anatomy study in 2013 described a new acellular layer equivalent to Bowman's membrane located in the posterior part of the stroma, separating the last row of keratocytes, the Dua layer. This layer would histologically form part of the stroma and it might have an impact on the understanding of corneal biomechanics and pathophysiology [20].

1.3.1.4. Descemet's membrane

Descemet's membrane is the basement membrane of the corneal endothelium and the second interface membrane of the cornea. It is an acellular layer mainly composed of type IV and type VIII collagen and other ECM proteins. It thickens from 3 μm at young ages to 10 μm in adults [21]. It is involved in maintaining corneal homeostasis, structure and transparency: it allows the entrance of nutrients to the corneal stroma, anchors the monolayer of endothelial cells that is essential for maintaining proper hydration and it seems to have an effect on maintaining the posterior corneal curvature [22].

1.3.1.5. Corneal endothelium

The endothelium is made up of a layer of hexagonal cells derived from the neural crest that are arranged in a polygonal mosaic fashion and do not have mitotic activity. The endothelium also contributes to the maintenance of such characteristic transparency of the cornea by regulating corneal hydration and nutrition. It maintains a balance between the amount of liquid directed towards the cornea from the aqueous humour and the energy expended by pumping the excess of it. The barrier function prevents the bulk passage of a very large amount of fluid from the aqueous humour

to the stroma, but in turn allows the regulated diffusion of small nutrients, water and other metabolites through 10 nm wide intercellular spaces [10].

1.4. The sclerocorneal limbus

The sclerocorneal limbus is the 1 mm wide transition zone between the transparent central cornea and the conjunctiva and sclera. Starting at the end of Bowman's layer, the limbus is a highly specialised area involved in many processes necessary for normal corneal function, such as peripheral corneal nutrition, source of stem cells for corneal regeneration and sensory responses.

In contrast to the central corneal epithelium, the limbal epithelium consists of 7-10 layers of non-keratinised and stratified epithelial cells and neighbouring cells, including melanocytes and Langherans cells. A subpopulation of the basal cells of this epithelium corresponds to limbal epithelial stem/progenitor cells (LES/PC), which are responsible for the regeneration of the central corneal epithelium.

The lack of stated biomarkers to unambiguously classify stem cells that regenerate the corneal epithelium has led to much debate about their terminology. Therefore, stem cells responsible for corneal epithelial regeneration will be referred to as limbal epithelial progenitor cells (LEPC) in this thesis.

1.4.1. The limbal niche

LEPCs are located in the limbus in the so-called limbal niche; a highly regulated, protective and specialised microenvironment that maintains the suitable conditions to ensure quiescence and stemness (Figure I.3).

The limbal stem cell niche provides not only a structural home for stem cells, but also a variety of soluble factors and key signalling pathways, biomechanical properties, functional extracellular matrix and interactions with surrounding elements, including niche cells. In the human cornea, the limbal epithelium undulates generating an arrangement of invaginations and projections into the limbal stroma described anatomically by the palisades of Vogt (POV). Histologically, the palisades contain the limbal crypts (LC), the downward invaginations of the limbal epithelium into the limbal stroma between the POV, and the subepithelial and vascularised stromal projections (SP), located around the corneal circumference and with melanin content [23]. These structures are proposed to harbour the LEPC in the limbus [23, 24].

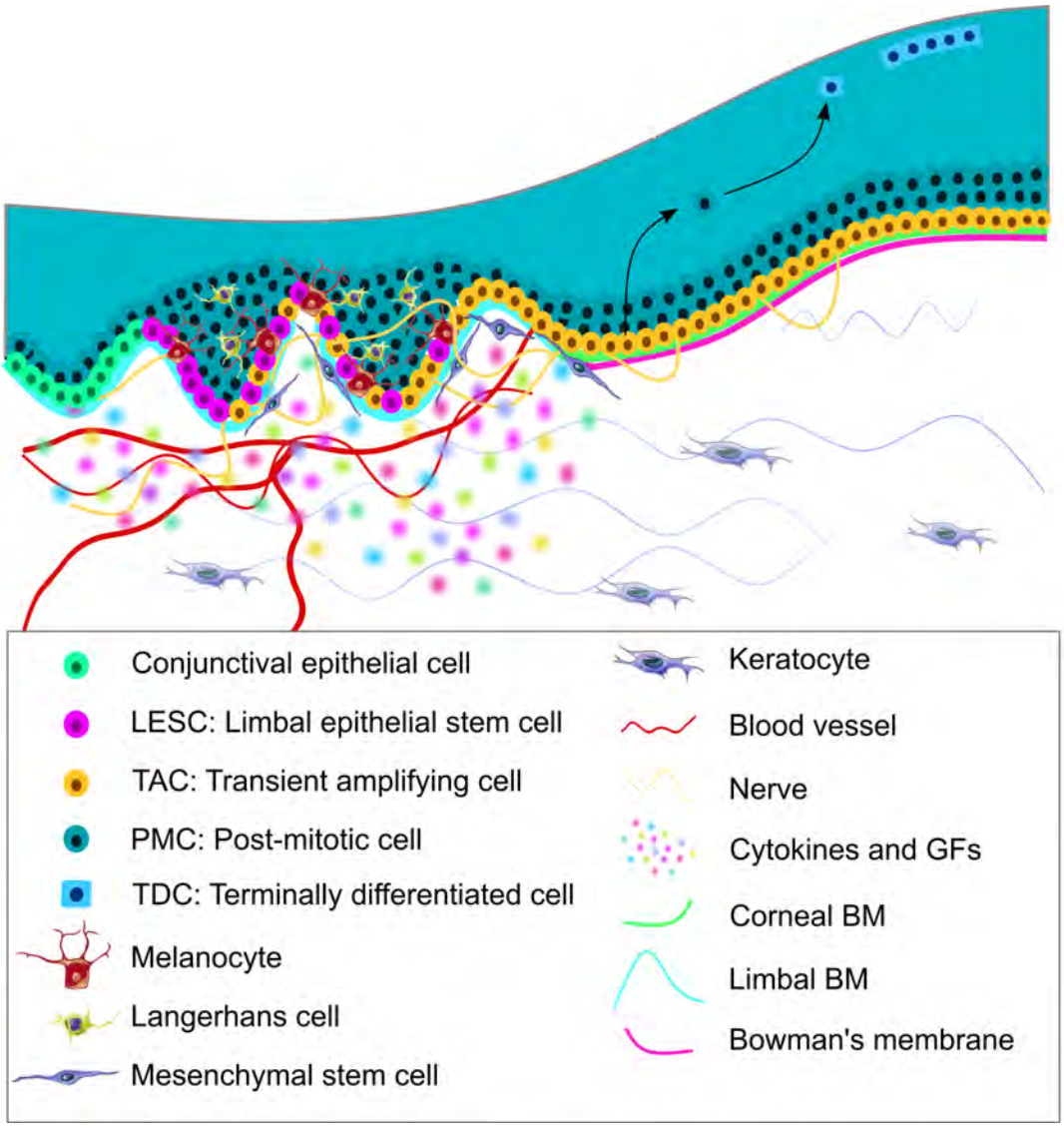

I.3. FIGURE: Detailed illustration of the limbal niche.

The characteristic structure resulting from the arrangement of the epithelium allows direct interaction between the epithelium and the stroma. In general, the corneal stroma is not extensively cellularised, but the density of stromal cells in contact with the epithelial protrusions increases in areas where limbal crypts are present.

The limbal niche contains immune cells, mesenchymal cells, melanocytes, vascular and nerve cells, ECM and signalling molecules. It has a vascularised and innervated structure that is essential for LEPC survival and the appropriate and integrated functionality of the niche components ensures proper maintenance, proliferation, migration and differentiation of LEPCs. Melanin from melanocytes protects LEPCs from ultraviolet (UV) irradiation and mesenchymal cells have a regulatory activity as they are in direct contact with LEPCs through elongated processes [25].

The ECM of the limbal stroma provides fundamental factors for stemness maintenance, contributing to mechanical strength, intracellular communication and interaction of basal epithelial and surrounding stromal cells.

It has been described that limbal epithelial cells interact directly with corneal stromal cells and melanocytes. In addition, melanocytes and limbal epithelial cells express N-cadherin, suggesting its importance in cell-cell interactions at the limbal niche [26]. Another fundamental aspect of stem cell phenotype maintenance is the crosstalk between quiescent and surrounding cells. Many signalling pathways are known to be involved in stem cell maintenance, including the Wnt or Notch signalling pathways.

Wnt proteins have been identified to be limbus specific (Wnt2, Wnt6, Wnt11 and Wnt16b) [27] and Notch1 receptor and HES-1/HEY-1 target genes have been identified at the basal layer of the human limbal epithelium, indicating the implication of Notch in the renewal of the corneal epithelium during normal homeostasis [28, 29].

1.4.2. Stem cells in the limbus

Adult stem cells are found in almost all tissues, including the human cornea. Progenitor cells are tissue-specific stem cells [30], known as limbal epithelial progenitor cells (LEPC) in the case of the corneal epithelium. There is controversy over the term limbal epithelial stem cells (LESC) or LEPCs for stem cells that are responsible for corneal regeneration. The lack of clear biomarkers to distinctly classify them has led to much debate.

LEPCs, located at the limbal epithelium, and corneal stromal stem cells (CSSC), located at the limbal stroma, play a key role in maintaining the optimal microenvironment for corneal homeostasis and thus successful vision. In addition, the existence of corneal endothelial progenitor cells has been proposed, although this remains controversial [31].

1.4.2.1. Corneal epithelial stem cells

Corneal epithelial stem cells are the most studied stem cells in the cornea and are known as LEPCs. These cells are located in the basal limbal area of the corneal epithelium and express different protein markers compared to the surrounding corneal cells. They have been catalogued as stem cells due to their stem cell-like

properties including slow cycling, colony forming capacity and expression of several biomarkers including ABCG2, ABCB5, KRT14 and KRT15, N-cadherin, ΔNP63α and Fzd7 [26, 32, 33].

1.4.2.2. Corneal stromal stem cells

CSSCs have mesenchymal stem cell properties and are located in the anterior limbal stroma. They are closely linked to limbal epithelial cells and both exhibit stem cell genes, despite having different protein phenotypes. CSSCs are in direct cell-cell contact with basal limbal epithelial cells [31].

The arrangement and cell-cell interaction of these cells, together with the presence of melanocytes in the epithelium in close proximity to the CSSCs, suggests the formation of a multicellular limbal niche complex that supports the stem cell nature of the LEPC population.

1.5. Corneal epithelium homeostasis

The cornea is a highly dynamic tissue that is mainly regenerated by the basal limbal epithelial cells known as LEPCs [16, 25]. Since it is not possible to define limbal epithelial stem cells (LESC) with a single biomarker, it has been reported that limbal epithelial cells in the basal zone are positive for ABCG2, PAX6, Fzd7, KRT14, KRT15, ABCB5, N-cadherin, KRT19, vimentin, KGF-r, metallothionein and α9-integrin staining, while they are negative for KRT3, KRT12, connexin 43, involucrin, P-cadherin, SSEA4, nestin and integrin α-2, α-6 and β-4, markers that are positive for central corneal epithelial cells [26, 34–45]. In addition, limbal epithelial stem cells with self-renewal capacity can be indentified by the co-expression of ΔNp63α, C/EBPδ and Bmi1 [46].

The corneal epithelium is constantly renewed every 7-10 days through different cell migration and proliferation mechanisms and LESC model is the most accepted hypothesis to explain corneal epithelium renewal and homeostasis (Figure I.4). As stated in this model, LESCs are located in the basal layer of the epithelium in the limbus, divide and give rise to transient amplifying (TAC) or progenitor cells. These cells migrate centripetally from the periphery to the central cornea as required. During migration, the cells continue to differentiate, giving rise to mitotic epithelial cells, which vertically proliferate and eventually become terminally differentiated

squamous cells that undergo desquamation [6, 25, 47, 48]. Thus, the flattened and uniform epithelial surface is maintained by a perfect balance among horizontal and vertical proliferation, migration and cell detachment, which is mainly induced by the friction generated when blinking eyelids voluntary or involuntarily [10, 49, 50]. This combination of processes is described in X, Y, Z hypothesis described by Thoft [48], where X (proliferation of basal limbal epithelial cells) + Y (centripetal migration and differentiation of corneal epithelial cells) = Z (loss of epithelial cells by eyelid blinking).

Considering some animal species, the repair and regeneration of the epithelium has been suggested to be facilitated by the presence of corneal epithelial stem cells (CESC) distributed over the entire surface of the cornea [25]. In some animal species such as pigs or rabbits, CESCs have been discovered in the central cornea, suggesting that stem cells may not be limited to the limbus, but rather that they are present in the basal layer of the entire cornea and are responsible for corneal renewal [47].

Studies concluding that human epithelial cells from the basal layer of the cornea do not have the capacity to form holoclones have reduced interest in this theory for humans [32].

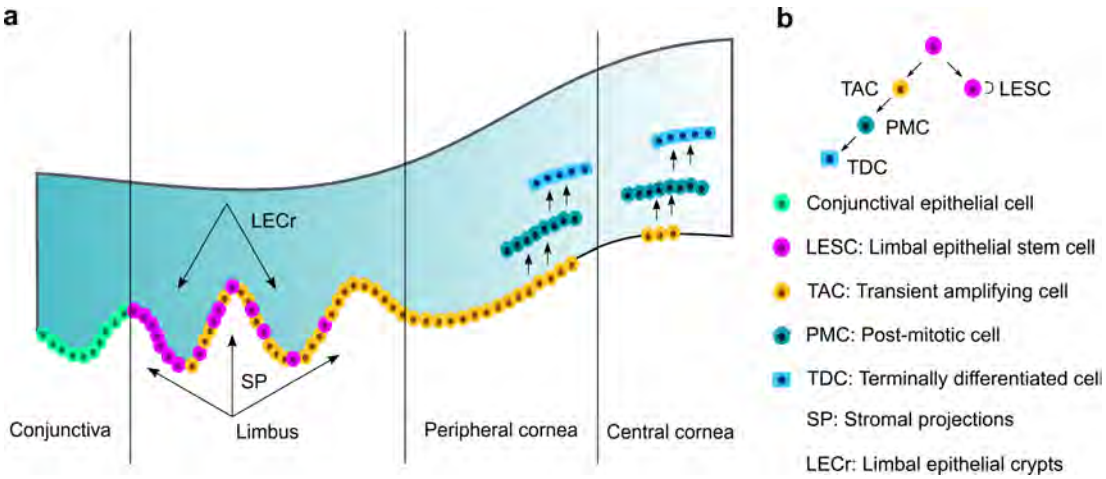

I.4. FIGURE: Schematic representation of LESC hypothesis. **a**) The stem cells located in the basal epithelium of the limbus divide asymmetrically to produce transient amplifying cells (TAC). These TACs migrate towards the central corneal epithelium, gradually transforming into post-mitotic cells (PMC) and then into terminally differentiated cells (TDC). LECr, SP, LESC, TAC, PMC and TDC refer to the limbal epithelial crypts, stromal projections, limbal epithelial stem cells, transient amplifying cells, post-mitotic cells and terminally differentiated cells, respectively. **b**) LESCs possess the ability to self-renew and differentiate into more specialised cells within the cornea.

1.6. Limbal stem cell deficiency (LSCD)

1.6.1. Epidemiology and pathology

Limbal stem cell deficiency (LSCD) is a disease of the ocular surface caused by the dysfunction or destruction of the limbal niche or the LEPCs, which are responsible for the normal homeostasis of the corneal epithelium. Loss of LEPCs or the functional properties of the limbal niche results in invasion of the conjunctival epithelium onto the corneal epithelium, which can lead to impaired epithelial healing, chronic ocular surface inflammation, neovascularisation and ultimately opacification and blindness. Other complications such as epithelial erosion, corneal ulceration or corneal perforation may also occur.

Orphanet considers LSCD to be a rare eye disease (ORPHA:171673) and according to the European Medicines Agency (EMA), LSCD is classified as an orphan disease affecting approximately 2 in 10,000 people in the European Union (EU). The causes of LSCD are diverse and include genetic conditions, systemic autoimmune diseases, trauma or injury to the ocular surface. Table III.1 lists the major causes of this disease according to a 10-year study involving 2,000 subjects, mostly children or young men with unilateral LSCD from different centres in Asia [51].

I.1. TABLE: Principal causes of LSCD.

Disease	Unilateral LSCD	Bilateral LSCD
Ocular burn	84%	30%
Steven-Johnson syndrome	4%	23%
Keratoconjunctivitis	3%	30%
Mucous membrane pemphigoid	2 %	4%
Traumatism	2%	-
Aniridia	-	9%

LSCD has been recognised for more than 2 decades, but until recently there has been no consensus on diagnostic criteria, staging, classification and management. The International LSCD Working Group has published general guidelines for the classification, diagnosis and standardised management of the disease [52].

1.6.2. Diagnosis and treatments

The diagnosis of LSCD is based on clinical history, clinical presentation and diagnostic tests. An irregular corneal epithelium and disruption or loss of the

palisades of Vogt are the earliest signs of LSCD. As the disease progresses, the conjunctival epithelium invades the corneal epithelium overlying the visual axis.

The processes involved in LSCD can be identified by techniques that detect corneal or conjunctival cells in the eye or structural changes in the limbus and cornea. These include i) impression cytology, which allows the identification of goblet cells in the cornea, indicating conjunctival cell invasion, ii) observation of significant microstructural changes of the limbus by *ex vivo* confocal laser scanning microscopy, and iii) anterior segment optical coherence tomography, which provides high-resolution images of the anterior segments of the eye, including the cornea and limbus.

LSCD progression can be classified into 3 severity stages (stages I-III) according to the area of the eye affected [52, 53]. The following diagram (Figure I.5) illustrates the 3 stages of the disease and describes the percentage of the ocular surface affected in each stage.

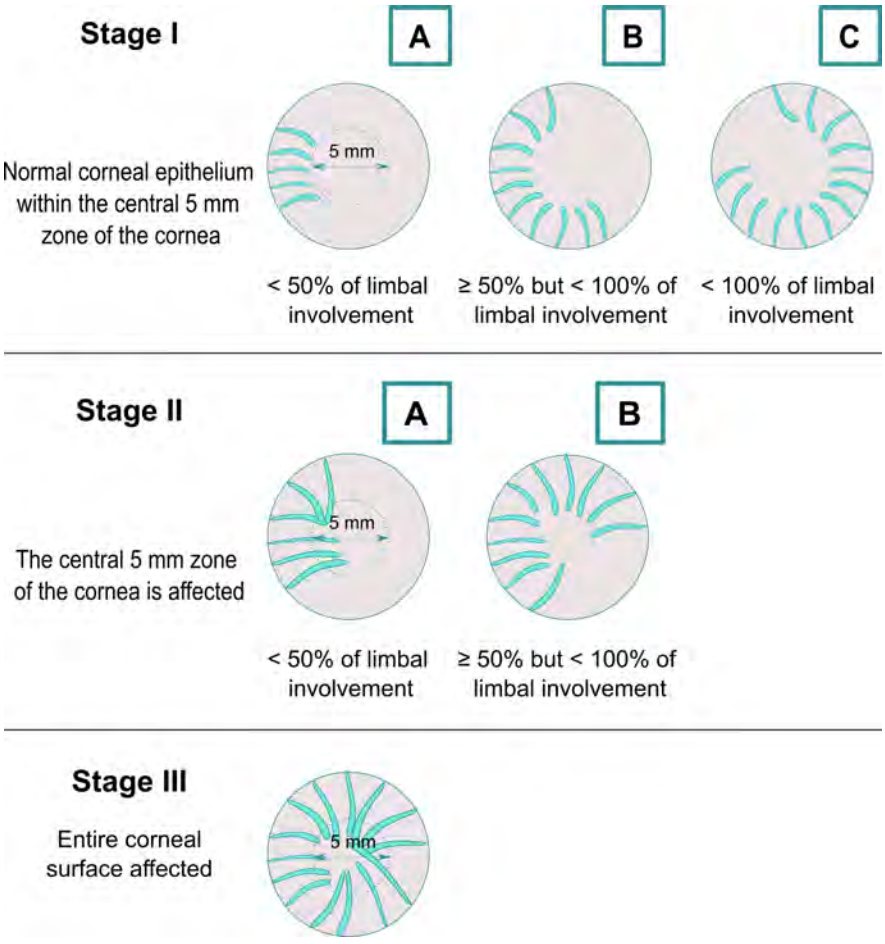

I.5. FIGURE: Schematic representation and description of the stages during LSCD.

To date, no topical or oral medication can replace missing, damaged or deficient LEPCs or can restore or mimic the limbal niche's functions. However, cell therapies are being developed to effectively replace them and restore corneal homeostasis [54, 55].

Management of the disease varies depending on the stage. The first approach is to resolve co-morbidities such as inflammation, tear film abnormalities, infection or others so as not to compromise any residual function of the LEPC that may still be present. In addition, improving the health of the ocular surface and reducing aggravating factors is beneficial for engraftment and long-term survival of potential grafts.

For unilateral or bilateral stage I and II LSCD, if the patient's vision is compromised or there are complications, surgery without LEPC transplantation is performed. The primary goal is to re-epithelialise the central corneal surface with existing or remaining corneal epithelial cells. This is done by removing a section of the conjunctiva to prevent further invasion of the visual axis. This procedure, called conjunctival epitheliectomy, is only indicated for non-severe conditions because of the potential for delayed re-epithelialisation. For other corneal defects, amniotic membrane (AM) may be transplanted to aid re-epithelialisation.

In more acute stages, such as stages II and III, once the ocular surface has been optimised by medical treatments, LEPCs are preferentially transplanted to restore the functional pool of LEPCs. The treatment approach differs depending on the laterality of the disease (unilateral disease affects only one eye, bilateral disease affects both eyes). In general, transplantation of a limbal graft or cultured LEPCs is enough as a treatment, which may differ between autologous and allogenic transplantation. Allogenic treatment uses limbal grafts from cadaveric o healthly living donors, while the cells of grafts in autologous transplants come from the patient's unaffectetd contralateral eye [53].

In recent decades, stem cell-based therapies have emerged as a promising field of regenerative medicine to develop methods to regenerate, repair or replace damaged or diseased cells, organs or tissues.

The first accepted therapy by the EMA for the treatment of LSCD was the Holoclar product of *ex vivo* expanded autologous human corneal epithelium containing stem

cells in 2008 [56]. Other products have been developed in the following years as a result of the need for more precise or effective solutions. The main drawback of stem cell-based therapies for LSCD is the inability to ensure LEPC rich cultures, as no specific stem cell marker has yet been established. There are currently 12 clinical trials underway or recruiting for the treatment of LSCD, most of them based on stem cell therapies (Table III.2). Other 15 clinical trials were completed between 2008 and 2023, although only HOLOCLAR has reached phase 4.

I.2. TABLE: List of active clinical trials related to LSCD.

NCT Number	Study Title	Phase	Locations
NCT03943797	Cultivated Autologous Oral Mucosal Epithelial Transplantation	Phase I	Core Laboratory for Cell Therapy, Veterans General Hospital, Taipei, Taiwan
NCT04021875	The Effects of Autologous SLET [1]	Observational study	National Taiwan University Hospital Taipei, Taiwan
NCT04704648	Feasibility Study of Ocular Surface Squamous Neoplasia Surgical Excision in People Living With HIV in Sub-Saharan Africa	NA	Uganda Cancer Institute Kampala, Uganda
NCT04995926	Labial Mucosal Epithelium Grafting for Corneal Limbus Substitution	NA	The S. Fyodorov Eye Microsurgery Federal State Institution, Moscow, Russia
NCT05494671	Studying Corneal Epithelial Stability Following Limbal Stem Cell Transplantation in Cases of LSCD	NA	Kasr Alainy, Cairo, Egypt
NCT03957954	Stem Cell Therapy for LSCD	Phase I	University of California Los Angeles, California, USA
NCT04021134	The Effects of Allogeneic SLET	Observational study	National Taiwan University Hospital Taipei, Taiwan
NCT05461469	Cornea Dome Lens Ocular Surface Imaging System Validation Study	Observational study	Universitätsklinik für Augenheilkunde und Optometrie Paracelsus Medizinische Privatuniversität Salzburg, Austria
NCT02886611	Limbal Stem Cell Deficiency of Genetic Origin: Genotype-phenotype Correlation	Observational study	Fondation Ophtalmologique Adolphe de Rothschild, Paris, France
NCT01756365	Autologous Cultured Corneal Epithelium (CECA) for the Treatment of Limbal Stem Cell Deficiency	NA	Toronto Western Hospital, Toronto, Ontario CIUSSS de l'Est-de-l'Île-de-Montréal, Canada
NCT03549299	Allogeneic ABCB5-positive Limbal Stem Cells for Treatment of LSCD	Phase I - Phase II	Massachusetts Eye and Ear Infirmary Boston, Massachusetts, US Universitäts-Klinikum Heidelberg, Germany
NCT03949881	Cultured Autologous Oral Mucosa Epithelial Sheet for the Treatment of Bilateral Limbal Stem Cell Deficiency	Phase I - Phase II	Ophthalmology department, Edouard Herriot hospital, Lyon, France

[1] SLET: Simple Limbal Epithelial Transplantation. SLET is a surgical procedure that involves transplanting small pieces of autologous or allogeneic limbal grafts over an amniotic membrane onto the damaged cornea. This is followed by the placement of a bandaged contact lens.

1.7. Overview of corneal regeneration

Due to the cornea's fundamental functions of protection and transmission and refraction of light, visual acuity is affected if any part of this tissue is compromised. Thus, the cornea contains a very effective regeneration mechanism to deal with this need of intact maintenance (Figure I.6).

1.7.1. Epithelial wound healing

When the corneal epithelium is injured by a trauma, infection or microbial damage, the attachment to the underlying basement membrane (BM) is disrupted and interleukin (IL)-1α and IL-1β are released by the damaged epithelial cells [11]. As it requires a rapid healing to maintain its barrier function, the cells from the wound margins that maintain cell-to-cell and BM contact migrate centripetally, so that a sliding cellular sheet covers the wound. Once the epithelial defect is covered, the basal cells begin to proliferate and differentiate to restore the different epithelial cell layers. Likewise, the basal cells start producing laminins 511 and 521 to regenerate the defective BM in cooperation with the keratocytes beneath the wound [57].

These processes of proliferation, differentiation and motility of epithelial repair are regulated by different growth factors such as the autocrine epidermal growth factor (EGF), transforming growth factor α (TGFα), TGFβ, insulin-like growth factor (IGF), platelet-derived growth factor (PDGF), fibroblast growth factor (FGF), Thymosin-β4 (Tβ4), or hepatocyte growth factor (HGF) and keratinocyte growth factor (KGF) released by stromal keratocytes [58, 59]. The corneal nerves that regulate eye blinking and therefore the turnover of epithelial cells and epithelial regeneration also provide factors such as substance P or nerve growth factor (NGF), among others [60–63].

1.7.2. Basement membrane wound healing

The integrity and timely regeneration of the BM is a deciding factor for a normal homeostatic corneal regeneration or a fibrotic healing response. The BM is disrupted in both, epithelial and stromal defects. First, the hemidesmosomal junctions of the epithelium to the basement membrane are disassembled to allow epithelial cell migration. This breakdown allows the introduction of epithelial derived IL-1, TGFβ, PDGF, vascular endothelial growth factor (VEGF) and other angiogenic and fibrotic

cytokines into the stroma that will trigger the myofibroblast transdifferentiation [18, 64].

A rapid regeneration of BM to stop the entry of growth factors requires a coordinated response from epithelial cells and keratocytes in the stroma. The basal epithelial cells deposit a layer of laminin 511 or 521 followed by a layer of laminin 332. Keratocytes add the remaining perlecan and nidogens [65]. These cells should be close to the wounded area so that their contribution to BM regeneration is not impeded by myofibroblasts. The restored BM downregulates the release of fibrotic factors from the epithelial cells and the myofibroblasts precursors undergo apoptosis [64, 66].

1.7.3. Stromal wound healing

Any damage to the stromal layer triggers a series of complex events that begins with the interactions between epithelial and stromal cells and the release of growth factors and cytokines through the damaged epithelial basement membrane.

Following epithelial damage, keratocyte apoptosis of the underlying stroma within the injured zone is the first response of stromal wound healing process. IL-1 (both α and β), tumour necrosis factor α (TNFα) and Fas-Fas ligand interactions are the main effectors of keratocyte apoptosis. These factors can come from the lacrimal gland, damaged epithelium, endothelium or inflammatory cells [67, 68]. Adjacent keratocytes proliferate, migrate and differentiate into their activated state, becoming fibroblasts that repopulate the wound site. These fibroblasts acquire the ability to produce IL-1 in an autocrine manner. IL-1 also increases the production of HGF and KGF by keratocytes and fibroblasts, which contribute to epithelial regeneration [69].

The increase of pro-inflammatory cytokines such as IL-1, IL-6 or TNFα in the stroma causes the infiltration of leukocytes from the limbal blood vessels [70]. The first inflammatory cells to infiltrate the stroma are the neutrophils, which accumulate at 18 and 30 hours after the injury and their number decreases after 48 hours. Neutrophils infiltrate the corneal stroma through the limbal blood vessels and keratocyte apoptosis facilitates their progression to the wound. Neutrophils eliminate pathogens and cellular debris through phagocytic functions and moreover, corneal nerve recovery has been reported to be affected by the absence of neutrophils due to their secretion of VEGF-A as a neurotrophic factor [71]. As the number of neutrophils normalises, macrophages from the limbal vessels enter the wound and migrate to the center. These

cells help to clear cell debris, secrete TGFβ to promote the differentiation of fibroblasts to myofibroblasts and mediate the formation of new blood and lymphatic vessels through VEGF release [72]. Langerhans cells also infiltrate the wound, increasing the ability to present foreign antigens in the cornea [18]. NK cell-infiltration from the limbal vessels to the central cornea has also been observed [73].

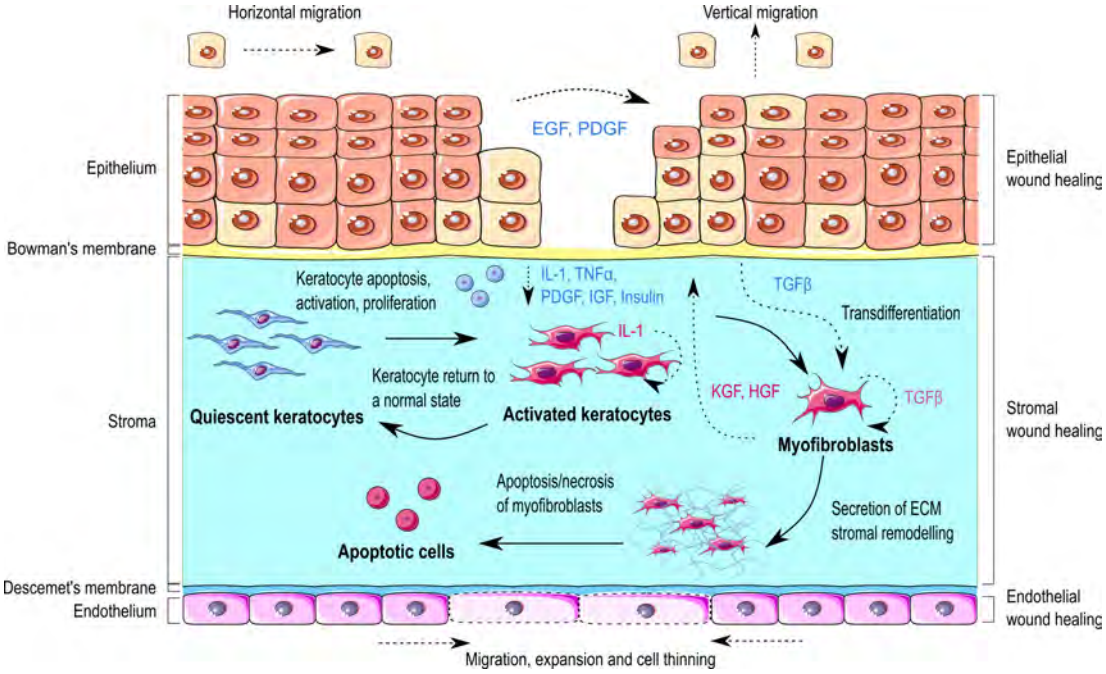

I.6. FIGURE: Overview of the corneal regeneration process. Following epithelial damage, growth factors including EGF, PDGF, IGF, insulin and other cytokines are released due to an intense biochemical activity triggered by damaged epithelial cells. Subsequently, healthy corneal epithelial cells undergo cell reorganisation, resulting in a series of morphological and functional changes. After this process begins, the epithelium closes as a result of the activation of LEPCs residing in the limbus, which proliferate and differentiate into increasingly differentiated epithelial cells, creating the stratification of the normal epithelium. In the corneal stroma, IL-1 and TNFα secreted by epithelial cells initiate keratocyte apoptosis. Within a few hours, the keratocytes neighbouring the acellular area begin to activate. Likewise, the initial apoptosis of subepithelial keratocytes is followed by the migration and proliferation of the neighbouring keratocytes, triggered by PDGF. This migration is then followed by the differentiation into myofibroblasts, a process mediated by TGF-β released by the epithelial cells. These myofibroblasts trigger the production of growth factors, namely HGF and KGF, which activate genes encoding extracellular matrix components and deactivate genes encoding molecules that preserve corneal transparency. Subsequently, there is an increased production of collagenases and other matrix MMPs, ultimately leading to stromal remodelling. The aforementioned processes lead to a significant increase in extracellular matrix production, stromal hypercellularity, and tissue contraction, resulting in tissue opacity or haze. Finally, stromal repair is completed through apoptotic mechanisms of the cells involved in stromal healing and by the restoration of keratocytes to their normal state. Concerning the endothelium, its regeneration is achieved through migration, expansion or thinning of cells to cover the maximum surface area. Epithelial cells secrete growth factors indicated in blue, while stromal cells secrete those indicated in red.

Concurrently to IL-1 and TNFα release, TGFβ, PDGF and FGF-2 are upregulated, activated and delivered by corneal epithelial cells. PDGF and FGF-2 trigger the migration, proliferation and transformation of keratocytes into fibroblasts [74]. TGFβ mediates the transdifferentiation from fibroblasts to myofibroblasts, which are responsible for secreting new ECM [74, 75].

Myofibroblasts are characterised by a high expression of α-smooth muscle actin (α-SMA) contractile stress fibers, vimentin, desmin and a reduced amount of crystalline proteins, which contribute to the reduction of light scattering by resembling the refractive index of the ECM in the cell cytoplasm [76–78]. They mainly come from the transformation of corneal keratocytes but bone marrow-derived fibrocytes have also been proposed as part of myofibroblasts' source in response to TGFβ [79].

The formation of new ECM is initially necessary for wound closure, but the secretion of this disorganised matrix results in tissue contraction and corneal haze. The survival of myofibroblasts over time and the constant production of new ECM hinders the contribution of keratocytes to restore the BM and inhibits the regeneration of corneal nerves in the stroma [72]. Besides, myofibroblasts can conduct their subsistence by a further autocrine production and release of TGFβ without the influx coming from the epithelium [18].

When the BM is restored, PDGF and TGFβ levels coming from the epithelial cells decrease. Once the BM heals and the entry of fibrotic factors ceases, the levels of TGFβ produced in an autocrine manner by the myofibroblasts will not be enough to maintain these cells persistently. Then, myofibroblasts enter apoptosis, the stroma is repopulated by keratocytes and the regeneration process overcome the fibrosis [80]. The necrosis/apoptosis of inflammatory cells also occur together with myofibroblasts' removal. Keratocytes are responsible for the resorption of the abnormal ECM and restoration of the normal stromal homeostatic state. This process can take months and in complex situations, transparency may not be restored.

1.7.4. Corneal endothelial wound healing

Due to their limited mitotic activity, endothelial regeneration is based on migration, expansion or cell thinning of the remaining cells to cover the largest area as possible. The IL-1 responsible for keratocyte death stimulates this migration [59].

When the cells close the wound, usually a few days after, they regain their pumping activity and they start secreting new BM.

Depending on the severity and extent of the endothelial injury, endothelial cells can also undergo Endothelial-Mesenchymal-Transition (EMT) process, where quiescent endothelial cells adquire fibroblast-like characteristics and begin to proliferate. This process is mainly stimulated by TGFβ, FGF-2 and IL-1β [81, 82]. These cells will detach from neighbouring cells and move independently along Descemet's membrane towards the damaged area, leading to quick wound healing. However, this process can compromise vision as they may secrete a fibrotic membrane known as retrocorneal fibrous membrane [83] that may alter the refractive capacity of the cornea.

As the endothelium is essential for the constant dehydration and thereby the transparency of the cornea, diseases or injuries leading to extensive loss of endothelial cells generally lead to corneal opacification due to excessive fluid accumulation and swelling.

1.8. Corneal defects

Corneal defects are defined as open sores on the corneal surface. They comprise defects that only involve epithelium, or epithelial-stromal ulcers, where the stroma is affected to a greater or lesser extent.

1.8.1. Epithelial defects

A corneal epithelial defect is defined as the loss of the superficial epithelial layer of the cornea caused by various aetiologies such as trauma, corneal dryness, different neurotrophic diseases, infections or burns. Patients suffer acute pain, redness, tearing, blurred vision and photophobia. They generally recover within 7-10 days without visual sequelae. However, inadequate treatment can lead to ocular complications such as corneal ulcers involving stroma, scarring or melting [84].

1.8.2. Persistent epithelial defects and neurotrophic ulcers

Persistent epithelial defects (PED) occur due to an inappropriate corneal epithelial repair response along with the eye's inability to close an epithelial wound. They result from an inappropriate re-epithelialisation and closure answer within 2 weeks despite the administration of conventional treatments [85, 86]. The remaining epithelial

cells or the stem cells of the limbus are unable to replenish the damaged area due to alterations in intercellular or cell membrane adhesions, such as tight junctions or hemidesmosomes. This causes a total epithelial thickness and corneal normal structure's loss [87].

Since each disease is characterised by the combination of different biochemical mechanisms that produce the epithelial wound and that can even generate stromal damage, the etiologies of PEDs are different. PEDs occur after exposure to toxic chemicals, mechanical trauma, or because of diseases such as dry eye syndrome, Vitamin A deficiency, Sjögren's Syndrome, herpes simplex or herpes zoster, diabetic keratopathy, limbal stem cell failure or neurotrophic keratopathy [88–91]. A lack of tear's growth factors, cytokines and neuropeptides released from trigeminal nerve involved in healing mechanisms can also lead to these defects [92].

They can lead to major complications such as infection and vision loss if they are not treated. Regardless of their origin, PEDs are associated with an increase in free plasmin on the ocular surface, an enzyme resposible for the degradation of a variety of plasma proteins, specially fibrin clots. This free plasmin in the ocular surface facilitates weak adhesions and induces the reduction and weakening of the junctional complexes between the corneal epithelium and the fibronectin of the extracellular matrix, thus contributing to the persistence of the defect itself [93]. The free plasmin is a chemoattractant for polymorphonuclear cells, which release certain metalloproteases with collagenase activity that favours corneal melting. Therefore, PEDs can progress to the anterior stroma and produce subsequent stromal ulceration by proteolytic degradation of stromal collagen and ECM.

1.8.2.1. Treatments for PEDs of the cornea

The management of PEDs remains one of the most challenging issues in ophthalmology due to the need to understand the disease etiology, the heterogeneity of causes and the long follow-up period. Different surgical alternatives have been described so far for the resolution of this clinical condition, but the most common and first-choice medical alternatives are usually non-invasive treatments that seek to reestablish the normal structure and function of the epithelium. These include ocular preservative free lubricants, reduction/withdrawal of drugs that may alter epithelial regeneration or the use of prophylactic topical antibiotics [94].

Soft bandage contact lenses aid in the healing of PEDs by protecting the epithelial cells from mechanical erosion by eyelids' blinking. The lenses are used together with antibiotics and preservative free lubricants to prevent their adhesion to the ocular surface. However, this treatment requires a close follow-up due to the risk of infection and lens' displacement [95, 96]. Pressure patching is another conventional alternative that offer similar benefits to the use of contact lenses. Alternatively, punctal occlusion (plugging the tear ducts) seeks to increase the contact time with the ointments and lubricants provided [94].

Medical treatments based on the application of specific molecules have also been proven as newer non-invasive therapies. EGF [87, 97], NGF [98, 99], substance P and IGF-1 [100], FGF [101, 102], amnion-derived cellular cytokine solution [103] or insulin eye drops [104, 105] are some examples that have shown their usefulness and potential for the treatment of PEDs.

Like so, the use of eye drops derived from the patient's own serum or other blood derivatives has proven to be effective [106–113]. Their positive effects may be linked to the high concentration of different growth factors, vitamins and components involved in epithelial proliferation and migration that are absent in artificial tears. However, the lack of standardised protocols, the variability in the concentrations used (from 20% to 100%) or the regulatory restrictions regarding their production, hinder the widespread use of this therapy.

Finally, surgical treatments aimed at improving ocular surface tropism are also available and include the epithelial debridement, amniotic membrane grafts [114–116], tarsorrhaphies [117–119] or corneal stem cell transplantations [120], especially needed in severe PED cases.

2. Regenerative medicine and Tissue engineering

Regenerative medicine (RM) is an interdisciplinary field of research and clinical application that aims to repair, replace or regenerate cells, tissues or organs to restore function lost due to congenital defects, disease, trauma or ageing. RM aims to activate the body's natural repair mechanisms to heal previously irreparable tissues or organs and includes solutions that regenerate damaged body parts by replacement or stimulation of the body's own mechanisms. It brings together several converging technological approaches, including the use of soluble molecules, gene therapy, stem and progenitor cell therapy, tissue engineering (TE), and reprogramming of cell and tissue types, among others [121] (Figure I.7).

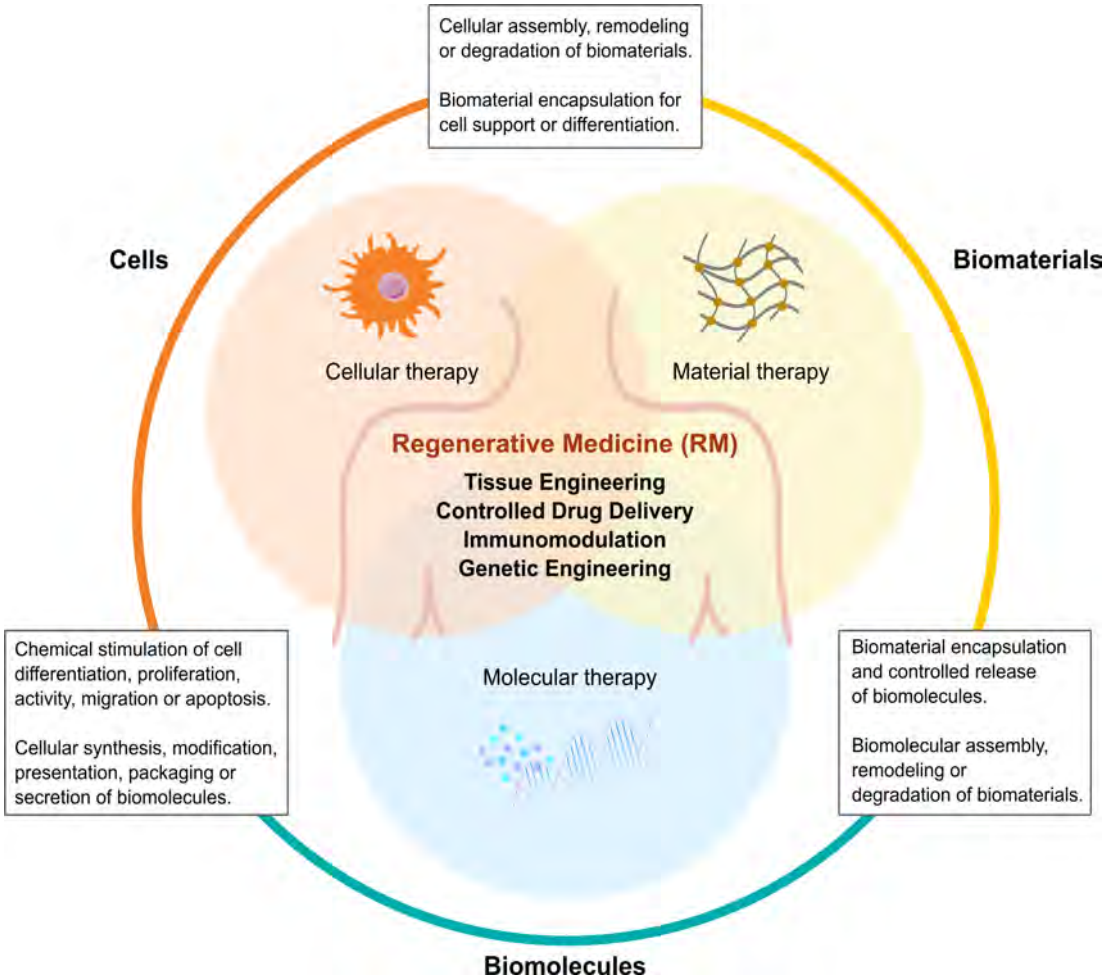

I.7. FIGURE: Overview of the strategies, components, and interactions used in RM. Regenerative medicine therapies involve delivering cells, biomaterials, or biomolecules, such as injecting regenerative cells or implanting acellular biomaterial scaffolds to stimulate endogenous tissue repair. Interdependent interactions can also be harnessed for tissue engineering, drug delivery, and immunomodulation. Although the solutions developed in this field are complex, these strategies offer the opportunity to target the most effective solutions for tissue regeneration and repair. Modified from [122].

Therefore, TE is a multidisciplinary field under the umbrella of RM that seeks to regenerate damaged tissues or organs by deliberate and controlled stimulation of target cells through a combination of mechanical and molecular stimuli [123]. It is closely associated with applications that repair or replace parts of tissues or entire tissues that require specific mechanical and structural properties and biochemical functions to work. Research in this field focuses on three aspects: the selection of cells to be used and expanded to replace the damaged ones, the selection of biomaterials that will favour tissue regeneration and the determination of physical, chemical and biological signals needed to regenerate functional tissues [124].

Depending on their application and placement within the body, biomaterials can be used in different forms such as hydrogels, membranes, sponges, fibre tubes or sphere-like structures.

2.1. Classification of biomaterials based on their origin

Considering their origin or source, natural and synthetic biomaterials can be differentiated.

2.1.1. Natural Biomaterials

Natural biomaterials are materials that originate during the growth cycle of animals, plants and microorganisms and include nucleic acids, polysaccharides, proteins, lipids and complex macromolecules such as proteoglycans. These materials exhibit a wide diversity of constituents, microstructures and complex physiological properties but show inherent bioactivity due to the presence of natural extracellular matrix motifs. They exhibit inherent biocompatibility and biodegradability and replicate the physiological ECM environment. They stimulate the cell adhesion, the subsequent tissue development and facilitate body integration. They are often the first choice when selecting a biomaterial.

They can be classified into three main groups: polysaccharide-based, protein-based or tissue/organ derived biomaterials.

2.1.1.1. Polyshaccaride-based biomaterials

Polysaccharides are carbohydrate polymers composed of monosaccharides (the fundamental units for all carbohydrates) linked by glycosidic bonds. They are

involved in various functions, including cell communication, energy storage, structural support, adhesion, or molecular recognition in the immune system.

Chitosan

Chitosan is a natural polysaccharide consisting of repeating units of glucosamine and N-acetylglucosamine derived from the partial deacetylation of chitin obtained from shells of shrimps and other crustaceans [125].

Its biocompatibility, biodegradability, large-scale availability and low cost, antimicrobial and antifungal properties and low immunogenicity make it a suitable material for biomedical applications [126]. Chitosan can be easily crosslinked and functionalised through modification of its amine and hydroxyl groups [127]. In addition, it shows a high water absorption and retention capacity beneficial for cartilage tissue engineering, corneal endothelial reconstruction and drug-loaded implants, and its cationic characteristics make it a good candidate for haemostasis [128, 129].

Hyaluronic acid (HA)

Hyaluronic acid (HA) is a natural polysaccharide ranging a wide scope of molecular weights (1-10000 KDa) and composed of D-glucuronic acid and D-N-acetylglucosamine units.

It exhibits good biodegradability, biocompatibility, viscoelastic and shear thinning behaviour [130] and tunable mechanical properties. Its repeating two-glucoside units contain carboxylic acid and hydroxyl groups that can be used for hydrogel functionalisation or crosslinking. It is one of the main components of connective tissues' ECM and its strong water absorption keeps the tissues hydrated, which benefits cellular infiltration and makes it a very suitable dressing material for chronic or poorly healed wounds [131]. Initially, HA was extracted from various animal connective tissues. However, due to its increasing demand, production shifted to microbiological sources. Currently, the most economical and reliable source for HA production is streptococcus A and C, from which HA was first isolated [132].

These characteristics make HA appropriate candidate for a wide range of applications, such as skin tissue engineering [133], dermal fillers [134, 135],

intraarticular adhesives [136, 137], vitreous substitutes [138–141], corneal wound healing [142–144] or drug carriers [145–147].

Alginate

Alginate is a linear polysaccharide composed of sequential or alternating blocks of β-D-mannuronic acid (M-block) and α-L-glucuronic acid (G-block), the M:G ratio of which influences the physicochemical properties obtained. A higher amount of M-blocks produces more flexible and elastic hydrogels, whereas a higher amount of G-blocks is associated with stiffer and more rigid hydrogels [148]. It is mainly obtained from brown seaweeds.

The carboxyl group of alginate G residues can crosslink with divalent cations such as calcium, strontium or barium to form alginate hydrogels [148]. It is an extrudable material, a beneficial property for gel injection or bioprinting applications, shows good biocompatibility, low cytotoxicity and is a non-immunogenic material. As it lacks cell adhesive elements, it can be mixed with other components such as proteins or arginine-glycine-aspartic acid (RGD) motifs to modify adhesion properties and cell-matrix interactions [149].

2.1.1.2. Protein-based biomaterials

Proteins constitute macromolecules consisting of linear chains of amino acids. Their fundamental role in biochemical, mechanical and structural functions in all living organisms make proteins ideal candidates as natural-derived building blocks for hydrogels.

Collagen

Collagen is a triple helix molecule mainly consisting of repeating units of glycine, proline and hydroxyproline [150]. It is the most abundant structural protein in the mammalian and human body, present in most soft or rigid connective tissues such as skin, cornea, bone, tendons or basement membranes [151].

Fibrillar (e.g. type I, II and III) and non-fibrillar (e.g. type IV or collagen-like proteins) collagens are differentiated and their functionality is diverse, participating in a large number of interaction systems with other micro- and macromolecular components [151, 152].

Fibrillar collagen and especially type I, besides serving as a scaffold for cells, is highly biocompatible, provides high tensile strength, controllable biodegradability and acts as a natural substrate for cell adhesion, proliferation and differentiation. It is also involved in various proregenerative interactions in the wound-healing process [153]. These properties make it the most widely used biomaterial so far in the field of tissue engineering, such as wound dressings, corneal implants, bone filling materials or drug delivery systems [154].

The majority of collagen is extracted from animal sources such as bovine (Achilles tendon bone or skin), rodent (rat-tail tendon), fish, mollusk and marine invertebrate, but recombinant methods have also been developed [153].

Gelatine

Gelatine is a polydisperse amphipathic protein obtained from the partial hydrolysis of collagen fibrils into polypeptides of lower molecular weight. Depending on the acid or alkali pretreatment of collagen, type A (acid hydrolysis) or type B (alkali hydrolysis) gelatine can be obtained [155].

Mammalian connective tissues and bones such as porcine skin, bovine hides or pork and cattle bones are the major sources of extraction, but fish by-products or even insects are some nonmammalian alternative sources that have gained importance recently [156–158]. The amino acid composition of gelatine varies depending on the extraction source and collagen pretreatment, but it can be defined as a linear chain predominantly composed of glycine, proline and hydroxyproline and a portion of variable amino acids [159]. Glycine stands for 1/3 to 1/2 of the total residues and about 1/4 of the total amino acids are represented by proline and hydroxyproline [160]. Although gelatine is derived from collagen, it shows better solubility and lower antigenicity than its precursor [161, 162], which is suitable for promoting cell adhesion and growth and regulating the degradation by matrix metalloproteinases.

Gelatine forms a physical gel when it is dissolved in hot water and subsequently cooled below room temperature. However, its instability at body temperature has led to the development of various chemical or enzymatic crosslinking strategies with or without functionalisation of gelatine side groups to be able to tune and control its properties [156].

Its versatility, low cost, and high biocompatibility have made it one of the most widely used biomaterials for hydrogel production.

Silk fibroin

Silk is a natural fibre composed of silk fibroin and sericin obtained from *Bombyx mori* silkworms' spinning. The fibrous protein silk fibroin (SF) is the main component (about 75%) and sericin is a sticky globular protein that surrounds the fibroin yarns. SF is the silk's component used for scaffold formation and regenerative medicine applications.

The aggregation structure of SF shows amorphous and crystalline regions responsible for different characteristics. The crystalline phase forms stable β-sheet crystallites that provide high strength to the silk and the amorphous region provides high toughness due to its energy absorption when the material is under stress. It is an easily processable biofiber, biocompatible with different biological tissues, modifiable in different formats such as hydrogels, membranes, nanofibers or scaffolds, and with controllable degradation (Figure I.8) [163, 164].

SF can be either physically or chemically crosslinked. The formation of β-sheet structure between contiguous chains produces the physical gelation, while, the phenolic hydroxyl groups of tyrosine and amino groups of lysine make chemical crosslinking possible [165]. The combination of both crosslinking techniques, blending with other polymers or the control of the molecular-level design and multiscale structure have recently been studied to produce hydrogels that are more resistant, injectable, with high self-healing capacity or with better adhesive and conductive properties [163].

I.8. FIGURE: Photographs of the synthesis process of silk fibroin-methacryloyl (Sil-MA) bioink and hydrogel. **a**) After measuring the weight of cocoons, the silk is degummed with 1 l of 0.05 M sodium carbonate for 1 h, rinsed twice with distilled water and dehydrated in the oven overnight. Then the silk is disolved in LiBr salt solution and filtered. Glycidyl methacrylate (GMA) is added dropwise to regenerated SF (RSF) and RSF-GMA solution is stirred on a hot plate (60 °C) at 800 rpm for 6 h to allow SF and GMA to react. The solution is then dyalised in distilled water during 7 days and lyophilised for another 5-7 days. The lyophilised Sil-MA sponge is disolved in 0.2% (wt/vol) LAP containing PBS and homogeneously mixed. Finally, the solution is centrifuged to remove air bubbles. **b**) A tracheal shape hidrogel printed with PKH67-labeled cells (green) and PKH26 labeled cells (red). From left to right, CAD design of a tracheal construct, images of the hydrogels that have been printed, fluorescence (FL) image using confocal or single plane illumination microscopy and merged image of fluorescent hydrogel and CAD design. Images taken from [164].

2.1.1.3. Tissue-derived biomaterials

Decellularised tissues or tissue-derived biomaterials are natural materials extracted from animals or humans that have undergone a process to eliminate cellular elements. This procedure conserves an acellular intricate structure made up of structural proteins, matrix macromolecules and growth factors that mimic the composition and organisation of the native ECM microenvironments. These materials offer both mechanical and biological support for cell seeding. Tissue-derived biomaterials can be classified into two categories: Organ/tissue-derived decellularised ECM (dECM) scaffolds or cell-derived dECM scaffolds [166].

Organ/tissue-derived dECM scaffolds

Decellularised extracellular matrix (dECM) scaffolds derived from organs or tissues undergo a decellularisation process, which removes all immunogenic cellular components. Decellularisation refers to the removal of cellular components from a tissue using physical stress and/or chemical/enzymatic agents, leaving only the non-cellular ECM. The resulting structure can then be used for therapeutic applications. Thus, the process preserves the original 3D architecture and bioactive molecules, enabling the regulation of cell adhesion, proliferation and differentiation, while maintaining similar mechanical properties to those of the tissue of origin [167].

Small intestinal submucosa [168], acellular dermis [169], adipose tissue [170] and heart valve-derived dECM [171] are some examples of the tissues and organs tested.

Cell-derived dECM scaffolds

Cell-derived dECM scaffolds are created by decellularising the specific ECM synthesised by cultured cells *in vitro*. For instance, to produce a cell-derived dECM from a culture of NIH-3T3 fibroblasts, 2×10^5 cells/well were seeded on a p24 plate with 1 ml of medium. Once they reached confluence, the medium was replaced, and ascorbic acid was added to stimulate collagen and matrix production. After 5 days of seeding, the cellular components were removed by decellularisation using lysis and wash buffers [172]. This method makes it more feasible to obtain cell type-specific dECMs such as stem cells dECMs and reduces the potential risk of infection by allogeneic/xenogeneic ECM [167]. Cellular components can be eliminated through physical methods such as freeze-thaw cycles, chemical methods like the application

of detergents such as sodium dodecyl sulfate and Triton X-100 to destroy cellular and nuclear membranes, or enzymatic methods such as the use of trypsin and nuclease solutions to degrade peptides, DNA, and RNA.

Cell-derived dECMs have been utilised to tailor specific cell and tissue niches for the purpose of enhancing cellular functions and interactions within the niche. For instance, it has been demonstrated that dECMs derived from human neonatal foreskin fibroblasts optimise the proliferation, differentiation and maintenance of the podocyte phenotype [173]. Additionally, mesenchymal stem cell (MSC)-derived dECMs have replicated the stem cell niche, thereby protecting re-seeded MSCs against oxidative stress [174].

2.1.2. Synthetic biomaterials

Synthetic biomaterials, which are artificially created in laboratories and typically derived from petroleum oil, can be divided into two categories: thermoplastic and thermosetting polymers. Thermoplastic polymers (Polyethylene glycol (PEG), vinyl polymers etc) soften when heat is applied and become hard again when cooled. Thermoset polymers (Silicone, Polyurethane, etc) react chemically with heat or chemicals and form insoluble materials that cannot melt.

The variety of available functional groups and preparation techniques for the design of synthetic polymers allows the modification of chemical, mechanical, biocompatibility or biodegradability properties in an easy and controlled fashion.

Acrylamide, vinyl acetate, ethylene glycol or lactic acid are some of the monomers from which synthetic polymers are derived. PEG, polycarbonate urethane (PU) or poly(ϵ-caprolactone) (PCL) are some of the three-dimensional networks of synthetic polymers [175].

2.2. Hydrogels

Hydrogels are polymeric networks formed by crosslinked monomers that depending on their hydrophilicity are capable of retaining up to 99% of water. This retention capacity makes them adequate solutions for biological systems such as the human body, which are mainly composed of water [176].

Since they were discovered in 1960 [177], the conduciveness of hydrogels to cell-biomaterial interactions in their hydrated environment and its versatile potential have contributed to the increasing interest and advancement in the field of hydrogel technology. Hydrogels can be used for different medical purposes: drug or cell delivery, tissue regeneration, improved reproduction of tissue microenvironments through 3D culture models, adhesion to moist tissues, haemorrhage prevention, tissue protection during radiotherapy or improved biocompatibility of implants, among others. In addition, as design and functionality features are constantly improved, the use of hydrogels is moving along towards complex applications such as enhanced wound healing, stem-cell differentiation or immune system reprogramming [178].

2.2.1. Main physicochemical properties of hydrogels

The key physicochemical properties of hydrogels that significantly influence their final properties and biological suitability are outlined below (Figure I.9).

2.2.1.1. Mesh size

Mesh size is crucial in determining the release kinetics of biomolecules or cells integrated into the hydrogel, with its control being essential to characterise the diffusion of these compounds. Additionally, pores serve as pathways for nutrient, metabolite or other substance transport to the cells [179]. Typically, pore size decreases with higher macromer concentration or crosslink density within the network.

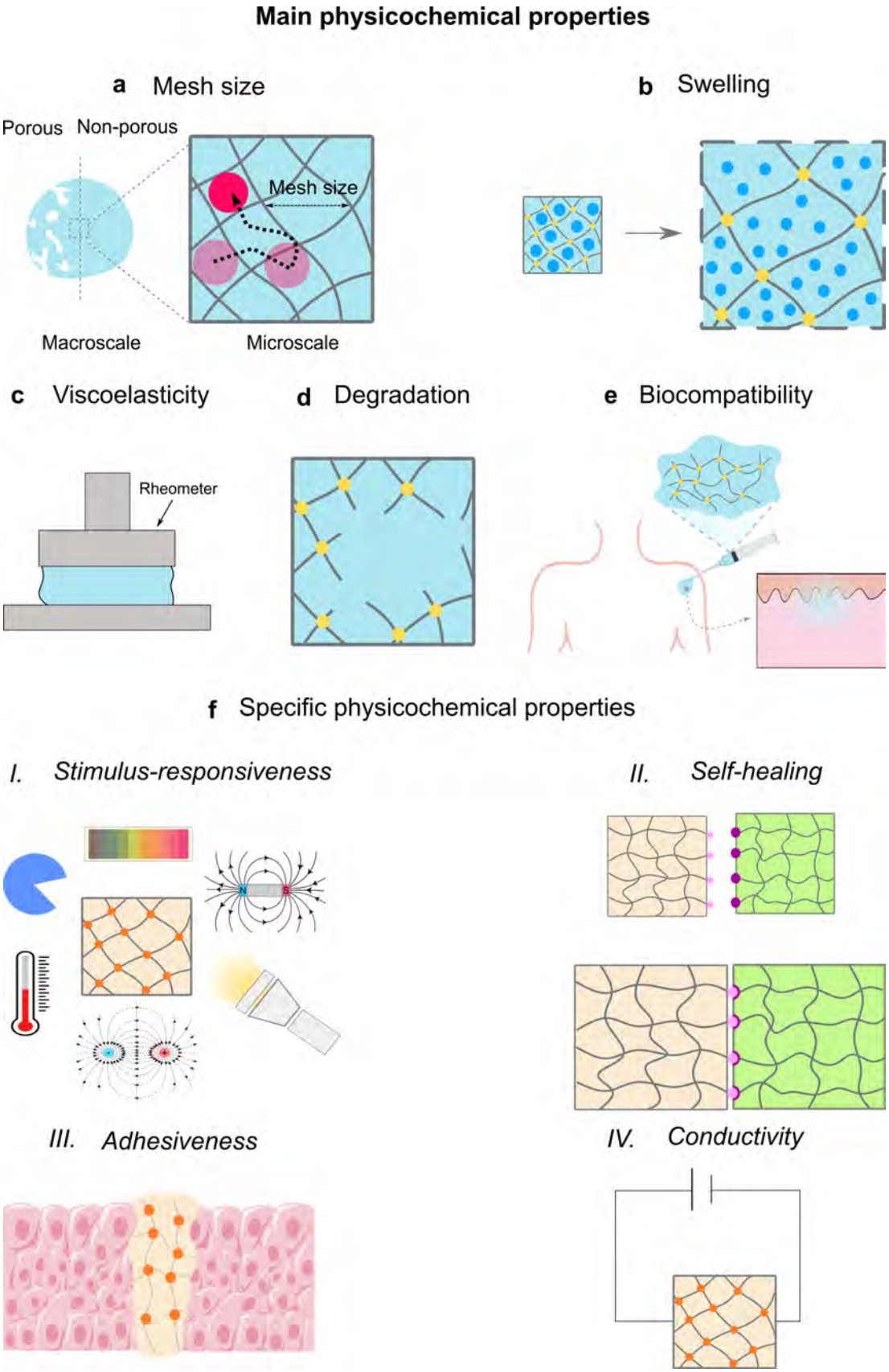

I.9. FIGURE: Schematic illustration of the main hydrogel properties related to hydrogel design guidance. **a**) Mesh size, **b**) swelling behaviour, **c**) viscoelastic behaviour, **d**) degradation profile, **e**) biocompatibility and **f**) properties related to application specificity.

2.2.1.2. Swelling behaviour

Swelling refers to the physical process of liquid absorption, resulting in an increase in material volume and mass. This process occurs due to the hydrogel's elastic and hydrophilic polymeric network that absorbs enough water to increase volume while generating elastic tension in the polymeric chains, thus impeding full dissolution. Swelling is one of the fundamental properties characteristic of most hydrogels and is affected by several factors such as the network structure, the chemical nature of the polymers (more hydrophilic or more hydrophobic), the media and the state of synthesis [180]. This property is important for the accommodation of hydrogels and it is directly linked to drug release and diffusion patterns.

2.2.1.3. Viscoelasticity

The viscoelasticity refers to the characteristic of showing both, elastic and viscous behaviour. Natural or tissue-derived biomaterials also exhibit viscoelastic properties, this is a very important feature for regulating cell-matrix interactions which can lead to differences in cell proliferation or differentiation. The concentration of the precursor polymer, molecular weight, composition, density or crosslinking method influence the viscoelasticity of the hydrogel [179].

The viscoelasticity of hydrogels is generally measured in a rheometer by dynamic mechanical analysis. In these analyses, the oscillatory response of a hydrogel is measured with respect to the variation of the amplitude and frequency of fixed oscillations. Small amplitude oscillatory shear (SAOS) is a frequently employed method for determining a hydrogel's viscoelastic response. The storage and loss moduli, which respectively account for the elastic and viscous responses of the hydrogel, describe the oscillatory response that is calculated in response to an oscillatory input. The material is classified as solid if the loss modulus exceeds the storage modulus, but liquid if the storage modulus is greater than the loss modulus. These moduli are determined through experiments conducted in the linear viscoelastic regime (LVR), where the hydrogel exhibits linear response to the magnitude of the imposed strain or stress. The storage and loss moduli are evaluated with respect to strain, time and frequency. Frequency sweeps are used to profile the material's time-dependent viscoelastic properties [176].

2.2.1.4. Biodegradability

Biodegradability is the process of hydrogel breakdown into harmless products for the body. It depends on various factors such as composition, preparation method, molecular weight, hydrophilicity, pH or temperature. Hydrogels can be removed from the body through bioabsorption and bioerosion. Degradation may occur through the hydrolysis or solubilisation of components [180]. Biodegradation *in vivo* occurs when the hydrogel is exposed to enzymes or body fluids in the biological environment. *In vitro*, degradation is measured by simulating the environment to which the hydrogel would be exposed, for instance, it can be included in a solution containing the enzymes found in a particular tissue.

2.2.1.5. Biocompatibility

Biocompatibility refers to a material's ability to function and respond in tissues without causing toxicity, potential harm or physiological or immunological reactivity. This concept encompasses biosafety and biofunctionality. The former requires that neither the product nor its degradation products produce adverse local or systemic effects, be carcinogenic, or produce harmful effects on reproduction and development. The latter defines the appropriate functionality of the biomaterial in a given application [180].

2.2.1.6. Properties related to application specificity

Stimulus-responsive properties

Stimulus-responsive hydrogels display modifications in their structural and mechanical characteristics in response to environmental stimuli. Endogenous and exogenous stimuli can be distinguished. Endogenous stimuli refer to modifications generated by the organism, such as changes in pH, metal ion concentrations, enzyme activity, redox environment, and antigens. In pathological tissues, abnormal signals such as changes in pH in tumour tissues can cause modifications in the hydrogel, which in turn can trigger an action like drug release or cell capture [181].

Conversely, light, temperature, magnetic field, electric field, and other external factors are exogenous stimuli. Hydrogels that react to these stimuli are designed for

non-invasive and remote functionality. Photocaged RGD hydrogels are an example that can guide fibroblast migration and angiogenesis via light stimulus [182].

Self-healing

The concept of self-healing is modelled from natural processes and refers to the hydrogel's ability to repair its structure and restore its properties without external intervention. For example, self-healing hydrogels can restore their mechanical properties after damage by external stimuli (light, heat, pH) or the interaction of the covalent and non-covalent bonds of the functional groups within. Various methodologies and mechanisms have been utilised to synthesise self-healing hydrogels, incorporating dynamic covalent and non-covalent bonds, or a combination of non-covalent and/or covalent permanent/dynamic interactions to fabricate hydrogels with rapid-healing, stable, and/or multi-responsive behaviour [183].

Adhesiveness

Hydrogel adhesion refers to the joining of two hydrogels or a hydrogel and a surface, which may be hard or soft in nature. Usually, the bonding between hydrogel and tissue is established through the formation of chemical crosslinks or physical interactions with the constituents of the biological surface [184].

Conductivity

All cells have the ability to produce and detect bioelectrical signals via the ion channels located in their cell membranes. These signals can be utilised as a crucial factor to regulate and control cell proliferation, migration, orientation, or differentiation. For instance, in case of a skin wound, the transepithelial potential of the skin is altered, resulting in the formation of an endogenous electric field from the edge into the wound, which could stimulate cell proliferation and migration and promote re-epithelialisation [185].

Conductive hydrogels comprise a hydrophilic polymer network with conductive fillers that enable efficient electron flow, including metallic nanoparticles, conductive polymers, or carbon-based materials. These hydrogels combine the beneficial features of hidrogel systems with the physiological and electrochemical characteristics of

conductive materials. Thus, they can detect electrical signals generated in biological systems and provide electrical stimulation to regulate cell and tissue activities [186].

2.2.2. Classification of hydrogels based on their crosslinking

Crosslinks are links or short sequences of links that bind polymer chains, resulting in network structures. This linking process makes the chains stiffer, stronger and tougher, allowing them to provide mechanical support for biological structures. Crosslinking between polymer chains occurs through functional groups, the fraction of the polymer chain responsible for the chemical reactions. The most common functional groups include amine (-NH_2), carboxyl (-COOH), thiol (-SH) or carbonyl (-CHO) groups.

Both natural and synthetic hydrogels are made by physically or chemically crosslinked polymers (Figure I.10). Crosslinks play a fundamental role in the formation of the hydrogel structure. They are responsible for generating stable network structures that are distinct from hydrogels' raw materials. Crosslinking is not a property itself but the crosslinking degree can be correlated with all the characteristics of a hydrogel. These crosslinks influence the physical properties of the polymer such as viscosity, melting point, strength or toughness [187]. Therefore, controlling the degree of crosslinking makes it possible to adjust the properties of the hydrogel and optimize it for different applications [156].

Depending on the type of crosslinking bonds physically crosslinked and chemically crosslinked hydrogels can be distinguished [188]. Chemical techniques for crosslinking result in improved mechanical properties and stability. Alternatively, physical methods are biocompatible by nature as they do not necessitate crosslinking agents.

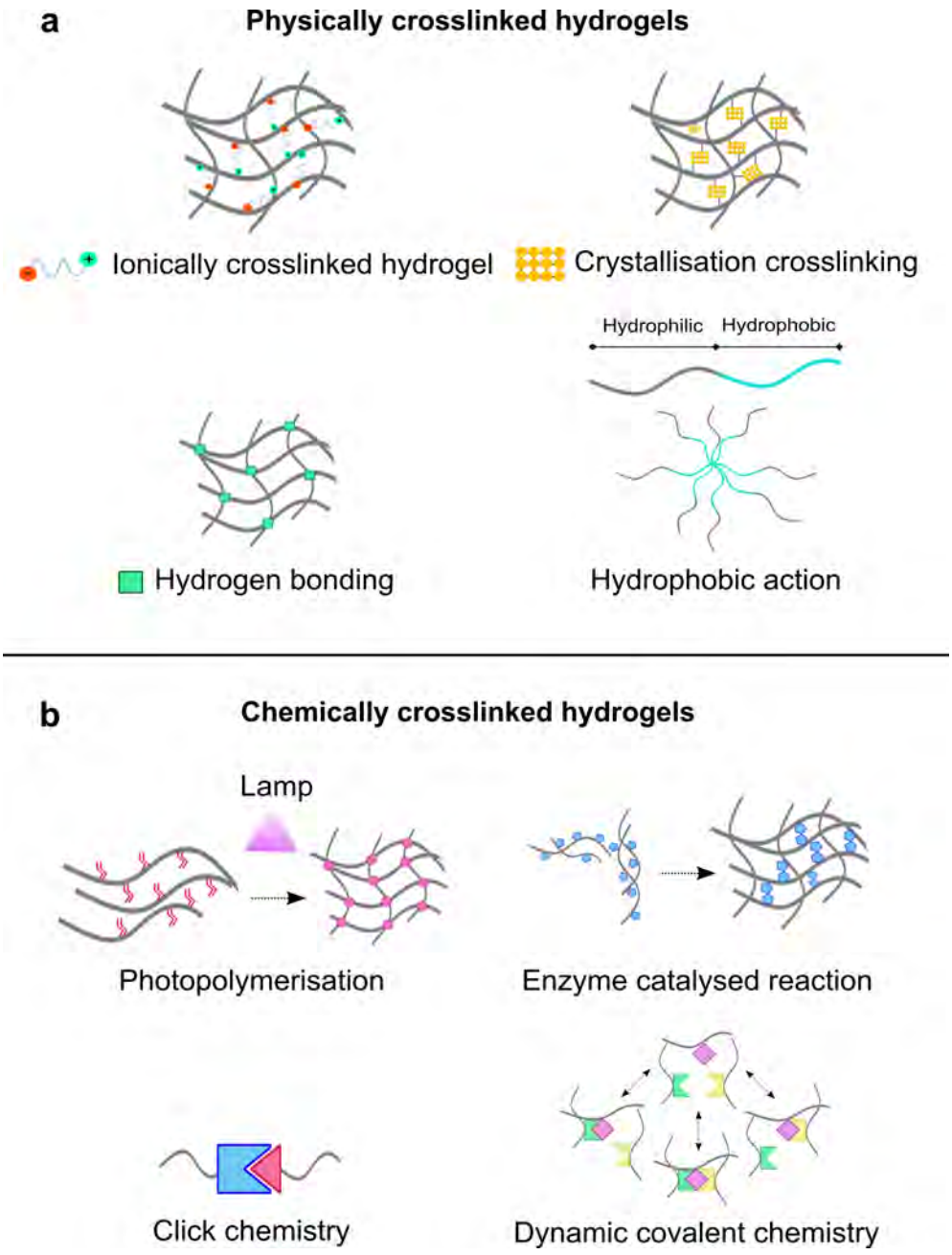

I.10. FIGURE: Schematic illustration of the different physical and chemical crosslinking strategies for hydrogel synthesis.

2.2.2.1. Physically crosslinked hydrogels

Physically crosslinked hydrogels lack crosslinking agents and are kept stable naturally by reversible transient bonds related to crystallinity, hydrogen bonding, hydrophobic interactions, electrostatic interactions or chain entanglements [189].

The mechanical properties of physical hydrogels are usually softer than the ones of chemically crosslinked hydrogels because physical interactions are weaker

than covalent bonds [190]. However, these interactions may be enough to keep the hydrogels from solubilising in aqueous media [187]. The gelation of physical hydrogels is related to the intrinsic properties of the polymers, which limits the modifications that can be made to the properties of the hydrogel. However, since gelation occurs without modifying the polymeric chains, it is easy to carry out and reverse when needed [191].

The study and understanding of ionic interactions, hydrophobic interactions or hydrogen-bonding interactions along with others has received greater interest recently to create hydrogels without the need for crosslinkers.

Ionically crosslinked hydrogels

Ionically crosslinked hydrogels form bonds from the electrostatic attraction between oppositely charged ions present in functional groups of polymer chains such as carboxyl or amino groups [192, 193]. Mono-, di- or trivalent metal ions such as Ag^1, $Ca_2{}^1$ or $Fe_3{}^1$ are some of the metal ions used to form such bonds. These networks present a self-healing behavior, i.e. they break under high stresses but re-form when the stress is removed, but the mechanical strength obtained is limited [194, 195].

For example, alginate or chitosan based hydrogels crosslinked with cations have been explored for diverse tissue engineering, drug delivery or wound healing applications [196–198].

Crystallisation crosslinking

Crystallisation crosslinking by repeated freeze-thawing cycles occurs when the renaturation of proteins generates crystallites that physically act as crosslinking sites to form the hydrogel. The use of this crosslinking technique has been described for gelatine, chitosan, cellulose or synthetic hydrogels [199–201]. For instance, a minocycline-loaded PVA-chitosan hydrogels formed by freezing-thawing cycles proved its efficacy as wound dressings in *in vivo* tests performed in rats [202].

Hydrogen bonding

Any molecule with a hydrogen atom attached directly to an oxygen or nitrogen can form hydrogen bonds, thus, the bonding of a hydrogen atom and a functional group such as amide, urea, carboxylic acid or hydroxyl group can act as a crosslinking

point in hydrogel formation and a crosslinked network can be generated [203, 204]. Hydrogen bonding is the main physical crosslinking form of natural polymers such as cellulose [205] alginate [206, 207] or chitosan [201].

Hydrophobic action between natural polymer groups

The hydrophobic association of hydrogels is formed by using amphiphilic polymers with hydrophobic end groups or by introducing a small amount of hydrophobic groups by a chemical reaction. The hydrophobic groups aggregate with each other and generate a three-dimensional network at a certain concentration [208].

2.2.2.2. Chemically crosslinked hydrogels

Chemically crosslinked or thermoset hydrogels have permanent covalent bonds. They can be formed by free radical polymerisation, radiation, crosslinking of small molecules or enzyme-induced crosslinking [209]. They generally exhibit greater stability, better mechanical properties and more tuneable degration performance than physical hydrogels.

Photopolymerisation

In photopolymerisation, reactive double-bonded carbons usually found in unsaturated groups, foster a free radical polymerisation when exposed to radiation. For example, water-soluble polymers containing hdroxyl, carboxyl and amino groups can react with acryloyl chloride, glycidyl methacrylate (GMA) and N-(3-aminopropyl) methacrylamide, thus introducing highly reactive vinyl groups [210]. The synthesis of photopolymerised hydrogels also requires photoinitiators that absorb specific light at different wavelengths such as Irgacure 2959, LAP, riboflavin phosphate, eosin Y etc [211–213]. These photoinitiators decompose or remove hydrogen from a donor molecule when they are exposed to light, forming reaction-initiating radicals that will react with reactive groups (Figure I.11).

This is a crosslinking method widely used to form cytokine encapsulating hydrogels [214–216] and it allows the modification of the mechanical properties and the precise selection of the crosslinked site by controlling light exposure [217].

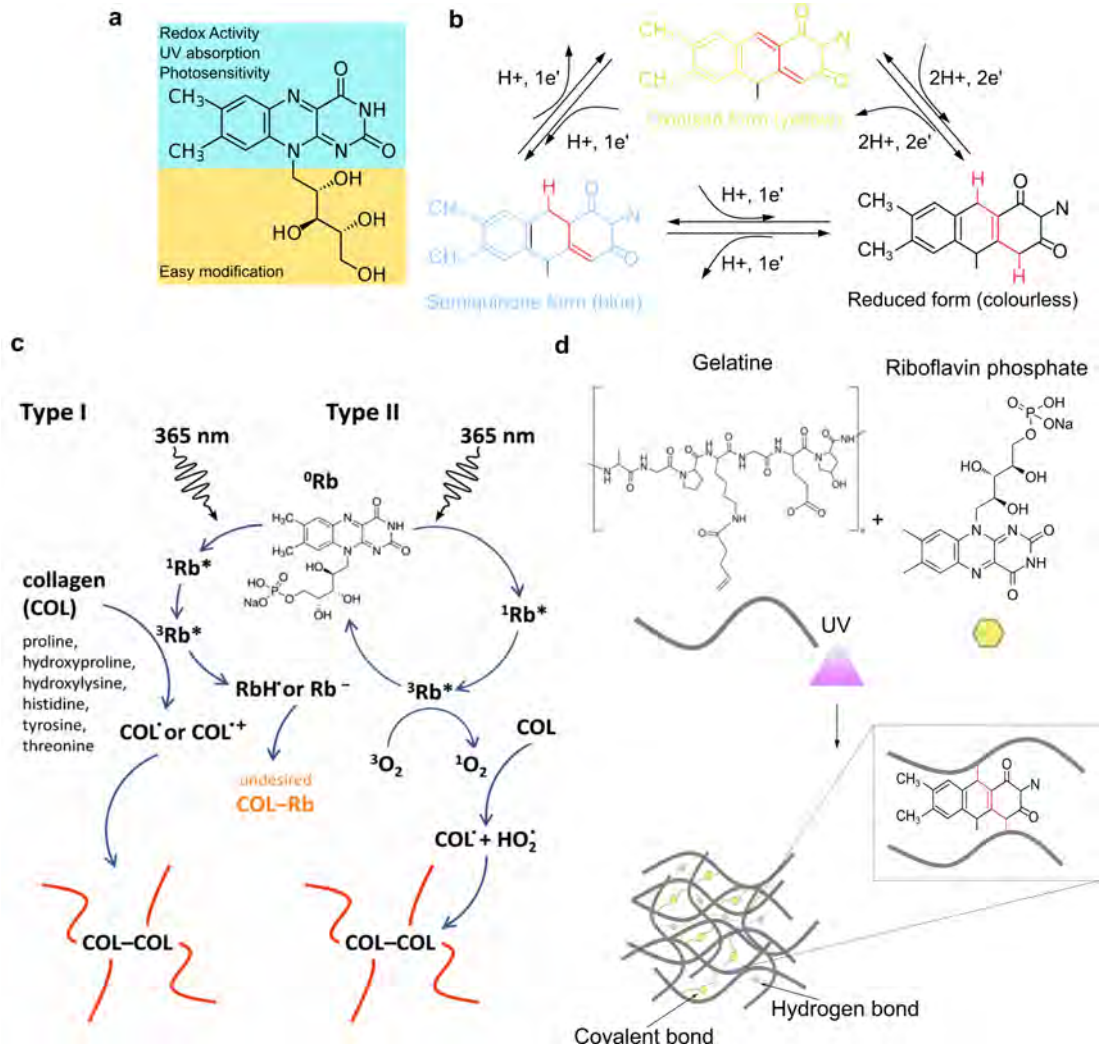

I.11. FIGURE: **a**) Structure of riboflavin; **b**) Oxidation states of riboflavin (**a** and **b** modified from [218]); **c**) Collagen and riboflavin crosslinking chemistry (modified from [219]); **d**) Possible crosslinking reaction between gelatine and riboflavin phosphate after UV irradiation.

Enzyme catalised reactions

Enzymes are proteins that accelerate the chemical reactions taking place within the cells of living organisms and play a fundamental role in almost all cellular processes. These catalysts typically participate in a wide range of reactions, such as oxidation and reduction, hydrolysis or chemical bond formation. Enzyme-mediated responses play a crucial role in mediating the crosslinking of native ECM. For example, lysis oxidase can lead to the production of aldehydes from lysine residues found in collagen or elastin fibers, which facilitate their assembly. Additionally, transglutaminase accomplishes protein crosslinking through the acyl transfer reaction between the carboxamide group of glutamate residues and the ε-amino group of lysyl residues.

Considering so, enzymes have been used to modify biomaterials' responses and change their chemical structures at desired sites.

Enzymatic crosslinking generates strongly covalent bonds within minutes under physiological conditions and makes it possible to modify polymerisation kinetics *in situ* by controlling the enzyme concentration [209]. The formation of bonds between carboxamide and amine groups by incorporating the enzyme transglutaminase and calcium ions [220], or the use of horseradish peroxidase (HRP) together with hydrogen peroxide (H_2O_2) to catalyse aniline [221], phenol [222] or tyramine groups [223] are several examples of enzyme catalysed crosslinking.

Click chemistry

Click chemistry refers to a way of generating products by simple reactions based on the formation of carbon-hetero bonds. Its name is intended to reflect a simple bonding of molecules like mechanical snap fasteners. These reactions are characterised as fast, simple, physiologically stable, modular, wide-ranging, regiospecific, versatile and high yield reactions that give a single reaction product [224].

Among the different click reactions that meet these criteria, Diels Alder, Schiff base, oxime and Michael-type addition are some of the classical crosslinking methods gathered in click chemistry.

Dynamic covalent chemistry

Dynamic covalent bonds have the ability to maintain their integrity or break in a relevant period of time for cell matrix remodelling [225]. The boronic ester for example is an excellent candidate for the synthesis of self-healing hydrogels, as it can rearrange bonds at different pH and temperature conditions [226, 227].

3. Regenerative medicine approaches for corneal regeneration

The shortage of high-quality donor tissues, endless waiting lists (only one cornea is available for every 70 needed) [228], graft rejection or other drawbacks such as donor-related infectious diseases have driven the development of RM techniques to restore or regenerate the cornea, leading to significant advances in effective corneal tissue alternatives for *in vitro* research and clinical purposes. Depending on the type of injury or disease desired to overcome, different solutions have been proposed, from the use of regenerative therapies with different types of stem cells to the development of biological scaffolds or innovative materials containing bioactive factors or stem cells.

Among all the therapies and solutions under research, 2 main TE strategies for treating corneal injuries are currently being investigated, which aim to reproduce or restore the microenvironment consisting of cells, extracellular matrix and molecular/mechanical signals: Cell sheet engineering and scaffold-based approaches.

3.1. Cell sheet engineering (CSE)

CSE involves the development of a confluent monolayer of cells *in vitro*, in which cell-cell and extracellular matrix interactions are strengthened [229]. The cells themselves play the main role in engineering the tissue construct, creating their own environment before being transplanted.

It is based on the use of culture substrates made of stimulus-responsive materials. By changing the stimulating factors such as temperature, enzyme, light, ions, redox, pH, sugar, etc., the adhesion behaviour of the substrate to the cells can be regulated so that the cells are naturally desorbed (Figure I.12).

In the most common widely studied CSE systems, the culture plates are coated with poly(N-isopropylacrylamide) (PIPAAm), a thermosensitive and hydrophobic material at 37 °C that allows cell proliferation and adhesion. After a monolayer is formed, the temperature is lowered to around 32 °C, the PIPAAm surface becomes hydrophilic and its rapid hydration prevents further cell attachment, causing the cell sheet to detach. Alternative methods for cell sheet detachment in addition to thermoresponsive surfaces have also been examined, including electrical triggers, light stimuli, magnetic forces, and pH changes. The resulting cell sheets are then

applied to the injured tissue. Generated cell sheets have been used for heart, liver, bone, skin, cartilage or periodontal tissue regeneration, among others [230].

The ocular surface is a suitable target for the application of CSE and this technique has been used to culture corneal epithelium *in vitro*, including the use of peripheral blood-derived mononuclear cells (PBMNC) [231], embryonic chondrogenic stem cell-derived cell sheets [232] or amniotic membrane stem cells [233]. The use of different substrates such as heat-responsive polymers [234] or elastin-like polypeptide (ELP) functionalised with RGD [235] has also been investigated.

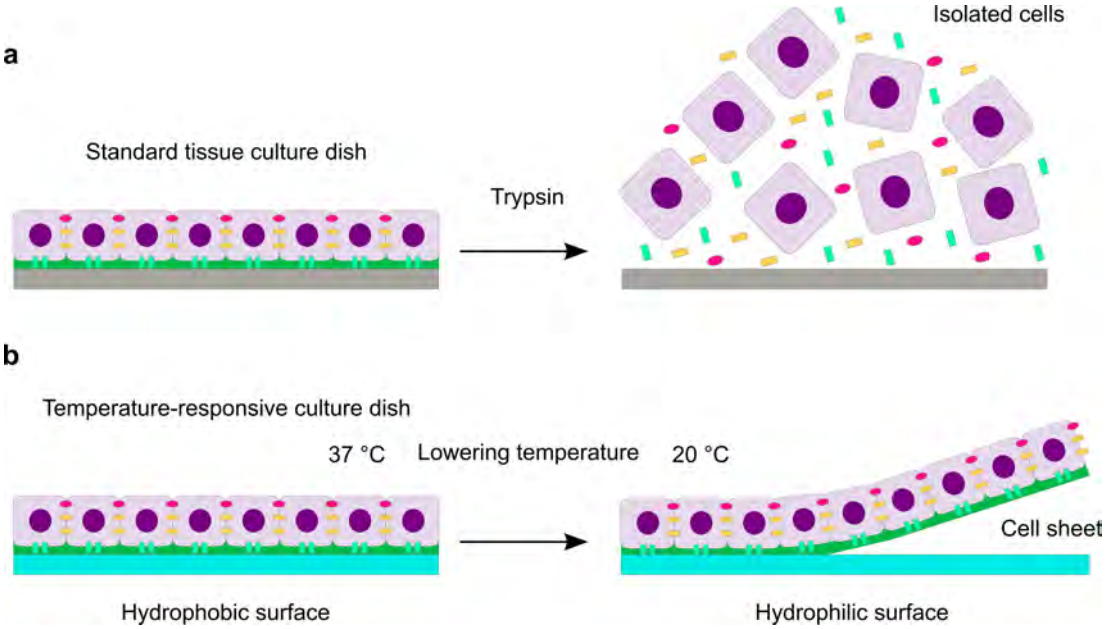

I.12. FIGURE: Cell sheet engineering (CSE) principle. **a**) Confluent cells are harvested individually using enzymatic digestion. **b**) Temperature-responsive culture dishes demonstrate the attachment and detachment of cell sheets. The dishes are composed of a thermoresponsive polymer that alters its hydrophilicity at specific temperatures, allowing for the formation and removal of cohesive cell sheets and providing an effective and non-invasive method for their creation and manipulation.

3.2. Scaffold-based approaches: Use of biomaterials

This approach focuses on the development of different types of substrates or matrices that mimic or stimulate the microenvironment and provide support for the cell population of interest.

The constructs developed vary in type (membranes, lenses, hydrogels etc.), composition (natural, synthetic or a combination of biomaterials) and may contain cells and molecules that would play an active role in the healing and restoration of the defect.

3.2.1. Development of therapeutic contact lenses

Contact lenses provide a physical barrier to allow tissue to heal, exert pressure to relieve pain and maintain adequate ocular surface hydration after surgery [236, 237].

They can be divided into two main groups: soft contact lenses made from polymer hydrogels or silicone-based polymer hydrogels, and rigid gas permeable contact lenses [238]. Silicone-based hydrogel lenses are the most used materials to fabricate soft contact lenses nowadays, as their softness, flexibility, water content, biocompatibility, transparency and gas permeability make them better candidates as drug or antimicrobial agent delivery systems [239–241]. Soft contact lenses account for 87% of fits [242, 243] in clinical practice and Balafilcon A (Pure Vision, Bausch & Lomb), Lotrafilcon A (Night & Day, Ciba Vision) and Lotrafilcon B (O2Optix, CIBA Vision) are some examples of Food and Drug Administration (FDA) approved solutions [244, 245].

The delivery of agents through contact lenses allows for a more gradual release over time with a more adjusted dose than traditional eye drops. Besides, they protect the epithelium from cell detachment that can occur with blinking and maintain a stable tear film on the stroma to promote epithelial cell migration [90].

Strategies to develop drug-loaded contact lenses include drug soaking [239, 246, 247], the introduction of a diffusion barrier by hydrophobic vitamin E [248–251], the incorporation of drug-loaded lipid-based nanoparticles (NP) or other colloidal nanostructured systems [252–256], molecular imprinting [257–259] or the addition of a drug film coating [260, 261]. The incorporation of lipid NPs, polymeric NPs, microemulsions or cyclodextrins shows high drug loading capacity, thermodynamic stability and great versatility to load both hydrophilic and hydrophobic drugs [262]. Molecular imprinting refers to the fabrication of a polymeric template with specific binding sites and unique geometric structures to which the drug can specifically bind. By controlling the affinity ratio between the polymeric network and the drugs, a higher affinity for the drug is achieved and the uptake and sustained release of the drug is improved [239]. All other techniques use hydrogels as carriers for drug-containing polymer nanoparticles or as polymer implants within contact lenses. Table I.3 lists some of the materials used as substrates [263].

I.3. TABLE: Characteristics of the polymers used as contact lenses' substrates. Table reproduced from [263].

Polymer	Characteristics
Propoxylated glyceryl triacrylate (PGT)	Polymer having multiple vinyl functionalities.
Polycaprolactone (PCL)	Hydrophobic and FDA-approved bioresorbable polymer without toxic byproducts.
Chitosan	Cationic polysaccharide polymer with good biocompatibility and biodegradability including lysozyme-related degradability.
poly-(lactic-co-glycolic acid) (PLGA)	Biocompatible, biodegradable and FDA-approved polymer that can change properties by varying the ratio of glycolic acid to lactic acid.
Poly (d,l-lactide)-dextran (Dex-b-PLA)	Core-shell structured nanoparticles consisting of PLA core and dextran outer shell.
Poly-Hydroxyethylmethacrylate(HEMA)	Hydrophilic hydrogel with high water content having excellent biocompatibility.
Ethyl cellulose (EC)	Hydrophobic, biocompatible,non-biodegradable polymer.
Fibrin	Protein-based natural biopolymer having biodegradability by plasmin-mediated fibrinolysis.
Eudragit S-100	pH-sensitive anionic copolymer having dissolving property in above pH 7.0.

3.2.2. Application of hydrogels for different corneal injuries

Biomaterials in the form of hydrogels are a very promising avenue for exploring scaffolding materials. They have favourable properties for the treatment of corneal lesions of varying degrees of severity. The tunable physical properties, biodegradability and bioactivity of hydrogels make it possible to simulate a cellular microenvironment favourable to cells. In addition, cells or biochemical molecules can be encapsulated in the hydrogels to promote regeneration of the corneal epithelium, stroma and full-thickness corneal wounds, promote corneal healing and potentially reduce the need for corneal donations.

Possible applications of hydrogels include (Figure I.13):

- Creation of dressings for superficial corneal epithelial wounds, where the hydrogel acts as a protector and accelerator of healing.
- Ocular adhesives as substitutes of sutures for small corneal incisions.
- Hydrogels as filling agents for corneal defects and corneal perforations.
- The creation of full corneal substitutes.

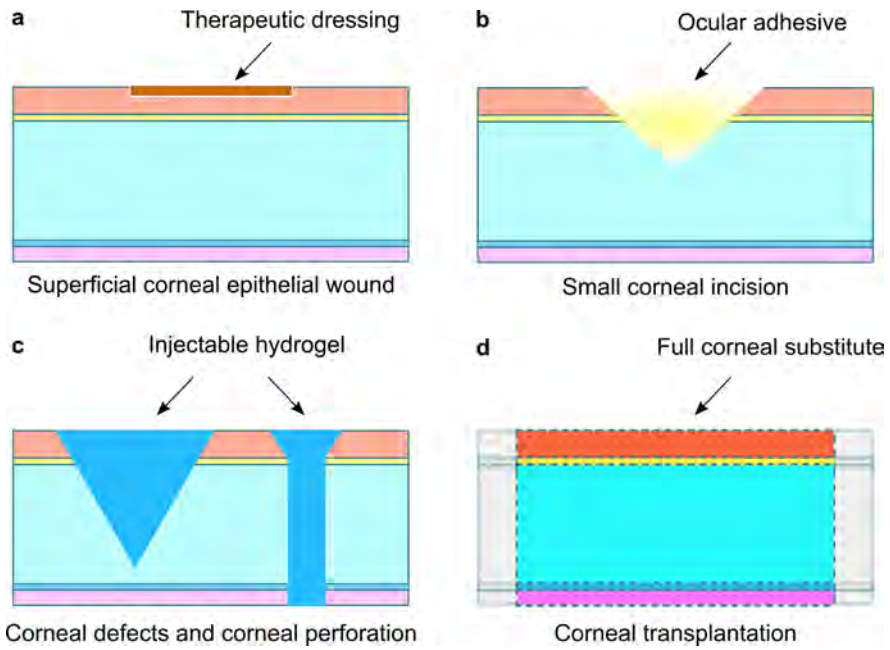

I.13. FIGURE: Hydrogel solutions for different corneal injuries. **a**) Therapeutic dressings for superficial corneal epithelial wounds. **b**) Ocular adhesives as suture replacement for small corneal incisions. **c**) Hydrogels as filling agents for corneal defects affecting the stroma and corneal perforations. **d**) The use of full corneal substitutes.

3.2.2.1. Therapeutic dressings

Therapeutic hydrogel sheets (THS) or membranes with a delivery system for drugs, growth factors or antibiotics have been used in the postoperative management of laser refractive surgery, corneal epithelial defects or corneal dystrophy to promote corneal healing, reduce inflammation and stabilise the microenvironment of the ocular surface. Amniotic membrane grafts or collagen vitrigels (CVs) are two examples of this application.

Amniotic membrane grafts

The amniotic membrane (AM) is the semi-transparent 0.02-0.05 mm thick layer of the placenta in contact with the foetus. It has no blood vessels and is composed of several layers: the epithelium (the innermost layer), formed by cuboidal cells secreting immunomodulatory factors; the basement membrane, secreted by epithelial cells and composed of collagen I, III, IV, V and VII, non-collagenous glycoproteins and hyaluronic acid; and the stromal layer. The latter is further subdivided into three layers: an inner compact layer containing mesenchymal stem cells (MSCs) and their secretome, a middle fibroblast layer, and the acellular spongy layer composed mainly of type III collagen and proteoglycans [264, 265].

Its composition based on collagen, cells and a variety of growth factors together with its anti-inflammatory, anti-fibrotic, antioxidant, antibacterial and non-immunogenic properties makes it an allograft with great potential in the field of ophthalmic tissue engineering and cell therapy [264].

Various commercial products derived from AM are available in the form of sheets. The cryopreserved ProKera membrane (Bio-Tissue, Miami, FL, USA) showed encouraging results in the treatment of bacterial keratitis [266], alkali burns [267], LSCD [268] or PEDs [269]. AmnioGraft (Bio-Tissue, Miami, FL, USA), AmnioGuard (Bio-Tissue, Miami, FL, USA) or AmbioDisk (Katena Products Inc, Denville, NJ, USA) are decellularised and lyophilised amniotic membrane grafts for office-based ophthalmic applications.

Taking into consideration all the interesting properties of AM, the use of human amniotic membrane (HAM) in ophthalmology has evolved from simple sheets to amniotic membrane extract eye drops (AMEED), amniotic membrane nanocomposites, drug carriers [270], powders or hydrogels consisting of a combination of amniotic membrane powder and other natural or synthetic materials [271, 272].

Collagen vitrigel (CV) membranes

Collagen vitrigels are membranes formed by compacted collagen I fibrils that simulate the architecture of corneal collagen. They are synthesised in 3 steps: formation of a collagen gel, vitrification, which consists of converting the gel into a rigid membrane through a drying process in which the collagen fibrils of the hydrogel are compacted into a dense network, and subsequent rehydration to convert the vitrified material into a thin, transparent gel membrane.

The effect of varying different vitrification variables such as temperature or humidity to subsequently culture keratocytes on the synthetised membranes has been studied [273]. CVs have been proposed for the reconstruction of endothelial, epithelial or stromal layer of the cornea [273, 274] or the combination of CVs and fibrin glue have been studied to repair corneas with LSCD or stromal wounds [275].

3.2.2.2. Ocular adhesives as substitutes of sutures for corneal incisions

Eye adhesives were developed as an alternative to sutures and their associated drawbacks. They can be broadly classified as synthetic, usually derived from cyanoacrylate or polyethylene glycol (PEG), or biological, usually fibrin-derived materials.

Cyanoacrylates

Cyanoacrylate (CTA) is an ester derived from cyanoacrylic acid that is readily polymerised by alcohols, water or amino acids present in living tissue. They are called superglues because of the strong bond of the adhesives to the tissues that results from the polymerisation reaction between the amino acid residues of the proteins and the CTA [276].

Although not FDA approved for ocular use, CTA has been used in ophthalmology for a variety of applications, including temporary tarsorrhaphy [277], corneal thining and perforation [278] or leaking blebs [279, 280].

Although it offers a quick and effective solution, the degradation of CTA to cyanoacetate and formaldehyde can induce acute and chronic inflammation, and its impermeability to fluids and metabolites, lack of transparency and rough surface limit the healing of the underlying tissue, impair vision and cause patient discomfort [281]. For these reasons, its use in ophthalmology has been limited.

PEG-based sealants

PEG and its derivatives are attractive synthetic materials for the development of ocular adhesives due to their tunable mechanical and biological properties, low immunogenicity and non-toxicity.

ReSure (Ocular Therapeutix Inc., MA, USA) and OcuSeal (Beaver-Visitec International, MA, USA) are two PEG-based adhesives that have been used in the clinic and tested in human clinical trials. ReSure is a FDA approved adhesive for closure of corneal incisions to prevent fluid leakage in cataract surgery [282]. The ReSure equivalent used in Europe is OcuSeal (Beaver-Visitec International, MA, USA), also an PEG-derived adhesive. Both sealants have shown improvements in

incision closure, astigmatism reduction or postoperative cataract recovery over nylon sutures [283–285].

However, their use is limited to sealing incisions that are not actively leaking. These sealants are unable to fill stromal defects, either because of poor adhesion if they are not covered by tissue [286, 287], or because of their uncontrollable and rapid polymerisation [284].

Fibrin glue

Along with CTAs, fibrin glues are the most used suture substitutes in ophthalmology and are based on mimicking the body's own clotting process. They combine a protein solution consisting of fibrinogen, plasminogen, fibronectin and factor XIII with a solution of thrombin and calcium chloride. Thrombin cleaves fibrinogen into fibrin, forming a three-dimensional network. Thrombin also cleaves Factor XIII, which allows the fibrin monomers to crosslink and polymerise in the presence of calcium ions. When this adhesive is applied to the cornea, fibrin and fibronectin crosslink with stromal collagen, generating a strong attachment to the tissue [288].

Since their first use in ophthalmology in the 2000s, fibrin adhesives have found many key applications as ocular sealants, including corneal perforation healing [289], pterygium surgery for conjunctival autografting [290], amniotic membrane transplantation [291] or sutureless lamellar keratoplasty [292]. Fibrin glue has also been combined with stem cells as an alternative to corneal transplantation [293, 294]. The advantages of these sealants lie in their rapid resorption, improved patient comfort, ease of use in the clinic and less corneal vascularisation compared to CTA. However, the main disadvantages are related to viral contamination and immunological problems. Although these risks are reduced with the use of autologous derivatives, they increase cost, time and reproducibility/consistency of product properties.

Commercial fibrin-based adhesives are available in liquid form for ophthalmic applications, such as TISSEEL (Baxter International, Deerfield, Illinois, USA), available in other countries under the name Tissucol (Baxter Hyland Immuno, Vienna, Austria), EVICEL (manufactured by OMRIX Biopharmaceuticals, New York, USA), Vitagel (Stryker, Kalamazoo, Michigan, USA), Greenplast Q (Green Cross Corp, Seoul, South

Korea) or Reliseal (Reliance Life Sciences, India), the latter two only available in Korea and India respectively.

Alternatives

In addition to the aforementioned materials, combinations of protein-based and synthetic materials have also been investigated for the repair or sealing of ocular wounds. For example, oxidised dextran (ODex) was incorporated into a gelatine methacrylate (GelMA)-based adhesive and crosslinked with visible light for sutureless keratoplasty, which outperformed commercial adhesives in improving re-epithelialisation and strong bonding between donor and recipient corneal beds [295].

3.2.2.3. Hydrogels as filling agents for corneal defects

Advances in chemical synthesis technology have led to the development of hydrogels using various materials such as collagen, gelatine, HA, etc. These are not limited to being simple wound fillers, but serve to promote lesion repair and induce corneal healing.

Collagen based hydrogels

The use of exogenous collagen to replace part of the corneal stroma aims to harness the inherent properties of collagen to promote wound healing by providing a framework for cell migration and colonisation. Exogenous animal-derived and recombinant collagens have been synthesised in various forms to produce ophthalmic sealants and fillers.

As for recombinant collagen, hydrogels based on recombinant human collagen types I and III have been shown to maintain optical clarity and promote the regeneration of corneal cells, nerves and tear film *in vivo* after 12 months of implantation in *Sus scrofa domesticus* minipigs [296]. Similarly, the hydrogel formed from recombinant human collagen with methacrylate anhydride and patterned to mimic the microstructure of natural corneal tissue induces the orderly growth of corneal limbal stromal stem cells, differentiates them into keratocytes and promotes the healing of damaged corneal stroma *in vivo* [297]. Alternatively, the LiQD Cornea hydrogel suggests a cheaper option to recombinant human collagen and shows

potential to reduce the immunological rejection associated with xenogeneic materials. This hydrogel consists of short synthetic collagen analog peptides conjugated with polyethylene glycol and mixed with fibrinogen and shows complete sealing of ocular wounds in rabbits and restoration of corneal thickness 3 months after surgery [298].

Considering animal-derived collagen versions, various crosslinking strategies and blends with other biomaterials such as HA or PEG with type I bovine collagen have also been reported to have great potential for promoting epithelialisation, improving corneal regeneration and reduced expression of fibrotic and inflammatory biomarkers [299–302]. In addition to just filling the wound, collagen-based hydrogels can be used as cell/drug delivery systems. Indeed, the sustained release of various therapeutic agents to improve corneal wound healing has also been proposed [303–305].

Gelatine based hydrogels

As a water-soluble polypeptide mixture derived from the hydrolysis of collagen, gelatine has been proposed as a suitable material for ocular tissue repair.

Although it is a widely used material in ocular tissue engineering, this material is presented chemically modified, as its popular derivative GelMA, combined with other materials or crosslinked by different strategies to obtain different viscoelastic and mechanical properties to facilitate its ocular application.

The functionalisation of gelatine with methacryloyl groups and its photocrosslinking by visible light allowed the development of a transparent, bicompatible adhesive hydrogel called GelCORE (gel for corneal regeneration) to repair corneal lesions without suturing (Figure I.14). In addition, the physical properties of the hydrogel could be fine-tuned by controlling the concentration of prepolymer and the duration of photocrosslinking [306]. By introducing glycidyl methacrylate into the gelatine backbone through chemical modification of the precursor and crosslinking with visible light, Sharifi et al. developed a protein-based elastic hydrogel (GELGYM) with excellent biomimetic properties approaching those of native tissue [307]. In addition, a light-curing hydrogel based on methacrylated gelatine (GelMA) was combined with Pluronic F127 diacrylate (F127DA) and bifunctional Pluronic F127 aldehyde (AF127) co-assembled micelles and collagen type I (COL I) to meet the requirements of transparency, epithelial and stromal regeneration, suture avoidance and strength. The hydrogel was shown to replace

deep corneal stromal defects and biointegrate well into the tissue within 4 weeks in rabbit models, showing great potential in keratoconus surgery and other corneal diseases [308].

Gelatine hydrogels mixed with DCM [309] or agarose [310] or incorporating keratocytes [311] or drugs [312] have also been used to optimise biomechanical and biological properties and induce healing of the defective cornea.

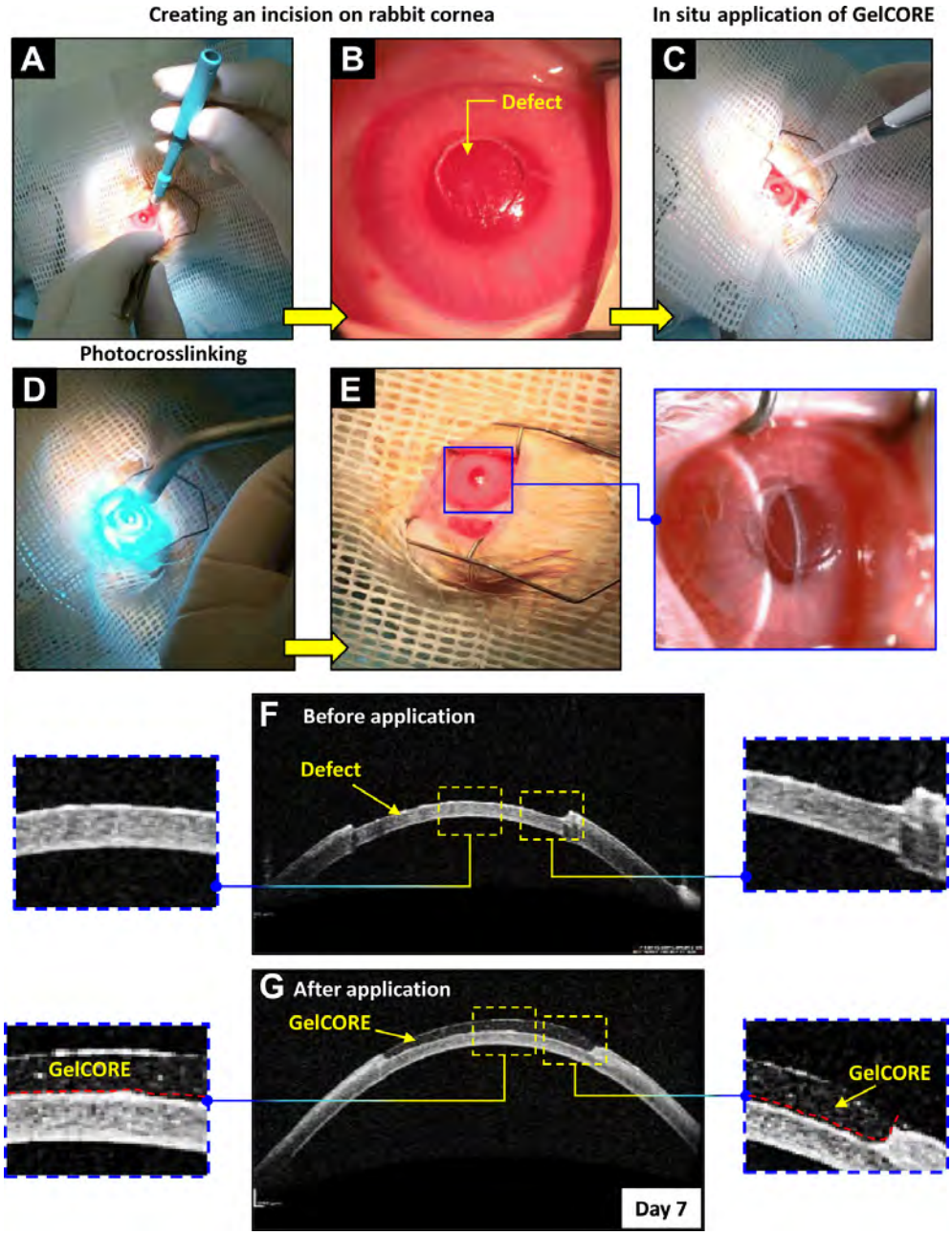

I.14. FIGURE: *In vivo* application of GelCORE bioadhesives into corneal defects in rabbits. **a**) and **b**), Creation of a stormal defect in rabbit corneas. **c**) *in situ* application of gelCORE solution, **d**) crossslinking process, **e**) formation of a transparent gelCORE adhesive on corneal stromal defect. Anterior segment optical coherence tomography images **f**) before and **g**) after treatment with GelCORE. Images reproduced from [306].

HA based hydrogels

HA is a component of the ECM of the cornea that has been linked to cell migration in the wound healing process, among other functions. This, together with its biocompatibility, transparency and mucoadhesive properties, has made HA a very attractive material for the development of tissue adhesives or scaffolds for the treatment of corneal wounds. For ophthalmic applications, crosslinkable HA derivatives with increased intraocular retention have been developed.

A bio-orthogonally crosslinked HA collagen hydrogel with increased transparency has been described that can fill and close corneal defects *in situ* through a sutureless incision [299]. Thiolene chemistry has also been used to develop a visible light photocrosslinkable HA-based hydrogel [313]. In addition, non-covalent supramolecular host-host interactions between HA-cyclodextrin and HA-adamantane have been used to form shear-thinning HA hydrogels that facilitate the adhesion and spreading of encapsulated human corneal epithelial cells *ex vivo*, improve corneal wound healing and reduce anterior stromal inflammation [142].

HA-based hydrogels have also been proposed to deliver cells and drugs to corneal wounds, such as corneal epithelial cells and dexamethasone [314].

Chitosan based hydrogels

Chitosan is also a natural, biodegradable mucoadhesive polymer that is attractive for wound filling. A dendronised (highly branched, tree-like fragments) chitosan hydrogel combined with oligoethylene glycol, whose sol-gel transition occurs at physiological temperature, has shown to rapidly fill and seal irregular corneal stromal defects, promote keratocyte proliferation and migration, and induce tissue regeneration in corneal stromal defects [315].

However, chitosan-based thermosensitive hydrogels show the added functionality of being promoted as payload carriers, such as drug delivery [316, 317], growth factors [129] or exosomes [318], which is more likely to attract research interest than the possibility of using these hydrogels solely as a wound filling material.

dECM-based hydrogels

Decellularised xenogenic corneal matrices have also been used to produce hydrogels for corneal applications. Due to their ability to retain bioactive components

of native tissues (e.g. collagen, glycosaminoglycans, growth factors and cell adhesion proteins), they have the advantage of mimicking the ECM composition of the native corneal stroma.

A thermosensitive hydrogel derived from decellularised porcine corneal ECM (COMatrix) with native protein content and proteins with regenerative capacity such as lumican, keratocan or laminins enhanced adhesion and proliferation and reduced inflammatory cytokine expression in human corneal epithelial cells [319, 320]. *In vivo*, it showed good adhesion to corneal defects after healing and promoted epithelial closure with an increase in the proliferation marker Ki-67 [321].

Furthermore, by crosslinking with N-cyclohexyl-N0-(2-morpholinoethyl) carbodiimide metho-p-toluenesulfonate (CMC)/N-hydroxysuccinimide (NHS), it was able to form a hydrogel capable of filling epithelio-stromal defects, forming a smooth surface that favoured wound healing by promoting ECM formation by corneal fibroblasts [322].

3.2.2.4. Full corneal substitutes

The development of whole corneal substitutes that attempt to mimic the microstructure and microenvironment of the different corneal layers for pathological corneas represents the most complex but promising avenue for corneal bioengineering. Corneal tissue models based on the principle of self-assembly have been developed to study physiological processes *in vitro*. Early models in the 90's included a stratified epithelium with a basement membrane, stromal fibroblasts embedded in a collagen hydrogel and an endothelial monolayer with a basement membrane [323] or immortalised corneal cell lines (epithelial, keratocyte and endothelial cells) dispersed in a collagen hydrogel [324].

These models have undergone further enhancement through the incorporation of human corneal endothelial cells, as well as primary and immortalised human corneal epithelial cells [325, 326]. Additionally, the study conducted by Wang et. al. utilised silk fibroin film stacks that were seeded with human corneal stromal stem cells (hCSSC) for the stroma, NGF stamped silk films that were seeded with human corneal epithelial cells (hCEC) for the epithelium, and a silk sponge that was seeded with chicken dorsal root ganglion (DRG) neurons to simulate the limbus. The silk film stacks of the stroma and the epithelium were embedded in type I rat tail collagen

hydrogel to integrate the scaffold. In addition, NGF-loaded collagen gels were combined with NGF-stamped silk films in the epithelium to guide the axons of DRG cells towards the centre of the scaffold. The incorporation of stromal, epithelial and innervated tissues allowed a more comprehensive study of corneal tissue innervation and development, corneal disease and tissue responses to environmental factors (Figure I.15) [327].

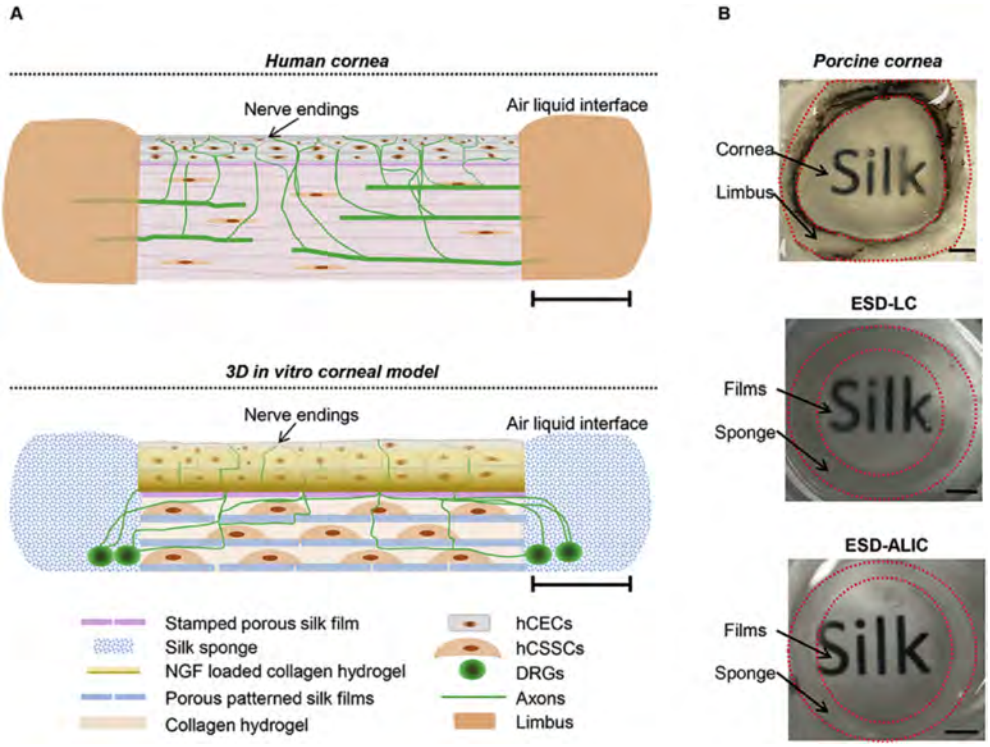

I.15. FIGURE: **a**) Illustration of human cornea and *in vitro* 3D corneal tissue model. Scale bar corresponds to 3 mm. **b**) Porcine cornea, co-culture of hCECs, hCSSCs and DRG explants in liquid and co-culture at air-liquid interface at day 28. Both co-cultures are soaked in glycerol. Scale bar corresponds to 3 mm. hCEC: human corneal epithelial cells; hCSSC: human corneal stromal stem cells; DRG: chicken dorsal root ganglion neurons; ESD-LC: tri-culture of all cell types in liquid interface; ESD-ALIC: tri-culture of all cell types in air-liquid interface. Image reproduced from [327].

Clinically, patients with severe LSCD and very opaque stromal scar tissue are usually treated with corneal stem cell transplantation followed by stromal replacement with a donor cornea. Recently, a nanostructured allogeneic artificial anterior lamellar cornea has been proposed to treat LSCD and stromal damage simultaneously. The model, called NANOULCOR, consists of fibrin-agarose combined with allogeneic corneal epithelial and stromal cells. After promising preclinical results [328–330], the model is currently in a phase I-II clinical trial to evaluate the safety and partial efficacy of this tissue-engineered product in humans [331].

II. HYPOTHESIS AND OBJECTIVES

1. Hypothesis

Persistent epithelial defects (PED) and chronic corneal ulcers are frequent ocular lesions that do not heal even after two weeks of treatment. The decreased sensitivity and inadequate healing of the corneal surface over time can lead to corneal lysis and even perforation. Although clinical diagnosis of PEDs is not difficult, managing this condition is a challenge. It is one of the most difficult corneal pathologies to treat and its management and follow-up are associated with high social and healthcare costs. PEDs can also occur in the context of limbal stem cell deficiency (LSCD) due to impaired re-epithelialisation caused by limbal progenitor cell involvement. LSCD is a chronic ocular surface pathology that clinically presents corneal neovascularisation, occasional corneal opacity, and can lead to vision loss or blindness. It is caused by damage to the number or microenvironment of limbal epithelial progenitor cells (LEPC) of the sclerocorneal limbus, which are responsible for renewing the corneal epithelium.

Conventional eye drops and topical antibiotics are typically used to treat PEDs. However, in the cases where the stroma is affected and the structural integrity of the eyeball may be compromised, surgical interventions such as tissue grafts or stem cell transplants may be required. The only current effective treatment for LSCD is the transplantation of *ex vivo* expanded limbal stem cells obtained from small fragments of healthy limbus. However, the success rates of this therapy leave much room for improvement, as it often needs to be repeated.

Thus, corneal tissue regeneration is necessary for the restoration of visual function in cases of LSCD, PEDs and corneal ulcers, and effective new treatments are needed to address the associated complications with the current therapies. In this context, the use of biocompatible hydrogels that would mimic the corneal stroma and would be functionalised with bioactive molecules that will support the biological mechanisms of tissue repair would restore ocular health and visual properties in patients with PEDs or stromal ulcers. Furthermore, corneal substitutes that promote the growth of LEPCs and resemble the native cornea in composition and anatomy for transplantation into LSCD patients would offer an effective therapeutic alternative that would reduce the use of donor corneas and fulfill the specific clinical characteristics of each patient.

2. Objectives

The main objective of this thesis was to develop and study the structural, rheological, optical, pharmacokinetic and biocompatibility properties of a hydrogel with similar characteristics to the native corneal extracellular matrix, and which was functionalised with bioactive molecules that favour the cellular and physiological processes necessary for corneal repair and regeneration in cases of PEDs. Besides, primary cultures of LEPCs were also characterised to optimise the conditions for preserving their multipotency in order to introduce these cells into future limbal constructs to transplant in LSCD cases.

For this purpose, the following specific objectives were defined:

1. Characterisation of the physicochemical and biocompatibility properties of different materials for the composition and functionalisation of hydrogels.
2. Functionalisation of the hydrogel through the addition of different bioactive components that promote corneal repair and regeneration and control inflammation.
3. *In vitro* evaluation of controlled release kinetics and therapeutic effects of supplements added to the hydrogel.
4. *Ex vivo* evaluation in a bovine and rabbit model and *in vivo* evaluation in a rabbit animal model of the therapeutic effect of functionalised hydrogels.
5. Immunohistochemical and immunocytochemical study of the human sclerocorneal tissues and primary human corneal cell cultures to determine the attributes of LEPCs and the diverse subpopulations existing in the limbal niche.

III. MATERIALS AND METHODS

1. Biomaterial characterisation

1.1. Film synthesis

Firstly, 4 biofilms of a protein nature were developed in order to study the potential of these biomaterials for their use in corneal engineering applications.

Collagen films were prepared by mixing porcine collagen (Tenerias Omega, Navarre, Spain), glycerol (20% wt based on dry collagen) (Panreac, Barcelona, Spain) and 0.05 M acetic acid (1:1 collagen/acetic acid ratio). The resulting mixtures were stored in a plastic bag at room temperature for 24 hours to hydrate the dough. The dough was placed in a caver laboratory press (Specac, Barcelona, Spain) between two aluminium plates previously heated to 90 °C, and then pressed at 0.5 MPa for 1 minute to obtain the collagen sheets, designated as COL.

Soy protein isolate (SPI) films were prepared by mixing SPI (ADM Protein Specialties Division, Amsterdam, Netherlands) and glycerol (40% wt based on dry SPI) for 5 minutes. These blends were placed in the laboratory press between two aluminium sheets previously heated to 120 °C, and pressed at 4 MPa for 2 minutes to obtain the SPI films, referred to as SPI.

Gelatine-lactose films were prepared by dissolving fish gelatine (Sigma Aldrich, St. Louis, MO, USA) and lactose (20% wt based on dry gelatine) (Panreac, Barcelona, Spain) in distilled water for 30 minutes at 80 °C with continuous stirring. Glycerol (10% wt based on dry gelatine) was then added to the solution and kept at 80 °C while stirring for further 30 minutes. The pH of the solution was adjusted to 10 with 0.1 M NaOH. Finally, the solutions were poured into Petri dishes and left to dry for 48 hours at room temperature to obtain the films. In addition, the films were heated at 105 °C for 24 hours to obtain the lactose-crosslinked gelatine films, designated as GEL-LAC.

Gelatine-citric acid films were prepared by mixing fish gelatine, citric acid (20% wt on dry gelatine basis) (Panreac, Barcelona, Spain) and agar (10% wt on dry gelatine basis) (Panreac, Barcelona, Spain) in distilled water. The solutions were heated at 80 °C and stirred for 30 minutes. Glycerol (20% wt on a dry gelatine basis) was then added and the pH of the solution was adjusted to pH 10 with 0.1 M NaOH. The heating procedure was repeated, the solutions were poured into Petri dishes and

allowed to cool at room temperature for 48 hours to obtain citric acid-crosslinked films, designated as GEL-CA.

1.2. Hydrogel synthesis

The assessment of four protein-based films resulted in the selection of gelatine as the primary material for developing a hydrogel to treat corneal defects. The gelatine from porcine skin (Sigma Aldrich, St. Louis, MO, USA) was crosslinked with riboflavin phosphate (RFP, Sigma Aldrich, St. Louis, MO, USA), a commonly used photoinitiator in clinical settings for crosslinking natural corneal collagen.

This hydrogel served as the basis for the biocompatibility and physicochemical evaluation of four different hydrogel versions, each with a different compound added. 4 different hydrogels were synthetised: the hydrogel designated as G, composed of 5% w/v gelatine and 0.01% w/v of RFP; the hydrogel named as G-D, containing 5% w/v gelatine, 0.01% w/v of RFP and 2.5% w/v dextran (Molecular weight: 450-650 KDa, Sigma Aldrich, St. Louis, MO, USA); the hydrogel referred as G-HA, composed of 5% w/v gelatine, 0.01% w/v of RFP and 0.4% w/v hyaluronic acid (Molecular weight: 1.01-1.80 MDa, Lifecore Biomedical, Chaska, MN, USA); and the hydrogel designated as G-MC, containing 5% w/v gelatine and 0.01% w/v of RFP 1% w/v methyl cellulose (Viscosity: 1200-1800 cP, Sigma Aldrich, St. Louis, MO, USA) (Chemical structures of each compound are shown in the figure III.1).

Gelatine hydrogel (G) was prepared by mixing 5% w/v gelatine and 0.01% w/v of RFP in deionized water and stirring the solution at 80 °C for 30 minutes. Gelatine hydrogels mixed with dextran or hyaluronic acid (G-D and G-HA) were similarly prepared: 5% w/v gelatine, 0.01% w/v of RFP and 2.5% w/v dextran (D) or 0.4% w/v hyaluronic acid (HA) were mixed in deionized water and stirred at 80 °C for 30 minutes. The gelatine hydrogel combined with methyl cellulose (G-MC) was prepared by mixing concentrated stocks of 2% w/v methyl cellulose (MC) solution and 10% w/v gelatine and 0.02% w/v RFP solution at 1:2 dilution. The solution was warmed up to 80 °C and thoroughly mixed pipetting up and down until a homogeneous solution was formed. Previously, 2% w/v MC stock solution in deionized water was stirred in an orbital shaker plate for 48 hours until the solution was completely dissolved. Gelatine stock solution was prepared by mixing 10% w/v gelatine and 0.02% w/v of RFP in deionized water and stirring the solution at 80 °C for 30 minutes.

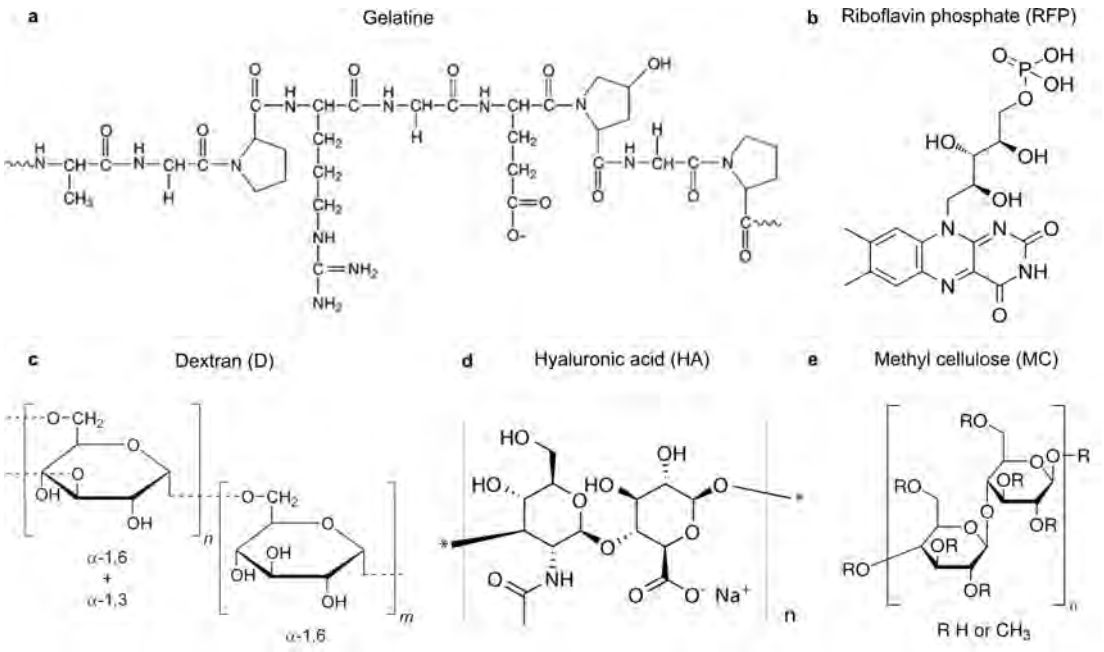

III.1. FIGURE: Chemical structures of the compounds used for the synthesis of the hydrogels. **a**) Gelatin, **b**) riboflavin phosphate (RFP), **c**) dextran (D), **d**) hyaluronic acid (HA) and **e**) methyl cellulose (MC).

The pH of all the hydrogels was adjusted to 7 with 1 M NaOH, warm solutions were filtered using 0.22 μm polyethersulfone (PES) hydrophilic membrane MILLEX® filters (Merck KGaA, Darmstadt, Germany) and stored at 4 °C until their use. When applied in the desired location, the hydrogels were crosslinked by exposing them to blue light for 2 minutes, resulting in manageable materials (Figure III.2). The Led.C curing lamp (Woodpecker Medical Instrument Co, Guilin, Guangxi, China) was used as the illuminating source for crosslinking (λ 420-480 nm).

1.3. Fourier Transform Infrared (FTIR) Spectroscopy

Attenuated total reflectance Fourier transform infrared (ATR-FTIR) spectroscopy was used to identify the distinctive, functional groups and characterise the chemical composition of the biofilms.

Nicolet Nexus FTIR spectrometer, with a MKII Golden Gate accessory (Specac, Barcelona, Spain), equipped with a diamond crystal as ATR element at a nominal incidence angle of 45° with a ZnSe lens was used to conduct the measurements. Measurements were recorded in the 4000-850 cm^{-1} range using 32 scans with a resolution of 4 cm^{-1}.

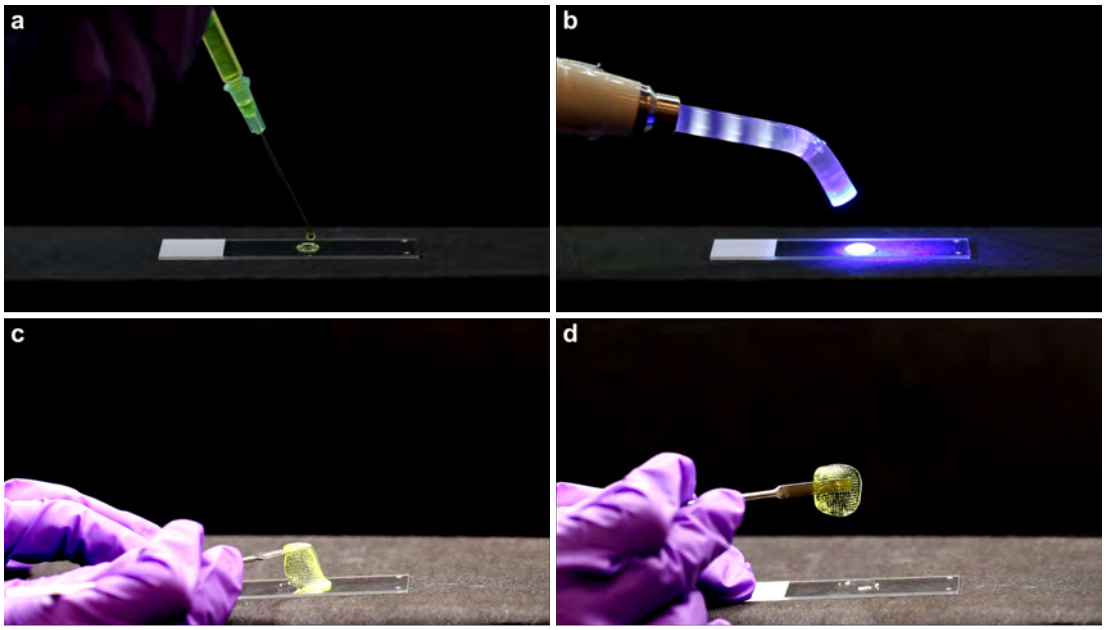

III.2. FIGURE: **a, b**) Injection and crosslinking process of gelatine-RFP hydrogel. **c, d**) Handling of the gelatine and RFP hydrogel after blue light crosslinking.

1.4. X-Ray Diffraction (XRD)

X-ray diffraction (XRD) analysis was used to analyse the microstructure of the films and identify their crystallinity, as well as distinguish between crystalline and amorphous phases of the biomaterials.

The analysis was conducted using a PANalytical Xpert PRO diffraction unit (PANalytical, Madrid, Spain) operating at 40 kV and 40 mA. The diffraction was generated by a Cu-Kα source (which corresponded to λ = 1.5418 Å), and the data were collected for 2θ values from 2 to 90°, where θ represented the angle of incidence of the X-ray beam on the sample.

1.5. Rheological measurements

The deformation, flow and viscous behaviour of the different hydrogels was assessed through rotational tests performed in the rheometer. They were carried out on a stress-controlled DHR-2 rheometer (TA Instruments, New Castle, DE, USA) using a 20 mm diameter serrated parallel plate with a solvent trap filled with water to prevent sample dehydration. All measurements were performed at 25 °C with a gap height of 500 μm.

The deformation behaviour of samples was assessed through amplitude sweeps. They were performed at a frequency of 10 rad/s to determine the deformation

required to damage the hydrogels. Frequency sweeps were used to describe the time-dependent behaviour of the samples within the non-destructive strain range. They were performed from 0.1 to 100 rad/s with a constant oscillatory strain within the linear viscoelastic regime (1%) to determine the time dependent behaviour of the samples. Both, amplitude and frequency sweeps were recorded at 20 points per decade.

Flow sweeps were performed from high (100 s^{-1}) to low (10^{-4} s^{-1}) shear rates with steady-state sensing to characterise the general flow performance.

Stress controlled yield stress measurements were taken from low to high stress with steady-state sensing and 10 points per decade.

Step-shear measurements were performed by alternating a low shear rate (0.1 s^{-1}) and a high shear rate (10 s^{-1}) for 60 seconds for 3 full cycles to describe the shelf-healing behaviour of the samples.

1.6. Swelling and expansion tests

The increase in volume and surface area of the hydrogels after soaking in phosphate-buffered saline (PBS) for 24 hours was characterised by swelling and expansion experiments.

50 μl drops of hydrogel were deposited in glass covers first to perform the swelling test. The initial weights (W_i) of glass covers containing the hydrogels were obtained before their immersion in PBS solution and incubation at 34 °C. After 24 hours, the PBS was removed from samples and the swollen weights (W_s) were measured. The swelling degree of samples was calculated following equation III.1.

$$S(\%) = \frac{W_s - W_i}{W_i} \times 100 \tag{III.1}$$

The expansion of the hydrogels was obtained by measuring the initial (A_i) and swollen areas (A_s) using ImageJ software (developed by Wayne Rasband at the Research Services Branch, National Institute of Mental Health, Bethesda, MD, USA). The expansion degree of samples was calculated following equation III.2.

$$E(\%) = \frac{A_s - A_i}{A_i} \times 100 \tag{III.2}$$

All measurements were performed in triplicate.

1.7. Light transmittance and transparency tests

Transmittance and transparency measurements were used to assess the optical properties of the hydrogels. The light transmission of each biomaterial in the visible spectrum (400-800 nm) was assessed by placing 3 mm diameter discs of each film or 100 μl of each hydrogel in a p96-well plate and determining its absorbance in the ELx800 Microplate Reader (BioTek® Instruments, Winooski, VT, USA). Both dried and hydrated states of the films and crosslinked and non-crosslinked hydrogel forms were examined for light absorption. Wells were filled with 1× PBS (Sigma Aldrich, St. Louis, MO, USA) solution and maintained for 1 h to measure the light absorption of hydrated films. PBS-filled wells were used as a control, while empty wells served as the baseline reference for the absorbance values of dried films. The measured absorbance values were transformed into transmittance percentages using equation III.3.

$$\%T\ (Transmittance) = 10^{(2-Absorbance)} \tag{III.3}$$

Apart from light transmission, the transparency was qualitatively measured by analysing specific photographic patterns positioned 12 cm away from the films and placing 500 μl of each hydrogel over a recognisable word pattern.

1.8. Biodegradability assay

Biodegradation tests were performed to determine weight loss of each film subjected to hydrolytic and enzymatic degradation. Initially weighed (W_0) square fractions of dried samples (6 mm × 6 mm) were immersed in a 200 μg/ml collagenase A solution (Roche, Mannheim, Germany) in PBS for different time points (15 min, 30 min, 1 h, 2 h, 4 h, and 24 h) and incubated at 37 °C. At each time point, samples were removed, freeze dried, and weighed (W_t). The *in vitro* hydrolytic degradation was equally assessed, but samples were incubated in PBS with no enzyme instead. Films soaked in deionized water were used as controls. The percentage of degradation was calculated considering the weight loss over time using the following equation III.4.

$$W(\%) = \frac{W_t}{W_0} \times 100 \tag{III.4}$$

All the measurements were performed in triplicate per time point and sample type.

1.9. *In vitro* release studies

3 different compounds were encapsulated within the hydrogels to measure their *in vitro* release kinetics:

- FITC-labelled immunoglobulin G (IgG): Purified rat IgG antibody (MP Biomedicals, Irvine, CA, USA) with a molecular weight of 150 kDa labelled with fluorescein isothiocyanate isomer I (FITC) (Sigma Aldrich, St. Louis, MO, USA) was used as a high molecular weight encapsulating compound. The antibody was introduced into the hydrogel with a final concentration of 1 mg/ml.
- FITC-labelled Albumin: Albumin protein with a molecular weight of 66 kDa labelled with FITC (Sigma Aldrich, St. Louis, MO, USA) was used as a medium molecular weight encapsulating compound. Albumin was introduced into the hydrogel with a final concentration of 1 mg/ml.
- Vigamox: The moxifloxacin hydrochloride ophthalmic solution Vigamox (Novartis, Barcelona, Spain) used to treat bacterial infections of the eye with a molecular weight of 0.44 kDa was used as a low molecular weight encapsulating compound. Vigamox was introduced into the hydrogel with a final concentration of 1 mg/ml.

The compounds' release from the hydrogels was analysed with fluorescence and absorbance measurements. To prepare each sample, 100 μl of the corresponding hydrogel was injected into the base of a glass capillary tube that was previously sealed at one end with epoxy. 400 μl of PBS was then added to the top of each hydrogel, and the tubes were incubated in the dark at 34 °C. The temperature of 34 °C was used because of being the average temperature of the eye surface. The supernatants were collected at established time points, and the same amount of solution was replaced with fresh PBS. The samples collected were inserted into a 96-well plate and analysed in a Synergy H1 Hybrid Multi-Mode Plate Reader (BioTek Instruments, Winooski, VT, USA).

The quantity of Vigamox released was determined by measuring the absorption at 290 nm. Moxifloxacin exhibits a peak absorbance in the UV spectrum at 290 nm due to the aromatic ring in its chemical structure. This property was utilised to determine

the released concentrations. The absorbance peaks were not observed in the structures of the IgG and albumin used, that is why it was decided to conjugate them with a well-characterised fluorochrome. This conjugation would enable the calculation of the concentrations released by means of a standard curve. The volume of FITC-IgG and FITC-Albumin released was computed by fluorescence measurements conducted with 485-520 excitation and emission wavelengths. The experiments were performed in quadruplicates. For each cargo, the cumulative release was calculated at each measurement time over the 2 week duration of the experiment and expressed as a percentage of the initial cargo released (considered as 100%).

1.9.1. FITC Labelling

FITC was manually conjugated to the purified rat IgG antibody. Purified rat IgG antibody as a lyophilized powder and FITC were dissolved in 12 ml of 0.1 M Na_2CO_3 buffer, pH 10. The quantity of FITC required to graft the desired amount of protein was calculated using the molar ratio between both compounds (Equation III.5).

$$Amount\ of\ FITC = \frac{MW_{FITC}}{MW_{IgG}} \times 100 \tag{III.5}$$

The solution was thoroughly mixed and the reaction was run in the dark overnight at 4 °C. After the incubation period, the solution was spun down to remove the excess of FITC using a Vivaspin® Turbo 15 PES filter (Sartorius, Göttingen, Germany). The solution was centrifuged at 3000g for 30 minutes for 6 cycles until no more FITC was seen in the filtrate solution.

1.10. Hydrogel functionalisation

1.10.1. Procurement of human amniotic membrane (HAM)

The placentas were obtained immediately after elective caesareans of healthy fetuses. Informed consent for donation and use of HAMs was obtained in advance. Donors were previously screened for human immunodeficiency virus (HIV) types 1 and 2, hepatitis B and C, and syphilis.

Placentas were collected in sterile stainless steel containers after childbirth. In the operating theatre, blood clots were removed with abundant saline washes. Once cleaned, the amnion, the innermost membrane of the placenta that surrounds the entire amniotic cavity during pregnancy, was carefully peeled away from the chorion up to the edge of the placenta. After separating the two membranes, sterilised nitrocellulose filter pieces (Merck KGaA, Darmstadt, Germany) were attached to the HAM to facilitate its division into 3 sections: distal amnion (10 cm wide section), medial amnion (10 cm wide section) and proximal amnion (up to the edge of the placenta) (Figure III.3).

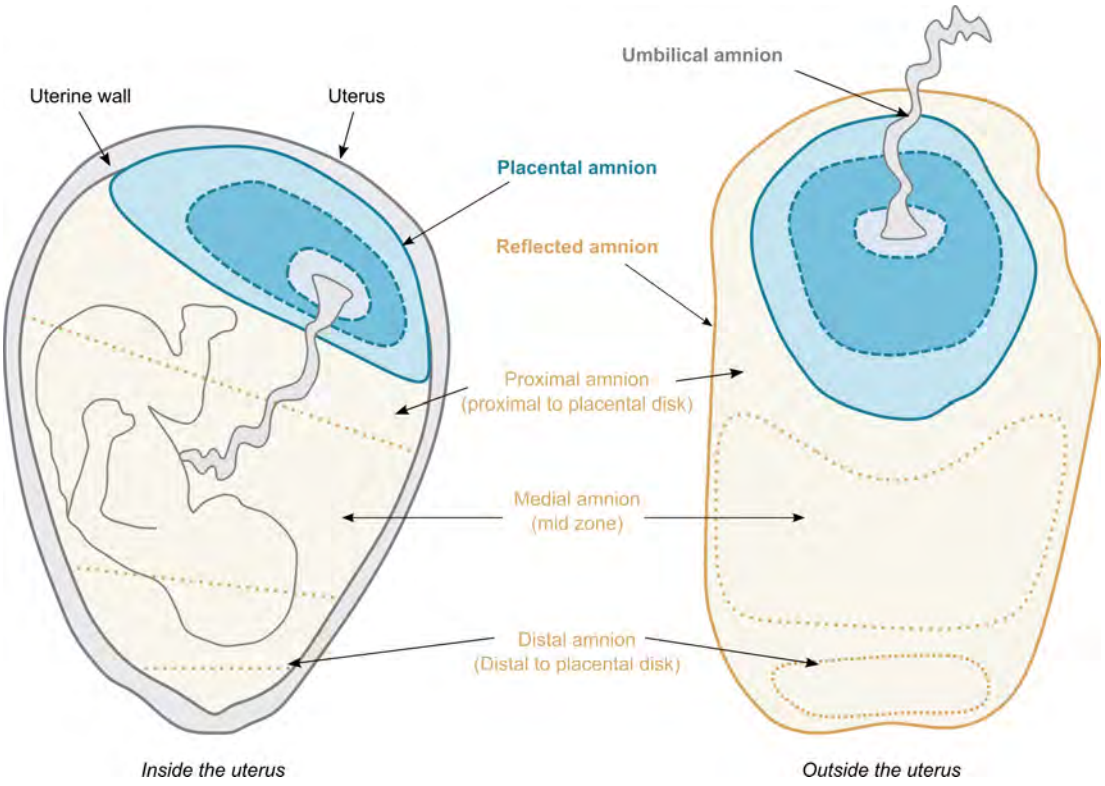

III.3. FIGURE: Schematic representation of the subregions of the human amniotic membrane (HAM) inside and outside the uterus. The placental amnion (blue, covering the placenta), the reflected amnion (orange, lining the uterine wall), and the umbilical amnion (gray, covering the umbilical cord). The reflected amnion can be divided into proximal amnion, the area that is closest to the placental disk, the medial amnion, and the distal amnion, the area farthest from the placental disk. Figure created based on [332].

The fragments were placed in bottles of sterile Dulbecco's Modified Eagle Medium (DMEM) solution (Lonza Bioscience, Basel, Switzerland) supplemented with 1.25 μg/ml amphotericin B (Gibco, Paisley, UK), 50 μg/ml penicillin-streptomycin (Sigma Aldrich, St. Louis, MO, USA) and 50 μg/ml neomycin (Gibco, Paisley, UK) for transport. The bottles were properly labelled with information about the HAM's region. The membranes were immediately taken to the laboratory.

In the laboratory and in a laminar flow hood, the distal, medial and proximal regions of each HAM were cut into pieces of 4-4.5 × 4-4.5 cm. The pieces were washed free of blood clots and blood residues were removed by brushing with clamps. They were washed 2 times for 5 minutes with DMEM solution containing antibiotics and another 2 washes for 5 minutes in DMEM medium without supplements. The fragments selected for eye drop preparation were washed with sterile PBS and frozen at -80 °C in 5 ml Eppendorf tubes until their use.

1.10.2. Human amniotic membrane extract (HAMe) preparation

Eppendorf tubes containing HAM fragments stored at -80 °C were immersed in liquid nitrogen for 5 minutes to harden the samples. Each sample was then crushed in a mortar pre-cooled at -80 °C until a soft powder was obtained. Each powdered sample was weighed, transferred to a 5 ml Eppendorf tube and resuspended in 3 ml PBS containing 5 ml/g protease inhibitor cocktail (P8340, Sigma Aldrich, St. Louis, MO, USA).

Sample tubes were placed on ice and sonicated for 20 minutes at 90% amplitude with 15 seconds and 15 seconds of recovery. The samples were then centrifuged at 3000g for 10 minutes at 4 °C and the supernatants were collected. Finally, the supernatants were filtered through 0.22 μm PES hydrophilic membrane MILLEX® filters, aliquoted into 0.2 ml tubes and stored at -80 °C until use.

1.10.3. Extraction of blood derivatives

Blood-derived compounds were chosen for hydrogel functionalisation. Human donor blood derivatives were used for *in vitro* assays, while rabbit samples were used for *in vivo* experiments.

1.10.3.1. Human

The blood-derived products incorporated into the hydrogels used in the *in vitro* assays were obtained from the blood of healthy, unmedicated 25-60 year-old donors.

Blood was collected by venipuncture after signing the informed consent following the Declaration of Helsinki and with a favourable report from the Ethics Committee for Research Involving Human Subjects of the University of the Basque Country UPV/EHU. The total volume of blood from each volunteer was divided into two equal parts to be processed by different methods to obtain two blood derivatives:

- Autologous serum (AS): Blood was collected in 5 ml Vacutainer® tubes containing a separating gel (BD, Franklin Lakes, NJ, USA), the tubes were allowed to clot for 2 hours at room temperature, centrifuged at 1000g for 15 minutes, and the entire supernatant fraction was collected, which constituted the AS.
- Serum derived from plasma rich in growth factors (sPRGF): Blood was collected in 5 ml Vacutainer® tubes containing 3.8% sodium citrate as anticoagulant (BD, Franklin Lakes, NJ, USA), the tubes were centrifuged at 460g for 8 minutes at room temperature and the complete supernatant fraction above the buffy coat was collected. 50 μl/ml calcium chloride (B. Braun, Melsungen, Germany) to a final concentration of 22.8 mM was added to neutralise the sodium citrate and activate platelet α-granule secretion and the coagulation cascade. The tubes were incubated at 36 °C for 2 hours to promote platelet activation and release of growth factors into the supernatant. Finally, the whole supernatant was collected after clot retraction, which constitutes the sPRGF.

Both AS and sPRGF were filtered using a 0.22 μm PES hydrophilic membrane MILLEX® filter, aliquoted and stored at -80 °C until their use.

1.10.3.2. Rabbit

New Zealand White rabbits weighing approximately 2 kg were used to obtain blood derivatives for *in vivo* assays. All experiments were performed in the general animal facility of the University of the Basque Country UPV/EHU (Sgiker) in accordance with experimental procedures approved by the Animal Research Ethics Committee of the University of the Basque Country UPV/EHU.

The methods for processing rabbit blood were developed based on our experience with human blood and the assays published in the literature.

After locally anaesthetising the rabbit with lidocaine, the blood was collected by central ear artery venipuncture into Vacutainer® tubes containing a poylmer gel for serum separation (BD, Franklin Lakes, NJ, USA).

After blood collection, it was allowed to clot for 2 hours at room temperature and centrifuged at 1000g for 15 minutes. The collected supernatant, which constituted the AS, was filtered through 0.22 μm PES hydrophilic membrane MILLEX® filter and stored at -80 °C until their use.

AS was the only blood product obtained from rabbits.

1.10.4. Quantification of growth factors

The different growth factors present in the AS, sPRGF and HAMe samples were quantified by enzyme-linked immunosorbent (ELISA) or Luminex assays.

ELISA is a highly sensitive biochemical assay used to detect and quantify specific analytes in a sample, including antibodies, antigens, proteins or biomolecular complexes.

ELISA assays rely on specific antigen-antibody interactions to produce a measurable result. The antigen is immobilized on a solid surface directly or indirectly by a specific capture antibody. A primary detection antibody is then added to form an antigen-antibody complex. After the detection antibody incubation, any unbounded sites are blocked using animal proteins such as bovine serum albumin (BSA) to prevent the binding of non-specific antibodies to the plate. The detection antibody is then labelled with a detection-susceptible molecule such as an enzyme or fluorophore (direct ELISA) or bound to a labelled secondary antibody (indirect ELISA). All the unbounded material is removed by washing with buffer solution between each step. Finally, the signal is detected by the addition of a substrate that generates colour in the presence of antigen and its measurement is directly proportional to the amount of antigen in the sample [333].

The detection of the growth factors of interest was performed with sandwich type ELISA assays, where the antigen of interest is sandwiched between a capture antibody previously coated on the wells of the plate and the detection primary antibody. After the incubation of the detection antibody, the secondary enzyme-conjugated antibody

is added. Table III.1 gathers the specific kits used for each molecule. The assays were performed following the manufacturer's protocol.

III.1. TABLE: List of the ELISA assays used for the quantification of growth factors.

Growth factor	Reference	Manufacturer
Glial derived neurotrophic factor (GDNF)	Ab100525	Abcam
Brain derived neurotrophic factor (BDNF)	E-EL-H0010	Elabscience
Pigment epithelium-derived factor (PEDF)	EH1048	FineTest (FineBiotech)
Substance P (SP)	EH4245	FineTest (FineBiotech)
Insulin-like growth factor 1 (IGF-1)	ELH-IGF1	RayBiotech
Nerve growth factor (NGF)	HEA105Hu	Cloud-Clone
Interleukin 1β (IL-1β)	HSLB00D	R&D Systems
Keratinocyte growth factor (KGF)	SBRS0581	Assay Genie

Luminex technology was also used to quantify some of the growth factors of the human AS, sPRGF and HAMe samples. This system is based on the same principle as sandwich ELISAs, but Luminex assays use distinctly coloured fluorescence-labelled beads to capture the targets, allowing the detection of multiple cytokines simultaneously (graphical description of both methods is shown on figure III.4).

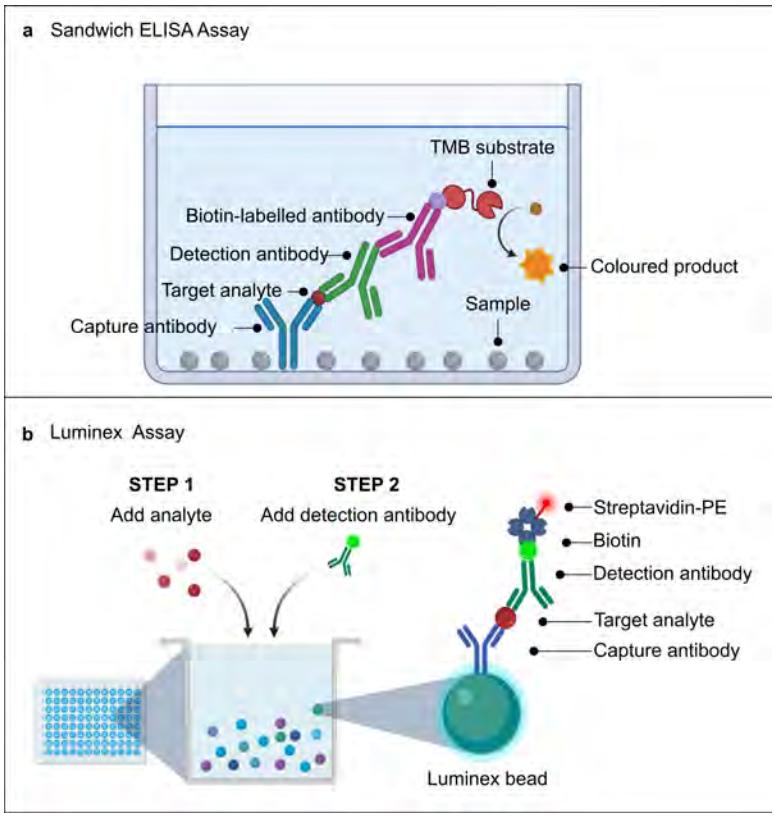

III.4. FIGURE: Schematic representation of **a**), sandwich ELISA and **b**), Luminex assay working principles.

Completed assays are read on a Luminex instrument where one laser classifies the type of bead to determine the analyte being detected, while a second laser determines the amount of analyte bound.

Human Angiogenesis/Growth Factor Panel 1 kit (HAGP1MAG-12K kit produced by Merck KGaA, Darmstadt, Germany) was used to quantify epidermal growth factor (EGF), fibroblast growth factor 2 (FGF2) and hepatocyte growth factor (HGF) according to the manufacturer's protocol.

Samples were loaded into a 96-well plate provided with the kit. An equal volume of a Luminex bead premix for the biomarkers of interest was added to each well and incubated overnight at 4 °C. The beads were then washed 3 times with 200 μl wash buffer and incubated with 25 μl of biotinylated secondary detection antibody for 1 hour at room temperature according to the manufacturer's protocol. The beads were then mixed with 25 μl of streptavidin-phycoerythrin (PE) conjugate, washed 3 times with 200 μl wash buffer and resuspended in 100 μl of sheath fluid. Finally, they were analysed using a Luminex-200™ instrument (Merck KGaA, Darmstadt, Germany) with xPONENT® software (Merck KGaA, Darmstadt, Germany).

1.10.5. Synthesis of functionalised hydrogels

Following the selection of the gelatine and RFP hydrogel, it was functionalized with 4 different compounds that could serve as candidates to aid in corneal wound healing. Infliximab (Merck KGaA, Darmstadt, Germany) is a human/murine chimeric monoclonal antibody of 150 kDa against tumour necrosis factor α (TNFα) and it was selected as an agent to combat inflammation. The two blood derived products, AS and sPRGF, as well as HAMe were also incorporated within the hydrogel as promoters of wound healing.

Functionalised hydrogels were prepared from 10% w/v gelatine and 0.02% w/v RFP stock solutions. Infliximab-loaded hydrogels were prepared by mixing 2 mg/ml Infliximab to a 10% w/v gelatine and 0.02% w/v RFP stock solution and adjusting them to a final concentration of 1 mg/ml Infliximab, 5% w/v gelatine and 0.01% w/v RFP with distilled water.

Hydrogels containing AS, sPRGF or HAMe were prepared by mixing a concentrated stock of 10% w/v gelatine and 0.02% w/v RFP solution and the AS/sPRGF/HAMe extracts at 1:1 dilution. Like so, the solutions were enriched with 50% of each blood derivative/HAMe and the final concentration of 5% w/v gelatine and 0.01% w/v RFP was maintained.

The pH of all the hydrogels was adjusted to 7 with 1M NaOH, warm solutions were filtered using 0.22 μm PES hydrophilic membrane MILLEX® filter and stored at 4 °C until their use.

2. Cell culture

Cell culture refers to the list of laboratory techniques that allow the maintenance and proliferation of eukaryotic or prokaryotic cells in a favourable physiological environment away from their original tissue source. Experimental applications of cell culture have served to provide *in vitro* model systems for the study of basic cell biology, toxicity testing of new drugs, gene therapy, disease mechanisms or the production of vaccines, antibodies and therapeutics.

Three cell culture models can be distinguished: primary cells, transformed cells or self-renewing cells. Primary cells are obtained directly from tissues by mechanical, chemical or enzymatic digestion; they are more representative of the cell types of the tissue of origin, but their lifespan is limited. Established cell lines are cells that have been transformed using genetic engineering tools to maintain their phenotype and allow continuous cell studies. Finally, self-renewing cells refer to a variety of stem cells that can differentiate into other cell types and survive long-term *in vitro*.

All of them require sterile conditions, an optimal incubation microenvironment and a regular supply of essential nutrients. Despite the need for specific culture conditions, cells are typically grown at 37 °C and 5% CO_2 in a cell incubator, and a different culture medium is used depending on the nutritional requirements of each cell type or the purpose of the study. This chemical formulation contains carbohydrates, vitamins, amino acids, minerals, growth factors and hormones in a special buffer formulation that maintains the pH level of the culture.

2.1. Established cell line culture

SV-40 immortalised human corneal epithelial (HCE) cells and NIH-3T3 fibroblasts commercial cell lines were used in this study for cytocompatibility evaluation (Figure III.5). Table III.2 summarises the specific culture media and culture conditions used to harvest each cell line.

III.2. TABLE: Detailed description of the used cell lines, culture medium and culture conditions.

Line	Culture medium	CO_2%	Tissue of origin	Company
HCE	DMEM:F12 1:1 (Lonza) + 10 % FBS (Gibco) + 2.5 mM glutamine (Sigma) + 50 U/ml penicilin/streptomycin (Sigma) + 0.5 % DMSO (Sigma) + 5 μg/ml insuline (Sigma) + 10 ng/ml EGF (Sigma) + 0.1 μg/ml choleric toxin (Sigma)	5 %	Cell line from human corneal epithelium	Kindly provided by Dr. K. Araki-Sasaki
NIH-3T3	DMEM:F12 1:1 + 10% FBS + 2.5 mM glutamine + 50 U/ml penicilin/streptomycin	5 %	Cell line from mouse embryonic fibroblast	Kindly provided by Dr. J. Sutherland

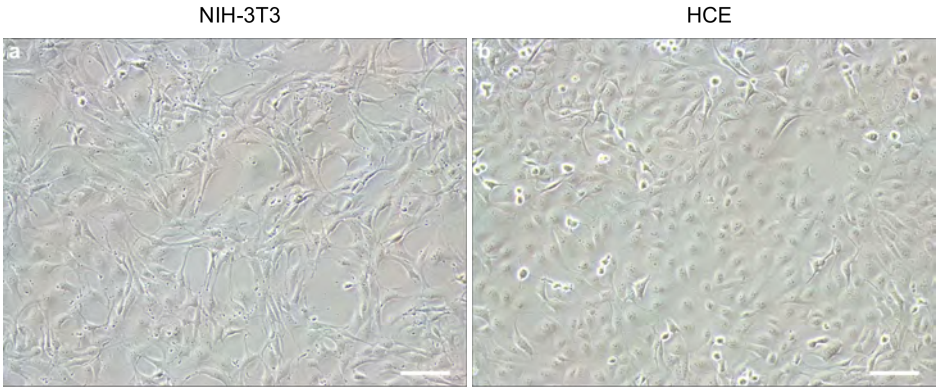

III.5. FIGURE: **a**) NIH-3T3 fibroblast cell line and **b**) HCE cell line. Images taken with 10× magnification lens. Scale bars correspond to 100 μm.

2.1.1. Thawing cryopreserved cells

Cell culture was initiated by thawing cryopreserved cells stored in liquid nitrogen. The vial containing the cells was warmed in a 37 °C water bath with constant stirring until the medium was thawed. The cell suspension was transferred to a sterile centrifuge tube containing 4 ml of warm culture medium and centrifuged at 300g for 5 minutes at room temperature. The supernatant was discarded and the cell pellet was resuspended in 1 ml of culture medium and seeded into a culture plate/flask containing the appropriate amount of medium.

2.1.2. Cell subculture

Cells were subcultured when grown to 80% of confluence. The culture medium was removed and the culture was washed with PBS to remove cell debris, detached dead cells and any residual media. The cells were then dissociated with an enzymatic solution of trypsin-EDTA (0.5% trypsin - 0.2% ethylenediaminetetraacetic acid) (Sigma Aldrich, St. Louis, MO, USA) for 5 minutes at 37 °C. After checking that the cells were rounded and detached from the culture dish, fetal bovine serum (FBS) (Lonza Bioscience, Basel, Switzerland) was added to inhibit trypsin's activity by substrate saturation. The cell suspension was centrifuged at 300g for 5 minutes. After discarding the supernatant, the cell pellet was first resuspended in 1 ml of fresh culture medium and then diluted in the appropriate volume according to the dish size and number of dishes to be seeded. The number of cells seeded was adjusted for each cell type and culture flask to achieve a subconfluent monolayer every 2-3 days.

2.1.3. Freezing cells

When needed, cells were frozen after trypsinisation and centrifugation at 300g for 5 minutes as described above. After removing the supernatant, suspending the cells in 1 ml of fresh culture medium and determining the total number of cells obtained from the passage, the desired amount of cells was diluted in 1 ml of a cryoprotectant solution consisting of 90% FBS and 10% dimethyl sulfoxide (DMSO, Sigma Aldrich, St. Louis, MO, USA). Each vial was labelled with the cell passage number, amount of cells and data details for proper registration in the laboratory cell bank records. Vials were progressively frozen (-1 °C/minute) in the Mr Frosty freezing container (Thermo Fisher Scientific, Waltham, MA, USA) stored at -80 °C for 24 hours. After 24 hours at -80 °C, the cell vials were transferred to an N_2 storage bank.

2.1.4. Cell counting

The number of cells in the culture before each reseeding or freezing step was determined by adding an aliquot of the cell suspension mixed with 1:1 trypan blue dye (Sigma Aldrich, St. Louis, MO, USA) to a haemocytometer or Neubauer chamber.

The cell count of the sample loaded into the Neubauer chamber was performed under an inverted optical microscope (Nikon, Tokyo, Japan) at 100× magnification. The number of cells per millilitre was calculated using the equation III.6, where M is the average number of cells counted per square of the haemocytometer and the volume correction factor was obtained by converting the volume of each square from 10^{-4} ml to 1 ml.

$$Cells/ml = M \times dilution\ factor \times 10^4 \tag{III.6}$$

Finally, the number of cells to be seeded was adjusted to the area of the dishes/plate wells used.

3. Cell isolation from human corneas

Cadaveric corneal tissues were provided by four tissue banks, including BSTN (Banco de Sangre y Tejidos de Navarra, Pamplona, Navarra, Spain), BST (Banc de Sang I Teixits, Barcelona, Catalonia, Spain), Biobanco Vasco (Vitoria-Gasteiz, Basque Country, Spain), and Biobanco A Coruña (A Coruña, Galicia, Spain) under Material Transfer Agreements (MTA).

3.1. Dissection of donor corneoscleral tissues and sclerocorneal rims

Donor corneas were received in refrigerated corneal chambers immersed in Eusol-C storage medium (Alchimia, Ponte San Nicoló, Italy). Immediately on arrival, the donor tissues were immersed in a Hank's solution containing 20 mM HEPES (Gibco, Paisley, UK), 500 U/ml penicillin-streptomycin, and 1.25 μg/ml amphotericin to wash out any remaining traces of storage medium. Once cleaned, the tissues were dissected under the Stemi 305 stereo dissection microscope (Zeiss, Oberkochen, Germany) to remove the iris, endothelium, Tenon's capsule and conjunctiva. The tissue was carefully scraped using surgical forceps and sponges.

Once the tissue was completely cleaned and prepared, the fragments of each cornea intended for tissue sectioning were cut and placed in optimal cutting temperature (OCT) compound (Sakura-Finetek, Alphen aan den Rijn, The Netherlands) blocks. The blocks were stored at -80 °C.

The central part of the cornea was separated from the peripheral corneal ring with an 8.5 mm punch. The conjunctiva was then removed by gently pulling on the tissue and cutting the base where the conjunctiva was separated from the cornea. Both the corneal ring and the central cornea were cut in half to facilitate the enzyme action during subsequent tissue digestion.

3.2. Tissue digestion and cell isolation

Cell culture samples were enzymatically digested. Dispase II (Roche, Mannheim, Germany) at a concentration of 2.4 U/ml in DMEM:F12 (Lonza Bioscience, Basel, Switzerland) medium supplemented with 5% FBS was used for 2 hours at 37 °C to separate the epithelium from the stroma.

Cell clusters from the limbal epithelium and supernatants containing suspended isolated cells were collected, centrifuged at 200g for 10 minutes and suspended in SHEM5 medium containing DMEM F12, 5% FBS, 1% penicillin-streptomycin, 1% N_2 supplement (Thermo Fisher Scientific, Waltham, MA, USA), 0.5 μg/ml hydrocortisone (Sigma Aldrich, St Louis, MO, USA), 0.5% DMSO, 8.4 ng/ml cholera toxin (Gentaur Molecular Products, Brussels, Belgium) and 2 ng/ml EGF (Sigma Aldrich, St Louis, MO, USA).

The remaining stromal tissues after digestion with dispase were placed in a mixture of 4 mg/ml collagenase A and 0.01% hyaluronidase (Sigma Aldrich, St Louis, MO, USA) at 37 °C overnight for stromal cell extraction. The next day, the digested tissue was scraped with a surgical spatula to release all possible stromal cells. The released cells, together with the supernatants obtained from this digestion, were centrifuged at 200g for 10 minutes and suspended in stromal cell medium (DMEM:F12, 10% FBS, 2.5 mM glutamine and 50 U/ml penicillin-streptomycin).

4. *In vitro* citocompatibility and biocompatibility assays

4.1. MTT assay

3-(4,5-dimethylthiazol-2-yl)-2-5-diphenyltetrazolium bromide (MTT) assays were used to indirectly measure the cytotoxicity of biomaterials in the form of sheets or hydrogels.

MTT is a colourimetric assay based on the measurement of metabolic activity. Living cells with active metabolism reduce the MTT compound to formazan, an insoluble purple product that accumulates inside cells or remains on the cell surface of cultures. When cells are dead or not metabolically active, they lose this MTT-formazan conversion ability [334]. The amount of formazan is proportional to the degree of metabolic activity of the culture in which the measurement is performed, which in turn may be related to the number of living cells. Formazan is solubilised with an organic solvent and the number of crystals formed can be determined by measuring changes in absorbance. The greater the number of formazan crystals, the higher the optical density and therefore the metabolic activity recorded [335].

Cells were seeded in flat bottom 96-well culture plates to perform MTT assays. Once ensured initial cell attachment (approximately 12 hours from their seeding), cells were starved for 16 hours with a solution of DMEM:F12 and 1% of BSA (Sigma Aldrich, St Louis, MO, USA) to synchronize cell cycles. Subsequently, the starving medium was replaced by the corresponding culture or treatment medium according to each assay. Time 0 hours was set at this step. Cells were seeded in triplicate and positive and negative controls and treatment blanks were included. Treatment wells were prepared by culturing cells with biofilm or hydrogel fractions in the corresponding cell culture media so as to directly expose cells to the biomaterial tested. After completing the starvation step and adding the appropriate culture media to each cell type, the biofilms or hydrogel fragments were introduced into the wells. The hydrogel portions were photocrosslinked for 2 minutes before adding them to the wells.

The metabolic activity of the cells was assessed at 0, 24, 48 and 72 hours. After the corresponding incubation period, the cultures were washed with $1\times$ PBS and 100 μl of 0.5 mg/ml MTT reagent (Sigma Aldrich, St Louis, MO, USA) dissolved in DMEM:F12 medium was added per well for 3 hours at 37 °C and 5% CO_2. The MTT containing medium was carefully removed and 100 μl of DMSO was added per well to dissolve the formazan crystals. Optical densities were determined at 570 nm using the ELx800 Microplate Reader and absorbance values in treatment and control wells were compared.

4.2. Live/Dead citotoxicity assay

Cell viability was assessed using the calcein AM-ethidium homodimer-1 (EthD1) staining assay. This assay is based on the uptake and conversion of the aceto-methoxyl (AM) calcein dye, which fluoresces in living cells with esterase activity, and the retention of the EthD1, which penetrates cells with damaged membranes and enhances its bright red fluorescence by binding to nucleic acids in dead cells [336].

The number of live/dead cells was determined at 24, 48 and 72 hours from cells seeded on the tested films or hydrogels using the calcein AM-EthD1 live/dead® viability/cytotoxicity assay (Thermo Fisher Scientific, Waltham, MA, USA). 2μM calcein-AM and 4μM EthD-1 were diluted in 1$\times$ PBS to prepare the assay solution. The culture medium was aspirated and a 1$\times$ PBS wash was performed before the cells were incubated with the dye solution for 40 minutes at room temperature in a dark environment. After incubation, the cells were imaged using a fluorescence microscope (Olympus, Tokyo, Japan) and automatically counted using ImageJ software. The assay was performed in triplicate. Biofilms or hydrogels without cells were included as blank.

4.3. Cell cycle analysis

Cell cycle analysis was used to quantify the DNA content and detect possible cell cycle changes in the cells incubated with the different hydrogel versions. Using the fluorescent nucleic acid dye propidium iodide (PI) and its ability to bind stoichimetrically to cellular DNA, the proportion of cells in each of the three interphase stages of the cell cycle (G0/G1 (2n), S (2n$\sim$4n) and G2/M (4n) phases, respectively) in each treatment group was determined.

Cells were trypsinised as previously described, centrifuged at 300g for 5 minutes and resuspended in 1ml PBS. This process was repeated twice to wash out the remaining medium. Cold 70% ethanol solution was added dropwise while vortexing the cell tube to ensure cell fixation and avoid cell clumping. The cells were incubated for 1 hour at 4 °C. After fixation, the cells were centrifuged and washed twice with PBS. The first centrifugation was performed at 1000g for 10 minutes and the second centrifugation was performed at 500g for 5 minutes. The cell pellet was treated with 250 μl of 100 μg/ml RNase (Thermo Fisher Scientific, Waltham, MA, USA) for 15 minutes at 37 °C to ensure removal of RNA and staining of DNA only. Finally, 10

μg/ml propidium iodide (PI) (Thermo Fisher Scientific, Waltham, MA, USA) was added to the cell solution and incubated for further 15 minutes at 37 °C, protected from light. The PI signal was excited with a 488 nm laser and detected through the phycoerythrin (PE)/Texas Red channel with a 610/10 nm bandpass filter. Analysis was performed using a Gallios flow cytometer (Beckman Coulter, Brea, CA, USA) and data were analysed using Kaluza 1.1 software (Beckman Coulter, Brea, CA, USA).

4.4. Migration assay

Migration of HCE and 3T3 cells over the biofilms was examined using two-well culture inserts (Ibidi, Gräfelfing, Germany) placed over the films. The silicone inserts consisted of two cell culture reservoirs separated by a defined cell-free gap. 20000 cells were seeded into each reservoir and left overnight to attach and form a monolayer over the films. The defined cell-free gap left by removal of the insert was recorded as the maximum area between the two cell fronts at time 0 hours. Cell migration was then quantified by using phase contrast microscopic images taken at 24, 48 and 72 hours. Distances were calculated processing the images in ImageJ software.

5. *In vitro* inflammation model

The initial tests to determine whether functionalised hydrogels could reduce inflammation were conducted using *in vitro* HCE cell cultures. To achieve so, an *in vitro* inflammation model was first established. After selecting the most effective method to inflame the cells, the complete assay was performed with different hydrogel treatments.

5.1. Establishment of the *in vitro* inflammation model

The model was established culturing HCE cells with TNFα (Abcam, Cambridge, UK) and lipopolysaccharide (LPS) (Sigma Aldrich, St. Louis, MO, USA). 400000 HCE cells were seeded per well of 6-well plates. 6 wells were incubated with 10 μg/ml LPS, three of them with HCE medium and the other 3 with DMEM:F12 medium. 6 wells were incubated with 100 ng/ml TNFα, three of them with HCE medium and the other 3 with DMEM:F12 medium. 3 wells cultured with HCE medium and 3 wells cultured with DMEM:F12 medium were used as controls. All the treatments were maintained in culture for 24 hours. The assay was performed in triplicate.

5.2. *In vitro* inflammation assay

HCE cells were inflamed with TNFα and then treated with the different versions of the functionalised hydrogels to test their ability to reverse inflammation.

65000 HCE cells were seeded per well of 6-well plates and exposed to 100 ng/ml TNFα for 72 hours to induce inflammation. Control wells were cultured with FBS-reduced HCE medium containing DMEM:F12 1:1, 2.5 mM glutamine (Sigma Aldrich, St. Louis, MO, USA), 50 U/ml penicilin/streptomycin, 0.5% DMSO, 0.5% FBS, 5 μg/ml insulin (Sigma Aldrich, St. Louis, MO, USA), 10 ng/ml EGF and 0.1 μg/ml choleric toxin.

After the incubation period, the inflammatory stimuli were removed and the cells were cultured with FBS-reduced HCE medium and 400 μl of the different versions of the functionalised hydrogels for 72 hours. Table III.3 summarises the hydrogels tested.

III.3. TABLE: Composition of the hydrogels tested in the *in vitro* inflammation assay.

Study group	Treatment
H	Hydrogel composed of 5% w/v gelatine and 0.01% w/v RFP.
H-Ab	Hydrogel composed of 5% w/v gelatine and 0.01% w/v RFP with 1 mg/ml Infliximab.
H-AS	Hydrogel composed of 10% w/v gelatine and 0.02% w/v RFP with human serum at a 1:1 dilution.
H-sPRGF	Hydrogel composed of 10% w/v gelatine and 0.02% w/v RFP with human serum rich in growth factors at a 1:1 dilution.
H-HAMe P	Hydrogel composed of 10% w/v gelatine and 0.02% w/v RFP with amniotic membrane extract from the amnion's proximal region at a dilution of 1:1.
H-HAMe M	Hydrogel composed of 10% w/v gelatine and 0.02% w/v RFP with amniotic membrane extract from the amnion's medial region at a dilution of 1:1.
H-HAMe D	Hydrogel composed of 10% w/v gelatine and 0.02% w/v RFP with amniotic membrane extract from the amnion's distal region at a dilution of 1:1.
H-HAMe Pool	Hydrogel composed of 10% w/v gelatine and 0.02% w/v RFP with amniotic membrane extract from a pool of the 3 regions of the amnion at a 1:1 dilution.

Cells exposed to TNFα for 6 days without any hydrogel treatment served as the inflammation positive control, whereas the wells cultured with FBS-reduced HCE medium for 6 days served as the negative control.

In addition, cells cultured with FBS-reduced HCE medium for the first 72 hours were exposed to H, H-Ab, H-sPRGF and H-HAMe pool for the following 72 hours to see if the hydrogels *per se* produced inflammation. Thus, a total of 14 conditions (8 different treatments stimulated with TNFα, 4 treatments without TNFα stimulus, 1 positive control and 1 negative control) were tested (Figure III.6).

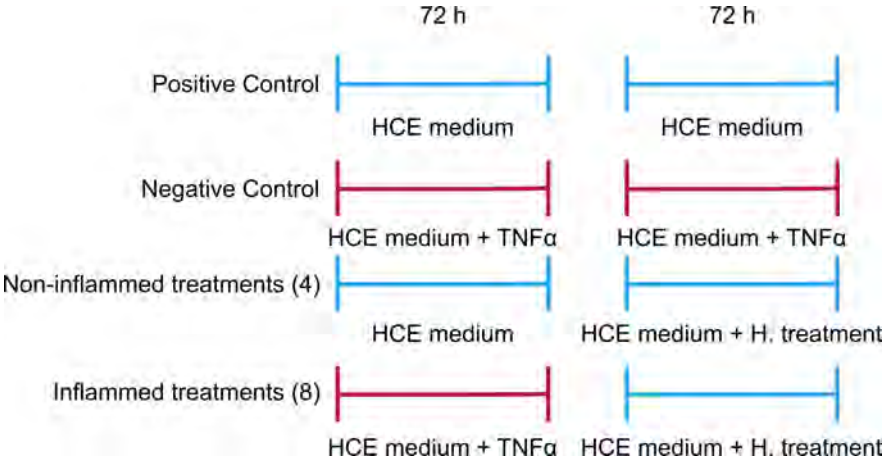

III.6. FIGURE: Scheme of treatments used in the *in vitro* inflammation assay.

6. *Ex vivo* eye model

Fresh bovine and rabbit eyes were obtained from local abattoirs and used as *ex vivo* models. These were used as a previous step to *in vivo* testing to optimise the *in situ* hydrogel application method and to assess the biocompatibility and efficacy of the hydrogel treatment.

6.1. *Ex vivo* surgical procedure

Fresh bovine and rabbit eyes obtained from local abattoirs were transported in DMEM:F12 solution supplemented with 1.25 μg/ml amphotericin B, 50 μg/ml penicillin-streptomycin and 50 μg/ml neomycin.

In the laboratory and in a laminar flow hood, the eyes were disinfected with 10% povidone-iodine solution, washed with PBS and the excess fat was removed with a surgical blade and small scissors (**a** and **b** of the figures III.7 and III.8). The eyes were wrapped circumferentially with clean gauze, they were held tightly in place and the centre of the cornea was wounded with a 8 mm trephine (**c** of the figures III.7 and III.8). The trephine deepened the wound to the mid of the stroma (approximately 150-200 μm). The epithelium and part of the anterior stromal flap were then lifted with a crescent blade (**d** of the figures III.7 and III.8) and the wounded corneas were removed from the globes (**e** of the figure III.7 and **f**) of the figure III.8). Approximately 1 mm of scleral rim was included in the organ culture model to keep the limbus intact.

Excised bovine corneas were transferred to preformed agar plugs. The agar plugs were fabricated in bioprinted polydimethylsiloxane (PDMS) moulds made to the anatomical dimensions of bovine corneas. Rabbit corneas were placed over p96 culture plates, epithelial side down, and filled with warm agar mixture and allowed to harden. In both cases, the agar mixture consisted of a 1:1 mixture of serum-free DMEM:F12 medium with 1% penicillin/streptomycin and 2% agar in distilled water.

The corneas were placed in culture dishes (60 mm dishes for bovine corneas and 30 mm dishes for rabbit corneas), the wounded areas were filled the hydrogels and crosslinked with blue light (**f** of the figure III.7). The samples were then incubated with SHEM5 culture medium at 37 °C in 5% CO_2. The corneal surfaces were moistened daily with culture medium, which was changed every 2 days.

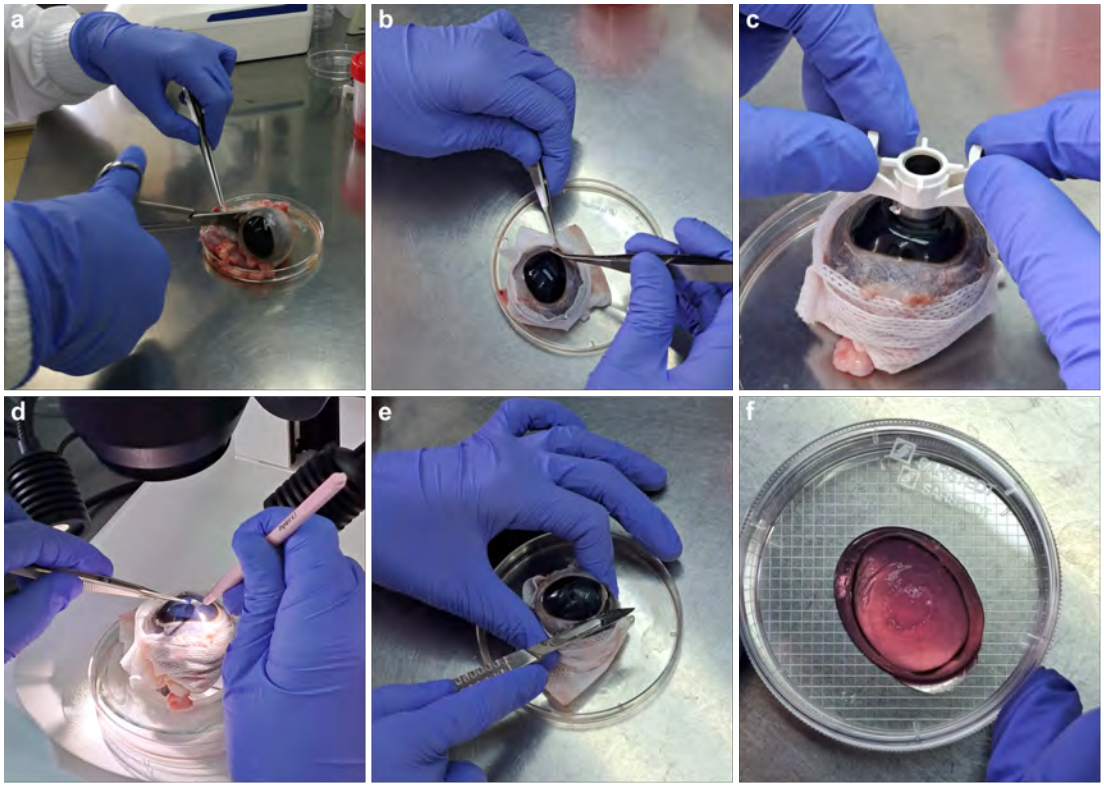

III.7. FIGURE: Extraction and processing procedure for the *ex vivo* bovine corneal model.

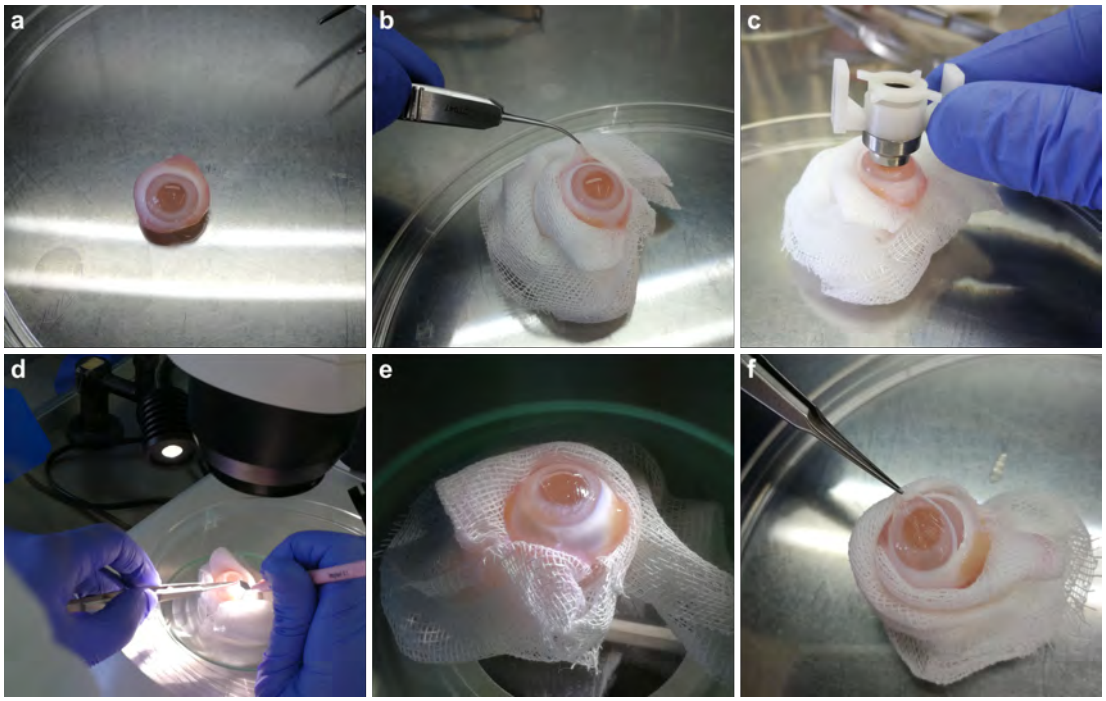

III.8. FIGURE: Extraction and processing procedure for the *ex vivo* rabbit corneal model.

7. Adhesion study

The adhesion properties of the gelatine and RFP hydrogel were determined using the TA.XT.Plus C texture analyser (Aname Instrumentación Científica, Madrid, Spain), equipped with a 5 kg load cell and a 3.5 mm diameter cylindrical probe, using bovine corneas as biological substrates. This characterisation method quantitatively determined the interaction between the hydrogel and the corneal surface and provided the work required to separate the hydrogel from the bovine cornea.

The corneal wounds were reproduced following the same procedure described in 6.1. Using a negative mould printed to the anatomical dimensions of the bovine cornea, paraffin blocks were produced to support the cornea and maintain its curvature during the test. The cornea-paraffin-support assembly was centred and adhered to the base of the texture analyser using double-sided adhesive tape.

Each hydrogel sample was placed on a 9 mm diameter upper cylinder probe, which was lowered at a constant rate of 1 mm/s until it reached the corneal surface. The probe was held in contact with the corneal surface for 30 s at a force of 0.2 N. After this time, the probe was returned to its initial position at the same speed (1 mm/s) (Figure III.9). During this separation, the force-displacement curve required to separate the bovine cornea from the tested formulation was recorded. Texture Exponent 32 software (Stable Micro Systems, Godalming, UK) was used to determine the maximum detachment force (F_{max}) and the work of adhesion (W_{adh}) calculated from the area under the curve (AUC) obtained from the force-displacement curve. All measurements were performed in triplicate.

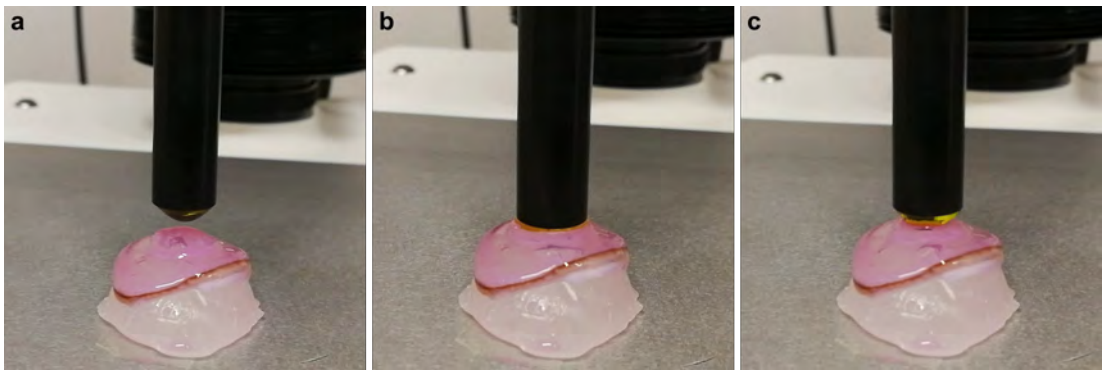

III.9. FIGURE: Representation of the vertical displacement of the cylindrical probe into the corneal wound in the adhesion test.

8. *In vivo* eye model

The *in vivo* assay was conducted to assess the potential and capability of hydrogel solutions as treatments for corneal ulcers.

Female New Zealand white rabbits weighing about 2 kg were used for *in vivo* studies. Animal experiments were carried out in accordance with the procedures and experimental designs approved by the Animal Research Ethics Committee of the University of the Basque Country UPV/EHU.

30 rabbits were randomly divided into 5 groups (n=6 for each group), 4 study groups (table III.4) and a control group. The control group consisted of eyes undergoing surgery and treated with 0.2% HA artificial tears 4 times daily until wound closure.

III.4. TABLE: Composition of the 4 hydrogel treatments used in the *in vivo* assay.

Study group	Treatment
Control	0.2% HA artificial tears 4 times daily until wound closure.
H	50 μl of 5% w/v gelatine and 0.01% w/v RFP hydrogel crosslinked for 2 minutes with blue light (day 0) + 0.2% w/v HA artificial tears 4 times daily until wound closure.
H-Ab	50 μl of 5% w/v gelatine and 0.01% w/v RFP hydrogel with 1 mg/ml Infliximab crosslinked for 2 minutes with blue light (day 0) + 0.2% HA artificial tears 4 times daily until wound closure.
H-AS	50 μl of 10% w/v gelatine and 0.02% w/v RFP hydrogel with rabbit autologous serum at a 1:1 dilution crosslinked for 2 minutes with blue light (day 0) + 0.2% HA artificial tears 4 times daily until wound closure.
H-HAMe	50 μl of 10% w/v gelatine and 0.02% w/v RFP hydrogel with amniotic membrane extract at a 1:1 dilution crosslinked for 2 minutes with blue light (day 0) + 0.2% HA artificial tears 4 times daily until wound closure.

The 30 rabbits were divided into 3 groups of 10 rabbits for surgery and data collection. For every 10 rabbits, the surgical procedure was performed in 2 rounds. The surgical procedure was first performed on the right eye of each animal (2 eyes per study group) and they were treated and evaluated for 1 week. After a 1-week rinsing period to remove any traces of topical or systemic medication, the same procedure was repeated on the left eye. After the evaluation period of the left eyes, the animals were euthanised and the corneas were collected for histological and inflammatory analysis.

Therefore, the *in vivo* study was divided into 6 separate experiments, with the odd-numbered experiments (E01/E03/E05) performed on the right eyes and the

even-numbered experiments (E02/E04/E06) performed on the left eyes.

Experiment E01 served as a pilot study to establish the conditions and surgical procedures for the subsequent experiments. In this pilot study, 5 rabbits were treated with 25 μl of 0.1% benzalkonium chloride (BAC) (Sigma Aldrich, St. Louis, MO, USA) and 5 rabbits with 25 μl of LPS at a concentration of 50 μg/ml once daily for 3 days before surgery and on the day of surgery to add an additional inflammation stimulus. The same surgical procedure described in the subsection 8.1 was used for this end, however, instead of tarsorrhaphy, a protective lens was placed in the treated eyes. The rabbits were evaluated for 10 days.

Following the evaluation of the pilot study, it was decided to replace contact lenses with tarsorrhaphy and remove the BAC or LPS stimulus. The evaluation period was also reduced from 10 to 7 days due to the early closure of some wounds.

Therefore, from E02 to E06, a total of 10 eyes per study group were used for the final *in vivo* analysis, 6 of them being evaluated 7 days after surgery (left eyes) and 4 of them 21 days after surgery (right eyes).

8.1. *In vivo* surgical procedure

Prior to surgery, rabbits were anaesthetised with an intramuscular injection of 1 ml/kg ketamine (Ketolar® 50 mg/ml, Pfizer, Madrid, Spain) and 0.3 ml/kg xylazine (Xylagesic 20 mg/ml, Laboratorios Calier SA, Barcelona, Spain) into the thigh. An anterior superficial stromal surface keratectomy was performed by placing a 6.5 mm diameter corneal Hessburg-Barron vacuum trephine (Jedmed, St. Louis, MO, USA) in the anatomical centre of the rabbit cornea and deepening to a thickness of approximately 187 μm (3 quarter turns of the trephine) (**a** of the figure III.10). A superficial keratectomy of the trephined area was then performed using a crescent blade (Alcon Laboratories, Barcelona, Spain) (**b** of the figure III.10). The defect was filled with 50 μl of the corresponding hydrogel solution preheated to 32 °C and illuminated with blue light for 2 minutes for *in situ* hydrogel crosslinking (**c** and **d** of the figure III.10). Finally, from experiments E02 to E06, partial tarsorrhaphy was performed and maintained for 72 hours to prevent the animal from touching the wound (**e** and **f** of the figure III.10).

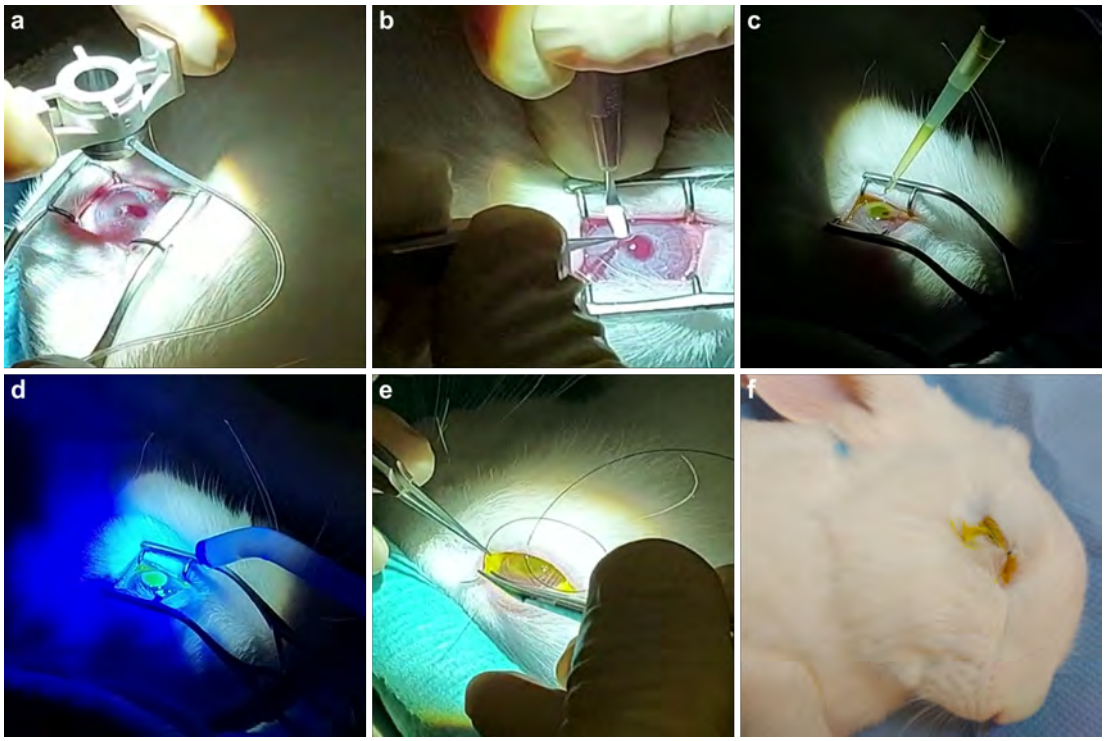

III.10. FIGURE: Steps followed for the *in vivo* surgical procedure.

0.05 mg/kg buprenorphine solution (Buprecare®, Ecuphar, Barcelona, Spain) was injected before the surgery and every 12 hours for 72 hours as an analgesic for pain relief, and 3 mg/ml Tobrex® antibiotic eye drops (Tobramycin solution, Novartis, Barcelona, Spain) were instilled until the wounds were closed to reduce the risk of infection. 0.2% HA artificial tears were also administered to all the study groups including the control to keep the eyes moist. Eyes were assessed from day 0 (day of surgery) to day 7.

At the end of the experimental procedure, the animals were anaesthetised with an intramuscular injection of 2 ml/kg ketamine and 0.6 ml/kg xylazine. For sacrifice, a volume of 10 ml of saturated potassium chloride was injected intravenously into the marginal ear vein. Death was confirmed by the onset of *rigor mortis*.

8.2. Clinical evaluation of eye injuries

Ocular morbidity in the rabbits was assessed during the *in vivo* assay using the Draize acute ocular toxicity test by slit lamp examination [337]. Ocular irritation was assessed on days 0, 1, 4 and 7 of the study.

The Draize test weighs and sums six parameters related to observable changes in the anterior segment of the eye, including density and area of corneal opacity, degree of iritis, conjunctival redness, oedema, and discharge (Table III.5). The ocular irritation index is the sum of all scores and can range from 0 to 110. A high score indicates a compound that would be irritating to the eye.

On the basis of the score obtained, each product was classified according to the value of the eye irritation index obtained, following the classification of Kay and Calandra (Table III.6, [338]).

The iris and conjunctiva were assessed first. Corneal reactions were then assessed by instilling 5 μl of 2% fluorescein Colicursí® Fluotest eye drops (Novartis, Barcelona, Spain) and illuminating the ocular surface with blue light. Fluorescein is a temporary dye that, together with blue light, helps to detect damage to the cornea.

The application of fluorescein to the ocular surface also helped to monitor the progress of wound closure by taking daily photographs. Photographs were taken on day 0 and from day 3 until wound closure. It was not possible to register wound evolution on day 1 and day 2 due to the partial tarsorrhaphy. The photographs were taken after removal of excess dye by rinsing the eye with saline eye drops.

III.5. TABLE: Draize scale's weighted scores for classifying the severity of eye injuries. Reproduced from [337].

Assesment			Score
CORNEA	A. Opacity-Degree of density (most dense area taken for reading)	Scattered or diffuse area; details of iris clearly visible.	1
		Easily discernible translucent areas; details of iris slightly obscured.	2
		Opalescent areas; no details of iris visible, size of pupil barely discernible.	3
		Opaque; iris invisible.	4
	B. Area of cornea involved	One quarter (or less) but not zero.	1
		Greater than one quarter, less than one half.	2
		Greater than one half, less than three quarters.	3
		Greater than three quarters, up to whole area.	4
			Score = A × B × 5 (range, 0 to 80)
IRIS	A. Reaction to light	Folds above normal, congestion, swelling, and/or circumcorneal injection; iris still reacting to light (sluggish reaction is positive).	1
		No reaction to light, hemorrhage, and/or gross destruction.	2
			Score = A × 5 (range, 0 to 10)
CONJUNCTIVAE	A. Redness of palpebral conjunctivae	Vessels definitely injected above normal.	1
		More diffuse, deeper crimson red; individual vessels not easily discernible.	2
		Diffuse beefy red.	3
	B. Chemosis	Any swelling above normal (includes nictitating membrane).	1
		Obvious swelling with partial eversion of the lids.	2
		Swelling with lids about half closed.	3
		Swelling with lids about half closed to completely closed.	4
	C. Discharge	Any amount different from normal.	1
		Discharge with moistening of the lids and hairs just adjacent to the lids.	2
		Discharge with moistening of the lids and considerable area around the eye.	3
			Score = (A + B + C) × 2 (range, 0 to 20)

III.6. TABLE: Eye irritation index values reported by Kay and Calandra [338].

MMTS	Irritation classification
0-0.5	Non-irritative
0.6-2.5	Practically non-irritative
2.5-15	Minimally irritative
15.1-25	Mildly irritative
25.1-50	Moderately irritative
50.1-80	Severely irritative
80.1-100	Extremely irritative
100.1-110	Maximally irritative
MMTS: Maximum mean total score	

9. Acquisition and analysis of tear samples

9.1. Collection and quantification of tear using Schirmer strips

Schirmer strips (Madhu Instruments, New Delhi, India) were used for tear sample collection. One strip was placed in the upper bulbar sac of the operated eye for 5 minutes on days 0, 1, 4 and 7 of the study (Figure III.11). Two samples were collected on each study day, one in the morning and one in the afternoon.

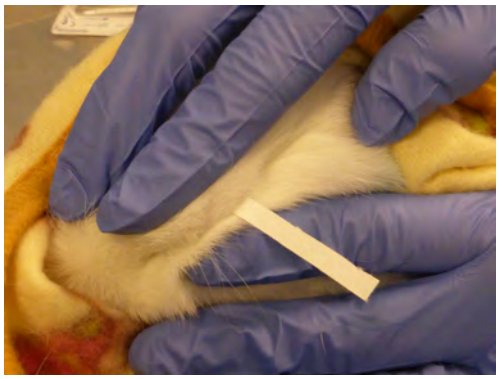

III.11. FIGURE: Tear adquisition procedure from Schirmer strip.

The amount of tear collected at each measurement was recorded, considering that 1 mm of strip corresponds to 1 μl of tear. Each strip was placed separately in a 1.5 ml Eppendorf tube without buffer and stored at -80 °C until use. Samples were preserved for subsequent tear elution and evaluation of inflammatory molecules. Samples were coded according to the day of tear collection, the rabbit used and the eye involved.

9.2. Protein elution from Schirmer strips

100 μl of PBS was added to each sample tube containing the Schirmer strip and kept in contact for 1 hour at room temperature to elute the tear content of the strip into the elution PBS buffer. The samples were then centrifuged at 400 rpm for 5 minutes at 4 °C using the Kubota 3500 tabletop refrigerated centrifuge (Kubota Corporation, Tokyo, Japan). After the first centrifugation, the Schirmer strips were transferred to 0.2 ml Eppendorf tubes and centrifuged at 1300 rpm and 4 °C for 5 minutes. The supernatant from the second centrifugation was added to the 1.5 ml Eppendorf tube with the volume previously collected for each sample.

6 μl aliquots per sample were taken for protein quantification by BCA assay and the tubes were stored at -80 °C until their further use for cytokine analysis.

9.3. Protein quantification-BCA assay

6 μl aliquot was used per tear sample for total protein quantification and bicinchoninic acid (BCA) assay was used for such purpose.

The BCA assay is a colourimetric assay based on the formation of a Cu^{2+}-protein complex under alkali conditions, followed by the reduction of Cu^{2+} to Cu^{+} [339]. The amount of Cu^{2+} reduced is proportional to the amount of protein present in the solution. The sodium salt of bicinchoninic acid reacts with Cu^{+} and causes a colour change from green to purple with a strong absorbance at 562 nm in a protein concentration-dependent manner.

Like so, the protein content of unknown samples can be spectrophotometrically determined compared with a known protein standard.

Protein levels were quantified using 0-1 mg/ml serial dilutions of BSA protein as a known protein standard. 10 μl of a 1:5 dilution of each sample or serial dilution of BSA and 200 μl of BCA and $CuSO_4$ working solution (50:1) (Sigma Aldrich, St. Louis MO, USA) were mixed in each well of a 96-well plate. Three replicates per sample or BSA serial dilution were quantified. The plate was incubated at 37 °C for 30 minutes in the dark and subsequently, the absorbance of each well was determined using a spectrophotometer at a wavelength of 562 nm (Thermo Fisher Scientific, Waltham, MA, USA). Finally, a standard curve for BSA was prepared and the protein concentration of each sample was calculated.

9.4. Evaluation of the expression of inflammatory molecules in tear samples by immunodetection-Antibody arrays

Quantification of cytokines in tear samples collected in the *in vivo* assay was performed using multiplex microarray technology with the QAL-CYT-1 Quantibody Rabbit Cytokine Array Kit (Raybiotech, Norcross, GE, USA).

This kit is based on the sandwich technique of a traditional ELISA, but allows the concentration of multiple cytokines to be accurately determined simultaneously by placing multiple cytokine-specific capture antibodies on a glass slide. A capture antibody is first bound to the glass surface of the array. After incubation with the sample, the cytokine of interest binds to the antibody on the solid surface. A second biotin-labelled detection antibody, capable of recognising a different epitope of the target cytokine, is then added. The cytokine-antibody-biotin complex is visualised using a laser scanner by adding the equivalent dye Cy3 conjugated to streptavidin. The microarray is divided into 16 wells with identical sets of cytokine antibodies and in each antibody along with the positive controls is arrayed in quadruplicate (Figure III.12).

For cytokine quantification, standards with predetermined concentrations of array-specific cytokines are provided to generate a standard curve for each cytokine. By comparing the signals of the unknown samples with the standard curve, the concentration of the cytokine in the samples is determined.

The QAL-CYT-1 Quantibody Rabbit Cytokine Array Kit allows the identification of interleukin 1α (IL-1α), interleukin 1β (IL-1β), interleukin 8 (IL-8), interleukin 17A (IL-17A), interleukin 21 (IL-21), leptin, macrophage inflammatory protein 1β (MIP-1β), matrix metallopeptidase 9 (MMP-9), neural cell adhesion molecule 1 (NCAM-1) and TNFα cytokines. All of these are related to the mitogen-activated protein kinase (MAPK) and the nuclear factor kappa-light-chain-enhancer of activated B cells (NF-κB) signaling pathways, processes that are strongly associated with the inflammatory cascade.

The experiment, scanning, data extraction and analysis were performed according to the manufacturer's protocol.

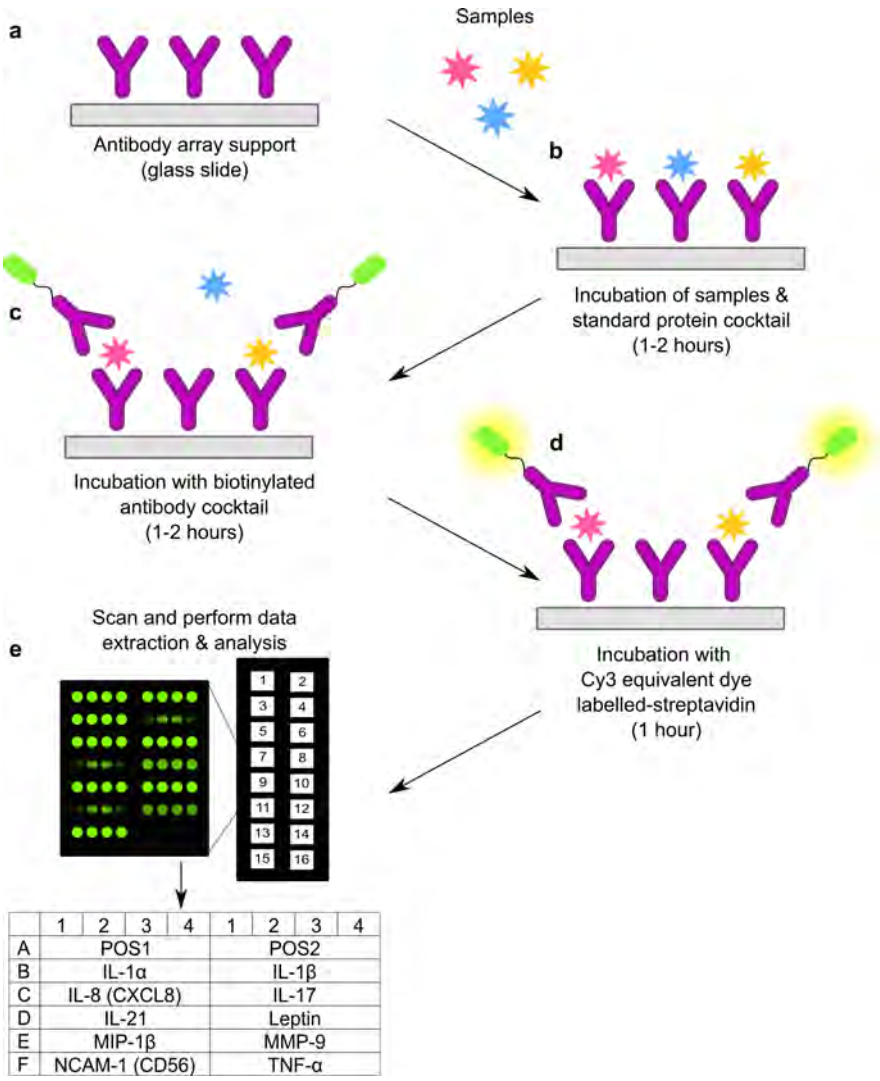

	1	2	3	4	1	2	3	4
A	POS1				POS2			
B	IL-1α				IL-1β			
C	IL-8 (CXCL8)				IL-17			
D	IL-21				Leptin			
E	MIP-1β				MMP-9			
F	NCAM-1 (CD56)				TNF-α			

III.12. FIGURE: Cytokine array working procedure. **a**) The glass slide containing the capture antibody is completely air dried before starting any incubation. **b**) Samples are added and inmobilized to the antibodies present in the solid support. **c**) The immobilized samples are then complexed with a biotinylated antibody. **d**) The enzyme complexes are incubated with Cy3 Equivalent Dye-Streptavidin to produce a detectable signal. **e**) The array is scanned and the data is analysed.

10. Gene expression analysis

Gene expression analysis studies how genes are transcribed to produce functional RNA or protein products. The study of gene regulation provides insight into normal and abnormal or pathological cellular processes.

10.1. RNA extraction from *in vitro* samples

RNA extraction from *in vitro* samples was performed from cultured HCE cells from *in vitro* inflammation experiments. The NucleoSpin RNA kit (Macherey-Nagel, Düren, Germany) was used and the manufacturer's instructions were followed for such purpose. The process was carried out at room temperature and using sterile RNAse-free material.

Cells in culture were dissociated with an enzymatic solution of trypsin-EDTA for 5 minutes at 37 °C. After cell detachment, FBS was added to inhibit trypsin's activity and cells were pelleted by centrifugation at 300g for 5 minutes. After removing the supernatant, cells were resuspended in 1× PBS, counted and centrifuged again to wash any residue of culture medium.

For RNA extraction, the cell pellet was lysed using 350 μl of RA1 buffer (Macherey-Nagel, Düren, Germany) and 3,5 μl β-mercaptoethanol reducing agent (Sigma Aldrich, St. Louis, MO, USA). RA1 is a prepared buffer for tissue and cell lysis before RNA isolation. Cell lysates were frozen at -80 °C until RNA purification, which was achieved following the manufacturer's instructions. The procedure included the DNA digestion step with DNase and a total of 60 μl of final RNA volume were obtained.

10.2. RNA extraction from *in vivo* samples

RNA from *in vivo* samples was extracted from corneal tissue samples obtained from the *in vivo* experiments. These tissues were comprised of the cornea, the sclerocorneal limbus and 1-2 mm of the sclera.

Rabbit corneas kept at -80 °C were defrosted, weighed and cut into long, thin strips to facilitate homogenisation. The samples were placed in threaded tubes with 0.5 mm zirconium oxide beads (Next Advanced, NY, USA). The volume of beads used in each tube was equivalent to 1× the volume of each sample. 1 ml of TRIzol (Thermo Fisher Scientific, Waltham, MA, USA) was introduced into each sample, the tubes were placed tightly closed in the Bullet blender (Next Advanced, NY, USA) and were homogenized at speed 8 for 3 minutes. After the run, the homogenised volume of the sample was divided into two 1.5 ml Eppendorf tubes, introducing 500 μl of the sample in each. 100 μl of chloroform were added per tube, samples were

shaken vigorously by hand and spun at 12000g for 15 minutes at 4 °C, which cause the sample to separate into a lower phenol red-chloroform phase containing cellular proteins, a cloudy interphase containing the DNA and a transparent upper aqueous phase containing the RNA. The aqueous phase was transferred to a clean Eppendorf tube and incubated for 1 hour at room temperature with 500 μl of isopropyl alcohol. Samples were centrifuged again at 12000g for 10 minutes at 4 °C, the supernatant was removed, the RNA pellet was washed with 1 ml of 70% ethanol and they were vortexed and spun again at 7500g for 5 minutes at 4 °C. After removing the supernatant, the RNA pellet was allowed to air dry and then dissolved in 20 μl of RNase-free water.

After RNA purification, samples were incubated with 1 unit/μl DNase I (Zymo-Research, Irvine, CA, USA) dissolved in DNase buffer (Zymo-Research, Irvine, CA, USA) for 15 minutes at RT to remove possible genomic DNA contamination. Finally, 2.5 μl of 25 mM EDTA solution was added to each sample and heated at 65 °C for 10 minutes.

10.3. RNA quantification

Total RNA concentration (ng/ml) was quantified measuring the absorbance (A) of each sample at 260 nm and 280 nm wavelength using the Take 3 Micro-Volume Plate for ELx800 Microplate Reader.

The Lambert-Beer law states that there is a linear relationship between absorbance and macromolecule concentration, up to an absorbance maximum of 1.2. RNA solutions exhibit maximum absorbance at a wavelength of 260 nm, while protein solutions exhibit maximum absorbance at a wavelength of 280 nm. The degree of RNA purity can be estimated by calculating the ratio of the values obtained at 260 nm and 280 nm (A_{260}/A_{280}). Pure RNA has an A_{260}/A_{280} ratio of approximately 2.0. Values outside of this range indicate sample contamination.

The concentration of RNA can be calculated from the absorbance measurement at 260 nm using the equation III.7, since each optical density unit measured at a wavelength of 260 nm corresponds to 40 μg/ml of single-stranded RNA.

$$RNA\ (\mu g/ml) = A_{260} \times Dilution\ factor \times 40 \tag{III.7}$$

After calculating RNA concentration, samples were stored at -80 °C to ensure their integrity until their use.

10.4. Retrotransciption

The most commonly used strategy in the retrotranscription reaction is the addition of an oligo deoxythymidine (dT) primer, a sequence of nucleotides containing only dT nucleobases, allowing it to hybridize to the poly-A tail of the mRNA of most eukaryotic organisms. The enzyme reverse transcriptase is responsible for synthesizing DNA of the sequence complementary to that of the mRNA acting as a template.

The iScriptTM cDNA Synthesis kit (BioRad, Hercules, CA, USA) was used for two-step reverse transcription. The cDNA was synthetized from 1 μg of RNA for each sample. 1 μg of total RNA was mixed with 4 μl of 5X iScript Reaction Mix, 1 μl of iScript Reverse Transcriptase and up to 20 μl of nuclease-free water. The complete reaction mix was incubated in a MJ Mini Personal Thermal Cycler (BioRad, Hercules, CA, USA) using the following protocol: 5 minutes at 25 °C for priming, 20 minutes at 46 °C for reverse transcription and 1 minute at 95 °C for reverse transcriptase inactivation. A final optional step at 4 °C was included until the sample was removed from the thermal cycler. cDNA samples were stored at -20 °C until qPCR analysis.

10.5. cDNA preamplification of *in vivo* samples

The cDNA samples obtained from the rabbit corneas of the *in vivo* assays were amplified using the Multiplex PCR Kit (Qiagen, Hilden, Germany). A volume of 5 μl was used for each sample, including 2.5 μl of 2X QIAGEN Multiplex PCR Master Mix, 0.5 μl of 500 nM primer mix, 1.25 μl of 1 μg cDNA template and 0.75 μl of RNAse-free water.

The thermal cycling protocol was configured with an initial heat activation cycle at 95 °C for 15 minutes to activate the DNA polymerase and 14 cycles of amplification. Each cycle was divided in a first denaturation step at 94 °C for 30 s, an annealing step at a temperature gradient of 57-63 °C for 90 seconds and an extension step at 72 °C for 60 seconds. A final extension step at 60 °C for 30 minutes was added after amplification. Samples were stored at –20 °C until their use.

10.6. Real time RT-qPCR

The cDNA obtained from reverse transcription was used as template for the real-time quantitative polymerase chain reaction (RT-qPCR). In this method, the amount of each specific target is determined by measuring the increase in fluorescence signal of DNA-binding dyes during consecutive enzyme-mediated amplification cycles.

The RT-qPCR was carried out in the CFX96 Real Time System and C1000 Touch Thermal Cycler (BioRad, Hercules, CA, USA) using SYBR® Green double-stranded DNA (dsDNA) binding dye (BioRad, Hercules, CA, USA). This fluorophore intercalates between DNA bases, where it becomes less mobile and hence released its energy as fluorescence intensity proportional to the amount of dsDNA product accumulated. Thus, it can be used for relative DNA quantification.

The reaction mix for each well of the PCR plate was made up of 10 μl of iTaq Universal SYBR® Green Supermix, 8 μl of Nuclease-free water, 0.5 μl of forward and 0.5 μl of reverse primers in a concentration of 500 nM and 1 μl of cDNA. The thermal cycling protocol consisted of an initial cycle at 95 °C for 3 minutes to activate the polymerase and 40 cycles of amplification. Each amplification cycle was divided in a first denaturation step at 95 °C for 30 seconds, a second step of annealing of the primers for 30 seconds and a third elongation step at 72 °C for 30 seconds. The information on the primers used is summarised in table III.7.

These cycles were followed by a cycle at 95 °C for 1 minute, another cycle at 65 °C for another minute and a 65-95 °C temperature gradient performed in 60 cycles by increasing the temperature 0.5 °C per cycle. The qPCR ended with a conservation step, where the PCR products were left at 4 °C until the equipment was turned off.

The dissociation protocol consisting of the temperature gradient where the temperature gradually increased from 65 °C to 95 °C induced the separation of the DNA strands synthesized during the PCR when the melting temperature (Tm) corresponding to each amplicon was reached. The intercalating SYBR® Green detached from the DNA strands when they were separated and it stopped emitting a fluorescence signal. This was represented as a fluorescence peak by the PCR equipment and made it possible to rule out the presence of multiple amplification products with different Tm values.

III.7. TABLE: Sequences and properties of the primers used in *in vitro* and *in vivo* assays.

Primer	Type	Sequence (5′-3′)	Amplicon size	Tm	GC%	Optimized Ta	Assay
IL-6	Fw primer Rv primer	GCAGATGAGTACAAAAGTCCTGA TTCTGTGCCTGCAGCTTC	120	58.43 57.93	43.48 55.56	59.6	*In vitro*
IL-1β	Fw primer Rv primer	CCATGGCAGAAGTACCTGAG CCTGGAAGGAGCACTTCATC	114	57.68 57.96	55 55	59.6	*In vitro*
TNFα	Fw primer Rv primer	TGCACTTTGGAGTGATCGG TCAGCTTGAGGGTTTGCTAC	145	57.77 57.81	52.63 50	59.6	*In vitro*
TBP	Fw primer Rv primer	GCTGTTTAACTTCGCTTCCG CAGCAACTTCCTCAATTCCTTG	104	57.77 57.83	50 45.45	59.6	*In vitro*
GusB	Fw primer Rv primer	GCCCATTATTCAGAGCGAGTA GTTTTTGATCCAGACCCAGATG	128	57.61 57.29	47.62 45.45	59.6	*In vitro*
IL-1β	Fw primer Rv primer	GTAGACCCCAACCGTTACCC AGACGGGCATGTACTCTGTC	145	57.4 56.5	60 55	56.4	*In vivo*
GADPH	Fw primer Rv primer	TCGGAGTGAACGGATTTG CTCGCTCCTGGAAGATGG	225	52.2 55.1	50 61.1	61	*In vivo*
Ki 67	Fw primer Rv primer	GCCAAGATAGTTGCTGATAC AAGTGTCCGATTCCGATTA	171	50.5 50.4	45 42.1	58.4	*In vivo*
HPRT1	Fw primer Rv primer	ACGTCGAGGACTTGGAAAGGGTGTT GGCCTCCCATCTCCTTCATCACATC	96	62.1 61	52 56	58.4	*In vivo*
p63	Fw primer Rv primer	CGCCCCTTTCGTCAGAACAC GTGCTGAGGAAGGTACTGCAT	165	61.57 60.07	60 52.38	57.2	*In vivo*
CK3	Fw primer Rv primer	GACTCGGAGCTGAGAAGCAT CAGGGTCCTCAGGAAGTTGA	198	59.54 58.65	55 55	59.8	*In vivo*
β-Actin	Fw primer Rv primer	AGATGACCCAGATCATGTTTGAG GTCACCGGAGTCCATCACG	119	58.22 60.15	43.48 63.16	57.2	*In vivo*
α-SMA	Fw primer Rv primer	CGGTGCTGTCTCTCTATGCC CACGCTCAGTCAGGATCTTCA	177	60.25 59.8	60 52.38	58.4	*In vivo*
RIG S15	Fw primer Rv primer	CATGGTGGGCGTCTACAAC ACTTGAGAGGGATGAAGCGG	161	58.53 59.46	57.89 55	58.4	*In vivo*
CD44	Fw primer Rv primer	GACACCATGGACAAGTTTTGG GAGATGCTGTAGCGACCATT	140	57.63 57.77	47.62 50	59.8	*In vivo*
PAX6	Fw primer Rv primer	AGAGAATACCAACTCCATCAG GATAATGGGTTCTCTCAAACTC	152	54.44 54.28	42.86 40.91	58.4	*In vivo*

Fw: Forward primer.
Rv: Reverse primer.
Tm: Melting temperature.
GC%: Guanine (G) and cytosine (C) content.
Ta: Annealing temperature.

10.6.1. Analysis of RT-qPCR results

The quantification cycles (Cq) results were corrected for each primer pair's RT-qPCR efficiency using the formula described by Pfaffl [340]. Additionally, the variation between plates was measured and corrected for each gene using internal calibrators. The expression of the study genes was then normalised with respect to the reference genes, which are genes whose expression remains constant within the assay conditions. After evaluating the coefficients of variation of various reference genes, Gusβ and TBP genes were selected for the *in vitro* inflammation assay, while GAPDH, HPRT1, and RIG S15 were chosen for the *in vivo* assay samples. The corrected Cqs of the reference genes were averaged and subtracted from the Cqs of the study genes to obtain the normalised ΔCq for each sample [341]. For each study gene, the

average ΔCq of all samples was substracted from the ΔCq of each sample, resulting in the ΔΔCq for each sample. This enabled us to calculate the relative expression (2-ΔΔCq) using Pfaffl's modification of the mathematical model described by Livak and Schmittgen [342]. The CFX Maestro software (BioRad, Hercules, CA, USA) was used for this purpose.

11. Histological analysis

Frozen 10 μm corneal tissue sections fixed in 4 % paraformaldehyde (PFA) and included in OCT compound were sectioned on a CM 3050S cryostat (Leica, Wetzlar, Germany). Slides were kept frozen at -20 °C until staining. Bovine and rabbit *ex vivo* cultured corneas and rabbit *in vivo* corneas were used for histological analysis.

11.1. Haematoxylin-Eosin (H-E) staining

Slides containing corneal tissues were placed in slide racks and passed through different solutions to perform the H-E staining. They were stained with Haematoxylin for 1 minute and 30 seconds, rinsed with 0.3% hydrochloric acid for 5 seconds and stained with working Eosin Y solution for 15 seconds. After each step, they were placed under tap water for 5 minutes.

After the last wash, the samples were dehydrated by immersing them in progressively concentrated ethanol solutions (50%, 70%, 96% and 2 solutions of 100%) for 10 seconds each.

Finally, the samples were cleared in 3 changes of Citrosol for 5 minutes each. Dibutylphthalate polystyrene xylene (DPX) solution was applied to the tissue on each slide and covered with a coverslip for microscopic visualisation.

11.2. Impression cytology

Impression cytology is a non-invasive technique based on the collection of cells from the superficial layers of the conjunctival epithelium for subsequent histological analysis.

Samples of conjunctival cells obtained from the animals used in *in vivo* experiments were obtained through this technique.

Samples were obtained by placing a 2×2 mm^2 0.45 μm filter paper (Merck KGaA, Darmstadt, Germany) with one end square and the other end tapered to identify the side that contained the cells. The filter was applied firmly to the upper conjunctival surface for 5-10 seconds, gently removed and placed on a 24-well plate containing 70% alcohol solution. They were kept in the alcohol solution at 4 °C until processing.

11.3. PAS staining of impression cytology samples

Impression cytology samples fixed in 70% alcohol were passed through a series of solutions to perform the periodic acid Schiff (PAS) staining. The samples were first rinsed with distilled water for 5 minutes. They were immersed in 1% periodic acid solution for 5 minutes, rinsed twice with distilled water and immersed in Schiff's reagent for 30 minutes in the dark. Schiff's reagent was washed off the samples with 3 changes of sulphuric acid bath for 2 minutes each, placed in tap water for 5 minutes and counterstained with Harris Haematoxylin for 30 seconds. They were then rinsed in tap water for 5 minutes.

After the last wash, the samples were dehydrated by immersing them in ethanol solutions of increasing concentrations (50%, 2 solutions of 96% and 2 solutions of 100%) for 1 minute each.

Finally, the samples were cleared in 2 changes of Citrosol for 5 minutes each. DPX was applied to the samples on each slide and covered with a coverslip for microscopic visualisation.

12. Inmunofluorescence

Immunofluorescence (IF) is a technique that allows visualisation of cellular antigens based on the specific binding of antigens and fluorophore-tagged antibodies.

Fluorophores, compounds that emit light when exposed to a certain wavelength, are conjugated to antibodies that are capable of binding to antigens within their original subcellular location in tissues or cell cultures. Thus, proteins or antigens can be visualized by fluorescence or confocal microscopy, depending on the biological question being addressed.

Antibodies or immunoglobulins (Ig) are glycoproteins produced by B-lymphocytes as a response to a previous exposition to any foreign molecule that triggers an immune response.

The basic structure of immunoglobins is composed of two identical pairs of heavy and light polypeptide chains linked together by disulfide bonds. The stem and lower arms are quite similar in the different classes of antibodies, but the polypeptide sequence in the tip of the arms gives specificity to bind its predetermined target while avoiding other similar targets. There are 5 described immunoglobulin classes in mammals (IgG, IgM, IgA, IgD and IgE) that differ in the activity and nature in the immune response.

The antibody affinity refers to the binding strength between the antibody's antigen binding site and the epitope and it is an important aspect to consider when designing an IF assay. The higher the affinity, the higher the speed of antibody-antigen interaction and the sensitivity of the assay.

IF assays offers the possibility to perform simultaneous detection of different structural and functional molecules. Firstly, samples must be attached to a solid support (slide or microscopy chamber) and should be fixed to preserve the life-like cellular morphology and prevent biochemical reactions that could damage tissue or cell integrity. The most commonly used fixatives are PFA, acetone or methanol and they are selected considering the sample and antibody type. PFA is usually used for membrane-associated protein staining, it crosslinks free amine groups and create a network of linked proteins to preserve cell morphology. However, it may react with the amine groups of proteins that can blur the final signal with autofluorescence. Moreover, it does not adequately permeabilize cell membranes therefore, permeabilisation step is required during the assay. Acetone and methanol are classified as precipitating fixatives because they cause protein precipitation, thus being effective in preserving cellular architecture. They do not require additional permeabilisation step.

Permeabilisation helps the antibody to pass through the cell membrane and enter the cell. After this step, the sample is blocked to minimize non-specific interactions and allow specific antigen-antibody binding. For blocking, samples are incubated with solutions containing blocking agents such as BSA, skimmed milk or serum. Once the sample blocked, high specificity primary antibody solution with

the adjusted dilution is applied. Direct and indirect antibody detection methods can be distinguished. Direct antibody detection uses fluorochrome conjugated primary antibodies while the indirect detection requires a secondary antibody that recognizes the primary antibody. Multiple antibodies specific for each protein can also be combined to stain multiple proteins within a unique tissue sample. In these cases, secondary antibodies should be conjugated to different fluorophores that do not overlap in their excitation and emission spectrum. Finally, samples are usually counterstained with florescent DNA- intercalant dyes like Hoechst or DAPI that are able to penetrate the nucleus and bind to AT-rich regions of the minor groove in DNA. This steps aids in the identification of individual cells and particular organelles.

12.1. Immunocytochemistry

Immunocytochemistry was performed on slides containing primary cells isolated directly from the corneoscleral human tissues and on 8-well chamber coverslips (Ibidi, Gräfelfing, Bayern, Germany) containing the cultured limbal cells fixed in 4 % PFA in PBS for 20 minutes at room temperature.

The samples were washed three times in PBS to remove any unreacted PFA. Fixed samples were permeabilized with 0.1% Triton TX-100 in PBS (PBST) for 10 min and blocked with a blocking solution containing 5% BSA and 10% FBS in PBST for 1 hour to reduce non-specific interactions that could lead to background and false positive staining. Samples were treated with the appropriate primary antibody solution (III.8) overnight at 4 °C, washed three times for 10 minutes each with PBST and stained with secondary antibodies for 2 hours at room temperature in the dark. Finally, samples were counterstained with 4 mg/ml Hoechst 33342 (Thermo Fisher Scientific, Waltham, MA, USA) diluted 1:1000 in PBS for 15 minutes at room temperature, washed twice with PBS for 5 minutes each, and mounted on microscope slides with Fluoromount G mounting medium (SouthernBiotech; Birmingham, UK). Slides were stored at 4 °C, protected from light, until fluorescence microscopy imaging. All images were captured using the Apotome.2 fluorescence microscope (Zeiss, Oberkochen, Germany).

12.1.1. Cytospin

To perform the immunocytochemical analysis of primary cells directly isolated from sclerocorneal human rims, part of the cells obtained from tissue digestion, both epithelial and stromal cells, were washed in 1× PBS and fixed in 2 % PFA for 20 minutes. Once fixed, they were washed in 1× PBS, centrifuged for 7 minutes at 300g and suspended in PBS-BSA (1%). The cell solution was then spun at 1300 rpm for 8 minutes using a cytospin (Thermo Fisher Scientific, Waltham, MA, USA) and precipitated over slides coated with poly-L-lysine (Sigma Aldrich, St. Louis, MO, USA). One hundred microlitres (100 μl) of cell suspension with a density of around 20000 cells were added per cytofunnel.

Immunocytochemistry assessed in slides containing cells directly isolated from tissues was performed as described above.

12.2. Immunohistochemistry

For immunohistochemistry, 10 μm slides were thawed at room temperature, marked with a hydrophobic pen and rinsed twice with PBS for 5 minutes each. Tissue sections were permeabilized twice for 10 minutes each with PBST and blocked for 10 minutes with 10% normal goat serum (NGS) (Thermo Fisher Scientific, Waltham, MA, USA) to reduce non-specific interactions that could lead to background and false positive staining. Samples were treated with the appropriate primary antibody solution (Table III.8), incubated in a blocking solution containing 0.1% BSA and 5% FBS in PBST overnight at 4 °C, washed with PBS for 10 minutes and twice with PBST for 15 minutes each, and stained with secondary antibodies diluted 1:1000 in blocking solution for 1.5 hours at room temperature in the dark. The samples were washed again with PBS 3 times for 10 min each and counterstained with 4 mg/ml Hoechst 33342 diluted 1:1000 in PBS for 15 min at room temperature. Finally, the samples were washed twice with PBS for 5 minutes each and mounted on slides with Fluoromount G mounting medium. Slides were stored at 4 °C, protected from light, until fluorescence microscopy imaging was performed. Images were taken using the Apotome.2 and Nikon Ti-U (Nikon, Tokyo, Japan) fluorescence microscopes.

III.8. TABLE: List of primary and secondary antibodies used for IF assays.

Inmmunogen	Reference	Company	Host	Class	Isotype	IHC/ICC dilution	Type	Conjugate
CK3/K76	CBL218	Millipore	Mouse	M	IgG1	1:50	1ry	Unc.
CK15	sc-47697	Santa Cruz	Mouse	M	IgG2a	1:50	1ry	Unc.
Intβ4	ab29042	Abcam	Mouse	M	IgG1	1:40	1ry	Unc.
Ki67	MAB4190	Millipore	Mouse	M	IgG1	1:40	1ry	Unc.
MelanA	ab785	Abcam	Mouse	M	IgG1	1:50	1ry	Unc.
PanCK	M3515	Dako	Mouse	M	IgG1	1:50	1ry	Unc.
ZO-1	ab190085	Abcam	Goat	M	IgG	1:40	1ry	Unc.
α-SMA	ab7817	Abcam	Mouse	M	IgG2a	1:400	1ry	Unc.
p63α	13109S	Cell signaling	Rabbit	M	IgG	1:800	1ry	Unc.
Vimentin	ab16700	Abcam	Rabbit	M	IgG	1:1000	1ry	Unc.
anti-Mouse IgG1	A21121	ThermoFisher	Goat	P	IgG	1:1000	2ry	AF® 488
anti-Mouse IgG1	A21124	ThermoFisher	Goat	P	IgG	1:1000	2ry	AF® 568
anti-Mouse IgG2a	A21131	ThermoFisher	Goat	P	IgG	1:1000	2ry	AF® 488
anti-Mouse IgG2a	A21134	ThermoFisher	Goat	P	IgG	1:1000	2ry	AF® 568
anti-Rabbit IgG	A11070	ThermoFisher	Goat	P	IgG	1:1000	2ry	AF® 488
anti-Rabbit IgG	ab175471	Abcam	Goat	P	IgG	1:1000	2ry	AF® 488
anti-Goat IgG	A11057	ThermoFisher	Donkey	P	IgG	1:1000	2ry	AF® 568

M: Monoclonal antibody. 1ry: Primary antibody. Unc.: Unconjugated.
P: Polyclonal antibody. 2ry: Secondary antibody. AF: Alexa Fluor®.

13. Microscopy techniques

13.1. Phase contrast microscopy

Morphological analysis of the cultures was performed using the Nikon Eclipse TS 100 inverted phase contrast microscope (Nikon, Tokyo, Japan). Images were captured using ProgRes CapturePro 2.6 software using 4×, 10× and 20× magnification lenses.

13.2. Bright-field microscopy

Samples prepared by H-E staining were observed using a Olympus BX50 microscope (Olympus, Tokyo, Japan) with 10×, 20× and 40× objectives. Images were taken using ProgRes CapturePro 2.6 software.

13.3. Fluorescence/confocal microscopy

Calcein AM-EthD1 live/dead® viability/cytotoxicity assays were imaged using a fluorescence microscope (Olympus IX71, Olympus, Tokyo, Japan). Images were taken using the Olympus DP71 camera and Olympus Cell B software.

Immunohistochemical and immunocytochemical slides were imaged using the Apotome.2 fluorescence microscope (Zeiss, Oberkochen, Germany). Images were taken using the Axiocam ER5c digital camera and Zeiss ZEN Blue capture software.

This microscope was used as a confocal microscope with the structured illumination system.

CK15 (red)-Melan A (green) stained cell colony images were observed using the Zeiss LSM880 Fast Airyscan superresolution microscope (Zeiss, Oberkochen, Germany). The images were taken using the Axiocam MRm digital camera and Zeiss ZEN Black capture software.

The immunohistochemical slides of the *in vivo* assays were photographed on the Nikon Ti-U (Nikon, Tokyo, Japan) fluorescence microscope. Images were taken using the Nikon DS-Qi2 camera and Nikon NIS Elements AR control software. This microscope was used as a confocal microscope with the deconvolution system.

The fluorescence analysis of both tissue sections and cell culture was performed using ImageJ software (developed by Wayne Rasband at the Research Services Branch, National Institute of Mental Health, Bethesda, MD).

13.4. Scanning electron microscopy (SEM)

Morphology of the film cross-section was visualized using a Hitachi S-4800 field emission scanning electron microscope (Hitachi High-Technologies Corporation, Madrid, Spain). The samples were mounted on a metal stub with a double-sided adhesive tape. Finally, they were coated under vacuum with gold (JFC-1100) in an argon atmosphere prior to observation. All samples were examined using an accelerating voltage of 15 kV.

SEM visualisation of cell cultures was also performed. Samples were fixed using 2% glutaraldehyde in 0.1 M Sorensen buffer with pH 7.4 at 4 °C overnight and then rinsed in Sorensen 0.1 M for three times during 10 min. Samples were dehydrated in increasing concentrations of 30, 50, 70, 90, and 96% ethanol for 30 minutes each. Two washes of absolute ethanol during 30 minutes were applied as the last ethanol dehydration step. Dehydrated samples were then immersed into hexamethyldisilazane (HMDS) for 30 minutes twice and were left in a desiccator to air-dry at room temperature. Once dried, samples were mounted into SEM sample stubs with a double-sided sticky tape. Finally, they were sputtered with gold in argon atmosphere for SEM visualisation.

14. Analysis and Statistics

The results were analysed using different statistical tests.

Regarding film-related results, The transparency analysis was conducted using the non-parametric Kruskal-Wallis test followed by Dunn's post hoc test. Two-way analysis of variance (ANOVA) was used to analyze the degradation and MTT values, with Bonferroni's test used for multiple comparisons.

The analysis of the hydrogel results involved the use of various statistical tests.

Swelling and expansion data were analyzed using the Non-parametric Kruskal-Wallis test, followed by Dunn's post hoc test. Transmittance and *in vitro* release assays were assessed using Two-way ANOVA with Sidak's and Dunnett's multiple comparisons, respectively. Two-way ANOVA was also used to analyze the results of Citocompatibility and growth factors' quantification, both of which followed Tukey's post hoc test.

The results of inflammation and adhesion *in vitro* were analysed using ordinary one-way ANOVA with Tukey's multiple comparisons. For the *in vivo* results, the re-epithelialisation data was analyzed using two-way ANOVA for wound closure evolution and ordinary one-way ANOVA for the percentage of wounds closed. Both analyses were followed by Dunnett's test for multiple comparisons. Two-way ANOVA was used to assess the Draize test scores and quantify tear volume, protein concentration from tear samples and for the cytokine concentration analysis of the 50 samples of the pilot study. Ordinary one-way ANOVA was used for gene expression analysis. All these tests followed Tukey's multiple comparisons.

Finally, the quantification results of primary cell cultures were subjected to the Kruskal-Wallis test, and the Dunn test was used for multiple comparisons.

All statistical differences were considered significant at the $p < 0.05$ level. The statistical calculations were performed using GraphPad Prism 8 software (San Diego, CA, USA).

IV. RESULTS

1. *In vitro* assessment of protein-based biofilms

The biomaterial candidates for corneal scaffolds aim to imitate the native cornea and must meet the requirements for the main corneal functions. They should be biocompatible and biodegradable, provide optical properties similar to those of the native tissue and have the ability to biointegrate by stimulating cell growth, proliferation, and migration.

The aim of this section was to assess the suitability of four protein-based biomaterials for use as corneal scaffolds *in vitro*. This evaluation is a crucial first step in developing new materials that can interact effectively with native tissues. The biofilms studied were based on porcine collagen (COL), soy protein isolate (SPI), fish gelatine crosslinked with lactose (GEL-LAC) and fish gelatine crosslinked with citric acid (GEL-CA), all of which were of animal or plant protein origin. COL and SPI films were obtained by compressing the blends in a laboratory press. Gelatine-based blends (GEL-LAC and GEL-CA) were poured into Petri dishes and left to dry for 48 hours at room temperature to obtain the films.

1.1. Physicochemical and morphological analysis

Attenuated total reflectance Fourier transform infrared (ATR-FTIR) spectroscopy was used to identify the characteristic functional groups of the chemical structures of the films. Chemical functional groups absorb infrared radiation at specific wavenumbers (cm^{-1}) due to the characteristic vibrations of their bonds and groups of bonds.

An amide bond is a chemical bond that joins an amino group (-NH_2) and a carboxyl group (-COOH). The peptide bond, which is an amide bond, determines the structure of a protein. To determine the structure of a protein, the infrared absorption peaks of amide I (1600-1800 cm^{-1}), amide II (1470-1570 cm^{-1}), amide III (1240-1350 cm^{-1}), and amide A (3300-3500 cm^{-1}) are used.

ATR-FTIR spectra of all films presented in figure IV.1 indicated a wide band between 3000-3500 cm^{-1}, attributed to free and linked O-H and N-H groups (amide A). The absorption peak at 2931 cm^{-1} was associated with CH_2 asymmetric stretching (**a** of the figure IV.1).

Principal absorption bands of proteins were associated with C=O stretching at 1635 cm^{-1} (amide I), N-H bending at 1545 cm^{-1} (amide II) and C-N stretching and N-H bending (amide III) at 1241 cm^{-1} (**b** of the figure IV.1). The absorption bands of glycerol, a plasticiser added to the films, appeared within the range of 800 cm^{-1} to 1155 cm^{-1}. Specifically, the absorption band located at 1051 cm^{-1} represented the stretching of the C-O bond. Concerning the crosslinking agents, the bands related to lactose were detected within the range of 953 to 1180 cm^{-1}. Correspondingly, the bands related to the carboxylic groups of citric acid were observed at 1743 cm^{-1}. The band vanished after the reaction of citric acid with gelatine, causing the gelatine band at 1545 cm^{-1} to shift to 1585 cm^{-1} due to the crosslinking reaction.

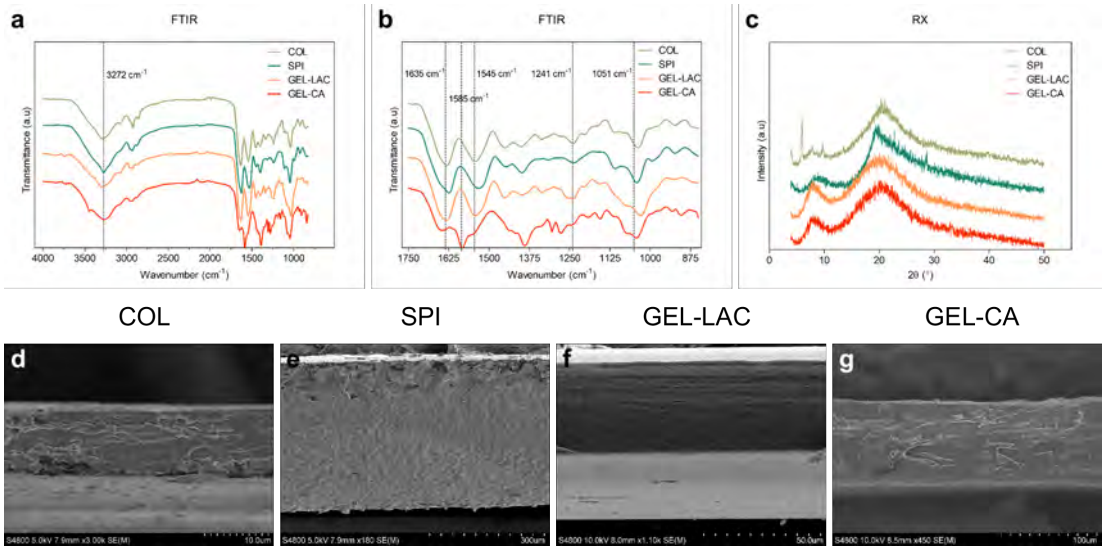

IV.1. FIGURE: FTIR spectra of the films **a**) from 4000 to 850 cm^{-1} and **b**) from 1750 to 850 cm^{-1}. X-ray diffraction patterns of films (**c**). SEM image sections of the films obtained with 3000 (**d**), 180 (**e**), 1100 (**f**), and 450× magnification (**g**). COL, collagen; SPI, soy protein isolate; GEL-LAC, lactose-crosslinked gelatine; GEL-CA, citric acid-crosslinked gelatine.

X-ray diffraction analysis (XRD) and scanning electron microscopy (SEM) were used to investigate the films' structure and its correlation with the measured physicochemical properties. XRD analysis identifies both crystalline and amorphous phases of the biofilms. These films are polymers with series of long chain molecules that can be arranged in two ways: crystalline, where their chains are orderly organised and oriented, or amorphous, where they are randomly packed with no discernible order. Although a polymer can be entirely amorphous, it can never be entirely crystalline. Instead, it will always contain regions that are partially amorphous.

c of the figure IV.1 showed that the COL films exhibited a XRD pattern characteristic of partially crystalline materials. The peak at 2θ = 7° indicated an intermolecular lateral packing distance between the molecular collagen chains, while the broad diffuse peak at 2θ = 20° was due to the diffuse scattering of collagen fibres, representing the amorphous structure of the films.

The diffraction pattern of SPI films showed a dominant amorphous halo with a broad band having a maximum at 2θ = 20°. This is characteristic of SPI, which has 7S and 11S amorphous globulins as its main components. GEL-LAC films showed two diffraction peaks: one at 21°, which was related to the crystallinity of gelatine, and another at 7.4°, which corresponded to the residual triple helix from native collagen. Similarly, the GEL-CA gelatine films displayed the gelatine peak at approximately 21° and a distinct diffraction peak corresponding to the triple-helix at a 2θ value of around 8°.

SEM analysis (**d-g** of the figure IV.1) demonstrated that all films had a tightly packed and consistent structure. The lateral arrangement of collagen chains in the COL films, as revealed by XRD analysis, was translated into a dense fibrillar structure in the SEM analysis. Conversely, the reduction in triple helix content in the gelatine films resulted in a less distinct fibrous morphology.

1.2. Light transmittance and transparency

The cornea plays a crucial role in transmitting incident light, accounting for over 60% of the eye's total refractive power. This function is closely related to its characteristic transparency. The orderly arrangement of collagen fibrils in addition to the thinness, morphology and distribution of keratocytes in the stroma, makes the cornea a transparent tissue. This organisation produces destructive interference from scattered light, which enhances light transmission. Therefore, corneal substitutes must transmit this amount of light, which is why it is so important to measure the optical properties of the selected materials.

The biofilms' direct transmittance and transparency were measured in both dry and hydrated forms. The former served as a control, while the hydrated versions represented their state on the corneal surface.

The films made of COL (**a** of the figure IV.2) and SPI (**b** of the figure IV.2) showed the lowest transmittance values, with the dried films being more translucent than the hydrated films. The disparities in light transmission values between dried and hydrated SPI films diminished with increasing wavelengths and from 620 nm onwards, the disparities were no longer statistically noteworthy. However, the dehydrated COL film transmitted approximately 30% more light than the hydrated counterpart across the full visible spectrum. In both dried and hydrated SPI films, as well as in dried COL films, approximately 60-80% of light was transmitted across almost all wavelengths of the visible spectrum. However, the photographs revealed blurred patterns, indicating that these films were translucent and allowed the passage of light but did not permit clear focus on objects placed at a specific distance (**e, f, i, j** of the figure IV.2).

Once hydrated, gelatine films exhibited higher light transmission. GEL-LAC film was the film that transmitted the highest amount of light and light transmission in both hydrated and dried GEL-LAC forms hardly fluctuated (**c** of the figure IV.2). Transmission dwindled to just 3% near the UV-A region (315-400 nm), which suggested a potentially beneficial protective effect against this particular form of radiation. The transmission of light remained low in the wavelengths close to the UV-A region but increased rapidly as it moved towards the yellow (570-580 nm), orange (580-620 nm), or reddish (620-780 nm) regions. The crosslinking method utilised in this film resulted in a yellowish tonality in comparison to the other films, however, its exceptional transparency remained unaffected. The patterns captured in the photographs were legible and distinct (**g, k** of the figure IV.2).

The GEL-CA films exhibited the highest increase in light transmission after hydration. Their transparency increased by approximately 20% across the entire visible spectrum, allowing over 80% of the incident light from 500 nm onwards to be transmitted (**d** of the figure IV.2). This improvement corresponded to an increase in transparency, as the hydrated film exhibited a clear and recognisable pattern (**h, l** of the figure IV.2).

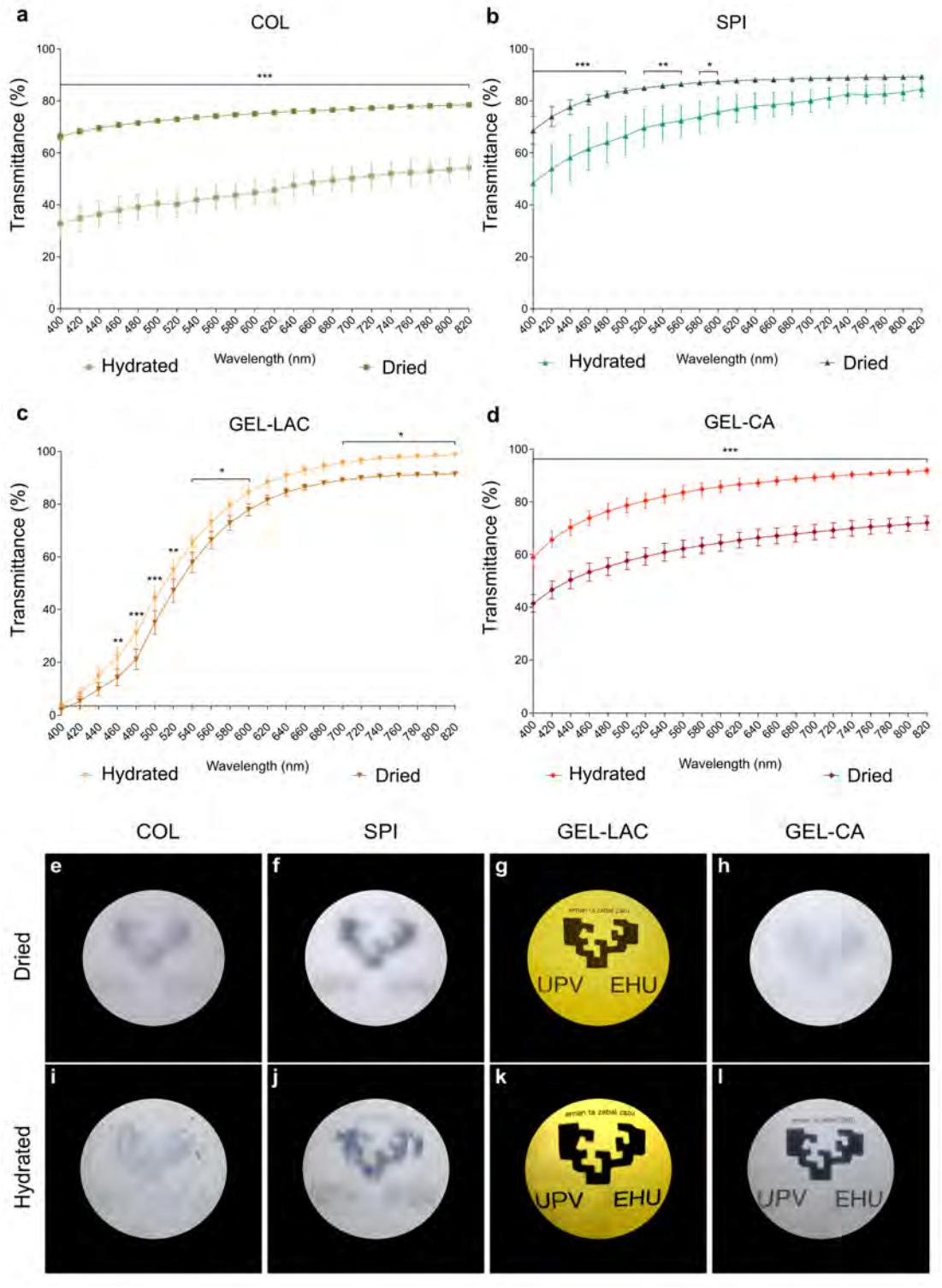

IV.2. FIGURE: Light transmittance spectra and transparency differences of dried and hydrated films. The graphs show the percentage of light transmitted by each film in the visible spectrum (**a-d**). Data are presented as the mean percentage of transmittance ± standard deviation (SD). Statistically significant differences indicate variations between the dried and hydrated states of each film ($* p < 0.05$, $** p < 0.01$, $*** p < 0.001$; $n = 9$). The figures **e-l** illustrate the transparency level of each film when placed at a distance of 12 cm from a specific pattern for both dried (**e-h**) and hydrated (**i-l**) films. All the images were taken of the same pattern and with the same conditions.

1.3. Biodegradability

The *in vitro* degradation assay demonstrated the response of the films to collagenase A enzyme, phosphate-buffered saline (PBS), or deionised water. After 15 minutes of immersion in the enzymatic solution, complete degradation of COL films occurred, possibly as a result of its solely physical crosslinking. This extensive degradation displayed noteworthy statistical differences in comparison to the control (degradation profile in deionised water, **a** of the figure IV.3). The degradation pattern was similar for both PBS and deionised water solutions; however, statistically significant differences were observed at various time points ($p < 0.001$ at 15 min, 4 h, and 24 h; $p < 0.01$ at 1 h; and $p < 0.05$ at 2 h). Deionised water caused a greater weight loss than PBS.

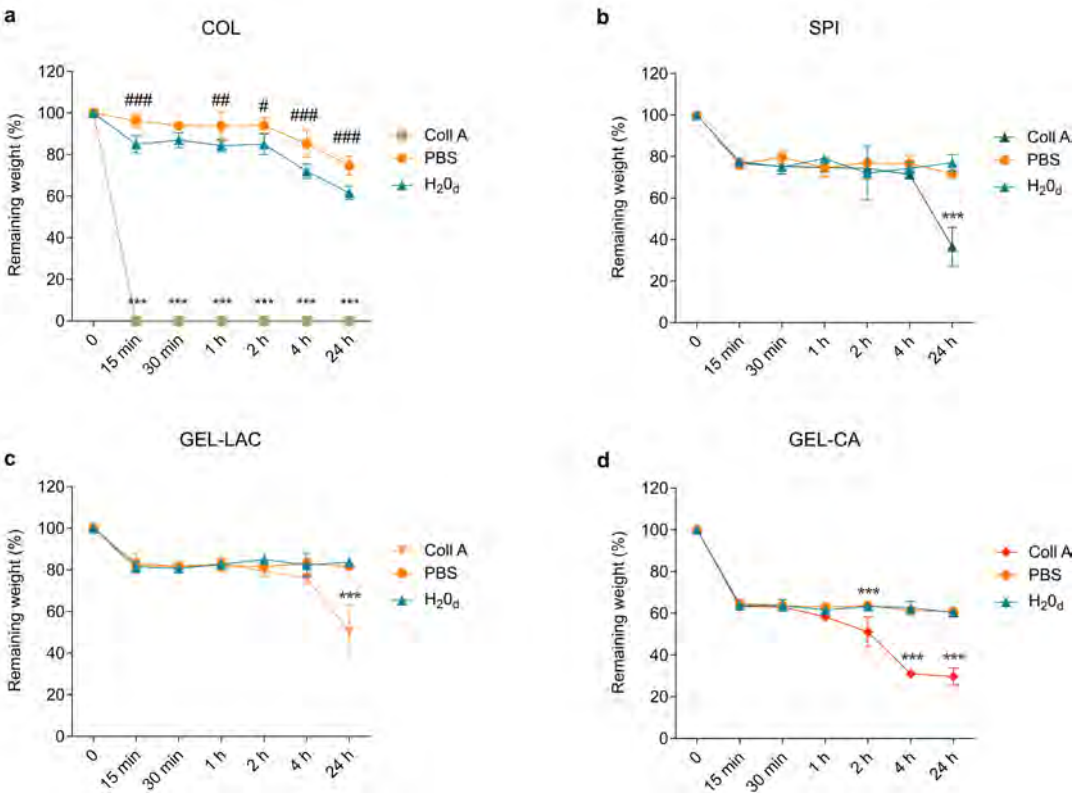

IV.3. FIGURE: *In vitro* degradation profiles of the films immersed in 200 μg/ml collagenase A solution or PBS at 37 °C over time. Films immersed in deionised water at 37 °C were used as control. **a**) Represents the degradation profiles of COL films, **b**) the degradation profiles of SPI films, **c**) the degradation profiles of GEL-LAC films and **d**) the degradation profiles of GEL-CA films. Data are reported as means ± SD, and statistically significant differences of films in collagenase A (∗) and PBS (#) are reported with respect to those in deionised water. ∗, # $p < 0.05$, ∗∗, ## $p < 0.01$, ∗∗∗, ### $p < 0.001$; n = 3.

A comparable decline pattern was observed for SPI, GEL-LAC, and GEL-CA films, as depicted in **b-d** of the figure IV.3. A rapid weight decrease was noticed within 15 minutes upon exposure to collagenase A, PBS, or deionised water. The weight of SPI and GEL-LAC films remained at approximately 70% and 80% during subsequent time points. The control showed significant differences only after 24 hours of enzymatic degradation, during which weight percentages decreased to 40% and 50%, respectively. Regarding the films made from GEL-CA, their weight was decreased by up to 60% after exposure to the three solutions for 15 minutes. This weight percentage was then constant until the 2-hour time point. The impact of collagenase A became significantly evident in relation to the hydrolysis caused by deionised water and PBS after 2 hours, when only 30% of the initial weight remained. There were no significant differences in weight loss between the control and PBS solution in the other films, compared to the COL films. The GEL-LAC films experienced the least weight decrease in the presence of the enzyme, followed by SPI, GEL-CA, and COL films. The degradation differences between the gelatine films emphasised the relevance of the employed crosslinking agent.

1.4. Cell proliferation and viability

Cell proliferation was examined at 0, 24, 48, and 72 hours in both NIH-3T3 fibroblasts and human corneal epithelial (HCE) cells, which were seeded in direct contact with the films. Positive control wells containing fresh medium but no biomaterials were also employed. The results related to 3T3 cultures indicated that all wells conditioned with the studied films showed an increase in cell proliferation over time similar to that of the control culture. However, the wells conditioned with collagen films exhibited a significantly lower proliferation rate compared to all other conditions (Figure IV.4).

Although viability values reaching approximately 70% were recorded wtih COL at 24 hours when compared to the control group, the exposure of the cells to this film in the subsequent time points resulted in a mild to moderate cytotoxic effect. Statistically significant differences were observed between the control group and the COL-conditioned cell culture at 48 and 72 hours resulting in an average metabolic activity of 40% and 50%, respectively.

Viability values for 3T3 cultures in contact with SPI, GEL-LAC, and GEL-CA films remained above 70% throughout the observation period. Viability was 82%, 89% and 73% at 72 hours for SPI, GEL-LAC, and GEL-CA films, respectively, compared to the control.

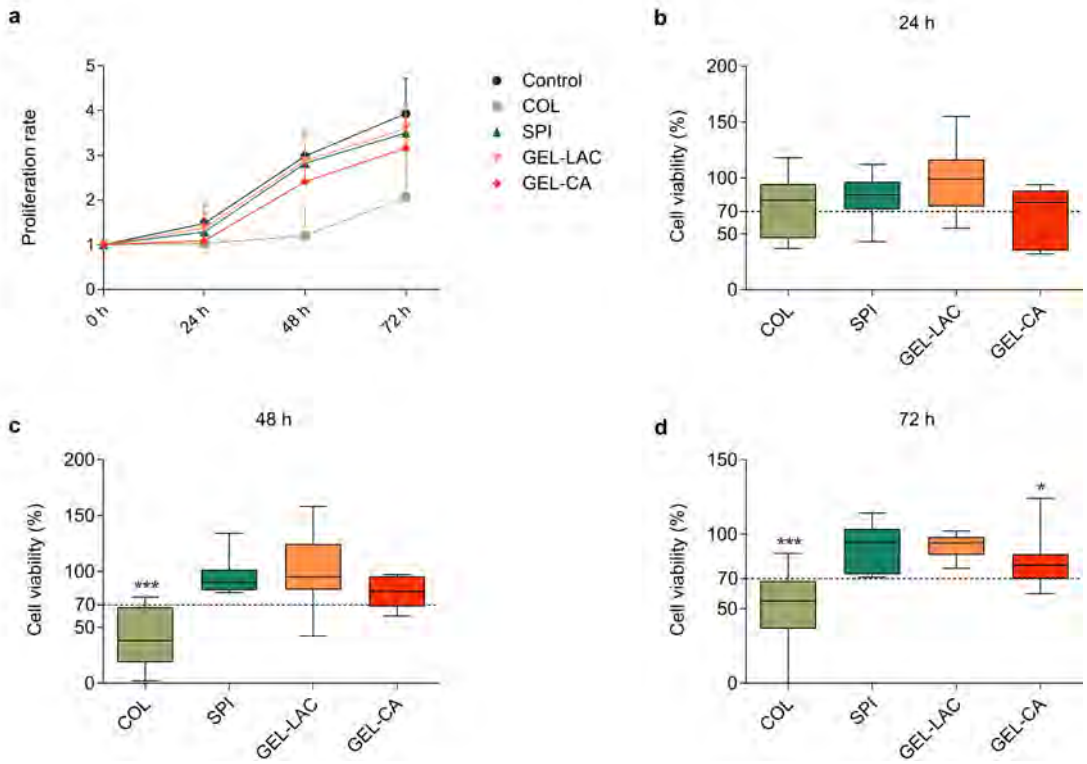

IV.4. FIGURE: Effects of film composition on the **a**) proliferation and **b-d**) viability of NIH-3T3 cells. Cells seeded in p96-well plates were exposed to each film for 24, 48, and 72 h. Cells seeded on wells without any biomaterial were used as controls. Proliferation results are represented as the proliferation rate mean ± SD of viable cells compared with viable cells at t = 0 h. Viability results are expressed as percentages of viable cells in relation to control wells (100% viability). The lines drawn inside each box represent the medians of viability values of each film. Statistically significant differences showed differences with respect to control (∗ $p < 0.05$, ∗∗ $p < 0.01$, ∗∗∗ $p < 0.001$; $n = 9$).

The results regarding HCE cultures displayed a time-dependent proliferation pattern (Figure IV.5). The HCE-containing wells that were conditioned with COL films had better proliferation patterns and higher values of viability compared to the 3T3 cultures. The viability was extensively above 70% in all instances for collagen films, except at 72 h time-point, when a median value of 60% of viability was recorded. The viability recorded for SPI, GEL-LAC, and GEL-CA was around 70% in all time points. The wells conditioned with GEL-LAC films were the only ones that did not show statistically significant differences with respect to the control at 72 h.

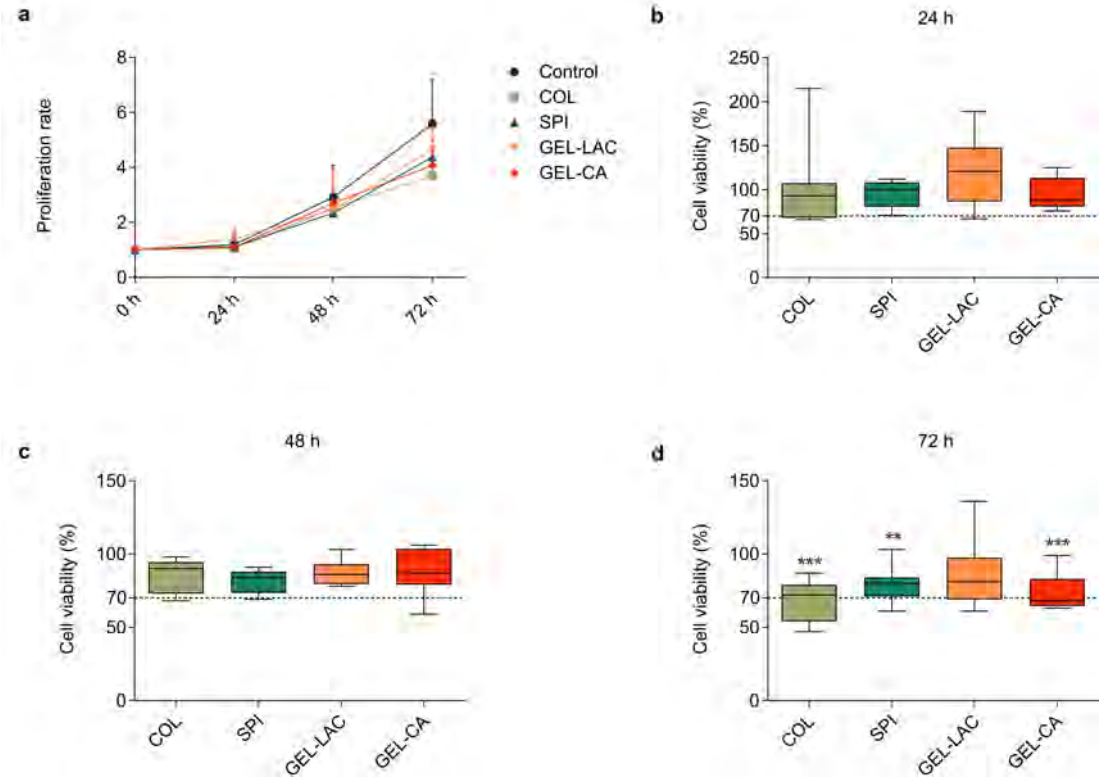

IV.5. FIGURE: Effects of film composition on the **a**) proliferation and **b-d**) viability of human corneal epithelial (HCE) cells. Cells seeded in p96-well plates were exposed to each film for 24, 48, and 72 h. Cells seeded on wells without any biomaterial were used as controls. Proliferation results are represented as the proliferation rate mean $\pm$ SD of viable cells compared with viable cells at t = 0 h. Viability results are expressed as percentages of viable cells in relation to control wells (100% viability). The lines drawn inside each box represent the medians of viability values of each film. Statistically significant differences showed differences with respect to control ($*$ $p < 0.05$, $**$ $p < 0.01$, $***$ $p < 0.001$; n = 9).

1.5. Cell adhesion

Cell adhesion and cytocompatibility of films were examined by observing cell cultures by a phase contrast microscope, conducting the Calcein AM-Ethidium homodimer-1 (EthD1) live/dead assay at different time points (24, 48, and 72 hours) by fluorescence microscopy, and by SEM images.

The 3T3 cells cultured on SPI, GEL-LAC, and GEL-CA films demonstrated similar cell morphology to the control culture, displaying the typical bi- and multipolar branched morphology of fibroblasts (**a-d** of the figure IV.6). Concerning the arrangement of cells on the films, both SPI and GEL-LAC films displayed a flat and elongated monolayer configuration similar to the control group. In contrast, GEL-CA films showed cell clustering instead of a monolayer configuration.

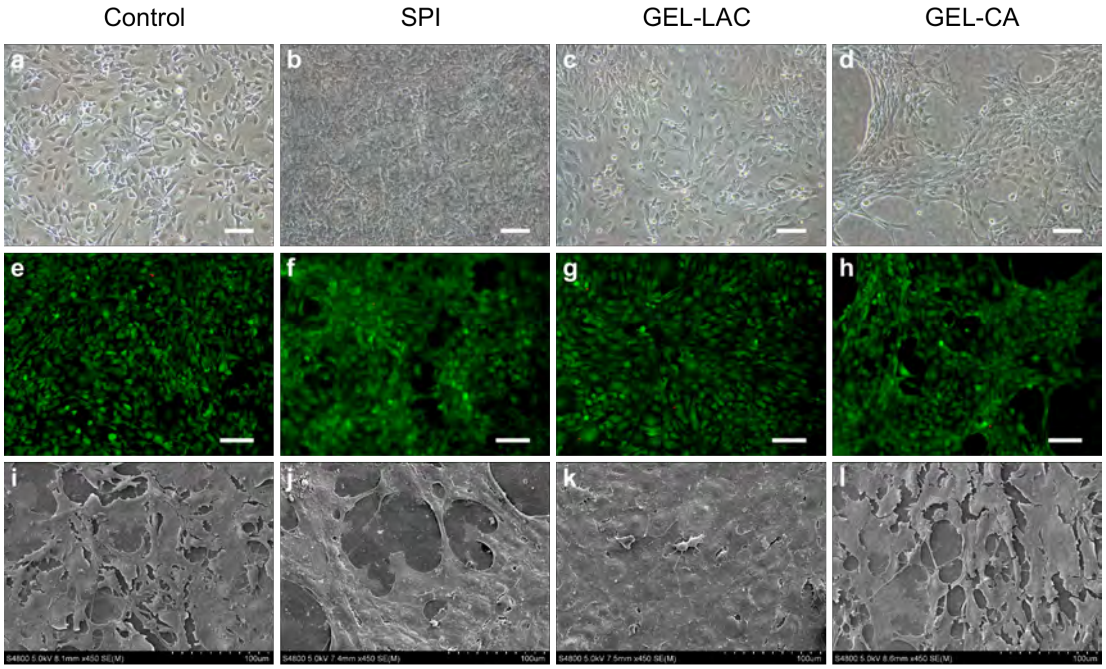

IV.6. FIGURE: Culture of 3T3 cells above the films. Contrast phase microscopic images of 3T3 cells on tissue culture well plate (control) and the films after 24 h of cell seeding (**a-d**). Representative Calcein AM-EthD1 live/dead assay images (**e-h**) and SEM images (**i-l**). **a-h**) Images taken with 10× magnification; scale bars correspond to 100 μm. **i-l**) Images taken with 450× magnification.

The live/dead Calcein AM-EthD1 assay showed minimal cell death on the films, with only approximately 1-5% of the adhered cells being stained with EthD-1 (**e-h** of the figure IV.6). Values were maintained for 72 hours. SEM images revealed a flat and stretched arrangement of cells across the films. At high magnification, there were no significant morphological differences observed among the different samples (**i-l** of the figure IV.6).

Morphological variations were observed in HCE cells seeded on different films (**a-d** of the figure IV.7). The corneal epithelial cells displayed the usual cobblestone-like arrangement in the control group and on the GEL-LAC film, whereas the cells seeded on SPI and GEL-CA films had more stretched and rounded shape. Similarly, the polygonal outline of cells observed in the control culture and GEL-LAC films was less apparent. Few dead cells were observed above the films on Calcein AM-EthD1 live/dead assays carried out at 24, 48, and 72 hours, as observed in **e-h** of the figure IV.7. The differences in morphology of HCE cultures were noticeable by phase contrast microscopy and these were further confirmed using Calcein AM staining. These cells exhibited larger cell volume and were not as flat as 3T3 fibroblasts, as discernable from SEM observations.

No differences were observed between the control wells and the cells seeded on the different films (**i-l** of the figure IV.7). A stratified arrangement of the cells was visible in all conditions.

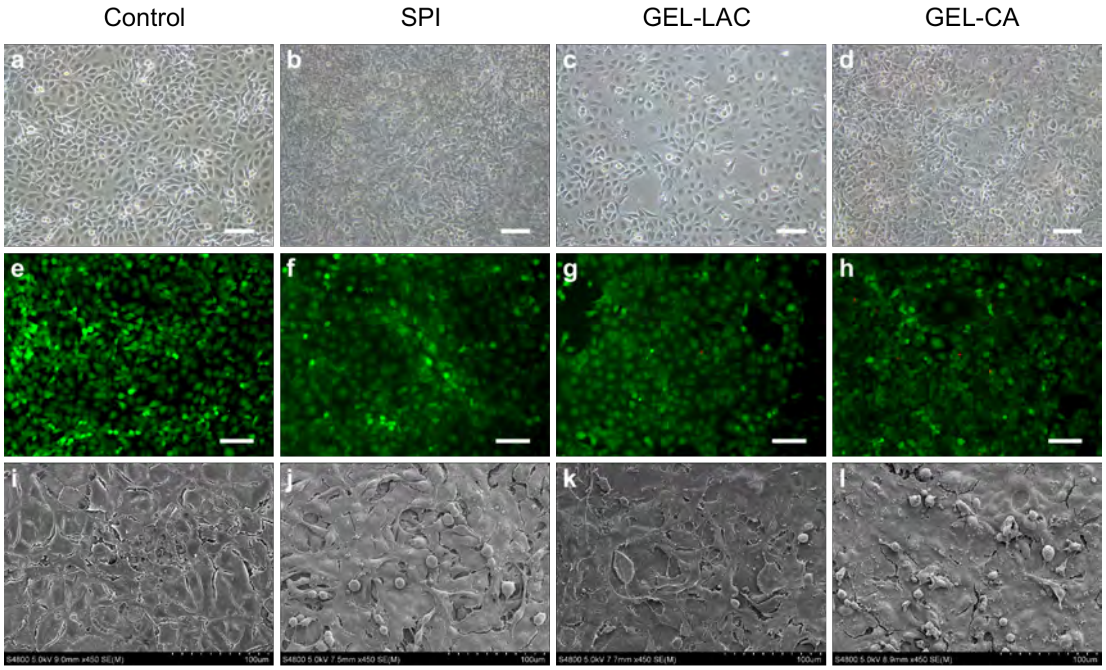

IV.7. FIGURE: Culture of HCE cells above the films. Contrast phase microscopic images of HCE cells on tissue culture well plate (control) and the films after 24 h of cell seeding (**a-d**). Representative Calcein AM-EthD1 live/dead assay images (**e-h**) and SEM images (**i-l**). **a-h**) Images taken with 10× magnification; scale bars correspond to 100 μm. **i-l**) Images taken with 450× magnification.

Regarding both cell types, cell cultures were clearly observed in GEL-LAC films under phase contrast microscope. However, it was not feasible to align the cells on the same plane within a particular quadrant of the SPI and GEL-CA films in some cases because of surface irregularities. It proved impossible to cultivate any type of cell on COL films due to poor adhesion, resulting in cell death and subsequent removal via PBS washes.

1.6. Cell migration

The migratory capacity of both types of cells on the films was evaluated by creating a gap free of cells and measuring the time required for the gap to close at 0, 24, 48, and 72 hours. Technical duplicates conducted on each film type revealed the potential for cellular migration on biomaterials for both cell types. The closure of gaps was quicker with 3T3 cells compared to HCE cells. In both cases, the cells seeded on GEL-CA required more time for closing gaps compared to other tested cells.

Nevertheless, the cell-free area was covered by all cultures within 72 hours (Figure IV.8). As was the case with adhesion assays, none of the cell types could be cultivated in COL films.

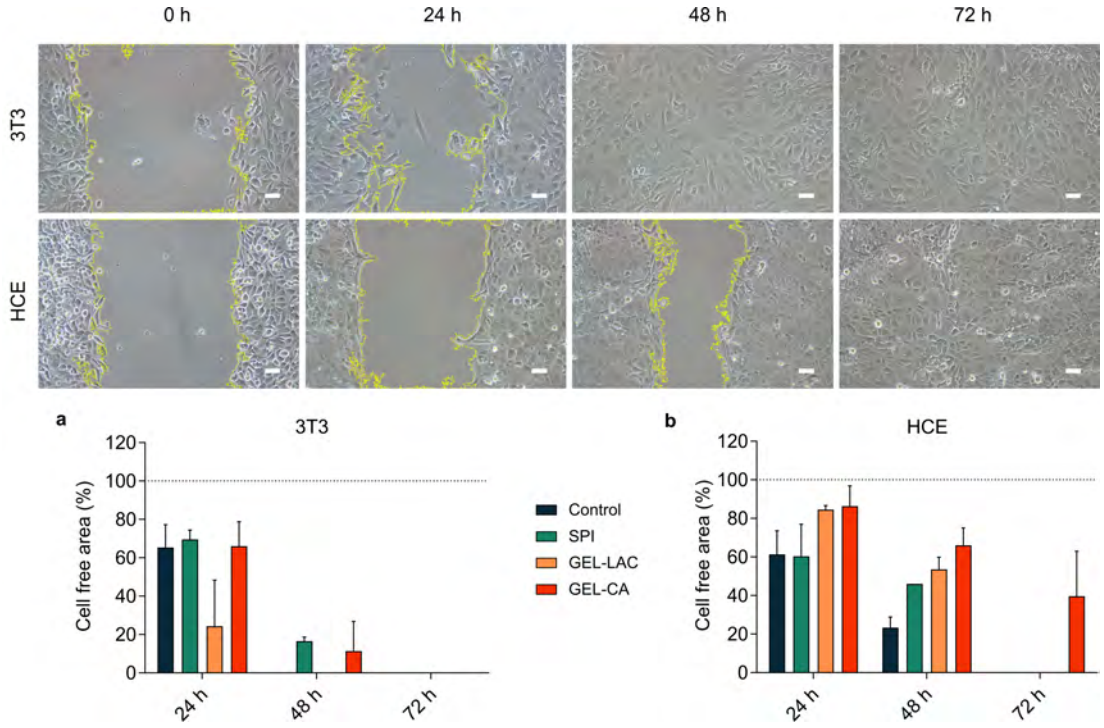

IV.8. FIGURE: Migration assay of HCE and 3T3 cells seeded above GEL-LAC after 24, 48, and 72 h. Images taken with 10 × magnification; scale bars correspond to 50 μm. Data in **a**) and **b**) represent the evolution of the gap closure by 3T3 (**a**) and HCE (**b**) cells in each film. No significant differences were recorded.

2. *In vitro* assessment of gelatine hydrogel

After testing various protein-based biomaterials in film conformation, gelatine was chosen as the starting material to develop a hydrogel that could act as a filler for corneal defects. Riboflavin phosphate (RFP) was selected as the hydrogel's crosslinking agent, a photocrosslinker widely used in clinics.

The physicochemical properties and the *in vitro* biocompatibility were assessed with different versions of the gelatine and RFP-based hydrogel, to each of which a different compound was added. The study employed four distinct hydrogels: The hydrogel referred as G, composed of 5% w/v gelatine and 0.01% w/v of RFP; the hydrogel named as G-D, synthetised with 5% w/v gelatine, 0.01% w/v of RFP and 2.5% w/v dextran (D); the hydrogel designated as G-HA, containing 5% w/v gelatine, 0.01% w/v of RFP and 0.4% w/v hyaluronic acid (HA); and the hydrogel referred as G-MC, composed of 5% w/v gelatine, 0.01% w/v of RFP and 1% w/v methyl cellulose (MC).

2.1. Rheological measurements

Shear rheology was used to characterise the viscoelastic, yielding and flow properties of the four versions of the hydrogel.

The amplitude sweep was used to describe the deformation behaviour of samples within the linear viscoelastic regime (LVR), the region where the test can be carried out without destroying the sample's structure. Its purpose is to determine the limit amount of deformation required for the internal structure to soften, start to flow or break. These measurements are obtained by changing the amplitude of the oscillatory signal over time while keeping the frequency constant. The frequency sweep is used to indicate the time-dependent behaviour of a sample within the LVR. Higher frequencies simulate fast motion at short times, while lower frequencies simulate slow motion at long times or at rest. In frequency sweeps, the oscillation frequency gradually increases or decreases over time while keeping the amplitude constant. The storage modulus G' represents the elastic part of the viscoelastic behaviour, describing the solid-like behaviour of the sample. The loss modulus G'' characterises the viscous part of the viscoelastic behaviour, which can be considered as the liquid-like performance of the sample.

The solid and liquid-like properties of the hydrogels were assessed through oscillatory amplitude and frequency sweeps.

Dynamic amplitude sweeps, conducted at a frequency of 10 rad/s, determined the yielding behaviour of the hydrogels and large LVR. For these hydrogels, the LVR could be deemed from 0 to roughly 100% strain values, wherein G′ and G″ displayed a plateau value, with G′ being higher than G″ in all instances. This indicated that all the hydrogels possessed a gel-like structure, demonstrating more of a solid's behaviour rather than that of a liquid within this regime. G hydrogel did not yield until stress values of approximately 250 Pa were attained. G-D, G-HA and G-MC displayed yield stresses of about 50 Pa, 500 Pa and 1800 Pa, respectively, at the crossover point of G′ and G″ (**a** of the figure IV.9).

These results suggested that a minimum threshold of stress was mandatory for all hydrogels to undergo flow but the inclusion of HA and MC increased this required stress level.

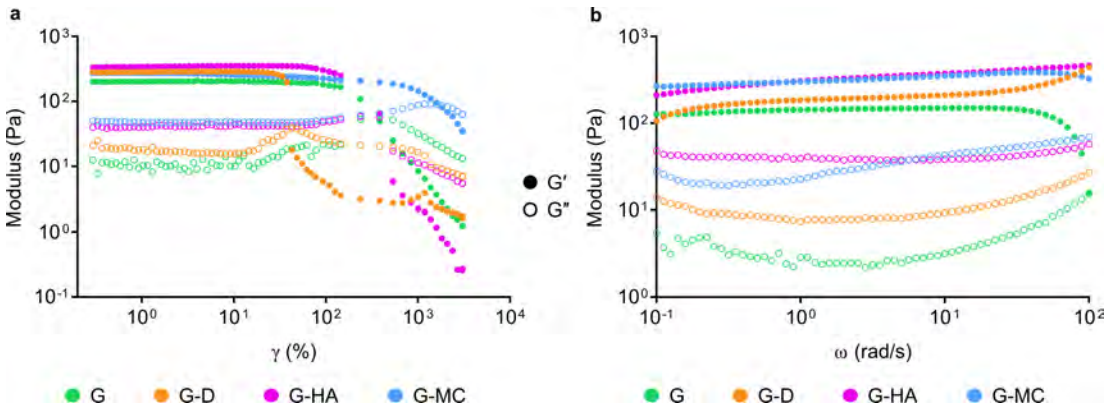

IV.9. FIGURE: **a**) Strain-dependent (angular frequency (ω) = 10 rad/s, 25 °C) and **b**) frequency-dependent (strain (ε) = 1%, 25 °C) oscillatory shear rheology of G, G-D, G-HA and G-MC hydrogel formulations.

Frequency-dependent oscillatory shear experiments conducted within the linear viscoelastic regime indicated that the frequency responses of G, G-D, G-HA, and G-MC hydrogels showed no significant difference. The storage modulus (G′) remained higher than the loss modulus (G″) over the entire frequency range assessed, without any crossover, suggesting that the hydrogels had solid-like properties when applied to the eye (**b** of the figure IV.9).

Frequency and amplitude sweeps were conducted on the hydrogels after being crosslinked with blue light to mimic their performance when applied to the corneal wound.

Flow sweeps were carried out to characterise the general flow performace of the samples. Shear-rate sweeps conducted on the hydrogels revealed a shear-thinning behaviour and shear dependent viscosities in all cases. The viscosity of the hydrogels decreased several orders of magnitude as the shear rate increased from 10^{-4} s^{-1} to 100 s^{-1}, resembling the mechanical conditions during injection (**a** of the figure IV.10). Thus, the results confirmed that all the hydrogels versions were easily injectable.

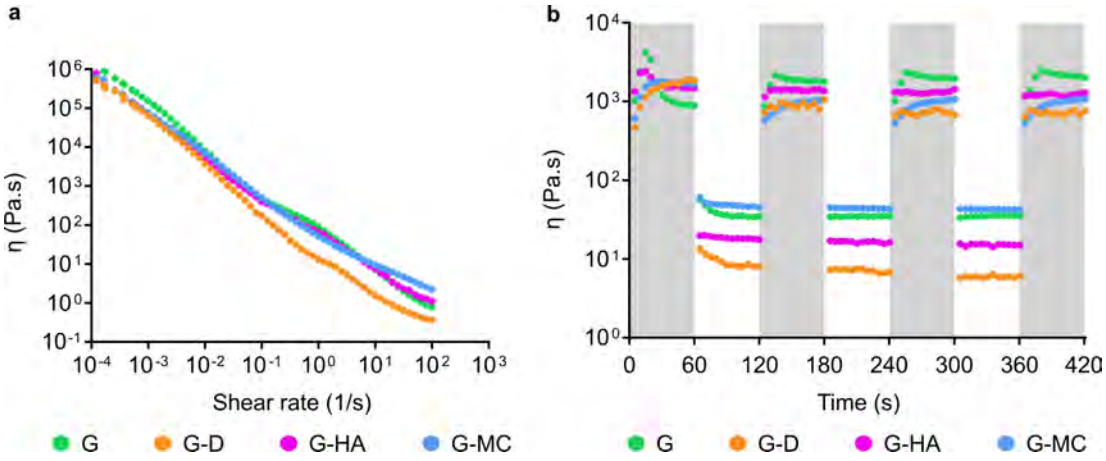

IV.10. FIGURE: **a**) Steady-shear reology of G, G-D, G-HA and G-MC hydrogels demonstrating highly shear-thinning behavior. **b**) Step-shear measurements of G, G-D, G-HA and G-MC hydrogels over four cycles of alternating low shear (gray; 0.1 s^{-1}) and high shear (white; 10 s^{-1}) rates.

The ability of the hydrogels to recover their properties and self-heal was assessed by step-shear measurements. The viscosity of all hydrogels lowered by one and a half to two orders of magnitude during high shear steps (10 s^{-1}), but rebounded to baseline viscosity within 5 seconds after the shear rate decline (0.1 s^{-1}) (**b** of the figure IV.10). Shear-induced thinning and self-healing test simulated the injection mechanism of hydrogels through a needle, where high shear rates would be employed to deposit the hydrogel on the corneal surface. This outcome demonstrated that a viscous hydrogel could be deposited and would persist in the corneal wound, thereby facilitating the controlled release of cargo.

Flow sweeps and step-shear measurements were performed before crosslinking the hydrogel with blue light at room temperature.

Stress-controlled yield stress measurements were also performed before light irradiation at room temperature. Static yield stress values were denoted on the corresponding graph of the figure IV.11.

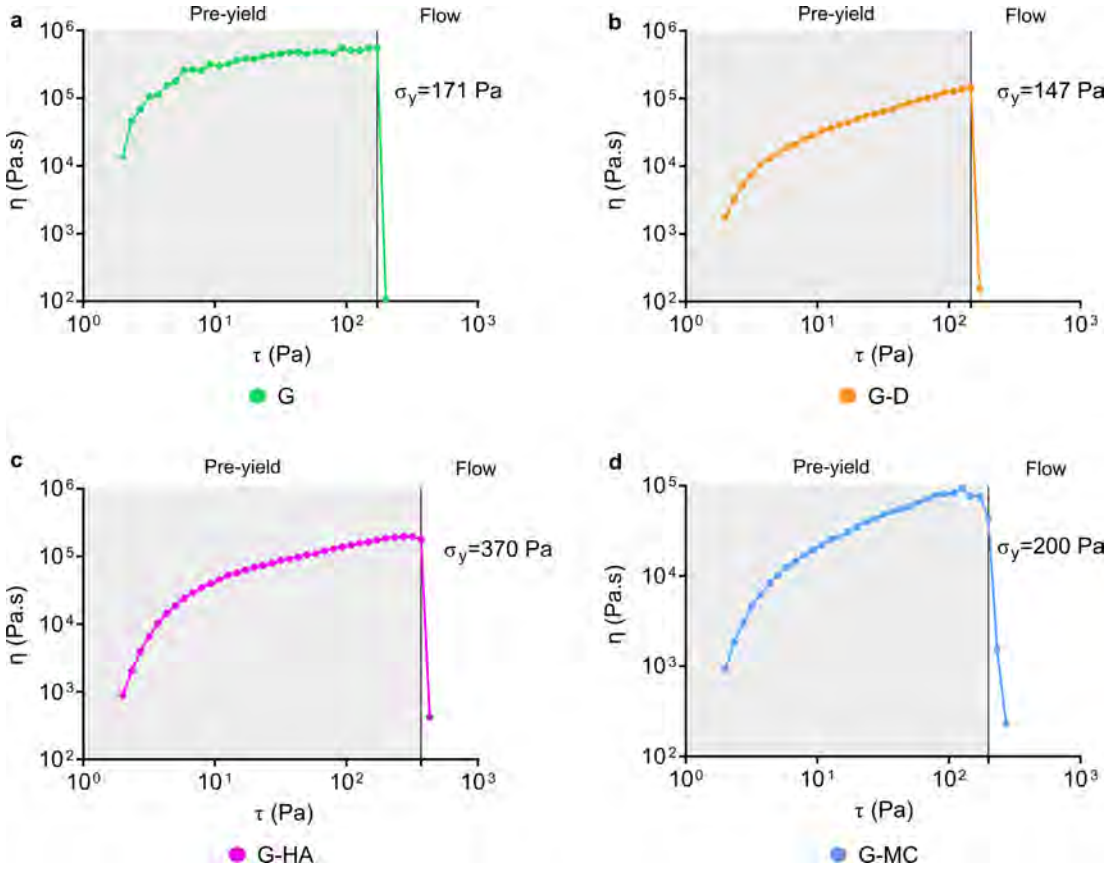

IV.11. FIGURE: Stress-controlled yield stress measurements of **a**) G, **b**) G-D, **c**) G-HA and **d**) G-MC hydrogels were performed from low to high stress with steady-state sensing. Static yield stress values are indicated on the corresponding graphs.

The stress required to initiate flow was higher when HA was added to the hydrogel (**c** of the figure IV.11), indicating that a higher stress would be required to pull the hydrogel through the syringe. The addition of MC also increased the static yield stress value compared to G and produced a more viscous hydrogel (**d** of the figure IV.11). However, G-D had the lowest σ_y value (**b** of the figure IV.11).

2.2. Swelling and expansion measurements

Swelling and expansion experiments were conducted to determine the increase in hydrogels' volume and surface area after immersion in PBS for 24 hours. The fold changes observed in the results were plotted in relation to the initial swelling and expansion values recorded before immersion in PBS (Figure IV.12).

In terms of the volume retained, G-D and G-HA displayed the highest increase, with fold-change values of 1.26 and 1.39 respectively (**a** of the figure IV.12). G hydrogel showed an increase of 1.12, which equaled a 10% increase, while the G-MC hydrogel underwent only a slight change (1.06 fold-change). Nevertheless, there were no statistically significant disparities between the volume retained by G-D, G-HA and G-MC with respect to G.

Regarding the increase in surface area, G hydrogel exhibited a 1.2 fold change, resulting in a 20% increase over its initial area. G-D recorded a 1.85 fold-change increase, G-HA a 2 fold-change increase, and G-MC a 1.74 fold-change increase. Significant differences were observed in the case of G-D and G-HA compared to G, with an increase of 85% and 100%, respectively, which was almost the double of the initial area (**b** of the figure IV.12).

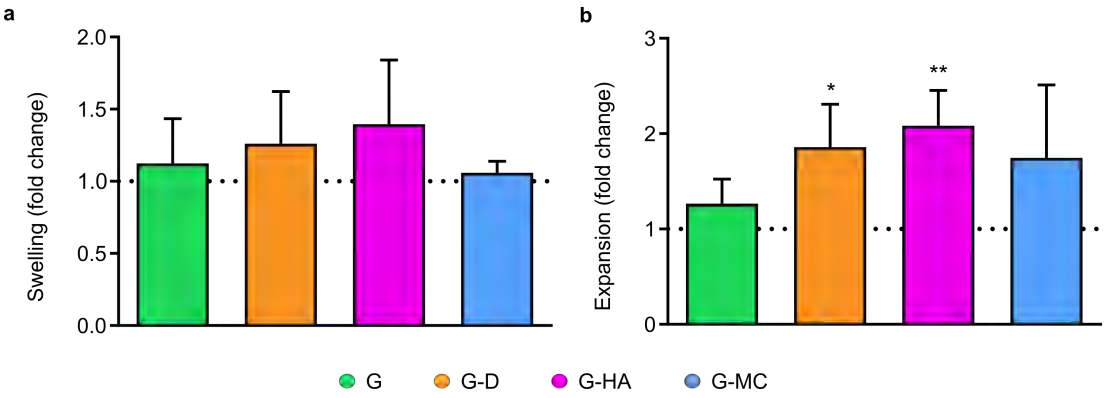

IV.12. FIGURE: **a**) Swelling and **b**) expansion measurements performed in G, G-D, G-HA and G-MC hydrogels 24 h after their immersion in PBS. Results are indicated as average fold-changes ± SD with respect to G hydrogel. Statistical significance is defined as p-value $*$ $p < 0.05$, $**$ $p < 0.01$, $***$ $p < 0.001$, $****$ $p < 0.0001$.

2.3. Light transmittance and transparency

The direct transmittance of the hydrogels before and after crosslinking was measured in the visible spectrum (400-800 nm). Transparency was assessed by placing 500 μl of each hydrogel before and after crosslinking over a recognisable pattern.

G and G-MC hydrogels exhibited the greatest transmittance, recording values of over 90% beyond 500 nm. Moreover, these hydrogels facilitated the clearest and most recognisable visualisation of the patterns positioned behind them (Figure IV.13). The variations in light transmission values for all hydrogels between their crosslinked and non-crosslinked forms showed a decrease as the wavelength increased.

Those differences became undetectable in the G and G-MC hydrogels from 520 nm onwards (**a, d** of the figure IV.13). The pre-crosslinked and the post-crosslinked versions of G-D hydrogel became indistinguishable from 600 nm (**b** of the figure IV.13). Although the differences in the two versions of G-HA remained evident across the complete visible spectrum, they were not statistically significant (**c** of the figure IV.13).

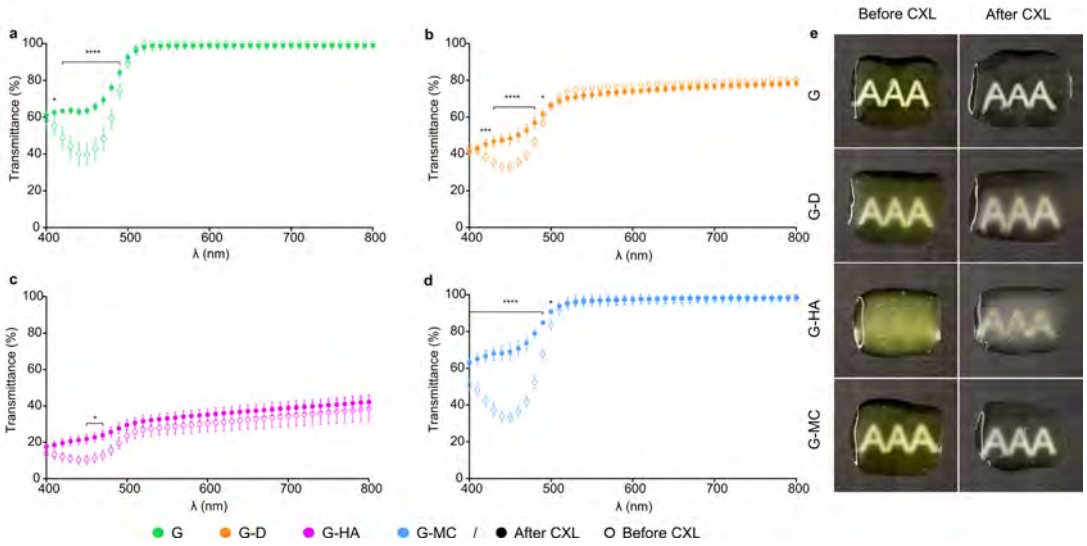

IV.13. FIGURE: Light transmittance spectra and transparency differences of G, G-D, G-HA and G-MC hydrogels before and after crosslinking. **a-d**) Graphs show the percentage of light transmitted by the crosslinked and non-crosslinked version of each film in the 400-800 nm range. Data are presented as the mean percentage of transmittance ± SD. Statistically significant differences indicate variations between the crosslinked and non-crosslinked states of each film (∗ $p < 0.05$, ∗∗ $p < 0.01$, ∗∗∗ $p < 0.001$, ∗∗∗∗ $p < 0.0001$). The figures in **e**) illustrate the transparency level of each hydrogels before and after their irradiation with blue light. The same pattern and the same conditions were used to take all the images.

The highest transmission value for G-D was about 80% starting at 600 nm (**b** of the figure IV.13). Similarly, a small yellow halo and a whitish halo could be observed in the non-crosslinked and crosslinked versions respectively (**e** of the figure IV.13). G-HA, the variant of the hydrogel that transmitted the least amount of light, reached a maximum transmission value of around 40%. This finding was consistent with the blurring effect seen in the corresponding images of **e** in figure IV.13, where the pattern located behind could not be in focus.

Adding RFP to the hydrogel imparted a yellow hue, which did not compromise its transparency. The four graphs showed noticeable differences in wavelengths beside the maximum absorption peak of riboflavin in the blue light spectrum, the wavelength employed by the lamp. This was associated with the absence of the yellowish tinge evident in the **e** of the figure IV.13.

2.4. *In vitro* release assays

The release of 3 different compounds from the four hydrogel versions was compared over the course of two weeks. FITC-IgG, FITC-Albumin, and Vigamox compounds were introduced within the hydrogels to observe their release kinetics and characterise the hydrogels' performance. These compounds represented high (150 kDa), medium (66 kDa), and low (0.44 kDa) molecular weight molecules, respectively.

FITC-IgG and FITC-Albumin release amounts were registered by fluorescence measurements conducted with 485-520 excitation and emission wavelengths. Vigamox release was computed by measuring the absorption at 290 nm. The outcomes were computed by incorporating a standard curve in the measurement of each compound. The concentration value at each time point was added to the previous concentration measurement. At the beginning of the experiment (t = 0 h), the concentration of each encapsulated compound was considered 100% and the percentage represented at each subsequent time point was calculated relative to this value. Four replicates were analysed for each treatment and compound released.

IgG release in either hydrogel formulation occurred progressively, with a tendency to reach a plateau from day 10 onwards. G hydrogels yielded half-life of release after the first week of the study (49% $\pm$ 4.4%), whereas G-D, G-HA and G-MC hydrogels released 36% $\pm$ 1.5%, 41% $\pm$ 3.9% and 37% $\pm$ 0.9% of the cargo respectively (**a** of the figure IV.14). Significant differences were observed between G-D and G-MC hydrogels and the control G at different time intervals (Table IV.1). For G-D, G-HA, and G-MC, important differences were observed up to day 1 when compared to hydrogel G. However, for G-HA, these differences were no longer observable from the third day of the study onwards.

Regarding Albumin release, G-HA and G-MC reached half-life release at day 3. G hydrogel released half-life of the cargo on the fourth day, while the hydrogel composed of G-D reached it on day 6. Unlike IgG, there was no plateau in the release kinetics of this compound and all hydrogels except G-D released 100% of the content after two weeks (**b** of the figure IV.14). Significant variations were observable among all three hydrogel versions (G-D, G-HA, and G-MC) in comparison to G at distinct time points (Table IV.1).

Vigamox demonstrated near-total cargo retention and minimal burst release. Two weeks later, the amount of released content did not surpass 35% (G, G-D, G-HA and G-MC hydrogels amounted to 30.16% $\pm$ 1.05%, 30.07% $\pm$ 1.45%, 32.37% $\pm$ 3.28% and 25.93% $\pm$ 0.61%, respectively) (**c** of the figure IV.14). In contrast to IgG and Albumin release, the differences from G were not statistically significant (Table IV.1).

When comparing Albumin and IgG, it was reasonable to expect a faster release of the smaller compound, Albumin, than IgG in all hydrogels. However, Vigamox, which was selected as the small encapsulating compound, exhibited the slowest release rate. The addition of Vigamox to the hydrogel could somehow adhered to the hydrogel structure, thus slowing its release.

IV.1. TABLE: Mean ± SD percentage values of the released amounts for each of the analysed cargoes in G, G-D, G-HA and G-MC hydrogels. Statistical significance is expressed with respect to G (* $p < 0.05$, ** $p < 0.01$, *** $p < 0.001$, **** $p < 0.0001$).

	IgG release				Albumin release				Vigamox release			
Time points	G	G-D	G-HA	G-MC	G	G-D	G-HA	G-MC	G	G-D	G-HA	G-MC
1h	1.58 ± 0.06	1.02 ± 0.04 ****	1.99 ± 0.08 ***	2.38 ± 0.31 *	4.47 ± 0.32	2.46 ± 0.13 ***	6.42 ± 0.34 ***	6.62 ± 0.62 **	1.37 ± 0.42	1.04 ± 0.31	1.22 ± 0.65	1.2 ± 0.47
2h	2.74 ± 0.12	1.9 ± 0.07 ***	3.32 ± 0.09 ***	4.07 ± 0.56 *	7.72 ± 0.35	4.56 ± 0.32 ****	10.7 ± 0.51 ***	10.5 ± 1.08 *	2.81 ± 0.13	1.98 ± 0.08 ***	2.39 ± 0.4	2.29 ± 0.07 **
4h	4.44 ± 0.21	3.23 ± 0.05 **	5.21 ± 0.17 **	5.99 ± 0.75 *	11.93 ± 0.35	7.21 ± 0.48 ****	14.99 ± 1.04 *	15.12 ± 1.25 *	4.01 ± 0.27	3.1 ± 0.31 *	3.35 ± 0.5	3.05 ± 0.21 **
6h	5.9 ± 0.28	4.54 ± 0.05 **	6.88 ± 0.19 **	7.79 ± 0.86 *	15.64 ± 0.23	9.81 ± 0.77 ***	19.32 ± 1.51 *	19.49 ± 1.36 *	5.07 ± 0.34	4.05 ± 0.37 *	4.28 ± 0.76	3.79 ± 0.38 **
8h	7.12 ± 0.31	5.64 ± 0.03 **	8.28 ± 0.25 **	9.29 ± 0.99 *	18.74 ± 0.19	12.06 ± 0.67 ***	23.03 ± 2.15	23.2 ± 1.47 *	6.3 ± 0.77	4.93 ± 0.61	5.21 ± 0.54	4.82 ± 0.07
12h	8.73 ± 0.37	7.09 ± 0.09 **	10.11 ± 0.32 **	11.07 ± 1.04 *	22.76 ± 0.19	15.42 ± 0.83 ***	27.84 ± 2.81	27.89 ± 1.58 *	7.46 ± 0.64	5.92 ± 0.55 *	5.93 ± 0.79	5.63 ± 0.36 *
1d	12.05 ± 0.41	9.76 ± 0.17 **	14.08 ± 0.21 **	14.89 ± 1.08 *	30.17 ± 0.31	20.9 ± 0.78 ****	36.11 ± 3.33	36.11 ± 1.59 **	9.75 ± 0.57	8.35 ± 0.83	8.55 ± 0.64	5.63 ± 0.32 *
2d	17.66 ± 0.57	13.02 ± 0.43 ****	19.03 ± 0.2 *	18.74 ± 0.79	38.42 ± 0.17	27.33 ± 0.82 ***	45.41 ± 3.66	45.6 ± 0.45 ****	12.13 ± 0.9	11.12 ± 0.86	11.15 ± 1.15	10.45 ± 0.23
3d	25.07 ± 1.28	17.49 ± 0.54 ***	24.01 ± 0.4	22.53 ± 0.92 *	46.57 ± 0.32	33.31 ± 1.01 ***	54.83 ± 3.86 *	53.96 ± 1.05 ***	16.06 ± 1.03	14.54 ± 1.48	15.75 ± 1.74	14.28 ± 0.28
4d	33.98 ± 4.85	22.29 ± 0.69 *	29.68 ± 1	26.44 ± 0.78	53.89 ± 0.44	38.87 ± 1.03 ****	65.59 ± 1.94 **	61.22 ± 1.63 **	20.18 ± 1.94	18.61 ± 1.47	19.47 ± 2.52	17.37 ± 0.02
5d	38.99 ± 4.22	26.31 ± 0.62 *	34.06 ± 2.3	30.13 ± 0.69 *	61.04 ± 0.47	44.49 ± 0.86 ****	73.91 ± 2.65 **	68.15 ± 1.27 **	22.87 ± 1.4	21.11 ± 1.44	22.66 ± 2.75	20.46 ± 0.43
6d	44.5 ± 4.39	31.43 ± 0.37 *	37.68 ± 2.61	33.44 ± 0.92 *	68.76 ± 0.96	50.17 ± 0.73 ****	82.74 ± 2.58 **	75.42 ± 1.03 ***	25 ± 1.45	23.69 ± 1.37	25.46 ± 2.71	22.25 ± 0.25
7d	49.11 ± 4.42	36.12 ± 1.52 *	41.45 ± 3.95	37.03 ± 0.93 *	77.1 ± 1.81	55.42 ± 0.77 ****	90.29 ± 2.73 ***	81.85 ± 1.68 *	27.03 ± 0.96	25.93 ± 1.2	27.99 ± 3.02	23.84 ± 0.16 *
10d	55.78 ± 4.73	46.92 ± 3.56	49.22 ± 4.87	41.65 ± 0.86 *	84.9 ± 1.61	64.12 ± 0.86 ****	99.74 ± 0.52 ***	92.17 ± 1.02 **	28.54 ± 0.9	27.96 ± 1.32	30.27 ± 3.08	24.88 ± 0.36 **
15d	63.93 ± 4.68	56.84 ± 1.77	57.02 ± 6.56	48.93 ± 0.9 *	97.47 ± 1.43	75.02 ± 1.81 ****	100 ± 0	100 ± 0	30.16 ± 1.05	30.07 ± 1.45	32.27 ± 3.28	25.93 ± 0.61 **

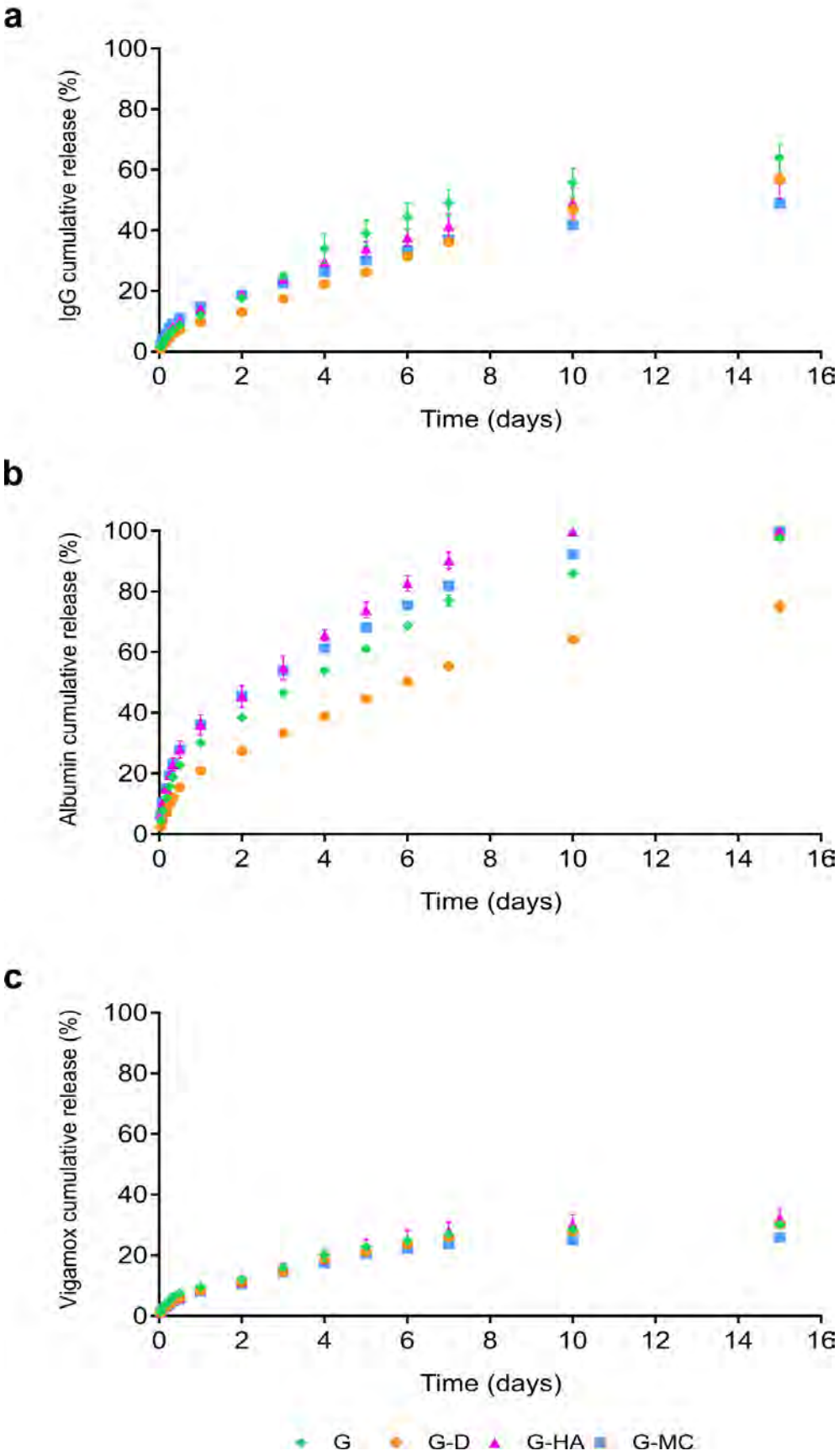

IV.14. FIGURE: **a**) FITC-labelled IgG, **b**) FITC-labelled Albumin and **c**) Vigamox release profiles of G, G-D, G-HA and G-MC hydrogels. The cumulative release was expressed as the normalised percentage of the total amount released over 15-day duration of the experiment.

2.5. Cytocompatibility assesment

The cytocompatibility of the hydrogels was assessed by Calcein AM-EthD1 live/dead viability/cytotoxicity assay kit, counting the number of cells seeded with the hydrogels and analysing their cell cycle. SV-40 immortalised human corneal epithelial (HCE) cells and NIH-3T3 fibroblasts commercial cell lines were used for the study. Both cell types were cultured on culture plates in contact with the corresponding hydrogel type. The cells were initially seeded and allowed to adhere to the plate. Subsequently, 20% of the total volume of medium in each well was replaced with the crosslinked hydrogel. The cultures were then maintained for 72 hours.

The viability of both cell types was almost 99% in all cases, with no statistically significant differences detected between the control and the cultures in contact with the hydrogels (**a, c** of the figure IV.15). Additionally, the cell count was similar to that of the control, with approximately 1 million of cells recorded after 72 hours (**b** of the figure IV.15).

There were no significant differences found between the control and each hydrogel-treated cultures regarding the cell cycle analysis by flow cytometry. The proportion of cells in the different phases of the cell cycle varied depending on the type of cell being investigated. Approximately 66% of NIH-3T3 fibroblasts were observed in the G0-G1 phase, which indicated that the majority of cells were not actively preparing to undergo cell division. They were rather carrying out their normal cellular functions (G0) or synthetising mRNA and proteins (G1). Approximately 11% of the cells were observed in the synthesis phase (S), and 23% were in the growth and preparation for mitosis or during full cell division (G2-M) (**d** of the figure IV.15).

HCE cells showed a higher percentage of cells in synthesis (S), preparing for mitosis (G2), or in cell division (M) compared to 3T3 fibroblasts. Overall, 56% of the total cell population was recorded in the G0-G1 phases, 16% of cells in synthesis (S) and 28% of cells in G2-M phases (**e** of the figure IV.15).

After analysing the rheological properties, transmittance, transparency, cargoes' release kinetics and cytocompatibility of the different hydrogels, it was concluded that only hydrogel G, consisting of 5% gelatine and 0.01% RFP, will continue to be studied.

The addition of dextran, hyaluronic acid, or methyl cellulose did not significantly enhance the properties of the hydrogel, hence the decision to proceed with the simplest composition.

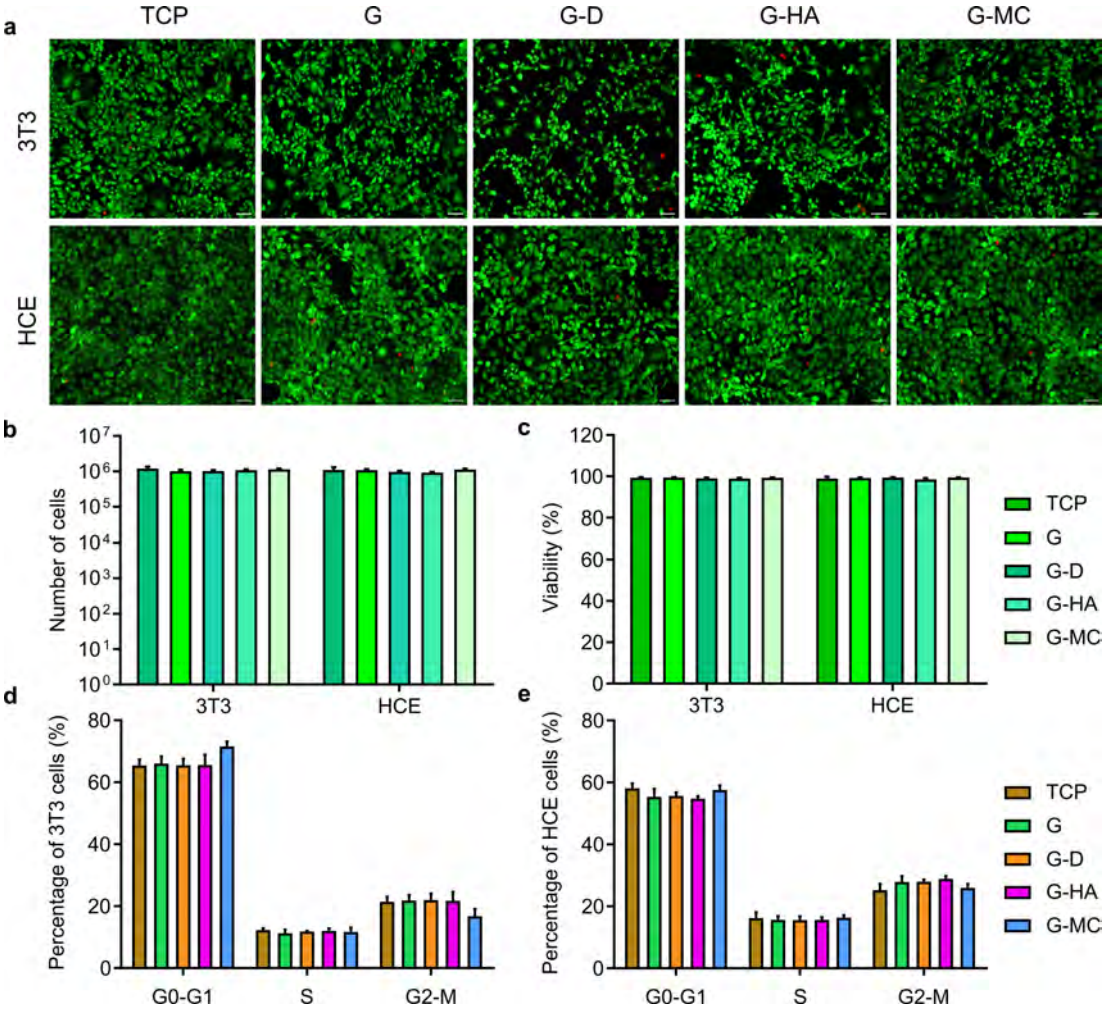

IV.15. FIGURE: Cytocompatibility results of NIH-3T3 and HCE cell cultures exposed to G, G-D, G-HA and G-MC hydrogels compared to cells seeded in a normal tissue culture plate (TCP). **a**) Representative Calcein AM-EthD1 live/dead assay images of NIH-3T3 and HCE cell cultures exposed to the different hydrogel versions. **b**) Cell counts after 72 h of culture. **c**) Percentage of viable cells registered in each group. **d, e**) Percentage of cells registered in each of the cell cycle phases for (**d**) NIH-3T3 and (**e**) HCE cultures.

2.6. Culture of corneal cells embedded in the hydrogel

The cytocompatibility of hydrogel G was confirmed by cultivating primary human corneal stromal cells within it and performing the Calcein AM-EthD1 live/dead assay after 48 hours in culture. The observed morphology diverged from that acquired in two-dimensional cultures, with cell clusters embedded at various depths and lacking the stretched and striated morphology typical of stromal cells. Nearly the whole culture was stained with Calcein AM, as observed in the figure IV.16.

While the cell arrangement was different, most of the cells were alive, confirming the cytocompatibility of the hydrogel one more time.

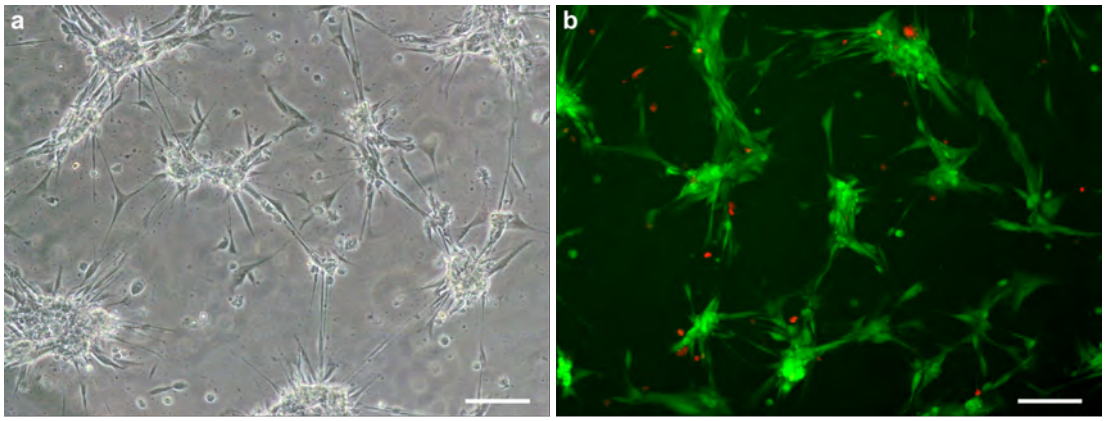

IV.16. FIGURE: Human stromal primary cells seeded by embedding them in G hydrogel. **a**) Phase-contrast microscopy image taken after 48 hours in culture. **b**) Calcein AM-EthD1 live/dead assay image conducted after 48 hours in culture. Scale bars correspond to 100 μm.

3. Quantification of growth factors

After selecting the composition of the gelatine-RFP hydrogel, various compounds were chosen to be released from the hydrogel in a controlled manner. These compounds included two blood-derived products, autologous serum (AS) and serum derived from plasma rich in growth factors (sPRGF), as well as human amniotic membrane extracts (HAMe), both of which would aid in corneal healing. Before their introduction into the hydrogels, these compounds were characterised by quantifying the content of 11 growth factors.

The mean and standard deviation of the quantification of two blood derivatives from six different patients were recorded. Two blood-derived products, AS and sPRGF, were obtained from the blood samples of each patient, resulting in a total of six samples per product. In addition, a pool of the 6 AS and another pool of the 6 sPRGF samples (x-AS, x-sPRGF) were quantified. Considering HAMe, the samples extracted from the distal, medial, and proximal parts (HAMe-D, HAMe-M, HAMe-P) of 3 different membranes were quantified. The average and standard deviation of these quantifications, along with those from the pools of the three parts performed by each membrane (x-HAMe), were calculated for HAMe.

3.1. Quantification of blood-derived products

There were notable differences in some growth factors between the two blood products across all patients, although these differences were unique to each individual. Patients 4 and 5 had no significant variations between AS and sPRGF in any of the analysed growth factors except HGF, whereas patients 1 and 6 exhibited significant differences in BDNF, PEDF, SP, EGF and HGF. Differences were found in the quantification of individual patient samples when compared with each version's pool. The production of pools from all AS and sPRGF samples reduced factor quantification when compared to the theoretical mean (T.x-AS, T.x-sPRGF), calculated from the average value of all patient's data, and this disparity became significant in some factors. The high temperatures needed for complement inactivation to create the pools may explain this reduction in quantification, which affected the loss of some growth factors and molecules of interest.

3.2. Quantification of HAMe samples

When examining HAMe, differences were most pronounced between the medial and proximal regions, although these differences may also differ between individuals.

A statistically significant decrease in all factors was observed when pooling each membrane part of the same patient.

Concerning the pools made from all parts of the three donor membranes, only 4 of the 11 factors studied showed significant differences between the three individuals, namely PEDF, IL-1β, SP and EGF. These results suggested that pool quantification remained consistent across individuals. As with blood products, the quantification of pooled samples was decreased compared to individual data.

IV.2. TABLE: Concentration of the growth factors measured in the extracted blood-derived products. The results are expressed as quantification mean ± SD. Statistically significant differences between AS and sPRGF samples are defined as p-value ∗ $p < 0.05$, ∗∗ $p < 0.01$, ∗∗∗ $p < 0.001$, ∗∗∗∗ $p < 0.0001$ for each patient.

GFs	BDNF (ng/ml)		NGF (pg/ml)		PEDF (ng/ml)		IL-1β (pg/ml)		GDNF (pg/ml)		Human S-P (pg/ml)	
Samples	AS	sPRGF	AS	sPRGF	AS	sPRGF	AS	sPRGF	AS	sPRGF	AS	sPRGF
p1	33.4 ± 0.82	13.93 ± 1.34 ****	0 ± 10.33	0 ± 18.77	1108.58 ± 22.23	720.36 ± 129.56 ***	0.19 ± 0.08	0.12 ± 0.02 *	27.99 ± 2.07	21.28 ± 0.47	1256.52 ± 293.92	436.61 ± 65.02 *
p2	19.45 ± 0.51	8.07 ± 0.43 ****	0	0 ± 4.71	762.69 ± 86.96	547.49 ± 39.82	0.01 ± 0.01	0 ± 0.08	63.79 ± 3.25	58.72 ± 0.87	122.84 ± 5.98	69.26 ± 0.13
p3	30.21 ± 2.28	23.70 ± 1.49 ***	0 ± 2.81	0.42 ± 1.86	1243.59 ± 79.54	1054.26 ± 109.31	0.04 ± 0.02	0,03	84.36 ± 5.59	69.60 ± 4.53	1935.65 ± 265.21	2485.92 ± 178.16
p4	26.96 ± 0.90	26.07 ± 1.85	96.25 ± 17.69	99.86 ± 12.59	914.09 ± 30.83	736.60 ± 113.50	0,09	0,09	264.81 ± 9.83	244.63 ± 11.46	510.16 ± 9.80	765.07 ± 126.64
p5	14.62 ± 0.43	10.51 ± 1.22	0 ± 4.63	0 ± 23.10	841.02 ± 96.50	734.58 ± 33.17	0 ± 0.02	0 ± 0.02	117.56 ± 7.09	92.12 ± 7.97	297.34 ± 28.73	403.11 ± 115.77
p6	18.34 ± 2.71	8.98 ± 1.02 ****	19.34 ± 6.40	0 ± 1.85	1283.91 ± 46.92	614.88 ± 19.62 ****	0 ± 0.01	0 ± 0.02	121.82 ± 9.15	112.73 ± 7.26	3866.38 ± 706.78	695.82 ± 204.19 ****
x	20.46 ± 0.04	12.96 ± 0.51 ****	22.54 ± 12.76	39.78 ± 13.43	863.08 ± 58.46	581.99 ± 5.39 *	0 ± 0.01	0 ± 0.01	266.48 ± 8.85	201.16 ± 10.26 ****	152.25 ± 0.25	154.05 ± 3.29
T.x	23.83 ± 7.18	15.21 ± 7.49	20.57 ± 36.54	20.85 ± 37.79	1025.65 ± 213.28	734.70 ± 177.91	0.06 ± 0.08	0.04 ± 0.05	113.39 ± 78.34	99.85 ± 73.98	1331.48 ± 1372.73	809.30 ± 823.62

GFs	EGF (pg/ml)		FGF2 (pg/ml)		HGF (pg/ml)		IGF (ng/ml)		KGF (pg/ml)	
Samples	AS	sPRGF	AS	sPRGF	AS	sPRGF	AS	sPRGF	AS	sPRGF
p1	393.27 ± 32.77	200.55 ± 1.19 ****	64.48 ± 33.03	82.55 ± 17.92	201.44 ± 16.36	80.45 ± 3.66 ***	0.21 ± 0.02	0.25 ± 0.02	0,00	0,00
p2	236.43 ± 9.87	85.71 ± 3.58 ****	156.88 ± 13.58	169.67 ± 14.91	296.60 ± 9.44	125.59 ± 10.37 ****	8.33 ± 0.05	8.12 ± 0.30	9.32 ± 1.44	8.67 ± 0.14
p3	300.66 ± 30.65	245.42 ± 15.11 *	160.98 ± 2.64	144.31 ± 20.94	823.61 ± 79.10	253.98 ± 19.17 ****	59.48 ± 3.35	45.42 ± 0.43	15.46 ± 0.04	9.55 ± 1.30
p4	133.76 ± 5.03	128.11 ± 4.31	134.21 ± 0	154.78 ± 16.55	268.66 ± 7.94	161.69 ± 0 **	122.73 ± 0.18	114.66 ± 1.86	85.66 ± 28.48	75.39 ± 0.53
p5	252.17 ± 7.89	229.42 ± 17.93	64.48 ± 33.03	55.50 ± 20.33	307.71 ± 6.27	155.72 ± 11.79 ****	4.59 ± 0.17	3.68 ± 0.18	8.67 ± 0.70	5.97 ± 0.48
p6	326.49 ± 20.11	130.08 ± 0.51 ****	98 ± 14.38	100.90 ± 18.48	370.39 ± 4.63	166.42 ± 0 ****	1.38 ± 0.05	0.97 ± 0.05	7.8 ± 0.33	6.57 ± 0.09
x	200.65 ± 10.67	145.07 ± 4.30 *	138.64 ± 6.27	137.96 ± 18.92	98.26 ± 14.27	100.84 ± 3.55	39.30 ± 21.55	27.58 ± 4.12	56.54 ± 0.95	45.56 ± 1.70
T.x	273.79 ± 85.86	169.88 ± 61.64	113.17 ± 44.52	113.96 ± 32.90	378. 07 ± 216.03	157.31 ± 55.07	32.79 ± 47.19	28.85 ± 43.27	21.15 ± 31.69	17.69 ± 27.14

BDNF: Brain-derived neurotrophic factor.
NGF: Nerve growth factor.
PEDF: Pigment epithelium-derived factor.
IL-1β: Interleukin 1β.
GDNF: Glial-derived neurotrophic factor.
S-P: Substance P.
EGF: Epidermal growth factor.
FGF2: Fibroblast growth factor 2.
HGF: Hepatocyte growth factor.
IGF: Insulin-like growth factor.
KGF: Keratinocyte growth factor.
p1-p6: Patients 1 to 6.
x: Pool of the samples of each blood derivative.
T.x: Theoretical pool.

IV.3. TABLE: Concentration of the growth factors measured in HAMe samples. The results are expressed as quantification mean ± SD. Statistically significant differences defined as p-value ∗, +, † $p < 0.05$, ∗∗, ++, †† $p < 0.01$, ∗∗∗, +++, ††† $p < 0.001$, ∗∗∗∗, ++++, †††† $p < 0.0001$ are shown with respect to "∗" HAMe-D, "+" HAMe-P and "†" HAMe-Pool.

GFs	BDNF (pg/ml)				NGF (pg/ml)				PEDF (ng/ml)			
Samples	D	M	P	x	D	M	P	x	D	M	P	x
p1	48.56 ± 4.71	21.33 ± 0.79 *	39.11 ± 5.50 †	6,33 **	901.33 ± 72.58	882.27 ± 84.43 †††	675.81 ± 137.03 ††	167.18 58.58 ***	33.85 ± 2.08	27.72 ± 3.20 $^{++}$	15.26 ± 0.28 ***†	0.06 ± 0.01 *
p2	8 ± 0.79	9.67 ± 1.57	19.11 ± 2.36	8,56	493.29 ± 71.43	348.10 ± 260.12	580.65 ± 144.18 ††	73.96 ± 45.93 *	36.73 ± 1.34	38.55 ± 0.02 $^{++++}$	12.95 ± 2.14 ****††††	0.17 ± 0.02
p3	39.11 14.93	64.11 ± 22 ††	43 ± 9.43	24.67 ± 0.79	1065.69 ± 33.01	1218.21 ± 45.85 $^{+\dagger\dagger\dagger\dagger}$	831.11 ± 201.99 ††††	148.18 ± 22.62 ****	20.04 ± 1	15.22 ± 1.16 $^{++\dagger\dagger\dagger}$	26.87 ± 1.15	0.28 ± 0.01 *

GFs	IL-1β (pg/ml)				GDNF (pg/ml)				Human S-P (pg/ml)			
Samples	D	M	P	x	D	M	P	x	D	M	P	x
p1	1 ± 0.06	0.49 ± 0.02 $^{****+++\dagger\dagger\dagger\dagger}$	0.86 ± 0.03 *††††	0.06 ± 0.01 ****	25.06 ± 0.69	21.77 ± 4.43 $^{++\dagger\dagger\dagger}$	10.92 ± 0.96 ***	8.70 ± 4.10 ****	6.25 ± 0.13	6.83 ± 0.60	6.01 ± 0.12	6.91 ± 1.26
p2	0.30 ± 0.06	0.19 ± 0.04 $^{++++}$	0.81 ± 0.02 ****††††	0.17 ± 0.02 *	0.26 ± 1.97	0.26 ± 1.97 $^{++++}$	15.13 ±0.71 ****††	6.49 ± 0.97	8.84 ± 0.65	7.57 ± 0.52	8.30 ± 0.23	8.14 ± 1.02
p3	0.17 ± 0.01	0.46 ± 0.08 $^{*****++\dagger\dagger}$	1.12 ± 0.01 ****††††	0.28 ± 0.01	4.77 ± 1.95	8.37 ± 0.24 $^{+}$	16.47 ± 0.71 ***††	7.68 ± 2.66	7.11 ± 0.03	6.04 ± 0.16 $^{++++\dagger\dagger\dagger\dagger}$	14.46 ± 0.08 ****††	11.28 ± 1.56 ***

GFs	FGF2 (pg/ml)				HGF (pg/ml)			
Samples	D	M	P	x	D	M	P	x
p1	1986.80 ± 53.75	2988.89 ± 189.24 $^{**++++\dagger\dagger\dagger\dagger}$	4638.27 ± 499.69 ****††††	421.62 ± 19.02 ****	16526.12 ± 831.18	17002.09 ± 2332.96 $^{++++\dagger\dagger\dagger\dagger}$	26283.42 ± 1351.62 ****††††	2542.30 ± 72.43 ****
p2	1923 ± 31.11	1718.88 ± 170.34 $^{++++\dagger\dagger\dagger}$	6878.22 ± 338.92 ****††††	521.08 ± 12.12 ****	6559.69 ± 27.10	4602.99 ± 0.55 $^{++++\dagger\dagger\dagger}$	28387.46 ± 2254.51 ****††††	862.38 ± 113 ***
p3	1534.62 ± 108.52	2311.04 ± 71.07 $^{**++++\dagger\dagger\dagger\dagger}$	5104.23 ± 67.58 ****††††	521.54 ± 18.60 **	8418.67 ± 579.61	7115.15 ± 610.87 $^{++++\dagger\dagger\dagger}$	31077.24 ± 278.15 ****†††	1176.67 ± 94.72 ***

GFs	EGF (pg/ml)				IGF (ng/ml)				KGF (pg/ml)			
Samples	D	M	P	x	D	M	P	x	D	M	P	x
p1	65.38 ± 0.26	118.86 ± 3.41 *****††	82.05 ± 1.65	80.26 ± 2.48	0.29 ± 0.04	0.27 ± 0.02 †	0.28 ± 0.03 †	0.07 ± 0.04 **	1.20 ± 0.17	2.57 ± 1.29 $^{*++++\dagger\dagger\dagger}$	11.17 ± 0.43 ****††††	N/A
p2	42.47 ± 3.44	24.45 ± 2.16	39.51 ± 2.00	27.81 ± 0.31	0.15 ± 0.01	0.19 ± 0.01	0.27 ± 0.05 †	0.10 ± 0.01	N/A	N/A $^{++++}$	15.13 ± 0.13 ****††††	N/A
p3	289.14 ± 5.65	284.47 ± 20.43 ††††	266.93 ± 17.96 ††	226.27 ± 7.22 ****	0.16 ± 0.10	0.10 ± 0.13 $^{+}$	0.28 ± 0.02	0.12	0.00	N/A $^{++++}$	14.51 ± 0.29 ****††††	0.49 ± 0.10

BDNF: Brain-derived neurotrophic factor.
NGF: Nerve growth factor.
PEDF: Pigment epithelium-derived factor.
IL-1β: Interleukin 1β.
GDNF: Glial-derived neurotrophic factor.
S-P: Substance P.
FGF2: Fibroblast growth factor 2.
HGF: Hepatocyte growth factor.
EGF: Epidermal growth factor.
IGF: Insulin-like growth factor.
KGF: Keratinocyte growth factor.
p1-p3: Patients 1 to 3.
D: Distal part of HAM.
M: Medial part of HAM.
P: Proximal part of HAM.
x: Pool of the samples of each membrane part.

IV.4. TABLE: Concentration of the growth factors measured in HAMe pool samples. The results are expressed as quantification mean ± SD. Statistically significant differences defined as p-value $*$, † $p < 0.05$, $**$, †† $p < 0.01$, $***$, † † † $p < 0.001$, $****$, † † †† $p < 0.0001$ are shown with respect to "$*$" patient 1 (p1) and "†" patient 3 (p3).

Samples	BDNF (pg/ml)	NGF (pg/ml)	PEDF (ng/ml)	IL-1β(pg/ml)	GDNF (pg/ml)	Human S-P (pg/ml)	EGF (pg/ml)	FGF2 (pg/ml)	HGF (pg/ml)	IGF (pg/ml)	KGF (pg/ml)
p1	6.33 ± 0.00	167.18 58.58	24.86 ± 6.14	0.06 ± 0.01	8.70 ± 4.10	6.91 ± 1.26	80.26 ± 2.48	421.62 ± 19.02	2542.30 ± 72.43	0.07 ± 0.04	N/A
p2	8.56 ± 0.00	73.96 ± 45.93	42.74 ± 3.19 ***	0.17 ± 0.02 *	6.49 ± 0.97	8.14 ± 1.02	27.81 ± 0.31 ***	521.08 ± 12.12	862.38 ± 113	0.10 ± 0.01	N/A
p3	24.67 ± 0.79	148.18 ± 22.62	30.23 ± 4.59 $^{++}$	0.28 ± 0.01 $^{***+}$	7.68 ± 2.66	11.28 ± 1.56 $^{***++}$	226.27 ± 7.22 $^{****++++}$	521.54 ± 18.60	1176.67 ± 94.72	0.12	0.49 ± 0.10

BDNF: Brain-derived neurotrophic factor.
NGF: Nerve growth factor.
PEDF: Pigment epithelium-derived factor.
IL-1β: Interleukin 1β.
GDNF: Glial-derived neurotrophic factor.
S-P: Substance P.
FGF2: Fibroblast growth factor 2.
HGF: Hepatocyte growth factor.
EGF: Epidermal growth factor.
IGF: Insulin-like growth factor.
KGF: Keratinocyte growth factor.
p1-p3: Patients 1 to 3.

4. *In vitro* inflammation assessment

In order to determine whether the functionalised hydrogels could reduce inflammation, *in vitro* assays were conducted first.

4.1. *In vitro* inflammation model

An *in vitro* inflammation model was established with HCE cells as the first step and 10 μg/ml LPS and 100 ng/ml TNFα were employed as two inflammation approaches to this end. The cells were exposed to one of the two agents for 24 hours in either HCE medium or DMEM:F12 medium. 6 different conditions were introduced in the assay: C-M.HCE, HCE cells cultured in HCE medium; C-DMEM, HCE cells cultured in DMEM:F12 medium; M.HCE-LPS, HCE cells cultured in HCE medium with LPS stimulus; DMEM-LPS, HCE cells cultured in DMEM:F12 medium with LPS stimulus; M.HCE-TNFα, HCE cells cultured in HCE medium with TNFα stimulus and DMEM-TNFα, HCE cells cultured in DMEM:F12 medium with TNFα stimulus. Cells cultured with HCE medium without the inflammation agent (C-M.HCE) served as control. Following this, the expression of inflammatory IL-6 and IL-1β genes were quantified to determine the inflammation level. Gusβ and TBP were used as reference genes.

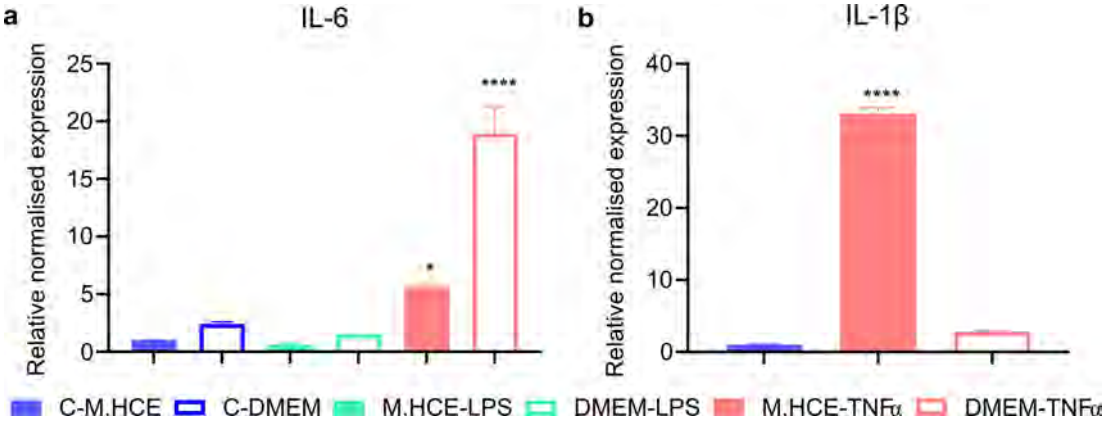

IV.17. FIGURE: Relative normalised gene expression ($\Delta\Delta$Cq) of **a**) IL-6 and **b**) IL-1β genes in inflamed and non-inflamed HCE cultures. Cells cultured with HCE medium and no inflammation stimuli were used as control (C-M.HCE). Statistical significance is defined as p-value $*$ $p < 0.05$, $**$ $p < 0.01$, $***$ $p < 0.001$, $****$ $p < 0.0001$ with respect to control (C-M.HCE).

Cultures subjected to TNFα showed higher expression of inflammatory genes in both instances, as evidenced by higher levels of IL-6 and IL-1β expression than LPS cultures (Figure IV.17). In addition to selecting TNFα as the inflammatory agent, HCE medium was chosen as the culture medium for dissolving TNFα. Apart from being the standard medium used in control samples, the cells cultured with HCE medium and exposed to TNFα showed statistically significant differences in the expression of IL-1β with respect to the control compared to those cultured with DMEM:F12 medium.

4.2. *In vitro* inflammation assay

After establishing TNFα and HCE medium as the preferred *in vitro* inflammatory stimulus and culture medium, the complete inflammation assay was performed. IL-1β gene expression was used to measure inflammation reversal in HCE cultures treated with the different functionalised hydrogels. The normalised expression of IL-1β was determined by using Gusβ and TBP as reference genes in the BioRadCFX Manager software. The outcomes were plotted against the geometrical mean of all samples and statistically analysed against the control (M-M).

Four conditions were tested using four variations of the functionalised hydrogel in the absence of an inflammatory stimulus to examine the effect of the hydrogels themselves (samples named with "M-" in the figure IV.18). To minimise the number of experimental conditions, only one option for each hydrogel variant was tested without TNFα stimulus: the non-functionalised hydrogel (M-H), the hydrogel containing antibody (M-H-Ab), the hydrogel containing sPRGF (M-H-sPRGF) as one of the two blood derivatives, and the pool of membrane extracts (M-H-HAMe (Pool)) for the hydrogels containing HAMe. The use of the hydrogel in any of its functionalised forms (M-H, M-H-Ab, M-H-sPRGF, M-H-HAMe (Pool)) without TNFα stimulation resulted in an inflammatory effect on the cells, with significant differences in the case of the non-functionalised hydrogel (M-H) in this regard. The addition of the antibody, sPRGF or the pool of HAMe reduced this effect to the point where there were no significant statistical differences compared to the control (M-M).

Higher levels of inflammation were observed in the cell cultures exposed to the TNFα-stimulated non-functionalised hydrogel (TNFα-H) than the cell cultures exposed to TNFα stimulus alone for 72 hours (TNFα-TNFα), but without statistically significant differences.

The addition of the hydrogel itself, which had already demonstrated an inflammatory effect (M-H), increased the culture's inflammation levels.

The addition of the antibody (TNFα-H-Ab), blood derivatives (TNFα-H-AS and TNFα-H-sPRGF) or the pool of HAMe (TNFα-H-HAMe) to the TNFα-stimulated cultures reduced the inflammation to the point where no significant differences were detected in comparison to the control. This confirmed the effectiveness of the products reversing inflammation. However, the hydrogels functionalised with HAMe taken from each part of the amniotic membrane (TNFα-H-HAMe (D), TNFα-H-HAMe (M), or TNFα-H-HAMe (P)) did not show such inflammation-reducing effect; statistically significant IL-1β levels were recorded in the three cases, with particularly notable differences in the case of the hydrogel functionalised with the HAMe obtained from the medial part (TNFα-H-HAMe (M)).

The *in vitro* outcomes served to select the 4 hydrogel versions employed in subsequent *ex vivo* and *in vivo* assays. AS was chosen as the blood derivative, given its superior reduction effect in comparison to sPRGF. The use of HAMe obtained from the proximal part of the membrane to functionalise the hydrogels was also based on the same criterion.

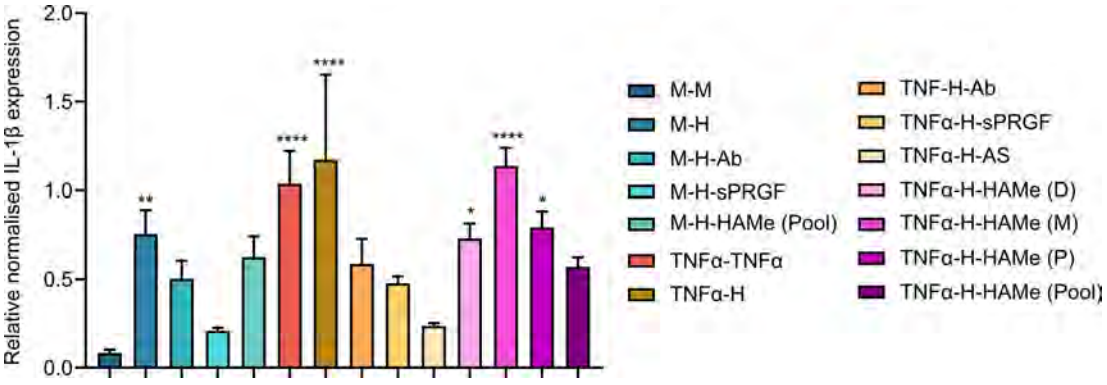

IV.18. FIGURE: Relative normalised gene expression ($\Delta\Delta$Cq) of IL-1β in HCE cultures seeded in the presence of different functionalised hydrogel versions. Statistically significant differences showed differences with respect to the cells cultured with HCE medium and no inflammation stimuli (M-M). Statistical significance is defined as p-value $*$ $p < 0.05$, $**$ $p < 0.01$, $***$ $p < 0.001$, $****$ $p < 0.0001$.

5. *Ex vivo* assays

So as to minimise the number of animals to be used in the *in vivo* experiments, *ex vivo* assays were performed to replicate the process of hydrogel application, adjust the dosage administered and duration of crosslinking, and verify the suitability of the hydrogel as a substrate for epithelial cell growth.

After testing a range of crosslinking times (40 s, 1 min, 1.5 min and 2 min) and hydrogel quantities (from 30 to 100 μl), 2-minute blue light crosslinking period and the introduction of 50 μl of the hydrogel were established to be enough to cover the wound and create a surface for the epithelial cells to proliferate upon.

Ex vivo cultured corneas were maintained for 8 days until epithelial cells closed the wound. Over the course of 8 days, a concentric and progressive closure evolution was observed (Figure IV.19).

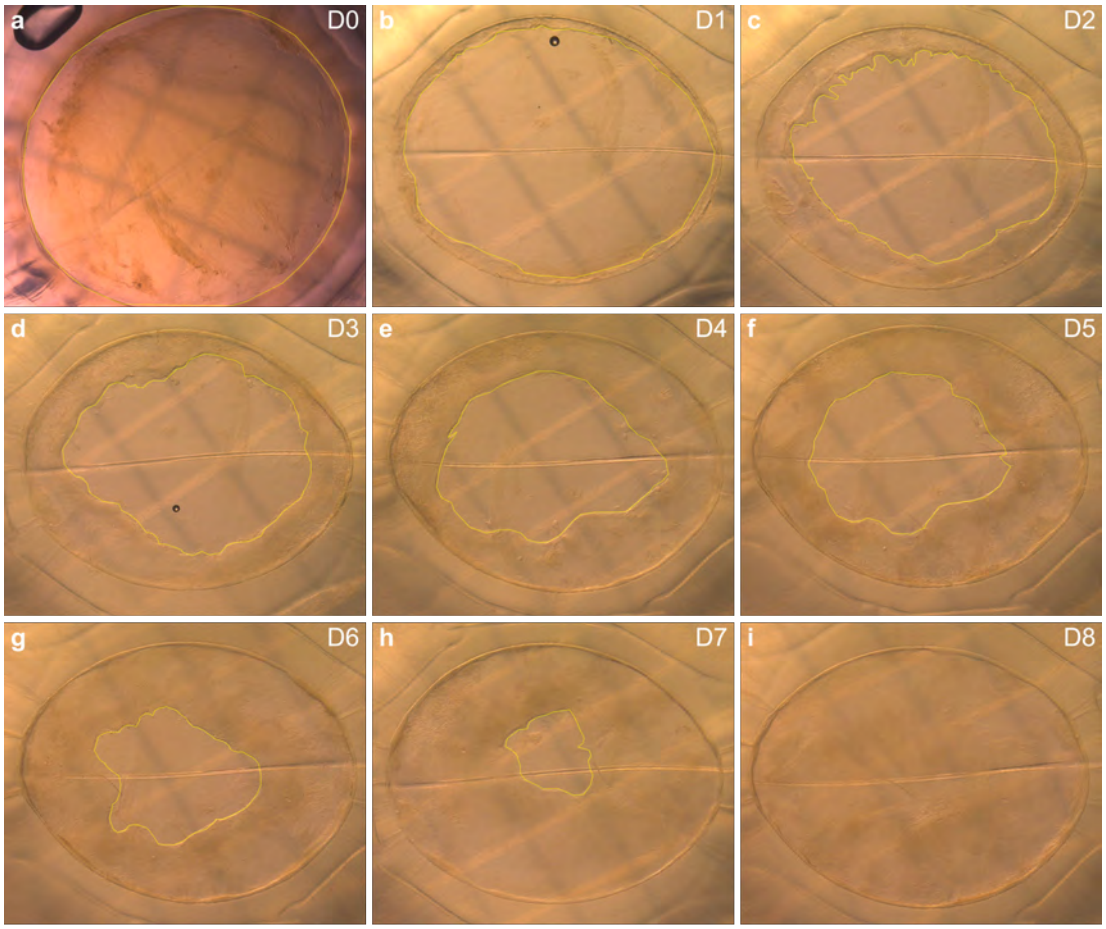

IV.19. FIGURE: Evolution of epithelial wound closure in the central cornea of an *ex vivo* bovine corneal model treated with the hydrogel over an 8-day period.

The hydrogel-treated cultured corneas required approximately 3 additional days to close compared to the control group (control group closed at day 5, hydrogel-treated group closed at day 8). It was observed that the epithelial cells in the control group were able to freely migrate without encountering any impediments, unlike the hydrogel-treated cultured corneas. Although the evolution in cases involving hydrogels was slower, a thicker epithelium was formed.

Whilst the hydrogel was occasionally lost when processing the corneas for OCT inclusion and histological staining, it was observed that the material remained attached to the damaged area as long as it was covered by the newly formed epithelium (Figure IV.20).

The experiments conducted on bovine eyes were replicated on rabbit corneas and the same wound evolution and closure characteristics were documented (Figure IV.21). Notably, the handling of the tissues differed significantly: bovine models provided improved observation of the closure process due to their larger size, but their tougher tissue composition made incision and wound replication less precise across different corneas.

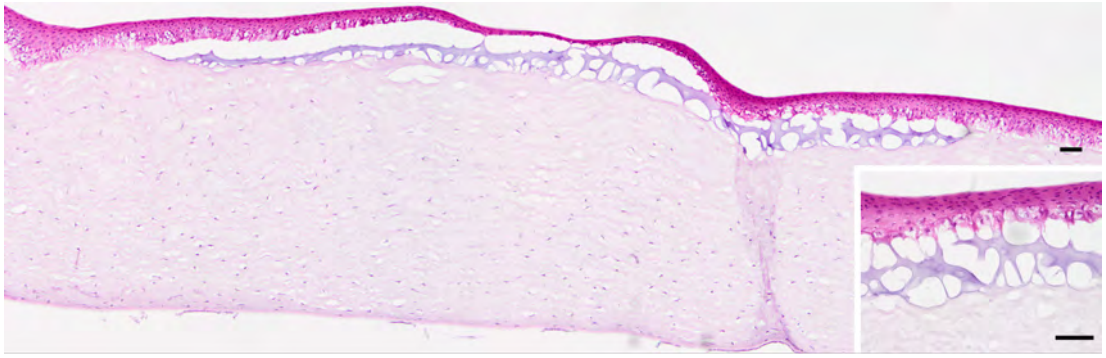

IV.20. FIGURE: Haematoxylin-Eosin staining of the histological section of the central cornea of the *ex vivo* bovine corneal model after re-epithelialisation and treatment with hydrogel H. The cornea was processed 8 days after wound reproduction. The large and small images were taken with 10× and 40× magnification lenses, respectively. The scale bars correspond to 50 μm. Complete epithelial repair was observed as well as maintenance of the applied hydrogel. Abundant adhesion points were observed for the hydrogel with the basal epithelium and with the anterior stroma at 400× magnification.

The histological analysis revealed a significant distinction between the two models in the limbal region. The basal layer of the bovine limbal epithelium exhibited a substantial concentration of melanin, which extended to the superficial layers. Conversely, melanin was barely detectable in rabbit corneal sections (Figure IV.22).

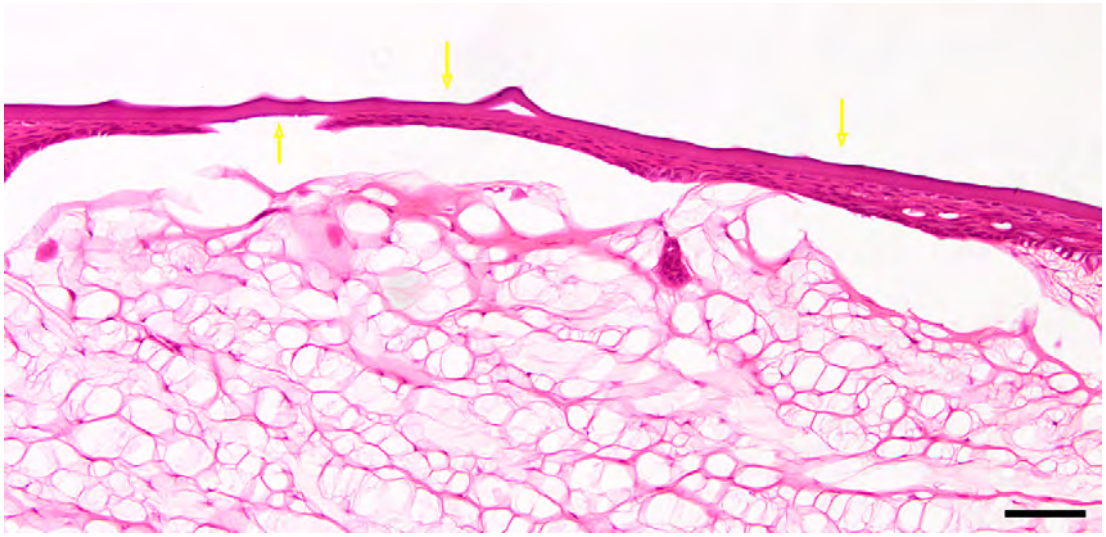

IV.21. FIGURE: Haematoxylin-Eosin staining of the histological section of the central cornea of the *ex vivo* rabbit corneal model after re-epithelialisation and treatment with hydrogel H. The cornea was processed 6 days after wound reproduction. Image was taken with 10× magnification lens and the scale bar corresponds to 100 μm. Complete epithelial repair was observed as well as maintenance of the applied hydrogel (marked with yellow arrows). A part of the applied hydrogel was noticeable above the new epithelium, indicating the long-lasting effect of the hydrogel throughout the wound healing process.

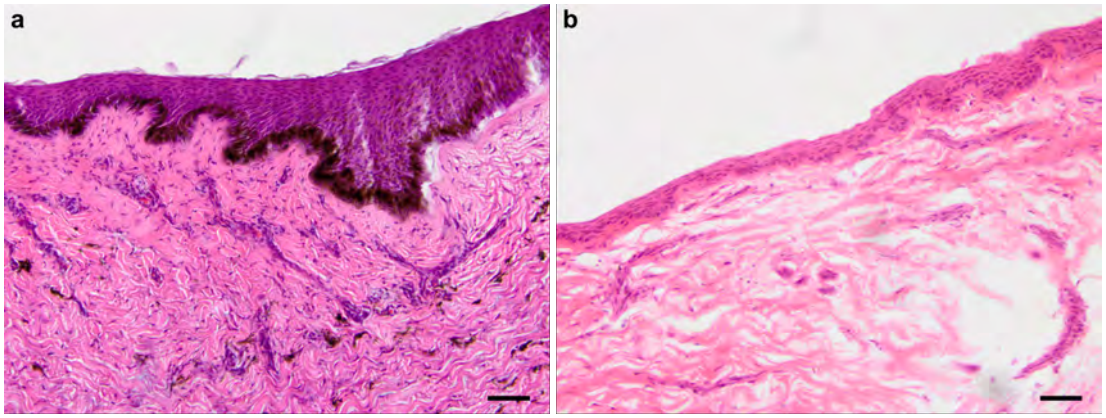

IV.22. FIGURE: Haematoxylin-Eosin staining of the histological sections of the limbal region from *ex vivo* models of **a**) bovine and **b**) rabbit corneas. The melanin concentration in the basal layer of the bovine limbus was significantly higher compared to that of the rabbit model. Images were taken with 20× magnification lens and the scale bars correspond to 50 μm.

6. *Ex vivo* adhesion test

The hydrogel's adherence to the wound was evaluated *ex vivo* by pressing a probe containing the hydrogel on the wound created in the bovine cornea in a TA.XT.Plus C texture analyser. The maximal force (F_{max}) and work of adhesion (W_{adh}) values were noted. The experiment was conducted with 3 biological replicates and performing 3 technical replicates with each.

The peak height in the graph in the figure IV.23 showed the maximum force (F_{max}) required to separate the hydrogel-containing probe from the bovine cornea. The work of adhesion (W_{adh}), estimated from the force vs. distance graph area, represented the total energy of probe withdrawal from the cornea.

The hydrogel exhibited a favourable adhesive force in the three biological samples that were examined, confirming the attachment of the hydrogel to the wound.

Statistically significant variations were observed among the distinct biological replicates in terms of work of adhesion, which could be associated with the irregularities of the wound areas (Figure IV.24).

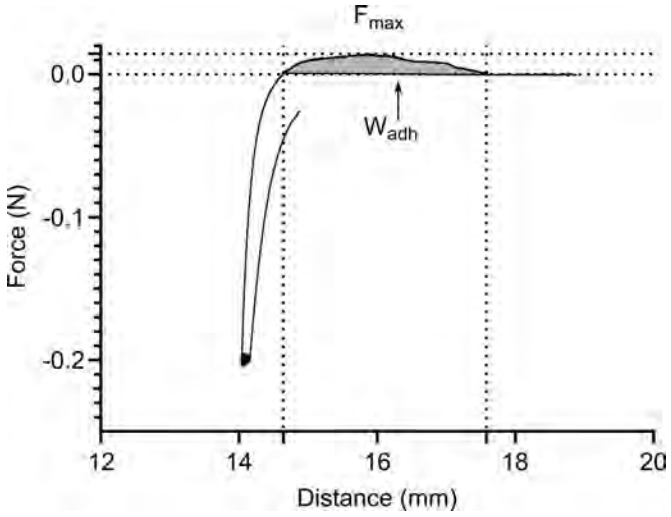

IV.23. FIGURE: Characteristic force displacement curve for H hydrogel in the mucoadhesion analysis. The maximum force required to separate the hydrogel-containing probe from the cornea is represented by the peak value of F_{max}. The area shaded in grey indicates the work of adhesion (W_{adh}) needed to detach the hydrogel from the cornea.

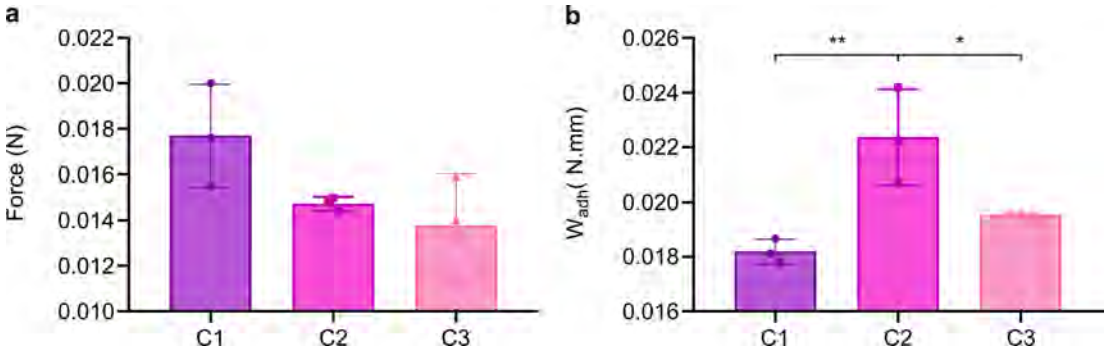

IV.24. FIGURE: Mucoadhesive properties of H hydrogel in terms of **a**) the detachment force (F_{max}) and **b**) the work of adhesion (W_{adh}). Measurements were performed in 3 biological replicates. Statistical significance is defined as p-value $*$ $p < 0.05$, $**$ $p < 0.01$, $***$ $p < 0.001$, $****$ $p < 0.0001$.

7. *In vivo* assays

To confirm the *in vitro* and *ex vivo* results, an *in vivo* experiment was conducted in a rabbit animal model. The corneal ulcers were reproduced through a superficial anterior stromal keratectomy on 30 rabbits. The animals were randomly divided into 5 groups and treated with:

- Control: 0.2% HA artificial tears 4 times daily until wound closure.
- H: 50 μl of 5% w/v gelatine and 0.01% w/v RFP hydrogel crosslinked for 2 minutes with blue light (day 0) + 0.2% HA artificial tears 4 times daily until wound closure.
- H-Ab: 50 μl of 5% w/v gelatine and 0.01% w/v RFP hydrogel with 1 mg/ml Infliximab crosslinked for 2 minutes with blue light (day 0) + 0.2% HA artificial tears 4 times daily until wound closure.
- H-AS: 50 μl of 10% w/v gelatine and 0.02% w/v RFP hydrogel with rabbit AS at a 1:1 dilution crosslinked for 2 minutes with blue light (day 0) + 0.2% HA artificial tears 4 times daily until wound closure.
- H-HAMe: 50 μl of 10% w/v gelatine and 0.02% w/v RFP hydrogel with HAMe at a 1:1 dilution crosslinked for 2 minutes with blue light (day 0) + 0.2% HA artificial tears 4 times daily until wound closure.

The 60 corneas were divided into 6 rounds of experiments.

7.1. Pilot study to fine-tune the experimental procedure conditions

The initial experiment (E01) served as a pilot test to fine-tune the conditions and create the established protocols. Two corneas for each condition were used (n = 10 corneas per group in total). Alongside the wound reproduction, 25 μl of 0.1% benzalkonium chloride (BAC) were instilled on surgery day to intensify the inflammatory outcome. In addition, safety contact lenses were applied to the treated corneas after reproducing the corneal wound and introducing the hydrogel. Due to the discomfort caused by the irritation of the BAC and the ulcer, the animals were constantly rubbing the damaged area. Consequently, only three of the ten rabbits maintained the lens until the second day after the surgery and all lenses were removed by the third day.

7.1.1. Re-epithelialisation

Re-epithelialisation was faster in the H and H-AS treatment groups, with mean percentage of opened wound area of 1.87% $\pm$ 2.65% for H and 0.00% $\pm$ 0.00%, that is, complete closure of defects, for H-AS-treated corneas within 5 days (Figures IV.25 and IV.26 and table IV.5). This was followed by H-HAMe hydrogel treatment, which registered a mean value of opened wound area of 0.89% $\pm$ 1.26% by day 6.

Similarly, H-AS hydrogel exhibited complete closure of all events on day 5, followed by the H treatment on day 6 and the H-HAMe treatment on day 7. Half of the control treatment and H-Ab treatment events had closed by day 8, but not all H-Ab events had completely closed by day 10 of the study (**b** of the figure IV.26).

The control treatment and H-Ab treatment showed a very similar closure evolution, although the closure rate did not reach 0% for H-Ab because one of the treated corneas did not completely re-epithelialise.

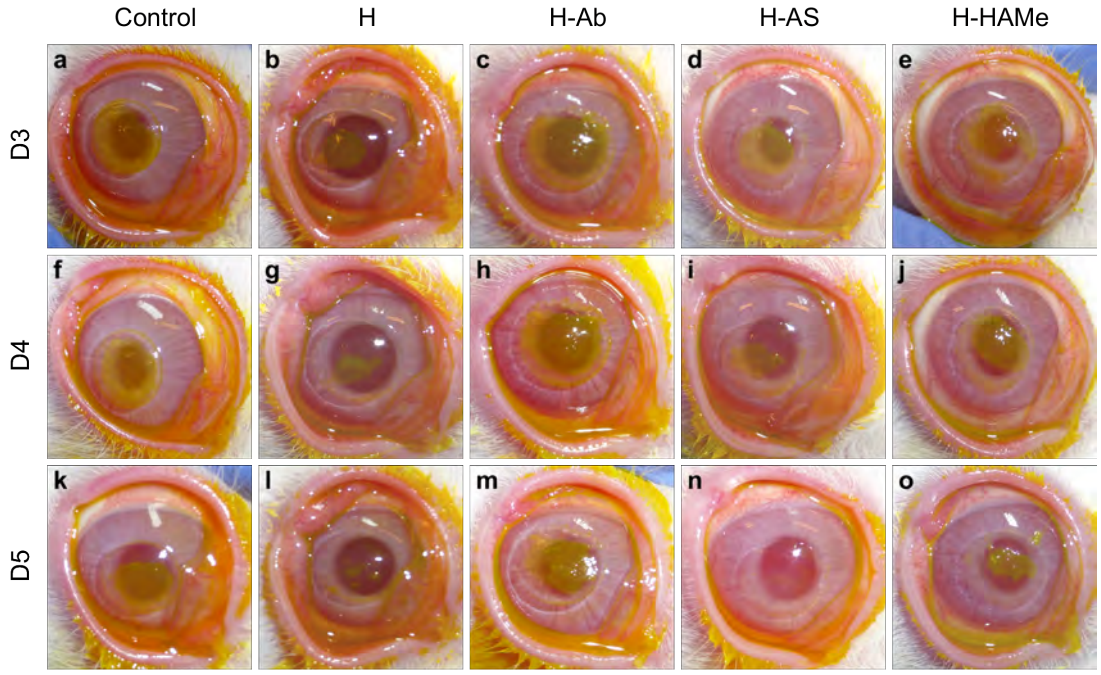

IV.25. FIGURE: Evolution of the epithelial defect *in vivo* in rabbit eyes of the pilot study treated with artificial tears (Control) or the different hydrogel versions (H, H-Ab, H-AS and H-HAMe) from day 3 (D3) to day 5 (D5). The epithelial injury was assessed using fluorescein staining.

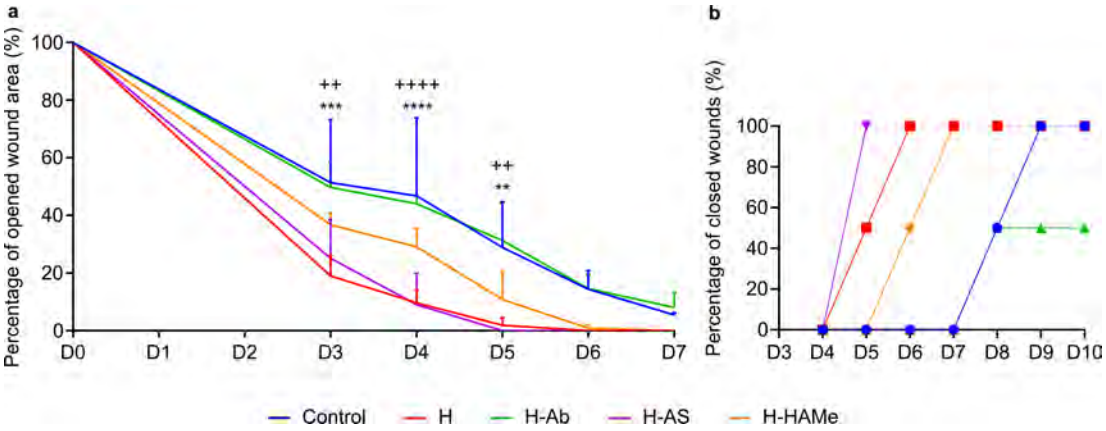

IV.26. FIGURE: Evolution of the epithelial defect *in vivo* in rabbit eyes of the pilot study. **a**) The percentage of the initial area of the surgical epithelial wound remaining open from the day of surgery (D0) to day 10 (D10). **b**) The percentage of wounds closed per day from day 4 (D4) to day 10 (D10). Statistically significant differences are defined as p-value $*$, + $p < 0.05$, $**$, ++ $p < 0.01$, $***$, +++ $p < 0.001$, $****$, ++++ $p < 0.0001$. "$*$" and "+" show significant differences of H and H-AS hydrogels with respect to the control treatment.

IV.5. TABLE: Progression of re-epithelialisation in rabbit eyes of the pilot experiment treated with the different hydrogels or the control treatment. Results are expressed as the mean of the percentage of opened wound area ± SD. Statistically significant differences are defined as p-value $*$, + $p < 0.05$, $**$, ++ $p < 0.01$, $***$, +++ $p < 0.001$, $****$, ++++ $p < 0.0001$. "$*$" and "+" show significant differences with respect to the control treatment and H-Ab hydrogel, respectively.

	Time (days)								
Treatment	0	3	4	5	6	7	8	9	10
Control	100.00	51.37 ± 21.83	46.80 ± 27.08	28.89 ± 15.79	14.43 ± 6.45	5.45 ± 0.79	0.40 ± 0.57	0.00 ± 0.00	0.00 ± 0.00
H	100.00	18.98 ± 7.11 $^{***+++}$	9.64 ± 4.70 *******	1.87 ± 2.65 ****	0.00 ± 0.00	0.00 ± 0.00	0.00 ± 0.00	0.00 ± 0.00	0.00 ± 0.00
H-Ab	100.00	49.71 ± 8.54	44.05 ± 2.75	31.30 ± 12.97	14.60 ± 4.87	8.05 ± 5.19	2.98 ± 2.12	1.80 ± 2.55	0.57 ± 0.81
H-AS	100.00	25.12 ± 13.39 ***	9.04 ± 10.88 *******	0.00 ± 0.00 $^{**++++}$	0.00 ± 0.00	0.00 ± 0.00	0.00 ± 0.00	0.00 ± 0.00	0.00 ± 0.00
H-HAMe	100.00	36.71 ± 4.02	29.11 ± 6.32	10.81 ± 9.91	0.89 ± 1.26	0.00 ± 0.00	0.00 ± 0.00	0.00 ± 0.00	0.00 ± 0.00

7.1.2. Clinical assesment

Clinical symptoms were evaluated using the Draize scale starting from day 3. Each treatment was then assigned an irritation index based on Kay and Calandra's classification.

All treatments, except for H hydrogel, recorded irritability scores in the minimally irritative range (2.5-15 range on the Kay and Calandra's classification) during the first few days after surgery (days 2, 3 and 4). Treatment H was classified as practically non-irritant (0.6-2.5 range on the Kay and Calandra's classification) from day 3 onwards. During the evaluation period, both the control and H-Ab groups consistently achieved the highest test scores from the beginning (Figure IV.27).

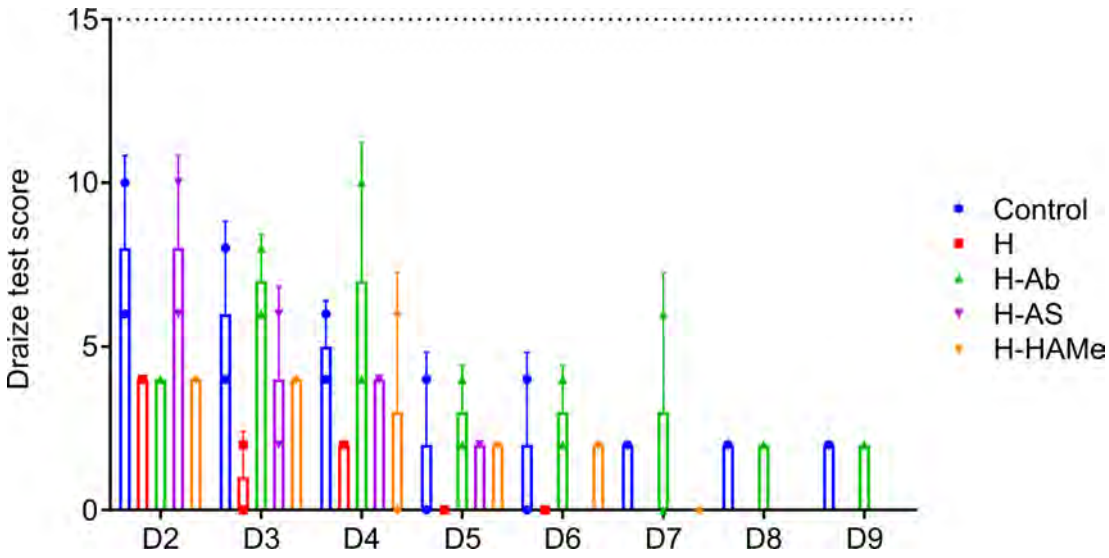

IV.27. FIGURE: Draize test score of the pilot study from day 2 (D2) to day 9 (D9). The range of scores on the Draize scale based on Kay and Calandra's classification from 2.5 to 15 represents the minimally irritative toxicity range. (Dotted line at y = 15). Any values exceeding 15 points would be classified as mildly irritative or higher. No statistically significant differences were found among the samples.

7.1.3. Evaluation of the expression of inflammatory cytokines in tear samples

Protein was extracted from tears through elution from Schirmer strips and centrifugation processes and it was quantified using BCA assays. 50 biological replicates were quantified (10 rabbits $\times$ 5 time points) in the first pilot experiment and the expression of inflamatory cytokines was assesed through QAL-CYT-1 Quantibody Rabbit Cytokine Array Kit (Raybiotech, Norcross, GE, USA).

Of all the cytokines analysed, the molecules that showed data with the highest confidence percentage and above the limit of detection were MIP-1β, MMP-9, NCAM-1 and IL-8. These four targets are related to the initial inflammatory response following an injury.

Figure IV.28 displayed the values of the four cytokines by day of study, grouping all treatments together. An increase in the expression of all four targets was observed on day 1, with a greater dispersion of quantity in the individual values (blue dots expressed in the graph). For MMP-9 and IL-8, this dispersion and increase also occurred on day 7. These differences corresponded to the differences that were recorded on those days for each treatment (Figure IV.29).

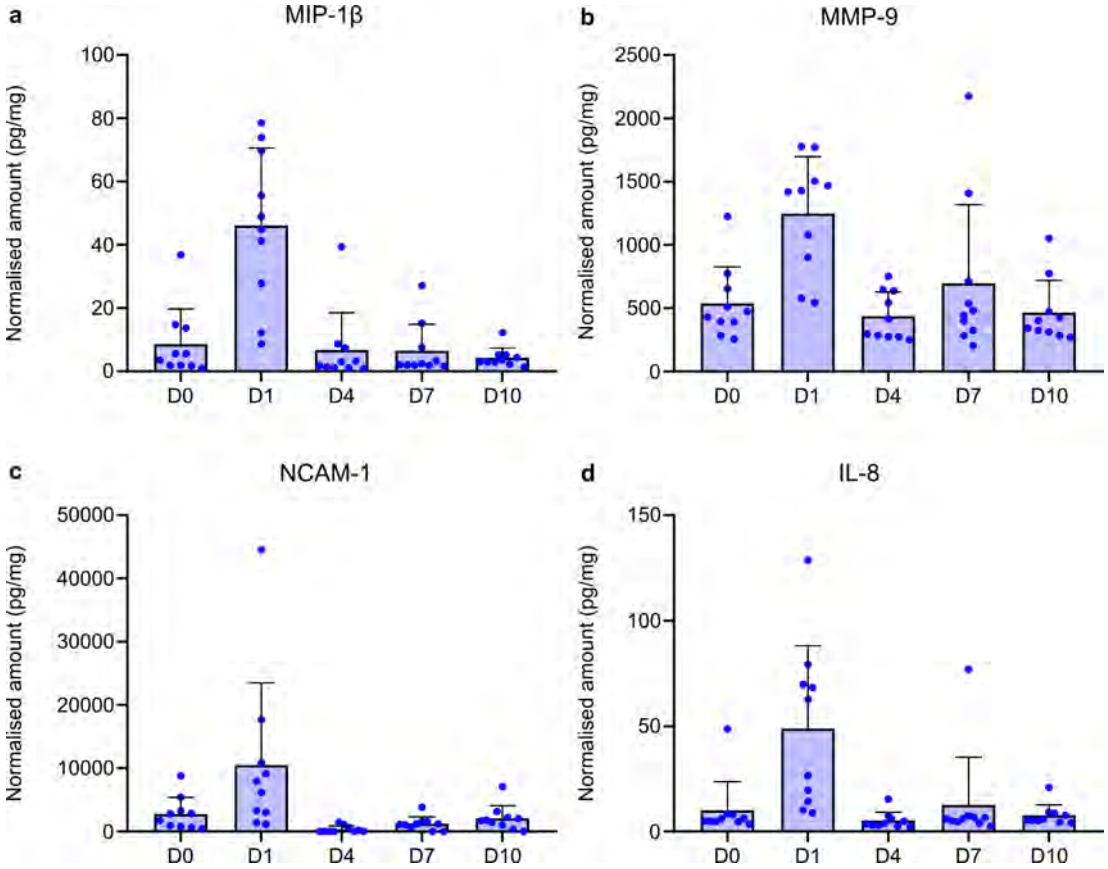

IV.28. FIGURE: The normalised amounts (pg/mg) of **a**) MIP-1β, **b**) MMP-9, **c**) NCAM-1, and **d**) IL-8 in the tear samples collected during the pilot study. The expression of each cytokine per study day is shown without distinguishing between treatments.

A comparable trend was observed for MIP-1β, MMP-9 and NCAM-1, with higher levels of expression at day 1 for both the H-AS and control groups. The results were consistent with those obtained from the Draize test on day 2, where the control treatment and the H-AS hydrogel showed higher irritation scores. From day 3 onwards, the Draize results were elevated for the H-Ab hydrogel, which coincided with the increase in MMP-9 on day 7 (Figure IV.29).

Cytokine expression decreased to minimal levels from day 4 of the study. A slight increase in MMP-9 and IL-8 was observed on day 7 in the H-Ab and H-HAMe groups for the former and in H-HAMe for the latter (**b** and **d** of the figure IV.29).

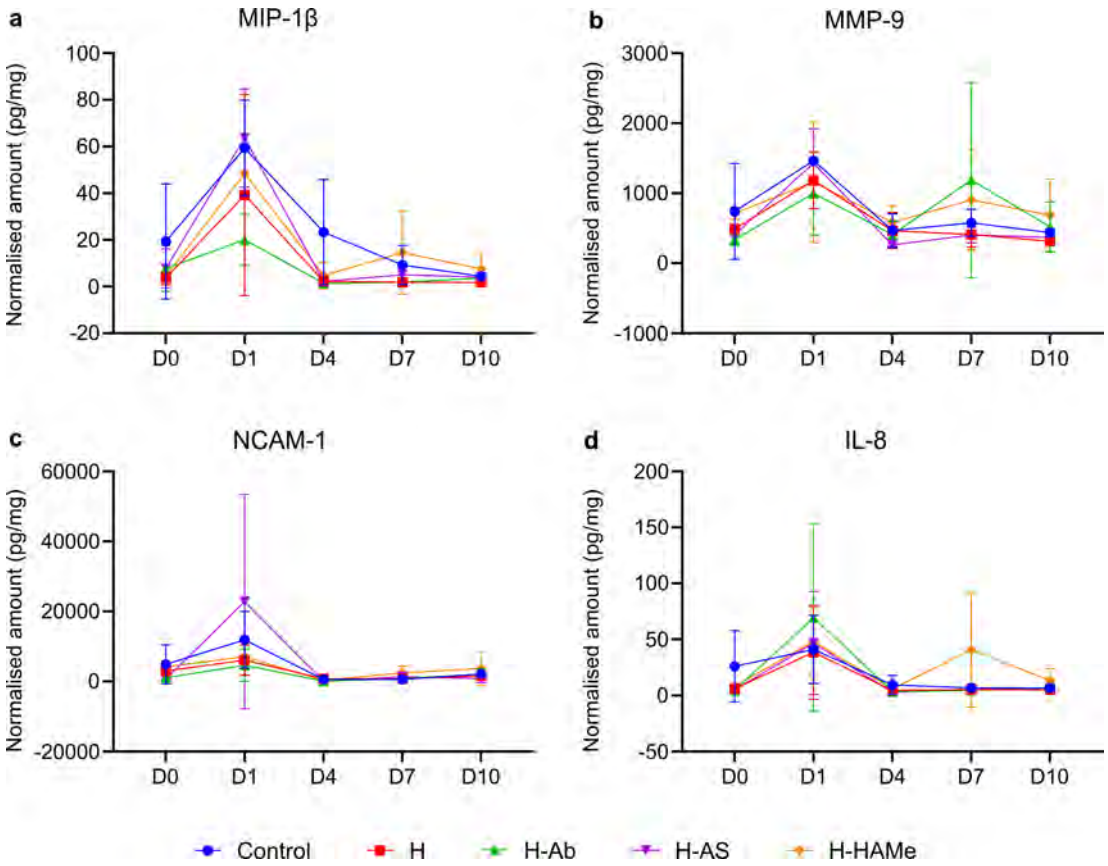

IV.29. FIGURE: The normalised amounts (pg/mg) of **a**) MIP-1β, **b**) MMP-9, **c**) NCAM-1, and **d**) IL-8 in the tear samples collected during the pilot study per day and per study group.

7.2. *In vivo* re-epithelialisation in a rabbit animal model

In view of the pilot study results, the contact lens was replaced by a three-day tarsorrhaphy for subsequent experiments. The added inflammatory stimulus caused by the BAC was also removed.

The five remaining rounds of experiments (E02-E06) were conducted with partial tarsorrhaphy maintained until the third day post-surgery. Therefore, all results presented hereafter show the results from experiments E02 to E06. The evolution of wound closure, which could not be recorded during the first two days due to the tarsorrhaphy, was accelerated by the surgical closure of the eyelids (Table IV.6, figure IV.30), being the mean percentage of opened area after 7 days 2.70% $\pm$ 3.81% for the 10 rabbits of the pilot experiment and 1.51% $\pm$ 2.60% for E02-E06 experiments.

IV.6. TABLE: Differences in the mean percentage of opened wound area ± SD for each experimental day between the pilot study (E01) and the remaining 5 experiments (E02-E06). Statistically significant differences are defined as p-value $*$ $p < 0.05$, $**$ $p < 0.01$, $***$ $p < 0.001$, $****$ $p < 0.0001$.

	Time (days)					
Experiment	0	3	4	5	6	7
E01	100,00	36.38 ± 14.42	27.73 ± 18.08	14.57 ± 14.77	5.98 ± 7.80	2.70 ± 3.81
E02-E06	100,00	18.60 ± 1.26 **	7.90 ± 1.46 **	4.61 ± 1.08	1.66 ± 1.47	1.51 ± 2.60

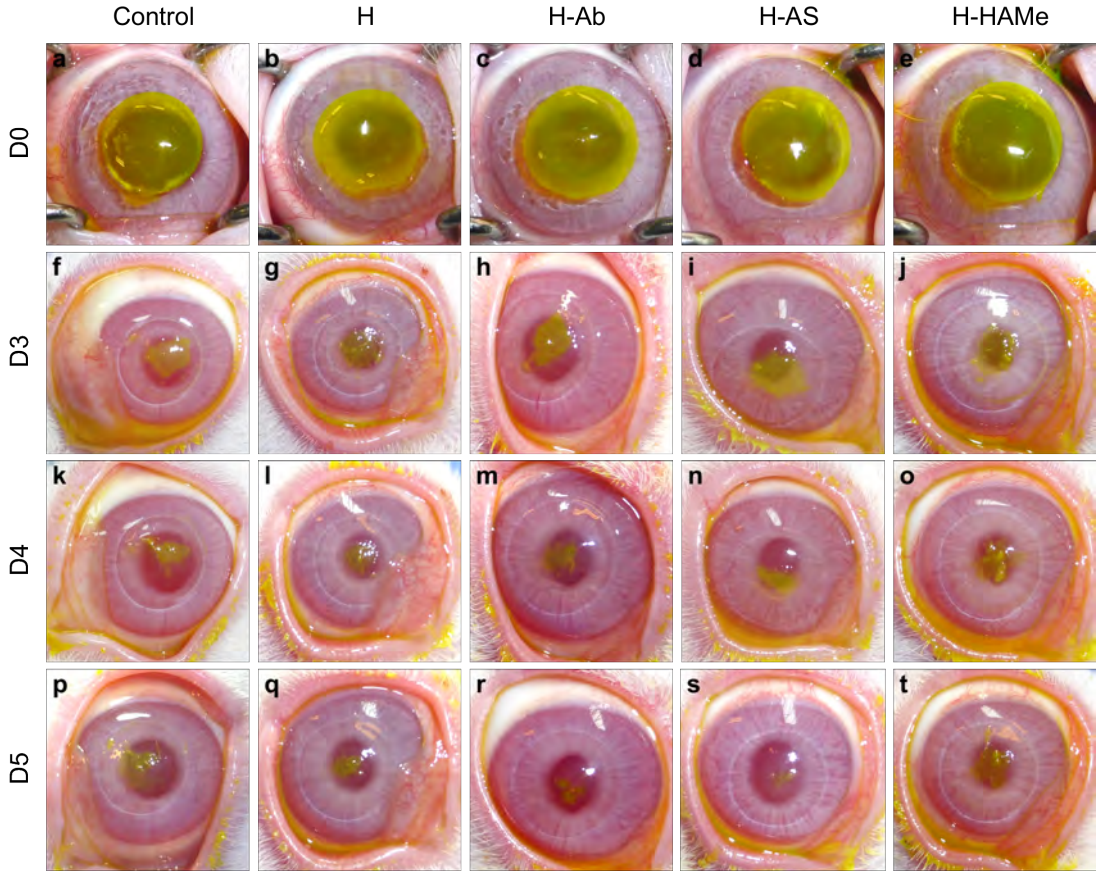

IV.30. FIGURE: Evolution of the epithelial defect *in vivo* in rabbit eyes treated with artificial tears (Control) or the different hydrogel versions (H, H-Ab, H-AS and H-HAMe) from the day of surgery (D0) to day 5 (D5). The epithelial injury was assessed using fluorescein staining.

The opened wound area barely exceeded a mean value of 20% after three days (Table IV.7, **a** of figure IV.31). The control group achieved the quickest closure of eye-cases by day 5 (shown in **c** of the figure IV.31) with a total of 60% cases closed (depicted as **b** in figure IV.31). Nevertheless, the closure process for some corneas seemed to stop at a plateau from day 5 onwards and even appeared to increase slightly by day 7, which suggested that some corneas may not had fully closed or may had closed falsely and reopened. About 20% of the control corneas failed to close (**b** in figure IV.31).

Regarding the hydrogel-based treatments, closure evolution was gradual and prolonged. The wound closure was quicker in the corneas treated with H-AS, with an average of 2.7% ± 3.19% of open wound on day 5 (**c** in figure IV.31). Half of the corneas were closed by day 5, 80% by day 6, and 100% by day 7 (**b** in figure IV.31).

IV.7. TABLE: Progression of re-epithelialisation in rabbit eyes treated with the different treatments or control. Results are expressed as the mean of the percentage of opened wound area ± SD. No statistically significant differences were found between the different treatments on different time points.

	Time (days)					
Treatment	0	3	4	5	6	7
Control	100,00	16.90 ± 12.00	6.06 ± 7.42	4.94 ± 8.14	3.99 ± 11.38	6.11 ± 16.10
H	100,00	18.63 ± 9.67	7.30 ± 8.32	5.10 ± 7.39	1.97 ± 4.12	0.79 ± 2.50
H-Ab	100,00	19.30 ± 15.22	10.05 ± 6.03	4.90 ± 3.44	0.63 ± 1.15	0.00 ± 0.00
H-AS	100,00	20.22 ± 9.64	7.83 ± 6.44	2.71 ± 3.19	0.23 ± 0.49	0.00 ± 0.00
H-HAMe	100,00	17.98 ± 8.67	8.27 ± 6.98	5.37 ± 6.17	1.50 ± 2.45	0.64 ± 2.03

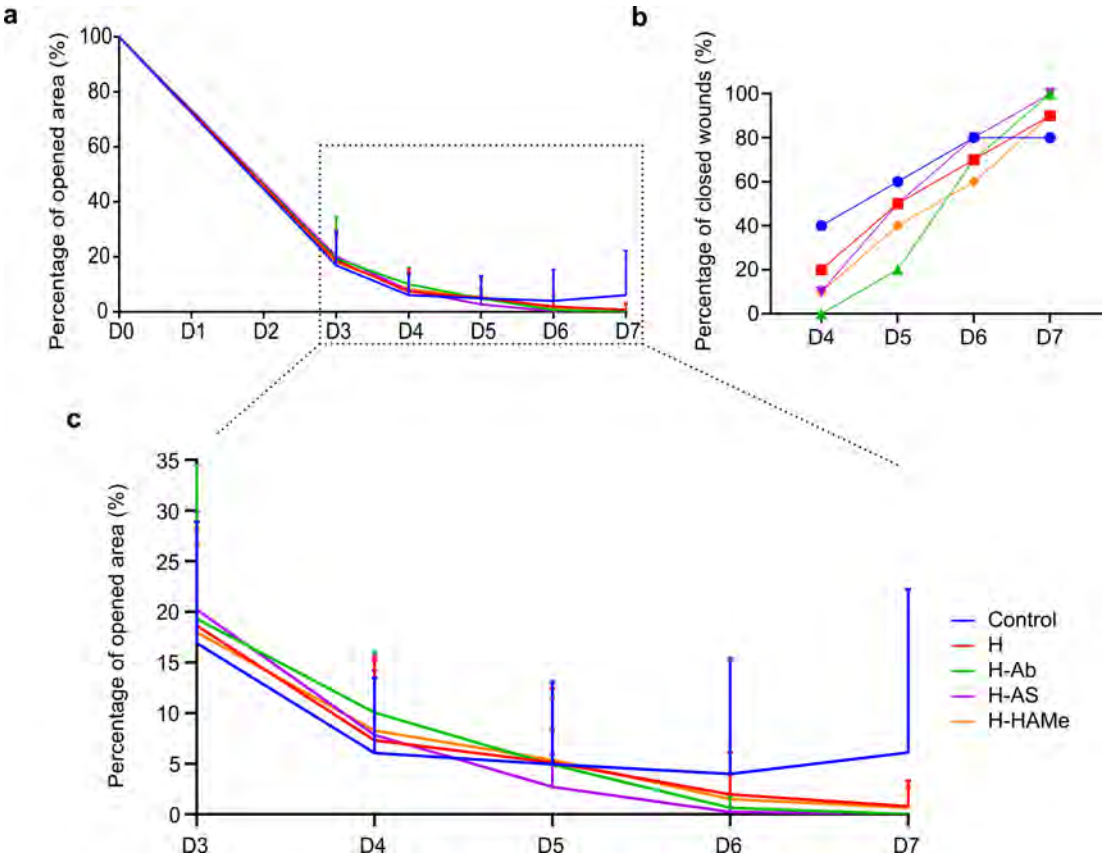

IV.31. FIGURE: Evolution of the epithelial defect *in vivo* in rabbit eyes. **a**) The percentage of the initial area of the surgical epithelial wound remaining open from the day of surgery (D0) to day 7 (D7). **b**) The percentage of wounds closed per day from day 4 (D4) to day 7 (D7). **c**) The percentage of the initial area of the surgical epithelial wound remaining open from the day 3 (D3) to day 7 (D7). No statistically significant differences were found between the samples.

Corneas treated with H-Ab exhibited the smallest percentage of closed area within the initial 4 days, with a mean of 10.05% ± 6.03% opened wound area on day 4 (Table IV.7). However all the wounds were closed by day 7. Graph **b** in figure IV.31 revealed that the majority of the wounds of H-Ab treated corneas closed between day 5 and 6 (from 20% to 70% of closed wounds). All corneas, as registered with H-AS treatment, exhibited complete wound closure by day 7.

The corneas treated with H and H-HAMe exhibited a similar trend. The percentage of wounded area on day 5 averaged 5.10% ± 7.39% and 5.37% ± 6.17%, respectively (Table IV.7 and **c** in figure IV.31), while 90% of the corneas were closed on day 7 in both cases. Therefore, 10% of the eyes did not re-epithelialise within 7 days, the final time-point established in this study.

No significant differences in wound closure were observed in any of the cases, possibly owing to the variability of the biological replicates.

7.3. Clinical assessment

All included treatments induced minimal signs of irritation on day 3 (Figure IV.32). The score was primarily due to redness of the palpebral conjunctivae, chemosis or, in some cases, discharge. The observed redness and chemosis on day 3 were most likely the result of surgery-related inflammation and irritation. In general, the H-AS treatment demonstrated a calming and alleviating impact on inflammation indicators.

During the study period of all the experiments, severe corneal opacity was only observed in one animal. However, it was deemed an outlier and excluded from the study. By day 4, all cases exhibited symptom improvement and the mean scores of the control group, H and H-AS indicated that these treatments were practically non-irritative (0.6-2.5 points range in the Kay and Calandra's classification). The H-Ab and H-HAMe groups entered this range from day 5 onwards.

The group that received H-AS treatment showed the most favourable clinical results. Any signs of irritability practically disappeared with this treatment from day 6 onwards (with a score of 0.2 ± 0.63), and by day 7, all corneas were scored at 0.

None of the records exceeded a score of 15 points, so the values obtained did not even reach the mildly irritating state (15.1-25 points on the Kay and Calandra's classification).

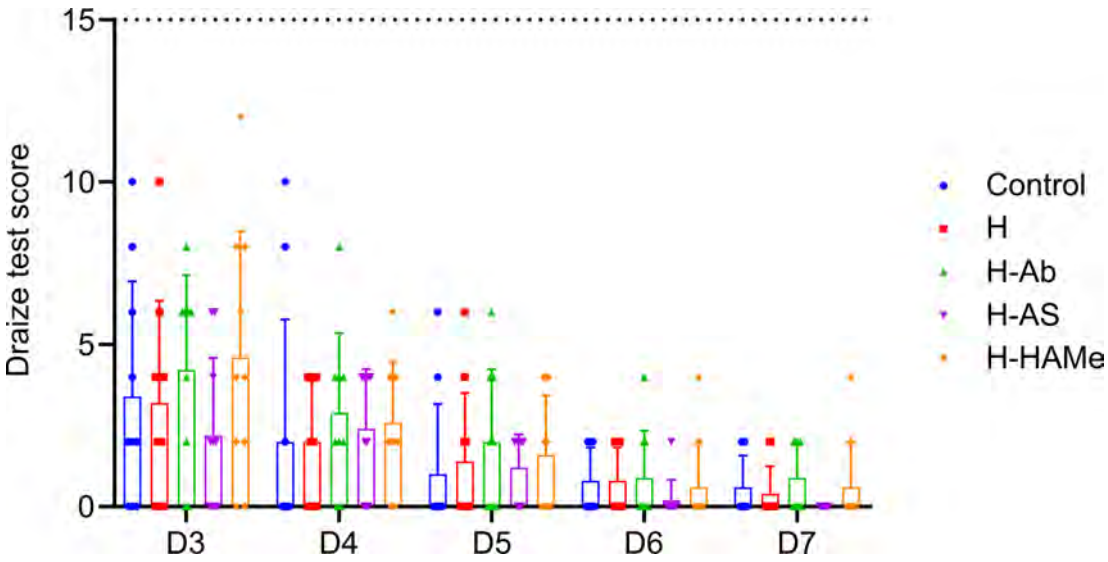

IV.32. FIGURE: Draize test score from day 3 (D3) to day 7 (D7). The range of scores on the Draize scale based on Kay and Calandra's classification from 2.5 to 15 represents the minimally irritative toxicity range. (Dotted line at y = 15). Any values exceeding 15 points will be classified as mildly irritative or higher. No statistically significant differences were found among the samples.

7.4. Quantification of tear volume and protein concentration

The total protein amount from experiments E02-E06 in tears extracted from Schirmer strips of 200 biological replicates (10 rabbits $\times$ 4 time points $\times$ 5 assays) was quantified in 5 independent quantification BCA assays (Figures IV.33 and IV.34).

Protein quantity followed a similar pattern to tear volume in most, but not all cases. The mean protein quantity value was lower than the corresponding tear volume value for the H-HAMe treatment on day 0 and the H-Ab treatment on days 4 and 7.

A lower volume of tears was collected in the samples acquired 1 day after the surgery and hence, a reduced protein was quantified (Figure IV.33 and figure IV.34). This happened due to the irritation and inflammation caused by the surgery which could hinder the production of tears. On the fourth and seventh days of the experiment, the tear volume collected and protein measured exhibited no marked deviations from the baseline.

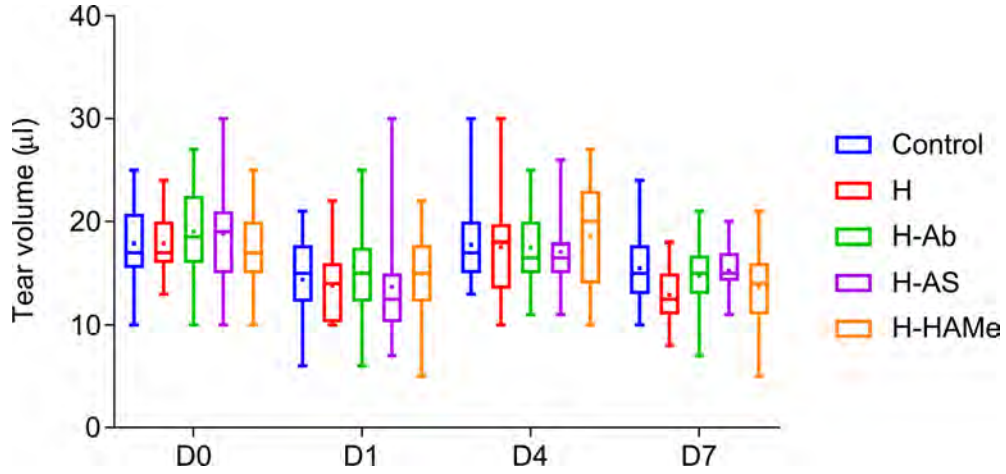

IV.33. FIGURE: Collected tear volume via Schirmer strips for each treatment on days 0, 1, 4, and 7 of the study. No statistically significant differences were found among the samples.

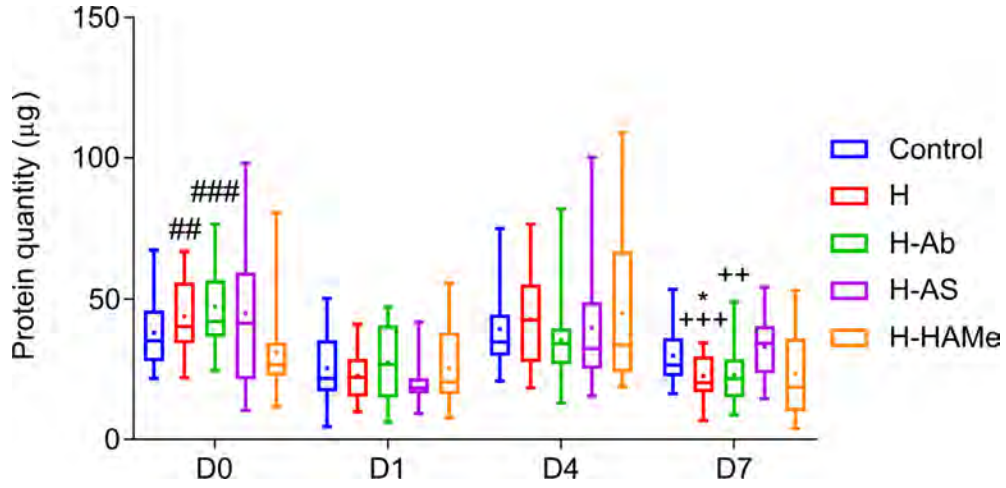

IV.34. FIGURE: Amount of protein quantified from the elution of tear samples collected by Schirmer strips for each treatment on days 0, 1, 4 and 7 of the study. Statistical significance is defined as p-value $*$, +, # $p < 0.05$, $**$, ++, ## $p < 0.01$, $***$, +++, ### $p < 0.001$, $****$, ++++, #### $p < 0.0001$."$*$", "+" and "#" show significant differences with respect to control, H-AS and H-HAMe hydrogels, respectively.

In experiments E02 to E06, the assessment of inflammatory cytokine expression by arrays could not be carried out due to transportation issues. Therefore, no cytokine evolution results were available.

7.5. Gene expression analysis of rabbit corneal samples

The expression of different genes was analysed in corneal samples acquired from rabbits 7 and 21 days after surgery (Experiments E02, E04, and E06 for day 7 and experiments E03 and E05 for day 21). Inflammation markers (IL-1β), markers commonly used for the identification of both limbal stem/progenitor cells (PAX6, p63) differentiated central corneal cells (KRT3), cell proliferation (Ki67), cell adhesion and migration (CD44) and fibrotic response (α-SMA) were included.

The normalised expression of each of the studied genes was calculated using GAPDH, HPRT1 and RIG S15 as reference genes in the BioRadCFX Manager software. The control group served as the control for plotting the data for each case (at 7 and 21 days). For the 21-day analysis, 2 biological replicates were utilised, including three technical replicates in each case. For the 7-day study, there were 3 biological replicates per group, with three technical replicates for each sample.

No statistically significant differences in IL-1β levels were found compared to the control group at 7 days (**a** in figure IV.35). IL-1β expression was similar to control for H, but decreased by half for H-Ab. However, the $\Delta\Delta$Cq value increased by an average of 0.5 value for H-AS and H-HAMe. Significant differences in the inflammation marker were evident in the corneas at 21 days (**b** in figure IV.35). In all hydrogel-based treatments, there was a reduction of more than 50% in inflammation compared to the control treatment, with H-HAMe (average $\Delta\Delta$Cq of 0.05), H-Ab (average $\Delta\Delta$Cq of 0.18), and H (average $\Delta\Delta$Cq of 0.17) showing notable results. The application of the non-functionalised hydrogel H also showed its effect in reducing inflammation.

Statistically significant differences were observed in both 7-day and 21-day corneal samples for α-SMA (**c, d** in figure IV.35). Hydrogel treatments lowered α-SMA levels in all cases, H-Ab and H-AS exhibiting the most substantial decrease in this marker. Furthermore, the application of H also reduced the expression of α-SMA in both time points.

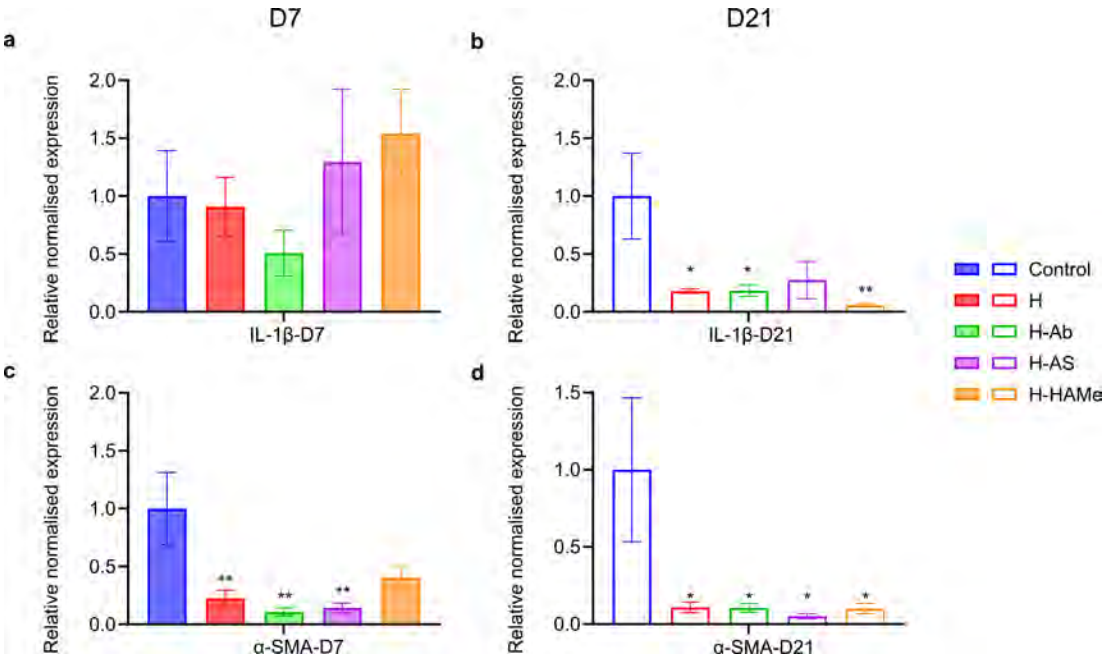

IV.35. FIGURE: Relative normalised gene expression (ΔΔCq) of IL-1β and α-SMA genes in rabbit corneal samples extracted 7 days (**a, c**) or 21 days (**b, d**) post surgery. Statistically significant differences defined as p-value $*$ $p < 0.05$, $**$ $p < 0.01$, $***$ $p < 0.001$, $****$ $p < 0.0001$ are shown with respect to the control of each time point.

Concerning the markers of limbal stem/progenitor cells (PAX6, p63) and differentiated central corneal cells (KRT3), no significant differences were observed between any of the treatments at either of the two analysed times (Figure IV.36). The expression of p63 and CK3 displayed similarities at both 7 and 21 days: at 7 days H-AS and H-HAMe treatments showed the highest expression values, however the expression of both markers decreased in the case of H-AS at 21 days.

Considering p63 at 7-day time point, the H-AS and H-HAMe treatments showed higher expression values compared to the control, while the expression was reduced for the H treatment. p63 expression remained similar to the control for the H-Ab treatment. After 21 days, the H and H-Ab treatments remained similar to the control but a decrease in H-AS expression and an increase in H-HAMe expression was noticeable.

At day 7, CK3 expression was similar in the control, H, and H-Ab groups. The H-AS and H-HAMe groups showed higher expression levels than the control group, but without significant differences. At 21 days, gene expression decreased in the H, H-Ab, and particularly H-AS treatments, while H-HAMe expression increased. No significant differences were observed.

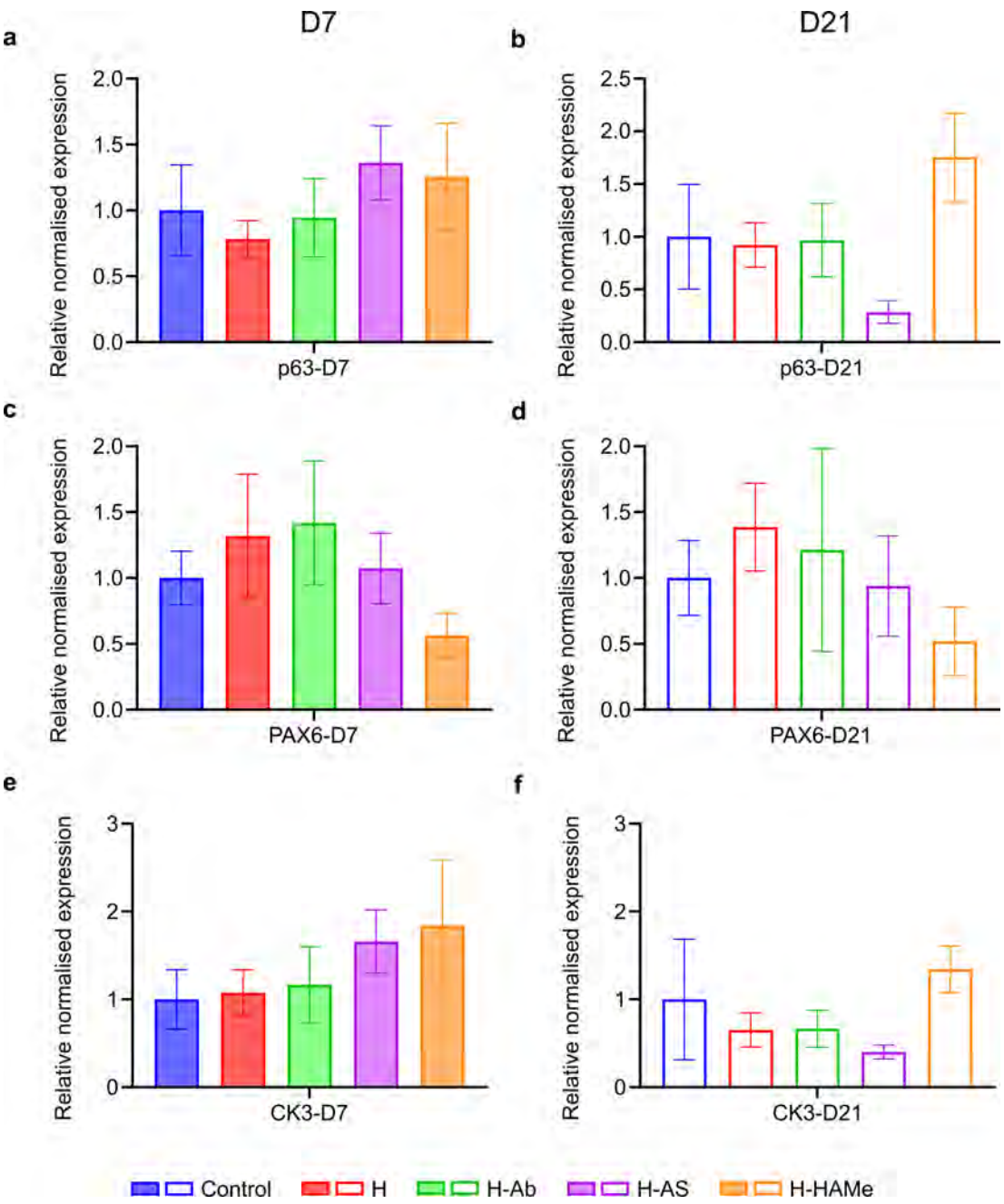

IV.36. FIGURE: Relative normalised gene expression (ΔΔCq) of p63, PAX6 and CK3 genes in rabbit corneal samples extracted 7 days (**a, c, e**) or 21 days (**b, d, f**) post surgery. Statistically significant differences defined as p-value $*$ $p < 0.05$, $**$ $p < 0.01$, $***$ $p < 0.001$, $****$ $p < 0.0001$ are shown with respect to the control of each time point.

For PAX6, the treatment patterns at 7 and 21 days showed remarkable similarity (**c, d** in figure IV.36): H and H-Ab were prominent above the control, H-AS remained at levels very similar to the control, and H-HAMe expression was reduced by almost half.

Statistically significant differences in the proliferation marker Ki67 arised upon analysing the treatments over the course of 21 days (**b** in figure IV.37). Ki67 expression was reduced at least 70% in H, H-Ab, H-AS, and H-HAMe, registering ΔΔCq mean values of 0.29, 0.18, 0.10, and 0.08, respectively. Despite lacking statistical significance, the 7-day treatment pattern mirrored the aforementioned findings (**a** in figure IV.37). The elevated Ki67 expression in the control group could be linked to the absence of any obstacle, like the hydrogel, which allowed epithelial cells to proliferate and migrate more effectively over the wound.

No statistically significant differences were observed in the cell adhesion and migration related marker CD44 at either of the 2 time points (**c, d** in figure IV.37), although H, H-Ab and H-AS showed major expression levels at both time points.

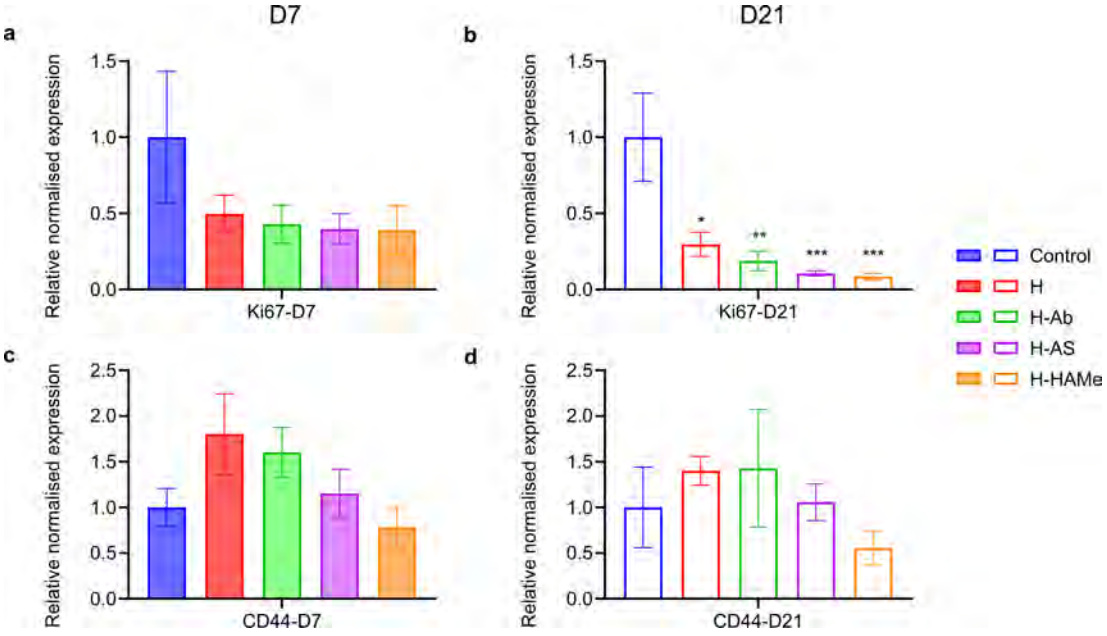

IV.37. FIGURE: Relative normalised gene expression (ΔΔCq) of Ki67 and CD44 genes in rabbit corneal samples extracted 7 days (**a, c**) or 21 days (**b, d**) post surgery. Statistically significant differences defined as p-value $*$ $p < 0.05$, $**$ $p < 0.01$, $***$ $p < 0.001$, $****$ $p < 0.0001$ are shown with respect to the control of each time point.

7.6. Histological analysis

7.6.1. Haematoxylin-Periodic Acid-Schiff (PAS) staining of impression cytology samples

Conjunctival cell samples from the upper bulbar conjunctiva were acquired through impression cytology before and after the surgery. The time before surgery (D0) represented the healthy eye, while the samples obtained 7 and 21 days after surgery represented the left and right eyes of each animal, respectively. All the samples were collected on the last day of the experiment, but both, 7- and 21-day samples were collected on the same day, i.e. the 7-day sample was from the left eye and the 21-day sample was from the right eye of each animal.

The results of the cytologies performed prior to surgery (D0) exhibited significant mucopolysaccharide labelling secreted of conjunctival goblet cells that had been marked with PAS staining (Figure IV.38). A lack of this staining was recorded in the cytologies obtained on days 7 and 21 after surgery, suggesting a reduction in globlet cells (Figure IV.39). Some differences were observed in cell morphology between the different treatment groups or time points under analysis. When comparing the 7-day samples, it was observed that the H and H-HAMe treatments had more goblet cells, despite not being stained with the dyes. Additionally, the nucleus-cytoplasm ratio decreased in the cells of the H-AS treatment. In the 21-day cytologies, goblet cells were observed in all treatments, but their morphology was appropriate only for the control and H-HAMe treated corneas. The cell morphology changed significantly with the H-Ab treatment at both 7 and 21 days. The cells appeared stretched compared to the other groups. These images show only one eye from each of the five samples for each time and treatment. They are intended for illustrative purposes only and do not aim to provide conclusive results regarding the effectiveness of the different treatments.

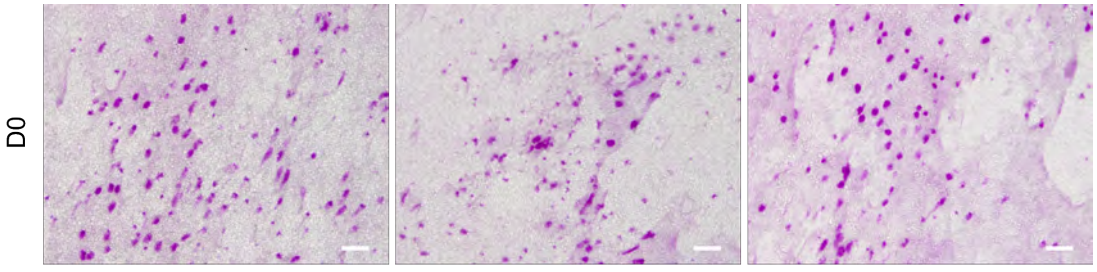

IV.38. FIGURE: Haematoxylin and PAS staining of impression cytology samples obtained before surgery (D0) from the bulbar conjunctivas of rabbit eyes of the *in vivo* assay. Images were taken with 20× magnification and the scale bars correspond to 50 μm.

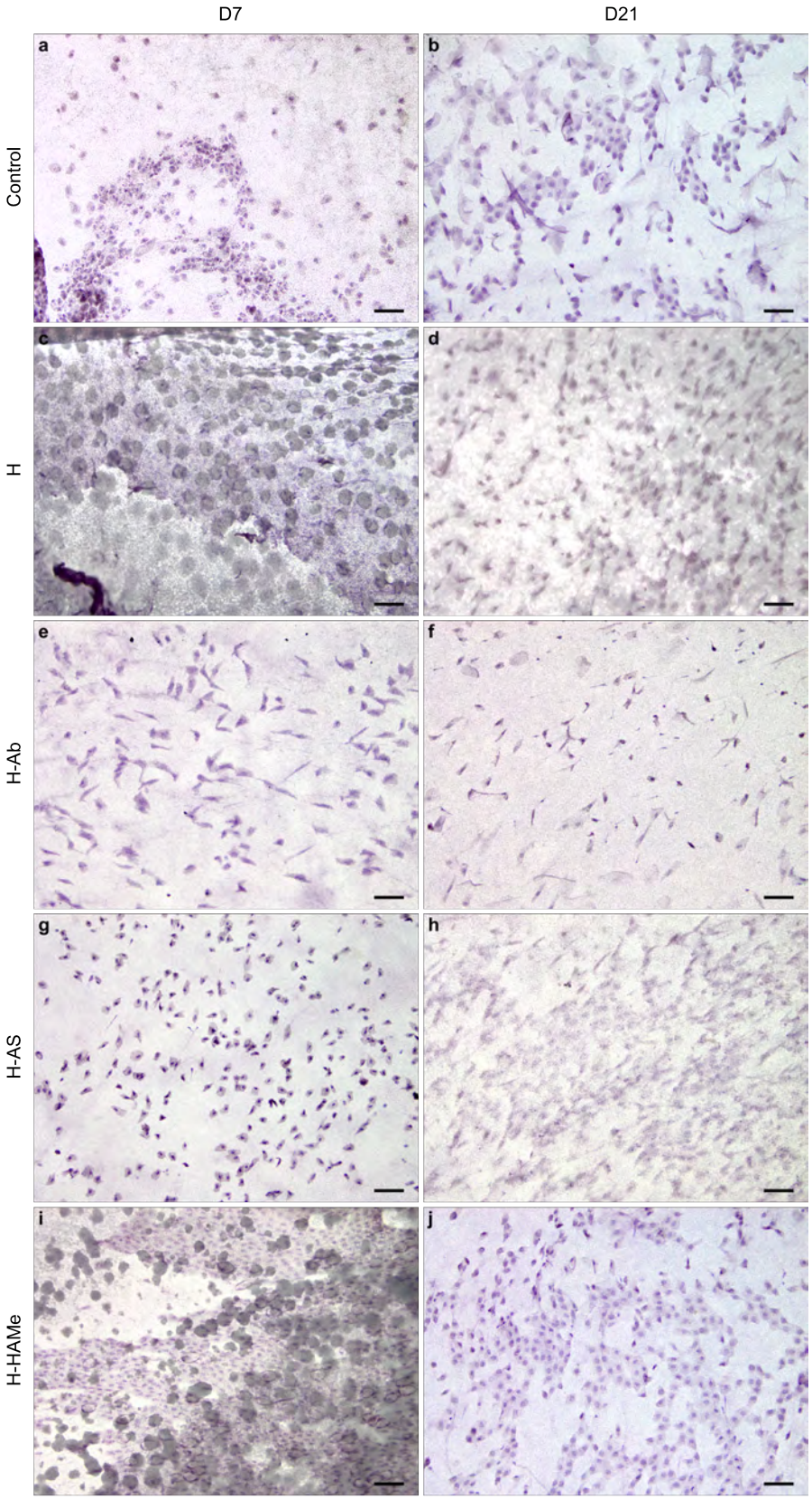

IV.39. FIGURE: Haematoxylin and PAS staining of impression cytology samples obtained from bulbar conjunctivas 7 (**a-e**) and 21 days (**f-j**) after surgery. Rabbit corneas were treated with artificial tears (Control) or with H, H-Ab, H-AS or H-HAMe hydrogels. Images were taken with 20× magnification and the scale bars correspond to 50 μm.

7.6.2. Haematoxylin-Eosin staining of rabbit corneal tissues

The histological images (Figures IV.40) displayed the wounded areas in different treatment groups. The growth of new epithelium was evident in all of them.

The tissue from these samples was processed by freezing and embedding them in OCT instead of paraffin, resulting in poorer preservation of tissue structure and making interpretation difficult, especially at the stromal level. Additionally, half of the stroma in these samples was reconstructed, rather than being compact tissue as found in a healthy cornea.

Although the hydrogel was probably lost in the sample processing, the blank spaces amidst the new epithelium and the impaired stroma in the hydrogel-based treatments proved that the hydrogel was present during healing, and was firmly attached to the tissue. The cavities recorded in the 7-day control treatment may be attributed to areas of poor adhesion between the epithelium and stroma (**a** of the figure IV.40).

In the control treatment, the histological analysis revealed a thick epithelium after 7 days, with stromal infiltration of myofibroblasts beneath it (**a** of the figure IV.40). After 21 days, the epithelium appeared more edematous, with a large presence of myofibroblast in the upper stroma (**b** of the figure IV.40). Overall, hydrogel-based groups exhibited a more compact epithelium compared to the control treatment.

Regarding hydrogel-based treatments, treatment H showed a re-epithelialised thick epithelium after 7 days, with myofibroblast infiltration observed particularly at the wound edges (**c** of the figure IV.40). However, after 21 days, the epithelium appeared thinner compared to the other treatments, and myofibroblast presence was visible (**d** of the figure IV.40). The epithelium appeared thicker and more compact following H-Ab treatment at 21 days compared to 7 days. The presence of myofibroblasts was less pronounced in this treatment at either time (**e** and **f** of the figure IV.40). **g** of the figure IV.40 showed that the epithelium of the H-AS treatment was detached from the stroma, indicating a loss of the deposited hydrogel. Additionally, myofibroblasts and a disordered extracellular matrix were visible. In contrast, an ordered extracellular matrix and no myofibroblasts infiltration was recorded at day 21 (**h** of the figure IV.40).

As for the H-HAMe treatment, **i** of the figure IV.40 taken at 7 days showed that the epithelium was detached from the stroma, likely due to the loss of the hydrogel during sample processing. At 21 days, there was infiltration of myofibroblasts and the extracellular matrix appeared slightly disordered beneath the epithelium (**j** of the figure IV.40).

Overall, epithelial growth and adhesion between the new epithelium and the stroma was observed in all samples, leaving cavities corresponding to the hydrogels in hydrogel-treated corneas.

As with the impression cytology samples, the presented results are purely illustrative and descriptive. It is not possible to provide an average of all biological replicates, as is done in other tests. Biological samples are inherently variable, and therefore, definitive conclusions or distinctions between treatments cannot be drawn solely based on these results.

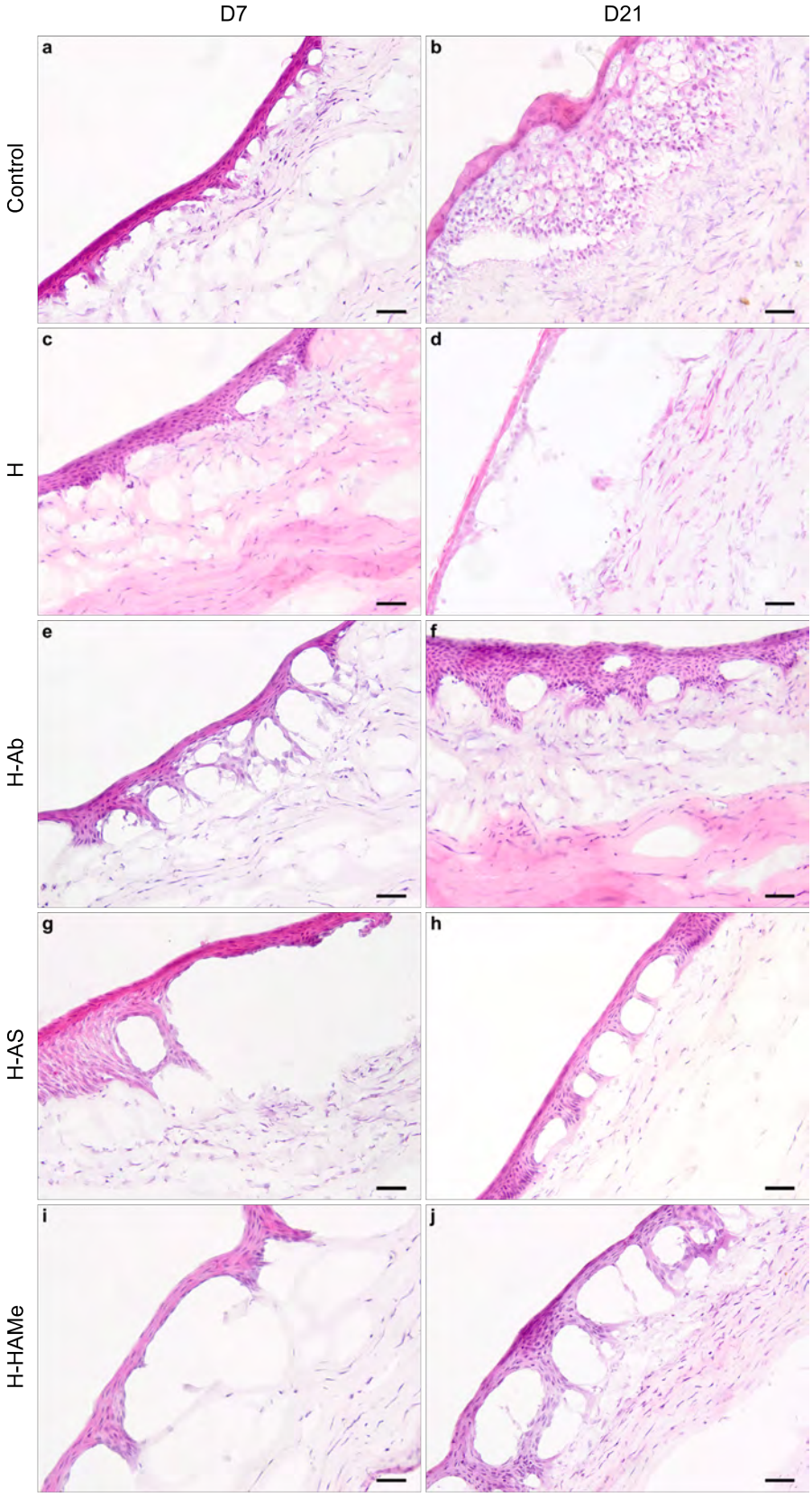

IV.40. FIGURE: Haematoxylin-Eosin staining of the histological sections of the central cornea of rabbit corneal samples obtained from the *in vivo* assay after re-epithelialisation. Rabbit corneas were treated with artificial tears (Control) or with H, H-Ab, H-AS or H-HAMe hydrogels, and processed 7 (**a, c, e, g, i**) and 21 days (**b, d, f, h, j**) after surgery. Images were taken with 20× magnification lens and the scale bars correspond to 50 μm.

7.7. Immunofluorescence analysis of rabbit corneal tissues

Immunohistochemistry was assessed in rabbit corneal tissues obtained 7 and 21 days after surgery (Experiments E02, E04, and E06 for day 7 and experiments E03 and E05 for day 21). Markers related to fibrosis (α-SMA), re-epithelialisation (CK3, PanCK) limbal activation (CK15), barrier function (ZO-1), cell adhesion (Int-β4) and cell proliferation (Ki67) processess were studied.

When corneal damage occurs, stromal keratocytes undergo transformation into corneal fibroblasts and subsequently into myofibroblasts. Myofibroblasts possess ultrastructural and physiological characteristics of smooth muscle cells, including the presence of prominent microfilament bundles or stress fibres. These characteristics enable them to exert contractile forces and direct extracellular matrix reorganisation at the site of injury. α-SMA serves as an indicator of smooth muscle cells and myofibroblasts.

α-SMA labelling was observed in the subepithelial stroma in all treatments of the 7-day processed corneas. Only small and thin patches of α-SMA were visible beneath the corneal epithelium in these samples, with alternating areas of negative α-SMA. The intensity of the staining was increased in 21 day processed-corneas. Strongly-stained band of α-SMA expression was registered in the subepithelial stroma of the control, H and H-HAMe groups obtained 21 days after surgery, thus confirming myofibroblast formation (**f, g, j** in figure IV.42). This staining was also observed to a lesser extent in the H-Ab treatment (**h** in figure IV.42). However, in the biological replicate illustrated in **i** of the figure IV.42, there was a complete absence of α-SMA positivity within the stroma for the H-AS group.

Overall, a disordered extracellular matrix and myofibroblasts were observed in all treatments to varying degrees.

Integrin β4 plays a role in hemidesmosome formation, acting as an adhesion marker between the epithelium and the underlying extracellular matrix. The protein displays polarised distribution in the basal cells of the corneal and limbal epithelium. In all groups, a discontinuity of integrin β4 labelling was observed in the wound site of the 7-day processed corneas. The control cornea showed an irregular Int-β4 positive interface with the stroma, while gaps or absence of labelling were observed in the wound site of the hydrogel-treated corneas.

Staining was more intense in all samples taken 21 days after surgery and it was positively expressed in both uninjured and injured areas of the corneal tissues (Figure IV.43).

The PanCK antibody detects most human cytokeratins and, as such, is capable of labelling the entire corneal epithelium accurately. Therefore, it was utilised as a marker for re-epithelialisation subsequent to injury. Strong PanCK positivity was detected across the epithelium in all corneas, in both the newly regenerated epithelium after wound (FigureIV.44) and the unharmed area (Data not shown).

CK3 is a cornea-specific cytokeratin that is specifically associated with differentiated epithelial cells. Its expression can be observed throughout the entire corneoscleral epithelium, but its pattern of expression varies depending on the area. It is present across the entirety of the epithelial thickness in the central cornea, its expression is limited to the superficial layers of the epithelium in the limbus and it is not present in the conjunctiva. CK3 labelling was detected throughout the central cornea in all samples regardless of treatment group and extraction time, similarly to PanCK labelling, as it is one of the cytokeratins contained within PanCK staining (Figure IV.45). CK3 positivity diminished in the limbal area.

CK15 is a specific epithelial cell cytoskeletal protein present in stratified epithelia and one of the proposed potential putative markes of the limbal stem cells. CK15 labelling was detected in the sclerocorneal limbal area and it was absent in the central cornea (Figure IV.45). Positive co-localisation of CK3 and CK15 was observed in certain cells located in the upper epithelial layers of the limbus close to the peripheral cornea. CK15 labelling in the corneas extracted 7 days post-surgery was very similar in all groups (**a-e** in figure IV.45). In all corneas extracted 21 days post-surgery, CK15 positivity was higher compared to the corresponding corneas extracted 7 days after surgery, suggesting limbal activation. Although CK15 positivity was present in all samples, it was noteworthy that eyes receiving H-Ab, H-AS and H-HAMe treatment 21 days post-surgery demonstrated significant clusters of undifferentiated CK15-positive cells in the basal limbal epithelium (**h, i, j** in figure IV.45).

ZO-1 is a protein belonging to the *zonula occludens* protein family. These proteins are situated in the plasma membrane of epithelial and endothelial cells, and are part of the intercellular junction complexes, known as tight junctions, occluding junctions or *zonula occludens*. ZO-1's primary role is to establish an impermeable barrier that blocks the free flow of substances between cells. As a result, substances pass selectively through the cells. In the cornea, the presence of ZO-1 indicates differentiated surface epithelial cells and the establishment of the corneal barrier effect, consistent with a functional corneal epithelium. ZO-1 labelling was observed in all corneas regardless of group and extraction time, predominantly in the superficial layers of the epithelium (Figure IV.46).

A greater proportion of positive cells for the proliferation marker Ki67 were noted in the corneas processed 7 days after surgery than those processed 21 days post-surgery, independent of the treatment received (Figure IV.46). Additionally, a higher amount of Ki67-stained cells was detected in the control group at both times (Figure IV.41 and **a, f** in figure IV.46). The percentage of positive cells was greater in H-AS comparing the different hydrogel treatment groups.

As with the histological samples, the results presented in this section are purely illustrative and complementary to other experiments where an average of all biological samples can be provided, such as qPCR or Draize test results. The presented images are consistent with the results from other assays, but may not accurately represent all biological replicates due to their significant variability.

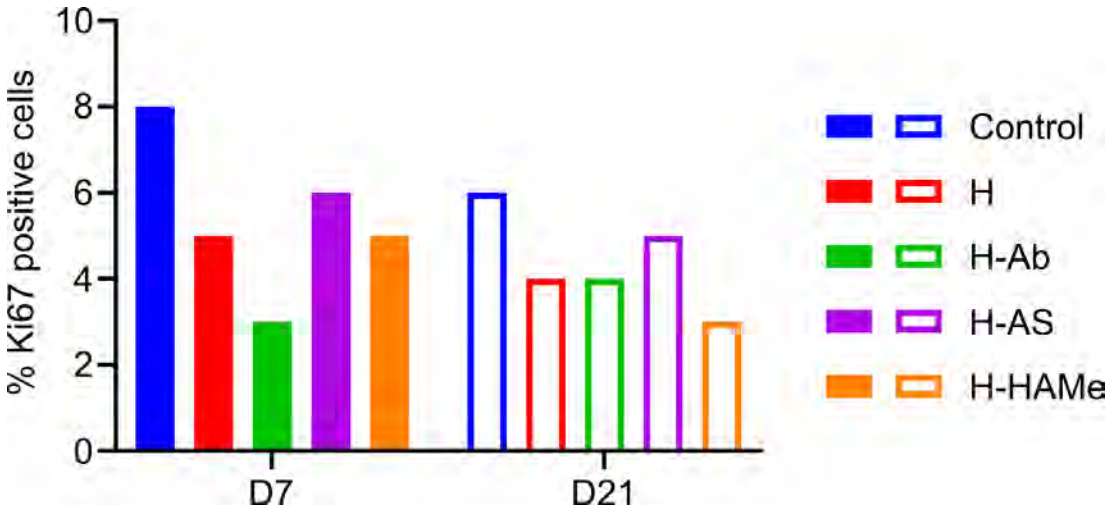

IV.41. FIGURE: Percentaje of Ki67 positive cells detected in rabbit corneal samples obtained from the *in vivo* assay. The corneas were treated with artificial tears (Control) or with H, H-Ab, H-AS or H-HAMe hydrogels and processed 7 and 21 days after surgery.

IV.42. FIGURE: Fluorescent immunostaining for α-SMA marker in the central cornea of rabbit corneal samples obtained from the *in vivo* assay. Rabbit corneas were treated with artificial tears (Control) or with H, H-Ab, H-AS or H-HAMe hydrogels and processed 7 (**a-e**) and 21 (**f-j**) days after surgery. The yellow arrows in images **c** and **h** indicated the real α-SMA labelling in the tissue. The green staining of the stroma in **c** and **h** mostly belonged to the autofluorescence acquired by the tissue itself. Images were taken with 20$\times$ magnification lens and the scale bars correspond to 100 μm.

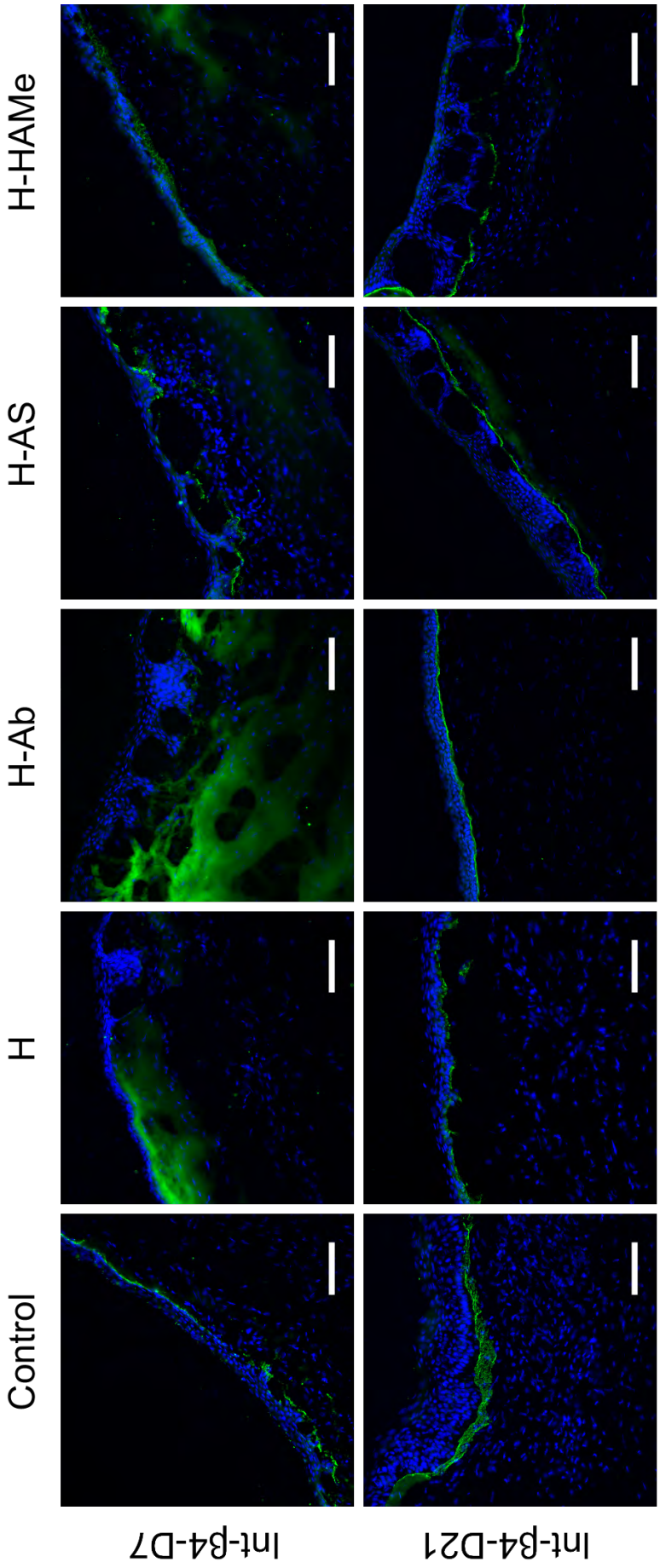

IV.43. FIGURE: Fluorescent immunostaining for Integrin-$\beta 4$ marker in the central cornea of rabbit corneal samples obtained from the *in vivo* assay. Rabbit corneas were treated with artificial tears (Control) or with H, H-Ab, H-AS or H-HAMe hydrogels and processed 7 (**a-e**) and 21 (**f-j**) days after surgery. Images were taken with 20× magnification lens and the scale bars correspond to 100 μm.

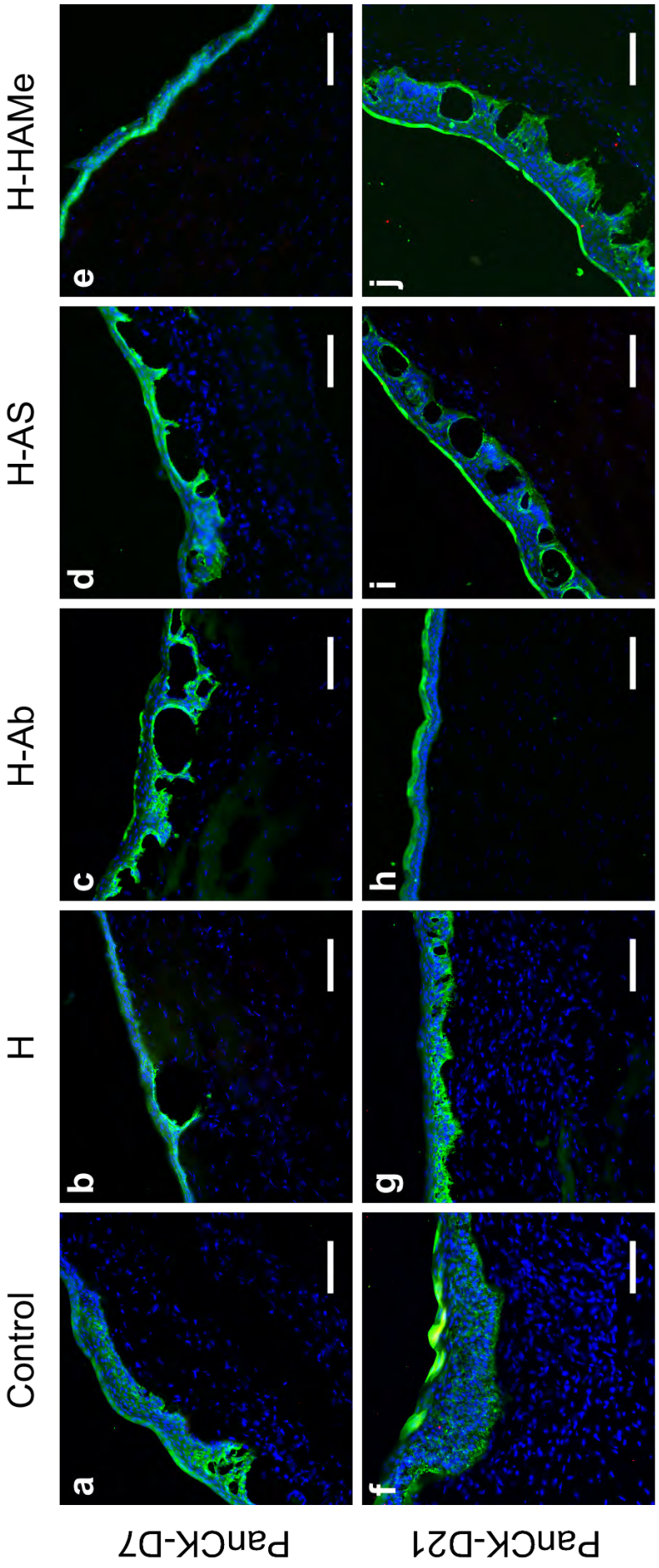

IV.44. FIGURE: Inmunofluoresce staining of PanCK marker in the central cornea of rabbit corneal samples obtained from the *in vivo* assay Rabbit corneas were treated with artificial tears (Control) or with H, H-Ab, H-AS or H-HAMe hydrogels and processed 7 (**a-e**) and 21 (**f-j**) days after surgery. Images were taken with 20× magnification lens and the scale bars correspond to 100 μm.

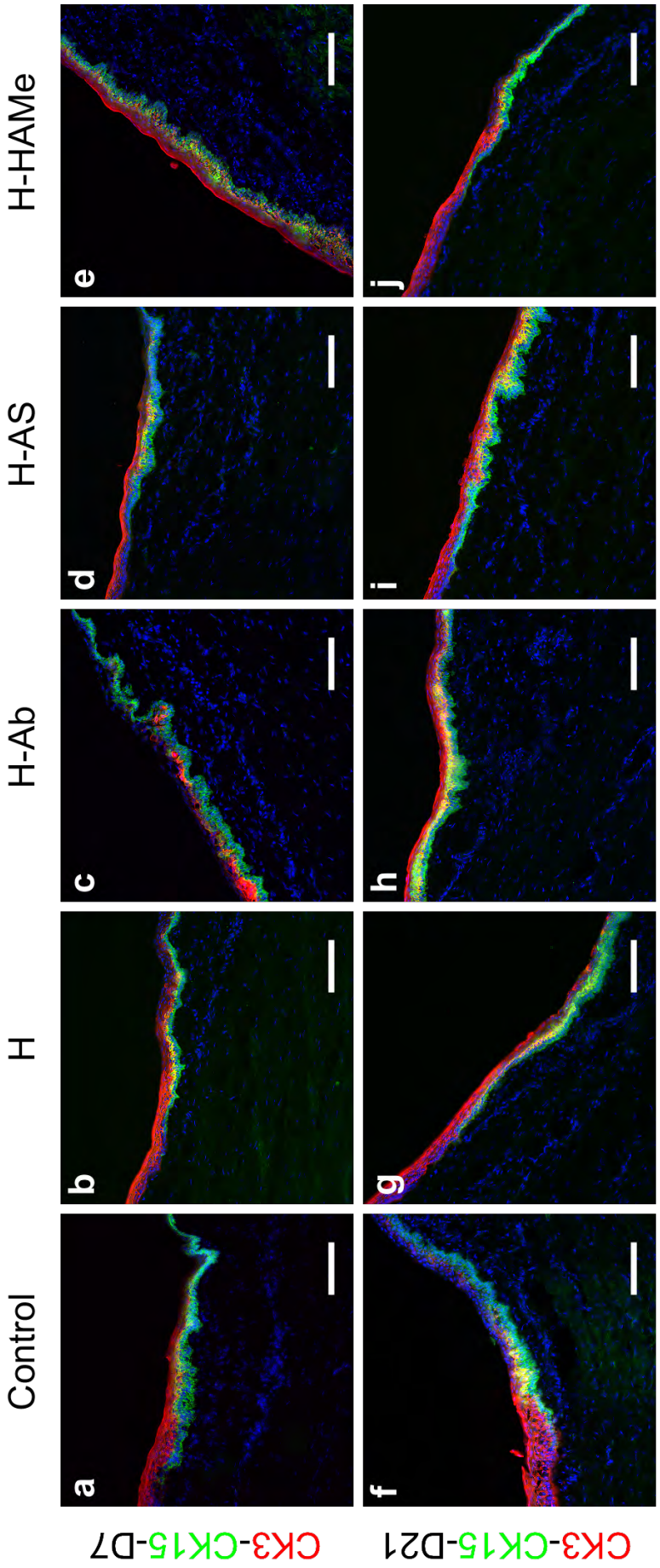

IV.45. FIGURE: Expression of CK3 (red) and CK15 (green) markers in the limbus of rabbit corneal samples obtained from the *in vivo* assay. Rabbit corneas were treated with artificial tears (Control) or with H, H-Ab, H-AS or H-HAMe hydrogels and processed 7 (**a-e**) and 21 (**f-j**) days after surgery. Images were taken with 20× magnification lens and the scale bars correspond to 100 μm.

IV.46. FIGURE: Expression of ZO-1 (red) and Ki67 (green) markers in the central cornea of rabbit corneal samples obtained from the *in vivo* assay. Rabbit corneas were treated with artificial tears (Control) or with H, H-Ab, H-AS or H-HAMe hydrogels and processed 7 (**a-e**) and 21 (**f-j**) days after surgery. Images were taken with 20× magnification lens and the scale bars correspond to 100 μm.

8. Primary limbal cell cultures

The primary cultures of cells extracted from human limbal rims were characterised as a first step in the development of a tissue-engineered limbal substitute for treating LSCD. The presence or absence of limbal stem cells, their quantity, and exact location in the epithelium of human sclerocorneal tissues were verified. Additionally, their potential to grow in culture and become a source of limbal stem-like epithelial cells for limbal cell transplantation was assessed. Immunohistochemical and immunocytochemical analyses were performed to determine the attributes of LEPCs and the various subpopulations present in the limbal niche.

8.1. ΔNp63α and melan A cell markers' expression in human sclerocorneal tissue

The Melan A marker was combined with p63 antibody to examine the relationship and location of both markers within the epithelium of sclerocorneal tissues. Although p63 is not a definitive limbal stem/progenitor cell marker, is one of the most used for the identification of these cells, being the ΔNp63α the predominant isoform in the limbal region.

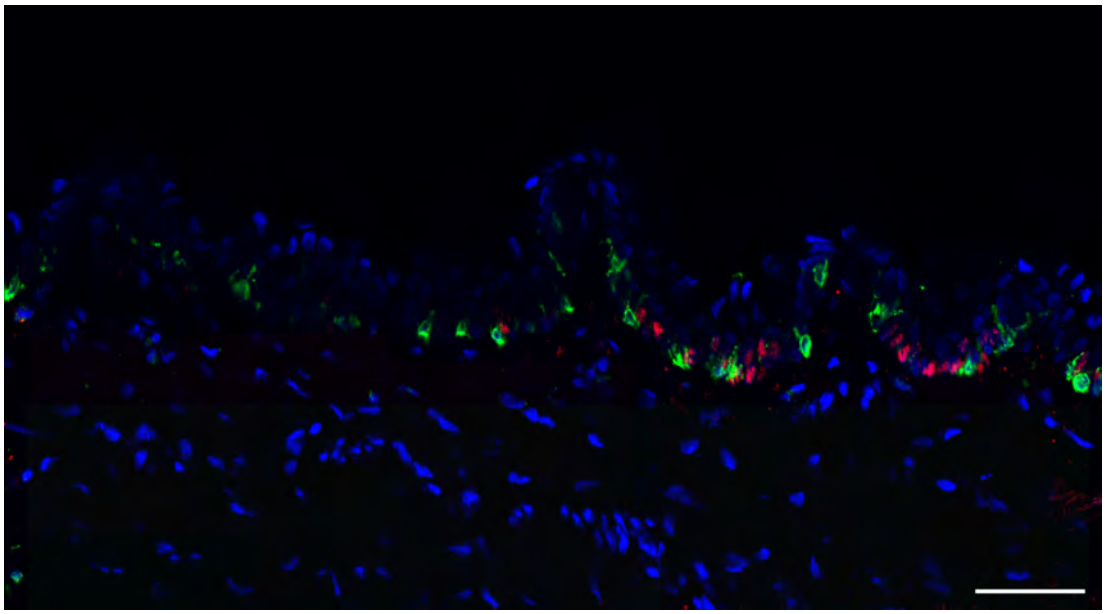

IV.47. FIGURE: Expressions of ΔNp63α and melan A-positive cells in a histological section of the limbal area of a human sclerocorneal tissue. The image was taken with a 20× magnification lens and scale bar corresponds to 50 μm. The image shows the specific localisation of ΔNp63α and melan A-positive cells in the limbal crypts.

Both markers were observed in the limbal region, more specifically in the limbal crypts (Figure IV.47). Melanocytes (green) were located among ΔNp63*α* bright cells (red), which potentially indicated undifferentiated stem/progenitor cells. Melan A-positive cells exhibited a branched morphology.

8.2. Isolation and culture of limbal epithelial cells

The effectiveness of cell extraction techniques from sclerocorneal tissues and their expansion *in vitro* were evaluated using multiple immunocytochemical procedures. The evolution of cell marker expression was measured across different culture phases. Epithelial cells obtained directly from the corneal limbal area were precipitated using a cytospin and their cell markers were analysed. Positive cells expressing CK15, vimentin, and ΔNp63*α* were detected in directly precipitated epithelial cells (**a, e** in figure IV.48). Subsequently, limbal epithelial cells isolated from sclerocorneal tissues were cultured for 12 $\pm$ 2 days (p0 passage) while preserving high CK15 marker staining (**b** in figure IV.48). As the cells were subcultured, the expression of the CK15 protein decreased. Only 40% of the cells precipitated from the cytospin were stained with CK15, whereas only 10% of passage 0 cultured cells were stained with CK15. CK15 expression was completely absent at the second passage of cultures (**c** in figure IV.48). Statistical differences were observed between p0 (Cytospin) and p1, p2 and p3 of the cultured cells for CK15 ($p = 0.005$) and vimentin ($p = 0.037$) cell markers (**d** in figure IV.48). Vimentin cell marker expression was only observed in a small cell proportion (roughly 7% of the total cells) derived from sclerocorneal tissues isolated and centrifuged using the cytospin. Furthermore, in p0 passage cultures, cells displaying the vimentin marker showed a branched and elongated morphology (**b** in figure IV.48) with some of these cells containing CK15-positive cells. The early passages of epithelial cultures exhibited varying morphological features compared to the cells containing vimentin found in second and later passages of epithelial cultures (**c** in figure IV.48).

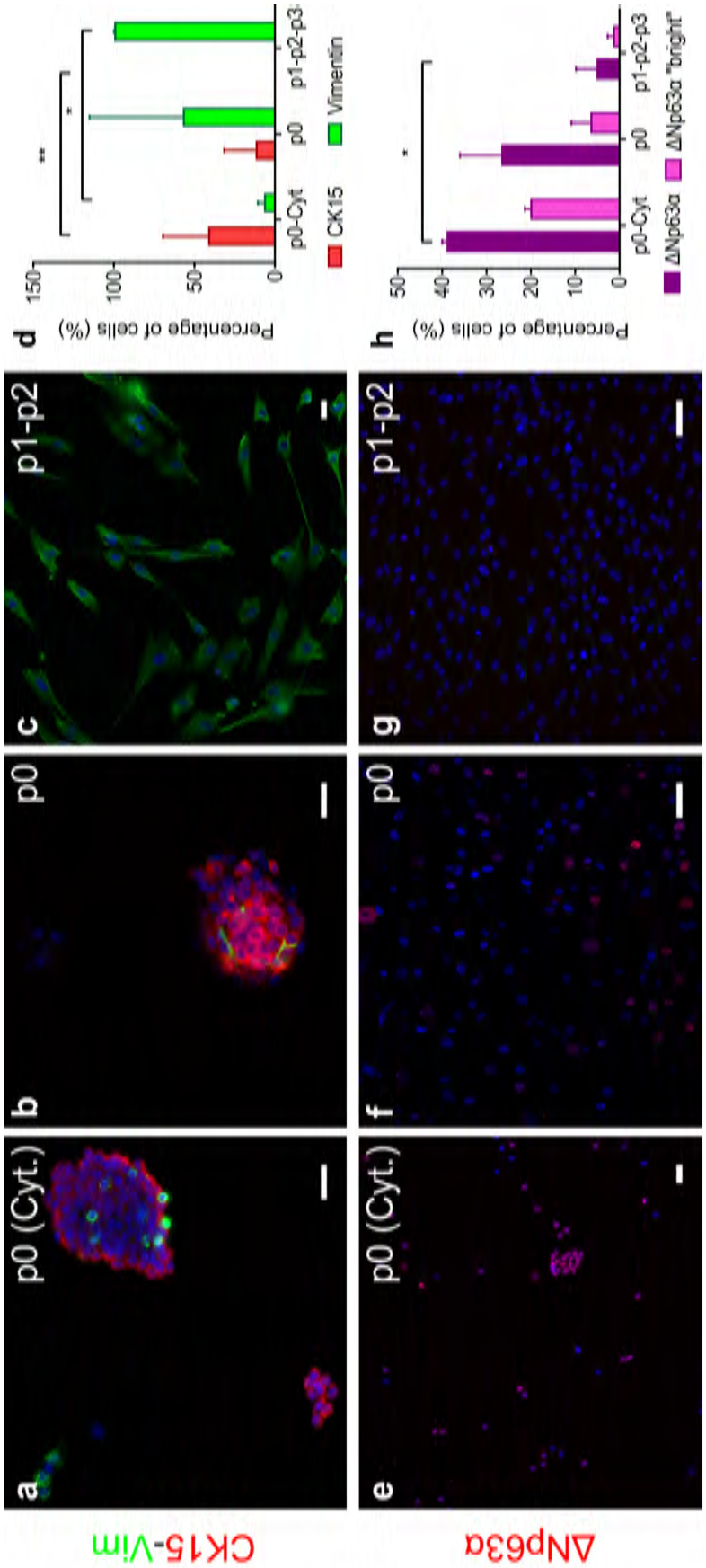

IV.48. FIGURE: Expressions of CK15, vimentin and ΔNp63α markers in human limbal epithelial cells directly isolated after tissue enzymatic digestion (**a** and **e**, p0 Cytospin) or cultured during several cell passages p0 (**b, f**) and p1-p2 (**c, g**). The images **a** and **e** show that the cells extracted directly after tissue digestion highly expressed the non-differentiation markers CK15 and ΔNp63α. An exponential decrease in the undifferentiation markers and a predominant vimentin staining were registered throughout the passages (Images **b, c, f, g**). The graphs show the evolution of the percentage of CK15- and vimentin-positive cells (graph **d**) and ΔNp63α bright cells (graph **h**) from several sclerocorneal tissues throughout the passages. Statistical significance is defined as p-value $*$ $p < 0.05$, $**$ $p < 0.01$, $***$ $p < 0.001$, $****$ $p < 0.0001$. Images were taken with 20$\times$ magnification and the scale bars correspond to 25 μm.

These vimentin positive cells from passage 2 showed a morphology that corresponded to differentiated stromal cells, but did not show the epithelial cell phenotype.

Both fresh and cultured sclerocorneal tissues generated epithelial cells that exhibited positive staining for ΔNp63*α* following tissue digestion. The evolution of the staining pattern remained uniform in all the cultures extracted from various tissues. The number of ΔNp63*α* bright cells decreased significantly between successive passages, while the number of cells with no or insignificant ΔNp63*α* signal increased (**e-h** in figure IV.48). The staining pattern decreased from 20% to 6% of the total number of counted bright cells in the passage of cells directly precipitated from the cytospin to the p0 culture. From the p0 passage onwards, the proportion of ΔNp63*α*-positive cells did not exceed 5%. Statistically significant differences were recorded amongst the cultured cells at p0 (Cytospin) and p1, p2, and p3 ($p = 0.043$) (**h** in figure IV.48).

8.3. Presence of melanocytes in the epithelial cell culture

Morphological variations were observed in vimentin-positive cells in epithelial and stromal cell cultures of p0 passage. The dendritic phenotype resembling melanocytes was seen in the vimentin-stained cells of the epithelial culture (**a** of the figure IV.49). Ramified cells were observed encircling the formation of epithelial cell colonies (**a** in figure IV.50). Melanocytes were also detected in epithelial cultures using the melan A marker (**b, c** in figure IV.50).

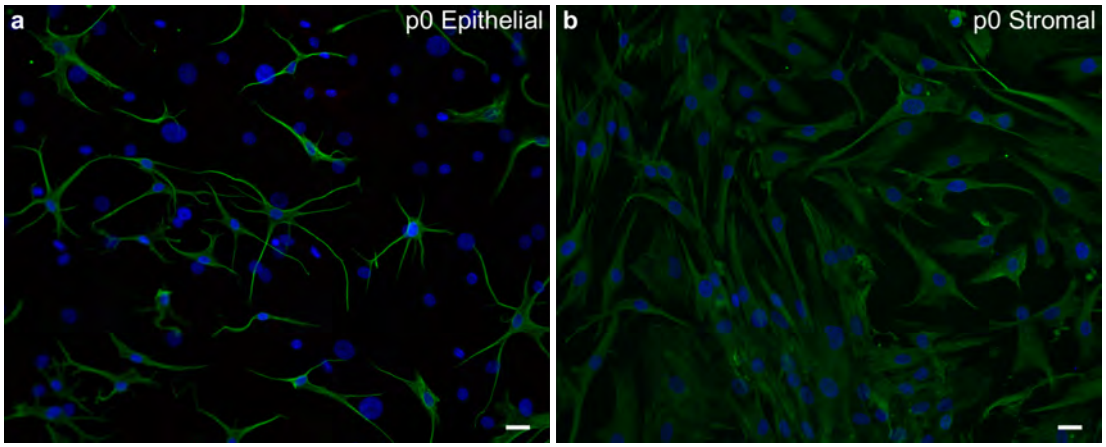

IV.49. FIGURE: Expression of the vimentin marker in human limbal epithelial (**a**) and stromal (**b**) cell cultures. Both cultures corresponded to p0 passage. Both images were taken with a 20× magnification lens and the scale bars correspond to 25 μm.

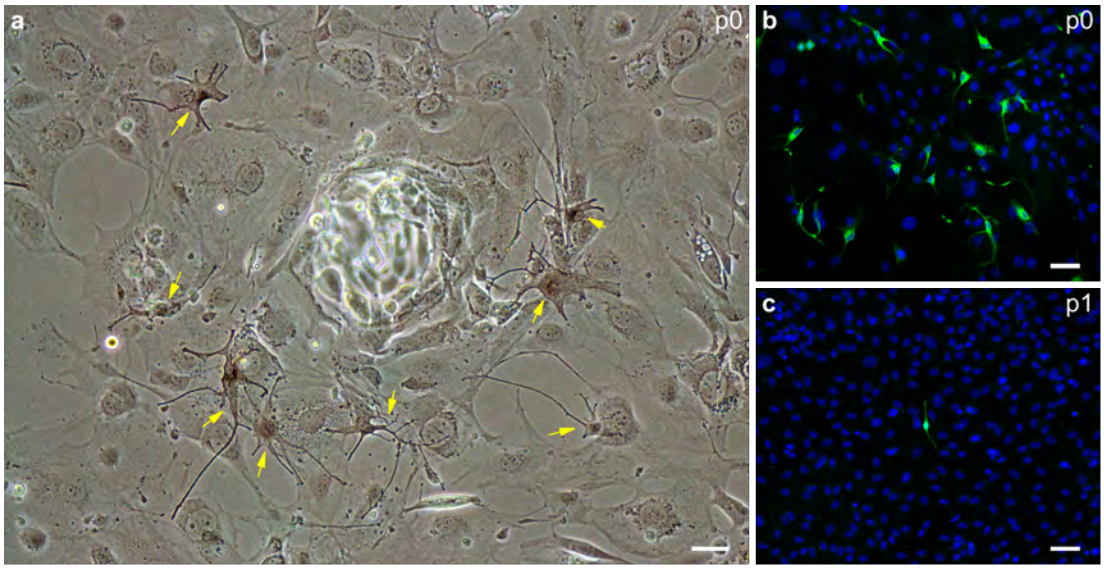

IV.50. FIGURE: Human limbal epithelial cell culture of passage p0 and passage p1. The phase-contrast microscopy image on the left (**a**) shows epithelial cells of passages p0 seeded above a *feeder layer* of 3T3 cells. Cells marked with yellow arrowheads correspond to the melanocytes that enclosed the forming epithelial stem cell colony. **b**) and **c**) fluorescence microscopy images show the expression of the melan A marker in epithelial cells of passages p0 and p1. All the images were taken with 20× magnification lens and all the scale bars correspond to 50 μm.

The p0 passages of the cultured cells from the analysed sclerocorneal tissues displayed prominent melan-A staining. Similar to the expression patterns of undifferentiated markers ΔNp63α and CK15, the staining for melan-A exhibited a significant decrease across all passages (Figure IV.50). Figure IV.51 illustrates the arrangement of melan A-positive melanocytes and CK15-positive cells in a colony of stem-like limbal epithelial cells of p0 passage. Melan-A positive melanocytes were observed between the CK15 cells, with their branches surrounding the CK15-positive cells in a protective manner.

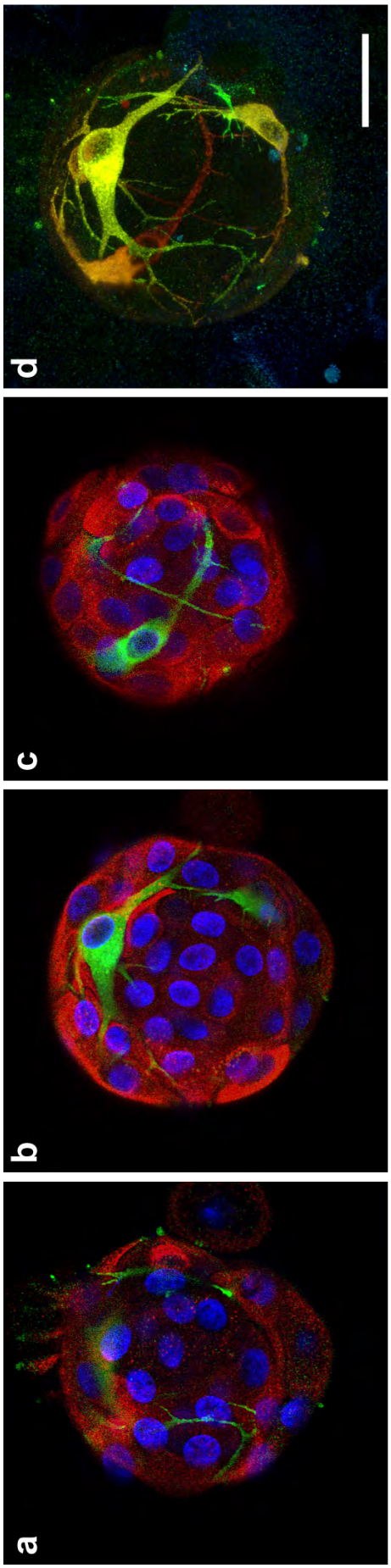

IV.51. FIGURE: Different confocal planes (**a-c**) of a holoclon of CK15-labelled epithelial stem/progenitor cells embraced by Melan A positive melanocytes. Figure **d** shows the reconstruction of all the acquired planes of the colony. The image was taken with a super-resolution microscope with 40× magnfication lens. The scale bar corresponds to 25 μm.

V. DISCUSSION

1. Evaluation of the films that could be used for corneal wound healing

Several materials are currently undergoing evaluation as prospective contenders for use as cell support platforms that can facilitate adhesion and viability of corneal cells [343–345]. Materials aiming to mimic the native cornea must meet the requirements set by the major corneal functions. This can be summarised as offering optical properties that are similar to those of native tissue, along with biocompatibility, biodegradability, and biointegration by stimulating cellular growth, proliferation and migration [346].

As an initial assessment of options, we aimed to conduct an *in vitro* analysis of various protein-based materials suitable for possible corneal bioengineering applications. The film format was employed due to its ease of use during *in vitro* cell culture assays.

The cornea is responsible for more than 60% of the total refractive power of the eye [347], which is why, in addition to the thinness, morphology and distribution of keratocytes in the stroma, the orderly arrangement of collagen fibrils makes the cornea a transparent tissue and, in turn, produces destructive interference from scattered light that enhances light transmission [10]. Because of this essential function of the cornea, measurement of the optical properties of materials selected for corneal applications is very important.

Chemically crosslinked gelatine films (GEL-LAC, GEL-CA) exhibited greater light transmission following hydration. The crosslinking that took place between the amino group of gelatine and the carbonyl group of lactose or the carboxyl group of citric acid led to enhanced optical properties and a more compact structure, illustrated in the SEM images. Compared to the COL and SPI films crosslinked by hydrogen bonding between the polar groups of proteins and the hydroxyl groups of glycerol, the GEL-LAC and GEL-CA films performed optically better.

The total transmittance of light is comprised of two components: direct transmittance, where the light propagation direction remains unchanged, and diffuse transmittance, which determines the clarity and haze of objects [348]. Measuring the effect of diffuse transmittance or scattering involved positioning the films at

a known distance from recognisable patterns, to prevent false contact clarity [349, 350]. The hydrated gelatine films showed favourable transparency, whereas COL and SPI, despite recording transmittance values between 60 and 80%, did not offer enough translucency to clearly distinguish patterns. The reason for this was associated with the partial structural order of the films, which hindered light scattering [351]. Subsurface light scattering is a phenomenon that explains the relationship between transparency, translucency, and opacity. It occurs when internal light scattering causes a transparent medium to become translucent and eventually opaque. Translucent materials scatter light, while fully transparent ones do not. However, in cases where part of the light is scattered and part is transmitted, if the amount of scattering is low enough or the object is thin enough, the background is clear through a translucent object. The transparency of a material can be affected by factors such as light absorption, microstructure, material thickness, or a refractive index mismatch [352]. In the case of the hydrated films, their transparency may have improved when they were immersed in water due to the closer refractive indexes between the material and water. The refractive index indicates the deflection of light as it passes through a material. If the two indices are close or coincide, the material is less likely to scatter or reflect light, which increases its transparency.

The results suggested the selection of gelatine as the best candidate if transparency would be the main concern. Gelatine is a versatile substance that inherently provides more transparency than collagen [345]. In addition to the excellent clarity and pattern definition observed in GEL-LAC and GEL-AC, GEL-LAC films could protect against UV radiation due to the yellowish tone caused by the Maillard reaction products formed from the non-enzymatic glycation of gelatine and lactose [353]. This is a very interesting feature for materials that would be used for the ocular surface. For instance, research suggested that yellow-tinted lenses offer protection against retinal cell damage [354].

The collagenase-mediated degradation findings emphasised the significance of the crosslinking agent, method, and crosslinking time in controlling degradation rates of biomaterials. The physically crosslinked COL and SPI films displayed early degradation, where COL degraded in just 15 minutes and SPI degraded by up to 40% in 24 hours. Additionally, the degradation profiles in gelatine films were influenced by the type of chemical reaction. After 24 hours, approximately 50% of the GEL-LAC

film remained, whereas slightly less than 40% of GEL-CA was retained. It should be noted that the initial weight loss experienced by all films corresponded to the glycerol, which was dissolved in solution. Following this initial drop, only COL was gradually degraded by hydrolysis.

The remodelling of the cornea's ECM is regulated by keratocyte-secreted metalloproteinases (MMP), which are zinc-dependent endopeptidases that degrade and remodel the ECM. MMPs are divided into membrane-type MMPs, collagenases, gelatinases, stromelysins, and matrilysins based on their chemical substrate and function. Inhibitors of metalloproteinases (TIMP) regulate the action of MMPs. Therefore, an imbalance between MMPs/TIMPs can lead to altered corneal surface homeostasis, resulting in higher levels of MMPs that are implicated in various pathologies [355]. For instance, in a hyperosmolar medium simulating dry eye disease, the amount of MMP-1 increased in a primary corneal epithelial cell culture from a mean of 12.02 ng/ml in the control group to 88.46 ng/ml in the cells exposed to high osmolarity [356]. Elevated MMP levels were also reported in the epithelium of patients with recurrent corneal erosions or in patients requiring penetrating and deep anterior lamellar keratoplasty, among others [357, 358].

The amount of collagenase used in this study was high (200 μg/ml) compared to the levels found in a real eye environment, and the films were continuously exposed to the enzyme. In reality, the degradation of the films would occur over a longer period of time than what was recorded in our results. Any substrate or scaffold created for the cornea must provide sufficient support to promote cell growth, migration, and proliferation during the tissue regeneration process, but it must also degrade concurrently with corneal stromal regrowth [306, 359]. The fact that the films were degraded by collagenases suggested that they were biodegradable and could facilitate internal tissue remodelling.

Regarding the cytotoxicity of the materials, viability values of less than 70% recorded with the collagen films implied that they could not be considered as cell-friendly films [360]. However, the unsatisfactory outcomes were not attributed to type I collagen itself, as the collagen is a material previously tested by other researchers [361, 362].

For instance, Isaacson and colleagues utilised a methacrylated form of this type I collagen combined with alginate in their constructs, and they observed a viability rate of 90% at 24 hours and 83% after 7 days with corneal keratocytes. These cells may be comparable to those utilised in our study [363]. Thus, this highlights the significance of material processing, crosslinking techniques, and the potential impact of adding different components on cell compatibility. The culture media was not changed throughout the entire study period, potentially influencing the observation of statistically significant differences in all treatment groups after 72 hours of exposure in comparison to the control. However, this scenario would not manifest in a real environment as the tears and blinking would continually renew the media in contact with the corneal cells [364].

Both cell types showed cell adhesion, viability, and migration on the films that were similar to the control. GEL-LAC and SPI demonstrated quicker wound closure than the control or GEL-AC.

The stiffness of support materials regulates cell behaviour and fate. Research indicates that corneal epithelial cells seeded on smooth surfaces are more likely to maintain their indifferentiation potential [365]. Furthermore, soft surfaces are considered advantageous for keratocytes to preserve their phenotype, as stiffer materials increase the likelihood of transformation into myofibroblasts, ultimately leading to accelerated deterioration of corneal tissue functions [366]. Hence, variations in cell behaviour on different films imply a need to investigate surface characteristics (e.g. roughness, topography or chemistry) that could affect cellular responses like adherence, cell proliferation and cell migration on materials [367].

2. Hydrogel solution for the treatment of corneal ulcers

Corneal epithelial defects are frequent wounds in ophthalmology practice. They usually heal with conventional treatments such as preservative-free artificial tears and antibiotics and/or topical corticosteroids, which may be in the form of eye drops or ointments. In some instances, however, ulcers are slow to heal and may progress to the corneal stroma or in the worst cases, even perforate the eye, which may lead to visual impairments and compromise the structural integrity of the eyeball. Various therapeutic options are available when this occurs, ranging from non-invasive eye drops that aim to restore the normal structure and function of the epithelium [94], soft

bandages contact lenses or pressure patching [94, 96], to surgical treatments such as grafts [114, 115], tarsorrhaphies [117–119] or stem cell transplants [120].

This thesis proposes an accessible intermediate solution for clinical applications that can temporarily fill corneal defects with a substrate that progressively delivers molecules that enhance healing, without requiring surgical intervention.

Based on the film characterisation results, gelatine was chosen as the primary material for hydrogel synthesis.

Gelatine is derived from acidic or alkaline hydrolysis of collagen and it was preferred due to its biocompatibility, non-immunogenicity, ease of handling and abundance, among other reasons. Compared to collagen, which is more sensitive to pH and buffer changes, gelatine is less complicated to work with and also more cost-effective, being very manageable for clinicians in medical centres.

When dissolved at concentrations exceeding 2% w/v, gelatine has the potential to generate physically crosslinked hydrogels at temperatures below 30-35 °C, due to a change in conformation of its molecules from a random spiral structure to a triple helix. Consequently, intermolecular hydrogen bonds are formed between large fractions of gelatine chains [368, 369]. However, this physical network disintegrates at higher temperatures, restricting its use to physiological temperatures of 37 °C.

2.1. Hydrogel's composition and crosslinking mechanism

Although the physiological temperature of the eye surface is around 34 °C [370], chemical crosslinking through photopolymerisation with riboflavin phosphate was selected to enhance the material's stability and mechanical characteristics. The decision to use RFP as a crosslinking agent for the hydrogel formation was based on its extensive usage in the field of ophthalmology.

In the cornea, collagen fibrils' structure and their spatial arrangement are responsible for the mechanical stability of the tissue. Moreover, their crosslinks also prevent collagen fibrils from slipping in the curved cornea. When the degree of crosslinking increases or decreases, the tissue's biomechanical properties get affected, causing a reduction in visual acuity [371]. For instance, corneal ectatic disorders comprise a group of medical conditions that lead to the thinning and bulging of the cornea. This condition reduces crosslinking, resulting in decreased corneal rigidity.

Keratoconus is one of the most frequently occurring ectatic conditions, which reduces corneal rigidity due to impaired crosslinking within or between collagen molecules [372].

The procedure of crosslinking applied to the affected stromal tissue is reliant on the utilisation of UVA rays in combination with a photosensitiser to create new covalent linkages between the collagen fibrils, consequently inducing an increase in corneal rigidity [373]. The use of UVA irradiated riboflavin solution was determined because of its localised effect, short treatment time and because it does not alter corneal transparency [371]. The first associated clinical trial was released in 2003 [374], and the technique was given FDA approval in 2016 [375], being the only crosslinking technique approved thus far for the creation of new collagen crosslinks.

Riboflavin, also known as vitamin B2, is a type of vitamin B that is primarily found in dairy products, meat, fish, dark green vegetables, grains, and cereals. It acts as a natural yellowish dye and has a photosensitive chemical structure that exhibits four light absorption peaks, one in the visible range of blue light (445 nm) and three in the UV range (375, 265, 220 nm) [376].

The substance is classified as a type II photoinitiator, meaning it requires an electron donor to act as a co-initiator for the initiation of photopolymerisation through the generation of radicals or radical ions [218]. Its configuration contains two components, the three-ring 7,8-dimethyl-10-alkylisoaloxazine portion responsible for its redox properties, photosensitivity, and UV absorption, this is also known as the Flavin core, and the ribitol tail comprising four hydroxyl groups that provides the scope for further modifications [377–379]. A common alteration to the original riboflavin structure involves the inclusion of a phosphate group. Flavin mononucleotide, or riboflavin phosphate (RFP), refers to the sodium salt of riboflavin that contains the core flavin or isoalloxazine ring. This renders RFP to maintain the identical photochemical properties as riboflavin, whilst enhancing its solubility [380].

Riboflavin's crosslinking mechanisms works as follows. The flavin core of riboflavin absorbs light and is excited to a short-lived singlet state reactive product, which subsequently reaches a highly reactive excited triplet state ($3RF^*$). Some singlet state products release their energy in the form of heat or fluorescence without reaching the triplet state, and part of the $3RF^*$ relaxes to a ground state [380]. The remaining portion of the $3RF^*$ is the one that triggers the crosslinking reaction, this triplet state

is an enduring birradical capable of oxidizing protein amino acid chains [381]. When oxygen is present in the reaction, the triplet state of riboflavin can produce singlet oxygen ($^1O_2$), which generates further radical and non-radical oxidation reactions resulting in crosslinking of the polymeric network [382]. RF-induced crosslinking density varies depending on the amino acid composition of the different proteins [383].

In the cornea, the stiffening is a result of the excitation of riboflavin to a triplet state upon UVA irradiation. This irradiation leads to the formation of reactive oxygen species of $HO^{\bullet}$, $O_2^{\bullet 2-}$, and $O_2^{\bullet -}$, in the case of type I mechanism, or the production of singlet oxygen that will subsequently generate peroxide and hydroxyl radicals, in the case of type II mechanism [384]. These riboflavin-induced free radicals or reactive oxygen species react with collagen molecules, resulting in covalent bonds between the amino acids of the collagen fibrils [374, 385, 386].

Riboflavin's oxidation results in the crosslinking of proteins that are high in amino acids, including histidine, lysine, tyrosine, and tryptophan. In addition, cysteine, methionine, tyrosine, tryptophan, and arginine can also be oxidised in the presence of riboflavin. Collagen comprises of proline, hydroxyproline, hydroxyllysine, histidine, tyrosine or threonine, which can undergo oxidation in the presence of riboflavin via type I or type II oxidative mechanisms [371]. Thus, the selection of riboflavin as a crosslinker for the gelatine hydrogel was based on its natural origin, non-toxicity and extensive clinical use. Our goal was to imitate established methods and mimick a real biological system, like the cornea, using our gelatine hydrogel solution.

All amino acids found in collagen are also present in gelatine, but it is low in methionine, cysteine and tyrosine due to degradation during hydrolysis [159]. No modifications were intended, such as the introduction of additional functional groups as methacrylate groups. Thus, it was hypothesised that the amino acids remaining in collagen [371] and retained in gelatine molecules after hydrolysis interact with RFP and crosslink to produce a crosslinking density sufficient for our intended use.

It was decided to use blue light as the illumination source rather than UV light. Riboflavin has light absorption peaks in both the UV range and the blue spectrum, with a peak at 445 nm, and is equally excited by both. In ophthalmology, blue light is employed to observe fluorescein stains in the cornea and is considered a safer option than UVA light. Although UVA light remains the most effective way of inducing

corneal crosslinking, research has also shown that blue light can initiate crosslinking and potentially be used as a substitute method [212, 215, 387].

The light source was positioned 10 cm away, administering a dosage of 100 mW/cm^2 for a duration of 2 minutes. This interval was chosen after evaluating multiple time periods on the *ex vivo* corneas.

Besides, the inclusion of various components was proposed to examine their impact on crosslinking and their possible advantageous properties when added to the hydrogel.

Dextran and methyl cellulose were selected based on their ophthalmic use and documented studies.

Dextran is a polysaccharide formed through the condensation of glucose and synthesised from sucrose by lactic acid bacteria. It is an α(1,6)-linked glucan with side chains linked to the backbone's C-3 position, with molecular weights that range from 1000 to 40000 Da [388]. In ophthalmology, dextran's lubricating properties make it a useful active ingredient in eye drops. The original and first approved corneal crosslinking procedure for the treatment of Keratoconus, the Dresden epithelial-off crosslinking protocol, for instance, employs a 20% (w/v) dextran solution as the main supplement for creating a 0.1% (w/v) riboflavin-5-phosphate solution [374]. This mixture increases the eye drop's viscosity and renders an isotonic solution via a hyperosmolar riboflavin solution [389].

Methyl cellulose (MC) is a water soluble polysaccharide derived from cellulose, which hydrates when exposed to cold water and forms a gel when heated. It is obtainable in different molecular weights ranging from 10-220 kDa and in ophthalmology, it can serve as a thickening agent in eye drops, a gelling agent in injections or as a constituent of films, filaments, or inserts [390, 391].

Both dextran and MC have been utilised in riboflavin solutions for corneal crosslinking procedures. Early research showed the effectiveness of crosslinking with riboflavin dextran solution, but MC has become the preferred method due to improved intraoperative central corneal thickness during crosslinking [392, 393], as well as increased diffusion velocity [394] and deeper stromal crosslinking [395], which may impact clinical outcomes.

Hyaluronic acid (HA) is a natural polysaccharide polymer with numerous functional groups and a high water-binding capacity. It is also a constituent of human ocular physiology and that is why it was decided to incorporate it into the hydrogel. In addition, HA is present in tear fluid, where it functions as follows: when blinking occurs, its molecules align, the HA temporarily loses its viscosity, and it spreads smoothly on the surface of the cornea. Between blinks, the solution increases in viscosity, thereby maximising its residence time on the ocular surface and improving hydration and lubrication [396]. These features together with its cell proliferation, anti-inflammatory, antioxidant and wound repair properties [144] make it a highly appropriate component for eye drops. The incorporation of HA was expected to generate similar outcomes as dextran or MC by interacting with gelatine and riboflavin molecules, leading to bond formation. Furthermore, it was expected to regulate or neutralise some of the free radicals produced by riboflavin [397].

The *in vitro* characterisation of the hydrogels resulted in the subsequent conclusions. The stress required to initiate flow was increased with the addition of HA or MC to the hydrogel. During the development of composite hydrogels made from phenolic hydroxyl possessing hyaluronic acid and gelatine, it was observed that viscosity values increased at low shear rates with increasing HA concentration. Conversely, viscosity decreased at higher shear rates, indicating an improvement in shear-thinning behavior [398]. Considering the aforementioned results and that cellulose and its derivatives are also commonly used as thickening agents [390, 391, 399], it was expected that both, HA and MC would have such an effect on the developed hydrogels. Dextran, however, caused the opposite outcome.

Concerning the *in vitro* release, the dextran hydrogel noticeably slowed down the release of compounds of different sizes. The performance of the hydrogels incorporating HA and MC was similar to each other, with a reduction in the release kinetics of IgG compared to hydrogel G, and an increase in the release kinetics of Albumin.

The results of transparency and transmittance measurements indicated that the introduction of any of the three components decreased both parameters. Notably, the patterns behind the hydrogels appeared more opaque and blurry, particularly with the use of HA, followed by dextran and MC. Silvestro et al. already reported that the transparency levels of their developed chitosan dressings decreased with

the addition of HA at different concentrations. They attributed the effect to the formation of polyelectrolytic aggregates between the two materials [400]. The addition of MC resulted in transmittance levels that were most comparable to those of gelatine; however, the images remained blurry. Ensuring high levels of transparency and transmittance is crucial for treating ocular surface conditions so this is one of the main parameters considered for the final selection.

The incorporation of components led to a higher degree of swelling and expansion. The effect of HA could be attributed to the compound's high water-binding capacity, the carboxylate group in hyaluronic acid results in negative charges that attract water molecules through hydrogen bonds [396, 401]. Dextran or cellulose and its derivatives are water-attracting compounds too. For example, 1 g of dextran with a molecular weight of 70 kDa can hold up to 25 ml of water [402]. Cellulose contains numerous hydroxyl groups that form strong hydrogen bonds with water molecules, making it a material with a high water-holding capacity [403]. Nonetheless, this property may not be advantageous for accommodating the hydrogel in the wound. The swelling ratio is a key indicator of the hydrogel's shape stability. A lower ratio guarantees that the hydrogel can affix to the host cornea, preventing detachment from the stromal bed owing to excessive swelling [404]. Finally, biocompatibility and cell cycle analysis outcomes were similar among all groups.

After conducting *in vitro* experiments, it was established that the addition of dextran, HA, or MC did not lead to a significant enhancement of the hydrogel's properties. Therefore, it was decided to stick with the fundamental composition of the hydrogel. The following functionalisation, *ex vivo* testing and *in vivo* testing experiments were carried out exclusively on the gelatine and RFP hydrogel.

2.2. Hydrogel's functionalisation

The hydrogel was modified to enrich the solution with constituents that reduce inflammation and accelerate the process of wound healing.

Haemoderivatives and human amniotic membrane extracts (HAMe) were chosen as rich sources of growth factors to functionalise the hydrogel.

Eye drops prepared from blood derivatives have been used to treat ocular surface diseases for nearly five decades [405]. The use of this therapy arises from the fact that a significant proportion of growth factors and proteins present in adult peripheral blood

are also found in tear fluid in similar concentrations. This finding is therapeutically valuable, as the ocular surface maintains its homeostasis through the trophic factors produced by the different cellular constituents of the lacrimal function unit that mutually support and protect each other [406].

Two blood-derived products were used in this study: autologous serum (AS) and serum derived from plasma rich in growth factors (sPRGF). AS consists of the supernatant collected after centrifugation of clotted blood samples, in which leukocytes' release is also included. sPRGF is obtained after inducing clotting with calcium chloride in the supernatant fraction above the white blood cell series resulting from centrifugation of unclotted blood. The release of growth factors in this case occurs in the absence of leukocytes, thus avoiding the effect of pro-inflammatory cytokines contained in white blood cells [407].

AS eye drops were the first blood-derived preparation used for the treatment of ocular surface pathologies [106, 408, 409]. At the ocular surface level, AS not only acts as a lubricant but also provides numerous substances essential for the recovery of the damaged epithelium, including vitamin A, epidermal growth factor (EGF), fibronectin and a variety of cytokines [410]. AS tears have also been found to promote epithelial healing and reduce post-operative pain in relation to crosslinking procedures [411].

sPRGF was introduced years later [110, 412] demonstrating potential as a therapeutic method for treating ocular surface disorders. It contains a wide range of factors involved in ocular regeneration [413], anti-inflammatory agents [414] and bacteriostatic/bactericidal molecules [415, 416], it affects the proliferation and migration of keratocytes and conjunctival fibroblasts and influences the modulation of myofibroblasts in the stroma of ocular surface tissues [417, 418]. It has demonstrated efficacy as a therapeutic option for neurotrophic keratitis [419], dry eye [420], ocular surface disease in glaucoma patients [421] and in aiding wound healing after photorefractive keratectomy [422, 423] or corneal wounds due to epithelial scraping [424, 425].

Human amniotic membrane (HAM) has been used in numerous ophthalmic applications due to its anti-inflammatory, immunomodulatory, low immunogenicity, antibacterial, angio-modulatory, antiscarring and haemocompatibility properties [426–430]. Its effects on corneal regeneration can be attributed to the various factors contained within, such as EGF, keratinocyte growth factor (KGF), vascular endothelial

growth factor (VEGF), basic fibroblast growth factor (bFGF), hepatocyte growth factor (HGF), platelet-derived growth factor (PDGF), the heavy chain (HC)-hyaluronan (HA)/pentraxin 3 (PTX3) complex and various structural proteins, including collagen (types I, III, VI, and VII), laminin, fibronectin, lumican, and osteoglycin [431–433]. The use of HAM has shown potential in ocular surface reconstruction and LSCD treatment [267, 434], as well as treating PEDs, chemical burns, and Stevens-Johnsons syndrome [435]. It has been used for the cultivation and release of various cell types [436, 437], as well as in corneal tissue engineering and delivery of corneal epithelial progenitor cells for LSCD [434].

Likewise, amniotic membrane extract (AMe) has successfully treated dry eyes and chemical burns when used as an eye drop, has proven to enhance corneal epithelial cell proliferation and differentiation, facilitate epithelial wound healing and inhibit corneal neovascularisation [432, 438, 439].

The absence of consistent standardisation of protocols has resulted in the development of various procedures for preparing AMe. The method used in this thesis involved washing the previously isolated amniotic membranes with a sterile solution containing an antibiotic cocktail, immersing the amniotic membranes in liquid nitrogen, manually pulverising them with a mortar and pestle to obtain a fine powder, and homogenising them with PBS. The pulverised samples were then sonicated to release more factors into the medium. After centrifugation, the supernatant was collected and sterilised by passing it through a filter. The membranes used in this study were stored at -80 °C until the extracts were obtained. Other methods have utilised pulverised dehydrated amniotic membranes [113] or extracts obtained from decellularised amniotic membranes [440].

2.2.1. Quantification of growth fators

The growth factors contained in blood-derivatives and HAMe are believed to have an impact on the corneal healing and regeneration process, thus their quantification may explain the different therapeutic effect of each product.

As sPRGF does not contains leucocytes but increases the concentration of platelets, it is expected to contain no proinflammatory cytokines but more growth factors than AS [407, 441]. However, unlike reported by other studies that suggested a higher concentration of epitheliotrophic factors in sPRGF [442–444], the quantification of

most of the studied growth factors in this work was higher in AS than in sPRGF samples.

The comparison of growth factors' concentration across various blood-derived preparations can be challenging due to the significant variability of results found within the literature. This variation in outcomes may be attributed to differences in processing and storage methods [441, 445] and the lack of standard AS preparation protocols, since this product still appears to be an ad hoc solution developed by each clinical centre. For instance, our research group's unpublished data indicate that increasing the time the blood remains clotted results in higher growth factor levels. In addition, the quantification results of this thesis revealed considerable concentration differences among individuals within blood products. This interindividual variability together with the differences with respect to literature made difficult to draw general conclusions about the relationship between the effectiveness of the blood product and growth factor concentration.

Furthermore, pools comprising all volunteers' samples were created for each blood product after previous complement factor inactivation. PEDF, SP, and HGF levels were considerably decreased with respect to a theoretical average value of all samples, with no reduction noted in the other factors. Most of our quantifications were therefore consistent with those of Anitua et al, showing that heating the samples has no impact on the quantified protein content [446, 447]. Even so, some other factors were temperature-sensitive and complement heat-inactivation destroyed them to a greater or lesser extent.

The *in vitro* inflammation tests revealed a higher decrease in IL-1β levels in TNFα-inflamed HCE cells treated with the AS-functionalised hydrogel. Taking into consideration the aforementioned factors, the choice of obtaining AS as the blood derivative for *in vivo* testing on rabbits was based on the increased growth factor's quantification achieved and the greater reduction in inflammation noticed in the *in vitro* assessments.

The amnion can be divided into various sub-regions based on its anatomical location. The placental amnion covers the placenta, and the reflected amnion covers the uterine wall and forms what is called the amniotic sac. Lastly, the umbilical or cord amnion covers the umbilical cord. The HAM fractions for this study were obtained from the reflected amnion. This part of the membrane was extracted rather than

placental HAM because its perceived to have more immunomodulatory potential than placental HAM, which appears to be more proinflammatory [332].

Quantification differences were observed among patients and between extracts obtained from different HAM regions. Regarding GFs' quantification of the extracts obtained from different HAM zones, our findings were consistent with prior studies. Gicquel et al. reported elevated EGF levels in the distal and medial component, which aligned with our results [448]. Similarly, greater concentrations of KGF, IGF1 or HGF were reported in the placental membrane [449–451], consistent with the increased levels observed in the proximal section of the reflected HAM, the region closest to the placenta.

The extracts' bioactive components may also vary depending on the preparation method. A study on HAMe preparation showed that pulverisation resulted in 20% more extractable factors than homogenisation because, in addition to being an easier method, the cell damage caused by liquid nitrogen caused more proteins and HGF to emerge. Similarly, the use of a protease inhibitor and repeated centrifugation increased the amount of extracted HGF. However, storing the extracts at -170 °F for 6 months resulted in a 50% decrease in the level of HGF and protein [452].

The variation amongst membranes in our case was also statistically significant, which was reasonably expected given the restricted number of biological samples available. As with blood products, extracts from various membrane regions were pooled for each patient. In this instance, heat inactivation was not required. However, a statistically significant decrease in the quantification of most of the analysed growth factors was noted.

Due to the influence of factors such as FGF2, HGF or KGF on proliferation, migration and corneal epithelial homeostasis during wound healing [59], and their high concentration in our results, the proximal part of the HAMe was selected to functionalise the hydrogels for the *in vivo* experiments. However, based on the quantifications, reduction of IL-1β in the *in vitro* inflammation assay and the literature, it may have been more appropriate to use the distal fraction for hydrogel functionalisation.

The hydrogel was functionalised with a 50% final concentration of blood derivatives and HAMe. This decision was based on our group's previous observation

that a 50% concentration of sPRGF in eye drops was a successful treatment for restoring the ocular surface in patients with PEDs who did not respond to other treatments [110, 425].

2.2.2. Anti-inflammatory agent: Infliximab

Infliximab was selected as a molecule to combat inflammation.

Infliximab is a human/murine chimeric monoclonal antibody against TNFα that binds to the free and transmembrane forms of TNFα to inhibit binding to its receptors [453]. Systemic use of this treatment has been described as effective in treating paediatric uveitis [454], as a stabiliser to avoid corneal melting in patients suffering from rheumatoid arthritis [455], and has proven to be effective in treating peripheral ulcerative keratitis [456]. Furthermore, it has shown to be highly efficient in suppressing inflammation after keratoprosthesis surgery in cases of autoimmune diseases and corneal ulceration [457–460].

Likewise, its use in eye drops is being investigated as a local therapy to reduce overall drug exposure, which occurs when the drug is injected into the bloodstream. Studies have shown its effectiveness in animal models for treating dry eye and neovascularisation [461, 462] and a clinical trial is currently underway in human patients to evaluate the tolerability and safety of Infliximab 10 mg/ml eye drops for treating corneal melt [463].

The rationale for incorporating a 1 mg/ml dose of Infliximab into the hydrogel is supported by previous studies that have encapsulated this antibody [464–466]. The ongoing clinical trial utilises Infliximab eye drops at a concentration of 10 mg/ml. The cornea's protective mechanisms limit the infiltration of external agents, resulting in a substantial decrease in the bioavailability of topically administered agents.

Only a small fraction, less than 5%, of the topical drug applied is absorbed by the cornea. The remaining amount is eliminated through the tear reflex, blinking, and nasolacrimal drainage [467]. Eyedrop dispensers provide an excess of solution beyond the ocular surface's capacity, thereby resulting in solution wastage. Furthermore, the efficient and uninterrupted flow of tears prevents the drops from remaining in contact with the cornea for the required duration. Since the developed hydrogel will act as a filler and remain localised in the wound, a lower dosage was considered appropriate to avoid overdose.

3. Application and effect of functionalised hydrogels on wound healing in *in vivo* experiments

In the context of tissue healing, replacement and regeneration are distinct concepts. Regeneration enables damaged tissue to fully restore affected parts to their original state by promoting new growth. Replacement refers to the healing of severely damaged area through the deposition of new abnormal tissue, it involves patching rather than restoring and it commonly implies scarring.

This dual restoration process is also evident in the cornea. The first phase following a corneal epithelial injury involves wound stabilisation whereby cellular debris is removed, cells become rounded and hemidesmosomes are reduced in the affected area [468]. This is followed by a **replacement** phase focusing on cell migration, proliferation, and production of ECM in the stroma. During this phase, cell mobility accelerates, allowing the area to be rapidly covered, while also restoring the barrier effect through an increase in cell surface area. New ECM formation is initially needed for wound closure; however, the secretion of this disorganised matrix results in corneal tissue contraction and opacity, leading to a fibrotic healing process [18].

Likewise, LEPCs become active and undergo proliferation. Once the cells coming from the limbus have covered the epithelial defect, the basal cells of the epithelium begin to proliferate and differentiate to restore the various epithelial cell layers [25]. They also produce laminins to regenerate the defective BM in cooperation with the keratocytes beneath the wound [57]. The re-establishment of the BM coincides with the formation of two out of the four intercellular junctions present in the corneal epithelium, the GAP junctions and the desmosomes. The other two junctions, adherens and tight junctions, are constitutively expressed in the migrating epithelium [469].

Ultimately, a **regeneration** phase occurs, during which the new tissue is organised and differentiated until, under favourable conditions, the original tissue characteristics are achieved [470, 471]. During the **replacement** phase, the epithelium typically requires 7-14 days to repair itself, without epithelial reinnervation, which usually takes place over a period of months [80, 472]. Considering **regeneration**, the release of cytokines, chemokines, and various growth factors from the epithelium,

endothelium, and keratocytes may take more than 2 years to restore proper stromal function and clarity [473].

Focusing on this issue, the goal of the functionalised hydrogel was to release compounds that would accelerate the repair of the stroma and promote the proper regeneration of the tissue. The gradual regeneration of the stroma is intended with the recovery of the epithelium and appropriate corneal curvature.

3.1. Establishment of *in vivo* surgical conditions

The conditions for systematic *in vivo* testing were established following a preliminary pilot study. The eyes were treated with 0.2% benzalkonium chloride (BAC) during the initial trial to induce further inflammation, and protective contact lenses were used to avoid the removal of the hydrogel. The anterior superficial stromal surface keratectomy led to inflammation as an inherent effect. Thus, it was decided that the inflammation resulting solely from the wound was sufficient, and therefore, the use of BAC was excluded to avoid unnecessary itching and discomfort. Furthermore, the use of contact lenses resulted in more discomfort than improvement to the damaged eyes. The inadequate size and poor fit of the lenses to the rabbits' eyes caused continuous rubbing of the wound and consequently, all rabbits had extracted the lens by day three.

Following these tests, it was decided to opt for partial tarsorrhaphy as a post-surgical measure up to the third day after surgery and not to include any additional inflammatory stimulus.

Tarsorrhaphy is a surgical technique that involves temporarily suturing the edges of the eyelids to reduce the size of the eyelid opening. This procedure has shown to have high success rates in treating PEDs. The reduction of the eyelid opening decreases the rate of tear evaporation, while immobilising the eyelid improves the healing process by reducing the traumatic impact of blinking [474].

Photographic records of the closure progression on the first and second days after the surgery were not possible due to the tarsorrhaphy. Moreover, the tarsorrhaphy led to faster re-epithelialisation across all treatments when compared to the results of the pilot study. Complete re-epithelialisation was observed in several cases on days 4 or 5 post surgery, along with a reduction in inflammation based on clinical observations weighted by the Draize scale. These findings are in line with

previous observations. Tarsorrhaphy has been demonstrated to accelarate the healing process of epithelial defects when compared to clinically utilised treatments, such as amniotic membrane transplantation [119]. Additionally, in conditions such as Sjögren's syndrome, tarsorrhaphy has been proven to aid in maintaining the tear film and promoting the healing of the corneal epithelium [475].

Regarding the variation in our results, it is important to consider that the presence of live animals greatly influences the outcome, given that there are certain aspects beyond our control that may affect the final results. The biological effect introduces uncontrolled variables, leading to differences amongst individuals, regardless of treatment. Therefore, having a large sample size is necessary for statistical differences to be truly significant and related to the different treatments.

3.2. Re-epithelialisation and healing

The average closed epithelial area was greater in the control group than in the hydrogel-treated groups during the initial days (day 3, 4 or 5) of the experiment. Nevertheless, a few eyes in the control group failed to close, and in some cases, the epithelium reopened by the end of the study.

The epithelial cells in the control group exhibited a high proliferative capacity. In accordance with the wound evolution findings, immunofluorescence analysis demonstrated a greater prevalence of Ki67-positive cells in the corneas of the control treatment, with particularly high expression observed in corneas extracted 7 days after surgery. Gene expression analysis further confirmed a higher expression in control-treated corneas than hydrogel-treated corneas, showing statistically significant decrease in Ki67 expression in the hydrogel-treated groups compared to the control treatment at 21 days. With the effect of tarsorrhaphy applied in healthy rabbits, that is, animals without any previous pathologies before practising the stromal surface keratectomy, the closure of the defects per se was evident and fast. It seemed that the absence of filler substances, such as the hydrogel, could have stimulated proliferation in the control corneas, resulting in faster wound closure due to the urgent need to close the wound [476]. The initial slowing of re-epithelialisation of hydrogel-treated corneas could be attributed to the hydrogel introduction to the corneal defect. If not carefully controlled, overflow of liquid hydrogels from the defect site may impede epithelial migration over the hydrogel [305, 477].

Despite the faster closure of the control-treated corneas, all hydrogel-based treatments achieved re-epithelialisation. In fact, considering all re-epithelisation cases, H-AS treatment resulted in the fastest closure of all eyes, with rapid closure being particularly noticeable from day 5 onwards. Besides, H-AS treated corneas exhibited the highest Ki67 labelling among hydrogel-based groups. This is consistent with studies showing that the presence of factors in blood products can enhance the proliferative capacity of epithelial cells [108, 422, 425, 478–480].

Following H-AS, H-HAMe exhibited a comparable closure evolution and a high count of Ki67 positive cells, as determined by immunohistochemistry, particularly during the initial 7-day period. The beneficial effects of AM or AM-derived products are attributed to their biomolecules and growth factors, such as HGF, EGF, TGF, or collagen types I, III, IV, and V, among others, which stimulate the migration, adhesion, and differentiation of the corneal epithelium. Choi et al. demonstrated that the suspension form of AM maintained its properties and had a beneficial effect on epithelial migration and proliferation as its concentration was increased in *in vitro* culture [481]. The proliferative effect of 0.1% AM extract on corneal epithelial cells in mechanical cell injuries was also demonstrated *in vitro* [438]. Additionally, amniotic membrane eye drops at concentrations of 0.1-1 mg/ml enhanced the proliferation of limbal stem cells, whereas these drops upregulated ABCG2, a putative stem cell marker, and downregulated CK3, a marker of differentiated corneal epithelial cells [432]. Likewise, the use of extracellular vesicles derived from human amniotic epithelial cells effectively enhanced the proliferation and migration of human corneal epithelial cells and human corneal stromal cells *in vitro*. It also promoted extracellular matrix reorganisation and cell adhesion to target tissues or cells by activating the focal adhesion signaling pathway in an orderly manner [482].

H-Ab treatment showed the slowest wound evolution until day 4 (Table IV.7) and the lowest number of closed cases until day 5 (**b** in figure IV.31), but it exhibited the most progressive closure evolution. It is worth noting that complete closure of all corneas was only observed in the H-Ab and H-AS groups. The treatment of ARPE (human retinal pigment epithelial cell line) cells with Infliximab did not affect cell proliferation, suggesting that Infliximab did not have an impact on the tested cells [483]. Additionally, no significant effect of Infliximab on the survival, phenotype, morphology, proliferation, cell cycle, and apoptosis of mouse and human

mesenchymal stromal cells was observed [484]. Infliximab controls inflammation by binding to both soluble and transmembrane forms of TNFα with high affinity. If the antibody controls inflammation, as observed in the pilot study of cytokines in tears, and the aforementioned results are considered, the cornea per se may carry out the remaining processes such as re-epithelialisation, proliferation, or cell migration in healthy animals with an intact neural pathway as in the case of the rabbits used. This could be one reason why the final closure results with H-Ab treatment were similar to those achieved with H-AS or H-HAMe.

Epithelial hyperplasia was observed in the re-epithelialised areas of some operated corneas in a greater or lesser extent regardless their treatment. The epithelium has extensive remodelling capabilities and its modifications correspond to the minimisation of curvature irregularities that impact visual acuity. While the primary mechanisms involved in this type of remodeling are still under debate, the epithelium thickens in regions with stromal tissue loss to compensate for the change in central curvature [485]. The developed hydrogels functioned as wound fillers, resulting in a smaller area needing epithelial coverage to compensate for the curvature change. This would explain why a thicker epithelium is apparent in the control corneal samples extracted 21 days after surgery.

As time passes and the stroma remodels, we would expect to observe an epithelium devoid of hyperplasia, confirming complete tissue regeneration. However, this process would take longer than the 21 days of our study.

Markers commonly used for identifying limbal stem/progenitor cells, PAX6 and p63, did not show any statistically significant differences in gene expression analysis across different times and treatments when compared to the control group. The RNA extraction was carried out on the entire sclerocorneal tissue comprising epithelium, stroma and endothelium, and since these markers are associated with specific cells present in the basal cell layer of the limbal epithelium, the total number of corneal cells might have influenced the results. If the limbal epithelium was specifically selected, the differences could have been more pronounced. However, CK15 labelling, a marker for corneal epithelial progenitor cells [37], which are positive exclusively in the basal layers of the limbal epithelium, revealed differences in immunohistochemical images among treatment groups. Our study confirmed the existence of these cells in the sclerocorneal limbus of all corneas analysed. Furthermore, there was a greater degree

of CK15 labelling observed in the H-Ab, H-AS and H-HAMe treated corneas extracted 21 days post-surgery. This outcome suggested that these treatments had a larger effect beyond the damaged area of the epithelium.

The higher expression of CK15 in H-AS and H-HAMe hydrogels could be explained by the contribution of growth factors from AS and HAMe. Our group previously reported the efficacy of sPRGF in maintaining the stemness potential of limbal stem/progenitor cells [425]. Similar results were also found in the use of platelet-rich plasma for maintaining stemness in human muscle-derived progenitor cells [486] and other mesenchymal stem/progenitor cells [487].

Regarding the AM, the combined use of AM transplantation and AM extract eye drops proved a synergistic effect on stem cell growth and differentiation of the corneal epithelium. Improved corneal clarity and decreased vascularity and conjunctivalisation using AM extract eye drops in combination with limbal transplant suggested that the cells lining the cornea were progenitor cells. This was verified by the presence of p63 and ABCG2 positive cells in the corneal buttons [433]. Interestingly, Lai and Luo demonstrated that cells cultured with AM substrate and riboflavin crosslinked with ultraviolet light were able to modulate stemness expression levels. Photoreticulated AM substrates were found to promote ABCG2 expression in limbal epithelial cells, and the concentration of riboflavin was shown to influence their stemness being [488].

CK15 positive cells also extend to the peripheral region of the cornea, generating an overall response to address the epithelial defect. As these cells divide and differentiate into corneal epithelial cells and move centripetally and upwards in the cornea, they display progressively more CK3 labelling [33, 35]. This was confirmed in all corneas regardless their treatment. Besides, immunohistochemical analysis demonstrated the expression of the epithelial marker PanCK in the wound, undamaged and limbal region.

Similarly, the epithelial cells located in the upper section of the corneal epithelium exhibit ZO-1, a protein linked to tight junctions. At both 7 and 21 days post-surgery, similar protein labelling was observed in all treatment groups, indicating successful re-epithelialisation of the impaired corneas and the development of a mature and functional corneal epithelium. It is worth noting the rapid establishment of the corneal epithelium's barrier function (demonstrated by ZO-1 positivity) during the initial

stages of the lesion repair, including in incipient epithelia. Therefore, prioritising the establishment of the corneal barrier function is crucial in promoting corneal healing [480, 489, 490].

3.3. Adhesion

CD44 is a transmembrane adhesion glycoprotein and crucial receptor for HA, which stimulates cellular proliferation and induces alterations in the cell cytoskeleton [491]. CD44 expression is mainly expressed in the basal epithelial layers of the uninjured cornea and increases after injury [492]. In corneal epithelial cells treated with HA, increased CD44 expression has been observed, leading to enhanced migration and reduced levels of inflammatory proteins [493]. CD44 synthesis was also found to have an impact on the migration phase of corneal wound healing [494].

While CD44 gene expression showed a slight increase in most of the hydrogel treatments compared to the control group during both studied time points, the observed differences were not significant. 0.2% HA drops were instilled in both the corneas treated with hydrogels and the control group. This may explain why no significant differences were observed between the groups.

Integrin β4 protein constitutes hemidesmosome-like junctions between epithelium and matrix and assists in forming a condensed and secure persistent tissue [495]. Integrin β4 labelling showed discontinuity at the wound site in all groups after 7 days. The control cornea had a jagged Int-β4 positive interface with the stroma, while gaps or absence of labelling were observed in the wound area of the hydrogel-treated corneas. However, the staining was more intense in all samples after 21 days, indicating stronger epithelial attachments and confirming the adhesion of the newly repaired epithelium to the underlying extracellular matrix.

Integrins play a crucial role in the adhesion of corneal epithelial cells to collagens, fibronectins, laminins, or vitronectin [496]. For instance, fibronectin is a glycoprotein that acts as an adhesive protein and plays a crucial role in various biological processes related to cell adhesion, detachment, and migration [497].

In corneal wound healing, fibronectin serves as a temporary matrix for epithelial cell adhesion and migration, playing an essential role in the healing process. Fibronectin-eye drops have been used after epithelial debridement in severe cases of ocular allergic disease, recurrent corneal erosion and reticular corneal dystrophy

to achieve rapid and complete epithelial regrowth after surgery [498, 499]. The clinical effectiveness of fibronectin-derived peptide PHSRN eye drops has been demonstrated for the treatment of PEDs, specially due to their rapid response, as evidenced by a marked decrease in the size of epithelial defects within 3 days [500]. Likewise, The Nap-FFPHSRN hydrogel, which included the fibronectin-derived peptide PHSRN with Nap-F self-assembled motifs, was found to facilitate corneal re-epithelialisation in *in vivo* tests on rabbits, resulting in complete morphological and architectural recovery [501]. Fibronectin is also found in blood products and amniotic membrane. Our group has previously reported the amount of fibronectin in different blood products and found no statistically significant differences between them [479]. The extracellular matrix of AM also contains collagens, laminins, fibronectin, elastin, proteoglycans and glycoproteins, as well as growth factors that promote cell migration and adhesion [502]. Perhaps the fibronectin present in the hydrogels functionalised with AS and HAMe may have stimulated epithelial cell migration and aided re-epithelialisation, especially during the first days of closure. This is supported by the previously discussed evolution of wound closure.

Considering this idea, the addition of fibronectin or other basement membrane components to the hydrogel composition could have enhanced epithelial cell adhesion.

3.4. Fibrosis

α-SMA is a reliable marker for activated myofibroblasts and its expression indicates fibrosis activation in the corneal stroma. In the normal healing process of the corneal stroma, infiltration of corneal fibroblasts followed by their conversion to myofibroblasts is observed [503]. Thus, keratocytes' activation and differentiation into myofibroblasts are essential physiological processes during the repair of corneal damage. Keratocytes are neural crest-derived cells responsible for maintaining corneal transparency by producing and remodelling extracellular matrix components, such as collagens, proteoglycans, and crystallins. They are small cells that branch between collagen lamellae to connect with each other and form a network throughout the stroma [504]. Keratocytes are identified by the expression of keratocan, as well as aldehyde dehydrogenases 1 and 3 (ALDH1A1 and ALDH3A1), CD34, lumican and vimentin [12, 504]. After an injury, keratocytes become active and transform into corneal fibroblasts, which then migrate to the wound site and begin repairing the

stroma. Corneal fibroblasts stop expressing keratocan and CD34 markers, lose their dendritic morphology and upregulate vimentin expression. However, they do not yet express α-SMA and desmin [505]. They play a role in matrix remodelling by producing extracellular matrix components and metalloproteinases, as well as modulating the regeneration of the epithelial basement membrane and the inflammatory response. When the lesion is severe, growth factors such as TGFβ are significantly increase in the stroma, which lead to the transformation of fibroblasts into myofibroblasts [506]. These growth factors are mainly released from the epithelium and tears [79]. Myofibroblasts are characterised by the expression of α-SMA, vimentin and desmin, and their contractile function [79]. They synthesise extracellular matrix components in large quantities and in a disorganised manner, leading to corneal opacity and contributing to scar formation. It is unclear what happens to these cells after tissue repair, but it is thought that they are eliminated by apoptosis once the flow of growth factors is diminished. This is because TGFβ signalling promotes myofibroblast survival [506]. *In vitro* studies have demonstrated that myofibroblasts can be inactivated and reverted to a fibroblast-like phenotype. However, this phenomenon has not yet been proven *in vivo* [505].

In this study, we observed myofibroblastic responses in both control and hydrogel-treated corneas, as expected after stromal injury. Nevertheless, the hydrogel-treated corneas exhibited less α-SMA expression.

While the initial fibrotic response is essential, the extracellular matrix secreted by myofibroblasts can often lead to stromal opacity in the cornea, a tissue that should be transparent. For this reason, keratocytes must subsequently reabsorb the matrix to restore normal transparency and prevent corneal haze.

Gene expression results demonstrated a significant decrease in α-SMA levels of the hydrogel treatments in comparison to the control treatment at both 7 and 21 days after the surgery. At day 7, the H-Ab and H-AS treated corneas exhibited the greatest reduction in α-SMA in contrast to the control group and maintained this effect for 21 days. Previous results from our group already indicated that the undiluted sPRGF blood-derived eye drops reduced α-SMA positivity resulting in less haze and scarring 30 days after surgery [425].

It is noteworthy that the use of the non-functionalised hydrogel (H) had a greater reduction effect compared to the HAMe-functionalised gel after 7 days.

However, after 21 days, the levels of α-SMA remained comparable among all hydrogel-based treatments, indicating a reduction in fibrosis for all hydrogel-treated corneas compared to the control group. The study showed that even the introduction of non-functionalised hydrogel, as in group H, produced a better antifibrotic effect than not introducing it.

The addition of gelatine may had influenced the tissue's fibrotic response. According to Chen et al., cells that penetrated GelMA inhibited the differentiation of keratocytes into myofibroblasts in the wound site, thus preventing the fibrotic response. Three months after the corneal surgery in rats, the cornea's fibrotic repair was still absent, and its thickness and refractive ability were similar to those of a healthy cornea [507]. Linking gelatine incorporation and surface stiffness, Ibañez et al. demonstrated a correlation between gelatine incorporation and surface stiffness. They found that increasing the stiffness of GelMA hydrogels influenced the activation of dermal myofibroblasts and the expression of fibrosis-related genes and proteins, such as α-SMA. Furthermore, the incorporation of pores into a stiff GelMA gel reduced stiffness and thus myofibroblast activation [508]. Based on these findings, the developed hydrogel may had provided an adequate stiffness that could have reduced the contractile forces of fibroblasts and, consequently, a high fibrotic response. However, it is important to note that this is simply a hypothesis based on the results obtained.

As for immunofluorescence, α-SMA labelling was recorded in the stroma as well as in the epithelium, both in the most basal epithelial region and in the most upper epithelium. Previous studies have established α-SMA staining in lens epithelial cells as a marker of epithelial-mesenchymal transition [509]. Furthermore, TGF-β, one of the growth factors found in AS or HAMe, has been shown to promote the epithelium-mesenchyme transition in damaged crystalline lenses [510, 511]. We hypothesise that a similar process may occur during corneal epithelial repair. The α-SMA staining in the upper part of the epithelium has also been documented in earlier studies with mice and rabbits [512, 513]. However, the causal explanation for this marking remains unknown. A potential explanation for the epithelial α-SMA positivity could be that the cells undergoing EMT, and therefore stained with α-SMA, could be the ones that migrate to close the wound and differentiate from the basal to the most anterior epithelium. The location of the staining in the basal or apical zone

could depend on the speed at which the epithelium stratifies. Similarly, the absence of epithelial staining after 21 days could be due to either the observation of a wound area that was more or less central or the shedding of cells that were previously positive for α-SMA.

Treatment for corneal scars is most effective when applied in the early stages after injury. The primary medical treatments for reducing corneal inflammation and fibrosis are topical corticosteroids. Agents such as prednisolone, dexamethasone, or fluorometholone are commonly used in clinical settings. However, they differ in their anti-inflammatory potency and ability to penetrate the cornea [514, 515]. Special contact lenses can treat the sequelae of milder cases [516], but when the scar is opaque and deep, leading to vision loss, an allograft or donor corneal transplant is necessary [517]. Limiting corneal opacification in the first few weeks may help avoid invasive surgery, long-term medication, and extensive follow-up.

Chameettachal et al. have made further progress in demonstrating a solution that promotes a microenvironment conducive to keratocyte expansion, without encountering transdifferentiation. They proved that the use of human cornea-derived extracellular matrix hydrogel as well as the xenogeneic bovine corneal hydrogel prevented scarring and the subsequent corneal opacification and facilitates normal stromal regeneration [518, 519]. Additionally, two recent studies have been conducted on hydrogel-based opacity reduction. One study involved an *in situ*-forming gellan gum hydrogel loaded with MSCs, which reduced the expression of mRNA encoding fibrosis markers such as α-SMA in rabbit stroma. The hydrogel also demonstrated a slow release of MSC cells into the stromal defect, preventing stromal opacity [520]. Like so, human amniotic epithelial stem cells-derived stromal keratocytes loaded gelMA hydrogel photocured with LAP was used to restore corneal tissue structure and microenvironment. This was achieved through the secretion of proteoglycans, promoting transparency, and inhibiting the inflammatory cascade, resulting in a 75% reduction of fibrosis [521].

Based on the qPCR and immunohistochemistry results, none of the treatments demonstrated complete antifibrotic properties. The potential to generate fibrosis varied among the treatments and was also influenced by the animal itself. However, the use of hydrogel appeared to have a positive effect in reducing fibrosis compared to not using it.

Since α-SMA expression decreased with hydrogel-treatments, it can be concluded that these products are highly attractive for addressing corneal defects by inducing a desirable α-SMA phenotype in the early stages of corneal injury and subsequently reducing it to prevent corneal opacification.

3.5. Eye irritation and inflammation

The expression of inflammatory cytokines was measured to assess inflammation using the extracted tear protein in the pilot study. The cytokines that had the most reliable expression values were those associated with the initial inflammatory response.

Macrophage inflammatory protein-1β (MIP-1β) is a factor produced by macrophages and monocytes in response to bacterial endotoxin or proinflammatory cytokines, such as IL-1β. It activates human granulocytes (neutrophils, eosinophils, and basophils) and is associated with acute neutrophilic inflammation [522]. MMP-9 degrades ECM proteins and activates cytokines to regulate tissue remodelling. It is produced primarily by neutrophils and macrophages and regulates inflammation in tissues and diseases [523]. IL-8 is an inflammation-related protein primarily released by macrophages following injury. It plays a key role in the recruitment of neutrophils and other immune cells to the site of infection [524]. Finally, NCAM-1 is expressed not only in dendritic cells and neural or mesenchymal stem cells but also in rare subsets of T and B lymphocytes and NK cells. In addition to its involvement in several brain-related biological processes, it is also involved in other biological functions such as cell adhesion, migration, proliferation or differentiation [525].

On the first day after surgery, both the control treatment and H-AS group showed the highest expression values for MIP-1β, MMP-9 and NCAM-1. The values for both treatments decreased on day 4, except for the control-treated corneas with the cytokine MIP-1β, for which a more progressive decrease was recorded. At day 1 after surgery, H-Ab-treated corneas exhibited the lowest expression values of MIP-1β, MMP-9, and NCAM-1, which could indicate the anti-inflammatory effect of the antibody.

The cytokine expression results up to day 4 were aligned with the irritation values recorded using the Draize scale. The control and H-AS groups showed the highest irritability scores on day 2. However, from day 4 onwards, cytokine expression

results were more reliable than the Draize scores because of the sensitivity of the array technology even in a context of low inflammation.

The pilot study had a low number of individuals (n=2 for each treatment) and the individual condition of each animal contributed to the large deviations recorded by each group. The results provided an approximate indication of the treatment trends, but a larger sample size study was needed to confirm them. Unfortunately, inflammation could not be assessed through the concentration of protein extracted from the tear with samples from studies E02-E06. These results would have been useful to confirm the validity of the pilot trends.

Regarding experiments E02-E06, the Draize scale's scores indicated that the H-AS treatment was the least irritating. H-Ab and H-HAMe had slightly higher scores on days 3, 4 and 5, but were practically non-irritating from day 6 onwards.

Although the H-Ab treatment showed higher irritability scores according to the Draize scale compared to the other treatments, functionalisation of the hydrogel with the antibody (H-Ab) was deemed the best option for reducing inflammation, as demonstrated by the IL-1β gene expression results. A reduction in inflammation was already observed at 7 days, though it was not statistically significant compared to the control treatment. However, significant differences were evident by day 21. The reduction of IL-1β levels through the topical administration of Infliximab was already demonstrated in a murine model of ocular surface scarring [526]. It was demonstrated that Infliximab effectively penetrated damaged corneas in a safe manner. Additionally, a reduction in fibrosis in the fornix was observed after Infliximab instillation, which was associated with a decrease in inflammatory cell infiltration in the conjunctiva. The study demonstrated that topical TNF-α blockade with Infliximab decreased inflammation and its consequences in the cornea, conjunctiva, and eyelids. This was observed clinically *in vivo*, with an increase in corneal transparency, and *ex vivo*, with a decrease in CD45 positive inflammatory cell infiltration in the eyelids, and a reduction in inflammatory cytokine expression in both the cornea and eyelids.

The most substantial reduction in inflammation was observed through qPCR results when using H-HAMe after 21 days. The benefits of H-HAMe are attributed to numerous growth factors included in HAMe that aid in the regeneration of the cornea. Regarding inflammation, it decreases the production of pro-inflammatory cytokines like TNFα and IL-6, as well as the expression of antigen-presenting cell markers such

as CD80, CD86, and major histocompatibility complex class 2 antigen that regulates immune responses. Moreover, it boosts the levels of anti-inflammatory cytokines like IL-10, leading to a reduction of inflammation and lower infection risk. Similarly, the decrease in TGF-1 and TGF-2 restricts fibrosis while all these mechanisms work in conjunction to promote wound healing and regeneration [113].

The benefits and properties of HAM and its various derivatives have been extensively studied. IL-1ra (human interleukin-1 receptor antagonist) and IL-10, which are factors capable of suppressing corneal inflammation, have been identified in the conditioned medium of human amniotic epithelial cells [527]. *In vitro* experiments have shown that utilising AM as a substrate can impede the increment of IL-1α and IL-1β caused by lipopolysaccharide [528]. Additionally, HAMe eye drops have demonstrated effectiveness in promoting corneal epithelial healing and reducing conjunctivalisation and vascularisation in cases of complete unilateral LSCD that underwent transplantation of a small limbal block from the healthy contralateral eye [433]. Furthermore, the matrix component HC-HA/PTX3 (heavy chain-hyaluronanpentraxin 3) has been demonstrated to effectively prevent inflammation, angiogenesis, and scarring, in addition to the previously mentioned growth factors [529].

All of these findings are in line with and correspond to the results obtained from corneas extracted 21 days after surgery. It is notable that the corneas treated with H-Ab and H-HAMe, the two hydrogels offering the greatest reduction in IL-1β, displayed the highest inflammation symptoms during the first days after surgery, including chemosis and redness, based on day-to-day clinical evaluations using the Draize scale.

Concerning H-AS treatment, IL-1β expression was higher in the H-AS-treated rabbit corneas extracted 7 days after surgery than in the control-treated ones. Although there was a decrease in IL-1β expression in H-AS-treated rabbits relative to the control treatment in samples taken 21 days post-surgery, this difference was not statistically significant. However, the administration of H-AS on rabbits resulted in a more beneficial day-to-day clinical evaluation, reduced Draize test scores, and lower levels of redness and chemosis compared to H-Ab and H-HAMe treatments.

AS contains beneficial factors for corneal repair and has shown potential benefits for treating ocular surface disorders such as dry eye disease. Dry eye disease (DED) is a multifactorial disorder of the tear film and ocular surface in which inflammation

is the main core mechanism of the disease. The insufficient lubrication and tear film homeostasis leads to symptoms such as discomfort, visual disturbances, irritation, foreign body sensation, light sensitivity and itching [530]. For severe DED, autologous serum eye drops and platelet-derived eye drops are recommended as treatments over artificial tears. This is because blood-derived eye drops not only provide lubrication but also contain additional factors that can improve the ocular surface and facilitate wound healing. Previous studies have shown that 20% autologous serum is effective in the treatment of severe dry eye and is regularly used in the clinics [412, 531–533], as well as platelet-derived eye drops, which resulted in significant improvement or disappearance of DED symptoms [534–536].

However, as the therapeutic potential of blood derivatives can be attributed to its similarity to natural tears, it is crucial to consider that the serum's composition may be influenced by the overall health of the patient being treated. The serum's composition is dependent on the blood composition, which can be influenced by the organism's current health status, despite the concentration and production levels. It has been demonstrated in humans that levels of VEGF and IL-6 increase in individuals with rheumatoid arthritis [537] and that serum from patients with Sjögren's syndrome contains elevated levels of pro-inflammatory cytokines, including TNFα, IL-1β, IL-6 or IL-8 [538, 539].

As a result, it is clear that the amount and quality of various factors in the serum differ, ultimately influencing the effectiveness and tolerance of blood products. Sera for the *in vivo* experiment were extracted before surgeries and treatments, so it was assumed that the rabbits did not contain any disease.

3.6. Overall *in vivo* response of the treatments

Among the hydrogel-treated corneas, the H-AS treatment resulted in faster epithelial closure compared to other hydrogel-based treatments. This was supported by the higher number of Ki67-positive cells observed in the immunohistochemistry analysis. Additionally, intense labelling of CK15-positive clusters was observed. In addition to reducing fibrosis and inflammation, as recorded by IL-1β and α-SMA in qPCR, clinical observations by Draize scale showed minimal signs of irritability.

It was expected that HAMe-functionalised hydrogels would have a similar effect to H-AS. While the inflammatory and fibrosis response was comparable, there was a

slower epithelial closure and higher *in vivo* signs of irritability.

Finally, the H-Ab hydrogel demonstrated its anti-inflammatory function by reducing IL-1β levels in qPCR recordings, as well as reducing fibrosis (α-SMA qPCR recordings). It had the slowest closure evolution, which was also confirmed by the amount of Ki67 positive immunohistochemistry. Together with H-AS, it achieved closure of all treated corneas. In terms of *in vivo* irritability and inflammation, this hydrogel-based treatment was found to produce the greatest irritability. However, the values were always within the range of minimally irritative or practically non-irritative.

In general, the introduction of hydrogel, whether functionalised or non-functionalised, improved wound healing. This was evidenced by a decrease in markers of inflammation, as observed by IL-1β through qPCR, achievement of re-epithelialisation in all cases and the drastic reduction of the fibrotic response, as evidenced by α-SMA through qPCR.

4. Characterisation of primary limbal cell cultures

The development of a limbal biosubstitute for LSCD treatment has also been among our objectives. To achieve so, two main areas of research have been identified: the synthesis of bioscaffolds and the optimisation of cell cultures to be included in the constructs.

Bioscaffolds should reproduce an environment that mimics the composition, structure, and properties of the *in vivo* ECM, providing both biological and physicochemical cues to cells. The ECM is a soft, tough and elastic three-dimensional structure that supports and maintains tissue and organ structure. It consists of a mixture of polysaccharides and various protein types, including collagen, elastin, and fibronectin. It performs pivotal functions in transportation, cellular communication, mechanotransduction, and growth factor signalling through interactions with cell surface receptors, binding growth factors and other signalling molecules.

The proper selection and development of bioscaffolds falls outside the scope of this thesis. Nevertheless, we have started working on the characterisation of primary cultures of cells extracted from human corneas. Immunohistochemical and

immunocytochemical analyses have been carried out to determine the attributes of LEPCs and the diverse subpopulations existing in the limbal niche.

LEPCs reside in the limbal niche and uphold corneal epithelial homeostasis. The limbal stem cell niche is characterised by a specific ECM composition, limbal vasculature and surrounding limbal niche cells (LNCs) that dictate the fate of LEPCs, delivering essential molecular signals for their maintenance and differentiation [24, 540–542].

Regarding primary cells cultures, CK15-positive labelling was observed in the epithelial cells directly precipitated from the cytospin, as well as some vimentin-positive cells. The high percentage of CK15-positive cells (approximately 40%) extracted via tissue digestion and the absence of this marker's expression in stromal cell cultures validated the sufficiency of the cell isolation methods employed, which resulted in reasonably pure epithelial and stromal populations. Whilst CK15 cytokeratin expression decreased throughout cell culture passages, vimentin staining increased and the vimentin-positive cells displayed a morphology similar to differentiated stromal cells. This suggests that stromal cells can rapidly proliferate and outcompete epithelial cultures if the cell culture does not prioritise epithelial stem cell preservation.

In addition to cytokeratins, the transcription factor p63 has also been used to ensure the presence of stem cells in corneal samples. Specifically, the ΔNp63α isoform has been identified as a positive marker of limbal stem cells located in the limbal niche [543].

Epithelial cells retrieved from freshly obtained and cultured sclerocorneal tissues displayed positive staining for ΔNp63α. However, a noticeable decline in ΔNp63α levels was recorded across all cell passages. A gradual reduction of p63 levels during the culture period was previously reported in human limbal explant cultures. Joseph et al. also documented a decrease in the number of p63-positive cells maintained for 1-3 weeks in culture. This study's findings, alongside their note on p63 staining in the limbus and central cornea, indicate that p63 might be a marker for both stem cells and transient amplifying cells. The study concludes that the decline in p63 positivity is relevant to the decline in cell proliferation after confluence [544].

Besides, since Rama et al demonstrated the need for a minimum of p63-bright

cells in the cell therapy product for successful transplantation, the staining of the transcription factor ΔNp63α has been used as a putative positive marker of stem cells in limbal biopsy cell expansions [545]. Holoclar is a stem cell-based treatment used to restore the corneal epithelium in adult patients with moderate to severe limbal stem cell deficiency [56]. The treatment involves taking cells from the patient's healthy limbus through a 1-2 mm^2 biopsy, which are then expanded *ex vivo* for subsequent transplantation. During product manufacture, cell cultures are expanded to recover as many stem cells as possible from the initial biopsy using ΔNp63α transcription factor staining as a putative positive stem cell marker.

No positive staining for CK15 was noted in directly isolated or cultivated stromal cells of the isolated stromal population. The predominant marker in these cultures was vimentin. A distinct orientation of these cells in culture was evident, as almost all cells were aligned in the same direction, imitating their organised disposition in the corneal stroma [12].

Concerning Melan A marker, a specific relationship between melanocytes and limbal epithelial stem cells has been suggested based on significant observations. Melan A cells showed positive staining in the limbal crypts and a ramified cell phenotype consistent with melanocytes was observed around forming limbal epithelial colonies. Additionally, a concurrent decrease in ΔNp63α-, CK15-, and Melan A-positive cells was recorded throughout the culture passages.

According to Dziasko et al., there is a close relationship between melanocytes and limbal stem cells in the niche [26, 546], where the former appear to have a protective role in potentially undifferentiated cells [24, 547]. The parallel decrease in both markers is consistent with the putative role of melanocytes in maintaining stemness. Besides, this could potentially be linked to the lack of vimentin expression seen in corneal epithelial cell cultures. Polisetti et al. demonstrated that pure melanocyte cultures stained positive for both melan A and vimentin [548]. Additionally, the ramified cells observed in the epithelium may also be associated with Langerhans cells that akin to melanocytes, reside within the limbal basal layer and exhibit positive staining for vimentin [549–552].

While isolating limbal niche cells is a challenge due to their small fraction in the total limbal population, these cells possess the ability to dictate the fate of LEPCs both *in vitro* and *in vivo* [547, 553–555]. Therefore, the intimate connection between

LEPCs and limbal melanocytes provides an opportunity to investigate their *in vitro* application to improve culture conditions that maintain the undifferentiated state of LEPCs. This approach enables enrichment of the culture with a higher number of stem cells, thereby enhancing their effectiveness in advanced ocular regeneration therapies or tissue-engineered products.

Co-culture of limbal melanocytes or their use as a feeder layer, rather than the gold standard mouse embryonic 3T3 fibroblasts, has demonstrated to preserve the stemness characteristics of LEPCs, their stem cell phenotype, and their ability to form clones [556]. Their low immunogenic profile and regulatory and anti-angiogenic properties make them suitable for enhancing stem cell therapies for LSCD patients. This eliminates the use of mouse 3T3 fibroblasts, which poses ethical and safety concerns due to contamination by xenogeneic molecules, immune rejection, and possible cross-species viral transmission.

Moreover, studies have illustrated that limbal melanocytes facilitate the proliferation and upkeep of LEPCs in corneal epithelial constructs generated through tissue engineering [547, 548, 557]. Additionally, when these two types of cells were co-cultured in fibrin hydrogels, a generation of multilayered epithelial constructs was achieved in merely ten days [548].

All these findings suggest that the incorporation of limbal melanocytes in the production of tissue-engineered constructs for reconstruction of the ocular surface may aid in maintaining the undifferentiated status of LEPCs and improve treatment effectiveness. Hence, further comprehension of the function of these cells and their interplay with LEPCs is crucial to harness their potential in the development of cell therapies or tissue-engineered constructs for the treatment of LSCD.

VI. CONCLUSIONS

1. The characterisation of four protein-based biofilms shows that, depending on the material, fabrication method, and type of crosslinking, they may be cytocompatible or not. Among the compressed and physically crosslinked COL and SPI and chemically crosslinked GEL films, gelatine is the most suitable candidate for hydrogel development. Additionally, empirical evidence indicates that RFP can react with the functional groups of unmodified gelatine.

2. The gelatine-RFP hydrogel maintains similar cell biocompatibility and rheological properties even when components such as dextran, hyaluronic acid or methyl cellulose are added. However, the addition of these components reduces the optical characteristics and increases the swelling of the hydrogel, what could hinder the hydrogel's accommodation to the corneal wound. Therefore, the gelatine-RFP hydrogel is defined as the simplest and most functional hydrogel composition.

3. The gelatine-RFP hydrogel functionalised with Infliximab or the blood derivatives prepared according to our protocols effectively reduces inflammation in TNFα-stimulated cells. Its effectiveness in inflamed situations counteracts the intrinsic inflammation that induces in non-inflamed *in vitro* cultures.

4. The gelatine-RFP hydrogel adheres to *ex vivo* and *in vivo* corneal wounds, promoting epithelial growth above the hydrogel. The introduction of the hydrogel, whether functionalised or not, improves the overall wound healing response *in vivo*. This is demonstrated by a reduction in inflammation, promotion of re-epithelialisation, and a decrease in the fibrotic response. Although no single treatment can be selected as optimal, the AS-functionalised hydrogel demonstrates the most rapid re-epithelialisation, the least clinical signs of irritation, and the least degree of fibrosis at 21 days. However, H-Ab and H-HAMe show a greater reduction in inflammation.

5. In relation to the maintenance of the limbal niche required for corneal regeneration, the simultaneous decrease in stemness and melanocyte markers during cell culture suggests a close association between primary LEPCs and melanocytes in this microenvironment. Understanding their interaction may help to develop new culture conditions that preserve the phenotype and function of LEPCs prior to their transplantation in the treatment of LSCD.

In response to the need for treatments for PEDs and corneal ulcers, the hydrogel developed from gelatine and RFP, functionalised with either blood-derived products, HAMe or an anti-inflammatory antibody, has proven to be a treatment that promotes re-epithelialisation, enhances tissue repair mechanisms by reducing fibrosis and controls the degree of inflammation to restore the overall ocular integrity. The treatment has proven to be easy to apply by the clinician and reduces the number of necessary interventions to just the application of the hydrogel on the first visit and the application of the antibiotic until epithelial wound closure.

Likewise, the characterisation of primary LEPC cultures and their interaction with other cells present in the sclerocorneal limbus, such as melanocytes, has opened a way to optimise the culture conditions required for future corneal cell-laden constructs. These constructs will be generated to promote oligo/unipotent growth of LEPCs and offer an alternative to the donor transplants currently used to treat LSCD.

I. SARRERA

1. Begiaren gainazala

Begiaren gainazala malko-geruza, konjuntiba, kornea, linbo esklerokorneala eta lotutako betazal-egiturak biltzen dituen unitate anatomiko funtzionala da (I.1 irudia). Osagai guztiak epitelioen jarraitasunagatik, inerbazioagatik eta sistema endokrino, baskular eta immunitate-sistemagatik funtzionalki batuta daude [1]. Osagai guzti hauek begiaren kanpoaldeko zatia osatzen dute, kanpoko mehatxuetatik babestu eta kornearen gardentasun egokia mantentzen laguntzen dutelarik. Horretarako, begi-gainazalaren homeostasi egokia, inmunitate-hesiaren egonkortasuna eta kornearen konponketa gaitasuna mantendu behar dituzte.

1.1. Malko-geruza

Malko-geruzak korneako eta konjuntibako epitelioen eta kanpo-ingurunearen arteko interfaze likidoa osatzen du eta begiaren lehen gainazal errefraktiboa da [2]. Begi gainazaleko agente lubrifikatzaile gisa dihardu, begia kliskatzean eta begi-mugimenduetan marruskadura murrizten baitu, eta korneako eta konjuntibako epitelioen oxigenaziorako, hidrataziorako eta metabolismorako beharrezkoa da [2].

Malko-geruza ehun eta epitelio anitzetatik datozen jariakinen nahasketa baten ondorioz sortutako lau geruzez osatuta dago. Korneako azken geruzako zelula epitelialen mikrobiloxken glikokaliza geruzarik barnekoena da eta kornea eta konjuntibako epitelioko zelula ezkatatsu geruzatuek sortutako muzinek osatzen dute. Geruza honek, malko-geruza korneako epiteliora itsatsita mantentzen du eta bakterioen inbasioen eta hantura-zelulen aurkako hesi gisa dihardu.

Honen gainetik muki geruza dago, MUC5AC muzinek, proteinek, elektrolitoek eta glikokaliza estaltzen duten konjuntibako zelula kaliziformeek jariatutako urez osatuta dagoena. Hirugarren geruza urtsua da, elektrolitoak, ura, proteinak eta malko-guruinek eta konjuntibako epitelioak sortutako muzina disolbagarri txikiak dituena. Geruza hau aurreko muki geruzarekin nahas daiteke. Kanpoko geruza Meibomio-ren guruinek jariatutako lipidoek osatzen dute eta lurruntzea saihesteko hesi gisa jarduten du, begia lehortasunetik babestuz [3]. Muki geruza eta geruza urtsuarekin gertatzen den bezala, geruza urtsua eta lipidikoa nahas daitezke.

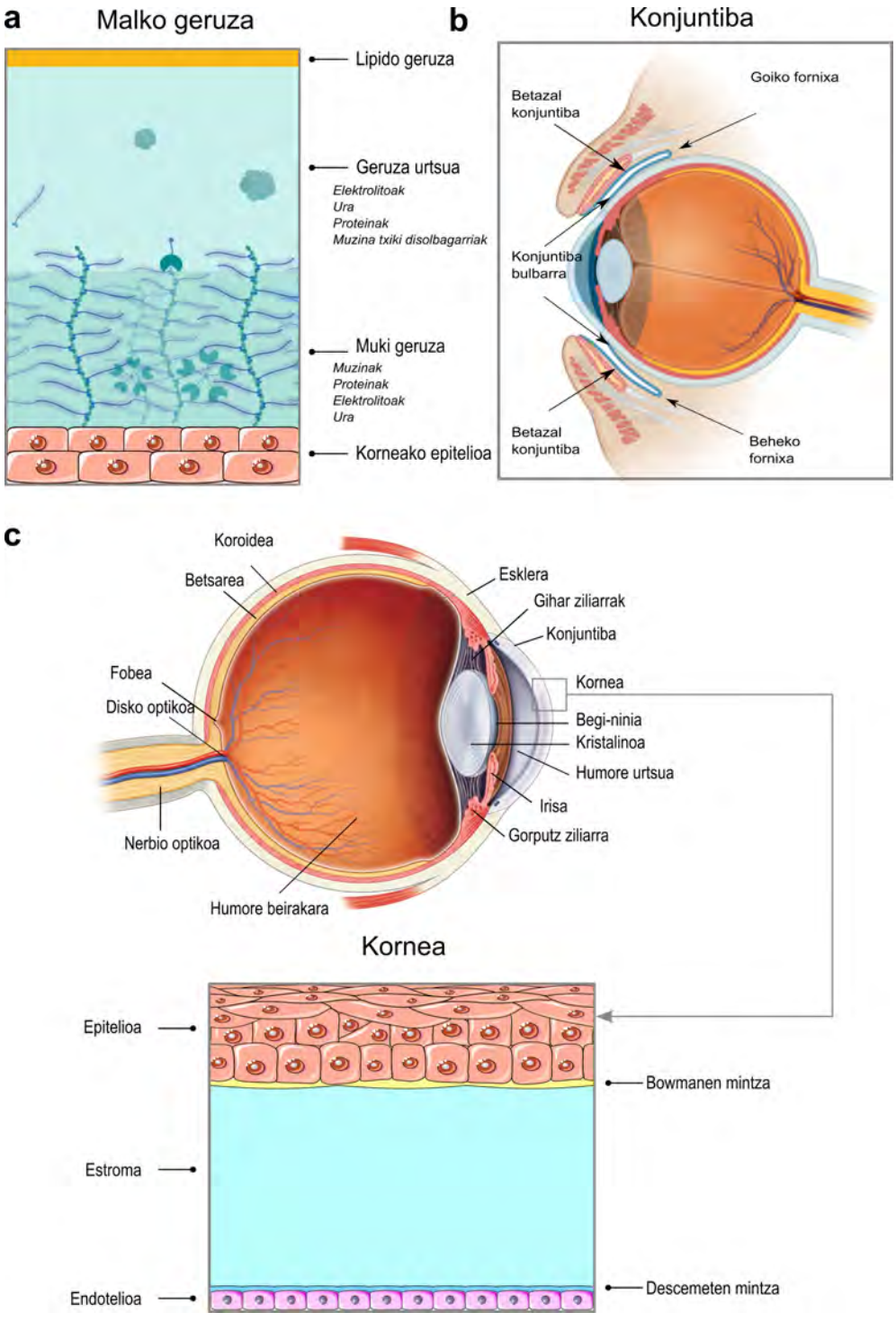

I.1. IRUDIA: Begiaren gainazalaren 3 osagai erakusten dituen eskema. **a**) Malko-geruzako 4 atalen diagrama. **b**) Konjuntibaren atalen kokapena; betazaleko konjuntiba, konjuntiba bulbarra eta konjuntiba-fornixa. **c**) Begi-globoaren osagai anatomiko nagusiak eta korneako geruzen ilustrazio xehatua.

Estimulu mekanikoek, kimikoek edo termikoek korneako eta konjuntibako nerbio sentsorialak aktibatzen dituzte, zeinak malko-guruinak eta konjuntibako zelula kaliziformeak inerbatu eta nerbio eferente parasinpatiko eta sinpatikoak aktibatzen

dituzten. Nerbio guzti horien aktibazioak muki geruza eta geruza urtsua jariatzea eragiten du. Azkenik, begien kliskak Meibomio-ren guruinak jariatutako eta guruin honen hodian biltegiratutako lipidoen askapena erregulatzen du.

1.2. Konjuntiba

Konjuntiba keratinizatu gabeko epitelio geruzatu batez osatutako muki mintz bat da. Epitelio horrek muzinak sintetizatzen dituzten zelula kaliziformeak ditu eta hauek malkoaren egonkortasuna eta kornearen gardentasuna mantetzeko funtsezkoak dira. Keratinizatu gabeko epitelio geruzatu hau, substantzia propio bezala ezagutzen den ehun konektibo fibrobaskular baten gainean dago, linfozitoak dituen azaleko geruza batez eta odol-hodiak, hodi linfatikoak eta nerbio-bukaerak dituen geruza sakonago batez osatuta dagoena [4].

Baskularizazioari, immunitate-zelula kantitate handiari eta inmunoglobulinak eta entzima bakterizidak jariatzeako ahalmenari esker, konjuntibak infekzioei erantzuteko potentzial handia du. Endozitosi edo difusio bidez, konjuntibako epitelioa malko-geruzan diluitutako substantziak xurgatzeko gai da. Ezaugarri horrek kolirioen instilazioaren eragin terapeutikoa errazten du.

1.3. Kornea

Kornea begiaren kanpoko aldean kokatzen den egitura da. Ehun garden abaskularra da, odol hodi gabekoa alegia, jatorri ektodermikoa (epitelioa) eta neuroektodermikoa (estroma eta endotelioa) duena. Kanpoko estimulu kaltegarrien aurrean babesteko lehen hesi gisa dihardu, eta begiaren errefrakzio gehiena ahalbidetzen du (1,33-ko errefrakzio-indizea), argia betsarera eta kristalinora igorriz [5].

1.3.1. Anatomia eta funtzioa

Gizaki heldu baten korneak 12 mm-ko zabalera eta 1 mm-ko luzera ditu batez beste. Ehun honen lodiera zertxobait handitzen da erdigunetik kanpoalderantz joan ahala, 0,55 mm inguruko lodiera du erdigunean eta 0,65 mm-ko lodiera periferian. Aurreko kurbadura-erradioak 7,8 mm neurtzen ditu eta atzekoak 6,5 mm inguru, neurri hauek guztiak gizabanakoen arteko aldaketen araberakoak izanik [5, 6].

Malko-geruzaren eta humore urtsuaren artean kokatutako egitura da, histologikoki eta funtzionalki ezberdinak diren 5 geruzez osatuta dagoena. Geruza

horiek, nerbio sentsorialekin batera, argia betsarera bideratzeko transdukzio-sistema osatzen dute. Epitelioak, Bowmanen mintzak eta estromak aurreko kornea deritzon egitura osatzen dute, Descemeten mintzak eta endotelioak, berriz, atzealdeko kornea eratzen dute (I.2 irudia).

1.3.1.1. Korneako epitelioa

Korneako epitelioa 50 μm inguruko lodiera duen eta 5-6 zelula geruzez osatuta dagoen epitelio ezkatatsu geruzatu ez keratinizatua da. Ilara bakarreko geruzarik sakonena, geruza basala, zutabe itxurako zelula basalek osatzen dute. Zelula horiek azpian kokatzen den mintz basalera eta Bowmanen mintzera lotuta daude, hemidesmosomen eta kolageno loturen sare konplexu baten bitartez. Zelula hauek IV motako kolagenoz, lamininaz, heparina sulfatoz, fibronektinaz eta VII motako kolagenoz osatuta dagoen mintz basala jariatzen dute eta bere funtzioa zelula epitelialen mugimendua eta migrazioa babestea da [7–9]. Epitelioaren hurrengo 2-3 geruzak, zelula basalen desberdintzapenetik eratorritako zelula suprabasalez osatuta daude. Azkenik, malko-geruzarekin kontaktu zuzenean dauden epitelioaren goialdeko bi edo hiru geruzak, forma zapal eta poligonala daukaten zelula ezkatatsuez osatuta daude. Zelula hauek lotura hertsiez osatutako banda jarraitu batez inguratuta daude [10].

Epitelio zelulen eta mintz basalaren arteko lotura sare konplexuari esker, epitelioak bere funtzio nagusia bete dezake: kanpoko estimulu kaltegarrien aurka babesteko hesi bat eskaintzea eta estroman malkoetatik datorren likidoa sartzea eragoztea. Horrez gain, kornean erasoak sumatu eta prebenitzeko epitelioa oso inerbatuta dago [10].

1.3.1.2. Bowmanen mintza

Bowmanen mintza 8-12 μm-ko lodiera duen korneako lehen mintz azelularra da. Epitelioa eta estroma fisikoki banatzen ditu eta ausaz antolatutako kolagenozko zuntz sare batez (batez ere I motako kolagenoa, baina baita III, V eta VII motakoak aurki daitezke) osatuta dago [11]. Gizakietan aurkitzen bada ere, animalia espezie guztiek ez daukate Bowmanen mintza [12].

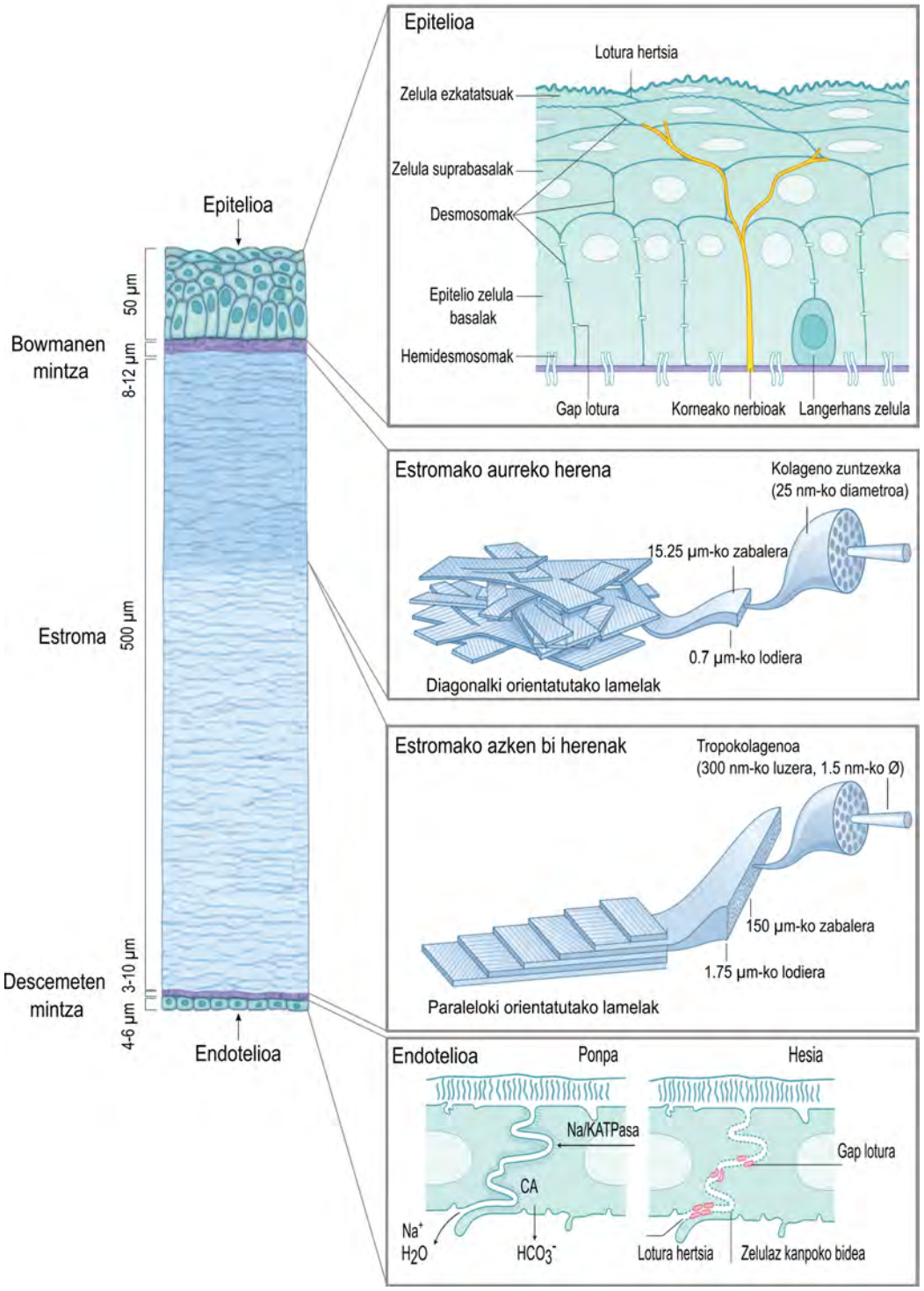

I.2. IRUDIA: Korneako osagaien ilustrazio xehatua. Epitelioa 5-6 geruzako epitelio estratifikatua da eta geruza zelular heterogeneoen arteko lotura-sare konplexua du. Estromaren aurreko herena diagonalean orientatutako xaflek osatzen dute, eta horiek z ardatzean aldaketa esanguratsuak eragiten dituzte. Aitzitik, estromaren atzeko bi herenak x eta y ardatzetan luzetarako erresistentzia eskaintzen duten xafla paraleloz osatuta daude. Kolageno-zuntzexkek lamela bakoitzaren barruan duten kokapenak zeregin garrantzitsua du zuntzexken ondulazioaren prebentzioan eta, beraz, banakako zuntxezka bakoitzaren trakzioarekiko erresistentziaren hobekuntzan. Azkenik, kornea-hesia eta ponpaketa metabolikoko lekuak korneako endotelioan zehazten dira. [10]-tik moldatutako irudia.

1.3.1.3. Estroma

Estroma kornea osoaren % 90-a osatzen duen geruza da eta oro har 500 μm-ko lodiera izan ohi du. Zelulaz kanpoko matrizeak (ZKM), keratozitoek eta korneako nerbioek osatzen dute. Zelulaz kanpoko matrizea heterodimerizatutako I eta V motako kolageno zuntzexkez, proteoglikanoez eta ura atxikitu eta kornearen gardentasuna mantentzen laguntzen duten glukosaminoglikanoez, hala nola keratan sulfatoz, kondroitin sulfatoz eta dermatan sulfatoz, osatuta dago [10, 13]. Estromaren ezaugarri den antolaketa espezifiko eta estrategiko honek, korneari gardentasun eta propietate mekaniko egokiak ematen dizkio [13].

Estromako kolageno zuntzexkak 300 lamelatan antolatzen dira erdialdean eta 500 lamelatan kanpoaldean, estromako eremu desberdinetan hauen tamaina, norabidea eta gurutzaketa maila aldatzen delarik. Bowmanen mintzetik hurbilen dagoen estromaren aurreko herena meheagoa eta estuagoa da, eta diagonalki orientatutako lamelez osatuta dago. Atzealdeko bi herenak aldiz lodiagoak eta zabalagoak dira eta paraleloki orientatuta daude. Bowmanen mintzarekin kontaktuan daudenak izan ezik, gainerako lamelak alderik alde banatzen dira kornearen kurbadura mantentzeaz arduratzen den eraztun zirkunferentzial bat osatuz [14].

Keratozitoak estromaren % 3-10 osatzen dute, kolageno-xaflen artean tartekatuta daude eta ZKM-ren antolaketa eta ordena zehatza mantentzearen arduradun nagusiak dira. ZKM-ren osagai nagusiak jariatzen dituzte, kolagenoa edo glukosaminoglikanoak kasu, kornearen egitura normala mantentzeko [15]. Jaioberrietan fibroblasto eraldatuen moduan dihardute eta estromako ZKM-ren zatirik handiena osatzen dute. Helduaroko estroman aldiz, egoera kieszentean mantentzen dira fibrozito eraldatuen moduan jardunez. Kornea kaltetzean, metabolikoki aktibo bihurtu eta ehuna konpontzeko indar kontraktilak aplikatu eta kolagenoa digeritzeko gai diren metaloproteinasak sortzen dituzten miofibroblasto bihurtzen dira. Horrez gain, erantzun inmunean bitartekari gisa dihardute beharrezkoa denean [16, 17]. Keratozitoez gain, monozitoak/makrofagoak, neutrofiloak, Langerhansen zelulak edo NK zelulak (ingelesetik, "Natural Killers", Zelula hiltzaileak) ere, estromaren jarduera immunitarioaren eta konponketaren parte gisa hauteman dira [18].

Kolageno eta keratozitoez gain, proteoglikanoak estromaren hirugarren osagairik ugariena dira. Kolageno zuntzekiko perpendikularki kokatuta daude eta ehunari bolumena, erresistentzia eta propietate biskoelastikoak ematen dizkiote, aldi berean estromako kolageno zuntzexken antolaketa mantentzen dutelarik [10].

Estromaren inerbazioak ere garrantzi handia du. Nerbio trigeminoaren adar oftalmikoko nerbio-zuntzak estromaren erdialdean sartu eta adar txikiagoetan banatzen dira. Adar horiek Bowmanen mintzean sartzen dira lehenik, eta epitelioaren xafla basalean ondoren, epitelioaren azpian, plexu subepiteliala sortuz. Honek estimulu mekaniko, kimiko eta tenperatura aldaketei erantzuten die, epitelioko zelula geruza basalaren inerbazioa ahalbidetu eta faktore trofikoak askatzen ditu begi gainazala osasuntsu mantentzeko [10, 19].

2013-an kornearen anatomiaren inguruan egindako azterketak, luzaroan finkatutako 5 geruzaz gain, seigarren geruza bat egon zitekeen eztabaida sortu zuen. Izan ere, Descemeten mintzaren eta endotelioaren artean Duaren geruza izeneko zelula gabeko beste geruza bat deskribatu zuten lehenengo aldiz. Geruza hau histologikoki estromaren parte izango litzateke, eta kornearen biomekanika eta fisiopatologia ulertzeko eragina izan lezake [20].

1.3.1.4. Descemeten mintza

Descemeten mintza korneako bigarren mintz azelularra da eta endotelioaren mintz basala. IV eta VIII motako kolagenoz osatuta dago batez ere, nahiz eta ZKM-ren beste proteina batzuk ere badituen. Gizaki gazteetan 3 μm-ko lodiera badu ere, 10 μm neurtzera irits daiteke helduetan [21]. Kornearen homeostasiaren, egituraren eta gardentasunaren mantenuan inplikatuta dago: mantenugaiak estromara sartzea ahalbidetu, zelula endotelialen monogeruza ainguratu eta hidratazio egokia mantendu ahal izateko funtsezkoa da. Horrez gain, atzealdeko kornearen kurbadura mantetzean ere eragina izan lezake [22].

1.3.1.5. Endotelioa

Endotelioa muino neuraletik eratorritako zelula zapal hexagonalez osatutako geruza batek osatzen du. Zelula horiek mosaiko poligonal baten forman daude antolatuta eta ez dute mitosi ahalmenik.

Endotelioak baita, korneako berezko gardentasuna mantentzen laguntzen du, korneako hidratazioa eta nutrizioa erregulatuz. Humore urtsutik kornearantz bideratutako likido kantitatearen eta gehiegizko likido hori ponpatzean gastatzen den energiaren arteko oreka mantentzen du. Endoteliaoren hesi funtzioak, humore urtsutik datorren likido kantitate handi bat estromara igarotzea eragozten du, aldi berean, 10 nm-tako zelulen arteko espazioetan zehar elikagai txikiak, ura eta beste metabolito batzuk modu erregularrean hedatzea ahalbidetzen duelarik [10].

1.4. Linbo esklerokorneala

Korneako linboa edo linbo esklerokorneala, kornea gardenaren eta konjuntibaren eta esklerotikaren arteko 1 mm-ko zabalera duen trantsizio eremuari deritzo. Linbo esklerokorneala Bowmanen geruzaren amaieran hasten den eremu oso berezia da eta kornearen funtzio egokirako beharrezkoak diren prozesu askotan esku hartzen du. Kornearen birsortzerako ezinbestekoak diren zelula amen iturria da, kornea periferikoaren elikaduran inplikatuta dago eta erantzun sentsorialetan parte hartzen du.

Korneako epitelioa ez bezala, linboko epitelioa 7-10 zelula geruzez osatuta dago. Geruza horiek geruzatutako eta keratinizatu gabeko epitelio zelulak eta inguruko beste zelula mota batzuk ditu, melanozitoak eta Langherans-en zelulak barne. Epitelio honen geruza basalean linboko epitelio zelula ama/progenitore (LEZA/P) bezala ezagutzen diren zelulak aurki daitezke, korneako epitelioaren birsorkuntzaren arduradunak direnak.

Korneako epitelioa birsortzen duten zelula amak zalantzarik gabe sailkatzeko biomarkatzailerik ez dagoenez, aipatutako zelula amak izendatzeko batasun eza gertatu da. Hala, korneako epitelioa birsortzea ahalbidetzen duten jatorrizko zelula amak, linboko zelula ama, linboko epitelio zelula ama, linboko epitelio zelula progenitore edo korneako epitelio zelula ama ala progenitore moduan ezagutzen dira. Lan honetan, zelula hauek linboko epitelio zelula ama edo progenitore LEZA/P deituko ditugu.

1.4.1. Linbo esklerokornealeko zelula amen nitxoa

Linboko zelula amak multzo txikietan nitxo zelular izeneko mikroingurune oso arautu, babesle eta espezializatu batean kokatzen dira, desberdindutako zelula espezifikoz inguratuta. Ingurune honek zelula amen sorkuntza eta hauen kieszentzia bermatzeko baldintza egokiak mantentzen ditu (I.3 irudia).

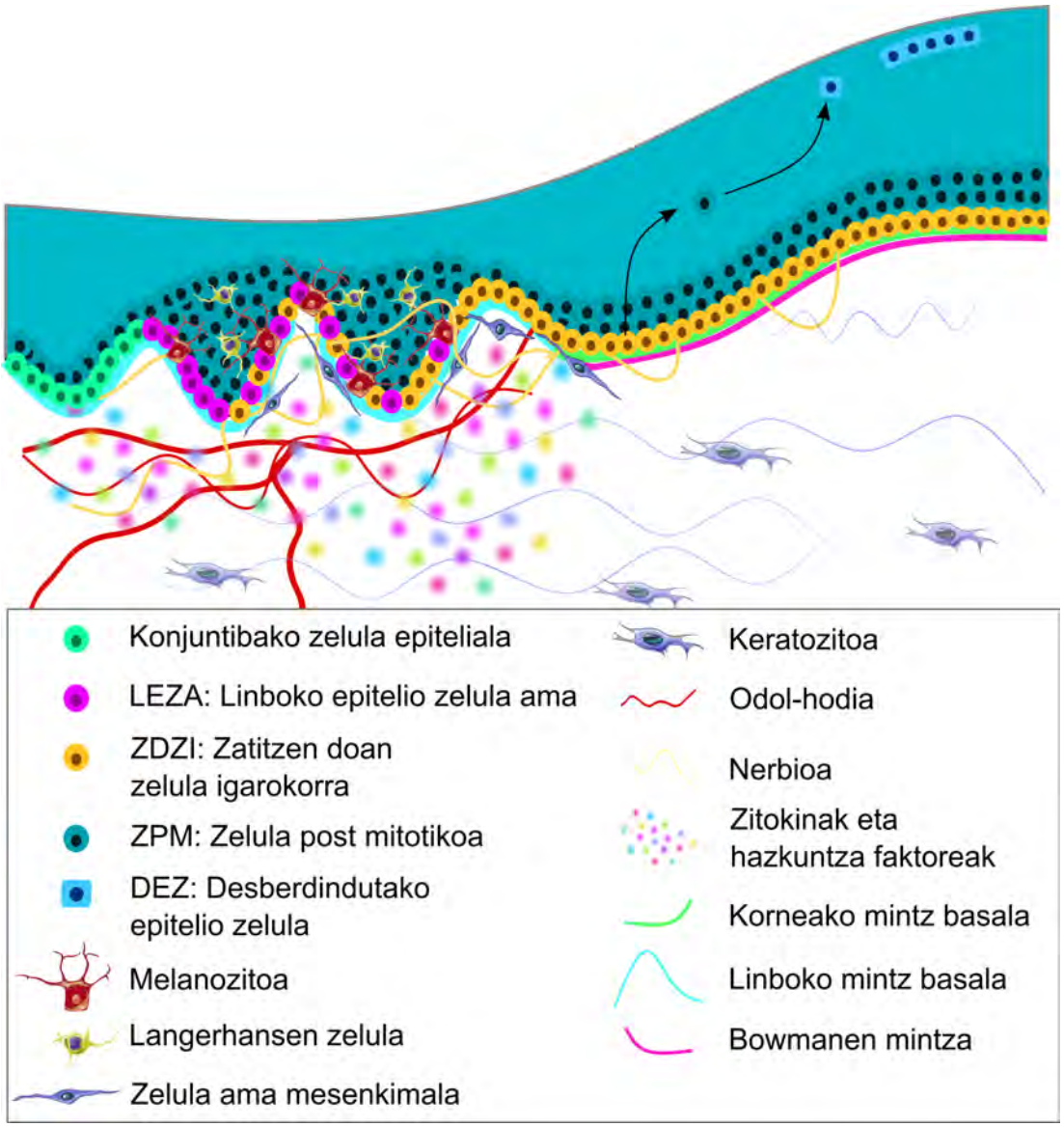

I.3. IRUDIA: Linbo esklerokornealeko zelulen nitxoa.

Zelula amentzako ingurune babesle bat eskaintzeaz gainera, faktore disolbagarriak, funtsezko seinaleztapen-bidezidor anitz, propietate biomekanikoak eta zelulaz kanpoko matrize funtzionala eskaini eta inguruko nitxoko zelulen eta beste elementuekiko interakzioak ere ahalbiditzen ditu. Giza kornearen kasuan, epitelioa eremu batzuetan tolestuta dago, uhin moduko egitura batzuk sortuz.

Egitura hauek anatomikoki Vogt-en tolesdurak bezala ezagunak dira. Histologikoki, Linboko kriptak, linboko epitelioaren beheranzko inbaginazioak, eta estromako proiekzioak aurkitu daitezke Vogt-en tolesduren baitan. Estromako proiekzioak kornearen zirkunferentzian zehar aurkitzen dira, baskularizatuta daude eta bere elementuen artean, melanina edukia duten zelulak aurki daitezke [23]. Bi egitura hauetan LEZA/P-k kokatzen dira [23, 24].

Epitelioaren tolesdura eta ondoriozko egitura bereizgarriak, epitelioaren eta estromaren arteko elkarrekintza zuzena ahalbidetzen du. Oro har, korneako estroman ez dira zelula asko aurkitzen, baina linboko kriptak kokatzen diren eremuetan, tolesdurekin kontaktu estuan dauden estromako zelula kopurua handitu egiten da.

Linboko zelulen nitxoak sistema immuneko zelulak, zelula mesenkimalak, melanozitoak, nerbio eta odol zelulak, zelulaz kanpoko matrizea eta seinaleztapen-molekulak ditu. Nitxoaren inerbazioa eta baskularizazioa funtsezkoak dira zelula amen biziraupenerako eta osagai guztien funtzionaltasun bateratuak, zelula amen mantentze, ugaltze, migrazio eta desberdintzapen egokia bermatzen ditu. Melanozitoen melaninak LEZA/P-k ultramore (UV) izpien irradiaziotik babesten ditu eta zelula mesenkimalek jarduera erregulatzailea dute, linboko zelula amekin zuzeneko kontaktuan baitaude [25].

Linboko estromaren zelulaz kanpoko matrizeak, zelula amen mantentzerako funtsezkoak diren faktoreak ematen ditu. Erresistentzia mekanikoa eman, zelulen arteko komunikazioa ahalbidetu eta epitelio basal eta inguruko estromako zelulen arteko elkarrekintzan laguntzen du.

Linbo eremuko zelula epitelialak, estromako zelulekin eta melanozitoekin kontaktu zuzenean daudela deskribatu izan da. Gainera, linboko melanozitoek eta zelula epitelialek N-kaderina adierazten dute, eta horrek linbo eremuan zelulen arteko interakzioen garrantzia iradokitzen du [26]. Zelula amen fenotipoa mantentzearen funtsezko beste alderdi bat zelula geldien eta ingurukoen arteko interakzioa da. Jakina da seinaleztapen-bidezidor asko zelula amen mantentze-lanetan inplikatuta daudela, Wnt edo Notch seinaleztapen-bideak barne.

Wnt/β-Katenina seinaleztapen-bidezidorra, mota ezberdinetako zelula amen mantentzean gakoa den bidezidorra izateagatik da ezaguna. Wnt familiako lau proteina ezberdin identifikatu dira linbo eremuan, Wnt2, Wnt6, Wnt11 eta

Wnt16b kasu [27]. Notch seinaleztapen-bidezidorra aldiz, giza garapenean zehar mantendutako mekanismoa da eta prozesu zelular ezberdinetan berebiziko garrantzia daukala dakigu. Notch1 hartzailea eta HES-1/HEY-1 geneak linboko epitelio geruza basalean identifikatu dira eta horrek, bidezidor honek linboko epitelioan duen presentzia baieztatzen du [28, 29].

1.4.2. Linboko zelula ama motak

Zelula ama helduak gorputzeko ia ehun guztietan daude, giza kornean barne.

Zelula progenitoreak ehun bateko berezkoak diren zelula amak dira [30], korneako epitelioaren kasuan, linboko epitelio zelula progenitore (LEZP) izenez ezagutzen direnak. Linboko epitelio zelula ama (LEZA) eta LEZP terminoaren inguruan eztabaida handia dago, korneako epitelioa birsortzen duten zelula amak zalantzarik gabe sailkatzeko biomarkatzailerik ez baitago.

Kornean mota ezberdinetako zelula amak daude eta bakoitzak bere funtzioa betetzen du. LEZA/P-k linbo eremuko epitelioan aurkitzen dira eta korneako estroma zelula amak (KSZA) berriz, linbo eremuko estroman. Bi zelula mota hauek kornearen birsortze eta homeostasirako beharrezkoak diren baldintzak sortzen dituzte, ondorioz ikusmena ziurtatuz. Aipatutako zelula amez gain, ikertzaile batzuk endotelioan zelula progenitoreak egon daitezkeela azaldu dute. Hala ere, hipotesi hau ez dago guztiz onartuta, eztabaida ugari sortu baititu [31].

1.4.2.1. Kornea edo linboko epitelio zelula ama edo progenitoreak

Linbo eremuan aurkitzen diren epitelio zelula amak (LEZA/P), korneako zelula ama motarik aztertuenak dira. Zelula hauek linboko epitelio geruza basalean talde txikietan multzokatuta kokatzen dira eta bereizgarriak diren ezaugarri fenotipikoak dituzte. Zelula ama gisa katalogatu dira, zelula amen berezko propietateak dituztelako, hala nola, ziklo zelular geldoa, koloniak sortzeko gaitasuna eta inguruko zelulek adierazten ez dituzten biomarkatzaileen adierazpena. LEZA/P-k adierazitako proteina hauek urteetan garatutako ustezko markatzaile zerrenda batean bilduta daude, eta esanguratsuenak ABCG2, ABCB5, KRT14, KRT15, N-kaderina, ΔNP63α eta Fzd7 dira [26, 32, 33].

1.4.2.2. Korneako estroma zelula amak

Korneako estroma zelula amek (KSZA), zelula ama mesenkimalekin antzekotasunak partekatzen dituzte eta linbo eremuko estromaren aurreko aldean kokatzen dira. Linboko epitelio zelula amekin harreman estua dute, eta markatzaile proteiko ezberdinak adierazten badituzte ere, biek zelula amekin lotutako ezaugarri fenotipikoak dituzte. Kornea-estromako zelula amek zuzeneko kontaktua dute linbo eremuko zelula epitelialekin [31]. Gainera, estromako zelula ama hauek melanozitoak dituzte inguruan. Guzti hau kontuan hartuta, zelula mota ezberdinez eratutako nitxo zelular konplexu baten eraketa argi dago, zeinak linboko epitelio zelula amen izaera mantentzen laguntzen duen.

1.5. Korneako epitelioaren homeostasia

Kornea birsortze ahalmen handia duen oso ehun dinamikoa da. Birsotze ahalmen horren arduradun nagusiak kornearen linbo eremuko epitelio basalean dauden LEZA/P-k dira [16, 25]. Ama izaera duten eta korneako epitelioa birsotzeko ezinbestekoak diren zelula hauek identifikatzeko, egun ez da markatzaile argirik aurkitu. Hala ere, urteetan egindako ikerketek ustezko markatzaileen sorta bat sortu dute, eta hauen konbinazioak erabiltzen dira LEZA/P-k identifikatzeko. Linboko epitelio basalean dauden zelulek markaketa positiboa dute ABCG2, ΔNp63α, Fzd7, KRT14, KRT15, ABCB5, N-kaderina, KRT19, bimentina, KGF-r, metalotioneina eta α-9 integrinarentzat. Aldiz, negatiboak dira KRT3, KRT12, 43 konexina, inbolukrina, P-kaderina, SSEA4, nestina, α-2, α-6 eta β-4 integrina proteinentzat [26, 34–45]. Halaber, eraberritzeko gaitasuna duten LEZA/P-k, ΔNp63α, C/EBPδ eta Bmi1 markatzaileen adierazpen bateratu bidez identifika daitezke [46].

Korneako epitelioa 7-10 egunetik behin berritzen da, hainbat migrazio eta zelulen ugaltze mekanismoren bitartez. Linboko epitelio zelula amak prozesu honen arduradunak direla dioen eredua korneako epitelioaren berrikuntza eta homeostasia azaltzeko hipotesirik onartuena da (I.4 irudia). Eredu honen arabera, LEZA-k linbo eremuko epitelioaren geruza basalean kokatzen dira eta banatzen doazen heinean, LEZA-en ondorengoak diren eta desberdinduago dauden zatitzen doazen zelula igarokorrak (ZDZI) sortzen dituzte. Zelula horiek modu zentripetuan migratzen dute linbo eremutik kornea erdialderantz, korneako epitelioaren beharraren arabera. Migrazio horretan, zelulak desberdintzen jarraitzen dute, epitelio zelula

post mitotikoak (ZPM) sortuz. Zelula hauek bertikalki ugaldu, migratu eta azkenik guztiz desberdindutako epitelio zelula (DEZ) ezkatatsuetan bihurtzen dira. Desberdindutako zelula hauek korneako epitelioaren gainazalera iritsi eta askatu egingo dira berriro ere, kornearen etengabeko homeostasi prozesuaren parte bihurtuz [6, 25, 47, 48]. Hala, ugaltze horizontalaren eta bertikalaren, migrazioaren eta zelula-askapenaren artean sortutako oreka perfektu batek, epitelioa osasuntsu eta uniforme mantentzen du [10, 49, 50]. Prozesuen konbinazio hau Thoftek deskribatutako X, Y, Z hipotesian deskribatzen da [48], non X (linbo eremuko zelula epitelial basalen ugaltzea) + Y (korneako zelula epitelialen migrazio zentripetua eta desberdintzapena) = Z (betazalen kliskatzeak eragindako epitelio zelulen askapena).

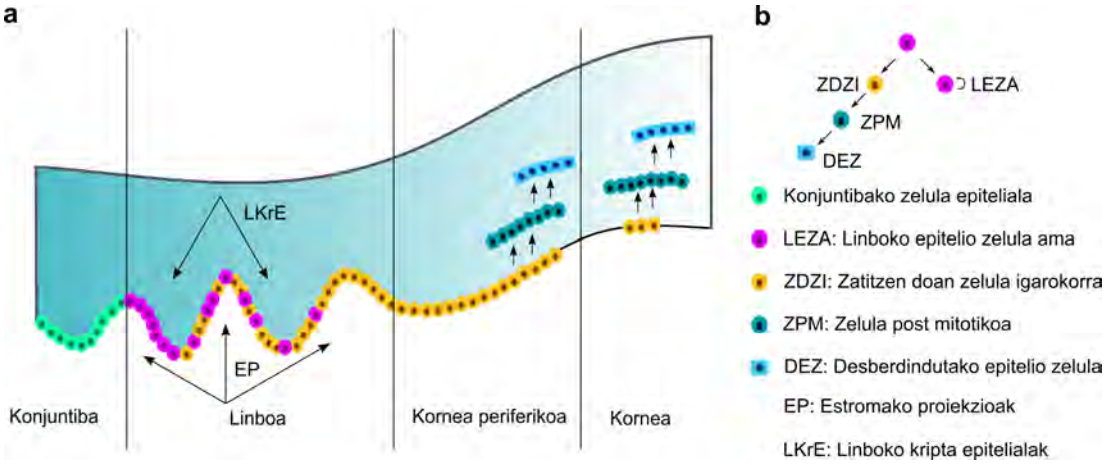

I.4. IRUDIA: LEZA bidezko kornearen birsortze hipotesiaren azalpen grafikoa. **a**) Linbo eremuko epitelio basalean kokatutako zelula amak asimetrikoki banatzen dira ZDZI-k sortzeko. ZDZI horiek kornea zentraleko eremura migratzen dute, pixkanaka ZPM eta, ondoren, DEZ bilakatuz. LKrE, EP, LEZA, ZDZI, ZPM eta DEZ linboko kripta epitelialei, estromako proiekzioei, linboko epitelio zelula amei, zatitzen doazen zelula igarokorrei, zelula post mitotikoei eta desberdindutako epitelio zelulei dagokie, hurrenez hurren. **b**) LEZA-ek autoberritzeko eta zelula espezializatuagoetan desberdintzeko gaitasuna dute.

Animalia-espezie batzuk kontuan hartuta, kornearen azalera osoan banatuta dauden korneako epitelio zelula amek (KEZA), epitelioaren birsortzea errazten dutela iradoki da [25]. Animalia-espezie batzuetan, hala nola txerrietan edo untxietan, KEZA-k aurkitu dira korneako erdiko gunean, eta horrek, zelula amak linbo eremura mugatuta ez daudela iradokitzen du [47].

Hala ere, gizakietan kornearen geruza basaleko zelulek holokloiak sortzeko gaitasunik ez dutela ondorioztatzen duten ikerketek, gizakientzat teoria honekiko interesa murriztu dute [32].

1.6. Linboko zelula amen gutxitasuna

1.6.1. Epidemiologia eta patologia

Linboko zelula amen gutxitasuna (LZAG) begiaren gainazaleko gaixotasun arraroa da. Gaixotasun hau linboko zelulen nitxoaren edo linbo eremuan dauden zelula amen disfuntzioak edo suntsipenak eragiten du, horiek baitira korneako epitelioaren birsortze eta homeostasi normala mantentzearen erantzuleak. LEZA/P-k edo linboko zelulen nitxoaren propietate funtzionalak galtzeak, konjuntibako epitelioak korneako epitelioa gainjartzea eragin dezake, eta horrek orbaintze epiteliala hondatzea, begi gainazalaren hantura kronikoa, neobaskularizazioa eta, kasu larrienetan, opazifikazioa eta itsutasuna ekar ditzake. Beste konplikazio batzuk, hala nola epitelioaren higadura, ultzerazioa edo kornea zulatzea ere gerta daitezke.

Europar Batasuneko Orphanet agentziak LZAG gaixotasun oftalmologiko arrarotzat jotzen du (ORPHA: 171673), eta Sendagaien Europako Agentziak (SEA), LZAG gaixotasun umezurtz gisa sailkatu du, Europar Batasunean (EB) 10.000 pertsonatik 2-k pairatzen baitute, gutxi gorabehera. LZAG emateko kausek jatorri ezberdina izan dezakete: afekzio genetikoak, gaixotasun autoimmuneak, traumatismoak edota begi gainazelako lesioak. Duela gutxi, 10 urteetan zehar eramandako ikerketa batek LZAG-ren demografia eta kausen inguruko deskribapen zabala argitaratu du. Ikerketa horrek, Asiako osasun-zentro ezberdinetan 2000 begitik gora kontutan izan zituen eta paziente gehienak LZAG begi bakarrean (unilaterala) pairatzen zuten haur edo gazte gizonezkoak izan ziren [51]. Ikerketan ondorioztatutako gaixotasunaren kausa nagusiak III.1 taulan zerrendatuta daude.

I.1. TAULA: LZAG-ren kausa nagusiak.

Gaixostasuna	LZAG unilaterala	LZAG bilaterala
Erredurak	% 84	% 30
Steven-Johnson sindromea	% 4	% 23
Keratokonjuntibitisa	% 3	% 30
Muki-mintzeko penfigoidea	% 2	% 4
Traumatismoa	% 2	-
Aniridia	-	% 9

LZAG duela bi hamarkada baino gehiagotik onartzen bada ere, duela gutxi arte ez da diagnostikoei, larritasun mailari, sailkapenari eta tratamenduari buruzko irizpiderik adostu. Hala, LZAG kudeatzeko nazioarteko lan taldeak, gaixotasuna era

bateratu eta estandarizatuan eramateko jarraibide orokor batzuk argitaratu ditu [52], gaixotasunaren diagnosi eta tratamenduak modu argiagoan egitearen aldera.

1.6.2. Diagnosia eta tratamenduak

Orokorrean LZAG-aren diagnostikoa historia klinikoan, pazienteak izan ditzakeen sintoma klinikoetan eta beste proba diagnostiko batzuetan oinarritzen da. Gaixotasun honen lehen agerpenak, korneako epitelioan nabaritzen dira. Epitelioa geroz eta irregularragoa bihurtzen da eta Vogt-en tolesdurak gutxitu egiten dira, zelula amen gordailua desagertzera iritsi arte. Gaixotasuna aurrera doan heinean, konjuntiba ehunak kornea inbadi dezake begiaren ikusmen ardatzera iritsi arte.

LZAG-rekin lotutako prozesuak diagnosi teknika desberdinen bidez identifika daitezke. Horien artean daude i) inprimatze zitologia, kornean zelula kaliziformeak identifikatzeko aukera ematen duena, horrek konjuntiba ehunak kornea inbaditu duela adieraziko du; ii) linboaren aldaketa mikroestruktural esanguratsuen behaketa laser eta eskaner bidezko *ex vivo* mikroskopia konfokalaren bidez; eta iii) aurreko segmentuaren koherentziazko tomografia, begiaren aurreko segmentuko elementuen bereizmen handiko irudiak ematen dituena, kornea eta linboa barne.

LZAG pazienteak aurkeztutako sintoma motaren eta hauek begiaren gainazalean hartzen duten eremuaren arabera 3 larritasun mailetan sailka daiteke (I-III mailak) [52, 53]. Hurrengo diagramak (I.5 irudia) gaixotasunak izan ditzakeen 3 mailak irudikatzen ditu eta maila bakoitzean erasandako begiaren gainazalaren ehunekoa zehazten du.

Gaur egun ez dago beraien funtzioa galdu, kaltetu edo desagertu diren LEZA-k ordezkatzeko edo linboko nitxoaren funtzioak berreskura ditzakeen sendagairik. Hala ere, korneako homeostasia modu eraginkorrean berrezartzeko zeluletan oinarritutako sendagai biologikoak garatzen dihardute [54, 55].

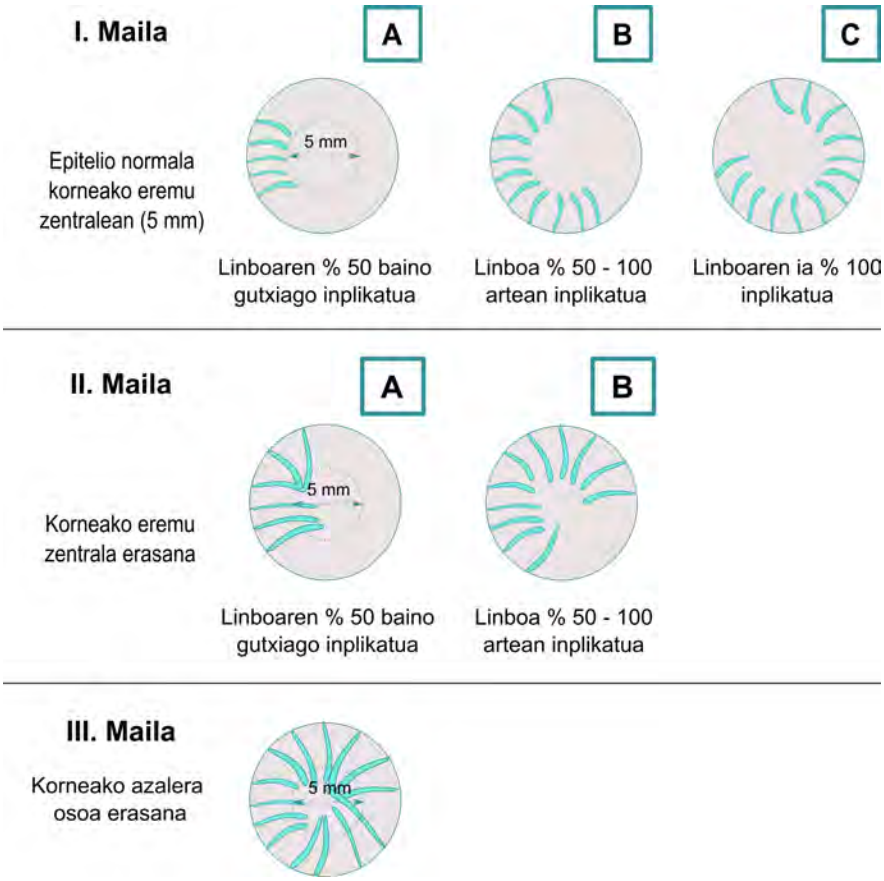

I.5. IRUDIA: LZAG-k izan ditzakeen aldi ezberdinen azalpen grafikoa.

Aplikatu beharreko tratamendua desberdina da gaixotasunaren mailaren arabera. Gaixotasunaren hedapen maila zehaztu ondoren, lehentasuna begiaren gainazalean ematen diren koerikortasunak ebaztean datza, hala nola, begiaren gainazaleko inflamazioa, malko-geruzaren anormaltasuna edo infekzioak. Begiaren gainazalean baldintza kritiko hauek eman ezkero, linbo eremuan gera daitezkeen LEZA/P apurren funtzioa kaltetu daiteke. Beraz, tratamenduaren lehen helburua kaltegarriak izan daitezkeen faktore hauek deuseztatzea da, era horretan begiaren gainazalaren osasuna hobetu eta arrisku faktoreak gutxitzeko. Aldi berean, arrisku faktoreak gutxitzeak aurrerago aplikatuko diren tratamenduetan hobekuntzak dakartza. Adibide gisa, koerikortasun gabeko transplanteetan, ehunaren biziraupena asko luzatzen da.

I. eta II. mailako begi bakarrean edo bietan emandako LZAG kasuetan, pazientearen ikusmena kaltetuta balego edo konplikazioak baleude, ez da LEZA/P-en transplanterik gomendatuko. Kasu hauetan linboan bertan gera daitezkeen zelula amek birsortzeko duten gaitasuna indartzea da helburu nagusia. Horretarako, linbo eremua hartu duen edo hartzeko gaitasuna izan dezakeen konjuntibako eremua

kirurgikoki kenduko da ikusmen ardatza garbi mantendu dadin. Prozedura kirurgiko hau konjuntibako epiteliotomia bezala ezagutzen da eta larriak ez diren kasuetan soilik da egokia. Teknika honek, kornearen berezko berrepitelizazioa du helburu. Bestelako korneako akatsetan, mintz amniotikoa erabil daiteke birsortze prozesuan laguntzeko.

Kasu akutuagoetan, hala nola II. eta III. mailatan, behin begi gainazalean egon zitezkeen koeritasunak tratatu ondoren, LEZA/P funtzionalak dituzten elementuak transplantatzea da aukerarik onena. Erabiliko den metodo kirurgikoa desberdina izango da gaixotasunaren lateraltasunaren arabera (alde bakarreko gaixotasunak begi bakarrari eragingo dio, alde biko gaixotasunak bi begiei). Oro har, linbo eremuko ehun zati baten edo LEZA/P-tan oinarritutako sendagai biologikoen transplantea nahikoa izaten da gaixotasunari aurre egiteko, transplante autologoa edo alogenikoa izan daitekeena. Transplante alogenikoetan hildako edo bizirik dauden emaileen linboko mentuak erabiltzen dira, transplante autologoetan erabilitako zelulak, berriz, pazientearen begi kontralateral osasuntsutik datoz [53].

Azken hamarkadan, zelula ametan oinarritutako terapiek medikuntza birsortzailean etorkizun handia erakutsi dute, kaltetutako edo gaixotutako zelulak, organoak edo ehunak birsortzeko, konpontzeko edo ordezkatzeko.

2008-an SEA-k LZAG tratatzeko zeluletan oinarritutako lehen sendagai biologikoa onartu zuen, Holoclar izenekoa hain zuzen. Produktu hau giza jatorriko korneako epitelioko zelula amen *ex vivo* hazkuntzan oinarritzen da [56]. Holoclar sendagaiaren onarpenetik aurrera, LZAG tratatzeko beste hainbat produktu garatzeko ikerketak eta saiakera klinikoak egin dira. Hala ere, LZAG tratatzeko zelula ametan oinarritutako terapien eragozpen handiena, LEZA/P-tan aberatsak diren hakuntza zelularrak bermatzeko ezintasuna da, oraindik ez baita zelula amak identifikatzeko biomarkatzaile zehatzik ezarri. Gaur egun, LZAG-ren tratamendurako 12 saiakuntza kliniko daude abian. Gehienak zelula ametan oinarritako saiakuntzak badira ere, teknika kirurgiko berriak aztertzen dituzten ikerketak ere badaude (III.2 taula). Horrez gain, 2008 eta 2023 urteen bitartean beste 15 saiakuntza burutu zituzten. Nolanahi ere, Holoclar izan da laugarren fasera iritsi den produktu bakarra.

I.2. TAULA: LZAG tratatzeko abian dauden saiakera klinikoen zerrenda.

NCT Zenbakia	Izenburua	Egoera	Lekua
NCT03943797	Kultibatutako Aho-Mukosa Epitelioaren transplante autologoa	I. fasea	Core Laboratory for Cell Therapy, Veterans General Hospital, Taipei,Taiwan
NCT04021875	SLET[1] Autologoaren jarraipena	Behaketazko azterketa	National Taiwan University Hospital Taipei, Taiwan
NCT04704648	Sahara hegoaldeko Afrikan GIB[2]-arekin bizi diren pertsonen begi gainazaleko neoplasia ezkatasuaren eszisio kirurgikoaren bideragarritasun azterketa	NA	Uganda Cancer Institute Kampala, Uganda
NCT04995926	Linboaren ordezkapenerako ezpain-mukosa mentuak	NA	The S. Fyodorov Eye Microsurgery Federal State Institution, Moscow, Russia
NCT05494671	LZAG kasuetan linboko epitelio zelula amak transplantatu ondoren, korneako epitelioaren egonkortasunaren azterketa	NA	Kasr Alainy, Cairo, Egypt
NCT03957954	Zelulan ametan oinarritutako LZAG-erako tratamendua	I. fasea	University of California Los Angeles, California, US
NCT04021134	SLET alogenikoaren jarraipena	Behaketazko azterketa	National Taiwan University Hospital Taipei, Taiwan
NCT05461469	Begi gainazelako irudiak lortzeko sistema balioztatzeko azterketa	Behaketazko azterketa	Universitätsklinik für Augenheilkunde und Optometrie Paracelsus Medizinische Privatuniversität Salzburg, Austria
NCT02886611	Jatorri genetikoko LZAG: genotipo eta fenotipoaren arteko korrelazioa	Behaketazko azterketa	Fondation Ophtalmologique Adolphe de Rothschild, Paris, France
NCT01756365	LZAGaren tratamendurako kultibatutako korneako epitelio autologoa	NA	Toronto Western Hospital, Toronto, Ontario CIUSSS de l'Est-de-l'Île-de-Montréal, Canada
NCT03549299	LZAGa tratatzeko ABCB5 markaketa positiboa duten linboko zelula ama alogenikoak	I/II faseak	Massachusetts Eye and Ear Infirmary Boston, Massachusetts, US Universitäts-Klinikum Heidelberg, Germany
NCT03949881	LZAG bilaterala tratatzeko aho-mukosa mentuak	I/II faseak	Ophthalmology department, Edouard Herriot hospital, Lyon, France

[1] SLET: Ingelez Simple Limbal Epithelial Transplantation, linboko epitelioaren transplante arrunta. Prozedura kirurgiko hau linboko mentu autologoaren edo alogeniakoren zati txikiak mintz amniotiko baten gainean transplantatzean datza. Ondoren, ukipen-lente bat jartzen da babes gisa.

[2] GIB: Giza immunoeskasiaren birusa

1.7. Kornearen birsortze prozesua

Kornea kanpoko mehatxuetatik babesteko eta argia transmititu eta errefraktatzeko funtsezkoa denez, ehun honetan jasandako edozein kaltek ikusmen-zorroztasuna kaltetzen du. Hori dela eta, korneak bere horretan mantentzeko oso eraginkorra den birsotze mekanismoa du (I.6 irudia).

1.7.1. Epitelioaren birsortze prozesua

Korneako epitelioa traumatismo, infekzio edo mikrobio-kalte baten ondorioz zauritzean, azpiko mintz basalarekin duen lotura apurtu eta kaltetutako zelula epitelialek 1α eta 1β motako interleukinak (IL-1α eta IL-1β) askatzen dituzte [11]. Babes hesi funtzioa mantendu ahal izateko orbaintze azkarra behar denez, euren artean eta mintz basalari lotuta jarraitzen duten ertzetako zelulek modu zentripetuan migratzen dute, horrela zelula-geruza irristakor batek zauria estaliz. Behin akats epiteliala estalita, epitelioko zelula basalak ugaltzen eta desberdintzen hasten dira epitelio geruza ezberdinak berritzeko. Era berean, zelula basal hauek, zauriaren azpian dauden keratozitoekin lankidetzan, 511 eta 521 lamininak ekoizten dituzte, mintz basal akastuna birsortzeko [57].

Konponketa epitelialaren ugaltze, desberdintzapen eta migrazio prozesu guzti horiek hainbat hazkuntza-faktoreek arautzen dituzte, hala nola hazkuntza faktore epidermiko (EGF) autokrinoak, α motako hazkuntza faktore eraldatzaileak (TGFα), β motako hazkuntza faktore eraldatzaileak (TGFβ), intsulina antzeko hazkuntza faktoreak (IGF), plaketetatik eratorritako hazkuntza faktoreak (PDGF), fibroblastoen hazkuntza faktoreak (FGF), timosina β4-k (Tβ4) edo estromako keratozitoek askatutako hepatozitoen hazkuntza faktoreak (HGF) eta keratinozitoen hazkuntza faktoreak (KGF) [58, 59]. Kliskatzea erregulatzen duten korneako nerbioek ere, P substantzia (S-P) edo nerbio hazkuntza faktorea (NGF) dakartzate, besteren artean [60–63].

1.7.2. Mintz basalaren birsortze prozesua

Mintz basala garaiz birsortzea faktore erabakigarria da kornearen birsortze homeostatiko egokia edo orbaintze fibrotikoa jasateko. Epitelioko zein estromako akatsek mintz basala erasaten dute. Lehenik eta behin, epitelio eta mintzaren arteko hemidesmosoma motako loturak bereizi egiten dira, epitelio zelulen migrazioa ahalbidetzeko. Kalte horri esker, IL1, TGFβ, PDGF, hazkuntza faktore endotelial

baskularra (VEGF) eta epiteliotik eratorritako beste zitokina angiogeniko eta fibrotiko batzuk estroman sar daitezke, transdesberdintzapen miofibroblastikoa eragin dezaten [18, 64].

Hazkuntza-faktoreen sarrera geldiarazi eta mintz basalaren birsortze azkar bat emateko, zelula epitelialek eta estromako keratozitoek erantzun koordinatu bat eskaini behar dute. Hala, epitelio zelula basalek, 511/521 eta 332 laminina geruzak ekoizten dituzte eta keratozitoek perlekanak eta nidogenoak gehitzen dizkiete geruza horiei [65]. Keratozito hauek zauritutako eremutik gertu egon behar dute, miofibroblastoek mintz basala birsortzeko laguntza oztopa ez dezaten. Azkenik, birsortutako mintz basalak epitelio zeluletatik eratorritako faktore fibrotikoen askapena gutxitzen du eta miofibroblasto aitzindariek apoptosia jasaten dute [64, 66].

1.7.3. Estromaren birsortze prozesua

Estromako edozein kalteren aurrean, epitelio zelulen eta estromako zelulen arteko elkarrekintzak hasi eta mintz basal kaltetutik igarotako hazkuntza-faktoreen eta zitokinen askapena ematen da lehendabizi. Epitelioa kaltetu ondoren, estromako orbaintze prozesuaren lehen erantzuna zauritutako eremuaren keratozitoen apoptosia da. Keratozitoen apoptosiaren eragile nagusiak IL-1 (α zein β) TNFα eta Fas-Fas estekatzailearen interakzioak dira. Faktore horiek malko-guruinetik, kaltetutako epiteliotik, endoteliotik edo hantura-zeluletatik etor daitezke [67, 68]. Hala, zauriaren ondoko keratozitoak ugaldu, migratu eta desberdindu egiten dira, zauriaren eremua birpopulatuko duten fibroblasto bihurtuz. Fibroblasto horiek IL-1 modu autokrinoan ekoizteko gaitasuna dute. IL-1-ak, keratozitoen eta fibroblastoen HGF eta KGF-en ekoizpena handituko du, zeinak epitelioaren birsortzean lagunduko duten [69].

IL-1, IL-6 edo TNFα bezalako zitokina proinflamatorioen kopurua handitzeak, linbo eremuko odol hodietatik eratorritako leukozitoen infiltrazioa eragingo du estroman [70]. Estromara iritsiko diren lehen inmunitate sistemako zelulak neutrofiloak dira. Hauek lesioa gertatu eta 18 eta 30 orduetara metatuko dira eta hauen kantitatea jeitsiz joango da 48 ordu igaro ostean. Neutrofiloak korneako estromara linboko odol-hodietatik iritsiko dira, eta keratozitoen apoptosiak, neutrofiloen zaurira bideratzea erraztuko du. Neutrofiloek patogenoak eta zelula-hondarrak ezabatuko dituzte funtzio fagozitikoen bidez, eta, gainera, nerbio kornealaren berreskurapenari neutrofilorik ez izateak eragiten diola deskribatu da, VEGF-A faktore neurotrofiko gisa jariatzen baita [71]. Neutrofilo kopurua

normalizatu ahala, linbo eremuko odol hodietatik eratorritako makrofagoak zaurian sartu eta erdialdera migratuko dute. Zelula horiek zelula-hondarrak garbitu, fibroblastoak miofibroblastoetara bereiztea sustatzeko TGFβ jariatu eta odol eta linfa hodi berrien eraketa sustatzeko VEGF askatuko dute [72]. Langerhansen zelulen eta NK zelulen infiltrazioa ere emango da [18, 73].

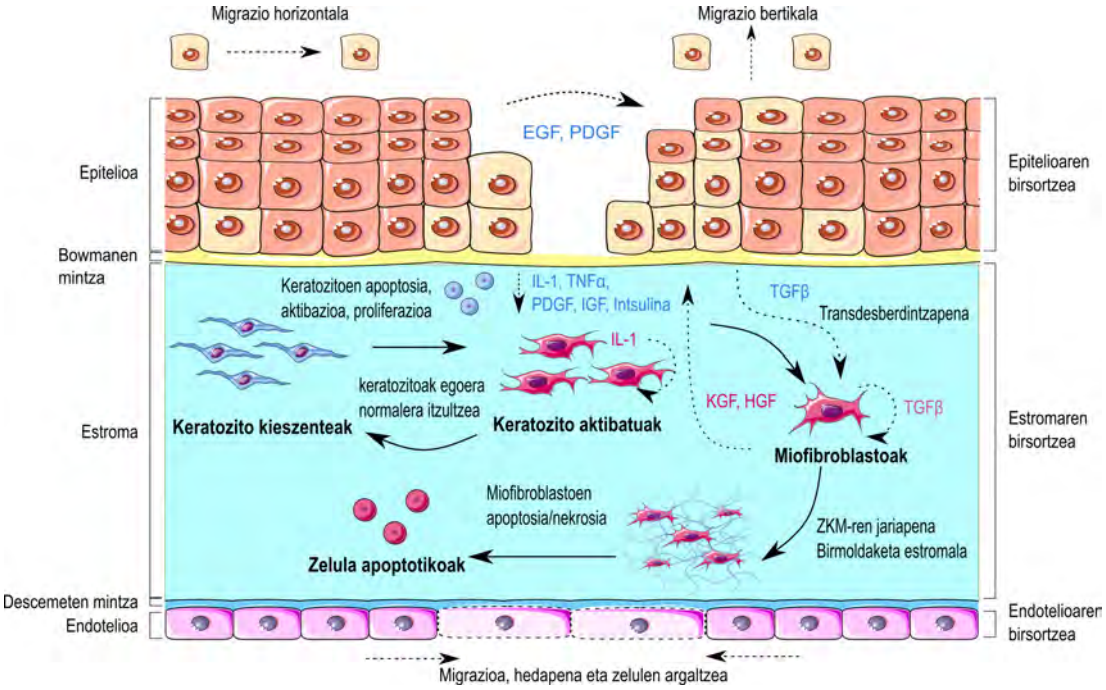

I.6. IRUDIA: Kornea birsortzeko prozesuaren ikuspegi orokorra. Kalte epitelial baten ondoren, hazkuntza faktoreak askatzen dira, hala nola EGF, PDGF, IGF, intsulina eta beste zitokina batzuk, kaltetutako zelula epitelialek eragindako jarduera biokimiko handi baten ondorioz. Ondoren, korneako zelula epitelial osasuntsuek berrantolaketa zelularra izaten dute, eta horrek aldaketa morfologiko eta funtzional batzuk eragiten ditu. Prozesu hori hasi ondoren, epitelioa itxi egiten da linboko eremuan kokatuta dauden LEZA/P-k aktibatzearen ondorioz, gero eta zelula epitelial desberdinduagoetan ugaldu eta bereizten baitira, epitelio arruntaren estratifikazioa sortuz. Korneako estroman, zelula epitelialek jariatutako IL-1 eta TNFα delakoek keratozitoen apoptosia eragiten dute. Ordu batzuen buruan, zelularik gabeko eremuaren ondoko keratozitoak aktibatzen hasten dira. Era berean, epitelioaren azpiko keratozitoen hasierako apoptosiaren ondoren, PDGF-k eragindako inguruko keratozitoen migrazioa eta ugaltzea ematen da. Migrazio horren ostean, aktibatutako keratozitoak miofibroblastoetara desberdintzen dira, zelula epitelialek askatutako TGF-β-ren eraginaren bitartez. Miofibroblasto horiek HGF eta KGF hazkuntza faktoreen ekoizpena eragiten dute. Faktore hauek zelulaz kanpoko matrizearen osagaiak kodetzen dituzten geneak aktibatu eta kornearen gardentasuna babesten duten molekulak kodetzen dituzten geneak desaktibatzen dituzte. Ondoren, kolagenasen eta matrizearen beste metaloproteinasa batzuen ekoizpena handitu egiten da, eta horrek estroma birmoldatzea dakar. Aipatutako prozesuek zelulaz kanpoko matrizearen, estromako zelula kantitatearen eta ehun-uzkurduraren ekoizpena nabarmen handitzea eragiten dute, eta horrek ehunaren opakutasuna eragiten du. Azkenik, estromaren konponketa estroma orbaintzean inplikatutako zelulen mekanismo apoptotikoen bidez eta keratozitoak egoera normalera berrezartzearen bidez osatzen da. Endotelioa, honen zelulak migratuz, hedatuz edo argalduz birsortzen da, ahalik eta azalera handiena estaltzeko. Zelula epitelialek urdinez adierazitako hazkuntza faktoreak jariatzen dituzte, eta estromako zelulek, berriz, gorriz adierazitakoak.

IL-1 eta TNFα askatzearekin batera, korneako epitelio zelulek TGFβ, PDGF eta FGF-2 ekoizpena eta askapena handituko dute. PDGF-ak eta FGF-2-ak keratozitoen migrazioa, ugaltzea eta fibroblasto bihurtzea eragingo dute [74]. TGFβ fibroblastoen eta miofibroblastoen arteko transdesberdintzapenean ezinbestekoa izango da, eta miofibroblasto horiek zelulaz kanpoko matrize berria jariatzeaz arduratuko dira [74, 75].

Miofibroblastoek muskulu leuneko α-aktina (α-SMA), estres-zuntz uzkurkorrak, bimentina, desmina eta proteina kristalinoen kantitate txikia adieraztea dute ezaugarri, eta horrek argiaren dispertsioa murrizten laguntzen du, zelulaz kanpoko matrizearen errefrakzio-indizearen antza baitu [76–78]. Miofibroblastoak korneako keratozitoen eraldaketatik datoz nagusiki, baina hezur-muinetik eratorritako fibrozitoak baita miofibroblasto iturri badirela proposatu da [79].

Zelulaz kanpoko matrize berriaren sorrera beharrezkoa da hasiera batean zauria ixteko, baina antolaketa zehatzik gabeko matrize nahasi hori jariatzeak ehuna uzkurtzea eta kornearen opakutasuna dakartza. Miofibroblastoen bizirauteak eta zelulaz kanpoko matrizearen etengabeko ekoizpenak, keratozitoek mintz basala sendatzeko laguntza zaildu eta korneako nerbioen birsortzea inhibitzen du [72]. Gainera, miofibroblastoek TGFβ era autokrinoan ekoiz eta aska dezakete iraun ahal izateko, epiteliotik datorren estimuluaren beharrik gabe [18].

Mintz basala berrezartzen denean, zelula epitelialetatik jariatutako PDGF eta TGF mailak gutxitu egiten dira. Mintz basala birsortu eta faktore fibrotikoen sarrera eteten denean, miofibroblastoek modu autokrinoan ekoiztutako TGFβ mailak ez dira nahikoak izango zelula horiek denbora luzez bizirauteko. Orduan, miofibroblastoak apoptosian sartzen dira, keratozitoek estroma birpopulatzen dute eta birsortze prozesuak orbaintze edo fibrosi prozesua gainjartzen du [80]. Sistema immuneko zelulen nekrosia/apoptosia miofibroblastoen desagerpenarekin batera ematen da. Keratozitoak ezohiko zelulaz kanpoko matrizearen birxurgapenaren eta estromaren ohiko egoera homeostatikoa berrezartzearen erantzuleak izango dira. Prozesu horrek hilabeteak iraun ditzake, eta, egoera konplexuetan, baliteke gardentasuna ez berrezartzea.

1.7.4. Endotelioaren birsortze prozesua

Endotelio zelulek mitosi ahalmen mugatua dutenez, endotelioaren birsortze prozesua kaltetu gabeko zelulen migrazioan, hedapenean edo hauen argaltzean oinarritzen da, zauritutako azalera estali ahal izateko. Endotelioko zelulen migrazio hau keratozitoen heriotzaren arduraduna den IL-1-k estimulatzen du [59]. Zauria itxi eta egun gutxira, endotelioko zelulek ponpaketa aktibitatea berreskuratu eta mintz basal berria ekoizten hasten dira.

Lesio endotelialaren larritasunaren arabera, zelula endotelialek trantsizio-prozesu endotelial-mesenkimala (EMT) ere jasan dezakete, non zelula endotelial kieszenteek fibroblastoen antzeko ezaugarriak hartzen dituzten eta ugaltzen hasten diren. Prozesu hau TGFβ-k, FGF-2-k eta IL-1β-k estimulatzen dute batez ere [81, 82]. Zelula horiek inguruko zeluletatik askatu eta modu independentean lekualdatzen dira Descemeten mintzean zehar kaltetutako eremura, zauriaren orbaintze azkarra ahalbidetzeko. Hala ere, prozesu honek ikusmena arriskuan jar dezake, zelulek kornearen errefrakzio-ahalmena alda dezakeen mintz fibrotsu bat jaria baitezakete [83].

Endotelioa kornearen gardentasuna eta deshidratazio konstante bat mantentzeko funtsezkoa denez, zelula endotelialen galera hedatua eragiten duten gaixotasunek edo lesioek, oro har, kornearen opazifikazioa eragiten dute, likidoaren gehiegizko metaketaren eta hanturaren ondorioz.

1.8. Korneako akatsak

Korneako akatsak korneako gainazalean egindako zauri irekiak dira. Hauen artean, epitelioari soilik eragiten dioten epitelio-akatsak zein estromari neurri handiagoan edo txikiagoan eragiten dioten ultzera epitelio-estromalak aurki daitezke.

1.8.1. Epitelio akatsak

Korneako epitelio akatsak korneako epitelioaren azaleko geruzaren galera dakar eta etiologia ezberdinek eragin dezakete, hala nola, traumatismoek, kornearen lehortasunak, gaixotasun neurotrofiko desberdinek, infekzioek edo erredurek. Pazienteek min akutua, gorritasuna, malko-jarioa, ikusmen lausoa eta fotofobia jasaten dituzte. Normalean 7-10 egunetan ikusmen ondorio gabe errekuperatzen dira.

Hala ere, tratamendu desegoki batek konplikazio ezberdinak eragin ditzake, hala nola estromari eragin diezaioketen ultzera kornealak [84].

1.8.2. Epitelio akats iraunkorrak eta ultzera neurotrofikoak

Epitelio akats iraunkorrak (EAI) korneako epitelioaren konponketa desegokiaren ondorioz gertatzen dira. Tratamendu konbentzionalak eman arren, akats hauetan begia ez da gai epitelioan sortutako zauria 2 asteko epean berrepitelizatzeko [85, 86]. Linbo eremuko epitelio zelula amak ez dira gai kaltetutako eremua betetzeko, zelulen arteko edo mintz zelularraren atxikiduran, lotura estuetan edo hemidesmosometan adibidez, arazoak direla medio. Horrek epitelioaren lodieraren eta kornearen ohiko egituraren erabateko galera dakar [87].

EAI-en etiologiak desberdinak izan daitezke eta hauek epitelioko zauria eta estromari kaltea eragin diezaioketen mekanismo biokimiko ezberdinen konbinazioagatik bereizten dira. EAI-k traumatismo mekaniko, substantzia kimiko toxikoekiko esposizio edo gaixotasun anitzengatik, hala nola, begi lehorra, A bitaminaren urritasuna, Sjögren sindromea, keratopatia diabetikoa, LZAG edo keratopatia neurotrofikoa besteren artean, sortzen dira [88–91]. Malkoak jariatutako hazkuntza faktoreen, zitokinen eta nerbio trigeminoak askaturiko neuropeptidoen faltak ere akats horiek eragin ditzake [92].

Zauri hauek tratatu ezean, infekzio edo ikusmen galera bezalako konplikazioak sor daitezke. Jatorria edozein dela ere, akats hauetan begiaren gainazaleko plasmina askearen kantitatea handitzen da. Plasmina aske horrek, korneako epitelioaren eta zelulaz kanpoko matrizearen arteko lotura konplexuak murriztu eta ahultzen ditu, eta horrek akatsak irautea eragiten du [93]. Plasmina askea zelula polimorfonuklearrentzat kimioerakargarria da, kolagenasa aktibitatea duten zenbait metaloproteinasa askatzen baitituzte, kornearen urtzea errazten dutenak. Beraz, EAI-ek aurreko estromara egin dezakete aurrera eta estromako ultzerazioa eragin, estromako kolagenoaren eta zelulaz kanpoko matrizearen degradazio proteolitikoaren bidez.

1.8.2.1. EAI-etarako tratamenduak

EAI-en tratamenduak oftalmologiaren erronka handienetako bat izaten jarraitzen du, gaixotasunaren etiologia eta kausen heterogeneotasuna ulertu eta epe luzeko jarraipena eskatzen dutelako. Orain arte, aukera kirurgiko ezberdinak deskribatu dira baina aukera mediko ohikoenak eta lehen hurrenkeran aukeratutakoak tratamendu ez-inbaditzaileak dira, epitelioaren egitura eta funtzioa berrezartzea bilatzen dutenak. Horien artean daude kontserbatzailerik gabeko lubrifikatzaileak, epitelioaren birsortzea eragotzi dezaketen farmakoak murriztea/kentzea edo antibiotiko topiko profilaktikoak erabiltzea [94].

Ukipen-lente bigunek EAI-ak sendatzen laguntzen dute, betazalen kliskatzeak eragindako higadura mekanikotik zelula epitelialak babestuz. Lente hauek antibiotikoekin eta kontserbatzailerik gabeko lubrifikatzaileekin batera erabiltzen dira, begien gainazalari atxiki ez dakizkion. Hala ere, tratamendu honek jarraipen zorrotza eskatzen du, lentea infektatzeko eta mugitzeko arriskua dagoelako [95, 96]. Presio-adabakiak ukipen-lenteen erabileraren antzeko onurak eskaintzen dituzten ohiko beste aukera bat dira. Bestetik, malko hodien buxadura aplika daiteke, adabaki eta lubrifikatzaileen eragina luzatzeko asmoz [94].

Molekula espezifikoen aplikazioan oinarritutako tratamenduak ere terapia ez-inbaditzaile bezala erabiltzen dira. Horien artean, EGF [87, 97], NGF [98, 99], P substantzia eta IGF-1 [100], FGF [101, 102], mintz amniotikotik eratorritako zitokina zelularren soluzioak [103] edo intsulinan oinarritutako kolirioak [104, 105] EAI-ak tratatzeko ahalmena frogatu duten adibide batzuk dira. Era berean, pazientearen odol serumetik eratorritako kolirioek ere eraginkortasuna erakutsi dute [106–113], hauen abantailak malko artifizialetan aurki ezin daitezkeen hazkuntza faktore, bitamina eta epitelio zelulen ugalketa eta migrazioan eragina duten osagaien kontzentrazio handiarekin lotuta egon baitaitezke. Hala ere, estandarizatutako protokolo faltak, erabilitako kontzentrazioen aldakortasunak (% 20-tik % 100-era) edo ekoizpenari dagozkion arauzko murrizketek terapia honen erabilera zailtzen dute.

Azkenik, begi gainazaleko tropismoa hobetzeko tratamendu kirurgikoak ere badaude, besteak beste, desbridatze epiteliala, mintz amniotikoko txertaketak [114–116], tarsorrafiak [117–119] edo linbo eremuko epitelio zelula amen transplanteak [120], EAI-en kasu larrietan bereziki beharrezkoak direnak.

2. Medikuntza birsortzailea eta Ehun-ingeniaritza

Medikuntza birsortzailea (MB) ikerkuntzako eta aplikazio klinikoko jakintza-adar anitzeko arloa da. Honek, sortzetiko akatsengatik, gaixotasunengatik, traumatismoengatik, edo zahartzeagatik galdutako funtzioak berrezartzeko zelulak, ehunak edo organoak konpontzea, ordezkatzea edo birsortzea du helburu. MB-k organismoaren konponketa-mekanismo naturalak aktibatu nahi ditu, konponezinak ziruditen ehunak eta organoak sendatzeko. Hala, organismoaren berezko mekanismoak ordezkatuz edo estimulatuz gorputzaren gune kaltetuak birsortzen dituzten soluzioak batzen dira MB-ren barruan. Hainbat ikuspegi teknologiko konbergente biltzen ditu, hala nola molekula disolbagarrien erabilera, terapia genikoa, zelula amekin egindako terapia, ehun-ingeniaritza eta zelula eta ehun moten birprogramazioa, besteak beste [121] (I.7 irudia).

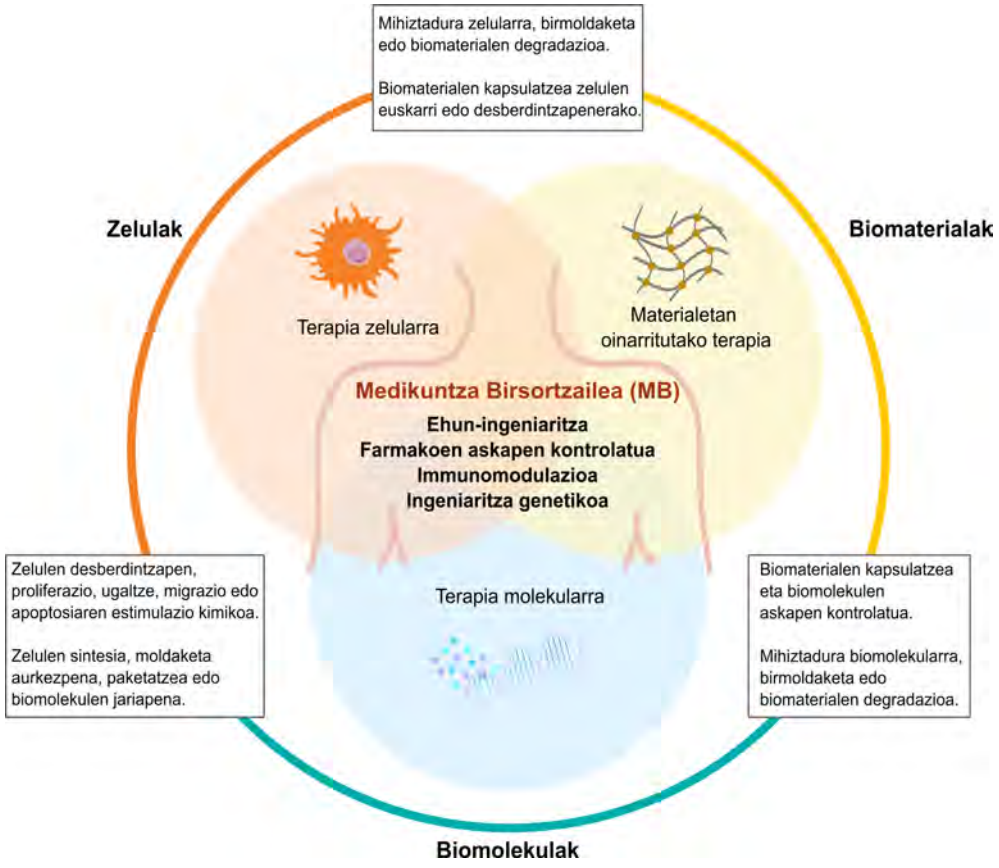

I.7. IRUDIA: Medikuntza birsortzailean erabilitako estrategien, osagaien eta interakzioen ikuspegi orokorra. Medikuntza birsortzaileko terapietan zelulak, biomaterialak eta biomolekulak sartzen dira jokoan, hala nola zelula birsortzaileak injektatzea edo ehun endogenoen konponketa sustatzeko biomaterial azelularren euskarriak sortzea. Arlo honetan garatutako soluzioak konplexuak badira ere, estrategia horiek ehunak birsortzeko eta konpontzeko erantzun eraginkorrenak bideratzeko aukera ematen dute. [122]-tik moldatutako irudia.

Beraz, ehun-ingeniaritza (EI) medikuntza birsotzailearen aterkipean kokatzen den jakintza alor anitzeko zientziari deritzo, funtsean ehunak eta organoak laborategian ekoiztu eta ondoren transplantatzea helburu duena [123]. Zientzia honek 3 alderdi ditu ardatz: kaltetutako zelulak ordezkatzeko erabiliko diren zelula egokien hautaketa, ehunen birsorkuntza erraztuko duten biomaterialen hautaketa eta ehun funtzionalak birsortzeko beharrezkoak diren seinale fisiko, kimiko eta biologikoen zehaztapena [124].

Gorputzean duten aplikazioaren eta kokapenaren arabera, biomaterialek hainbat forma har ditzakete, hala nola, hidrogelak, mintzak, belakiak, hodiak edo egitura esferikoak aurki daitezke.

2.1. Jatorriaren araberako biomaterialen sailkapena

Jatorri edo iturriaren arabera, biomaterial naturalak eta sintetikoak bereiz daitezke.

2.1.1. Biomaterial naturalak

Biomaterial naturalak animalien, landareen eta mikroorganismoen hazkuntza-zikloan sortzen diren materialak dira eta azido nukleikoak, polisakaridoak, proteinak, lipidoak eta proteoglikanoak bezalako makromolekula konplexuak barne hartzen dituzte. Osagai ezberdinez osaturiko biomaterial hauek mikroegitura eta propietate fisiologiko konplexuak dituzte. Berezko bioaktibitate, biobateragarritasun eta biodegradagarritasuna dute, eta zelulaz kanpoko matrizearen ingurune fisiologikoa erreproduzitzen dute. Zelulen atxikipena eta ondorengo ehunaren garapena sustatzen dute, biomaterial eta gorputzaren arteko integrazioa erraztuz. Biomaterialen aukeraketan lehen hautagaiak izaten dira.

Hiru multzo nagusitan sailka daitezke: polisakaridoetan oinarritutako biomaterial naturalak, proteinetan oinarritutako biomaterial naturalak eta ehun edo organoetatik eratorritako biomaterial naturalak.

2.1.1.1. Polisakaridoetan oinarritutako biomaterial naturalak

Polisakaridoak lotura glukosidikoez elkartutako hainbat monosakaridoz osatutako polimeroak dira. Hainbat funtzio betetzen dituzte, hala nola zelulen arteko komunikazioa, energia biltegiratzea, egituren euskarri izatea, atxikipena edo immunitate-sistemaren ezagutza molekularra.

Kitosanoa

Kitosanoa ganben eta beste krustazeo batzuen oskoletatik lortutako kitinaren deazetilazio partzialetik eratorritako eta glukosamina eta N-azetilglukosamina unitate errepikakorrez osatutako polisakarido naturala da [125].

Bere biobateragarritasunak, biodegradagarritasunak, eskuragarritasunak, kostu baxuak, propietate antimikrobiano eta antifungikoek eta immunogenizitate baxuak biomedikuntzako aplikazioetarako material egoki bihurtzen dute [126]. Amina eta hidroxilo taldeak aldatuz, kitosanoa erraz erretikula eta funtzionaliza daiteke [127]. Gainera, ura xurgatzeko eta atxikitzeko duen gaitasunak, kartilago ehunen ingeniaritzarako, korneako endotelioaren birsortzerako edo farmakoz betetako inplanteetarako onuragarri bihurtzen du, eta bere ezaugarri kationikoek hemostasirako hautagai on bihurtzen dute [128, 129].

Azido hialuronikoa

Azido hialuronikoa (AH), azido D-glukuronikozko eta D-N-azetilglukosaminazko unitatez osatutako polisakarido naturala da, 1-10000 KDa bitarteko pisu molekularra izan dezakeena.

Biodegradagarritasun ona, biobateragarritasuna, izaera biskoelastikoa, ebakidura bidezko mehetze portaera [130] eta propietate mekaniko doigarriak ditu. AH-ren unitate errepikakorrek, hidrogelak funtzionalizatzeko edo gurutzatzeko erabil daitezkeen azido karboxiliko eta hidroxilo taldeak dituzte. Ehun konektiboen zelulaz kanpoko matrizearen osagai nagusietako bat da, eta ura xurgatzeko duen ahalmen handiak ehunak hidratatuta mantentzen ditu. Horrek, zelulen infiltrazioa erraztu eta zauri kronikoetarako edo gaizki sendatutako zaurietarako apositu-material egokia bihurtzen du [131]. Hasiera batean, animalien ehun konektiboak ziren AH lortzeko iturri nagusia. Hala ere, eskaria gero eta handiagoa zenez, honen ekoizpenak iturri mikrobiologikoetara egin zuen salto. Gaur egun, AH ekoizteko iturri ekonomiko eta fidagarriena A eta C estreptokokoak dira, hauetatik isolatu baitzen AH lehen aldiz [132].

Ezaugarri horiek direla eta, AH aplikazio ugarietarako hautagai egokia da, hala nola larruazaleko ehun-ingeniaritzarako [133], akats dermikoak betetzeko [134, 135], itsasgarri bezala jarduteko [136, 137], humore beirakarako ordezkoak sortzeko [138–141], korneako zaurietarako [142–144] edo farmakoak garraiatzeko [145–147].

Alginatoa

Alginatoa azido β-D-manuronikoaren (M blokea) eta azido α-l glukuronikoaren (G blokea) bloke sekuentzialez edo alternoz osatutako polisakarido lineala da. M eta G blokeen erlazioak, materialak har ditzakeen propietate fisikokimikoetan eragina du. M bloke gehiago izateak hidrogel malguagoak eta elastikoagoak sortzen ditu, aldiz, G blokeen kopuru altuak hidrogel zurrunagoekin lotzen dira [148]. Batez ere alga arreetatik lortzen da.

Alginatoaren G blokeko karboxilo multzoa kaltzioa, estrontzioa edo barioa bezalako katioi dibalenteekin gurutza daiteke alginato hidrogelak sortzeko [148]. Erraz moldatu daitekeen materiala da, biobateragarritasun ona du, zitotoxikotasun txikia, eta material ez-immunogenikoa da. Zelulen atxikipena errazteko elementurik ez duenez, beste osagai batzuekin nahas daiteke, hala nola proteinekin edo azido aspartiko-argina-glizina (RGD) sekuentziekin, atxikitze-propietateak eta zelula eta matrizearen arteko interakzioak aldatzeko [149].

2.1.1.2. Proteinetan oinarritutako biomaterial naturalak

Proteinak aminoazidoen kate linealez osatutako makromolekulak dira. Organismo bizidun guztien funtzio biokimiko, mekaniko eta egitura funtzioetan duten oinarrizko eginkizunaren ondorioz, proteinak hidrogelen fabrikaziorako jatorri naturaleko hautagai ezin hobeak dira.

Kolagenoa

Kolagenoa batez ere glizina, prolina eta hidroxiprolina unitate errepikakorrez osatutako helize hirukoitzeko egitura duen molekula bat da [150]. Egiturazko proteina ugariena da ugaztunen gorputzean, ehun konektibo bigun edo zurrun gehienetan aurki daitekeena, hala nola larruazalean, kornean, hezurrean, tendoietan edo mintz basaletan [151].

Zuntz-kolagenoak edo kolageno fibrilarrak (I, II eta III motakoak adibidez) eta kolageno ez fibrilarrak edo zuntz-kolagenoak ez direnak (IV motako kolagenoa edo honekin antzekotasunak dituzten proteinak esaterako) bereiz daitezke, askotariko funtzioak betetzen dituzte eta beste osagai mikro eta makromolekular batzuekiko interakzio-sistema askotan parte hartzen dute [151, 152].

Zuntz-kolagenoa eta, bereziki, I motako kolagenoa, zelulentzako euskarri gisa baliatzeaz gain, oso biobateragarria da, trakzio indarrekiko erresistentzia handia du, biodegradagarritasun kontrolagarria, eta substratu natural gisa jarduten du zelulen atxikitze, ugaltze eta desberdintzapenerako. Halaber, zaurien orbaintze prozesuan birsortze mekanismoetan parte hartzen du [153]. Propietate horiengatik, ehun-ingeniaritzaren arloan orain arte gehien erabili den biomateriala izan da, hala nola zaurietarako aposituak, kornea inplanteak, hezurrentzako betegarriak edo botikak garraiatzeko sistemak garatzeko erabili izan da [154].

Kolageno gehiena animalia-iturrietatik dator, hala nola behietatik (hezurretatik, Akilesen tendoietatik, larruazaletik), karraskarietatik (arratoi-isatseko tendoietatik), arrainetatik, moluskuetatik eta itsas ornogabeetatik, baina kolagenoa sortzeko metodo birkonbinatzaileak ere garatu dituzte [153].

Gelatina

Gelatina, kolageno zuntzexken hidrolisi partzialetik lortutako pisu molekular txikiagoa duten polipeptidoek osatutako proteina anfipatikoa da. Kolagenoaren aurretratamendu azidoaren edo alkalinoaren arabera, A motako gelatina (hidrolisi azidoa) edo B motakoa (hidrolisi alkalinoa) lor daiteke [155].

Ugaztunen ehun konektiboak eta hezurrak dira erauzketa-iturri nagusiak, hala nola txerri-azala, behi-larruak edo txerri- eta behi-hezurrak, baina arrainetatik eratorritako hondakinak edo intsektuak ere badira duela gutxi garrantzia hartu duten beste iturri batzuk [156–158]. Gelatinaren egitura nagusiki glizinaz, prolinaz eta hidroxiprolinaz eta aminoazido aldakorren zati batez osatutako kate lineal bezala defini daiteke, baina erauzketa-iturriaren eta kolagenoaren aurretratamenduaren arabera, aminoazidoen konposizioa aldatzen da [159]. Aminoazido kopuru osoaren 1/3-tik 1/2-ra, glizinak osatzen du, eta aminoazido guztien 1/4-a prolinak eta hidroxiprolinak osatzen dute [160]. Gelatina kolagenotik eratorritako materiala den arren, bere aitzindariak baino disolbagarritasun eta antigenizitate txikiagoa du [161, 162]. Propietate horiek, zelulaz kanpoko matrizearen metaloproteinasen degradazioa erregulatzeko eta zelulen atxikimendua eta hazkuntza sustatzeko material egoki bihurtzen dute.

Gelatina gelifikatzen da ur berotan disolbatu eta jarraian giro-tenperaturaren azpitik hozten denean. Hala ere, gorputzeko tenperaturan duen ezegonkortasunak gelatina erretikulatzeko hainbat estrategia kimiko edo entzimatiko garatzea ekarri du, materialaren propietateak hobetu eta kontrolatzeko [156].

Honen modalkortasunak, kostu baxuak eta biobateragarritasun handiak hidrogelak sortzeko gehien erabiltzen den biomaterialetako bat bihurtu dute.

Zeta fibroina

Zeta *Bombyx mori* harrek irundutako fibroinaz eta serizinaz osatutako zuntz naturala da. Fibroina proteina da osagai nagusia (% 75 inguru) eta serizina fibroinazko hariak inguratzen dituen proteina globular itsaskorra da. Fibroina da ehun-ingenieritzaren arloan euskarriak sortzeko erabiltzen den zetaren osagaia.

Fibroinak eremu amorfo eta kristalinoak ditu eta horietako bakoitzak propietate desberdinak ematen dizkio zetari. Fase kristalinoak β-xaflez osatutako kirstalito egonkorrak eratzen ditu, zetari erresistentzia handia ematen diotenak. Eremu amorfoek tinkotasun handia ematen diote, materiala tentsiopean dagoenean energia xurgatzen baitute. Erraz prozesatu daitekeen biozuntza da, hainbat ehun biologikorekin biobateragarria, degradazio kontrolagarria duena eta hainbat forma har ditzakeena, hidrogelak, mintzak edo nanozuntzak kasu (I.8 irudia) [163, 164].

Zeta fibroina fisikoki edo kimikoki erretikula daiteke. Alboko kateen arteko β-xaflen eraketak gelifikazio fisikoa sortzen du, tirosinaren talde hidroxilo fenolikoek eta lisinaren amino taldeek erretikulazio kimikoa ahalbidetzen dutelarik [165]. Duela gutxi, hidrogel hauen propietateak hobetzeko teknika ezberdinak aztertu dituzte, hala nola, erretikulazio fisiko eta kimikoa konbinatzea, zeta beste polimero batzuekin nahastea edo maila molekularrean materialaren diseinua kontrolatzea [163].

I.8. IRUDIA: Metakriloil-zeta fibroinazko (Sil-MA) biotinta eta hidrogela prestatzeko prozesua. **a**) Kapuluak pisatu ondoren, zeta 1 l 0,05 M sodio karbonatoarekin nahastu, ur destilatuarekin bi aldiz garbitu eta gau osoan zehar berogailuan deshidratatzen da. Ondoren, zeta LiBr gatz-disoluzio batean disolbatu eta iragazi egiten da. Glizilato metakrilatoa (GMA) tantaz tanta gehitzen zaio zeta fibroinari (RZF), eta RZF-GMA soluzioa plaka bero baten gainean (60 °C) nahasten da 6 orduz 800 b/min-tara, zeta fibroinak eta GMA-k erreakziona dezaten. Ondoren, disoluzioa ur destilatuan diluitzen da 7 egunez, eta beste 5-7 egunez liofilizatzen da. Sil-MA liofilizatuaren belakia LAP konposatua % 0,2-ko kontzentrazioa duen PBS soluzio baten disolbatu eta homogeneoki nahasten da. Azkenik, soluzioa zentrifugatu egiten da aire-burbuilak ezabatzeko. **b**) PKH67 (berdea) markatutako zelulekin eta PKH26 (gorria) markatutako zelulekin inprimatutako trakea forma duen hidrogela. Ezkerretik eskuinera: trakea baten CAD diseinua, inprimatu diren hidrogelen irudiak, fluoreszentzia-irudia (FL) mikroskopia konfokala edo plano bakarreko argiztapen-mikroskopia erabiliz, eta hidrogel fluoreszentearen eta CAD diseinuaren irudi bateratua. [164]-tik hartutako irudiak.

2.1.1.3. Ehun edo organoetatik eratorritako biomaterial naturalak

Ehunetatik edo organoetatik eratorritako biomaterialak, animalietatik edo gizakietatik ateratako eta osagai zelularrak kentzeko tratamendu bat jasan duten material naturalak dira. Ehunak, zelulaz kanpoko matrizearen jatorrizko mikroingurune eta antolamendu trinkoa mantentzen du osagai zelularrak ezabatu ondoren, zelulak ereiteko euskarri mekaniko eta biologikoa eskainiz. Ehunetatik eratorritako biomaterialak bi kategoriatan sailka daitezke: Organo edo ehunen zelulaz kanpoko matrizea deszelularizatu ondoren lortutako euskarriak, edo ereindako zelulek sortutako zelulaz kanpoko matrizea deszelularizatu ondoren lortutako euskarriak [166].

Organo edo ehunen zelulaz kanpoko matrizea deszelularizatu ondoren lortutako euskarriak

Organo edo ehunen zelulaz kanpoko matrizetik eratorritako euskarriek, osagai zelular immunogeniko guztiak ezabatzen dituen tratamendua jasaten dute. Deszelularizazioa ehun baten osagai zelularrak tentsio fisikoaren eta/edo agente kimiko edo entzimatikoen bidez ezabatzeari deritzo. Honen ondoren lortutako zelula gabeko zelulaz kanpoko matrizea, aplikazio terapeutikoetarako erabil daiteke. Tratamendu honek, jatorrizko arkitektura tridimentsionala eta molekula bioaktiboak babesten ditu. Horri esker, zelulen atxikipena, ugalketa eta zelulen desberdintzapena erregula daitezke, jatorrizko ehunaren antzeko propietate mekanikoak mantenduz [167].

Heste meharreko submukosa [168], zelula gabeko dermisa [169], ehun adipotsua [170] eta bihotz-balbuletatik eratorritako zelulaz kanpoko matrizea [171] dira frogatutako ehun eta organoen adibide batzuk.

Zelulek sortutako zelulaz kanpoko matrizea deszelularizatu ondoren lortutako euskarriak

Biomaterial hauek *in vitro* ereindako zelulek sortutako zelulaz kanpoko matrizetik eratorritako materialak dira. Adibidez, NIH-3T3 fibroblastoen kultibo batetik abiatuta zelulaz kanpoko matrize deszelularizatu bat sortzeko, 2×10^{5} zelula erein ziren 1 ml bitarteko p24 plaka baten kikara bakoitzeko. Zelulak konfluentziara iristean, medioa ordezkatu eta azido askorbikoa gehitu zitzaion, kolagenoaren eta matrizearen

ekoizpena estimulatzeko. Ereindako egunetik 5 egun igaro ondoren, zelulen osagaiak deszelularizazio bidez ezabatu ziren, lisi- eta garbiketa-tanpoiak erabiliz [172]. Metodo honek zelula-mota jakin bateko zelulaz kanpoko matrize espezifikoak lortzea ahalbidetzen du, zelulaz kanpoko matrize alogeniko/xenogeniko bidezko infekzio-arriskua murrizten duelarik [167]. Osagai zelularrak metodo fisiko, kimiko edo entzimatikoak erabiliz ezaba daitezke. Adibidez, izozte eta desizozte zikloak erabiliz, dodezil sulfato sodikoa eta Triton X-100 bezalako detergenteak aplikatuz mintz zelularrak eta nuklearrak suntsitzeko, edo tripsina-soluzioak eta nukleasak erabiliz, peptidoak, ADN eta RNA degradatzeko.

Zeluletatik eratorritako zelulaz kanpoko matrizeak nitxo zelular espezifikoak egokitzeko eta honen barruko funtzioak hobetzeko erabili izan dira. Adibidez, jaioberrien prepuzioko fibroblastoetatik eratorritako zelulaz kanpoko matrizea deszelularizatu ondoren lortutako euskarriek, podozitoen ugaltzea, desberdintzapena eta mantentzea optimizatzen dutela frogatu dute [173]. Gainera, zelula ama mesenkimalen zelulaz kanpoko matrizetik eratorritako euskarriek, zelula amen nitxoa erreplikatzeko ahalmena erakutsi dute, berrereindako zelula ama mesenkimalak estres oxidatibotik babesten dituztelarik [174].

2.1.2. Biomaterial sintetikoak

Biomaterial sintetikoak laborategietan artifizialki sortutako eta orokorrean petroliotik eratorritako materialak dira eta bi kategoriatan bana daitezke: polimero termoplastikoak eta termoegonkorrak. Polimero termoplastikoak (polietilenglikola (PEG), polimero binilikoak, etab.) berotzean bigundu eta hoztean berriro gogortzen diren materialak dira. Polimero termoegonkorrek (silikona, poliuretanoa, etab.) kimikoki erreakzionatzen dute beroarekin edo produktu kimikoekin eta urtu ezin diren material disolbaezinak eratzen dituzte.

Eskura dauden talde funtzionalen eta polimero sintetikoak diseinatzeko tekniken aniztasunari esker, propietate kimikoak, mekanikoak, hauen biobateragarritasuna edo biodegradagarritasuna erraz eta modu kontrolatuan alda daitezke.

Akrilamida, binilo-azetatoa, etilenglikola edo azido laktikoa dira polimero sintetikoak sortzen dituzten monomeroetako batzuk. PEG, polikarbonato uretanoa (PU) edo poli (ϵ-kaprolaktona) (PKL) polimero sintetikoen adibideak dira [175].

2.2. Hidrogelak

Hidrogelak gurutzatutako monomeroez osatutako sare polimerikoak dira, hidrofilizitate mailaren arabera, % 99-rarteko ura atxikitzeko ahalmena izan dezaketenak. Gaitasun horrek, giza gorputza bezalako sistema biologikoen aplikazioetarako hautagai egoki bihurtzen ditu, giza gorputza gehienbat urez osatutako sistema baita [176].

1960-an ezagutzera eman zirenetik [177], hidrogelen moldakortasunari eta zelulentzako ingurune egokia izateari esker, hidrogelen teknologiaren alorrak garrantzi handiagoa lortu du. Hidrogelak hainbat helburu medikorako erabil daitezke: farmakoak edo zelulak garraiatzeko, ehunen birsorkuntzarako, 3D hazkuntza-ereduen bidez zelulen ugalketa sustatuko duten ehunen mikroinguruneak sortzeko, odol jarioen prebentziorako, erradioterapian ehunak babesteko edo inplanteen biobateragarritasuna hobetzeko, besteak beste. Gainera, diseinuaren eta funtzionaltasunaren ezaugarriak etengabe hobetzen diren heinean, gero eta aplikazio konplexuagoetan erabiltzen hasi dira, hala nola zaurien orbaintzea hobetzeari, zelula amen desberdintzapenari edo immunitate-sistemaren birprogramazioari lotutako aplikazioetan [178].

2.2.1. Hidrogelen propietate fisiko-kimiko nagusiak

Jarraian, hidrogelen ezaugarrietan eta egokitasun biologikoan eragin nabarmena duten funtsezko propietate fisiko-kimikoak deskribatzen dira (I.9 irudia).

2.2.1.1. Sarearen tamaina

Sarearen tamaina funtsezkoa da hidrogeletan integratutako biomolekulak edo zelulak askatzeko zinetika zehazteko, eta haren kontrola funtsezkoa da konposatu horien hedapena zehazteko. Gainera, sareko poroek elikagaiak, metabolitoak edo beste substantzia batzuk zeluletara garraiatzeko bide gisa balio dute [179]. Normalean, makromero kontzentrazioa edo saretze dentsitatea handiago den heinean, poroen tamainak behera egiten du.

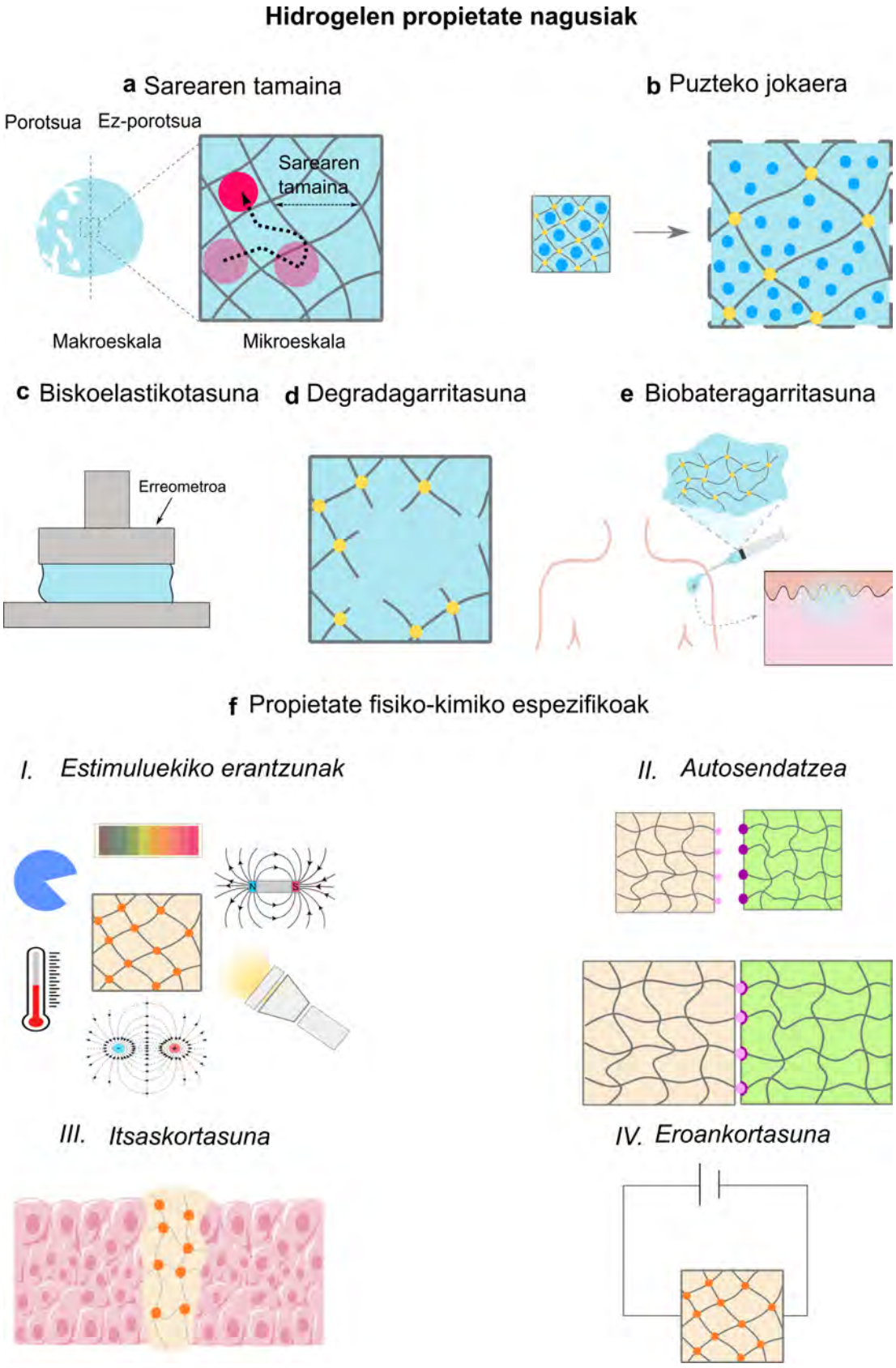

I.9. IRUDIA: Hidrogelen diseinuan kontuan izan beharreko propietate nagusiak. **a**) Sarearen tamaina, **b**) puzteko jokaera, **c**) biskoelastikotasuna, **d**) biodegradagarritasuna, **e**) biobateragarritasuna eta **f**) aplikazioaren espezifikotasunari lotutako propietateak.

2.2.1.2. Puzteko jokaera

Puztea likidoak xurgatzeko prozesuari dagokio, eta horrek materialaren bolumena eta masa handitzea dakar. Prozesu hori hidrogelaren sare polimeriko elastiko eta hidrofiloaren ondorioz gertatzen da. Sare horrek bolumena handitzeko nahikoa ur xurgatzen du, eta, aldi berean, tentsio elastikoa sortzen du kate polimerikoetan, materiala erabat disolbatzea eragozten dutenak. Puztea hidrogel gehienen ezaugarri nagusietako bat da eta hainbat faktorek eragiten diote, hala nola sarearen egiturak, polimeroen izaera kimikoak (hidrofiloagoak edo hidrofoboagoak izatea), inguruneak eta sintesi-egoerak [180]. Propietate honek lotura zuzena du farmakoak askatzeko eta garraiatzeko ezaugarriekin.

2.2.1.3. Biskoelastikotasuna

Biskoelastikotasuna portaera elastikoa eta likatsua erakusteko ezaugarriari dagokio. Biomaterial naturalek edo ehunetatik eratorritako biomaterialek ere propietate biskoelastikoak dituzte. Propietate hau zelulen eta hidrogelaren arteko interakzioak erregulatzeko oso garrantzitsua da, desberdintasunak eragin baititzake zelulen ugalketan edo desberdintzapenean. Polimero aitzindariaren kontzentrazioak, pisu molekularrak, konposizioak, dentsitateak edo erretikulazio-metodoak hidrogelaren biskoelastikotasunean eragiten dute [179].

Hidrogelen biskoelastikotasuna erreometroan egindako analisi mekaniko dinamikoen bidez neurtu ohi da. Analisi horietan, hidrogel baten oszilazio-erantzuna oszilazio finkoen anplitudearen eta maiztasunaren aldakuntzarekiko neurtzen da. Anplitude txikiko oszilazio-ebakidura hidrogel baten erantzun biskoelastikoa zehazteko maiz erabiltzen den metodoa da. Biltegiratze- eta galera-moduluek hidrogelaren erantzun elastikoa eta likatsua adierazten dituzte hurrenez hurren, eta oszilazio-sarrerari erantzunez kalkulatzen den oszilazio-erantzuna deskribatzen dute. Materiala solido gisa sailkatzen da galera-moduluak biltegiratze-modulua gainditzen badu, baina likido gisa biltegiratze-modulua galera-modulua baino handiagoa bada. Modulu horiek eremu biskoelastiko linealean (EBL) egindako saiakuntzen bidez zehazten dira. Eremu horretan hidrogelak ezarritako deformazioaren edo tentsioaren magnitudeari emandako erantzun lineala erakusten du. Biltegiratze- eta galera-moduluak deformazioaren, denboraren eta maiztasunaren arabera ebaluatzen

dira. Bestalde, denboraren menpeko materialaren propietate biskokelastikoak zehazteko maiztasun-ekorketak erabiltzen dira [176].

2.2.1.4. Biodegradagarritasuna

Biodegradagarritasuna hidrogela organismoarentzat kaltegarriak ez diren produktuetan deskonposatzeko prozesuari deritzo. Hainbat faktoreren menpe dago, hala nola konposizioa, fabrikazio metodoa, pisu molekularra, hidrofilizitatea, pH-a edo tenperatura. Hidrogelak organismotik ezaba daitezke xurgapen eta higaduraren bidez. Degradazioa hidrolisiaren edo osagaien disolbatzearen ondorioz gerta daiteke [180]. Biodegradazioa *in vivo* hidrogela ingurune biologikoan entzimen edo gorputz-fluidoen eraginpean jartzen denean gertatzen da. *In vitro* aldiz, hidrogela egongo litzatekeen ingurunea simulatuz neurtzen da, adibidez, ehun jakin batean dauden entzimak dituen soluzio batean sar daiteke.

2.2.1.5. Biobateragarritasuna

Biobateragarritasuna material batek toxikotasunik, kalte potentzialik edo erreaktibitate fisiologiko edo immunologikorik eragin gabe, ehunetan funtzionatzeko eta erantzuteko duen gaitasunari deritzo. Biobateragarritasunak biosegurtasun eta biofuntzionaltasun kontzeptuak biltzen ditu. Biosegurtasunak, produktuak berak edo produktutik degradatutako elementuak ondorio kaltegarri lokal edo sistemikoak ez eragitea, kartzinogenoak ez izatea edo zelulen ugalketa eta garapenean ondorio kaltegarriak ez sortzea eskatzen du. Biofuntzionaltasunak, materialak aplikazio jakin baterako duen egokitasuna definitzen du [180].

2.2.1.6. Aplikazioaren espezifikotasunari lotutako propietateak

Estimuluei emandako erantzunen araberako propietateak

Estimuluekiko sentikorrak diren hidrogelek egituran eta ezaugarri mekanikoetan aldaketak jasaten dituzte ingurumen-estimuluen aurrean. Estimulu endogenoak organismoak sortutako aldaketei dagozkie, hala nola pH-aren aldaketak, ioi metalikoen kontzentrazioak, jarduera entzimatikoa edo erredox ingurunea. Ehun patologikoetan, seinale anormalek, hala nola tumore-ehunetan pH-a aldatzeak, hidrogela aldatzea eragin dezakete, eta horrek, aldi berean, farmakoen askapena edo zelulak bahitzea eragin dezake [181].

Aitzitik, argia, tenperatura, eremu magnetikoa, eremu elektrikoa eta kanpoko beste faktore batzuk estimulu exogenoak dira. Estimulu horiei erantzuten dieten hidrogelak urrutiko funtzionaltasunerako edo funtzionaltasun ez-inbaditzailerako diseinatuta daude. Argiarekiko sentikorrak diren RGD domeinuak dituzten hidrogelek adibidez, fibroblastoen migrazioa eta angiogenesia argiaren bidez gida ditzakete [182].

Autosendatzea edo egitura birmoldatzeko ahalmena

Autosendatze kontzeptua prozesu naturaletan oinarritzen da, eta hidrogelak bere egitura konpontzeko eta bere propietateak kanpoko esku-hartzerik gabe berrezartzeko duen gaitasunari deritzo. Adibidez, hidrogel autobirsotzaileek kaltea jasan ondoren beren propietate mekanikoak berrezarri ditzakete kanpoko estimuluen (argia, beroa, pH) edo barneko talde funtzionalen lotura kobalenteen eta ez-kobalenteen elkarrekintzen bidez. Hidrogel autobirsotzaileak sintetizatzeko hainbat mekanismo erabili dira, lotura dinamiko kobalenteak eta ez-kobalenteak txertatuz, edo interakzio iraunkor/dinamiko kobalente/ez-kobalenteen konbinazio bat gehituz, orbaintze azkarreko, egonkorreko eta erantzun anitzeko portaerak dituzten hidrogelak sortzeko [183].

Itsaskortasuna

Hidrogelak itsastea edo atxikitzea bi hidrogelen edo hidrogel baten eta gainazal gogor edo bigun baten arteko loturari dagokio. Normalean, hidrogela eta ehunaren arteko lotura, lotura kimikoen edo interakzio fisikoen bitartez gauzatzen da [184].

Eroankortasuna

Zelula guztiek beren zelula-mintzetan kokatutako kanal ionikoen bitartez seinale bioelektrikoak sortzeko eta detektatzeko gaitasuna dute. Seinale horiek faktore erabakigarri gisa erabil daitezke zelulen ugalketa, migrazioa, orientazioa edo desberdintzapena erregulatzeko eta kontrolatzeko. Adibidez, larruazaleko zauri baten kasuan, larruazalaren potentzial transepiteliala aldatu egiten da, eta horrek zauriaren ertzetik barrualdera eremu elektriko endogenoa sortzea eragiten du, ugalketa eta migrazio zelularra suspertu eta berrepitelizazioa susta dezakeena [185].

Hidrogel eroaleek elektroien fluxu eraginkorra ahalbidetzen duten polimero hidrofiloen sare batez osatuta daude, hala nola, nanopartikula metalikoak, polimero eroaleak edo karbonoz egindako materialak. Hidrogel horiek hidrogelen berezko ezagarri onuragarriak material eroaleen ezaugarri fisiologiko eta elektrokimikoekin konbinatzen dituzte. Horrela, sistema biologikoetan sortutako seinale elektrikoak detektatu eta zelulen eta ehunen jarduerak erregulatzeko estimulazio elektrikoa eman dezakete [186].

2.2.2. Gurutzaketa edo erretikulazio metodoaren araberako hidrogelen sailkapena

Lotura gurutzatuak polimeroen kateak lotzen dituzten eta sare-egiturak sortzen dituzten lotura edo lotura-sekuentzia laburrak dira. Gurutzaketa edo erretikulazio horri esker, polimero-kateak zurrunagoak, indartsuagoak eta erresistenteagoak dira, eta horrek egitura biologikoei euskarri mekanikoa ematen die. Kate polimerikoen arteko gurutzaketa talde funtzionalen bidez gertatzen da. Talde funtzional ohikoenak amina (-NH_2), karboxilo (-COOH), tiol (-SH) edo karbonilo (-CHO) taldeak dira.

Hidrogel naturalak zein sintetikoak fisikoki edo kimikoki erretikulatutako polimeroz osatuta daude (I.10 irudia) eta lotura horiek sare-egitura egonkorrak sortzeko ardura dute. Gurutzaketa ez da berez propietate bat, baina gurutzatze-maila hidrogel baten ezaugarri guztiekin lotu daiteke. Gurutzaketa mailak eragina du polimeroaren propietate fisikoetan, hala nola biskositatean, fusio-puntuan, erresistentzian edo tinkotasunean [187]. Beraz, saretze-mailaren kontrolak hidrogelaren propietateak doitzeko eta hainbat aplikaziotara optimizatzeko aukera ematen du [156].

Loturen arabera, fisikoki erretikulatutako hidrogelak eta kimikoki erretikulatutakoak bereiz daitezke [188]. Erretikulazio-teknika kimikoek propietate mekanikoak eta egonkortasuna hobetzen dituzte. Bestalde, metodo fisikoek berezko biobateragarritasuna dute, ez baitute erretikulazio agenterik behar.

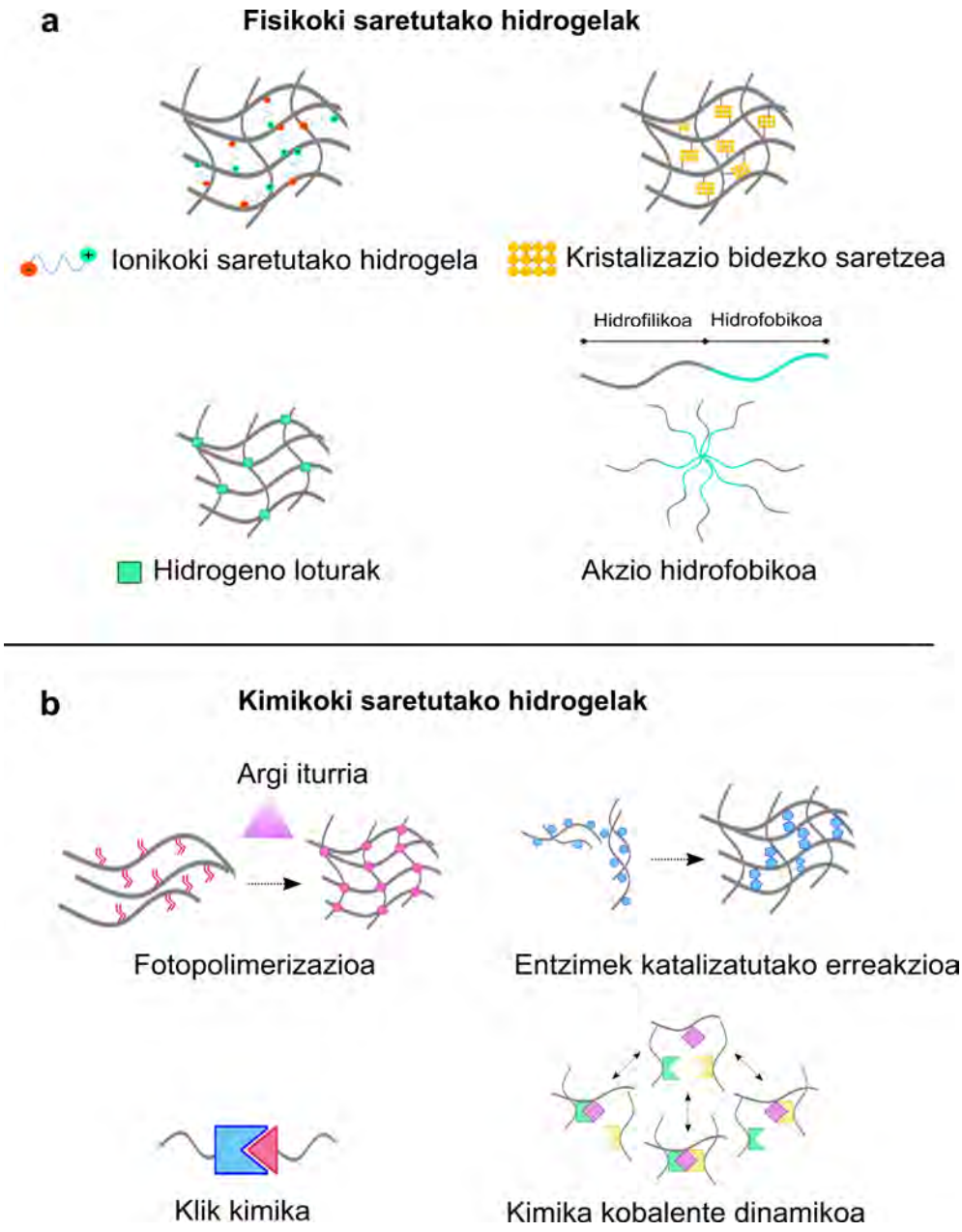

I.10. IRUDIA: Hidrogelen sintesirako erretikulazio estrategia fisiko eta kimikoen sailkapena.

2.2.2.1. Fisikoki gurutzatutako hidrogelak

Interakzio fisikoen bitartez gurutzututako hidrogelek ez dute erretikulazio eragilerik. Hauek egonkor mantentzen dira, kristalinotasunari, hidrogeno-loturei, interakzio hidrofobikoei, interakzio elektrostatikoei edo kateen korapilatzeari lotutako lotura iragankorrei esker [189].

Interakzio fisikoak lotura kobalenteak baino ahulagoak dira, beraz, hidrogel fisikoen propietate mekanikoak kimikoki erretikulatutako hidrogelenak baino ahulagoak dira orokorrean [190]. Hala ere, interakzio horiek nahikoak izan daitezke

hidrogelak ingurune urtsuetan disolbatzea saihesteko [187]. Hidrogel fisikoen gelifikazioa polimeroen berezko propietateekin lotuta dago, eta horrek hidrogelaren propietateetan egin daitezkeen aldaketak mugatzen ditu. Hala ere, gelifikazioa kate polimerikoak aldatu gabe gertatzen denez, erraza da gauzatzea eta prozesua alderantzizkatzea beharrezkoa denean [191].

Erretikulazio eragilerik gabeko hidrogelak sortzeko, interakzio ionikoak, interakzio hidrofobikoak edo hidrogeno-loturak besteak beste, aztertu eta ulertzeak interes handiagoa izan du berriki.

Ionikoki gurutzatutako hidrogelak

Ionikoki gurutzatutako hidrogelen loturak, kate polimerikoen talde funtzionaletan dauden kontrako karga-ioien arteko lotura elektrostatikotik abiatuta eratzen dituzte, hala nola karboxilo edo amino taldeak [192, 193]. Ioi metaliko mono-, di- edo tribalenteak, hala nola Ag^1, Ca_2^1 edo Fe_3^1, ioi-loturak osatzeko erabiltzen diren ioi metalikoetako batzuk dira. Sare horiek autosendatze portaera dute, hau da, tentsio altuen pean hausten dira, baina tentsioa kentzean propietateak berrezartzen dituzte. Hala ere, lortutako erresistentzia mekanikoa mugatua da [194, 195].

Adibidez, katioiekin erretikulatutako alginato edo kitosanoan oinarritutako hidrogelak ehun-ingeniaritzarako, farmakoak askatzeko edo zauriak orbaintzeko hainbat aplikazioetan aztertu dituzte [196–198].

Kristalizazio bidezko gurutzaketa

Kristalizazio bidezko gurutzaketa izozte- eta desizozte-ziklo errepikakorren bitartez gertatzen da. Prozesu honetan, proteinen birnaturalizazioak, hidrogela osatzeko erretikulazio-gune gisa jardungo duten kristalitoak sortzen ditu. Erretikulazio-teknika honen erabilera gelatina, kitosano, zelulosa edo hidrogel sintetikoetarako deskribatu da [199–201]. Esate baterako, izozte-desizozte zikloez osatutako eta minoziklinaz kargatutako PVA eta kitosanoz osatutako hidrogel baten apositu gisa jarduteko eraginkortasuna frogatu zuten, arratoietan egindako *in vivo* probetan [202].

Hidrogeno-loturak

Oxigeno edo nitrogeno bati zuzenean lotutako hidrogeno atomo bat duen edozein molekulak hidrogeno loturak sor ditzake. Beraz, hidrogeno atomo baten eta talde funtzional baten arteko elkarketak (amida, urea, azido karboxilikoa edo talde hidroxilo bat kasu) gurutzaketa puntu gisa jardun dezake hidrogelen eraketan [203, 204]. Hidrogeno-loturak zelulosa [205], alginatoa [206, 207] edo kitosanoa [201] bezalako polimero naturalen lotura fisiko nagusiak dira.

Polimero naturalen taldeen arteko interakzio hidrofoboak

Polimeroen interakzio hidrofoboak, talde terminal hidrofoboak dituzten polimero anfifilikoak erabiliz edo erreakzio kimiko baten bidez multzo hidrofobo kopuru txiki bat sartuz eratzen dira. Talde hidrofoboak euren artean gehitu eta hiru dimentsioko sare bat sortzen dute [208].

2.2.2.2. Kimikoki gurutzatutako hidrogelak

Kimikoki gurutzatutako hidrogelek edo hidrogel termoegonkorrek lotura kobalente iraunkorrak dituzte. Erradikal askeen polimerizazioz, erradiazioz, molekula txikien erretikulazioz edo entzimek eragindako erretikulazioz osa daitezke [209]. Oro har, hidrogel kimikoek hidrogel fisikoek baino egonkortasun handiagoa, propietate mekaniko hobeak eta degradazio-portaera doigarriagoa dute.

Fotopolimerizazioa

Fotopolimerizazioan, lotura bikoitzeko karbono erreaktiboek erradikal askeen bidezko polimerizazioa sustatzen dute argi erradiazioaren eraginpean jartzean. Adibidez, uretan disolba daitezkeen eta hidroxilo, karboxilo eta amino multzoak dituzten polimeroek, akriloilo kloruroarekin, glizilo metakrilatoarekin (GMA) eta N-(3 aminopropilo)-metakrilamidarekin erreakzionatu dezakete, binilo talde oso erreaktiboak sartuz [210]. Fotopolimerizatutako hidrogelen sintesiak uhin-luzera desberdinetan argi espezifikoa xurgatzen duten fotoabiarazleak behar ditu, hala nola Irgacure 2959, LAP, erriboflabina fosfatoa, Eosina Y, etab [211–213]. Fotoabiarazle horiek molekula emaile baten hidrogenoa deskonposatzen edo ezabatzen dute argiaren eraginpean, talde erreaktiboekin erreakzionatuko duten erreakzio-abiarazle erradikalak eratuz (I.11 irudia).

Erretikulazio-metodo hau zitokinak kapsulatuta dituzten hidrogelak sortzeko asko erabiltzen da [214–216]. Argiaren esposizioa kontrolatuz, propietate mekanikoak aldatzeko eta polimerizatutako gunea zehaztasunez hautatzeko aukera ematen du [217].

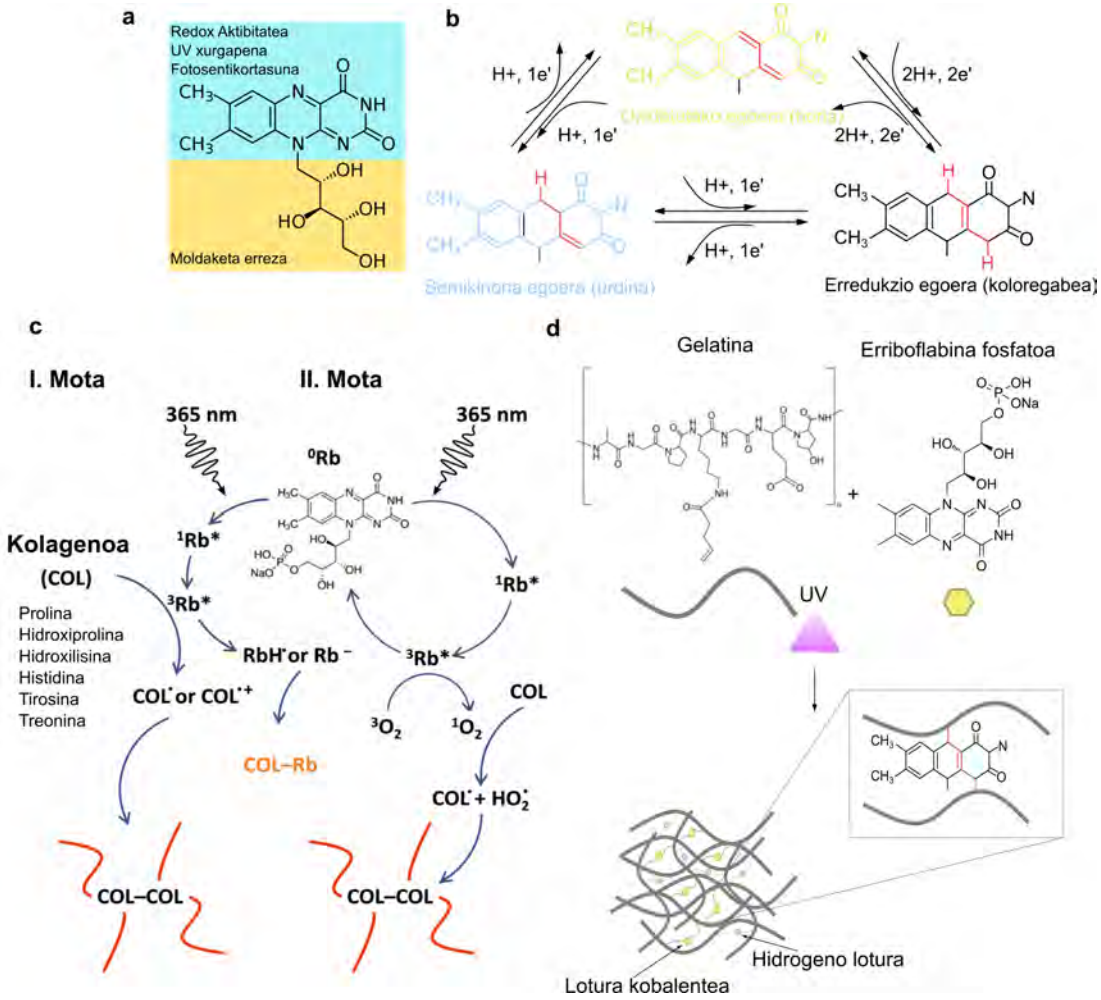

I.11. IRUDIA: **a**) Erriboflabinaren egitura; **b**) Erriboflabinaren oxidazio egoerak (**a** eta **b** [218]-tik moldatuta); **c**) Kolageno eta erriboflabinaren arteko gurutzaketa prozesua ([219]-tik moldatuta); **d**) UV izpiekin irradiatu ondoren, gelatina eta erriboflabina fosfatoaren arteko erretikulazio prozesuaren erreakzio posiblea.

Entzimek katalizatutako erreakzioak

Entzimak organismo bizidunen zelulen barruan gertatzen diren erreakzio kimikoak azkartzen dituzten proteinak dira, eta funtsezko eginkizuna betetzen dute ia prozesu zelular guztietan. Katalizatzaile horiek erreakzio sorta zabal batean parte hartzen dute, hala nola oxidazioan eta erredukzioan, hidrolisian edo lotura kimikoen eraketan. Entzimen bidez emandako erantzunek berebiziko garrantzia dute zelulaz kanpoko matrizearen saretze prozesuan. Adibidez, oxidasa-lisiak

aldehidoak sor ditzake kolageno edo elastina-zuntzetan dauden lisina hondakinetatik abiatuta, eta horrek zuntzen antolaketa erraztuko du. Gainera, transglutaminasak proteinak gurutzatzen ditu, glutamato-hondakinen karboxamida taldearen eta lisilo-hondakinetako ε-amino taldearen arteko azil-transferentziaren erreakzioaren bidez. Horrela, entzimak biomaterialen erantzunak aldatzeko eta egitura kimikoak nonahi aldatzeko erabili dira.

Erretikulazio entzimatikoak lotura kobalenteak sortzen ditu denbora tarte laburrean eta entzima-kontzentrazioa kontrolatuz, polimerizazio-zinetika zuzenean aldatzeko aukera ematen du [209]. Transglutaminasa entzima eta kaltzio ioiak gehituz karboxamida eta amina taldeen arteko loturak sortzea [220], edo HRP peroxidasa eta hidrogeno peroxidoa (H_2O_2) erabiltzea, anilina [221], fenol [222] edo tiramina [223] taldeak katalizatzeko, entzimek katalizatutako gurutzaketen hainbat adibide dira.

Klik kimika

Klik kimika karbono-hetero loturen eraketan oinarritutako erreakzio sinpleen bidez produktuak sortzeko moduari dagokio. Bere izenak molekulen lotura sinplea presiozko itxitura mekanikoak bezalako lotura sinple batekin alderatu nahi du. Erreakzio horiek erreakzio azkarrak, errazak, fisiologikoki egonkorrak, moldagarriak, espektro zabalekoak, espezifikoak, aldakorrak eta errendimendu handikoak dira, eta erreakzio-produktu bakarra ematen dute [224].

Irizpide hauek betetzen dituzten klik erreakzio ezberdinen artean, Diels Alder, Schiff-en erreakzioa, oxima bidezko erreakzioa eta Michael motako erreakzioa dira klik kimikan bildutako gurutzaketa metodo klasikoetako batzuk.

Kimika kobalente dinamikoa

Lotura kobalente dinamikoek, zelula eta hidrogelaren arteko birmoldatze beharraren arabera beren osotasunari eusteko edo denbora tarte baten ondoren hausteko gaitasuna dute [225]. Ester boronikoa, adibidez, hautagai bikaina da orbaintzeko gaitasuna duten hidrogelen sintesirako, loturak pH-aren eta tenperaturaren baldintza desberdinetan berrantola baititzake [226, 227].

3. Medikuntza birsortzaileari lotutako kornea birsortzeko konponbideak

Emaileen ehun-eskasiak, itxarote-zerrenda amaigabeek (behar diren 70 korneako, kornea bakarra dago) [228], mentua errefusatzeak edo beste eragozpen batzuek, hala nola emailearekin lotutako gaixotasun infekziosoek, kornea birsortzeko MB-ak barnean hartzen dituen tekniken garapena bultzatu dute, eta horrek aurrerapen handiak ekarri ditu *in vitro* ikerketa eta klinikarako kornea-ehuna ordezteko alternatiba eraginkorretan. Gainditu nahi den lesio edo gaixotasun motaren arabera, hainbat konponbide proposatu dituzte, zelula ama mota desberdinekin terapia birsortzaileak erabiltzetik hasi eta faktore bioaktiboak edo zelula amak dituzten euskarri biologikoak edo material berritzaileak garatzeraino.

Gaur egun ikertzen ari diren terapia eta soluzio guztien artean, korneako zauriak tratatzeko ehun-ingeniaritzari lotutako 2 estrategia dira nagusi: Zelula-xaflen ingeniaritza edo 3 dimentsiotako euskarrietan oinarritutako ingeniaritza. Estrategia horien helburua zelulek, zelulaz kanpoko matrizeak eta seinale molekular/mekanikoek osatutako mikroingurunea berrezartzea da.

3.1. Zelula-xaflen ingeniaritza

Zelula-xaflen ingeniaritzak (ZXI) zelulen monogeruza baten *in vitro* garapena dakar, zeinetan zelulen arteko interakzioak eta zelulen eta zelulaz kanpoko matrizearen arteko interakzioak indartzen diren [229]. Zelulek beraiek ehunarentzako euskarria izango dena sortzen dute transplantatu aurretik.

Estimuluei erantzuten dieten materialekin egindako zelulentzako hazkuntza-substratuen erabileran oinarritzen da. Faktore estimulatzaileak aldatuz, hala nola tenperatura, entzimak, argia, ioiak, erredox erreakzioak, pH-a, azukrea, etab., zelulak substratura atxikitzeko portaera erregula daiteke, zelulak modu naturalean askatzeko (I.12 irudia).

ZXI-sistema ohikoenetan, hazkuntza-plakak poli(N-isopropilakrilamida)-z (PIPAAm) estaltzen dira, 37 °C-tan termosentikorra eta hidrofoboa den materiala, zelulen ugaltzea eta atxikitzea ahalbidetzen dituena. Zelulen monogeruza eratu ondoren, tenperatura 32 °C ingurura jaisten da, PIPAAm-ren azalera hidrofiloa bilakatu eta haren hidratazio azkarrak zelulen atxikipena eragozten du, zelulen

xafla askatzea eragiten duelarik. Gainazal termosentikorrez gain, zelula-xaflak askatzeko metodo alternatiboak ere aztertu dira, hala nola aktibatzaile elektrikoak, argi-estimuluak, indar magnetikoak eta pH-aldaketak. Prozesu honetatik lortutako zelula-xaflak kaltetutako ehunari aplikatzen zaizkio. Zelula-xaflak bihotz-ehuna, gibel-ehuna, hezurra, larruazala, ehun kartilaginosoak edo ehun periodontalak birsortzeko erabili dira, besteak beste [230].

Begiaren gainazala itu oso egokia da ZXI aplikatzeko. Teknika hau, odol periferikotik eratorritako zelula mononuklearrak [231], enbrioi-zelula ama kondrogenikoak [232] edo mintz amniotikoko zelula amak [233] erabiliz, korneako epitelioa *in vitro* hazteko erabili da. Hainbat substraturen erabilera ere ikertu da, hala nola polimero termoiraunkorrak [234] edo RGD bidez funtzionalizatutako elastinaren antzeko polipeptidoa (EAP) [235].

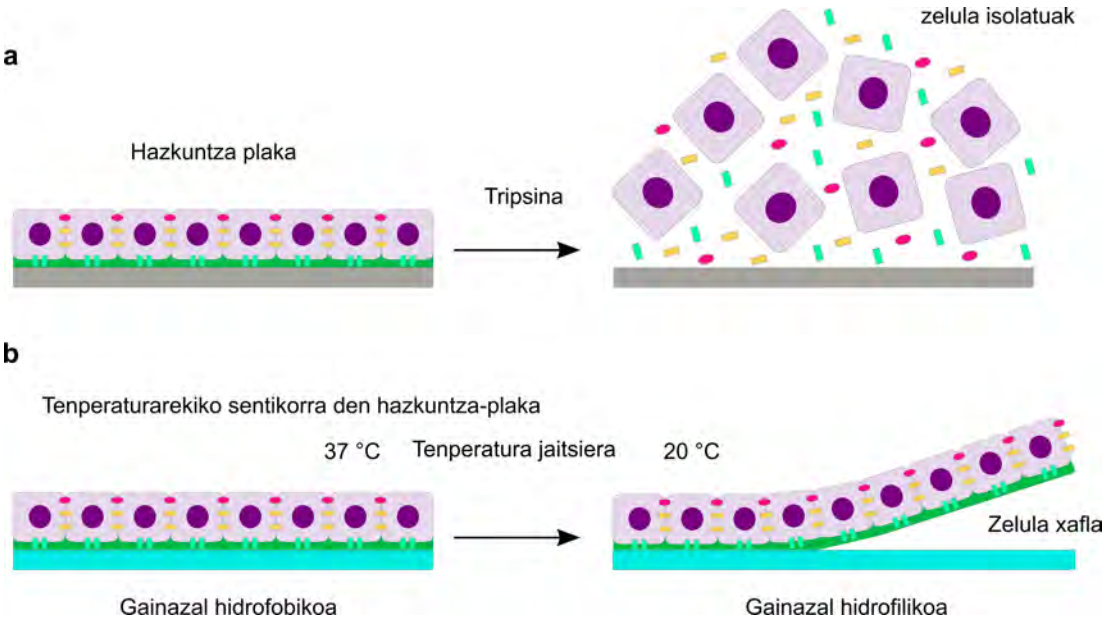

I.12. IRUDIA: Zelula-xaflen ingeniaritza. **a**) Konfluentzian dauden zelulak banaka askatzen dira digestio entzimatikoaren bidez. **b**) Zelula-xaflen atxikipena eta askatzea termoiraunkorrak diren hazkuntza plaketan. Plakak polimero termoiraunkor batez estalita daude, eta horrek bere hidrofilia tenperatura espezifikoetan aldatzea baimentzen du. Metodo eraginkor eta ez-inbaditzailea izanik, xafla zelularrak eratu, zelulak elkarri lotuta mantendu eta xafla osoa aska daiteke.

3.2. 3 dimentsiotako euskarriak: biomaterialen erabilera

Estrategia hau ehunaren mikroingurunea antzeratzen eta estimulatzen duten eta zelulentzako euskarri izango diren substratu edo matrize mota ezberdinen garapenean oinarritzen da.

Garatutako euskarriek, mota (mintzak, lenteak, hidrogelak, etab.) eta osaera (naturala, sintetikoa edo hauen konbinazio bat) anitza eta zelulak eta/edo molekulak izan ditzakete, lesioa sendatzeko eta berrezartzeko zeregin aktiboa izango luketenak.

3.2.1. Ukipen-lente terapeutikoen garapena

Ukipen-lenteek ehunen orbaintzea ahalbidetzeko hesi fisiko bat ezartzen dute, mina arintzeko presioa eragiten dute eta kirurgiaren ondoren begiko gainazalaren hidratazio egokia mantentzen laguntzen dute [236, 237].

Bi multzo nagusitan bana daitezke: hidrogel polimerikoz edo silikonazko hidrogel polimerikoz egindako ukipen-lente bigunak, eta gasarekiko iragazkorrak diren ukipen-lente zurrunak [238]. Silikona gaur egun ukipen-lente bigunak egiteko gehien erabiltzen den materiala da, honen leuntasunak, malgutasunak, ur-edukiak, biobateragarritasunak, gardentasunak eta gasarekiko iragazkortasunak, farmakoak garraiatzeko sistemak garatzeko hautagai hobea bilakatzen baitute [239–241]. Klinikan erabiltzen diren lenteetatik % 87-a ukipen-lente bigunak dira [242, 243]. Balafilcon A (Pure Vision, Bausch & Lomb), Lotrafilcon A (Night & Day, Ciba Vision) edo Lotrafilcon B (O2Optix, CIBA Vision) dira Elikagai eta Sendagaien Administrazioak (FDA) onartutako soluzioen adibide batzuk.

Molekulak ukipen-lenteen bidez garraiatzeak, askapen mailakatuagoa dakar eta honek, kolirio tradizionaletan ez bezala, beharrezko dosia hobeto doitzea ahalbidetzen du. Gainera, begien kliskaren ondorioz gerta daitekeen epitelioko zelulen askapena babesten dute, eta zelula epitelialen migrazioa errazteko estromaren gaineko malko-geruza egonkor bat mantentzen laguntzen dute [90].

Farmakoz kargatutako ukipen-lenteak garatzeko estrategia ezberdinak aurki daitezke: lenteak farmakoz blaitzea [239, 246, 247], E bitamina hidrofobikoaren bidez hedapen-hesi bat ezartzea [248–251], farmakoz kargatutako nanopartikula (NP) lipidikoak edo bestelako sistema nanoegituratu koloidalak gehitzea [252–256], inprimaketa molekularra [257–259] edo farmakoz bustitako estaldura bat gehitzea [260, 261]. NP lipidikoek, NP polimerikoek, mikroemultsioek edo ziklodextrinek, farmakoak kargatzeko gaitasun handia, egonkortasun termodinamikoa eta farmako hidrofilikoak zein hidrofobikoak kargatzeko moldakortasun handia erakutsi dute. Inprimaketa molekularra, berariazko lotura-guneak eta egitura geometriko bakarrak dituen txantiloi polimeriko bat fabrikatzeari dagokio, farmakoa lotura horiei berariaz

lotu dakiekeena. Sare polimerikoaren eta farmakoen arteko harremana kontrolatzean, farmakoarekiko afinitatea hobetzen da, eta horrek farmakoaren atzemate eta askapen mailakatua hobetzen du [239]. Gainerako teknikek hidrogelak erabiltzen dituzte farmakoak dituzten nanopartikula polimerikoen eramaile gisa edo ukipen-lenteen barruko material polimeriko gisa. I.3 taulan substratu bezala erabilitako materialetako batzuk aurki daitezke [263].

I.3. TAULA: Ukipen-lenteetan erabilitako polimeroen ezaugarriak. [263]-tik hartutako taula.

Polimeroa	Ezaugarriak
Propoxilatutako glizerilo-triakrilatoa (PGT)	Hainbat funtzio biniliko dituen polimeroa.
Polikaprolaktona (PKL)	FDA-k onartutako eta azpiproduktu toxikorik gabeko polimero biodegradagarri hidrofoboa.
Kitosanoa	Polimero polisakarido kationikoa, biobateragarritasun eta biodegradagarritasun ona dituena,degradagarritasun lisozimatikoa barne.
Poli-(azido laktiko-koglikolikoa) (PLGA)	FDA-k onartutako polimero biobateragarria eta biodegradagarria, azido glikolikoaren eta azido laktikoaren proportzioa aldatuz bere propietateak alda ditzakeena.
Poli (d, l-laktida)-dextranoa (Dex-b-PLA)	PLA-zko nukleoa eta dextranozko kanpoko estalkia duten nanopartikulak.
Poli-hidroxietilmetakrilatoa (HEMA)	Ur eduki handiko eta hidrogel hidrofilo biobateragarria.
Etilzelulosa (EZ)	Polimero hidrofoboa, biobateragarria eta biodegradaezina.
Fibrina	Proteinetan oinarritutako biopolimero naturala, plasminak gidatutako fibrinolisi bidezko biodegradagarritasuna duena.
Eudragit S-100	pH-arekiko sentikorra den kopolimero anionikoa, pH-7-tik gorako propietate disolbatzailea duena.

3.2.2. Hidrogelen erabilera korneako zauri ezberdinetan

Hidrogel formako biomaterialak larritasun desberdineko korneako zauriak tratatzeko etorkizun handiko konponbideak dira. Hidrogelen propietate fisiko moldagarriek, biodegradagarritasunak eta bioaktibitateak zelulen aldeko mikroingurunea antzeratzea ahalbidetzen dute. Gainera, zelulak edo molekula biokimikoak hidrogeletan kapsulatu daitezke, korneako epitelioaren, estromaren eta kornearen lodiera osoa hartzen duten zaurien birsorkuntza sustatzeko eta kornea-donazioen beharra murrizteko.

Hidrogelen aplikazio posibleen artean, honako hauek aurki daitezke (I.13 irudia):

- Korneako sakonera txikiko epitelio-zaurietarako aposituak edo mintz terapeutikoak, non hidrogelak orbaintzea bizkortu eta babes gisa jarduten duen.

- Josturak ordeztuko dituzten begietako itsasgarriak, korneako ebakidura txikiak sendatzeko.
- Korneako akats sakonak eta zulaketak betetzeko hidrogelak.
- Kornea bere osotasunean ordeztuko duten konstruktuak.

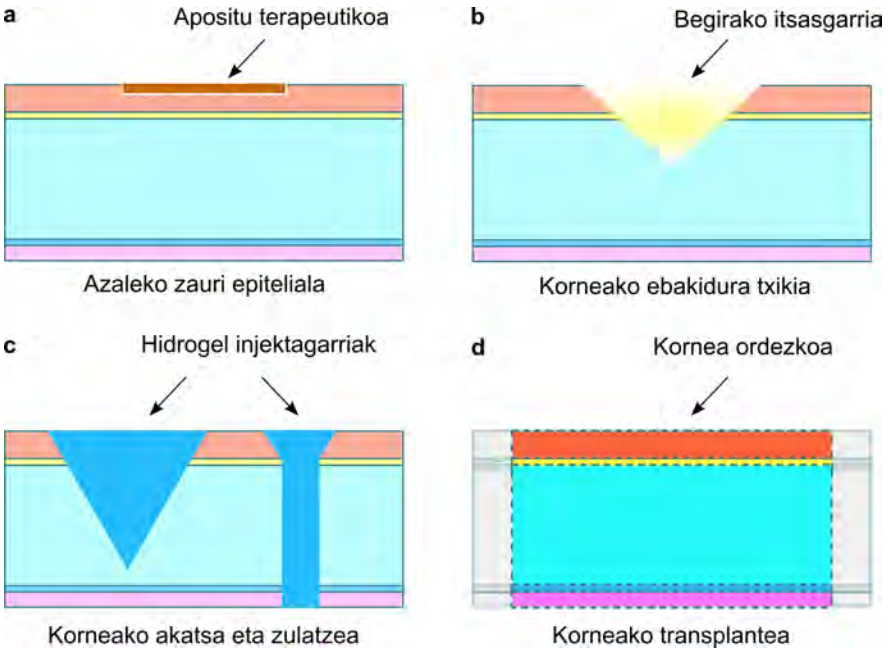

I.13. IRUDIA: Korneako akats ezberdinetarako hidrogelen aplikazioak. **a**) Korneako sakonera txikiko epitelio-zaurietarako apositu terapeutikoak. **b**) Ebakidura txikietarako josturen ordezko gisa erabiliko diren begietako itsasgarriak. **c**) Korneako akats sakonak eta zulaketak betetzeko hidrogelak. **d**) Kornea bere osotasunean ordeztuko duten konstruktuen erabilera.

3.2.2.1. Mintz terapeutikoak

Apositu terapeutikoak edo farmakoak, hazkuntza faktoreak edo antibiotikoak dituzten hidrogel mintzak, laser bidezko errefrakzio-kirurgian, korneako epitelio-akatsen edo korneako distrofiaren ebakuntza ondoko tratamenduan erabili dira. Apositu hauek, kornea-orbaintzea errazten, hantura murrizten eta begi gainazaleko mikroingurunea egonkortzen laguntzen dute. Mintz amniotikoko mentuak edo kolagenozko bitrigelak dira aplikazio honen bi adibide.

Mintz amniotikoko mentuak

Mintz amniotikoa (MA) fetuarekin kontaktuan dagoen plazentaren 0,02-0,05 mm-ko lodiera duen geruza erdi-gardena da. Ez du odol-hodirik eta hainbat geruzaz osatuta dago: epitelioa (geruzarik barnekoena), faktore immunomodulatzaileak jariatzen dituzten zelula kuboidalez osatua; mintz basala, zelula epitelialek jariatu eta

I, III, IV, V eta VII motako kolagenoz, kolagenozkoak ez diren glikoproteinez eta azido hialuronikoz osatua; eta geruza estromala. Azken hau, aldi berean, hiru geruzatan bana daiteke: zelula ama mesenkimalak eta horien sekretoma dituen barne-geruza trinkoa, tartean kokatutako geruza fibroblastikoa eta geruza azelularra, nagusiki III motako kolagenoak eta proteoglikanoek osatzen dutena [264, 265].

Kolagenoz, zelulez eta hainbat hazkuntza faktorez osatutako konposizioak, bere propietate antiinflamatorioekin, antifibrotikoekin, antioxidatzaileekin, antibakterianoekin eta ez-immunogenikoekin batera, ehun-ingeniaritza oftalmikoaren eta terapia zelularraren baitan potentzial handiko alomentu bihurtzen dute [264].

Mintz formako MA-etatik eratorritako hainbat produktu komertzial aurki daitezke. Kriokontserbatutako ProKera mintzak (Bio-Tissue, Miami, FL, AEB) emaitza onuragarriak erakutsi zituen keratitis bakteriarraren tratamentuan [266], erreduretan [267] edo LZAG [268] eta EAI-ak sendatzeko tratamentuetan [269]. AmnioGraft (Bio-Tissue, Miami, FL, AEB), AmnioGuard (Bio-Tissue, Miami, FL, AEB) edo AmbioDisk (Katena Products Inc, Denville, NJ, AEB), aplikazio oftalmologikoetarako erabiltzen diren zelula gabeko eta liofilizatutako MA-tik eratorritako mentuak dira.

MA-ren propietate interesgarri guztiak kontuan hartuta, oftalmologian giza mintz amniotikotik eratorritako hainbat produktu garatu dituzte, hala nola, mintz arruntak, MA-tik eratorritako kolirioak, mintz amniotikoko nanokonposatuak, farmakoen garraiatzaileak [270] edo MA eta beste material natural edo sintetiko batzuen konbinazio batez osatutako hidrogelak [271, 272].

Kolagenozko bitrigelak

Kolagenozko bitrigelak korneako kolagenoaren arkitektura antzeratzen duten I motako kolageno zuntzexkez osatutako mintzak dira. Hiru pausotan sintetiza daitezke: kolagenozko gel baten eraketa; beiratzea, hau da, gela lehortze-prozesu baten bidez mintz zurrun bihurtzea, lehortze-prozesu horretan hidrogelaren kolageno zuntzexkak sare trinko bat osatzen dutelarik; eta, azkenik, berhidratatzea, beiraztatutako materiala mintz fin garden bihurtzeko.

Beiratze prozesuaren aldagai ezberdinak aldatzearen eragina, hala nola tenperatura edo hezetasuna, aztertu da, sintetizatutako mintzetan keratozitoak kultibatu ahal izateko ondoren [273]. Kolagenozko bitrigelak korneako geruza

epiteliala, estromala edo endoteliala berreraikitzeko proposatu dira [273, 274] edo kolagenozko bitrigelaren eta fibrinazko itsasgarriaren konbinazioa LZAG-a edo zauri estromalak dituzten korneak konpontzeko aztertu dute [275].

3.2.2.2. Josturen ordezko begietako itsasgarriak

Begietako itsasgarriak josturen eta horiekin lotutako eragozpenen alternatiba gisa garatu ziren. Oro har, sintetikoak, zianoakrilatotik edo polietilenglikol (PEG) delakotik eratorritakoak kasu gehienetan, edo biologikoak, fibrinatik eratorritako materialak normalean, izan daitezke.

Zianokrilatoak

Zianoakrilatoa azido zianoakrilikotik eratorritako ester bat da, ehunetan dauden alkoholekin, urarekin edo aminoazidoekin erraz polimerizatzen dena. Zianoakrilatoak superitsasgarri bezala ezagunak dira, proteinen aminoazidoen hondakinen eta zianoakrilatoaren arteko polimerizazio-erreakzioaren ondorioz, ehunei gogor lotzen zaizkielako [276].

FDA-k zianoakrilatoa begiko erabilerarako zehazki onartu ez duen arren, oftalmologian hainbat aplikaziotarako erabili da, hala nola aldi baterako tarsorrafian [277] edo argaltze, zulatze edo besikulen askapenari lotutako arazoetan [278–280].

Konponbide azkarra eta eraginkorra izan arren, zianoakrilatoa zianoazetato eta formaldehidoan degradatzeak hantura akutu eta kronikoa eragin dezake. Gainera, honen iragazgaiztasunak, gardentasun faltak eta gainazal zimurtsuak azpiko ehunaren orbaintzea mugatu, mina eragin eta ikusmena kaltetu dezake [281]. Horregatik, oftalmologian erabilera mugatua du.

PEG-etik eratorritako itsasgarriak

PEG-a eta honen eratorriak begietako itsasgarriak garatzeko material sintetiko erakargarriak dira, propietate mekaniko eta biologiko moldagarriak, immunogenizitate txikia eta toxikotasun eza erakutsi baitute.

ReSure (Ocular Therapeutix Inc., MA, AEB) eta OcuSeal (Beaver-Visitec International, MA, AEB) PEG-an oinarritutako eta saiakuntza klinikoetan erabilitako bi itsasgarri dira. ReSure katarata-kirurgian likido-ihesak saihesteko FDA-k onartutako itsasgarria da [282]. OcuSeal (Beaver-Visitec International, MA, AEB)

Europan erabiltzen den ReSure-ren baliokidea da. Nailonezko josturen aldean bi itsasgarriek onurak erakutsi dituzte ebakiduren itxieran, astigmatismoaren murrizketan edo katarata ebakuntzaren osteko errekuperazioan [283–285].

Hala ere, itsasgarri hauen erabilera jario aktiborik ez duten ebakidurak ixtera mugatuta dago. Itsasgarri hauek ez dira gai akats estromalak betetzeko, bai itsaspen txikiagatik [286, 287], bai polimerizazio kontrolaezin eta azkarra izateagatik [284].

Fibrinazko itsasgarriak

Zianoakrilatoarekin batera, fibrinazko itsasgarriak oftalmologian gehien erabiltzen diren josturen ordezkoak dira, zeinak organismoaren koagulazio-prozesua imitatzean oinarritzen diren. Fibrinazko itsasgarriek fibrinogenoz, plasminogenoz, fibronektinaz eta XIII faktoreaz osatutako soluzio proteiko bat tronbina eta kloruro kaltzikoko disoluzio batekin konbinatzen dute. Tronbinak fibrinogenoa fibrinan banatzen du, hiru dimentsioko sare bat osatuz. Tronbinak XIII. faktorea ere zatitzen du, eta horri esker, fibrinazko monomeroak gurutzatzen eta polimerizatzen dira kaltziozko ioien presentzian. Itsasgarri hau korneako zauri edo ebakiduretan aplikatzen denean, fibrina eta fibronektina kolageno estromalarekin gurutzatu eta ehunarekiko atxikimendu handia sortzen dute [288].

2000-ko hamarkadan oftalmologian lehen aldiz erabili zirenetik, fibrinazko itsasgarriek funtsezko aplikazio asko aurkitu dituzte itsasgarri gisa, hala nola kornea-zuloak orbaintzeko [289], pterigiona kentzeko ebakuntzan konjuntibako automentua itsasteko [290], MA-ren transplanterako [291] edo josturarik gabeko keratoplastia lamelarrerako [292]. Fibrinazko itsasgarria korneako transplantearen alternatiba gisa zelula amekin ere konbinatu da [293, 294]. Itsasgarri hauen abantailen artean birxurgapen azkarra, pazientearen erosotasun handia, klinikan erabiltzeko erraztasuna eta zianoakrilatoarekin alderatuta kornearen baskularizazio txikiagoa lortzea aipa daitezke. Hala ere, eragozpen nagusiak kutsadura birikoarekin eta arazo immunologikoekin lotuta daude. Deribatu autologoen erabilerak arrisku horiek murrizten baditu ere, produktuaren propietateen kostua, denbora eta erreproduzigarritasuna handitzen dira.

Badira aplikazio oftalmikoetarako fibrina likidoz egindako itsasgarri komertzialak, hala nola TISSEEL (Baxter International, Deerfield, Illinois, AEB), beste herrialde batzuetan Tissucol izenarekin (Baxter Hyland Immuno, Viena,

Austria) eskuragarri, EVICEL (OMRIX Biopharmaceuticals, New York, AEB), Vitagel (Stryker, Kalamazoo, Michigan, AEB), Greenplast Q (Green Cross Corp, Seul, Hego Korea) edo Reliseal (Reliance Life Sciences, India), azken bi hauek Hego Korean eta Indian bakarrik eskuragarri daudelarik, hurrenez hurren.

Beste konponbide batzuk

Aipatutako materialez gain, begietako zauriak konpontzeko edo ixteko material proteiko eta sintetikoen konbinazioak ere ikertu dituzte. Adibidez, dextrano oxidatua (ODex) gehitu eta argi ikusgarriz gurutzatutako gelatina metakrilatozko (GelMA) itsasgarri batek, berrepitelizazioa hobetzeko itsasgarri komertzialek baino propitate hobeak erakutsi ditu [295].

3.2.2.3. Korneako akats sakonak eta zulaketak betetzeko hidrogelak

Sintesi kimikoaren teknologian egindako aurrerapenek hainbat material erabiltzen dituzten hidrogelak garatzea ekarri dute, hala nola kolagenoa, gelatina, AH etab. Horiek ez dira zauria betetzera mugatzen, korneako orbaintzea eta lesioen itxiera sustatzeko balio dute.

Kolagenoan oinarritutako hidrogelak

Korneako estroma ordezteko kolageno exogenoa erabiltzeak, kolagenoaren berezko propietateak aprobetxatzea du helburu, zelulen migrazio eta kolonizaziorako ingurune bat eskainiz. Korneako akatsak betetzeko animalia-jatorriko kolageno exogenoak eta kolageno birkonbinatzaileak hainbat formatan sintetizatu dira.

Kolageno birkonbinatzaileari dagokionez, I eta III motako giza kolageno birkonbinatzailean oinarritutako hidrogelek argitasun optikoa mantentzen dutela eta korneako zelulen, nerbioen eta malko geruzaren birsorkuntza *in vivo* sustatzen dutela erakutsi dute *Sus scrofa domesticus* txerrietan aplikatu ondoren [296]. Era berean, giza kolageno birkonbinatzailetik abiatuta eta anhidrido metakrilatoarekin nahastutako hidrogelak, linbo eremuko estromako zelula amen hazkuntza ordenatua sustatzen, hauen keratozitoetarako desberdintzapena eragiten eta kaltetutako estroma *in vivo* orbaintzen laguntzen duela erakutsi du [297]. Bestalde, LiQD Cornea delako hidrogela, giza kolageno birkonbinatzailearen aukera merkeago bezala eta material xenogenikoei lotutako errefusa immunologikoa murrizteko aukera gisa proposatu

dute. Hidrogel hau PEG-arekin eta fibrinogenoarekin konbinatutako kolagenoaren antzeko peptido sintetiko laburrez osatuta dago, eta untxien begietako zaurien itxiera osoa eta kornearen lodiera osoa berrezartzen duela erakutsi du kirurgia egin eta 3 hilabetera [298].

Animalia-jatorriko kolagenoaren bertsioak kontuan hartuta, beste biomaterial batzuekin nahastutako, hala nola AH edo PEG, eta estrategia desberdinekin gurutzatutako I motako behi kolagenoak, epitelizazioa sustatzeko, kornea-birsorkuntza hobetzeko eta biomarkatzaile fibrotikoen eta inflamatorioen adierazpena murrizteko potentzial handia erakutsi du [299–302]. Zauria betetzeaz gain, kolagenoz egindako hidrogelak zelulak/farmakoak askatzeko sistema gisa erabil daitezke, korneako zaurien orbaintzea hobetuko duten hainbat agente terapeutiko etengabe askatzeko sistema gisa ere proposatu baitituzte [303–305].

Gelatinan oinarritutako hidrogelak

Kolagenoaren hidrolisiaren ondoriozko nahasketa polipeptidiko hidrodisolbagarri gisa, gelatina begi-ehuna konpontzeko material egoki bezala proposatu dute.

Begietako ehun-ingeniaritzan asko erabiltzen den materiala bada ere, orokorrean kimikoki eraldatuta, beste material batzuekin konbinatuta edo hainbat estrategiaren bidez gurutzatuta erabiltzen da, begietako aplikazioa erraztuko duten propietate biskoelastiko eta mekaniko desberdinak lortzeko.

Josturarik gabeko kornea-lesioak konpontzeko GelCORE izeneko hidrogelaren garapena, kimikoki eraldatutako gelatinan oinarritutako hidrogel baten adibidea da. Ikerketa honetan gelatina talde metakriloilikoekin funtzionalizatu eta argi ikusgarriaren bitartez gurutzatu zuten (I.14 irudia) [306]. Bestetik, gelatinaren kate nagusia glizilato metakrilatoarekin nahastuz eta hidrogela argi ikusgarriarekin gurutzatuz, Sharifi-k eta kolaboratzaileek GELGYM deituriko hidrogel elastiko bat garatu zuten. Hidrogel honek propietate biomimetiko bikainak erakutsi zituen [307]. Horrez gain, metakrilatutako gelatinan (gelMA) oinarritutako hidrogela, F127 (F127DA) pluroniko diakrilatoarekin eta F127 pluroniko aldehido mizelekin eta I motako kolagenoarekin konbinatu zen. Hidrogel honek, untxietan egindako korneako estromako akats sakonak ordezteko ahalmena erakutsi zuen 4 asteetan, keratokonoaren kirurgian eta korneako beste gaixotasun batzuetan potentzial handi izan zezakeela frogatuz [308].

Zelulaz kanpoko matrize deszelularizatuarekin edo agarosarekin nahastutako gelatinazko hidrogelak [309, 310], edo keratozitoak [311] zein farmakoak [312] garraiatzen dituzten gelatinazko hidrogelak ere erabili dira, propietate biomekanikoak eta biologikoak optimizatu eta zauritutako kornearen orbaintzea sustatzeko.

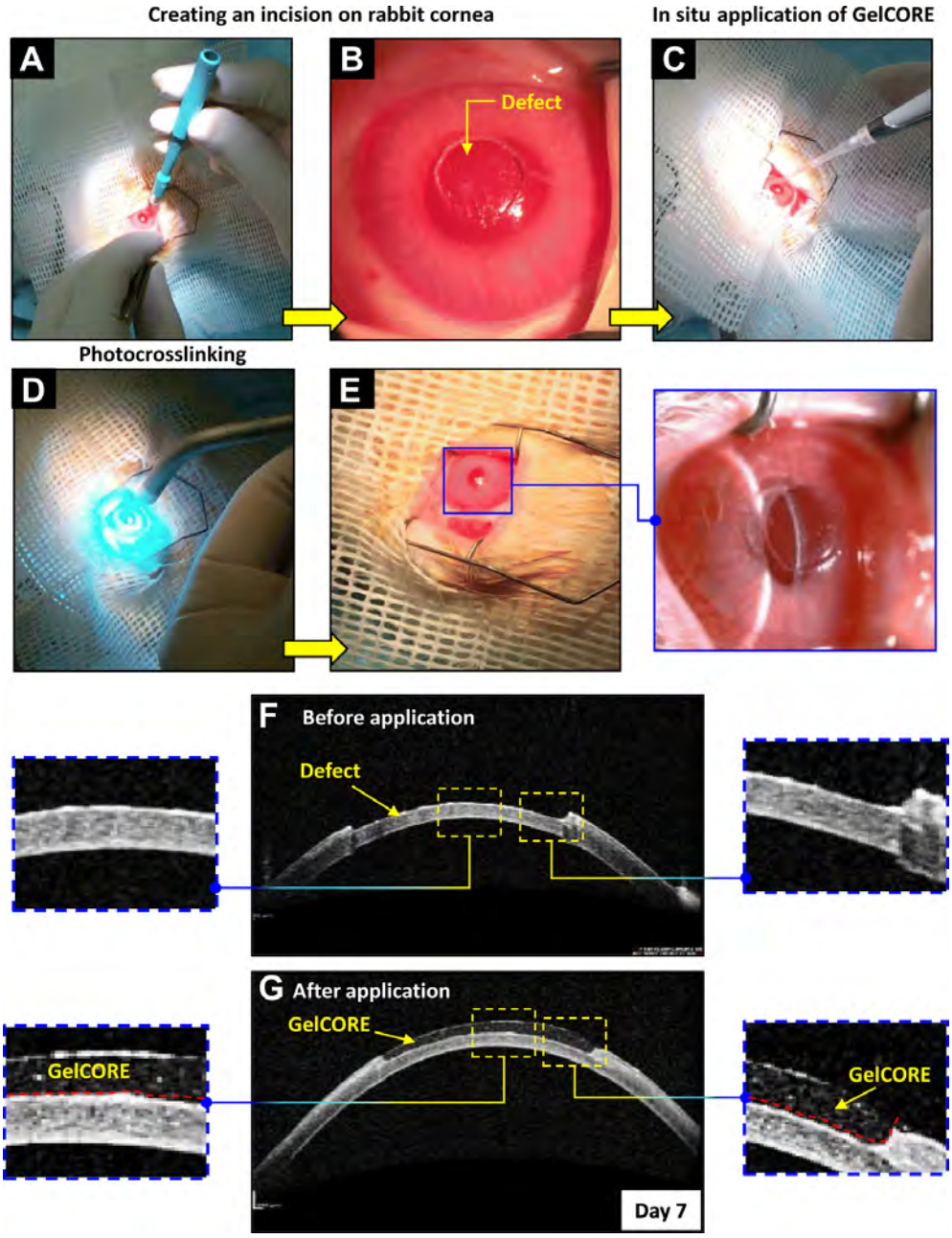

I.14. IRUDIA: GelCORE itsasgarriaren *in vivo* aplikazioa untxien korneako zaurietan **a**) eta **b**) Untxien korneetan sortutako akats estromalak. **c**) GelCORE itsasgarriaren zuzeneko aplikazioa, **d**) erretikulazio prozesua, **e**) akats estromalaren gaineko gelCORE itsasgarri gardenaren eraketa. GelCORE tratamenduaren **f**) aurretik **g**) ostean ateratako aurreko segmentuaren koherentziazko tomografia bidez lortutako irudiak. [306]-tik hartutako irudiak.

AH-an oinarritutako hidrogelak

AH korneako zelulaz kanpoko matrizearen osagaia da eta zauriak orbaintzeko prozesuan zelulen migrazioarekin lotuta dago besteak beste. Horrek, biobateragarritasun, gardentasun eta propietate mukoitsasgarriekin batera, korneako itsasgarriak edo euskarriak garatzeko oso material erakargarria bihurtu du. Aplikazio oftalmikoetarako, gurutzatu daitezkeen AH-aren eratorriak garatu dira, begi barneko atxikipen handiagoa erakutsi dutenak.

Adibidez, bio-ortogonalki erretikulatutako AH-z eta kolagenoz egindako hidrogel bat deskribatu dute, kornea-akatsak zuzenean bete eta itxi ditzakeena [299]. Tiol talde kimikoak ere erabili dira argi ikusgarriarekin gurutzatutako AH-hidrogela garatzeko [313]. Gainera, interakzio supramolekular ez-kobalenteez baliatuz, AH-ziklodextrina eta AH-adamantano hidrogelak sortu dituzte, hauetan kapsulatutako giza zelula epitelialen *ex vivo* atxikipena errazten, korneako zaurien orbaintzea hobetzen eta estromaren hantura murrizten dutenak [142].

Halaber, zelulak eta farmakoak kornea-zaurietara garraiatzeko AH-n oinarritutako hidrogelak ere proposatu dituzte [314].

Kitosanoan oinarritutako hidrogelak

Kitosanoa, halaber, polimero mukoitsasgarri natural eta biodegradagarria da. Oligoetilenglikolarekin kobinatutako kitosanozko hidrogelak korneako estromaren akats irregularrak azkar betetzeko ahalmena erakutsi du, keratozitoen ugaltzea eta migrazioa sustatu eta estroma ehunaren birsorkuntza sustateaz gainera [315].

Kitosanoz egindako hidrogel termosentikorrek karga ezberdinen eramaile gisa jardun dezakete, hala nola farmakoak [316, 317], hazkuntza faktoreak [129] edo exosomak [318] garraiatzeko ahalmena erakutsi dute besteak beste. Ezaugarri horrek, material honekiko ikertzaileen interesa gehiago erakarri du.

Deszelularizatutako zelulaz kanpoko matrizeetan oinarritutako hidrogelak

Deszelularizatutako kornea-ehun xenogenikoak, hidrogelak ekoizteko ere erabili dira. Jatorrizko ehunen osagai bioaktiboak atxikitzeko gaitasuna dutenez (adibidez, kolagenoa, glukosaminoglikanoak, hazkuntza faktoreak eta zelula-atxikipeneko proteinak), berezko estroma kornealaren zelulaz kanpoko matrizearen konposizioa imitatzeko abantaila erakusten dute.

Zelulaz kanpoko matrize kornealetik eratorritako hidrogel termosentikor deszelularizatu batek (COMatrix), giza zelula epitelial kornealen atxikipen eta ugaltzea hobetu eta zitokina inflamatorioen adierazpena murrizteko gaitasuna erakutsi du [319, 320]. Halaber, deszelularizatutako korneako zelulaz kanpoko matrizetik eratorritako hidrogelak, orbaindu ondorengo akats kornealekiko atxikimendu ona erakutsi eta itxiera epiteliala *in vivo* sustatzen duela frogatu dute [321].

Zelulaz kanpoko matrize deszelularizatutik eratorritako hidrogela N-ziklohexil-N0-(2-morfolinoetil) karbodiimida meto-p-toluenosulfonato (CMC)/N-hidroxisukzinimida (NHS) bidez ere erretikulatu izan da eta akats epitelio-estromalak betetzeko ahalmena erakutsi du, zauria orbaintzen laguntzen duen gainazal lau bat eratuz eta fibroblasto kornealak zelulaz kanpoko matrizea ekoiztea sustatuz [322].

3.2.2.4. Kornea bere osotasunean ordezteko konstruktuak

Korneako geruza ezberdinen mikroegitura eta mikroingurunea imitatzen saiatzen diren kornea-ordezkoen garapena, korneako ehun-ingeniaritzako etorkizun handiko esparrua da. Prozesu fisiologikoak aztertzeko automihiztaduraren printzipioan oinarritutako kornea ereduak garatu izan dira *in vitro*. 90-eko hamarkadan garatutako lehen ereduen artean, mintz basal eta epitelio estratifikatu batez sortutako eredua, kolagenozko hidrogel batean txertatutako fibroblastoak eta mintz basala zuen endotelio monogeruza bat [323], edo kolagenozko hidrogel batean sakabanatutako korneako zelula epitelialak, keratozitoak eta zelula endotelialak zituen euskarria aurki daitezke [324].

Eredu horiek giza zelula endotelial kornealak eta giza zelula epitelial primarioak gehituz are gehiago hobetu dira [325, 326]. Wang eta kolaboratzaileak epitelioa, estroma eta linboko eremua antzeratzen saiatu dira euren konstruktuan. Giza korneako zelula ama estromalekin ereindako zetazko fibroinazko filmen pilak erabili dituzte estroma sortzeko, giza korneako zelula epitelialekin ereindako eta NGF-rekin estalitako zetazko filmak erabili dituzte epitelioa irudikatzeko, eta oilasko-erro dortsaleko neurona ganglionarrekin (DRG) ereindako zetazko belaki batek linboaren eremua simulatu du. Estromaren eta epitelioaren zetazko filmen pilaketak, I motako kolagenozko hidrogelean txertatu dira, euskarri osoa bateratua geratu dadin. Gainera,

epitelioko NGF-rekin estalitako zetazko filmak NGF-rekin kargatutako kolagenozko gelekin konbinatu dituzte, DRG zelulen axoiak euskarriaren erdigunerantz gidatzeko asmoz. Eredu konplexu honek, korneako ehunaren inguruko azterketa sakonoagoa egitea ahalbidetu du (I.15 irudia).

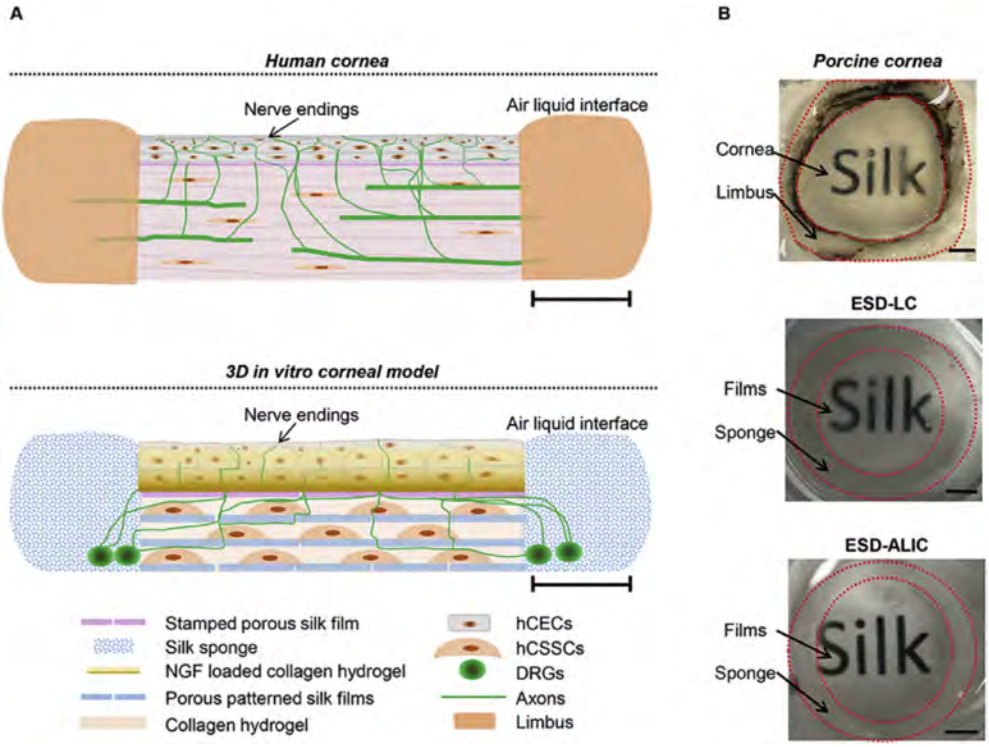

I.15. IRUDIA: **a**) Giza kornearen eta *in vitro* 3D kornea-ehunaren eredua. 3 mm-tako eskala lerroa. **b**) Txerri kornea, interfaze likido eta aire-likido interfazean hCEC, hCSSC eta DRG zelulen hazkuntza bateratua 28. egunean. Hazkuntza biak glizerolez busti dira. 3 mm-tako eskala lerroa. hCEC: giza korneako zelula epitelialak; hCSSC: giza korneako zelula ama estromalak; DRG: oilasko-erro dortsaleko neurona ganglionarrak; ESD-LC: interfaze likidoko mota zelular guztietako hazkuntza bateratua; ESD-ALIC: aire-likido interfazeko zelula-mota guztietako hazkuntza bateratua. [327]-tik hartutako irudia.

Klinikoki, LZAG larria eta orbaindutako estroma-ehun oso opakua duten pazienteak, korneako zelula amen transplantearekin tratatzen dira lehendabizi eta estroma ordeztuko duen emaile baten kornea transplantatuz ondoren. Duela gutxi, LZAG eta estroma-kaltea aldi berean tratatzeko aurreko kornearen konstruktu alogeniko nanoegituratu bat proposatu da. NANOULCOR izeneko eredua korneako zelula epitelialekin eta zelula estromal alogenikoekin konbinatutako fibrinaz eta agarosaz osatuta dago. Emaitza prekliniko oparoen ondoren [328–330], konstruktua I-II faseko saiakuntza kliniko batean dago gaur egun, honen segurtasuna eta eraginkortasun partziala gizakietan ebaluatzeko [331].

II. HIPOTESIA ETA HELBURUAK

1. Hipotesia

Epitelio akats iraunkorrak (EAI) eta korneako ultzera kronikoak begietako lesio ohikoak dira, zeinetan 2 asteko tratamenduaren ondoren ere, begia ez den gai epitelioan sortutako zauria berrepitelizatzeko. Denborak aurrera egin ahala, sentikortasuna gutxitzeak eta korneako gainazalaren orbaintze desegokiak kornea-lisia edota zulaketa eragin dezakete. EAI-en diagnostiko klinikoa zaila ez den arren, hauen tratamenduak erronka handia suposatzen du oraindik. Korneako patologiarik zailenetako bat da, eta haren kudeaketa eta jarraipena gizarte- eta osasun-kostu handiekin lotzen dira. Linboko zelula amen gutxitasunaren (LZAG) testuinguruan ere EAI-k gerta daitezke, linboko zelula ama erasanek eragindako berrepitelizazio desegokiaren ondorioz. LZAG-a begiaren gainazaleko gaixotasun kronikoa da, klinikoki neobaskularizazio korneala, kornea-opakutasuna eta ikusmen-galera edo itsutasuna eragin ditzakeena. Linbo esklerokornealeko zelula ama epitelialen kopuruan edo linboko zelulen nitxoan izandako kalteek eragiten dute, horiek baitira korneako epitelioaren birsortze eta homeostasi normala mantentzearen arduradunak.

EAI-k kolirio konbentzionalekin eta antibiotiko topikoekin tratatu ohi dira. Hala ere, estroma kaltetuta dagoen eta begi-globoaren osotasuna arriskuan egon daitekeen kasuetan, ebakuntza kirurgikoak egitea beharrezkoa izan daiteke, hala nola ehun-mentuak edo zelula amen transplanteak egitea. LZAG-erako egungo tratamendu eraginkor bakarra, linbo osasuntsuaren zati txikietatik lortutako eta *ex vivo* kultibatutako linboko zelula ama epitelialen transplantea da. Hala ere, terapia honen arrakasta-tasak asko hobetu daitezke oraindik, askotan errepikatu egin behar izaten baita.

Beraz, kornea-ehuna birsortzea beharrezkoa da LZAG, EAI-en eta korneako ultzeren kasuetan ikusmen-funtzioa berrezartzeko, eta tratamendu eraginkor berriak behar dira egungo terapiekin lotutako zailtasunei aurre egiteko. Testuinguru horretan, korneako estroma imitatuko luketen hidrogel biobateragarriak erabiltzeak eta ehunak konpontzeko mekanismo biologikoak bermatuko lituzketen molekula bioaktiboekin funtzionalizatuta egoteak, EAI-k edo estromako ultzerak dituzten pazienteen begietako osasuna eta propietate bisualak lehengoratuko lituzke.

Gainera, LEZA/P-en hazkuntza sustatzen duten eta jatorrizko kornearen konposizioa eta anatomia antzeratzen duten kornea-ordezkoek, alternatiba terapeutiko eraginkorra eskainiko lukete LZAG-a duten pazienteetan transplantatzeko. Hauek emaileen kornea-erabilera murriztuko lukete eta paziente bakoitzaren ezaugarri kliniko espezifikoak beteko lituzkete.

2. Helburuak

Tesi honen helburu nagusia jatorrizko korneako zelulaz kanpoko matrizearen antzeko ezaugarriak dituen hidrogel bat garatzea eta honen egitura, erreologia, propietate optikoak, farmakozinetika eta biobateragarritasuna aztertzea izan da. Hidrogela, EAI-en kasuan kornea birsortzeko beharrezkoak diren prozesu fisiologiko eta zelularrak errazten dituzten molekula bioaktiboekin funtzionalizatu dugu. Gainera, LEZA/P-en hazkuntza primarioak ere karakterizatu ditugu, haien ama izatea babesteko baldintzak optimizatu eta LZAG kasuetarako etorkizunean sortuko diren kornea-ordezkoetan txertatzeko.

Horretarako, helburu espezifiko hauek zehaztu ditugu:

1. Hidrogelak sintetizatu eta funtzionalizatzeko material ezberdinen propietate fisiko-kimikoen eta bateragarritasunaren karaterizazioa.
2. Hidrogelaren funtzionalizazioa, kornearen birsorkuntza sustatzen duten eta hantura kontrolatzen duten hainbat osagai bioaktibo gehituz.
3. Hidrogelean txertatutako osagaien askapen zinetika eta efektu terapeutikoa *in vitro* ebaluatzea.
4. Funtzionalizatutako hidrogelaren efektu terapeutikoaren ebaluazioa behi eta untxi-korneen *ex vivo* ereduetan eta *in vivo* untxi-korneetan.
5. Giza ehun esklerokornealen eta giza korneako zelulen hazkuntza primarioen azterketa immunohistokimiko eta immunozitokimikoa, linboko nitxoan dauden populazio ezberdinak eta LEZA/P-en ezaugarriak zehazteko.

III. MATERIALAK ETA METODOLOGIA

1. Biomaterialen karakterizazioa

1.1. Biofilmen sintesia

Lehenik eta behin, izaera proteikoko 4 biofilm garatu genituen, biomaterial horiek kornea-ingeniaritzako aplikazioetarako eduki zezaketen potentziala aztertzeko.

Kolagenozko filmak txerri larruazaletik eratorritako kolagenoa (Tenerias Omega, Nafarroa, Espainia), glizerola (pisatutako kolageno lehorraren pisuarekiko % 20-a) (Panreac, Bartzelona, Espainia) eta 0,05 M azido azetiko (kolageno/azido azetiko proportzioa 1:1) nahastuz prestatu genituen. Sortutako nahasketak plastikozko poltsa batean sartu genituen 24 orduz giro-tenperaturan, lortutako orea hidrata zedin. Orea laborategi-prentsa batean sartu genuen (Specac, Bartzelona, Espainia), aldez aurretik 90 °C-tan berotutako aluminiozko bi plaken artean, eta ondoren minutu batez 0,5 MPa-eko indarrarekin prentsatu genuen kolageno-xaflak lortzeko. Kolageno xaflak KOL izenaz adierazi ditugu lan honetan.

Soja-proteina isolatuz egindako filmak, soja-proteina isolatua (SPI) (ADM Protein Specialties Division, Amsterdam, Herbehereak) eta glizerola (pisatutako SPI lehorraren pisuarekiko % 40-a) 5 minutuz nahastuz prestatu genituen. Nahasketa horiek aldez aurretik 120 °C-tan berotutako aluminiozko bi xaflen artean laborategiko prentsan sartu genituen, eta 2 minutuz 4 MPa-etara prentsatu genituen SPI izeneko filmak lortzeko.

Gelatina eta laktosaz egindako filmak arrain-azaletik eratorritako gelatina (Sigma Aldrich, St. Louis, MO, AEB) eta laktosa (pisatutako gelatina lehorraren pisuarekiko % 20-a) (Panreac, Bartzelona, Espainia) 30 minutuz ur destilatuan 80 °C-tara eta etengabe irabiatuz prestatu genituen. Ondoren, soluzioari glizerola gehitu (pisatutako gelatina lehorraren pisuarekiko % 20-a), eta 80 °C-tara beste 30 minutuz irabiatu genuen. Soluzioaren pH-a 10-era 0,1 M NaOH-rekin egokitu genuen. Azkenik, soluzioa Petri plaketan isuri eta 48 orduz giro tenperaturan lehortzen utzi genuen filmak lortzeko. Gainera, filmak 105 °C-tara 24 orduz berotu genituen, laktosarekin erretikulazioa gerta zedin. Lortutako film hauek GEL-LAK bezala izendatu ditugu lan honetan.

Gelatina eta azido zitrikoz osatutako filmak arrain-azaletik eratorritako gelatina, azido zitrikoa (pisatutako gelatina lehorraren pisuarekiko % 20-a) (Panreac, Bartzelona, Espainia) eta agarra (pisatutako gelatina lehorraren pisuarekiko % 10-a) (Panreac, Bartzelona, Espainia) ur destilatuarekin nahastuz prestatu genituen. Nahasketa 30 minutuz 80 °C-tara berotuz eta irabiatuz lortu genuen. Ondoren, glizerola (pisatutako gelatina lehorraren pisuarekiko % 20-a) gehitu eta disoluzioaren pH-a 10-era 0,1 M NaOH-rekin egokitu genuen. Berotze-prozedura hau errepikatu, nahasketa Petri plaketan isuri eta hauek giro-tenperaturan 48 orduz hozten utzi genituen azido zitrikoarekin erretikulatutako filmak lortzeko. Lortutako film hauek GEL-AZ bezala izendatu ditugu lan honetan.

1.2. Hidrogelen sintesia

Proteinetan oinarritutako lau biofilmak ebaluatu ondoren, gelatina hautatu genuen kornea-akatsak tratatzeko hidrogela garatzeko material nagusi gisa. Txerri-larruazaletik eratorritako gelatina (Sigma Aldrich, St. Louis, MO, AEB) erriboflabina fosfatoarekin (RFP, Sigma Aldrich, St. Louis, MO, AEB) erretikulatuz sortu genuen hidrogela. Erriboflabina klinikan korneako kolageno naturala saretzeko erabili ohi den fotoabiarazlea da.

Hidrogel honetan oinarriturik, 4 bertsio ezberdin garatu genituen bakoitzari konposatu desberdin bat erantsiz, biobateragarritasun eta ebaluazio fisiko-kimikoaren azterketa gauzatzeko. Garatutako hidrogelak hurrengo hauek izan ziren: G izeneko hidrogela, % 5 p/bol gelatinaz eta % 0,01 p/bol RFP-z osatua; G-D izeneko hidrogela, % 5 p/bol gelatinaz, % 2,5 p/bol dextranoz (Pisu molekularra: 450-650 KDa, Sigma Aldrich, St. Louis, MO, AEB) eta %0,01 p/bol RFP-z osatua; G-AH izeneko hidrogela, % 5 p/bol gelatinaz, % 0,4 p/bol azido hialuronikoz (Pisu molekularra: 1,01-1,80 MDa, Lifecore Biomedical, Chaska, MN, AEB) eta % p/bol 0,01 RFP-z osatua; eta G-MZ izeneko hidrogela, % 5 p/bol gelatinaz, % 1 p/bol metilzelulosaz (Biskositatea: 1200-1800 cP, Sigma Aldrich, St. Louis, MO, AEB) eta % 0,01 p/bol RFP-z osatua (Konposatuen egitura kimikoak III.1 irudian ikus daitezke).

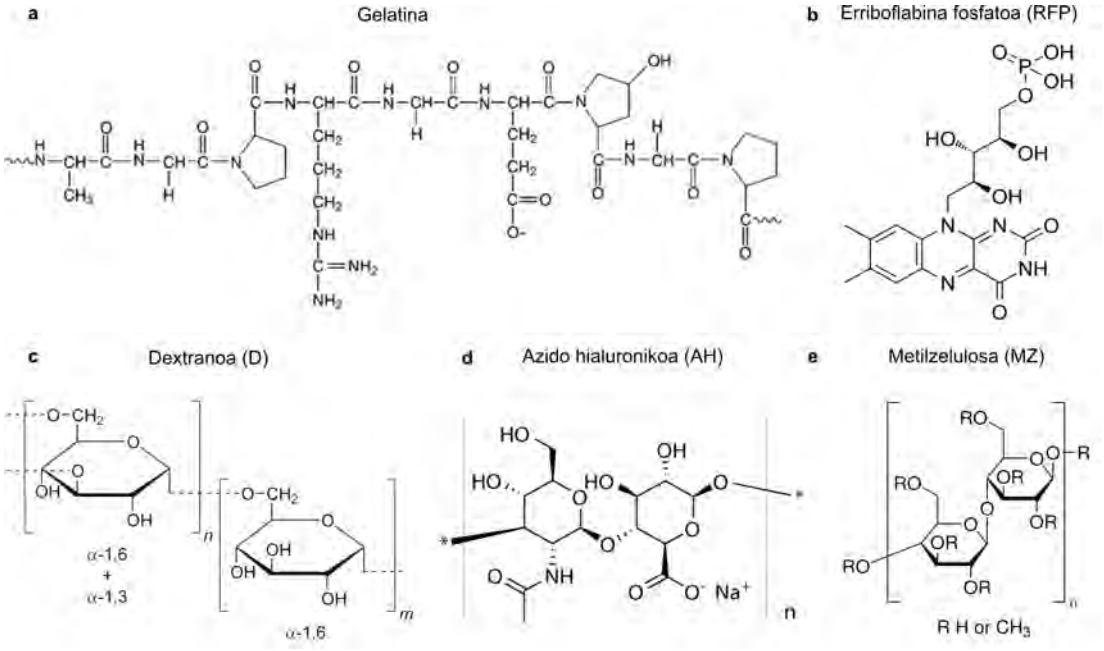

III.1. IRUDIA: Hidrogelen sintesirako erabilitako konposatuen egitura kimikoa. **a**) Gelatina, **b**) erriboflabina fosfatoa (RFP), **c**) dextranoa (D), **d**) azido hialuronikoa (AH) eta **e**) metilzelulosa (MZ).

Gelatinazko hidrogela (G), % 5 p/bol gelatina eta % 0,01 p/bol RFP ur destilatuan nahastuz eta soluzioa 80 °C-etan 30 minutuz irabiatuz prestatu genuen.

Dextrano edo azido hialuronikoarekin nahastutako gelatinazko hidrogelak (G-D eta G-AH), antzera prestatu genituen: % 5 p/bol gelatina eta % 0,01 p/bol RFP, % 2,5 p/bol dextrano edo % 0,4 p/bol azido hialuronikoarekin ur destilatuan nahastu eta 80 °C-tan irabiatu genituen 30 minutuz.

Metilzelulosarekin konbinatutako gelatinazko hidrogela (G-MZ), % 2 p/bol metilzelulosa (MZ) eta % 10 p/bol gelatina eta % 0,02 p/bol RFP soluzioen stock-ak 1:2 diluzioan nahastuz prestatu genuen. Soluzioa 80 °C-tara berotu eta etengabe pipeteatuz nahastu genuen, soluzio homogeneo bat lortu arte. Lehendabizi, % 2 p/bol MZ stock-a sortzeko, irabiagailu batean mantendu genuen 48 orduz, MZ erabat disolbatu arte. Gelatina eta RFP stock-a % 10 p/bol gelatina eta % 0,02 p/bol RFP ur destilatuan nahastuz eta soluzioa 80°C-etan 30 minutuz irabiatuz prestatu genuen.

Hidrogel guztien pH-a 1 M NaOH-rekin 7-ra egokitu genuen, soluzioak 0,22 μm-ko polietersulfonezko (PES) MILLEX® iragazkiak (Merck KGaA, Darmstadt, Alemania) erabiliz iragazi eta 4 °C-tan gorde genituen erabili arte.

Beharrezko tokian aplikatu ondoren, hidrogelak bi minutuz argi urdinarekin erretikulatu genituen, hidrogel moldagarriak lortu zirelarik (III.2 irudia). Led.C (Woodpecker Medical Dagoen, Guilin, Guangxi, Txina) erretikulazio lanpara erabili genuen argiztapen-iturri gisa (λ 420-480 nm).

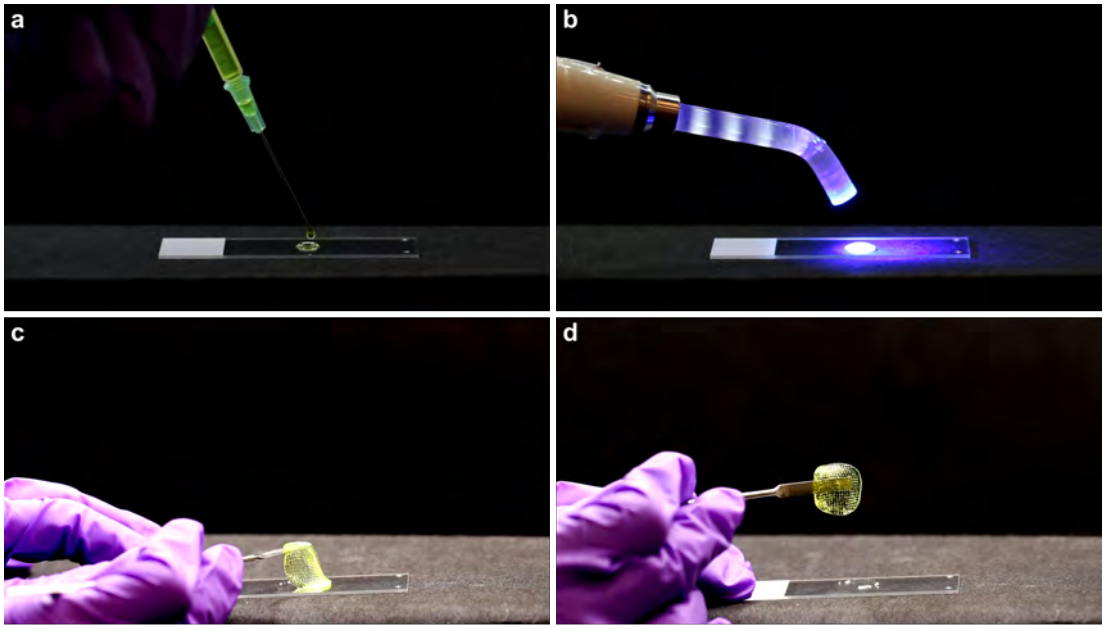

III.2. IRUDIA: Gelatina eta RFP hidrogelaren injekzio eta erretikulazio prozesua.

1.3. Fourierren transformatuaren bidezko espektroskopia infragorria (FTIR)

Fourierren transformatuaren bidezko espektroskopia infragorria (FTIR) biofilmen talde funtzional bereizgarriak eta konposizio kimikoaren osagaien arteko elkarrekintzak karakterizatzeko erabili genuen.

Neurketak Golden Gate MKII osagarria eta ATR (ingelesez, *Attenuated Total Reflectance*) elementu gisa diamantezko kristal bat zuen Nicolet Nexus FTIR (Specac, Bartzelona, Espainia) espektrofotometroa erabiliz burutu genituen, 45 °-tako intzidentzia-angelua eta ZnSe-zko lentea erabiliz. Guztira 32 ekorketa egin genituen, 4 cm^{-1}-eko bereizmenarekin eta 4000-850 cm^{-1} arteko uhin-zenbakietan.

1.4. X izpien difrakzioa (XRD)

X izpi bidezko difrakzio-analisia (XRD) biofilmen mikroegitura eta kristalinitatea aztertzeko erabili genuen, bai eta biomaterialen fase kristalinoak eta amorfoak bereizteko ere.

Azterketak 40 kV eta 40 mA-tan lan egindako PANalytical Xpert PRO (PANalytical, Madril, Espainia) difrakzio-unitatea erabiliz egin genituen. Erradiazioa Cu-Kα (λ = 1,5418 Å) iturritik sortu eta datuak 2 eta 90° tarteko 2θ balioetatik lortu genituen. θ laginarekiko X-izpien elektroi-sortaren eraso-angeluari deritzo.

1.5. Erreologia neurketak

Hidrogelen deformazioa, fluxua eta portaera likatsua erreometroan egindako oszilazio-saiakuntzen bidez ebaluatu genuen. Neurketak DHR-2 erreometroan (TA Instruments, New Castle, DE, AEB) 20 mm-ko diametroko horzdun plaka paralelo bat erabiliz egin genituen, urez betetako disolbatzaile-koska bat zuena, laginaren deshidratazioa saihesteko. Neurketa guztiak 25 °C-tara egin genituen, 500 μm-ko altuera tartearekin.

Laginen deformazio-portaera, 10 rad/s-ko maiztasunarekin egindako anplitude-ekorketen bidez ebaluatu genuen. Maiztasun-ekorketak, eremu biskoelastiko linealean (EBL) laginen denboraren araberako portaera deskribatzeko erabili genituen. Hauek, EBL-ren barruan oszilazio-deformazio konstante batekin (% 1) eta 0,1 eta 100 rad/s artean egin genituen. Bai anplitude zein maiztasun-ekorketetan 20 balio erregistratu genituen hamarkadako.

Fluxu-ekorketak deformazio abiadura altuetatik (100 s^{-1}) baxuetara (10^{-4} s^{-1}) egin genituen fluxuaren errendimendu orokorra karakterizatzeko.

Tentsioaren bidez kontrolatutako muga elastikoaren neurketak ebakidura-tentsio baxuetatik altuetara egin genituen, hamarkadako 10 balio erregistratuz.

Tartekatutako ebakidura neurketak 60 segundutako hiru ziklotan neurtu genituen, laginen sendatze ahalmena deskribatzeko. Deformazio abiadura baxua (0.1 s^{-1}) eta altua (10 s^{-1}) txandakatu genituen horretarako.

1.6. Puzte- eta hedatze-saiakuntzak

Hidrogelen bolumen eta azaleraren handitzea, puzte- eta hedatze-saiakuntzen bidez hidrogelak 24 orduz PBS-tan murgildu ondoren neurtu genituen.

Puzte portaera ebaluatzeko, 50 μl-ko hidrogel tantak beirazko estalkietan jarri genituen. Hidrogelak zituzten estalkien hasierako pisuak (W_i) erregistratu genituen PBS disoluzioan murgildu eta 34 °C-tan inkubatu aurretik.

24 ordu igaro ondoren, PBS-a kendu eta puztutako laginen pisuak (W_s) erregistratu genituen. Laginen puzte-maila III.1 ekuazioaren bitartez kalkulatu genuen.

$$S(\%) = \frac{W_s - W_i}{W_i} \times 100 \tag{III.1}$$

Hidrogelen hedapena hasierako azalerak (A_i) eta handitutako azalerak (A_s) neurtuz kalkulatu genuen ImageJ softwarearen bidez (Wayne Rasbandek garatua, Research Services Branch, National Institute of Mental Health, Bethesda, MD, AEB). Laginen hedapen-maila III.2 ekuazioren bidez kalkulatu genuen.

$$E(\%) = \frac{A_s - A_i}{A_i} \times 100 \tag{III.2}$$

Neurketa guztiak 3 aldiz errepikatu genituen.

1.7. Transmitantzia eta gardentasun saiakuntzak

Transmitantzia eta gardentasun saiakuntzak hidrogelen propietate optikoak ebaluatzeko egin genituen. Biomaterial bakoitzaren transmitantzia espektro ikusgarrian (400-800 nm) ebaluatzeko, biofilm bakoitzaren 3 mm-ko diametroko zatiak edo hidrogelen 100 μl 96 kikaradun hazkuntza-plaketan jarri genituen eta argiaren xurgapena ELx800 plaka-irakurgailuan (BioTek® Instruments, Winooski, VT, AEB) zehaztu genuen. Biofilmen egoera lehorrak zein hidratatuak eta erretikulatutako zein erretikulatu gabeko hidrogelak erabili genituen argiaren xurgapena zehazteko.

Plakakako kikara bakoitza 1× PBS-arekin (Sigma Aldrich, St. Louis, MO, AEB) bete genuen biofilm hidratatuen argi-xurgapena neurtzeko. PBS-z betetako kikarak kontrol gisa erabili genituen, eta kikara hutsak, berriz, biofilm lehorren xurgapen-balioetarako erreferentzia gisa. Neurtutako xurgapen-balioak transmitantzia-ehuneko bihurtu genituen III.3 ekuazioaren bidez.

$$\%T\ (Transmitantzia) = 10^{(2-xurgapena)} \tag{III.3}$$

Argiaren transmisioaz gain, gardentasuna kualitatiboki neurtu genuen, biofilmetatik 12 cm-tara jarritako argazki-patroi espezifikoak aztertuz eta hidrogel bakoitzaren 500 μl ezagut daitekeen hitz-patroi baten gainean jarriz.

1.8. Biodegradazio saiakuntza

Biodegradazio-probak biofilm bakoitzak jasandako degradazio hidrolitikoa eta entzimatikoa zehazteko egin genituen. Hasieran pisatutako (W_0) lagin lehorren (6 mm $\times$ 6 mm-tako zatiak) zatiak 200 μg/ml A kolagenasa (Roche, Mannheim, Alemania) soluzioan eta 37 °C-tan inkubatu genituen denbora-tarte ezberdinetan (15 min, 30 min, 1 h, 2 h, 4 h eta 24 h). Neurketa-denbora bakoitzean, laginak atera, liofilizatu eta pisatu genituen (W_t). *In vitro* degradazio hidrolitikoa ere ebaluatu genuen, laginak entzimarik gabeko PBS-etan inkubatuz. Ur destilatuan sartutako biofilmak kontrol gisa erabili genituen. Denboran zeharreko degradazio-ehunekoa pisu-galera kontuan hartuta eta III.4 baliatuz kalkulatu genuen.

$$W(\%) = \frac{W_t}{W_0} \times 100 \tag{III.4}$$

Neurketa-denbora eta lagin bakoitzeko 3 neurketa egin genituen.

1.9. *In vitro* askapen saiakuntzak

Hidrogeletan 3 konposatu ezberdin kapsulatu genituen hauen *in vitro* askapen zinetika neurtzeko:

- FITC-z markatutako G immunoglobulina (IgG): Pisu molekular handiko konposatu gisa, Fluoreszeina Isotiozianato I isomeroarekin (FITC) (Sigma Aldrich, St. Louis, MO, AEB) markatutako eta 150 kDa-eko IgG arratoi antigorputza (MP Biomedicals, Irvine, CA, AEB) erabili genuen. Antigorputza 1 mg/ml-ko kontzentrazio finalarekin kapsulatu genuen.
- FITC-z markatutako albumina: FITC-z markatutako eta 66 kDa-eko albumina proteina (Sigma Aldrich, St. Louis, MO, AEB) pisu molekular ertaineko konposatu gisa erabili genuen. Albumina hidrogelean sartu genuen 1 mg/ml-ko kontzentrazio finalarekin.
- Vigamox: Pisu molekular txikiko konposatu gisa Vigamox (Novartis, Bartzelona, Espainia) moxifloxazino soluzio oftalmikoa erabili genuen. Konposatu honek 0,44 kDa-ko pisu molekularra du eta begiko infekzio bakterianoak tratatzeko erabiltzen da. Vigamox-a 1 mg/ml-ko kontzentrazio finalarekin kapsulatu genuen.

Hidrogeletako konposatuen askapena fluoreszentzia- eta xurgapen-balioen bidez neurtu genuen. Lagin bakoitza prestatzeko, hidrogel bakoitzaren 100 μl injektatu genituen beirazko hodi baten oinarrian. Hodi horren muturretako bat epoxiz zigilatu genuen hidrogela injektatu aurretik, hau jausi ez zedin. Ondoren, 400 μl PBS gehitu genituen hidrogel bakoitzaren goiko aldean, eta hodiak 34 °C-tan inkubatu genituen argitik babestuta. Inkubazioa 34 °C-tan gauzatu genuen begi-gainazalaren batez besteko tenperatura delako. Gainjalkinak ezarritako denbora-puntuetan bildu eta disoluzio-kantitate bera PBS berriarekin ordezkatu genuen. Jasotako laginak 96 kikaradun hazkuntza-plaketan sartu eta Synergy H1 (BioTek Instruments, Winooski, VT, AEB) plaka irakurgailuan aztertu genituen.

Askatutako Vigamox kantitatea zehazteko, absorbantzia 290 nm-tan neurtu genuen. Moxifloxazino soluzioak bere egitura kimikoaren eraztun aromatikoaren ondorioz xurgapen-gailur bat du 290 nm-tara. Propietate hau askatutako kontzentrazioak zehazteko erabil daiteke. IgG eta albuminak ordea, xurgapen-tontorrik erakutsi ez zutenez, konposatu hauek fluorokromo batekin uztartzea erabaki genuen. Hala, askatutako FITC-IgG eta FITC-Albuminaren bolumena kalkulatzeko, 485-520 nm-ko kitzikapen eta igorpen uhin luzeerekin egindako fluoreszentzia-neurketak erabili genituen. Esperimentuak lau aldiz errepikatu genituen. Karga bakoitzerako, metatze-askapenaren bolumena kalkulatu genuen 2 asteetan zehar. Ehunekoetan adierazitako balioak hasierako kargaren kontzentrazioa % 100 gisa hartuta kalkulatu genituen.

1.9.1. FITC markaketa

IgG arratoi antigorputza FITC-rekin markatzeko, antigorputza eta FITC, 0,1 M Na_2CO_3 disoluzioaren (pH 10) 12 ml-tan disolbatu genituen. FITC kantitatea bi konposatuen arteko erlazio molarra erabiliz kalkulatu genuen (III.5 ekuazioa).

$$FITC\ kantitatea\ = \frac{MW_{FITC}}{MW_{IgG}} \times 100 \tag{III.5}$$

Soluzioa ondo nahastu eta 4 °C-tan inkubatzen utzi genuen gau osoan. Ondoren, FITC soberakina ezabatzeko soluzioa Vivaspin® Turbo 15 PES iragazkiekin (Sartorius, Göttingen, Alemania) 3000g-tan zentrifugatu genuen 30 minutuz 6 aldiz, FITC soberakin guztia ezabatu arte.

1.10. Hidrogelen funtzionalizazioa

1.10.1. Giza mintz amniotikoa (GMA)-ren erauzpena

GMA emateko eta erabiltzeko baimen informatua lortu ondoren, karenak progamatutako fetu osasuntsuen zesareetatik lortu genituen. Aurretik, 1. eta 2. motako giza immunoeskasiaren (GIB) birusa, B eta C hepatitisa eta sifilia detektatzeko probak egin zitzaizkien emaileei.

Karenak ontzi esteriletan bildu genituen erditzearen ondoren. Ebakuntza-gelan, odol-koaguluak PBS garbiketekin kendu genituen lehenengo. Garbitu ondoren, amniosa, haurdunaldian barrunbe amniotiko osoa inguratzen duen karenaren mintzik barnekoena, arreta handiz askatu genuen korionetik. Bi mintzak banandu ondoren, GMA nitrozelulosazko iragazki esterilizatuetan (Merck KGaA, Darmstadt, Alemania) kokatu genuen 3 sekziotan errazago zatitzeko. Hala, mintz bakoitza 3 atal ezberdinetan banatu genuen: hurbileko amniosa (10 cm-ko zabalerako sekzioa), erdiko amniosa (10 cm-ko zabalerako sekzioa) eta urruneko amniosa (karenaren ertzeraino doana) (III.3 irudia).

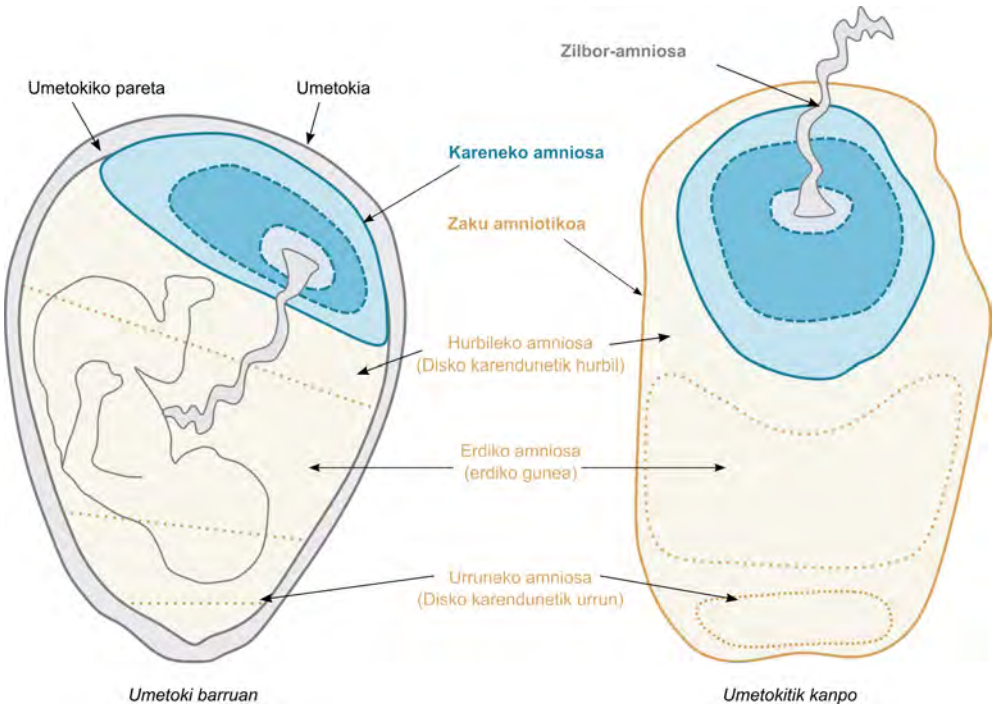

III.3. IRUDIA: Giza mintz amniotikoaren eskualdeen irudikapen eskematikoa umetokiaren barruan eta kanpoan. Kareneko amniosa (urdinez markatuta, karena estaltzen du), zaku-amniotikoko amniosa edo islatutako amniosa (laranjez markatuta, umetoki-pareta estaltzen du) eta zilbor-amniosa (grisez markatuta, zilbor-hestea estaltzen du). Zaku-amniotikoko amniosa 3 gunetan bana daiteke, disko karendunetik hurbilen dagoen gunea, erdiko gunea eta urruneko amniosa, disko karendunetik urrunen dagoen gunea. [332]-tik abiatuta moldatutako irudia.

Amnios zatiak 1,25 μg/ml B anfoterizinaz (Gibco, Paisley, Erresuma Batua), 50 μg/ml penizilina-estreptomizinaz (Sigma Aldrich, St. Louis, MO, AEB) eta 50 μg/ml neomizinaz (Gibco, Paisley, Erresuma Batua) osatutako DMEM (Lonza Bioscience, Basilea, Suitza) soluzioz betetako ontzietan garraiatu genituen. Ontziak behar bezala etiketatu genituen GMA-ren eskualdeari buruzko informazioarekin.

Laborategian, GMA bakoitzeko eremuak (urrunekoa, erdikoa eta hurbilekoa) 4-4,5 $\times$ 4-4,5 cm-ko zatitan moztu genituen. Zati bakoitzean gera zitezkeen odol-koaguluak garbiketen bidez eta pintzekin eskuilatuz kendu genituen. Antibiotikodun DMEM soluzioarekin 5 minutuz 2 aldiz garbitu genituen lehenengo, eta beste 2 aldiz 5 minutuz gehigarririk gabeko DMEM soluzioarekin.

Kolirioa prestatzeko laginak PBS esterilarekin garbitu eta -80 °C-tan gorde genituen 5 ml-ko Eppendorf hodietan erabili arte.

1.10.2. Giza mintz amniotikoko estraktuen (GMAe) prestakuntza

-80 °C-tan biltegiratutako GMA zatiak zituzten Eppendorf hodiak nitrogeno likidotan sartu genituen 5 minutuz, laginak gogortzeko. Ondoren, lagin bakoitza -80 °C-tara hoztutako zaparri batean birrindu genuen hauts fin bat lortu arte. Lortutako hautsa pisatu eta 5 ml/g proteasa-inhibitzaile koktela (P8340, Sigma Aldrich, St. Louis, MO, AEB) zuen 3 ml PBS-tan berreseki genuen 5 ml-ko Eppendorf hodi batean.

Lagin-hodiak izotzetan jarri eta 20 minutuz sonikatu genituen % 90-eko anplitudearekin, 15 segundu eta 15 segunduko errekuperazioarekin. Ondoren, laginak 3000g-tan 4 °C -tara zentrifugatu genituen 10 minutuz eta gainjalkinak jaso genituen. Azkenik, laginak 0,22 μm ko MILLEX® iragazkien bidez iragazi, 0,2 ml-ko hodietan banatu eta -80 °C-tan biltegiratu genituen erabili arte.

1.10.3. Odol-eratorrien prestakuntza

Odoletik eratorritako konposatuak hidrogelak funtzionalizatzeko aukeratu genituen. *In vitro* saiakuntzetarako giza emaileen odol eratorriak erabili genituen, *in vivo* saiakuntzetan aldiz untxien laginak erabili genituen.

1.10.3.1. Giza emaileen odol-eratorriak

In vitro saiakuntzetan erabilitako hidrogeletan kapsulatutako odol eratorriak, 25-60 urte bitarteko emaile osasuntsuen odoletik atera genituen. Emaileek baimen informatua sinatu ondoren, Helsinkiko adierazpenari jarraituz eta Euskal Herriko Unibertsitateko UPV/EHU-ko Gizakiekin lotutako Ikerketetarako Etika Batzordearen (GIEB) aldeko txostenarekin, odola benopuntzio bidez atera genuen. Emaile bakoitzaren odol-bolumen osoa bi zati berdinetan banatu genuen, metodo desberdinen bidez bi produktu lortzeko:

- Serum autologoa (SA): Odola gel banatzailea zuten 5 ml Vacutainer® hodietan (BD, Franklin Lakes, NJ, AEB) bildu, hodiak giro-tenperaturan 2 orduz koagulatzen utzi eta 1000g-tara 15 minutuz zentrifugatu genituen. SA prozesu honetatik lortutako gainjalkinari deitu genion.
- Hazkuntza faktoreetan aberatsa den plasmatik eratorritako seruma (sPRGF): Odola % 3,8 sodio zitratoa antikoagulatzaile gisa zuten 5 ml-ko Vacutainer® hodietan (BD, Franklin Lakes, NJ, AEB) bildu, hodiak 460g-tara 8 minutuz zentrifugatu eta leukozitoen frakzioaren gaineko gainjalkinak jaso genituen. 22,8 mM-ko kontzentrazio finala lortzeko 50 μl/ml kaltzio kloruro (B. Braun, Melsungen, Alemania) gehitu genizkion hodi bakoitzari, sodio zitratoa neutralizatzeko eta koagulazio kaskada aktibatzeko. Hodiak 2 orduz 36 °C-tan inkubatu genituen, plaketen aktibazioa eta hazkuntza faktoreen askapena sustatzeko. sPRGF prozesu honetatik lortutako gainjalkinari deitu genion.

SA eta sPRGF laginak 0,22 μm ko MILLEX® iragazkien bidez iragazi, alikuotatu eta -80 °C-tan biltegiratu genituen erabili arte.

1.10.3.2. Untxien odol eratorriak

2 kg inguruko *New Zealand White* untxiak erabili genituen *in vivo* saiakuntzarako odol eratorriak lortzeko. Saiakuntzak Euskal Herriko Unibertsitateko animaliategi zerbitzu orokorrean (Sgiker) egin genituen, UPV/EHU-ko Animaliekin egiten den Esperimentaziorako Etika Batzordeak (AEEB) onartutako prozedura esperimentalak jarraituz.

Untxi-odola prozesatzeko metodoak giza odolarekin izandako esperientzian eta bibliografian argitaratutako saiakuntzetan oinarrituta garatu genituen.

Untxia lidokainarekin anestesiatu ondoren, odola arteria aurikular zentraletik jaso genuen seruma bereizteko polimero-gela zuten Vacutainer® hodietan (BD, Franklin Lakes, NJ, AEB). Odola atera ondoren, laginak 2 orduz giro-tenperaturan koagulatzen utzi eta 1000g-tan zentrifugatu genituen 15 minutuz. SA prozesu honetatik lortutako gainjalkinari deitu genion. SA 0,22 μm ko MILLEX® iragazkien bidez iragazi, alikuotatu eta laginak -80 °C-tan biltegiratu genituen erabili arte. SA untxietatik lortutako odol eratorri bakarra izan zen.

1.10.4. Hazkuntza faktoreen kuantifikazioa

SA, sPRGF eta GMAe laginetako hazkuntza faktoreak saiakuntza immunoentzimatikoen (ELISA) edo Luminex teknologiaren bidez kuantifikatu genituen.

ELISA (ingelesetik, *Enzyme-Linked ImmunoSorbent Assay*) lagin bateko analito espezifikoak detektatzeko eta kuantifikatzeko erabiltzen den sentikortasun handiko saiakuntza biokimikoa da, antigorputzak, antigenoak, proteinak edo konplexu biomolekularrak detektatzen dituena.

ELISA saiakuntzak antigeno-antigorputz interakzio espezifikoetan oinarritzen dira emaitza neurgarri bat sortzeko. Antigenoa azalera solido batean immobilizatzen da, modu zuzenean edo ez-zuzenean, atzemate-antigorputz espezifiko baten bidez. Ondoren, detekzio-antigorputz primario bat gehitzen da antigeno-antigorputz konplexu bat osatzeko. Detekzio-antigorputzaren inkubazioaren ondoren, aske geratutako materiala blokeatu egiten da animalia-proteinak erabiliz, hala nola behi-seroalbumina (BSA), berariazko antigorputzak plakari lotzea saihesteko. Ondoren, detekzio-antigorputza molekula detektagarri batekin markatzen da, entzima edo fluoroforo batekin adibidez (ELISA zuzena), edo markatutako bigarren mailako antigorputz batekin (ELISA ez-zuzena). Plakan aske geratutako material guztia inkubazio urratsen artean egindako tanpoi bidezko garbiketen bidez kentzen da. Azkenik, seinalea antigenoa detektatu eta kolorea sortzen duen substratu bat gehituz neurtzen da, eta haren balioa laginean dagoen antigeno kopuruarekiko zuzenki proportzionala da [333].

Intereseko hazkuntza faktoreak sandwich motako ELISA saiakuntzen bidez detektatu genituen. Saiakuntza horietan, intereseko antigenoa atzemate-antigorputz baten eta detekzio-antigorputz primarioaren artean tartekatzen da aldez-aurretik.

Detekzio-antigorputzen inkubazioaren ondoren, entzimekin lotutako antigorputz sekundarioa gehitzen zaio. III.1 taulak molekula bakoitzerako erabilitako kit espezifikoak jasotzen ditu. Saiakuntzak fabrikatzailearen protokoloari jarraiki egin genituen.

III.1. TAULA: Hazkuntza faktoreak kuantifikatzeko erabilitako ELISA saiakuntzen zerrenda.

Hazkuntza faktorea	Erreferentzia	Fabrikatzailea
Glia-lerro zelularretik eratorritako faktore neurotrofikoa (GDNF)	Ab100525	Abcam
Garunetik eratorritako faktore neurotrofikoa (BDNF)	E-EL-H0010	Elabscience
Epitelio pigmentariotik eratorritako faktorea (PEDF)	EH1048	FineTest (FineBiotech)
P Substantzia (SP)	EH4245	FineTest (FineBiotech)
Intsulina antzeko hazkuntza faktorea 1 (IGF-1)	ELH-IGF1	RayBiotech
Nerbio hazkuntza faktorea (NGF)	HEA105Hu	Cloud-Clone
Interleukina 1β (IL-1β)	HSLB00D	R&D Systems
Fibroblastoen hazkuntza faktorea 7 (FGF7)	SBRS0581	Assay Genie

SA, sPRGF eta GMAe laginen hazkuntza faktoreetako batzuk kuantifikatzeko Luminex teknologia erabili genuen. Sistema hau sandwich motako ELISA-ren printzipio berean oinarritzen da, baina Luminex saiakuntzek fluoreszentziaz markatutako mikroesferak erabiltzen dituzte analitoak atzemateko, zeinak zitokina anitzak aldi berean detektatzea ahalbidetzen duten (bi metodoen deskribapen grafikoa III.4 irudian ikus daiteke). Saiakuntzak Luminex tresna berezian irakurtzen dira. Laser batek detektatutako analitoa mikroesfera motaren arabera sailkatzen du lehendabizi, eta bigarren laser batek aldiz, lotutako analitoaren kantitatea zehazten du.

Human Angiogenesis/Growth Factor Panel 1 kita (HAGP1MAG-12K, Merck KGaA, Darmstadt, Alemania) hazkuntza faktore epidermikoa (EGF), fibroblastoen hazkuntza faktorea 2 (FGF2) eta hepatozitoen hazkuntza faktorea (HGF) kuantifikatzeko erabili genuen. Laginak 96 kikaradun hazkuntza plaka batean kargatu genituen. Kikara bakoitzari, Luminex mikroesferen nahasketaren laginaren adinako bolumena gehitu eta plaka gauez 4 °C-tara inkubatu genuen. Ondoren, mikroesferak 200 μl garbiketa-tanpoiarekin 3 aldiz garbitu eta 25 μl antigorputz biotinilatuarekin inkubatu genituen ordubetez giro-tenperaturan, fabrikatzailearen protokoloa jarraituz. Inkubazio honen ostean, mikroesferak 25 μl estreptabidina-fikoeritrina (PE) konjugatuarekin nahastu, 3 aldiz 200 μl garbiketa-tanpoiarekin garbitu eta 100 μl herrestatze-likidotan berreseki genituen. Azkenik, Luminex-200™ (Merck KGaA, Darmstadt, Alemania) tresna eta xPONENT® software-a (Merck KGaA, Darmstadt, Alemania) erabiliz aztertu genituen.

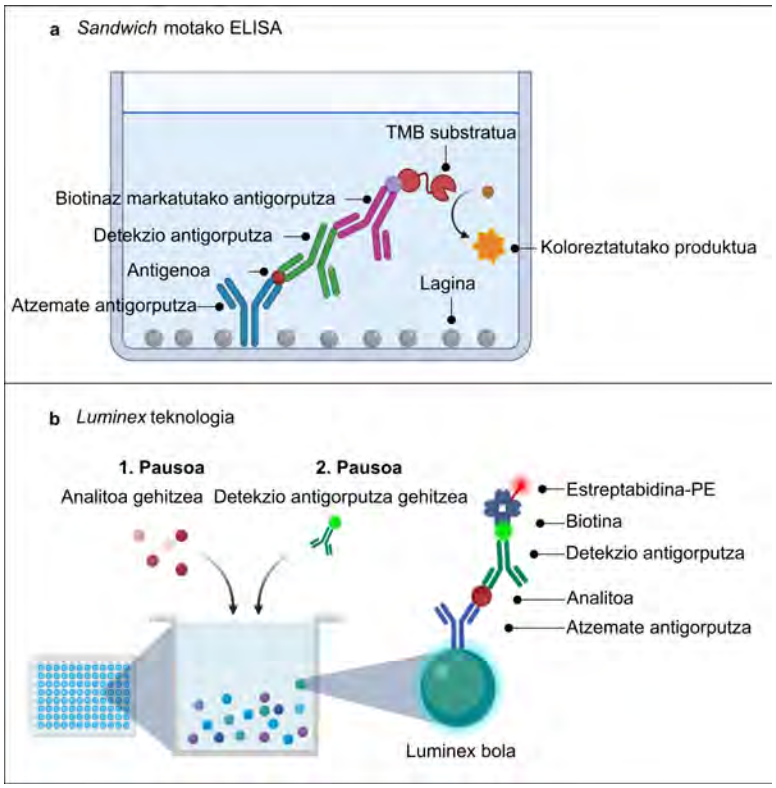

III.4. IRUDIA: **a**) Sandwich motako ELISA eta **b**) Luminex teknologiaren funtzionamenduaren irudikapen eskematikoa.

1.10.5. Funtzionalizatutako hidrogelen sintesia

Gelatina-RFP hidrogela hautatu ondoren, korneako zauriak orbaintzen laguntzeko hautagai gisa balio zezaketen 4 konposatu desberdinekin funtzionalizatu genuen. TNFα-ren aurkako Infliximab (Merck KGaA, Darmstadt, Alemania) 150 kDa-eko giza antigorputz monoklonala hanturari aurre egiteko agente gisa hautatu genuen. Zaurien orbaintze-prozesuaren sustatzaile gisa, odoletik eratorritako bi produktuak, SA eta sPRGF, zein GMAe, aukeratu genituen.

Funtzionalizatutako hidrogelak % 10 p/bol gelatina eta % 0,02 p/bol RFP stock soluzietatik hasita prestatu genituen. Antigorputzarekin kargatutako hidrogelak prestatzeko, 2 mg/ml Infliximab, % 10 p/bol gelatina eta % 0,02 p/bol RFP soluzio batekin nahastu eta ur destilatuarekin 1 mg/ml Infliximab, % 5 p/bol gelatina eta % 0,01 p/bol RFP kontzentrazio finaletara egokitu genituen.

SA-z, sPRGF-z edo GMAe-z funtzionalizatutako hidrogelak, % 10 p/bol gelatina eta % 0,02 p/bol RFP stock-a eta SA/sPRGF/GMAe 1:1-ko diluzioan nahastuz prestatu genituen. Hala, % 5 p/bol gelatina eta % 0,01 p/bol RFP-ren kontzentrazioak mantendu eta hidrogelak % 50 odol eratorri/GMAe-rekin aberastu genituen.

Hidrogel guztien pH-a 1 M NaOH-rekin 7ra egokitu, 0,22 μm ko MILLEX® iragazkien bidez iragazi eta 4 °C-tara biltegiratu genituen erabili arte.

2. Hazkuntza zelularrak

Hazkuntza zelularra, jatorrizko ehun-iturritik urrun dagoen ingurune fisiologiko egoki batean zelula eukariotoak edo prokariotoak mantentzea eta ugaltzea ahalbidetzen duten laborategiko tekniken zerrendari dagokio. Hazkuntza zelularren garapenak, oinarrizko zelulen biologia, farmako berrien toxikotasun-probak, terapia genikoa, gaixotasunen mekanismoak edo txertoen, antigorputzen eta terapien ekoizpena aztertzeko *in vitro* eredu-sistemak sortzeko balio izan du.

Hazkuntza zelularren barruan hiru eredu bereiz daitezke: zelula primarioak, zelula eraldatuak edo zelula autoberritzaileak. Zelula primarioak digestio mekaniko, kimiko edo entzimatiko bidez, zuzenean ehunetatik lortzen dira, jatorrizko ehunaren zelula motaren adierazgarri dira baina haien bizitza mugatua da. Zelula-lerroak, zelulen fenotipoa mantentzeko eta azterketa zelularrak ahalbidetzeko ingeniaritza genetikoko tresnen bidez eraldatu diren zelulak dira. Azkenik, zelula autoberritzaileak beste zelula-mota batzuetan bereiz daitezkeen eta epe luzera *in vitro* biziraun dezaketen zelula ama mota bati dagozkio.

Zelula mota guzti hauen hazkuntzak, baldintza esterilak, inkubazio-ingurune egokia eta funtsezko mantenugaien hornidura erregularra eskatzen du. Baldintza espezifikoak behar diren arren, zelulak 37 °C-tan eta % 5 CO_2-tan kultibatzen dira, eta hazkuntza-medio desberdina erabiltzen da zelula-mota bakoitzaren nutrizio-beharren edo azterketaren helburuaren arabera. Ingurunearen formulazio kimiko horrek karbohidratoak, bitaminak, aminoazidoak, mineralak, hazkuntza faktoreak eta hormonak ditu, pH-maila egokia mantentzen duen tanpoi batean.

2.1. Zelula lerroak

Ikerketa honetan, SV-40-rekin hilezkortutako giza korneako zelula epitelialak (KZE) eta NIH-3T3 fibroblastoen zelula lerro komertziala erabili genituen biobateragarritasuna ebaluatzeko (III.5 irudia). III.2 taulan, zelula-lerro bakoitza lortzeko erabilitako hazkuntza-medio eta baldintza zehatzak laburbiltzen dira.

III.2. TAULA: Erabilitako lerro zelularren, hazkuntza-medioen eta hazkuntza-baldintzen deskribapena.

Lerroa	Hazkuntza-medioa	% CO_2	Jatorrizko ehuna	Jatorria
KZE	DMEM:F12 1:1 (Lonza) + % 10 FBS (Gibco) + 2.5 mM glutamina (Sigma) + 50 U/ml penizilina/estreptomizina (Sigma) + % 0.5 DMSO (Sigma) + 5 μg/ml intsulina (Sigma) + 10 ng/ml EGF (Sigma) + 0.1 μg/ml koleraren toxina (Sigma)	% 5	Giza epitelio kornealetik eratorritako zelula lerroa	K. Araki-Sasaki doktoreak lagata
NIH-3T3	DMEM:F12 1:1 + % 10 FBS + 2.5 mM glutamina + 50 U/ml penizilina/estreptomizina	% 5	Saguen enbrioi fibroblastoen zelula lerroa	J. Sutherland doktoreak lagata

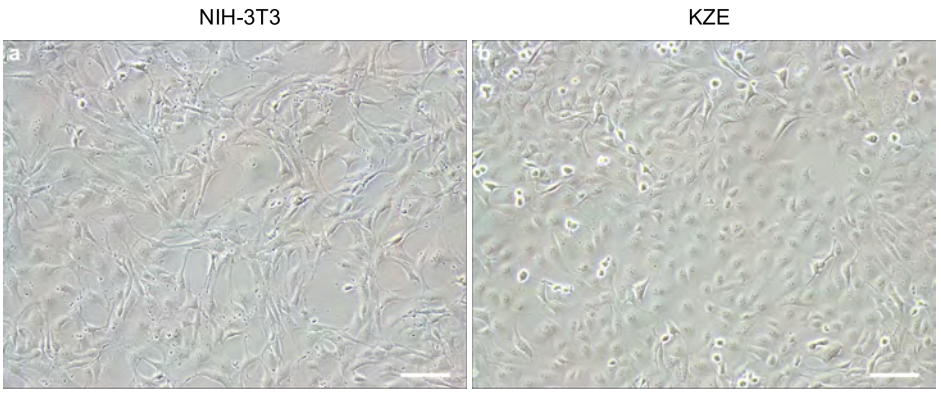

III.5. IRUDIA: **a**) NIH-3T3 fibroblastoen zelula lerroa eta **b**) KZE zelula lerroa. 10× handipen objektiboarekin ateratako irudiak. Eskala lerroek 100μm-ko neurriak adierazten dituzte.

2.1.1. Kriokontserbatutako zelulak desizoztea

Hazkuntza zelularra nitrogeno likidotan kriokontserbatutako zelulak desizoztuz hasi genuen. Zelulen hodia 37 °C-ko ur-bainu batean berotu genuen hau desizoztu zen arte. Zelula-esekidura 4 ml hazkuntza-mediorekin batera zentrifugazio-hodi esteril batera transferitu eta 300g-tan zentrifugatu genuen 5 minutuz giro-tenperaturan. Gainjalkina bota, zelulen pelleta 1 ml hazkuntza-mediotan berreseki eta medio kantitate egokia zuen hazkuntza-plakan erein genuen.

2.1.2. Zelulen hazkuntza

Zelulak % 80-ko konfluentziara heltzean kultibatu genituen. Hazkuntza-medioa kendu eta kultiboa PBS-rekin garbitu genuen, zelula-hondarrak eta zelula hilak baztertzeko. Ondoren, zelulak tripsina-EDTA (% 0,5 tripsina - % 0,2 azido etilendiaminotetraazetikoa) (Sigma Aldrich, St. Louis, MO, AEB) soluzio entzimatiko batekin 5 minutuz 37 °C-tara disoziatu genituen. Zelulak hazkuntza-plakatik askatuta zeudela egiaztatu ondoren, behi-serum fetala (FBS) gehitu genuen, substratua

asetzearen ondorioz tripsinaren jarduera inhibitzeko. Ondoren, zelula-esekidura 300g-tara 5 minutuz zentrifugatu genuen. Zentrifugazioaren ostean gainjalkina baztertu, zelulen pelleta 1 ml hazkuntza-mediotan berreseki eta plakaren tamainaren eta erein behar ziren plaka-kopuruaren arabera zelulak bolumen egokian diluitu genituen. Ereindako zelulen kopurua zelula-mota eta hazkuntza-plaka bakoitzerako doitu genuen, 2-3 egunean behin zelulen geruza konfluente bat lortzeko.

2.1.3. Zelulak izoztea

FBS-rekin tripsinizatu eta 300g-tara 5 minutuz zentrifugatu ondoren, zelulak izoztu genituen beharrezko kasuetan. Horretarako, gainjalkina baztertu, zelulak 1 ml hazkuntza-medioan berreseki eta hodian batutako zelula kopurua zehaztu ondoren, % 90 FBS eta % 10 dimetilsulfoxidoz (DMSO, Sigma Aldrich, St. Louis, MO, AEB) osatutako soluzio kriobabesle baten 1 ml-tan berreseki genituen zelulak. Zelula-hodi bakoitza zelulen pase-zenbakiarekin, zelula kopuruarekin eta datuen xehetasunekin etiketatu genuen, laborategiko zelulen biltegiko zerrendan behar bezala erregistratzeko. Zelula-hodiak Mr. Frosty delako edukiontzian (Thermo Fisher Scientific, Waltham, MA, AEB) gorde genituen -80 °C-tan 24 orduz, pixkanaka izoz zitezen. 24 ordu igaro ondoren, zelula-hodiak N_2 biltegiratze-depositura transferitu genituen.

2.1.4. Zelula-zenbaketa

Zelulen kopurua berriro erein edo izozteko urrats bakoitzaren aurretik zehazteko, tripan urdinarekin (Sigma Aldrich, St. Louis, MO, AEB) nahastutako zelula-esekiduraren alikuota bat hemozitometro edo Neubauer ganbera batera gehitu genuen. Neubauerren ganberan kargatutako laginaren zelulak, alderantzizko mikroskopio optikoa (Nikon, Tokio, Japonia) $100\times$ handipenekin erabiliz zenbatu genituen. Mililitro bakoitzeko zelula-kopurua III.6 ekuazioaren bidez kalkulatu genuen. Ekuazio horretan, M-k hemozitometroaren karratu bakoitzeko zenbatutako zelulen batez besteko kopurua adierazten du. Bolumenaren zuzenketa-faktorea, karratu bakoitzaren bolumena 10^{-4} ml-tik 1 ml-ra aldatuz kalkula daiteke.

$$Zelulak/ml = M \times diluzio\ faktorea \times 10^4 \tag{III.6}$$

Azkenik, erein beharreko zelulen kopurua erabilitako plakaren eremura egokitu genuen.

3. Giza korneetako zelulen erauzketa

Hilotzen kornea-ehunak, BSTN-tik (Nafarroako Odol eta Ehun Bankua), BST-tik (Banc de Sang I Teixits, Bartzelona, Katalunia, Espainia), Euskal Biobankutik (Gasteiz, Euskadi, Espainia) eta Biobanco A Coruña-tik (A Coruña, Galizia, Espainia) lortu genituen MTA akordioak jarraituz.

3.1. Emaileen ehun eta eraztun esklerokornealen disekzioa

Emaileen korneak Eusol-C (Alchimia, Ponte San Nicoló, Italia) biltegiratze-medioz betetako kornea-ganbera hoztuetan jaso genituen. Iritsi eta berehala, emaileen ehunak 20 mM HEPES (Gibco, Paisley, Erresuma Batua), 500 U/ml penizilina-estreptomizina eta 1,25 μg/ml anfoterizinaz osatutako Hank's soluzio batean garbitu genituen, biltegiratze medioaren edozein hondakin kentzeko. Garbitu ondoren, ehunak Stemi 305 disekzio mikroskopio estereoskopikoan (Zeiss, Oberkochen, Alemania) disekzionatu genituen, irisa, endotelioa, Tenonen kapsula eta konjuntiba kentzeko. Ehunak kontu handiz karrakatu genituen, pintza kirurgikoak eta belakiak erabiliz.

Ehunak erabat garbi eta prest izandakoan, ehun-ebaketetarako erabiliko ziren kornea bakoitzaren zatiak moztu eta ebaketa tenperatura optimoko (OCT, Sakura-Finetek, Alphen aan den Rijn, Herbehereak) konposatu-blokeetan jarri genituen. Blokeak -80 °C-tan biltegiratu genituen erabili arte.

Kornea bakoitzaren erdiko zatia kornea-eraztun periferikotik bereizi genuen 8,5 mm-ko puntzoi batekin. Ondoren, konjuntiba kendu genuen ehunetik leunki tira eginez eta konjuntiba korneatik bereizita zegoen oinarria moztuz. Kornea-eraztuna eta erdiko kornea erditik moztu genituen, ehunaren digestio entzimatikoa errazteko asmoz.

3.2. Ehunen digestioa eta zelulen erauzketa

Zelulen hazkuntzako laginak entzimatikoki digeritu genituen. Lagin bakoitza DMEM:F12 (Lonza Bioscience, Basilea, Suitza) eta % 5 FBS (Lonza Bioscience, Basilea, Suitza) medioan disolbatutako 2,4 U/ml dispasa II (Roche, Mannheim, Alemania) soluzioan sartu eta 2 orduz 37 °C-tan mantendu genuen epitelioa estromatik bereizteko.

Linbo eremuko epitelio zelula taldeak eta askatutako zelula isolatuak bildu, 10 minutuz 200g-tara zentrifugatu eta DMEM:F12-z, % 5 FBS-z, % 1 penizilina-estreptomizinaz, % 1 N_2 suplementuz (Thermo Fisher Scientific, Waltham, MA, AEB), 0,5 μg/ml hidrokortisonaz (Sigma Aldrich, St Louis, MO, AEB), % 0,5 DMSO-z, 8,4 ng/ml koleraren toxinaz (Gentaur Molecular Products, Brusela, Belgika) eta 2 ng/ml EGF-z (Sigma Aldrich, St Louis, MO, AEB) osatutako SHEM5 medioan berreseki genituen.

Dispasarekin digeritu gabeko estroma-ehunak 4 mg/ml A kolagenasa (Roche, Mannheim, Alemania) eta % 0,01 hialuronidasa (Sigma Aldrich, St Louis, MO, AEB) entzimen soluzioan 37 °C-tan mantendu genituen gau oso batez, estromako zelulak erauzteko. Hurrengo egunean, digeritutako ehuna espatula kirurgiko batekin karrakatu genuen, estromako zelula gehienak aska zitezen. Askatutako zelulak, digestio horretatik lortutako gainjalkinarekin batera, 200g-tara zentrifugatu genituen 10 minutuz, eta estromako zelulen medioan (DMEM:F12, % 10 FBS, 2,5 mM glutamina eta 50 U/ml penizilina-estreptomizina). berreseki genituen ondoren.

4. *In vitro* zitobateragarritasun eta biobateragarritasun saiakuntzak

4.1. MTT saiakuntza

(3-(4,5-dimetilthazol-2-il)-2,5-difenil tetrazolio bromuroarekin (MTT) egindako saiakuntzak filmen eta hidrogelen zitotoxikotasuna neurtzeko erabili genituen.

MTT saiakuntza kolorimetrikoa zelulen jarduera metabolikoaren neurketan oinarrituta dago. Metabolismo aktiboa duten zelulek, MTT konposatua formazan bihurtzen dute, zelulen barruan edo zelulen gainazalean metatzen den more koloreko produktu disolbaezina. Hildako edo metabolikoki aktiboak ez diren zelulek, MTT-formazan bihurtzeko ahalmena galtzen dute [334]. Neurtutako formazan kantitatea zelulen jarduera metabolikoaren mailarekiko proportzionala da, eta, aldi berean, zelula bizien kopuruarekin erlaziona daiteke.

Formazana disolbatzaile organiko batekin disolbatu eta sortutako kristal kopurua absorbantzia aldaketak neurtuz zehaztu daiteke. Zenbat eta handiagoa izan formazan-kristalen kopurua, dentsitate optikoa orduan eta handiagoa izango da eta, beraz, erregistratutako jarduera metabolikoa baita [335].

MTT saiakuntzak egiteko zelulak 96 kikaradun hazkuntza-plaketan erein genituen. Hasierako atxikipen zelularra ziurtatu ondoren (erein eta 12 ordura gutxi gorabehera), zelulak 16 orduz DMEM:F12 eta % 1 BSA (Sigma Aldrich, St Louis, MO, AEB) medioan mantendu genituen ziklo zelularrak sinkronizatzeko. Ondoren, medio hau saiakuntza bakoitzari zegokion hazkuntza-medioagatik ordezkatu genuen, urrats horretan saiakuntzaren hasierako denbora (t = 0 h) finkatuz. Kontrol positibo, negatibo, eta zuriak sartzeaz gain, tratamendu bakoitzeko 3 erreplika gehitu genituen. Tratamenduak, biofilm zatiak edo hidrogelak alegia, zegokion hazkuntza zelularraren medioarekin inkubatuz prestatu genituen, zelulak eta biomaterialak kontaktu zuzenean jartzeko. Hala, zelula mota bakoitzari zegokion hazkuntza-medioa gehitu ondoren, biofilm edo hidrogel zatiak gehitu genituen. Hidrogel zatiak kikaretara gehitu baino arinago 2 minutuz argi urdinarekin erretikulatu genituen.

Zelulen jarduera metabolikoa 0, 24, 48 eta 72 ordutan ebaluatu genuen. Inkubazio-aldi bakoitzaren ondoren, hazkuntza zelularrak 1× PBS-rekin garbitu eta DMEM:F12 medioan disolbatutako 100 μl 0,5 mg/ml MTT erreaktiboan (Sigma Aldrich, St Louis, MO, AEB) mantendu genituen 3 orduz % 5 CO_2-rekin eta 37°C-tara. MTT medioa kontu handiz kendu eta 100 μl DMSO gehitu genituen kikarako, formazan kristalak desegin zitezen. Dentsitate optikoak 570 nm-ko uhin luzera eta ELx800 mikroplaken irakurgailua erabiliz zehaztu eta tratamendu eta kontrolen arteko absorbantzi balioak alderatu genituen.

4.2. Zitotoxikotasun saiakuntza

Zelulen bideragarritasuna AM-Kaltzeina eta Etidio-1 homodimero (EthD1) tindaketa-saiakuntzaren bidez ebaluatu genuen. Saiakuntza hau azeto-metoxilo (AM)-Kaltzeina koloratzailearen zelulen xurgapen eta kobertsioan eta EthD1-ren atxikipenean oinarritzen da. AM-Kaltzeina esterasa-jarduera duten zelula bizietan fluoreszentzia berdea erakusten du, eta EthD1-k, mintza kaltetuta duten zeluletan sartu, hildako zelulen azido nukleikoekin elkartu eta fluoreszentzia gorri distiratsua sortzen du [336].

Zelulak biofilm edo hidrogelekin erein eta AM-Kaltzeina-EthD1® (Thermo Fisher Scientific, Waltham, MA, AEB) bideragarritasun/zitotoxikotasun-saiakuntza erabiliz, bizitako/hildako zelulen kopurua 24, 48 eta 72 ordutan zehaztu genuen. 2 μM AM-Kaltzeina eta 4 μM EthD-1 1× PBS-tan diluitu genituen saiakuntzaren soluzioa prestatzeko. Hazkuntza-medioa erretiratu, 1× PBS-rekin garbiketa bat

egin eta zelulak koloratzaile-disoluzioarekin 40 minutuz ingurune ilun batean eta giro-tenperaturan inkubatu genituen.

Inkubazioaren ondoren zelulen irudiak atera genituen fluoreszentziazko mikroskopio batekin (Olympus, Tokio, Japonia) eta automatikoki kontatu genituen ImageJ softwarra erabiliz. 3 erreplika egin genituen saiakuntza bakoitzeko eta zelularik gabeko biofilm edo hidrogelak erabili genituen kontrol zuri gisa.

4.3. Ziklo zelularraren analisia

Ziklo zelularraren analisia, hidrogelaren bertsio desberdinekin inkubatutako zeluletan DNA edukia kuantifikatzeko eta zikloan gerta daitezkeen aldaketak detektatzeko erabili genuen. Azido nukleikoak tindatzen dituen eta DNA zelularrari estoikiometrikoki lotzeko gaitasuna duen propidio ioduro (PI) fluoreszentea erabiliz, zelulen proportzioa zelula-zikloaren hiru interfaseetako bakoitzean (G0/G1 (2n), S (2n $\sim$ 4n) eta G2/M (4n) faseak, hurrenez hurren) zehaztu genuen. Neurketa hau tratamendu bakoitzarekin errepikatu genuen.

Zelulak aurretik deskribatu bezala tripzinizatu, 5 minutuz 300g-tara zentrifugatu eta 1 ml PBS-tan berreseki genituen. Prozesu hau bi aldiz errepikatu genuen egon zitezkeen medioen hondakinak kentzeko. % 70-eko etanol soluzio hotza tantaz tanta gehitzen joan ginen zelula-hodia irabiatu bitartean, zelulen finkapena ziurtatu eta hauen aglutinazioa saihesteko. Zelulak ordubetez 4 °C-tara inkubatu genituen ondoren. Behin finkatuta, zelulak zentrifugatu eta PBS-arekin 2 aldiz garbitu genituen, lehenengo zentrifugazioa 10 minutuz 1000g-ra eta bigarrena 5 minutuz 500g-tara eginez. Zelulen pelleta 250 μl 100 μg/ml RNasarekin (Thermo Fisher Scientific, Waltham, MA, AEB) tratatu genuen 15 minutuz 37 °C-tara, RNA ezabatu eta DNA bakarrik tindatuko zela ziurtatzeko. Azkenik, 10 μg/ml PI (Thermo Fisher Scientific, Waltham, MA, AEB) gehitu genizkion soluzio zelularrari, eta beste 15 minutuz 37°C-tara inkubatu genituen, argitik babestuta. PI-ren seinalea 488 nm-ko laserrarekin kitzikatuz eta Texas fikoeritrina (PE)/gorriaren kanalaren bidez detektatu genuen, 610/10 nm-ko banda-paseko iragazki batekin. Analisiak Gallios fluxu-zitometroarekin (Beckman Coulter, Brea, CA, AEB) egin eta datuak Kaluza 1.1 softwarearekin aztertu genituen (Beckman Coulter, Brea, CA, AEB).

4.4. Migrazio-saiakuntza

Biofilmen gaineko KZE eta 3T3 zelulen migrazioa aztertzeko, biofilmen gainean jarritako bi kikaradun insertoak (Ibidi, Gräfelfing, Alemania) erabili genituen. Silikonazko insertoak zelula-hazkuntzako bi kikaraz osatuta daude, definitutako zelularik gabeko espazio batez bereiziak. 20000 zelula kikara bakoitzean erein eta gau osoan utzi genituen filmen gainean atxiki eta monokapa bat osa zezaten. Insertoa kentzean zelularik gabe geratutako espazioa bi fronte zelularren arteko gehieneko azalera gisa erregistratu genuen (t = 0 h). Ondoren, 24, 48 eta 72 ordutan hartutako faseen kontrasteko irudi mikroskopikoen bidez migrazio zelularra kuantifikatu genuen. Distantziak, irudiak ImageJ programan prozesatuz kalkulatu genituen.

5. *In vitro* inflamazio saiakuntza

KZE zelulak, funtzionalizatutako hidrogelen *in vitro* inflamazioa murrizteko gaitasuna zehazteko erabili genituen. Horretarako, *in vitro* inflamazio-eredu bat ezarri genuen lehendabizi. Zelulak inflamatzeko metodorik eraginkorrena hautatu ondoren, saiakuntza hidrogel-tratamendu desberdinekin egin genuen.

5.1. *In vitro* inflamazio ereduaren ezarpena

Inflamazio eredua aukeratzeko, KZE zelulak TNFα (Abcam, Cambridge, Erresuma Batua) eta lipopolisakaridoarekin (LPS) (Sigma Aldrich, St. Louis, MO, AEB) kultibatu genituen. 400000 KZE zelula kikarako erein genituen p6 hazkuntza-plaka batean. 6 kikara 10 μg/ml LPS-rekin kultibatu genituen, horietako hiru KZE hazkuntza medioarekin eta beste 3-rak DMEM:F12 medioarekin. Halaber, 6 kikara 100 ng/ml TNFα-rekin inkubatu genituen, horietako hiru KZE hazkuntza medioarekin eta beste 3-rak DMEM:F12 medioarekin. KZE hazkuntza medioarekin kultibatutako 3 kikara eta DMEM:F12 medioarekin kultibatutako beste 3 kikara kontrol gisa erabili genituen. Tratamendu guztiak 24 orduz mantendu genituen kultiboan eta saiakuntzaren 3 erreplika egin genituen guztira.

5.2. *In vitro* inflamazio saiakuntza

KZE zelulak TNFα-rekin inflamatu eta funtzionalizatutako hidrogelekin tratatu genituen, hauek hantura murriz zezaketela egiaztatzeko.

p6 hazkuntza plaka baten kikarako 65000 KZE zelula erein eta 100 ng/ml TNFα soluzio batean inkubatu genituen 72 orduz, zelulak inflama zitezen. Kontrolak DMEM:F12 1:1, 2,5 mM glutamina (Sigma Aldrich, St. Louis, MO, AEB), 50 U/ml penizilina/estreptomizina, % 0,5 DMSO, % 0,5 FBS, 5 μg/ml intsulina (Sigma Aldrich, St. Louis, MO, AEB) 10 ng/ml EGF eta 0,1 μg/ml koleraren toxina zuen KZE hazkuntza-medioarekin kultibatu genituen.

Inkubazio-denboraren ondoren, inflamazio-estimuluak kendu eta zelulak 400 μl hidrogel eta aipatutako KZE hazkuntza-medioarekin kultibatu genituen 72 orduz. III.3 taulan probatutako hidrogelen konposizioa aurki daiteke.

III.3. TAULA: *In vitro* inflamazio-saiakuntzan erabilitako hidrogelen konposizioa.

Taldea	Tratamendua
H	% 5 p/bol gelatinaz eta % 0,01 p/bol RFP-z osatutako hidrogela.
H-Ag	% 5 p/bol gelatinaz eta % 0,01 p/bol RFP-z osatutako hidrogela, 1 mg/ml Infliximab-ekin funtzionalizatua.
H-SA	% 10 p/bol gelatinaz eta % 0,02 p/bol RFP-z osatutako hidrogela, 1:1 diluzioan gehitutako SA-rekin funtzionalizatua.
H-sPRGF	% 10 p/bol gelatinaz eta % 0,02 p/bol RFP-z osatutako hidrogela, 1:1 diluzioan gehitutako sPRGF-rekin funtzionalizatua.
H-GMAe P	% 10 p/bol gelatinaz eta % 0,02 p/bol RFP-z osatutako hidrogela, 1:1 diluzioan gehitutako hurbileko eremutik ateratako GMAe-rekin funtzionalizatua.
H-GMAe M	% 10 p/bol gelatinaz eta % 0,02 p/bol RFP-z osatutako hidrogela, 1:1 diluzioan gehitutako erdiko eremutik ateratako GMAe-rekin funtzionalizatua.
H-GMAe D	% 10 p/bol gelatinaz eta % 0,02 p/bol RFP-z osatutako hidrogela, 1:1 diluzioan gehitutako urruneko eremutik ateratako GMAe-rekin funtzionalizatua.
H-GMAe nahasketa	% 10 p/bol gelatinaz eta % 0,02 p/bol RFP-z osatutako hidrogela, 1:1 diluzioan gehitutako 3 eskualdeetatik lortutako GMAe-ren nahasketarekin funtzionalizatua.

TNFα-ren eraginpean inolako hidrogel tratamendurik gabe 6 egunez kultibatutako zelulak kontrol positibo gisa jarri genituen. Aldiz, KZE hazkuntza-medioarekin 6 egunez kultibatutako kikarak kontrol negatibo gisa balio izan ziguten. Lehenengo 72 orduetan KZE medioarekin kultibatutako zelulak, H, H-Ag, H-sPRGF eta H-GMAe taldeen eraginpean egon ziren hurrengo 72 orduetan, hidrogelek izatez hantura sor zezaketen ala ez ikusteko. Hala, 14 baldintza ezberdin probatu genituen guztira (TNFα-rekin estimulatutako 8 tratamendu, TNFα estimulurik gabeko 4 tratamendu, kontrol positibo bat eta kontrol negatibo bat) (III.1 irudia).

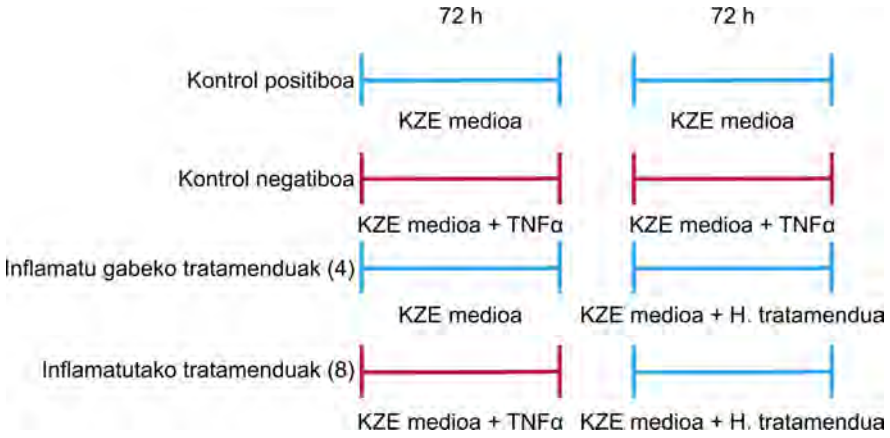

III.1. IRUDIA: *In vitro* inflamazio saiakuntzan erabilitako tratamenduen eskema.

6. *Ex vivo* begi eredua

Hiltegietatik lortutako behi- eta untxi-begiak *ex vivo* hazkuntza-eredu bezala erabili genituen. Proba hauek zuzeneko hidrogelaren aplikazioa optimizatzeko eta tratamenduaren biobateragarritasuna eta eraginkortasuna ebaluatzeko balio izan ziguten, *in vivo* saiakuntzaren aurreko urrats gisa.

6.1. *Ex vivo* prozedura kirurgikoa

Behi- eta untxi-begiak 1,25 μg/ml B anfoterizinarekin, 50 μg/ml penizilina-estreptomizinarekin eta 50 μg/ml neomizinarekin osatutako DMEM:F12 soluzioan garraiatu genituen hiltegietatik.

Laborategian, fluxu laminarreko kanpaian lan eginez, begiak % 10 iodopobidona soluzio batekin desinfektatu, PBS-rekin garbitu eta ehun eta koipe soberakinak labana kirurgiko eta guraize txikiekin kendu genituen (III.6 eta III.7 irudietako **a** eta **b**). Begi bakoitza gaza garbi batekin bildu (III.6 eta III.7 irudietako **c**), tinko eutsi eta kornearen erdialdea 8 mm-ko trepano batekin zauritu genuen estromaren erdiraino sakonduz (150-200 μm gutxi gorabehera). Ondoren, ebakitako epitelioa eta aurreko estromaren zatia baztertu genituen Crescent motako hortz batekin (III.6 eta III.7 irudietako **d**) eta korneak begi-globoetatik bereizi genituen (III.6 irudiko **e** eta III.7 irudiko **f**), gutxi gorabehera 1 mm-ko lodierako esklera ehuna utziz, linboa bere horretan mantentzeko.

Behi-korneak agarrezko moldeetan kokatu genituen. Hauek behien korneetako dimentsio anatomikoekin inprimatutako polidimetilsiloxanozko (PDMS) moldeetan fabrikatu genituen. Untxi-korneak 96 kikaradun hazkuntza-plaken gainean kokatu genituen epitelioa beherantz begira zutela, agar beroarekin bete eta gogortzen utzi genituen, agarrak kornearen forma har zezan. Bi kasuetan, agar-nahasketa % 2 agar soluzioa eta % 1 penizilina/estreptomizinaz aberastutako DMEM:F12 soluzioa 1:1 diluzioan nahastuz lortu genuen.

Korneak hazkuntza-plaketan jarri (60 mm-ko plakak behi-korneetako kasuan eta 30 mm-ko plakak untxien korneetarako), zauritutako eremuak hidrogelez bete eta argi urdinez (III.6 irudiko **f**) erretikulatu genituen. Ondoren, laginak SHEM5 hazkuntza-medioarekin inkubatu genituen 37 °C-tara eta % 5 CO_2-rekin. Kornea gainazalak egunero busti genituen hidratatuta mantentzeko eta hazkuntza-medioa bi egunetik behin aldatu genuen.

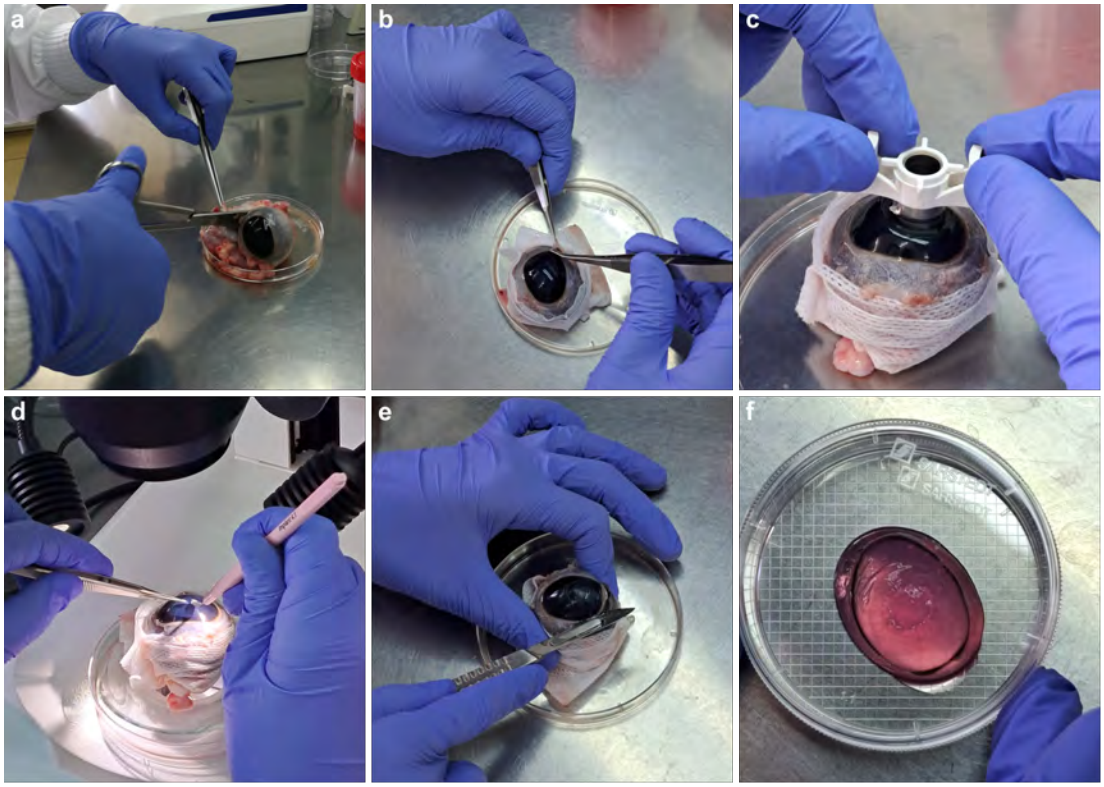

III.6. IRUDIA: *Ex vivo* eredurako behi-kornearen prozesamendua.

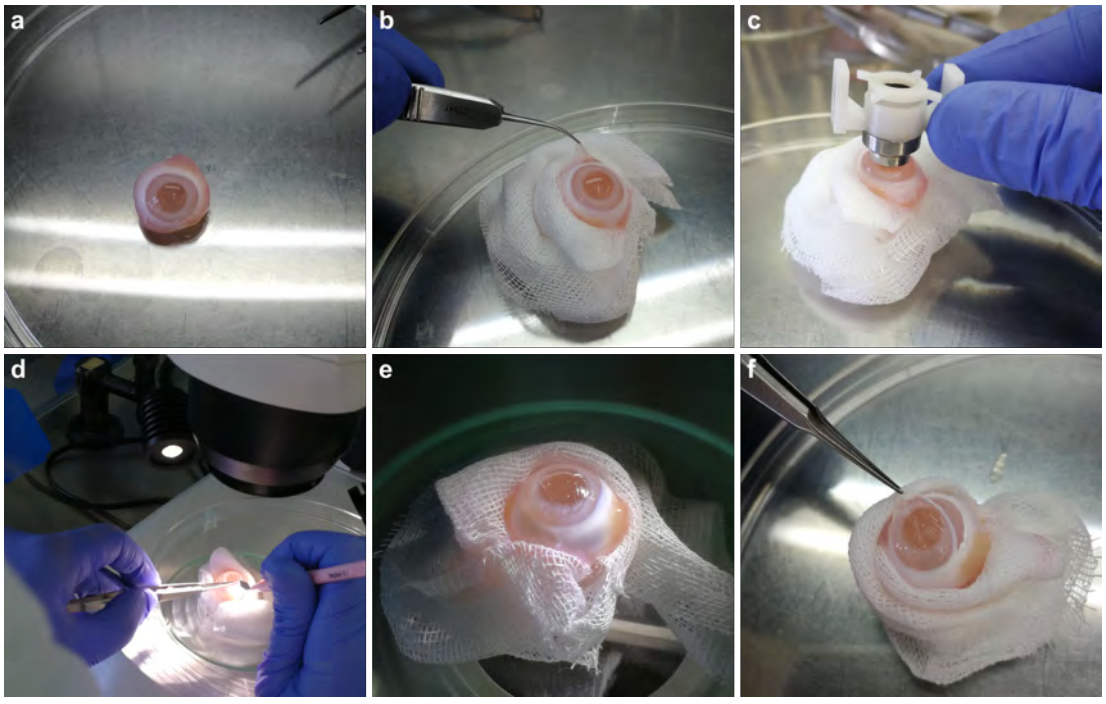

III.7. IRUDIA: *Ex vivo* eredurako untxi-kornearen prozesamendua.

7. Atxikidura proba

Gelatina eta RFP hidrogelaren atxikipen-propietateak zehazteko, 5 kg-ko karga-unitatez eta 3,5 mm-ko diametroko zunda zilindrikoz hornitutako TA.XT.Plus C (Aname Instrumentación Científica, Madril, Espainia) gailua erabili genuen, behi-korneak substratu biologiko gisa erabiliz. Neurketa honek, hidrogelaren eta kornea-gainazalaren arteko elkarreragina eta hidrogela behi-korneatik bereizteko beharrezko lana kuantitatiboki zehaztea ahalbidetu zuen.

Behi-korneetako zauriak *ex vivo* prozedura kirurgikoa jarraituz egin genituen. Behi-kornearen dimentsio anatomikoekin inprimatutako molde negatibo bat erabiliz, kornea eusteko eta proban zehar honen kurbadura mantentzeko parafina-blokeak fabrikatu genituen.

Kornea-parafina-euskarri multzoa, bi aldeko zinta itsaskorraren bidez zentratu eta gailuaren oinarrira itsatsi genuen. Hidrogel-lagin bakoitza 9 mm-ko diametroko zunda zilindrikoan jarri, eta 1 mm/s-ko abiadura konstantean jaitsiarazi genuen, kornea-gainazalera iritsi arte. Zunda 30 segunduz mantendu genuen kornea-gainazalarekin kontaktuan eta 0,2 N-ko indarrarekin. Denbora hori igaro ondoren, zunda abiadura berdinarekin (1 mm/s) hasierako posiziora altxatu genuen (III.8 irudia).

Zunda korneatik bereizteko denbora tarte horretan, kornea eta hidrogela bereizteko beharrezko indar-desplazamendu kurba erregistratu genuen. Texture Exponent 32 software-a (Stable Micro Systems, Godalming, Erresuma Batua) erabili genuen indar maximoa (Fmax) eta atxikitze-lana (Wadh) zehazteko, indar-desplazamendu kurbaren azpiko eremutik abiatuta. 3 erreplika egin genituen neurketako.

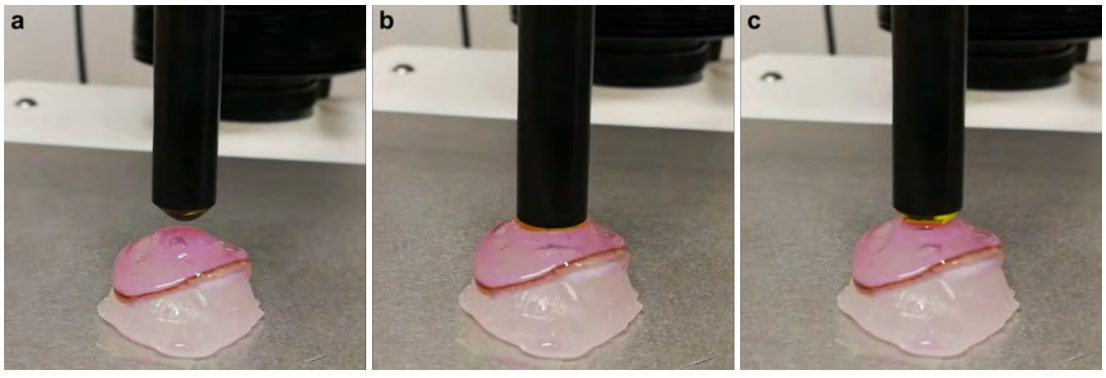

III.8. IRUDIA: Zunda zilindrikoaren korneako zauriarekiko desplazamendu bertikala.

8. *In vivo* begi eredua

In vivo saiakuntza hidrogelek korneako zaurien tratamendu gisa zuten ahalmena ebaluatzeko balio izan zigun.

Hala, *New Zealand White* motako 2 kg inguruko untxi emeak erabili genituen. Animaliekin egindako esperimentuak UPV/EHU-ko AEEB-k onartutako prozedura eta diseinu esperimentalak jarraituz egin genituen.

30 untxi ausaz banatu genituen 5 taldetan (n = 6 talde bakoitzeko), 4 azterketa-talde eta kontrol-talde bat (III.4 taula). Kontrol-taldea kirurgia egin eta zauria itxi arte % 0,2-ko AH-zko malko artifizialekin tratatutako untxiek osatu zuten.

III.4. TAULA: *In vivo* saiakuntzan erabilitako tratamenduen konposizioa.

Taldea	Tratamendua
Kontrola	% 0,2 AH-zko malko artifizialak 4 aldiz egunean zauria itxi arte.
H	50 μl % 5 p/bol gelatinaz eta % 0,01 p/bol RFP-z osatutako eta 2 minutuz argi urdinarekin erretikulatutako hidrogela + % 0,2 AH-zko malko artifizialak 4 aldiz egunean zauria itxi arte.
H-Ag	50 μl % 5 p/bol gelatinaz, % 0,01 p/bol RFP-z eta 1 mg/ml Infliximab-ez osatutako eta 2 minutuz argi urdinarekin erretikulatutako hidrogela + % 0.2 AH-zko malko artifizialak 4 aldiz egunean zauria itxi arte.
H-SA	50 μl % 10 p/bol gelatinaz, % 0,02 p/bol RFP-z eta SA-z 1:1 diluzioan osatutako eta 2 minutuz argi urdinarekin erretikulatutako hidrogela + % 0,2 AH-zko malko artifizialak 4 aldiz egunean zauria itxi arte.
H-GMAe	50 μl % 10 p/bol gelatinaz, % 0,02 p/bol RFP-z eta GMAe-z 1:1 diluzioan osatutako eta 2 minutuz argi urdinarekin erretikulatutako hidrogela + % 0,2 AH-zko malko artifizialak 4 aldiz egunean zauria itxi arte.

30 untxiak 10 untxiz osatutako 3 taldetan banatu genituen. Prozedura kirurgikoa 2 txandatan egin genuen 10 untxiko. Kirurgia animalia bakoitzaren eskuineko begian egin genuen lehenik (2 begi azterketa-talde bakoitzeko), astebetez tratatuz eta ebaluatuz. Medikazio topiko edo sistemikoen edozein arrasto ezabatzeko astebeteko epearen ondoren, prozedura bera errepikatu genuen ezkerreko begian. Ezkerreko begien ebaluazioaren ostean, animaliak hil eta korneak jaso genituen, histologia aldaketak eta hantura aztertzeko.

Beraz, *in vivo* azterketa 6 esperimentutan banatu genuen, esperimentu bakoitiak (E01/E03/E05) eskuineko begietan eta esperimentu bikoitiak (E02/E04/E06) ezkerreko begietan eginez.

E01 esperimentua azterketa pilotu gisa erabili genuen ondorengo esperimentuetako baldintzak eta prozedura kirurgikoa ezartzeko. Azterketa pilotu honetan, 5 untxi 25 μl % 0,1 benzalkonio kloruroarekin (BAK) (Sigma Aldrich, St. Louis, MO, AEB) eta 5 untxi 25 μl 50 μg/ml LPS-rekin tratatu genituen egunean behin kirurgia baino 3 egun lehenago zein kirurgia egunean, hantura estimulu gehigarri bat izan zezaten. 1.10.3.2 azpiatalean deskribatutako prozedura kirurgiko bera erabili genuen horretarako; hala ere, tarsorrafiaren ordez, lente babesle bat ezarri genuen tratatutako begietan. Untxiak 10 egunez ebaluatu genituen.

Proba pilotua ebaluatu ostean, ukipen-lenteen ordez tarsorrafia jartzea eta BAK edo LPS estimulua kentzea erabaki genuen. Halaber, ebaluazio-denbora 10 egunetik 7-ra murriztu genuen, zauri batzuen itxiera azkarra zela eta.

Beraz, E02tik E06ra, *in vivo* analisia egiteko 10 begi erabili genituen azterketa-taldeko, horietako 6 kirurgia egin eta 7 egunetara (ezkerreko begiak) eta horietako 4 kirurgia egin eta 21 egunetara (eskuineko begiak) batu genituelarik.

8.1. *In vivo* prozedura kirurgikoa

Kirurgia egin aurretik, untxiak 1 ml/kg ketamina (Ketolar® 50 mg/ml, Pfizer, Madril, Espainia) eta 0,3 ml/kg xilazina (Xylagesic 20 mg/ml, Laboratorios Calier SA, Bartzelona, Espainia) izterrean injektatuz anestesiatu genituen.

Aurreko estromako keratektomia egiteko, 6,5 mm-ko diametroko Hessburg-Barron motako trepanoa (Jedmed, St. Louis, MO, AEB) kornearen erdialdean jarri eta 187 μm inguruko lodieraraino sakonduz gauzatu genuen (III.9 irudiko **a**). Jarraian, Crescent motako hortz batez baliatuz (Alcon Laboratories, Bartzelona, Espainia), trepanoarekin markatutako eremua kornea osotik bereizi genuen (III.9 irudiko **b**). Zauria 32 °C-tan berotutako 50 μl hidrogelarekin bete eta 2 minutuz argi urdinarekin irradiatu genuen, hidrogelaren erretikulazioa gerta zedin (III.9 irudiko **c** eta **d**). Azkenik, E02-tik E06-ra arteko esperimentuetako korneetan tarsorrafia partzial bat egin eta 72 orduz mantendu genituen, animaliek zauria uki ez zezaten (III.9 irudiko **e** eta **f**) .

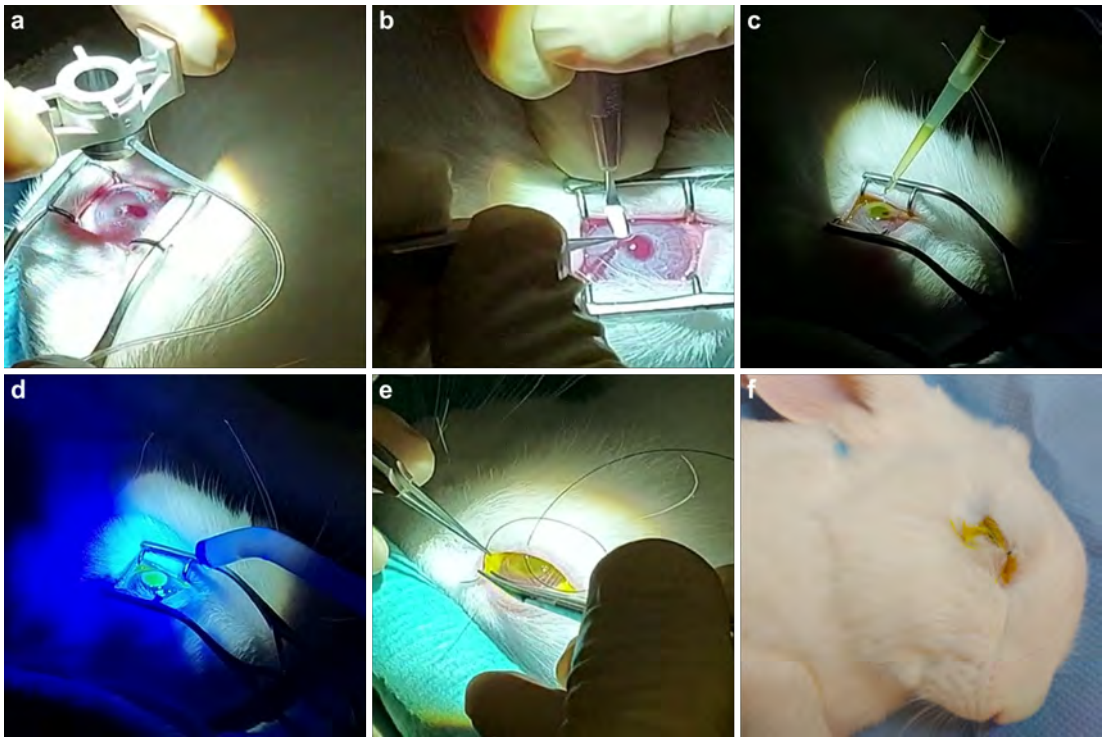

III.9. IRUDIA: *In vivo* prozedura kirurgikoa egiteko jarraitutako pausuak.

0,05 mg/kg buprenorfina (Buprecare, Ecuphar, Bartzelona, Espainia) kirurgia egin aurretik eta 12 ordutik behin injektatu genien untxiei, mina arintzeko analgesiko gisa, eta 3 mg/ml Tobrex (Novartis, Bartzelona, Espainia) tanta oftalmiko antibiotikoak instilatu genizkien begiko zauriak itxi ziren arte, infekzio-arriskua murrizteko. Halaber, % 0,2 AH malko artifizialak bota genizkien untxi guztiei, kontrolei barne, begiak heze mantentzeko. Begiak kirurgiaren egunetik (t = 0 egun) 7. egunera arte ebaluatu genituen.

Prozedura esperimentalaren amaieran, animaliak 2 ml/kg ketamina eta 0,6 ml/kg xilazina injektatuz anestesiatu genituen. Hiltzeko, belarriko zain marjinaletik 10 ml potasio kloruro saturatu injektatu genien. Heriotza *rigor mortis* ezaugarriak agertzeagatik berretsi genuen.

8.2. Korneako zaurien ebaluazio klinikoa

Untxien begi-erikortasuna Draizeren begietako toxikotasun akutuaren proba erabiliz eta arraildura-lanpara bidez aztertuz ebaluatu genuen *in vivo* [337]. Begietako narritadura kirurgiaren egunean (t = 0 egun) eta 1., 4. eta 7. egunetan ebaluatu genuen.

Draizeren probak begiaren aurreko segmentuan ikus daitezkeen aldaketekin lotutako sei parametro neurtu eta hauen balioak batzen ditu, kornea-opakutasunaren dentsitatea eta azalera, iritis maila, konjuntibaren gorritasun maila, edema eta muki-sekrezioa barne (III.5 taula). Begiko narritadura-indizea puntuazio guztien baturari dagokio, eta 0 eta 110 artekoa izan daiteke. Puntuazio altu batek, aztertutako konposatua begiarentzat narritagarria izan daitekeela adieraziko du.

Lortutako puntuazioaren arabera, produktu bakoitza narritadura-indizearen arabera sailkatzen da, Kay eta Kalandraren sailkapena jarraituz (III.6 taula, [338]).

Irisa eta konjuntiba ebaluatu genituen lehendabizi. Jarraian, kornea ebaluatu genuen, 5 μl % 2 Colicursí® Fluotest fluoreszeina begi tantak (Novartis, Bartzelona, Espainia) instilatuz eta begi-gainazala argi urdinez argiztatuz. Fluoreszeina aldi baterako koloratzailea da, eta, argi urdinarekin batera, korneako zauriak detektatzen laguntzen du.

Begi-gainazalean fluoreszeina aplikatzeak ere zauriaren itxieraren eboluzioa ikuskatzen lagundu zigun, egunero argazkiak ateraz. Argazkiak kirurgia egunean (t = 0 egun) eta 3. egunetik aurrera atera genituen, zauriak itxi arte. Tarsorrafia partzialaren ondorioz, zauriaren bilakaera ezin izan genuen 1. eta 2. egunetan erregistratu.

III.5. TAULA: Begiko zaurien larritasuna sailkatzeko Draize eskalaren puntuazio sistema. [337]-tik hartuta.

Ebaluazioa			Puntuazioa
KORNEA	A. Opakutasuna Dentsitate maila	Eremu lausoa; irisaren xehetasunak argi eta garbi ikus daitezke.	1
		Erraz bereizteko moduko eremu zeharrargiak; irisaren xehetasunak apur bat ilunduta.	2
		Eremu opaleszenteak; ez dago irisaren xehetasunik, ia ez da begi-niniaren tamaina bereizten.	3
		Opakoa; iris ikusezina.	4
	B. Kaltetutako kornea eremua	Laurden bat (edo gutxiago).	1
		Laurden bat baino gehiago, erdia baino gutxiago.	2
		Erdia baino gehiago, 3 laurden baino gutxiago.	3
		Hiru laurden baino gehiago, azalera osora arte.	4
			Puntuazioa = A × B × 5 (0-tik 80-ra)
IRISA	A. Argiarekiko erreakzioa	Tolesturak normalean baino gorago, hantura eta/edo injekzio zirkunkorneala; irisak argitan erreakzionatzen jarraitzen du (erreakzio motela positiboa da).	1
		Argiaren aurkako erreakziorik gabe, odoljarioa eta/edo suntsipen makroskopikoa.	2
			Puntuazioa = A × 5 (0-tik 10-era)
KONJUNTIBA	A. Betazaleko konjuntibaren gorritzea	Odol-hodien ohikoa baino gorritasun handiagoa.	1
		Lausoagoa, gorritasun biziagoa; banakako odol-hodiak ez dira erraz bereizten.	2
		Gorritasun lausoa.	3
	B. Hantura	Ohikoa baino hantura handiagoa (mintz niktitantea barne).	1
		Begi-bistako hantura, betazalen ebertsio partzialarekin.	2
		Hantura, betazalak erdi itxita daudela.	3
		Betazalak erdi itxita eta erabat itxita dituen hantura.	4
	C. Muki sekrezioa	Normala ez den edozein sekrezio kopurua.	1
		Betazalak eta betazalen ondoan dauden ileen bustitzea muki jariakinaren ondorioz.	2
		Betazalak muki jariakinaren bidez bustitzea, eta begiaren inguruko eremuan eragitea.	3
			Puntuazioa = (A + B + C) × 2 (0-tik 20-ra)

III.6. TAULA: Kay eta Calandrak ezarritako begiko narritaduraren indizearen balioak [338].

GBBP	Narritadura sailkapena
0-0.5	Ez-narritagarria
0.6-2.5	Ia ez-narritagarria
2.5-15	Minimoki narritagarria
15.1-25	Apur bat narritagarria
25.1-50	Nahiko narritagarria
50.1-80	oso narritagarria
80.1-100	Izugarri narritagarria
100.1-110	Guztiz narritagarria
GBBP: Gehieneko batez besteko puntuazioa	

9. Malko-laginak eskuratzea eta aztertzea

9.1. Schirmer-en tiren bidez malkoa biltzea eta kuantifikatzea

Schirmer-en tirak (Madhu Instruments, New Delhi, India) malko-laginak biltzeko erabili genituen. Kirurgia (t = 0 egun) zein 1. 4. eta 7. egunetan, operatutako begiaren goiko zaku bulbarrean tira bat kokatu eta 5 minutuz mantendu genuen (III.10 irudia). Bi lagin jaso genituen aipatutako egun bakoitzean, bata goizez eta bestea arratsaldez.

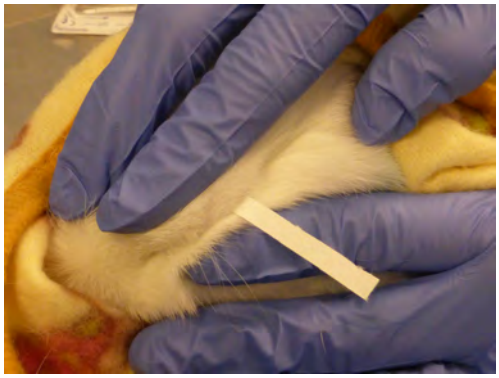

III.10. IRUDIA: Schirmer tiratik malkoa jasotzeko prozedura.

Tira bakoitzeko 1 mm 1 μl malko zela kontuan hartuta, lagin bakoitzean jasotako malko kantitatea erregistratu genuen. Lagin bakoitza 1,5 ml-ko Eppendorf hodi batean sartu eta -80 °C-tara biltegiratu genuen erabili arte. Laginak malkoa erauzi eta hantura-molekulak ebaluatzeko gorde genituen. Hauek erregistro eguna, erabilitako untxia eta ezker edo eskuin begiaren arabera kodetu genituen.

9.2. Schirmer-en tiretatik lortutako laginetako proteinen eluzioa

100 μl PBS gehitu genizkion lagin-hodi bakoitzari eta ordubetez giro tenperaturan mantendu genituen malko-edukia PBS tanpoian eluitzeko. Ondoren, laginak 400 b/min eta 4 °C-tara 5 minutuz zentrifugatu genituen Kubota 3500 (Kubota Corporation, Tokio, Japonia) zentrifuga erabiliz. Lehen zentrifugazioaren ondoren, Schirmer-en tirak 0,2 ml-ko Eppendorf hodietara transferitu eta 1300 b/min eta 4 °C-tara zentrifugatu genituen beste 5 minutuz. Bigarren zentrifugazioaren gainjalkina 1,5 ml-ko Eppendorf hodira gehitu genuen aldez aurretik bildutako bolumenarekin.

Lagin bakoitzeko 6 μl-ko alikuotak baztertu genituen proteina edukia BCA saiakuntzaren bidez kuantifikatzeko eta hodiak -80 °C-tara biltegiratu genituen zitokina edukia aztertu arte.

9.3. Proteina edukiaren kuantifikazioa-BCA saiakuntza

Malko-lagin bakoitzeko 6 μl-ko alikuota bat erabili genuen proteina eduki totala azido bizinkoninikoaren (BCA) saiakuntzaren bidez kuantifikatzeko.

BCA saiakuntza saiakuntza kolorimetriko bat da, baldintza alkalinoetan Cu^{2+}-proteina konplexu baten eraketan eta ondorengo Cu^{2+}-tik Cu^{+}-rako erredukzioan oinarrituta dagoena [339]. Erreduzitutako Cu^{2+} kantitatea disoluzioan dagoen proteina kantitatearekiko proportzionala da. Azido bizinkoninikoaren gatzak Cu^{+}-rekin erreakzionatzen du, 562 nm-tara argia proteina kontzentrazioaren arabera xurgatu eta berde koloretik more kolorera aldatzen da. Hala, lagin ezezagunen proteina-edukia ezagutzen den proteina-eredu batekin alderatuz espektrofotometrikoki zehaztu daiteke.

Proteina-edukia kuantifikatzeko, proteina-patroi ezagun gisa BSA proteinaren 0-1 mg/ml-ko diluzio seriatuak erabili genituen. BSA edo lagin bakoitzeko 1:5 diluziotik 10 μl, 200 μl BCA eta $CuSO_4$ (50:1) (Sigma Aldrich, St. Louis MO, AEB) disoluzioarekin nahastu genituen 96 kikaradun hazkuntza plakako kikara bakoitzeko. Hiru erreplika kuantifikatu genituen BSA diluzio seriatu edo lagin bakoitzeko. Plaka 37 °C-tara 30 minutuz iluntasunean inkubatu eta, ondoren, kikara bakoitzaren argi xurgapena kuantifikatu genuen espektrofotometroan (Thermo Fisher Scientific, Waltham, MA, AEB) 562 nm-ko uhin luzera erabiliz. Azkenik, lagin bakoitzaren proteinen kontzentrazioa kalkulatu genuen BSA kurba estandar batekin alderatuz.

9.4. Immunodetekzioaren eta antigorputz-array bidezko malko-laginetako hantura-molekulen adierazpenaren ebaluazioa

In vivo saiakuntzan jasotako malko-laginetako zitokinen kuantifikazioa, multiplex microarray teknologia eta QAL-CYT-1 Quantibody Rabbit Cytokine Array (Raybiotech, Norcross, GE, AEB) kita erabiliz egin genuen.

Kit hau sandwich motako ELISA teknikan oinarritzen da, baina aldi berean zitokina anitzen kontzentrazioa zehaztasunez kuantifikatzeko aukera ematen du, zitokinak atzemateko antigorputz espezifiko ugari erabiltzen baititu. Atzemate-antigorputza array-aren gainazalera itsasten da lehenik. Laginarekin inkubatu ondoren, intereseko zitokina gainazaleko antigorputzarekin lotzen da. Ondoren, biotinarekin markatutako bigarren detekzio-antigorputz bat gehitzen da, zitokinaren beste epitopo bat ezagutzeko gai dena. Zitokina-antigorputz biotina konplexua laser eskaner baten bidez eta estreptabidinarekin konjugatutako Cy3 tindaketa gehituz irakurtzen da. Array-a, zitokinen antigorputzen multzo berdinekin osatutako 16 kikaratan banatuta dago eta horietako bakoitzean 4 erreplika aurki daitezke, kontrol positiboekin batera (III.11 irudia).

Zitokinak kuantifikatzeko, zitokinen kontzentrazio zehatzak dituzten estandarrak gehitzen dira zitokina bakoitzerako kurba estandar bat sortzeko. Lagin ezezagunen seinaleak kurba estandarrarekin alderatuz, zitokinak laginetan duen kontzentrazioa zehaztu daiteke.

QAL-CYT-1 Quantibody Rabbit Cytokine Array kitak, honako zitokina hauek identifikatzeko aukera ematen du: interleukina 1α (IL-1 α), interleukina 1β (IL-1 β), interleukina 8 (IL-8), interleukina 17A (IL-17A), interleukina 21 (IL-21), leptina, 1β makrofagoetako proteina inflamatorioa (MIP-1β), metalopeptidasa 9 (MMP-9), nerbio zelulei atxikitzeko 1 motako molekula (NCAM-1) eta TNFα. Horiek guztiak lotuta daude mitogenoek aktibatutako kinasa proteina (MAPK) eta NF-κB (aktibatutako B zelulen kappa kate arinak indartzen dituen faktore nuklearra) seinaleztapen-bidezidorrekin, inflamazio kaskadarekin lotura handia duten prozesuak hain zuzen.

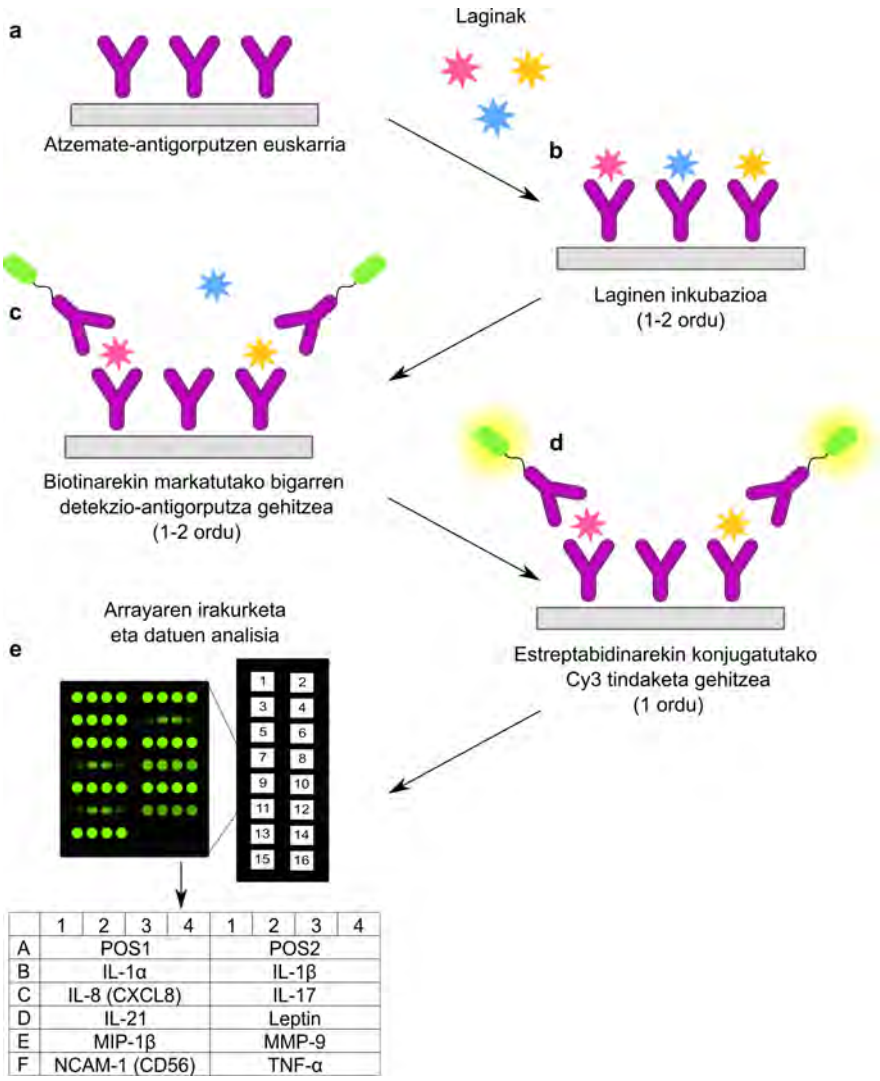

	1	2	3	4	1	2	3	4
A	POS1				POS2			
B	IL-1α				IL-1β			
C	IL-8 (CXCL8)				IL-17			
D	IL-21				Leptin			
E	MIP-1β				MMP-9			
F	NCAM-1 (CD56)				TNF-α			

III.11. IRUDIA: Zitokinen arrayaren lan-prozedura. **a**) Atzemate-antigorputzak dituen beirazko euskarria erabat lehortzen da edozein inkubazio hasi aurretik. **b**) Laginak gehitu eta euskarrian dauden antigorputzekin lotzen dira. **c**) Ondoren, biotinarekin markatutako bigarren detekzio-antigorputz bat gehitzen da, zitokinaren beste epitopo bat ezagutzeko gai dena. **d**) Estreptabidinarekin konjugatutako Cy3 tindaketa gehitzen da seinale detektagarri bat sortzeko. **e**) Array-a irakurri eta datuak aztertzen dira.

Esperimentua eta datuen analisia fabrikatzailearen protokoloa jarraituz gauzatu genuen.

10. Gene-adierazpenaren analisia

Gene-adierazpenaren analisiak RNA edo proteina funtzionalak ekoizteko geneak nola transkribatzen diren aztertzen du. Azterketa honek, prozesu zelular normalak edo patologikoak ulertzea ahalbidetzen du.

10.1. RNA-ren erauzketa *in vitro* lortutako laginetatik

In vitro laginen RNA-ren erauzketa inflamazio-saiakuntzetan lortutako KZE zeluletatik egin genuen. NucleoSpin RNA (Macherey-Nagel, Düren, Alemania) kita eta fabrikatzailearen jarraibideak jarraitu genituen horretarako. Prozesua giro-tenperaturan eta RNAsa-rik gabeko material esterila erabiliz gauzatu genuen.

Kultiboan zeuden zelulak 5 minutuz 37 °C-tara gehitutako tripsina-EDTA soluzioarekin bereizi genituen. Zelulen askapenaren ondoren, tripsinaren jarduera inhibitzeko FBS gehitu eta zelulak 300g-tara 5 minutuz zentrifugatu genituen. Gainjalkina kendu ondoren, zelulen pelleta 1× PBS-tan berreseki, zenbatu eta berriro zentrifugatu genituen gera zitekeen edozein medioren hondar garbitzeko.

RNA erauzteko, zelulen pelleta 350 μl RA1 tanpoia (Macherey-Nagel, Düren, Alemania) eta 3,5 μl merkaptoetanol (Sigma Aldrich, St. Louis, MO, AEB) erabiliz lisatu genuen. RA1 tanpoia RNA isolatu aurretik ehunen eta zelulen lisirako prestatutako tanpoia da. Lisatutako laginak -80°C-tara gorde genituen RNA purifikatu arte. RNA-ren purifikazioa fabrikatzailearen jarraibideak betez gauzatu genuen, DNA-ren digestio-urratsa ere jasotzen zuena. Guztira, 60 μl RNA bolumen lortu genituen.

10.2. RNA-ren erauzketa *in vivo* lortutako laginetatik

In vivo laginen RNA, *in vivo* saiakuntzan lortutako kornea-ehunen laginetatik erauzi genuen. Lagin hauek korneaz, linbo esklerokornealaz eta eskleraren 1-2 mm-z osatuta zeuden.

-80 °C-tara gordetako untxi-korneak desizoztu, pisatu eta zati luze eta finetan ebaki genituen ondorengo homogeneizazioa errazteko. Laginak hari-hodietan sartu genituen 0,5 mm-ko zirkonio oxidozko (Next Advanced, NY, AEB) aleekin batera, hodi bakoitzean erabilitako ale bolumena 1× lagin bakoitzaren bolumenaren baliokidea izanik. Hodiko 1 ml TRIzol (Thermo Fisher Scientific, Waltham, MA, AEB) gehitu eta Bullet Blender (Next Advanced, NY, AEB) homogeneizagailuan 3 minutuz homogeneizatu genituen. Ondoren, homogeneizatutako laginaren bolumena 1,5 ml-ko bi Eppendorf hoditan banatu genuen, bakoitzean laginaren 500 μl sartuz. 100 μl kloroformo gehitu genituen hodiko, laginak eskuz gogor astindu eta 15 minutuz 12000g-tara zentrifugatu genituen 4 °C-tan. Prozesu honetan, lagina 3 fase desberdinetan bereiztea lortu genuen: gorri fenol-kloroformo behe fase bat, proteina

zelularrak zituena, DNA-z osatutako interfase uher bat eta RNA-z osatutako goi fase urtsu eta gardena. Fase urtsuak Eppendorf hodi garbietara transferitu eta laginak ordubetez 500 μl alkohol isopropilikoarekin inkubatu genituen. Laginak 12000g-ra zentrifugatu genituen 10 minutuz 4 °C-tara, gainjalkina kendu, RNA pelleta 1 ml % 70 etanolekin garbitu eta 5 minutuz 7500g eta 4 °C-tara zentrifugatu genituen berriro ere. Azkenik, gainjalkina kendu, RNA pelleta airean lehortzen utzi eta ondoren 20 μl RNasa-rik gabeko uretan disolbatu genituen.

RNA purifikatu ondoren, laginak, DNasa tanpoian (Zymo-Research, Irvine, CA, AEB) disolbatutako 1 unitate/μl I DNasa-rekin (Zymo-Research, Irvine, CA, AEB) inkubatu genituen 15 minutuz giro-tenperaturan, DNA genomiko posiblea ezabatzeko. Azkenik, entzimaren jarduera eteteko 2,5 μl 25 mM EDTA gehitu genizkion lagin bakoitzari eta 10 minutuz 65 °C-tara berotzen utzi genituen.

10.3. RNA-ren kuantifikazioa

RNA kontzentrazioa (ng/ml) lagin bakoitzaren absorbantzia (A) 260 nm eta 280 nm uhin-luzeratan neurtuz kuantifikatu genuen Take 3 Micro-Volume Plate unitatea ELx800 plaka-irakurgailua erabiliz.

Lambert-Beer legearen arabera, erlazio lineala dago xurgapenaren eta makromolekularen kontzentrazioaren artean. RNA disoluzioen gehieneko xurgapena 260 nm-ko uhin-luzeran gertatzen da, eta proteina-disoluzioak, berriz, 280 nm-ko uhin-luzeran. 260 nm-tan eta 280 nm-tan (A_{260}/A_{280}) lortutako balioen ratioak RNA-ren purutasun-mailaren zenbatespena ematen du. RNA puruaren A_{260}/A_{280} ratioa 2,0 ingurukoa da. Maila horretatik gorako edo beheragoko balioek laginen kutsadura adierazten dute.

RNA kontzentrazioa 260 nm-ko xurgapen-neurketatik abiatuta kalkula daiteke III.7 ekuazioaren bidez; izan ere, 260 nm-ko uhin-luzeran neurtutako dentsitate optikoko unitate bakoitza 40 μg/ml RNA monokatenariori dagokio.

$$RNA\ (\mu g/ml) = A_{260} \times Diluzio\ faktorea \times 40 \tag{III.7}$$

Behin kontrentrazioa neurtuta, laginak -80 °C-tara gorde genituen erabili arte.

10.4. Erretrotranskripzioa

Erretrotranskripzio-erreakzioan gehien erabiltzen den estrategia oligodesoxitimidina (dT)-abiarazle bat gehitzea da. Nukleotido-sekuentzia horrek dT nukleobaseak baino ez ditu, eta horri esker, organismo eukarioto gehienen RNA mezulariaren (RNAm) poli-A sekuentziarekin hibrida daiteke. Alderantzizko transkriptasa entzima RNAm-ren sekuentzia osagarriaren DNA sintetizatzeaz arduratzen da, eredu gisa jarduten baitu.

Bi urratsetako alderantzizko transkripzioa egiteko iScriptTM cDNA Synthesis (BioRad, Hercules, CA, AEB) kita erabili genuen. DNA osagarria (cDNA), lagin bakoitzeko 1 μg RNA-tik abiatuta sintetizatu genuen. 1 μg RNA, 4 μl 5X iScript erreakzio nahasketa, 1 μl iScript alderantzizko transkiptasa eta 20 μl osatzera arteko nukleasarik gabeko urarekin nahastu genituen. Erreakzio osoaren nahasketa MJ Mini (BioRad, Hercules, CA, AEB) termozikladorean hurrengo protokoloa jarraituz inkubatu genuen: 5 minutu 25 °C-tara erreakzioa abiarazteko, 20 minutu 46 °C-tara alderantzizko transkripziorako eta 1 minutu 95 °C-tara alderantzizko transkriptasa inaktibatzeko. Amaieran, 4 °C-tako azken urrats bat gehitu genuen lagina termozikladoretik atera arte. cDNA laginak -20°C-tara gorde genituen qPCR analisira arte.

10.5. *In vivo* laginetatik lortutako cDNA-ren preanplifikazioa

In vivo saiakuntzako untxien korneetatik lortutako cDNA laginak Multiplex PCR (Qiagen, Hilden, Alemania) kita erabiliz anplifikatu genituen. 2,5 μl 2X QIAGEN Multiplex PCR nahasketa, 0,5 μl 500 nM-eko kontzentrazioan jarritako abiarazleen nahasketa, 1.25 μl 1 μg cDNA eta 0.75 μl RNAasa-rik gabeko ur nahastu genituen lagin bakoitzeko.

Protokoloa, DNA polimerasa aktibatzeko 95 °C-tara 15 minutuz egindako hasierako aktibazio termikoko ziklo batekin eta 14 anplifikazio-zikloekin konfiguratu genuen. Anplifikazio-ziklo bakoitza honela banatu genuen: 30 segunduz 94 °C -tara egindako desnaturalizazioa, 90 segunduz 57-63 °C -ko tenperatura-gradientean egindako hibridazioa eta 60 segunduz 72 °C-tara egindako luzapen urratsa. Anplifikazioaren ondoren, 30 minutuz 60 °C-tara egindako azken urratsa gehitu genuen. Laginak -20 °C-tan biltegiratu genituen erabili arte.

10.6. Polimerasaren kate-erreakzio kuantitatiboa denbora errealean (RT-qPCR)

Alderantzizko transkripziotik lortutako cDNA RT-qPCR-aren molde gisa erabili genuen. Metodo honetan, produktu espezifiko bakoitzaren kantitatea zehazteko, DNAri lotzen zaizkion fluoreszentzia markatzaileen seinalearen gehikuntza neurtzen da entzimek neurtutako anplifikazio-ziklo jarraietan.

RT-qPCR-a CFX96 eta C1000 Touch termozikladorea (BioRad, Hercules, CA, EE.UU.) eta SYBR® Green double-stranded DNA (dsDNA) (BioRad, Hercules, CA, USA) tindaketa erabiliz gauzatu genuen. Fluoroforo hau DNA baseen artean tartekatzen da, eta, bertan bere energia askatzen du, metatutako dsDNA produktuaren kantitatearekiko proportzionala den fluoreszentzia-intentsitate gisa. Horrela, DNA modu erlatiboan kuantifika daiteke. Hurrengo erreakzio-nahasketa gehitu genion PCR plakaren kikara bakoitzari: 10 μl, iTaq Universal SYBR® Green nahasketa, 8 μl nukleasarik gabeko ura, 0,5 μl *forward* eta 0,5 μl *reverse* abiarazleak eta 1 μ 500 nM cDNA. Protokoloa, polimerasa aktibatzeko 95 °C-tara 3 minutuz egindako hasierako aktibazio ziklo batekin eta 40 anplifikazio-zikloekin konfiguratu genuen. Anplifikazio-ziklo bakoitza honela banatu genuen: 30 segunduz 95 °C -tara egindako desnaturalizazioa, 30 segundoz abiarazleen hibridazioa eta 30 segundoz 72 °C-tara egindako azken luzapen urratsa. Erabilitako abiarazleei buruzko informazioa III.7 taulan laburbilduta ikus daiteke.

Ondoren, minutu batez 95 °C-tara egindako ziklo bat, beste minutu batez 65 °C-tara egindako beste ziklo bat eta ziklo bakoitzeko tenperatura 0,5 °C handitzen joandako 60 ziklo gehitu genituen, 65-95 °C bitarteko tenperatura-gradientean. Azkenik qPCR-ko produktuak 4 °C-tara mantendu genituen ekipoa itzali arte. Disoziazio protokoloan, tenperatura pixkanaka 65 °C-tik 95 °C-tara igotzeari esker, PCR-an sintetizatutako DNA kateak bana daitezke anplikoi bakoitzari dagokion fusio-tenperaturara (Tm) iristean. SYBR Green tindaketa DNA kateetatik askatzen da kateak banatzean eta fluoreszentzia igortzeari uzten dio. Hori, PCR-ak fluoreszentzia-gailur gisa irudika dezake, Tm-ren balio desberdinekin anplifikazio-produktu ugariren presentzia baztertzeko aukera emanez.

III.7. TAULA: *In vitro* eta *in vivo* saiakuntzetan erabilitako abiarazleen sekuentziak eta propietateak.

Abiarazlea	Mota	Sekuentzia (5′-3′)	Anplikoi tamaina	Tm	% GC	Optimizatutako Ta	Saiakuntza
IL-6	Fw abiarazlea	GCAGATGAGTACAAAAGTCCTGA	120	58.43	43.48	59.6	*In vitro*
	Rv abiarazlea	TTCTGTGCCTGCAGCTTC		57.93	55.56		
IL-1β	Fw abiarazlea	CCATGGCAGAAGTACCTGAG	114	57.68	55	59.6	*In vitro*
	Rv abiarazlea	CCTGGAAGGAGCACTTCATC		57.96	55		
TNFα	Fw abiarazlea	TGCACTTTGGAGTGATCGG	145	57.77	52.63	59.6	*In vitro*
	Rv abiarazlea	TCAGCTTGAGGGTTTGCTAC		57.81	50		
TBP	Fw abiarazlea	GCTGTTTAACTTCGCTTCCG	104	57.77	50	59.6	*In vitro*
	Rv abiarazlea	CAGCAACTTCCTCAATTCCTTG		57.83	45.45		
GusB	Fw abiarazlea	GCCCATTATTCAGAGCGAGTA	128	57.61	47.62	59.6	*In vitro*
	Rv abiarazlea	GTTTTTGATCCAGACCCAGATG		57.29	45.45		
IL-1β	Fw abiarazlea	GTAGACCCCAACCGTTACCC	145	57.4	60	56.4	*In vivo*
	Rv abiarazlea	AGACGGGCATGTACTCTGTC		56.5	55		
GADPH	Fw abiarazlea	TCGGAGTGAACGGATTTG	225	52.2	50	61	*In vivo*
	Rv abiarazlea	CTCGCTCCTGGAAGATGG		55.1	61.1		
Ki 67	Fw abiarazlea	GCCAAGATAGTTGCTGATAC	171	50.5	45	58.4	In vivo
	Rv abiarazlea	AAGTGTCCGATTCCGATTA		50.4	42.1		
HPRT1	Fw abiarazlea	ACGTCGAGGACTTGGAAAGGGTGTT	96	62.1	52	58.4	*In vivo*
	Rv abiarazlea	GGCCTCCCATCTCCTTCATCACATC		61	56		
p63	Fw abiarazlea	CGCCCCTTTCGTCAGAACAC	165	61.57	60	57.2	*In vivo*
	Rv abiarazlea	GTGCTGAGGAAGGTACTGCAT		60.07	52.38		
CK3	Fw abiarazlea	GACTCGGAGCTGAGAAGCAT	198	59.54	55	59.8	*In vivo*
	Rv abiarazlea	CAGGGTCCTCAGGAAGTTGA		58.65	55		
β-Actin	Fw abiarazlea	AGATGACCCAGATCATGTTTGAG	119	58.22	43.48	57.2	*In vivo*
	Rv abiarazlea	GTCACCGGAGTCCATCACG		60.15	63.16		
α-SMA	Fw abiarazlea	CGGTGCTGTCTCTCTATGCC	177	60.25	60	58.4	*In vivo*
	Rv abiarazlea	CACGCTCAGTCAGGATCTTCA		59.8	52.38		
RIG S15	Fw abiarazlea	CATGGTGGGCGTCTACAAC	161	58.53	57.89	58.4	*In vivo*
	Rv abiarazlea	ACTTGAGAGGGATGAAGCGG		59.46	55		
CD44	Fw abiarazlea	GACACCATGGACAAGTTTTGG	140	57.63	47.62	59.8	*In vivo*
	Rv abiarazlea	GAGATGCTGTAGCGACCATT		57.77	50		
PAX6	Fw abiarazlea	AGAGAATACCAACTCCATCAG	152	54.44	42.86	58.4	*In vivo*
	Rv abiarazlea	GATAATGGGTTCTCTCAAACTC		54.28	40.91		

Fw: Forward abiarazlea. Tm: Fusio tenperatura. Ta: Hibridazio tenperatura.
Rv: Reverse abiarazlea. % GC: Guanina (G) eta zitosina (C) edukia.

10.6.1. RT-qPCR emaitzen analisia

Lortutako emaitzak (Cq), Pfaffl-ek deskribatutako formularen bidez abiarazle bikote bakoitzaren eraginkortasunarekiko zuzendu genituen [340]. Gainera, barne-kalibratzaileen presentziari esker, gene bakoitzerako plaken arteko aldakuntza neurtu eta zuzendu genuen. Ondoren, azterketa-geneen adierazpena erreferentziazko geneekiko normalizatu genuen. Azken hauek, saiakuntzan zehar haien adierazpena konstante mantentzen duten geneak dira. Erreferentziazko gene ezberdinen aldakuntza-koefizienteak ebaluatu ondoren, Gusβ eta TBP geneak erabili genituen *in vitro* inflamazio-saiakuntzako laginetan, eta GAPDH, HPRT1 eta RIG S15 geneak *in vivo* saiakuntzako laginetan. Normalizaziorako, azterketako geneen Cq-ei erreferentziazko geneen Cq-en batez besteko geometrikoa kendu genien, lagin bakoitzerako normalizatutako ΔCq lortuz [341]. Ondoren, azterketako gene bakoitzari, lagin guztien ΔCq-ren batez bestekoa kendu genion, lagin bakoitzaren $\Delta\Delta$Cq lortuz. Honen bitartez adierazpen erlatiboa (2-$\Delta\Delta$Cq) kalkulatu ahal izan

genuen [342]. Guzti hau, CFX Maestro softwarearen (BioRad, Hercules, CA, AEB) bidez egin genuen.

11. Analisi histologikoa

OCT konposatu blokeetan sartutako kornea-ehunak 10 μm-ko sekzioetan ebaki genituen CM 3050S kriostatoan (Leica, Wetzlar, Alemania) eta % 4 paraformaldehidoarekin (PFA) finkatu genituen. Ebaketak -20 °C-tara biltegiratu genituen tindatu arte. Analisi histologikoa egiteko *ex vivo* esperimentuetatik lortutako behi- eta untxi-korneak eta *in vivo* saiakuntzatik lorturako untxi-korneak erabili genituen.

11.1. Hematoxilina-Eosina (H-E) tindaketa

Kornea-ehunen portak kubetetan jarri eta soluzio desberdinekin buzti genituen H-E tindaketa egiteko. Hematoxilinarekin minutu bat eta 30 segunduz tindatu genituen lehendabizi, % 0,3 azido klorhidrikoarekin 5 segunduz garbitu ondoren eta 15 segundoz Eosinarekin tindatu genituen azkenik. Urrats bakoitzaren ondoren, uretan sartu genituen 5 minutuz.

Azken garbiketaren ostean, laginak pixkanaka kontzentratutako etanol-disoluzioetan (% 50, % 70, % 96 eta % 100-eko 2 soluzio) 10 segundoz buztiz deshidratatu genituen.

Azkenik, 3 Zitrosol aldaketa egin genituen, laginak 5 minutuz kubeta bakoitzean mantendu genituelarik. Amaitzeko, DPX-a aplikatu genion portako ehun bakoitzari eta objektu-estalki batekin estali genituen laginak, mikroskopioan bistaratzeko.

11.2. Inprimatze zitologia

Inprimatze zitologia konjuntiba-epitelioko azaleko geruzetako zelulak biltzean oinarritzen den teknika ez-inbaditzailea da, ondoren analisi histologikoa egitea ahalbidetzen duena.

Teknika honen bidez, *in vivo* saiakuntzan erabilitako animalien konjuntiba-zelula laginak lortu genituen.

Laginak 2 $\times$ 2 mm^2-ko 0,45 μm-ko iragazki-paper (Merck KGaA, Darmstadt, Alemania) zatietan jaso genituen. Iragazki-papelak goiko konjuntibara 5-10 segunduz

itsatsi, emeki-emeki erretiratu eta % 70-eko alkohol-disoluzioan sartu genituen. Hauek alkohol-disoluzioan bertan 4 °C-tara gorde genituen prozesatu arte.

11.3. Inprimatze zitologia bidez lortutako laginen PAS tindaketa

% 70-eko alkohol-disoluzioan finkatutako inprimatze zitologiaren laginak soluzio desberdinekin buzti genituen Azido periodiko-Schiff-en tindaketa (PAS) egiteko. Laginak 5 minutuz ur destilatuarekin garbitu genituen lehendabizi. % 1 azido periodikotan sartu genituen 5 minutuz, bi aldiz ur destilatuarekin garbitu eta Schiff-en erreaktiboan mantendu genituen 30 minutuz argitik babestuta. Azido sulfurikozko 3 soluziotan sartu genituen laginak Schiffen erreaktiboko hondarrak garbitzeko, bainu bakoitzean 2 minutuz mantendu genituelarik. Ondoren, 5 minutuz uretan sartu eta 30 segundoz Harrisen hematoxilinarekin tindatu genituen. Tindaketaren ostean, laginak 5 minutuz garbitu genituen iturriko urarekin. Azken garbiketaren ondoren, laginak pixkanaka kontzentratutako etanol-disoluzioetan (% 50, % 96-ko 2 soluzio eta % 100-eko 2 soluzio) minutu batez buztiz deshidratatu genituen.

Amaitzeko, 2 Zitrosol aldaketa egin genituen, laginak 5 minutuz kubeta bakoitzean mantendu genituelarik. DPX-a aplikatu genion portako lagin bakoitzari eta objektu-estalki batekin estali genituen, mikroskopioan bistaratzeko.

12. Immunofluoreszentzia

Immunofluoreszentzia (IF) antigeno eta fluoroforoekin markatutako antigorputzen berariazko loturetan oinarritzen den teknika da eta zeluletako antigenoak detektatzeko aukera ematen du.

Fluoroforoak, uhin-luzera jakin baten aurrean argia igortzen duten konposatuak dira. Hauek antigorputzei batu eta ehunetan edo hazkuntza zelularretan aurki daitezkeen antigenoekin lotu daitezke. Honek, proteinak edo antigenoak fluoreszentzia bidezko mikroskopiaren edo mikroskopio konfokalaren bidez ikuskatzea ahalbidetzen du.

Antigorputzak edo immunoglobulinak (Ig), erantzun immunitarioa aktibatzen duen edozein molekularen aurreko esposizio bati erantzuteko B linfozitoek sortutako glukoproteinak dira.

Immunoglobulinen oinarrizko egitura kate polipeptidiko astun batek eta 2 kate arin pare berdinek osatzen dute, disulfuro loturez elkarri lotuta daudenak.

Zurtoina eta beheko besoak nahiko antzekoak dira antigorputz mota desberdinetan, baina beso-puntetako sekuentzia polipeptidikoa antigenoekiko espezifikoa da. Ugaztunetan erantzun immunitarioan jarduera desberdina duten 5 immunoglobulina mota aurki daitezke (IgG, IgM, IgA, IgD eta IgE).

Antigorputzen afinitatea antigenoarekiko lotura-gune eta epitopoaren arteko lotura-indarrari deritzo, eta IF saiakuntza bat diseinatzerakoan kontuan hartu beharreko alderdi garrantzitsua da. Zenbat eta afinitate handiagoa izan, orduan eta handiagoa izango da antigorputz eta antigenoaren arteko interakzio-abiadura eta sentikortasuna.

IF saiakuntzek hainbat molekula estruktural eta funtzional aldi berean detektatzeko aukera ematen dute. Lehenik eta behin, laginak euskarri solido batera (mikroskopio-porta batera esaterako) finkatu behar dira zelulen morfologia zaintzeko eta ehunaren edo zelulen osotasuna kaltetu dezaketen erreakzio biokimikoak saihesteko. Gehien erabiltzen diren finkatzaileak PFA, azetona edo metanola dira, eta lagina eta antigorputz motaren arabera hautatzen dira. PFA, normalean, mintzekin lotutako proteinak tindatzeko erabiltzen da, amina talde askeak erretikulatzen ditu eta gurutzatutako proteinen sare bat sortzen du zelulen morfologia babesteko. Hala ere, irakurri beharreko seinalea autofluoreszentziaz lausotu dezaketen proteinen amina taldeekin erreakziona dezake. Gainera, ez ditu zelula-mintzak behar bezala iragazkortzen, eta, beraz, erabiliko den protokolora urrats hau gehitu beharra dago. Azetona eta metanola finkatzaile prezipitatzaile gisa sailkatzen dira, proteinen prezipitazioa eragiten dutelako, eta, beraz, eraginkorrak dira zelulen arkitektura zaintzeko. Ez dute iragazkortasun-urrats gehigarririk behar.

Lagina iragazkortzeak antigorputzari zelula-mintza zeharkatzen eta zelulan sartzen laguntzen dio. Urrats horren ondoren, lagina blokeatu egiten da, antigeno-antigorputz berariazko loturak ahalbidetzeko eta interakzio ez espezifikoak minimizatzeko. Honetarako, laginak agente blokeatzaileak dituzten soluzioekin inkubatzen dira, hala nola BSA, esne gaingabetua edo seruma. Blokeoaren ondoren, laginak espezifikotasun handiko antigorputz primarioarekin inkubatzen dira. Antigorputzak modu zuzen edo ez-zuzenean detektatzeko metodoak bereiz daitezke. Antigorputzak zuzenean detektatzeko, fluorokromoekin elkartutako antigorputz primarioak erabiltzen dira; modu ez-zuzenean detektatzeko, berriz, antigorputz primarioa ezagutzen duen antigorputz sekundario bat erabiltzen da.

Proteina bakoitzarentzat zenbait antigorputz espezifiko ere konbina daitezke, lagin berean proteina ezberdinak tindatzeko. Kasu horietan, bigarren mailako antigorputzak kitxikapen- eta igorpen-espektroan gainjartzen ez diren hainbat fluoroforekin elkartu behar dira. Azkenik, laginak DNA-ren (Hoechst edo DAPI) koloratzaile fluoreszenteekin markatzen dira, nukleoan sartu eta DNA-rekin bat egin dezaketenak. Honek zelula indibidualak eta organulu zehatzak identifikatzen laguntzen du.

12.1. Immunozitokimika

Immunozitokimika analisiak giza ehun korneoeskleraletatik zuzenean isolatutako zelula primarioak zituzten portetan zein 8 kikaradun ganberatan (Ibidi, Gräfelfing, Bayern, Alemania) egin genituen. Laginak 20 minutuz % 4 PFA-rekin finkatu genituen aldez aurretik.

Laginak hiru aldiz PBS-arekin garbitu genituen lehendabizi, erreakzionatu gabeko PFA kentzeko. Finkatutako laginak PBST-arekin (PBS-tan disolbatutako % 0,1 Triton TX-100-eko soluzioa) iragazkortu genituen 10 minutuz, eta % 5 BSA eta % 10 FBS PBST soluzioarekin ordubetez blokeatu ondoren, interakzio ez-espezifikoak murrizteko. Laginak antigorputz primarioen soluzio egokiarekin inkubatzen utzi genituen 4 °C-tara gau osoan zehar (III.8 taula). Ondoren, 10 minutuko 3 alditan PBST-arekin garbitu eta antigorputz sekundarioekin inkubatu genituen 2 orduz ilunpetan eta giro-tenperaturan. Azkenik, laginak 4 mg/ml Hoechst 33342-rekin (Thermo Fisher Scientific, Waltham, MA, EE.UU.) 15 minutuz markatu, bi aldiz 5 minutuz PBS-arekin garbitu eta mikroskopiozko portetan muntatu genituen Fluoromount G (SouthernBiotech; Birmingham, Erresuma Batua) konposatuarekin. Portak 4 °C-tan gorde genituen argitik babestuta fluoreszentzia-mikroskopiako irudiak lortu arte. Irudiak Apotome.2 fluoreszentzia mikroskopioarekin (Zeiss, Oberkochen, Alemania) atera genituen.

12.1.1. Zitospina

Giza ehun esklerokornealetatik zuzenean isolatutako zelula primarioen analisi immunozitokimikoa egiteko, ehunen digestiotik lortutako zelulen kantitate bat, epitelialak zein estromalak, 1× PBS-etan garbitu eta % 2 PFA-tan finkatu genituen 20 minutuz. Behin finkatuta, 1× PBS-tan garbitu, 7 minutuz 300g-tara zentrifugatu eta PBS-% 1 BSA-n berreseki genituen. Ondoren, zelulen soluzioa 8 minutuz 1300

b/min-tan zitospinean (Thermo Fisher Scientific, Waltham, MA, AEB) zentrifugatu eta poli-L-lisinaz (Sigma Aldrich, St. Louis, MO, AEB) estalitako portetan prezipitatu genituen. Berresekitako zelulen 100 μl 20000 zelula inguruko dentsitatearekin gehitu genituen zitospinaren euskarri bakoitzeko.

12.2. Immunohistokimika

Immunohistokimikarako, 10 μm-ko ehun-ebaketak zituzten portak desizoztu, arkatz hidrofobo batekin markatu eta bi aldiz PBS-rekin 5 minutuz garbitu genituen. Ehun-portak bi aldiz iragazkortu genituen 10 minutuz PBST-arekin, eta 10 minutuz % 10 NGS-arekin (ingelesetik *normal goat serum*) (Thermo Fisher Scientific, Waltham, MA, AEB) blokeatu genituen, interakzio ez-espezifikoak murrizteko. Laginak antigorputz primarioekin inkubatu genituen 4 °C-tara gaba oso batez (III.8 taula). Ondoren, PBS-rekin 10 minutuz eta bi aldiz PBST-rekin 15 minutuz garbitu eta 1:1000 diluitutako antigorputz sekundarioekin inkubatu genituen 1,5 orduz ilunpetan eta giro-tenperaturan. Laginak PBS-rekin 3 aldiz 10 minutuz berriro garbitu eta 4 mg/ml Hoechst 33342-ekin markatu genituen 15 minutuz giro-tenperaturan. Azkenik, laginak 5 minutuz PBS-rekin bi aldiz garbitu eta Fluoromount G konposatuarekin estalkiekin muntatu genituen. Portak 4 °C-tara gorde genituen argitik babestuta, fluoreszentzia-mikroskopiako irudiak atera arte. Irudiak Apotome.2 eta Nikon Ti-U (Nikon, Tokio, Japonia) fluoreszentzia-mikroskopioekin atera genituen.

III.8. TAULA: IF saiakuntzetan erabilitako antigorputz primario eta sekundarioen zerrenda.

Immunogenoa	Erreferentzia	Etxe komertziala	Ostalaria	Klasea	Isotipoa	Diluzioa	Mota	Konjugatua
CK3/K76	CBL218	Millipore	Mouse	M	IgG1	1:50	1ry	Unc.
CK15	sc-47697	Santa Cruz	Mouse	M	IgG2a	1:50	1ry	Unc.
Intβ4	ab29042	Abcam	Mouse	M	IgG1	1:40	1ry	Unc.
Ki67	MAB4190	Millipore	Mouse	M	IgG1	1:40	1ry	Unc.
MelanA	ab785	Abcam	Mouse	M	IgG1	1:50	1ry	Unc.
PanCK	M3515	Dako	Mouse	M	IgG1	1:50	1ry	Unc.
ZO-1	ab190085	Abcam	Goat	M	IgG	1:40	1ry	Unc.
α-SMA	ab7817	Abcam	Mouse	M	IgG2a	1:400	1ry	Unc.
p63α	13109S	Cell signaling	Rabbit	M	IgG	1:800	1ry	Unc.
Bimentina	ab16700	Abcam	Rabbit	M	IgG	1:1000	1ry	Unc.
anti-Mouse IgG1	A21121	ThermoFisher	Goat	P	IgG	1:1000	2ry	AF® 488
anti-Mouse IgG1	A21124	ThermoFisher	Goat	P	IgG	1:1000	2ry	AF® 568
anti-Mouse IgG2a	A21131	ThermoFisher	Goat	P	IgG	1:1000	2ry	AF® 488
anti-Mouse IgG2a	A21134	ThermoFisher	Goat	P	IgG	1:1000	2ry	AF® 568
anti-Rabbit IgG	A11070	ThermoFisher	Goat	P	IgG	1:1000	2ry	AF® 488
anti-Rabbit IgG	ab175471	Abcam	Goat	P	IgG	1:1000	2ry	AF® 488
anti-Goat IgG	A11057	ThermoFisher	Donkey	P	IgG	1:1000	2ry	AF® 568

M: Antigorputz monoklonala. 1ry: Antigorputz primarioa. Unk.: Konjugatu gabea.
P: Antigorputz poliklonala. 2ry: Antigorputz sekundarioa. AF: Alexa Fluor®.

13. Mikroskopia teknikak

13.1. Fase-kontraste mikroskopia

Hazkuntza-zelularren analisi morfologikoa Nikon Eclipse TS 100 fase-kontraste alderantzizko mikroskopioa (Nikon, Tokio, Japonia) erabiliz egin genuen, Irudiak ProgRes CapturePro 2.6 software-arekin atera genituen, 4× 10× eta 20× handipen objektiboak erabiliz.

13.2. Eremu argiko mikroskopia

H-E-az tindatutako laginak Olympus BX50 mikroskopioa (Olympus, Tokyo, Japan) eta 4× 10× eta 20× handipen objektiboak erabiliz aztertu genituen. Irudiak ProgRes CapturePro 2.6 software-arekin atera genituen.

13.3. Fluoreszentziazko mikroskopia eta mikroskopia konfokala

Bideragarritasun/zitotoxikotasun AM-Kaltzeina-EthD1 tindaketa-saiakuntzetako laginak Olympus IX71 fluoreszentziako mikroskopioarekin (Olympus, Tokio, Japonia) aztertu genituen. Irudiak Olympus DP71 kamera eta Olympus Cell B softwarearekin atera genituen.

Immunohistokimikako eta immunozitokimikako laginak Apotome.2 fluoreszentzia-mikroskopioarekin aztertu genituen (Zeiss, Oberkochen, Alemania). Irudiak Axiocam ER5c kamera digitalarekin eta Zeiss ZEN Blue software-arekin atera genituen. Mikroskopio hau mikroskopio konfokal gisa erabili genuen baita, egituratutako argiztapen-sistema zuela.

CK15 (gorria)-Melan A (berdea) tindatutako zelulen koloniak Zeiss LSM880 Fast Airyscan (Zeiss, Oberkochen, Alemania) bereizmen handiko mikroskopioarekin aztertu genituen. Irudiak Axiocam MRm kamera digitalarekin eta Zeiss ZEN Black atzemateko softwarearekin atera genituen.

In vivo saiakuntzako laginak Nikon Ti-U fluoreszentzia-mikroskopioan (Nikon, Tokio, Japonia) aztertu genituen. Nikon DS-Qi2 kamera eta Nikon NIS Elements AR kontrol software-a erabili genituen irudiak sortzeko. Mikroskopio hau dekonboluzio-unitatea erabiliz mikroskopio konfokal gisa erabili genuen.

Ehun eta hazkuntza zelularren portetako fluoreszentzia-analisia ImageJ software-a erabiliz gauzatu genuen (Wayne Rasbandek garatua Research Services Branch, National Institute of Mental Health, Bethesda, MD).

13.4. Ekorkuntz mikroskopia elektronikoa (SEM)

Biofilmen ebaketak Hitachi S-4800 (Hitachi High-Technologies Corporation, Madril, Espainia) ekorkuntz-mikroskopio elektronikoa erabiliz aztertu genituen. Laginak bi aldeko zinta itsaskorra zuen metalezko euskarri batean muntatu genituen lehenik. Azkenik, urrearekin (JFC-1100) argon atmosferan estali genituen behaketa egin aurretik. Lagin guztiak 15 kV-ko azelerazio-tentsioa erabiliz aztertu genituen.

Hazkuntza zelularrak SEM bitartez ere aztertu genituen. Laginak 0,1 M Sorensen tanpoian gehitutako % 2 glutaraldehido soluzioan finkatu genituen, pH 7,4 eta 4 °C-tara, gau osoan zehar mantenduz. Ondoren, 0,1 M Sorensen soluzioan garbitu genituen 10 minutuz. Laginak % 30, 50, 70, 90 eta 96-ko etanol kontzentrazioetan deshidratatu genituen 30 minutuz. Etanol absolutuarekin 30 minutuko bi garbiketa egin genituen deshidratazioaren azken urrats gisa. Ondoren, dishidratatutako laginak hexametildisilazanoan (HMDS) sartu genituen 30 minutuz bi aldiz eta lehortzen utzi genituen giro-tenperaturan. Behin lehortuta, laginak SEM euskarrietan muntatu genituen alde biko zinta itsasgarriarekin. Azkenik, urrearekin argon atmosferan estali ziren SEM bidez bistaratzeko.

14. Analisia eta estatistika

Emaitzak hainbat proba estatistikoren bidez aztertu genituen.

Biofilmekin lotutako emaitzei dagokienez, gardentasun-analisia Kruskal-Wallisen proba ez-parametrikoa eta ondorengo Dunnen proba aplikatuz egin genuen. Degradazio eta MTT balioak aztertzeko, Two-way ANOVA bariantza-analisia konparazio anitzentzako Bonferroniren testarekin erabili genuen.

Hidrogelaren emaitzen analisirako hainbat proba estatistiko erabili genituen.

Puzte- eta hedapen-datuak Kruskal-Wallisen proba ez-parametrikoaren eta ondorengo Dunnen testarekin aztertu genituen. *In vitro* igorpen- eta askapen-saiakuntzak Two-way ANOVA bariantza-analisiarekin eta Sidak eta Dunnetten konparazio anitzetarako testekin ebaluatu genuen, hurrenez hurren. Two-way ANOVA bariantza-analisia zitobateragarritasunaren eta hazkuntza

faktoreen kuantifikazioaren emaitzak aztertzeko erabili genuen, bi kasuetan Tukey-ren post hoc testa erabiliz.

In vitro inflamazio saiakuntzaren eta atxikipenaren emaitzak one-way ANOVA bariantza-analisi arruntarekin eta Tukey-ren konparazio anitzetako testarekin aztertu genituen.

In vivo emaitzei dagokienez, zaurien itxierari buruzko datuak two-way ANOVA bariantza-analisiaren bidez aztertu genituen, eta one-way ANOVA arruntaren bidez, zauri itxien ehunekoak ebaluatu genituen. Bi analisien ondoren, konparazio anitzetarako Dunnett-en proba erabili genuen. Draize probaren puntuazioak, malko-laginen malko-bolumena eta proteinen kontzentrazioa eta proba pilotuko zitokinen kontzentrazioa kuantifikatzeko, Two-way ANOVA bariantza-analisia erabili genuen baita. Adierazpen genikoa aztertzeko aldiz, one-way ANOVA arrunta erabili genuen. Froga guzti hauek Tukeyren konparazio anizkoitzak jarraituz egin genituen. Azkenik, hazkuntza zelular primarioen kuantifikazio emaitzak Kruskal-Wallisen proba eta konparazio anitzetarako Dunnen testa erabiliz ebaluatu genituen.

Analisi estatistiko guztiak adierazgarritzat jo genituen $p < 0,05$ mailan. Kalkulu estatistikoak GraphPad Prism 8 (San Diego, CA, AEB) programarekin egin genituen.

IV. EMAITZAK

1. Izaera proteikoko biofilmen *in vitro* ebaluazioa

Kornea-euskarriak sortzeko erabiliko diren biomaterialek jatorrizko kornea imitatzea dute helburu, beraz kornearen funtzio nagusietarako baldintzak bete behar dituzte. Biobateragarriak eta biodegradagarriak izan behar dira, jatorrizko ehunaren antzeko propietate optikoak eskaini behar dituzte eta biointegratzeko gaitasuna izan behar dute, hazkuntza, ugalketa eta migrazio zelularra estimulatuz.

Atal honen helburua proteinetan oinarritutako lau biomaterialen egokitasuna ebaluatzea izan zen, kornea-euskarri gisa *in vitro* erabiltzeko. Ebaluazio hau, material berriak jatorrizko ehunekin modu eraginkorrean elkarreragin dezaketen balioztatzeko lehen urrats erabakigarria da. Aztertutako biofilmak txerri larruazaletik eratorritako kolagenoz (KOL), soja-proteina isolatuz (SPI), laktosarekin erretikulatutako arrain-gelatinaz (GEL-LAK) eta azido zitrikoarekin erretikulatutako arrain-gelatinaz (GEL-AZ) sintetizatu genituen, guztiek animalia-edo-landare proteinak oinarri zituztelarik. KOL eta SPI filmak laborategiko prentsa batean nahasketak konprimituz lortu genituen. Gelatinaz egindako nahasketak (GEL-LAK eta GEL-AZ) Petri plaketan isuri genituen eta 48 orduz giro-tenperaturan lehortzen utzi genituen, filmak lortzeko.

1.1. Analisi fisiko-kimikoa eta morfologikoa

Fourierren transformatuaren bidezko espektroskopia infragorria (FTIR) filmen egitura kimikoaren ezaugarri diren talde funtzionalak identifikatzeko erabili genuen. Talde funtzional kimikoek erradiazio infragorria xurgatzen dute uhin-zenbaki espezifikoetan (cm^{-1}), loturen eta lotura-multzoen bibrazio bereizgarrien ondorioz.

Lotura amida bat amino talde bat (-NH_2) eta karboxilo talde bat (-COOH) lotzen dituen lotura kimikoa da. Lotura peptidikoak, lotura amida alegia, proteina baten egitura definitzen du, eta hau zehazteko I. amidaren (1600-1800 cm^{-1}), II. amidaren (1470-1570 cm^{-1}), III. amidaren (1240-1350 cm^{-1}) eta A amidaren (3300-3500 cm^{-1}) xurgapen infragorriko tontorrak erabiltzen dira.

IV.1 irudian aurkeztutako film guztien ATR-FTIR espektroek 3000-3500 cm^{-1} arteko banda zabala erakutsi zuten, O-H eta N-H talde libre eta lotuei esleitua (amida A). 2931 cm^{-1}-ko xurgapen-tontorra CH_2 luzatze asimetrikoari zegokion (IV.1 irudiko **a**).

Proteinen xurgapen-banda nagusiak honako hauekin lotu genituen: 1635 cm^{-1}-ko tontorra C=O luzatzearekin (amida I), 1545 cm^{-1}-ko tontorra N-H tolesdurarekin (amida II) eta 1241 cm^{-1}-ko tontorra C-N luzatze eta N-H tolesdurarekin (amida III) (IV.1 irudiko **b**). Glizerolaren xurgapen-bandak, filmei erantsitako plastifikatzailea, 800 cm^{-1} eta 1155 cm^{-1} bitarteko tartean erregistratu genituen. Zehazki, 1051 cm^{-1}-ra identifikatutako xurgapen-bandak C-O loturaren luzatzearekin lotu genuen. Agente gurutzatzaileei dagokienez, laktosarekin erlazionatutako bandak 953 eta 1180 cm^{-1} artean detektatu genituen. Era berean, azido zitrikoaren talde karboxilikoekin lotutako bandak 1743 cm^{-1}-ra ikusi genituen. Azido zitrikoak gelatinarekin erreakzionatu ondoren banda hau desagertu eta 1545 cm^{-1}-ra kokatutako gelatinaren banda 1585 cm^{-1}-tan erregistratu genuen, erretikulazio-erreakzioaren ondorioz.

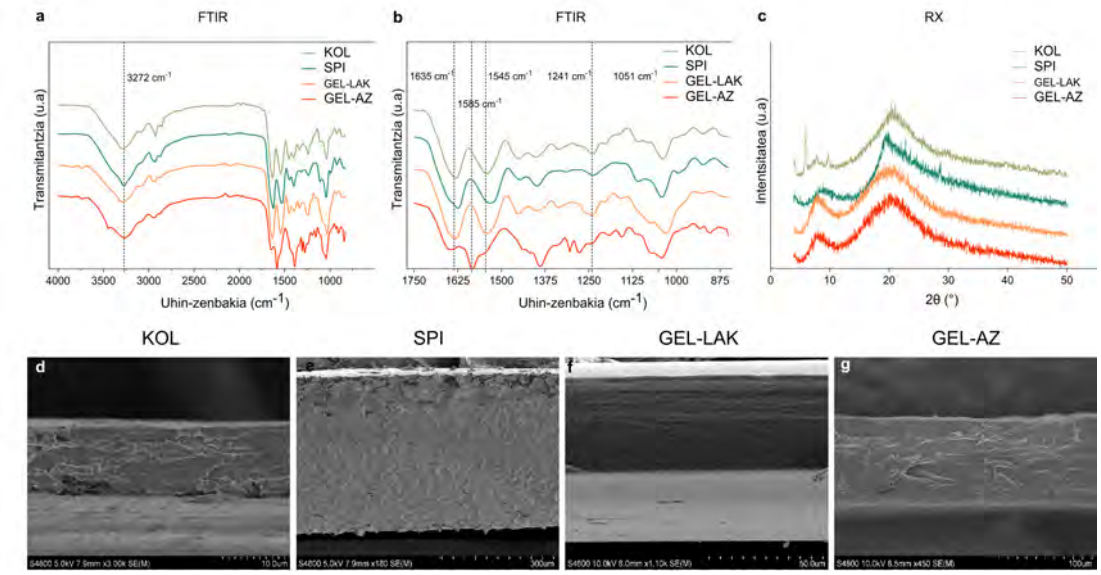

IV.1. IRUDIA: Filmen **a**) 4000-850 cm^{-1} eta **b**) 1750-850 cm^{-1} bitarteko FITR espektroak. **c**) Filmetako X izpien difrakzio-analisia. 3000 (**d**), 180 (**e**), 1100 (**f**) eta 450× (**g**) handipenekin lortutako filmen SEM irudiak. KOL: Kolagenoa; SPI: Soja-proteina isolatua; GEL-LAK: Laktosarekin erretikulatutako gelatina; GEL-AZ: Azido zitrikoarekin erretikulatutako gelatina.

X izpi bidezko difrakzio-analisia (XRD) eta ekorkuntz mikroskopia elektronikoa (SEM) erabili genituen filmen egiturak aztertu eta hauek neurtutako propietate fisiko-kimikoekin duten korrelazioa ikertzeko. XRD analisiak biofilmen fase kristalinoak eta amorfoak identifikatu zituen. Film hauek kate luzeko molekulen serieak dituzten polimeroak dira, bi modutara antolatuta egon daitezkeenak: kristalinoak, kateak ordenean antolatuta eta orientatuta dituztenak, edo amorfoak, ausaz multzokatuta daudenak, ordena bereizgarririk gabe. Polimero bat erabat amorfoa izan daitekeen arren, inoiz ezin da guztiz kristalinoa izan. Aitzitik, beti

izango ditu zati batean amorfoak diren eskualdeak.

KOL filmek partzialki kristalinoak diren materialei dagokien XRD eredua erakutsi zuten (IV.1 irudiko **c**). 2θ = 7°-ko tontorrak kolagenozko kate molekularren arteko alboko paketatze intermolekularraren distantzia adierazi zigun; aldiz, 2θ = 20°-ko tontor zabal lausoa kolagenozko zuntzen sakabanatzearen ondorioz erregistratu genuen, filmen egitura amorfoaren adierazgarria.

SPI filmen difrakzio-ereduek eremu amorfo nabarmena erakutsi zuten 2θ = 20°-tan zuen banda zabalarekin. Hori SPI-ren ezaugarria litzateke, 7S eta 11S globulina amorfoak baititu osagai nagusi gisa. GEL-LAK filmek bi difrakzio-tontor erakutsi zituzten: bata 21°-tara, gelatinaren kristalinotasunarekin lotutakoa, eta bestea 7,4°-tara, jatorrizko kolagenoaren helize hirukoitzari zegokiona. Era berean, GEL-AZ gelatinazko filmek gelatinazko tontorra erakutsi zuten, 21°-tan gutxi gorabehera, eta kolagenoaren helize hirukoitzari zegokion difrakzioko tontor desberdin bat, 2θ-tan 8° ingurukoa.

IV.1 irudiko SEM (**d-g**) analisiaren bitartez film guztiek egitura estu eta sendoa zutela frogatu genuen. XRD analisiaren bidez ikusitako KOL filmetako kolageno-kateen albo-antolaketa, zuntz-egitura trinko bezala erregistratu genuen SEM irudietan. Haatik, gelatinazko filmetan helize hirukoitzaren edukia murrizteak zuntz-morfologia ez hain definitua izatea eragin zuen.

1.2. Transmitantzia eta gardentasuna

Korneak argiaren transmisioan berebiziko garrantzia du, begiaren errefrakzio-ahalmenaren % 60 baino gehiago esleitzen baitzaio. Funtzio hori estuki lotuta dago kornearen gardentasun bereizgarriarekin. Kolageno-zuntzen antolaketa ordenatuak, estromako keratozitoen morfologia eta banaketarekin batera, ehun garden bihurtzen dute kornea. Antolaketa horrek, barreaitutako argiarekiko interferentzia suntsitzaileak eragin eta argiaren transmisioa hobetzen du. Beraz, kornea-ordezkoek argi kopuru hori transmititzeko gai izan behar dute, horregatik garrantzitsua da hautatutako materialen propietate optikoak neurtzea. Biofilmen argi-transmisioa eta gardentasuna egoera lehorrean zein hidratatuan neurtu genituen. Lehenengoak kontrol gisa balio izan zuten, eta hidratatutako bertsioak korneako gainazalean izan zezaketen egoera irudikatzeko balio izan ziguten.

IV.2 irudiko KOL (**a**) eta SPI (**b**) filmek transmisio-baliorik baxuenak erakutsi zituzten, pelikula lehorrak hidratatuak baino zeharrargiagoak izanik. SPI film lehor eta hidratatuen arteko argi-transmisioaren balioen ezberdintasunak murriztuz joan ziren uhin-luzerak handitu heinean, eta 620 nm-tik aurrera, ezberdintasunak estatistikoki esanguratsuak izateari utzi zioten. Hala ere, KOL biofilm lehorrek espektro ikusgai osoan hidratatuek baino % 30 argi gehiago transmititzen zutela erakutsi zuten. SPI film lehor eta hidratatuetan eta KOL film lehorretan, gutxi gorabehera % 60-80-ko argi transmisioa erregistratu genuen espektro ikusgaiaren uhin-luzera ia guztietan. Hala ere, gardentasun-argazkiek eredu lausoak erakutsi zituzten. Horrek, filmak zeharrargiak zirela eta argia pasatzen uzten zutela baina irudiak garbi fokatzeko gai ez zirela erakutsi zigun (IV.2 irudiko **e, f, i, j**).

Behin hidratatuta, gelatinazko filmek argi transmisio handiagoa erakutsi zuten. GEL-LAK filmek transmititu zuten argi gehien, eta GEL-LAK-en forma hidratatuetan zein lehorretan argi transmisioak ia ez zuen aldaketarik jasan (IV.2 irudiko **c**). Transmisioa % 3-ra jaitsi zen UV-A eskualdetik gertu (315-400 nm), erradiazio mota horren aurkako babes-ezaugarri izatea iradokiz. Argiaren transmisioak txikia izaten jarraitu zuen UV-A eskualdetik gertuko uhin-luzeretan, baina azkar handitu zen eskualde horira (570-580 nm), laranjara (580-620 nm) edo gorrixkara (620-780 nm) hurbildu ahala. Film hauek kolore horixka erakutsi zuten erabilitako erretikulazio-metodoa zela eta, baina kolore horrek ez zuen gardentasunean eraginik izan. Argazki-patroiak irakurgarriak izan ziren film hauekin (IV.2 irudiko **g, k**). GEL-AZ filmek erakutsi zuten hidratazioaren ondorengoko argi-transmisioaren hobekuntzarik handiena. Hauen gardentasuna % 20 inguru handitu zen espektro ikusgai osoan, eta, horri esker, argiaren % 80 baino gehiago transmititu ahal izan zuten 500 nm-tik aurrera (IV.2 irudiko **d**). Hobekuntza hori bat zetorren gardentasuna handitzearekin, film hidratatuek argazki-patroi argiak eta fokatuak erakutsi baitzituzten (IV.2 irudiko **h, l**).

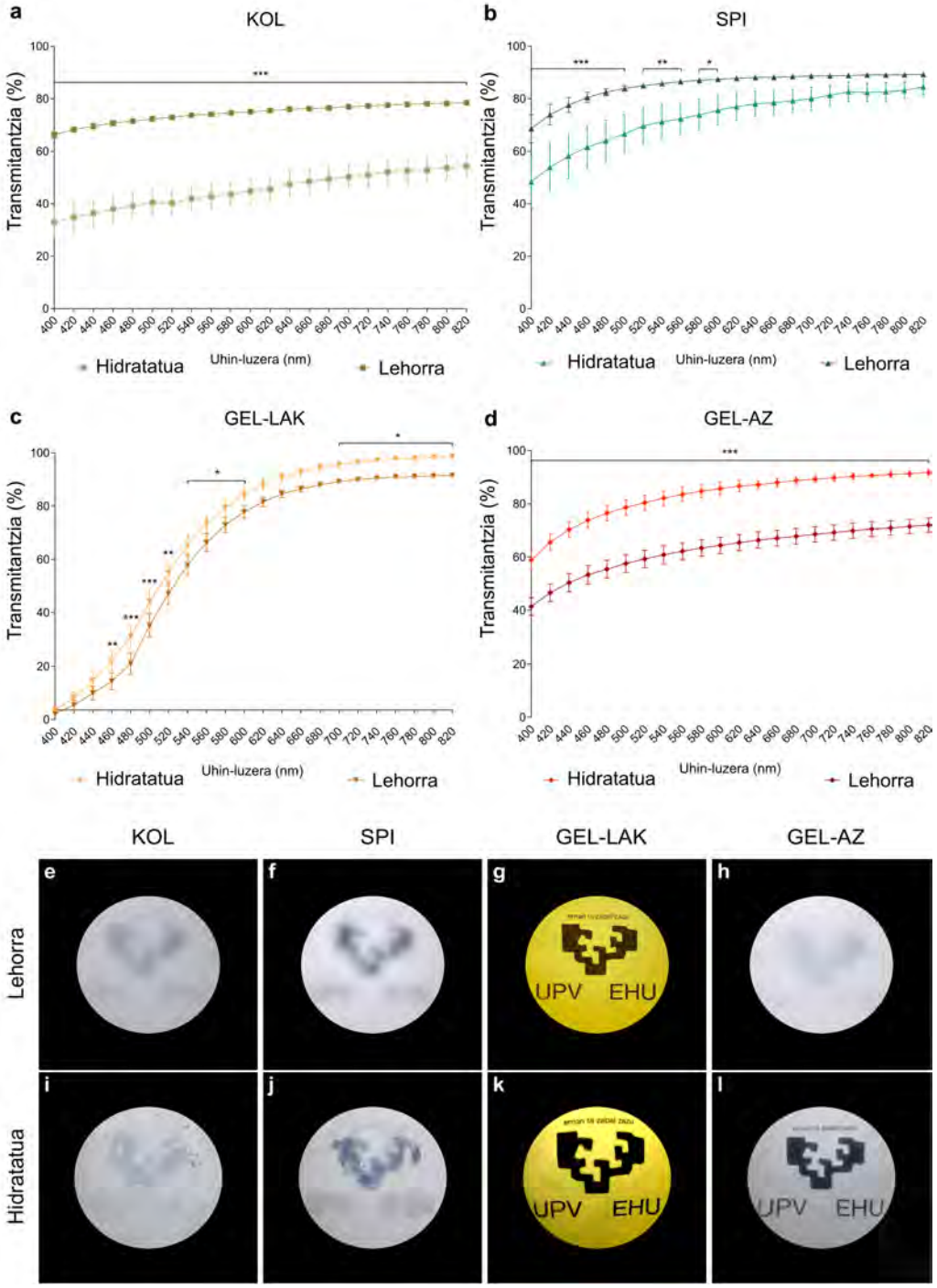

IV.2. IRUDIA: Film hidratatuen eta lehorren transmitantzia eta gardentasuna. **a-d**) Grafikoek film bakoitzak espektro ikusgaian transmititutako argiaren ehunekoa erakusten dute. Datuek transmitantzia-ehunekoaren batez bestekoa $\pm$ desbideratze estandarra (DE) adierazten dute. Ezberdintasun estatistikoki esanguratsuek film bakoitzaren egoera lehor eta hidratatuen arteko aldaketak adierazten dituzte ($*$ p < 0,05, $**$ p < 0,01, $***$ p < 0,001; n = 9). **e-l**) irudiek film bakoitzaren gardentasun-maila erakusten dute, bai film lehorretan (**e-h**), bai hidratatuetan (**i-l**). Irudi guztiak baldintza berdinekin atera genituen.

1.3. Biodegradazioa

In vitro degradazio-saiakuntza, filmek kolagenasa A entzimarekiko, PBS-arekiko edo ur desionizatuarekiko portaera ikusteko balio izan zigun. Soluzio entzimatikoan 15 minutuz murgildu ondoren, KOL filmak guztiz degradatu ziren, ziur aski soilik fisikoki erretikulatzearen ondorioz. Degradazio azkar horrek desberdintasun estatistiko nabarmenak erakutsi zituen kontrolarekin alderatuta (ur desionizatuaren degradazio-profila, IV.3 irudiko **a**). Degradazio-eredua antzekoa izan zen PBS eta ur desionizaturako; hala ere, alde estatistikoki esanguratsuak erregistratu genituen hainbat denbora-puntutan ($p < 0{,}001$ 15 minutu, 4 ordu eta 24 ordutan; $p < 0{,}01$ 1 ordutan; eta $p < 0{,}05$ 2 ordutan). Desionizatutako urak PBS-ak baino pisu gehiago galtzea eragin zuen.

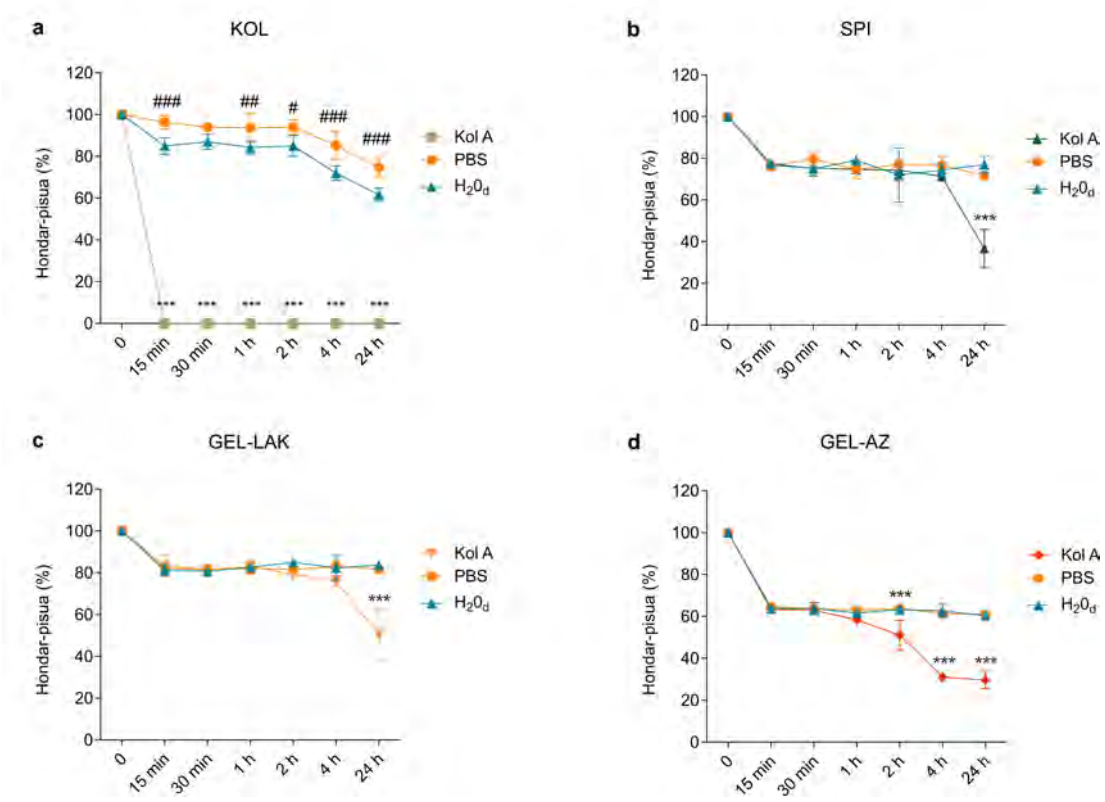

IV.3. IRUDIA: 24 orduz 37 °C-tan 200 μg/ml-ko kolagenasa A soluzioan edo PBS-tan mantendutako filmen *in vitro* degradazio-profilak. Ur desionizatuan murgildutako filmak kontrol gisa erabili genituen. **a**) KOL filmen degradazio-profilak, **b**) SPI filmen degradazio-profilak, **c**) GEL-LAK filmen degradazio-profilak eta **d**) GEL-AZ filmen degradazio-profilak. Datuek batez bestekoa $\pm$ DE adierazten dute, eta kolagenasa A-n ($*$) eta PBS-n (#) sartutako filmen eta ur desionizatuan sartutako filmen arteko alde estatistikoki esanguratsuak adierazten dituzte. $*$, # $p < 0{,}05$, $**$, ## $p < 0{,}01$, $***$, ### $p < 0{,}001$; $n = 3$.

SPI, GEL-LAK eta GEL-AZ filmek degradazio-eredu konparagarriak erakutsi zituzten (IV.3 irudiko **b-d**). Kolagenasa A, PBS edo ur desionizatuaren eraginpean egon ondoren, pisua 15 minututan azkar murriztu zela ikusi genuen. SPI eta GEL-LAK filmen pisua % 70 eta % 80 inguruan mantendu zen hurrengo denbora-puntuetan. Kontrolek (ur desionizatuan murgildutako filmek) aldaketa estatitikoki esanguratsuak 24 orduren ondoren jasandako degradazio-entzimatikoarekin soilik erakutsi zituzten, pisuen ehunekoak % 40-ra eta % 50-era jaitsiz, hurrenez hurren. GEL-AZ filmei dagokienez, pisua % 60-ra jaitsi zen 15 minutuz hiru soluzioekiko esposizioaren ondoren. Pisuaren ehuneko hori konstante mantendu zen 2 ordura arte. Hortik aurrera, kolagenasa A-ren inpaktua nabarmendu zen ur desionizatuak eta PBS-ak eragindako hidrolisiarekin konparatuz, hasierako pisuaren % 30 bakarrik mantendu baitzen. KOL filmekin izan ezik, gainontzeko filmetan ez zen ezberdintasun esanguratsurik egon kontrolaren eta PBS soluzioaren arteko pisu-galeran, eta GEL-LAK filmek pisu galera txikiena erregistratu zuten entzimaren presentzian. Gelatinazko filmen arteko degradazio-desberdintasunek erabilitako agente erretikulatzailearen garrantzia nabarmendu zuten.

1.4. Zelulen proliferazioa eta bideragarritasuna

Zelulen proliferazioa 0, 24, 48 eta 72 ordutan aztertu genuen filmekin kontaktu zuzenean ereindako NIH-3T3 fibroblastoetan zein giza korneako zelula epitelialetan (KZE). Biomaterialik gabeko baina hazkuntza medioz betetako kikarak kontrol positibo gisa gehitu genituen. 3T3 emaitzek adierazi zutenez, zelulak ugalduz joan ziren denboran zehar filmekin kontaktuan jarritako baldintza guztietan, KOL filmekin kontaktuan jarritako hazkuntzek ezberdintasun nabarmenak erakutsi zituztelarik (IV.4 irudia).

24 ordutan, KOL taldean kontrol-taldearekin alderatuta % 70 inguruko bideragarritasun-balioak erregistratu genituen arren, ondorengo denbora-puntuetan zelulak KOL filmaren eraginpean egoteak efektu zitotoxikoa eragin zuen. Alde estatistikoki esanguratsuak ikusi genituen kontrol-taldearen eta KOL filmekin ereindako zelula-hazkuntzen artean 48 eta 72 ordutan, % 40-ko eta % 50-ko jarduera metabolikoa erregistratu baikenuen, hurrenez hurren. SPI, GEL-LAK eta GEL-AZ filmekin kontaktuan zeuden 3T3 hazkuntzen bideragarritasun-balioak % 70-etik gora mantendu ziren saiakuntza osoan zehar. Bideragarritasuna % 82, % 89 eta % 73-koa izan zen 72 ordura SPI, GEL-LAK eta GEL-AZ filmetarako kontrolarekin alderatuta.

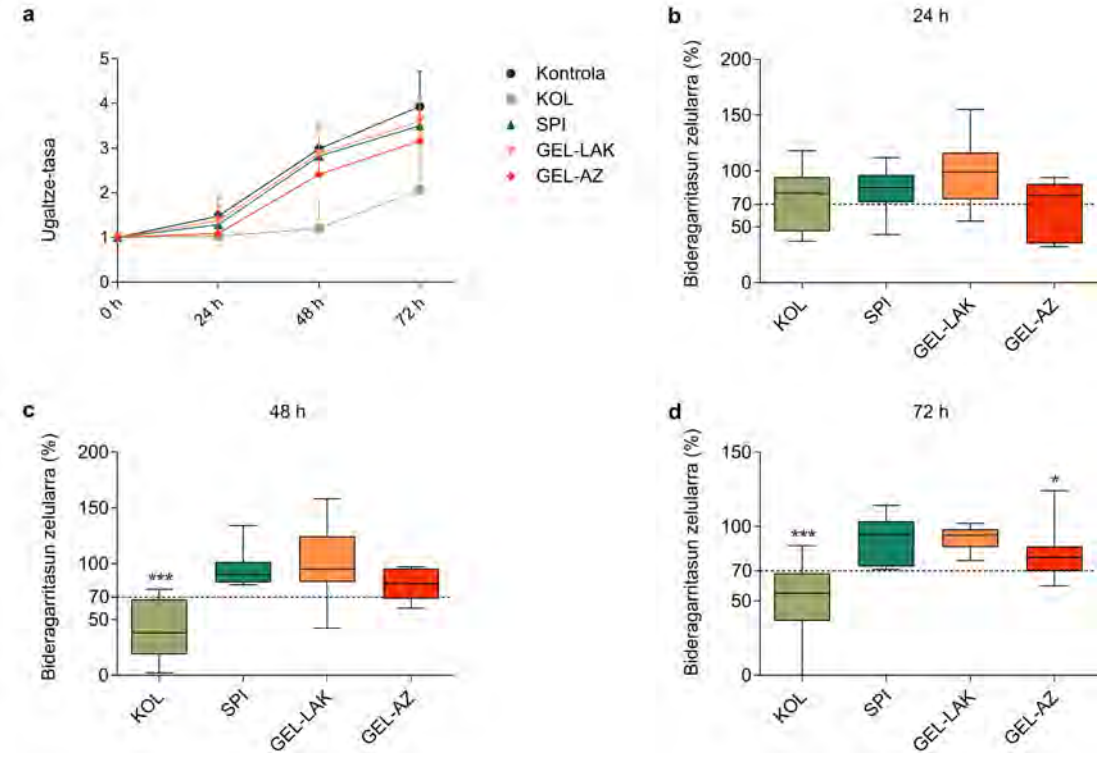

IV.4. IRUDIA: Filmen eragina NIH-3T3 zelulen **a**) proliferazioan eta **b-d**) bideragarritasunean. 3T3 zelulak film bakoitzarekin kontaktuan jarri genituen 24, 48 eta 72 orduz. Inolako biomaterialik gabe ereindako zelulak kontrol gisa erabili genituen. Proliferazio-emaitzek zelula bideragarrien ugaltze-tasaren batez bestekoa $\pm$ DE adierazten dute, t = 0 h-ko zelula bideragarriekin alderatuta. Bideragarritasun-emaitzek zelula bideragarrien ehunekoa adierazten dute, kontrolarekin alderatuta (% 100-eko bideragarritasuna). Grafikoen kutxa bakoitzaren barruan marraztutako lerroek film bakoitzaren bideragarritasun-balioen medianak adierazten dituzte. Kontrolarekiko desberdintasun estatistikoki esanguratsuak ikusi daitezke ($*$ $p < 0,05$, $**$ $p < 0,01$, $***$ $p < 0,001$; $n = 9$).

KZE hazkuntzei buruzko emaitzek denboraren menpeko ugaltzea erakutsi zuten (IV.5 irudia). KOL filmekin ereindako KZE-k ugalketa-patroi hobeak eta bideragarritasun-balio handiagoak erakutsi zituzten 3T3 hazkuntzekin alderatuta. Bideragarritasuna % 70-etik gorakoa izan zen KOL filmekin kasu guztietan, 72 orduan izan ezik, puntu honetan % 60 inguruko bideragarritasuna erregistratu baikenuen (% 60 medianaren balioa). Hala ere, KOL filmetarako erregistratutako balioak baxuenak izan ziren gainerako filmekin konparatuz. SPI, GEL-LAK eta GEL-AZ-rentzat erregistratutako bideragarritasuna % 70-etik gorakoa izan zen denbora-puntu guztietan.

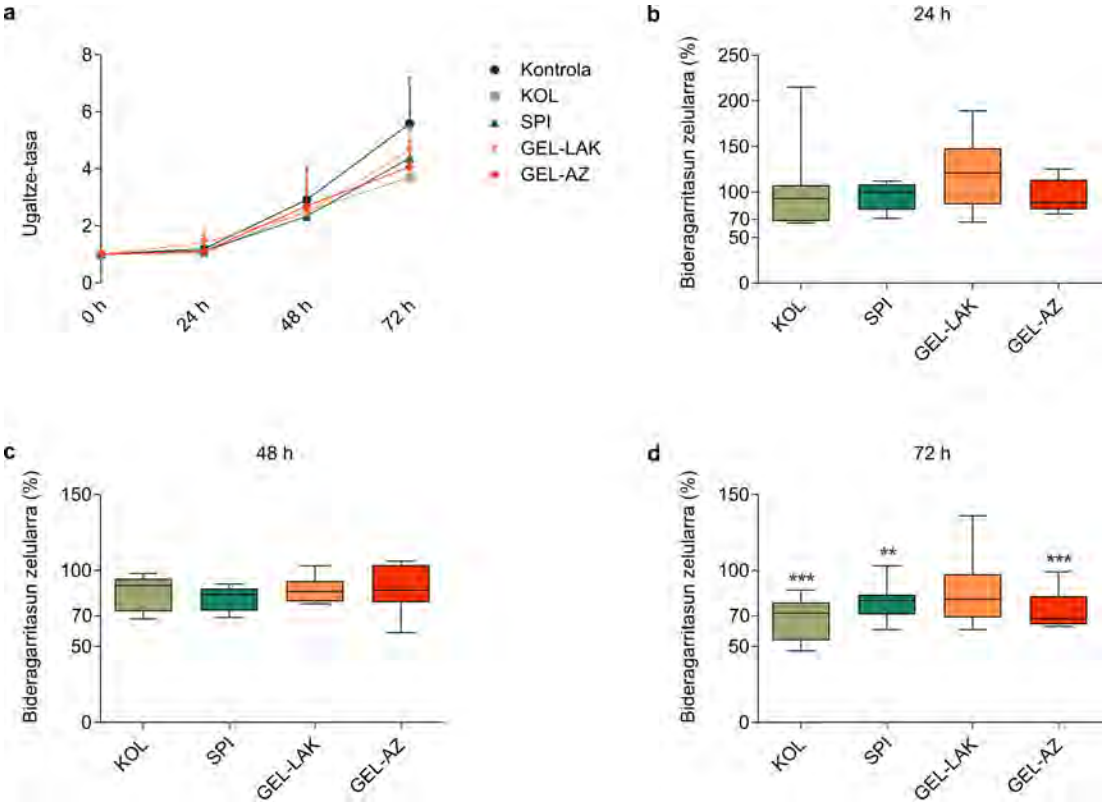

IV.5. IRUDIA: Filmen eragina KZE zelulen **a**) proliferazioan eta **b-d**) bideragarritasunean. KZE zelulak film bakoitzarekin kontaktuan jarri genituen 24, 48 eta 72 orduz. Inolako biomaterialik gabe ereindako zelulak kontrol gisa erabili genituen. Proliferazio-emaitzek zelula bideragarrien ugaltze-tasaren batez bestekoa ± DE adierazten dute, t = 0 h-ko zelula bideragarriekin alderatuta. Bideragarritasun-emaitzek zelula bideragarrien ehunekoa adierazten dute, kontrolarekin alderatuta (% 100-eko bideragarritasuna). Grafikoen kutxa bakoitzaren barruan marraztutako lerroek film bakoitzaren bideragarritasun-balioen medianak adierazten dituzte. Kontrolarekiko desberdintasun estatistikoki esanguratsuak ikusi daitezke (∗ $p < 0,05$, ∗∗ $p < 0,01$, ∗∗∗ $p < 0,001$; $n = 9$).

1.5. Zelulen atxikidura

Zelulen atxikidura eta filmen zitobateragarritasuna, AM-Kaltzeina eta Etidio-1 homodimero (EthD1) saiakuntza denbora-puntu desberdinetan (24, 48 eta 72 ordu) eginez eta SEM irudiak aztertuz ebaluatu genituen.

SPI, GEL-LAK eta GEL-AZ filmen gainean ereindako 3T3 zelulek kontrol-tratamenduaren antzeko morfologia erakutsi zuten, fibroblastoen ohiko morfologia adardun bipolar eta multipolarra alegia (IV.6 irudiko **a-d**). Zelulek filmetan zuten kokapenari dagokionez, SPI eta GEL-LAK filmek geruza bakarreko konfigurazio lau eta luzea erakutsi zuten, hau da, kontrol-taldearenaren antzekoa. GEL-AZ filmetan ordea, zelulak multzokatuta ikusi genituen monogeruza-konfigurazio baten ordez.

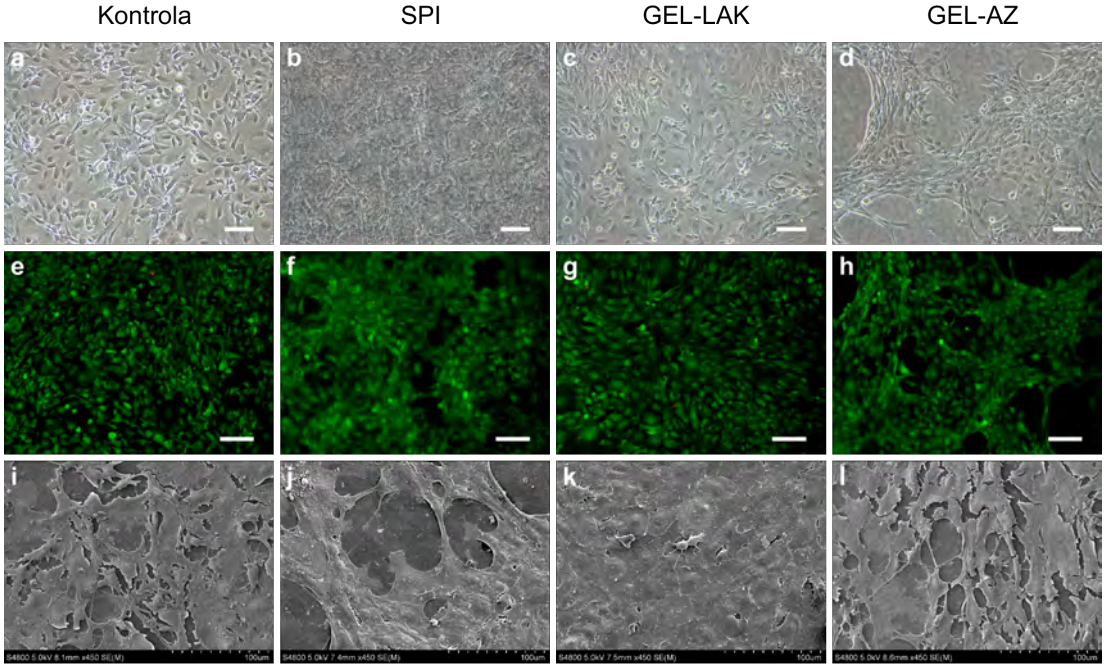

IV.6. IRUDIA: 3T3 zelulen hazkuntza filmen gainean. **a-d**) Fase-kontrasteko mikrospioaren bidez, 3T3 zelulen hazkuntza-plakaren (Kontrola) edo filmen gaineko hazkuntzen irudiak 24 orduz kultibatu ondoren. **e-h**) AM-Kaltzeina-EthD1 saiakuntzaren irudiak eta **i-l**) SEM bidez ateratako irudiak. **a-h**) Irudiak 10× handipen objektiboarekin atera genituen eta eskala lerroek 100 μm-ko neurriak adierazten dituzte. **i-l**) Irudiak 450× handipenarekin atera genituen.

AM-Kaltzeina-EthD1 saiakuntzetan zelulen % 1-5-a soilik tindatu zen EthD-1-z, heriotza-tasa minimo bat adieraziz. Balioak 72 orduz mantendu ziren. SEM irudiek zelulen antolaketa laua eta zabala erakutsi zuten filmetan, taldeen arteko desberdintasun morfologiko esanguratsurik gabe (IV.6 irudiko **i-l**).

Aldaketa morfologikoak erregistratu genituen film ezberdinen gainean ereindako

KZE zeluletan (IV.7 irudiko **a-d**). Korneako epitelio-zelulek mosaiko formako ohiko kokapena erakutsi zuten kontrol eta GEL-LAK filmetan, SPI eta GEL-AZ filmetan ereindako zelulek, berriz, forma luzatuagoa eta biribilagoa erakutsi zuten, antolaketa poligonal lausoago batekin. 24, 48 eta 72 ordutan egindako AM-Kaltzeina-EthD1 saiakuntzetan hildako zelula gutxi erregistratu genituen (IV.7 irudiko **e-h**). KZE hazkuntzen morfologian desberdintasunak, fase-kontraste mikroskopiaren bidez hauteman eta AM-Kaltzeina-EthD1 tindaketaren bidez baieztatu genituen. Zelula horiek bolumen zelular handiagoa erakutsi zuten 3T3 zelulekin konparatuz, SEM behaketetatik ondorioztatu bezala. Ez genuen taldeen arteko desberdintasunik ikusi, eta zelulen antolaketa estratifikatua erregistratu genuen kasu guztietan (IV.7 irudiko **i-l**).

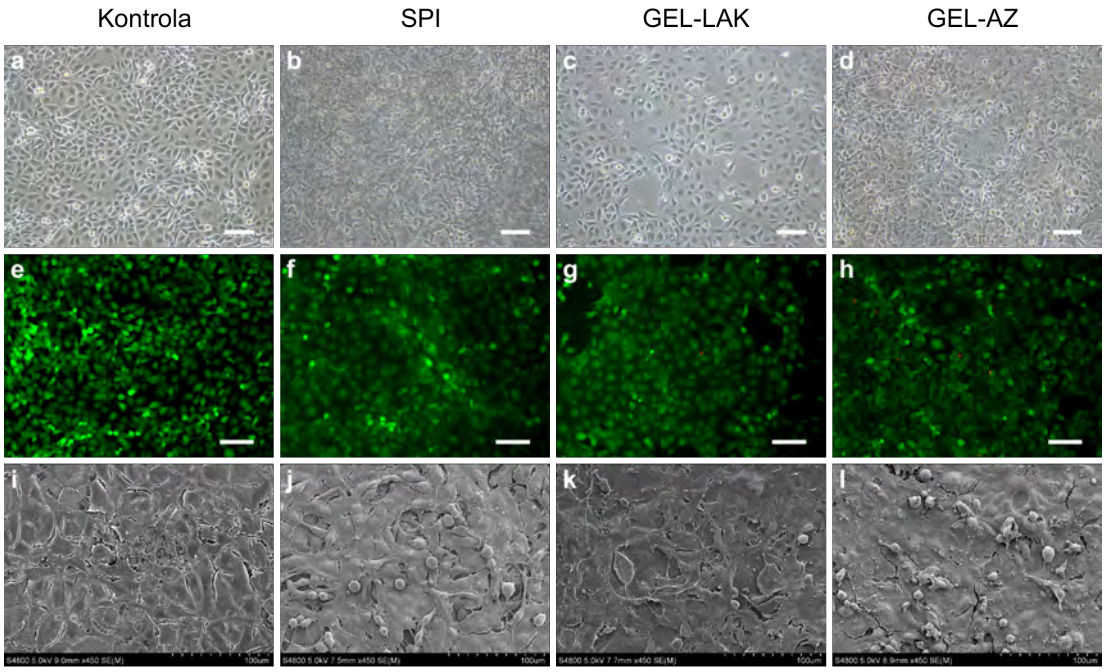

IV.7. IRUDIA: KZE zelulen hazkuntza filmen gainean. **a-d**) Fase-kontrasteko mikrospioaren bidez, KZE zelulen hazkuntza-plakaren (Kontrola) edo filmen gaineko hazkuntzen irudiak 24 orduz kultibatu ondoren. **e-h**) AM-Kaltzeina-EthD1 saiakuntzaren irudiak eta **i-l**) SEM bidez ateratako irudiak. **a-h**) Irudiak 10× handipen objektiboarekin atera genituen eta eskala lerroek 100 μm-ko neurriak adierazten dituzte. **i-l**) Irudiak 450× handipenarekin atera genituen.

Bi zelula motei dagokienez, zelula-hazkuntzak argi ikusi genituen GEL-LAK filmetan fase-kontrasteko mikroskopiaren bidez. Hala ere, SPI eta GEL-AZ filmetan ezin izan genituen zelulak plano berean lerrokatu koadrante zehatz baten barruan, gainazalaren irregulartasunak zirela medio. Atxikidura eskasaren ondorioz, ezin izan genuen KOL filmen gainean zelularik erein eta beraz, film mota hau saiakuntza honetatik baztertu genuen.

1.6. Zelulen migrazioa

Biofilmen gaineko KZE eta 3T3 zelulen migrazio-ahalmena zelularik gabeko hutsune bat sortuz eta hau 0, 24, 48 eta 72 ordutan ixteko beharrezko denbora neurtuz ebaluatu genuen. Film-mota bakoitzean egindako erreplikek bi zelula-moten biomaterialen gaineko migrazio potentziala erakutsi zuten. Arrakalen itxiera azkarragoa izan zen 3T3 zelulekin KZE zelulekin baino. Bi kasuetan, GEL-AZ-ren gainean ereindako zelulek denbora gehiago behar izan zuten hutsuneak ixteko. Hala ere, hazkuntza guztiek zelularik gabeko eremua estali zuten 72 ordutan (IV.8 irudia). Atxikitze-saiakuntzen kasuan bezala, zelula-motetako bat ere ezin izan genuen KOL filmen gainean erein.

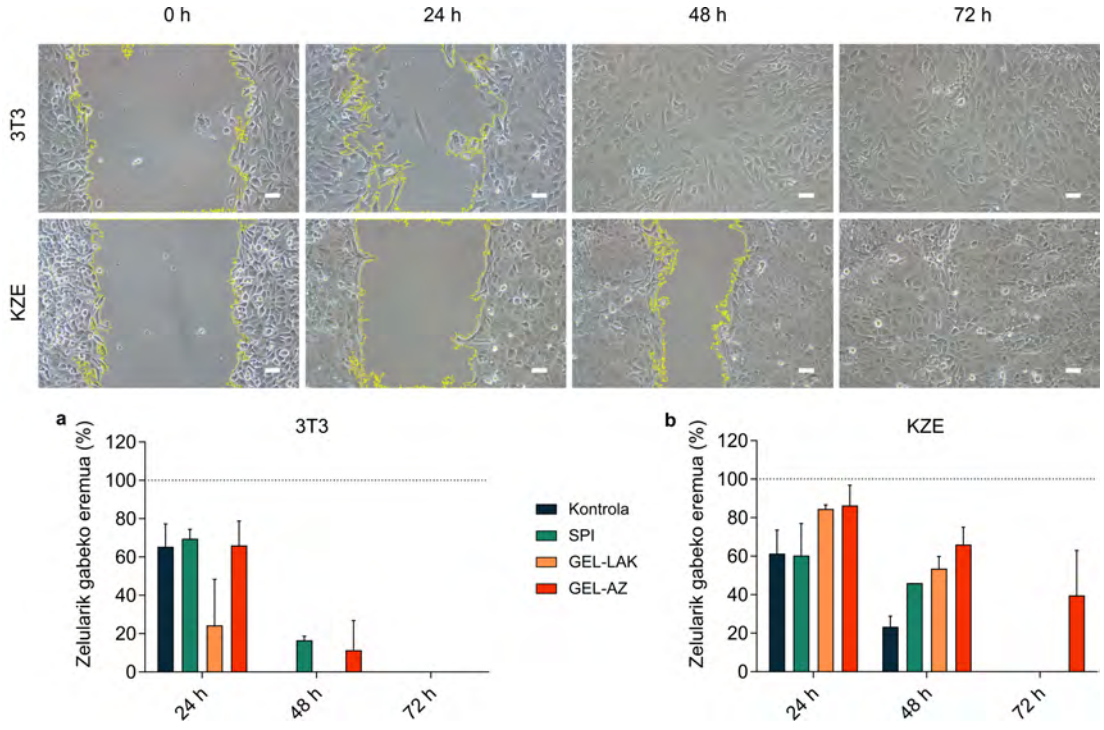

IV.8. IRUDIA: GEL-LAK-en gainean ereindako KZE eta 3T3 zelulen migrazio-saiakuntza, 24, 48 eta 72 orduz kultibatu ondoren. Irudiak 10× handipen objektiboarekin atera genituen; eskala lerroek 50 μm-ko neurriak adierazten dituzte. **a,b**) grafikek film bakoitzean 3T3 (**a**) eta KZE (**b**) zelulen hutsune-itxieraren bilakaera adierazten dute.

2. Gelatinazko hidrogelen *in vitro* ebaluazioa

Biofilm forman landutako proteinetan oinarritutako hainbat biomaterial probatu ondoren, gelatina aukeratu genuen kornea-akatsak betetzeko hidrogela garatzeko abiapuntuko material gisa. Hidrogelaren agente erretikulatzaile bezala erriboflabina fosfatoa (RFP) hautatu genuen, klinikan asko erabiltzen den fotogurutzatzailea.

Gelatina eta RFP oinarri zituen hidrogelaren bertsio desberdinak egin eta hauen propietate fisiko-kimikoak eta *in vitro* biobateragarritasuna ebaluatu genituen. Azterketan lau hidrogel-bertsio erabili genituen: G izeneko hidrogela, % 5 gelatinaz eta % 0,01 RFP-z osatua; G-D izeneko hidrogela, % 5 gelatinaz, %0,01 RFP-z eta % 2,5 dextranoz (D) osatua; G-HA izeneko hidrogela, % 5 gelatinaz, %0,01 RFP-z eta % 2,5 azido hialuronikoz (AH) osatua eta G-MZ izeneko hidrogela, % 5 gelatinaz, %0,01 RFP-z eta % 1 metilzelulosaz (MZ) osatua.

2.1. Erreologia neurketak

Ebakidura-erreologia lau hidrogel bertsioen propietate biskoelastikoak eta fluentzia eta jariakortasun ezaugarriak bereizteko erabili genuen.

Anplitude-ekorketak eremu biskoelastiko linealean (EBL), saiakuntza laginaren egitura suntsitu gabe egin daitekeen eremua alegia, laginen deformazio-portaera deskribatzeko erabili genituen. Saiakuntza honek aztertutako materiala jariatzen hasteko edo hausteko beharrezkoa den deformazio-muga zehaztea du helburu. Neurketa horiek lortzeko, seinale oszilatorioaren anplitudea aldatu beharra dago denboran zehar, maiztasuna konstante mantentzen den bitartean. Maiztasun-ekorketa lagin batek EBL tartearen barruan duen denboraren araberako portaera adierazteko erabiltzen da. Maiztasun altuenek mugimendu azkarra simulatzen dute denbora laburretan; maiztasun baxuenek, berriz, mugimendu geldoa denbora-tarte luzeetan edo atsedenean. Maiztasun-ekorketetan, oszilazio-maiztasuna pixkanaka handitzen edo gutxitzen da denboran, anplitudea konstante mantentzen den bitartean. Biltegiratze-moduluak (G') portaera biskoelastikoaren zati elastikoa adierazten du, eta laginaren portaera solidoa deskribatzen du. Galera-moduluak (G'') aldiz, portaera biskoelastikoaren zati likatsua ezaugarritzen du, laginaren portaera urkaritzat har daiteke.

Hidrogelen propietate solido eta likidoak anplitude eta maiztasun oszilazio-ekorketen bidez ebaluatu genituen.

10 rad/s-ko maiztasunarekin eginiko anplitude-ekorketa dinamikoek, hidrogelen isuri-portaera eta EBL eremua zehaztu zituzten. Hidrogel horietarako, EBL-a 0tik % 100-era bitarteko deformazio-baliotzat har zitekeen, gutxi gorabehera. Eremu horretan, G′ eta G″ balio egonkortuak erregistratu genituen, kasu guztietan G′ G″ baino handiagoa izanik. Horrek hidrogel guztiek gel baten antzeko egitura zutela adierazi zuen, erregimen horren barruan jokaera urkaria baino solido bati dagokion portaera erakutsiz. G hidrogela 250 Pa inguruko tentsio-balioak lortu arte ez genuen isurtzen ikusi. G-D-k, G-AH-k eta G-MZ-k 50 Pa, 500 Pa eta 1800 Pa-ko fluentzia-tentsioak erakutsi zituzten, hurrenez hurren, G″ eta G′-ren arteko gurutzagunean (IV.9 irudiko **a**).

Emaitza horiek, hidrogel guztiak isuri zitezen gutxieneko tentsio-maila bat behar zela iradoki zuten, baina AH eta MZ gehitzeak handitu egin zuen beharrezko tentsio-maila hori.

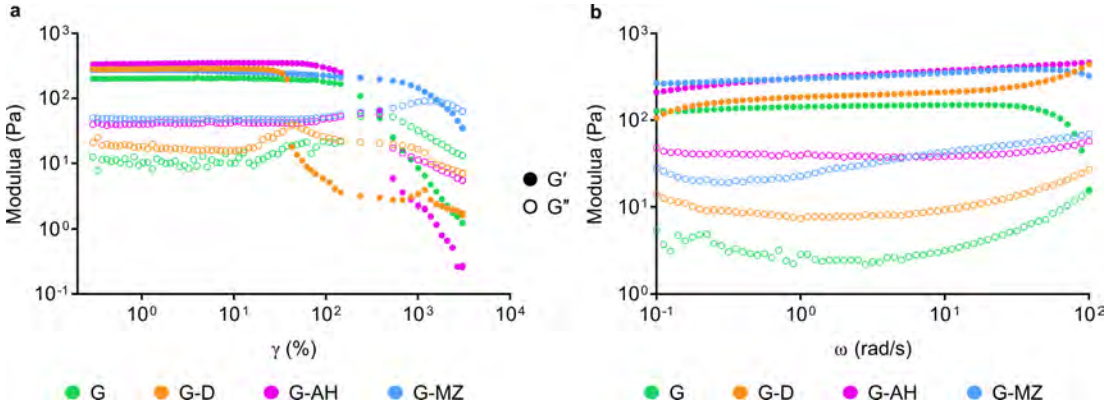

IV.9. IRUDIA: **a**) G, G-D, G-AH eta G-MZ hidrogelen anplitude-ekorketak (frekuentzia angeluarra (ω) = 10 rad/s, 25 °C) eta **b**) G, G-D, G-AH eta G-MZ hidrogelen maiztasun oszilazio-ekorketak (tentsioa (ε) = % 1, 25 °C).

EBL-ren barruan egindako maiztasun oszilazio-ekorketen bitartez, G, G-D, G-AH eta G-MZ hidrogelen maiztasun-erantzunek ezberdintasun esanguratsurik ez zutela ikusi genuen. Biltegiratze-modulua (G′) galera-modulua (G″) baino handiagoa izan zen ebaluatutako maiztasun-tarte osoan, inolako gurutzaketarik gabe. Emaitza horrek, begirako aplikazio posible batean hidrogelek solidoen antzeko propietateak izango zituztela iradoki zuen (IV.9 irudiko **b**).

Hidrogeletan egindako maiztasun eta anplitude ekorketak argi urdinarekin

erretikulatu ondoren egin genituen, korneako zauriari aplikatzean hidrogelak edukiko lukeen portaera imitatzeko.

Laginen fluxu-portaera orokorra ezaugarritzeko fluxu-ekorketak egin genituen. Ebakidura-abiaduraren ekorketek, hidrogelen ebakidura bidezko argaltze-portaera eta ebakiduraren mendeko biskositatea erakutsi zuten kasu guztietan. Hidrogelen biskositateak behera egin zuen ebakidura-abiadura 10^{-4} s^{-1}-tik 100 s^{-1}-ra handitu ahala, xiringa bidez injektatzean izango luketen baldintza mekanikoen antza hartuz (IV.10 irudiko **a**) . Beraz, emaitzek hidrogelen bertsio guztiak erraz injektatu zitezkeela egiaztatu zuten.

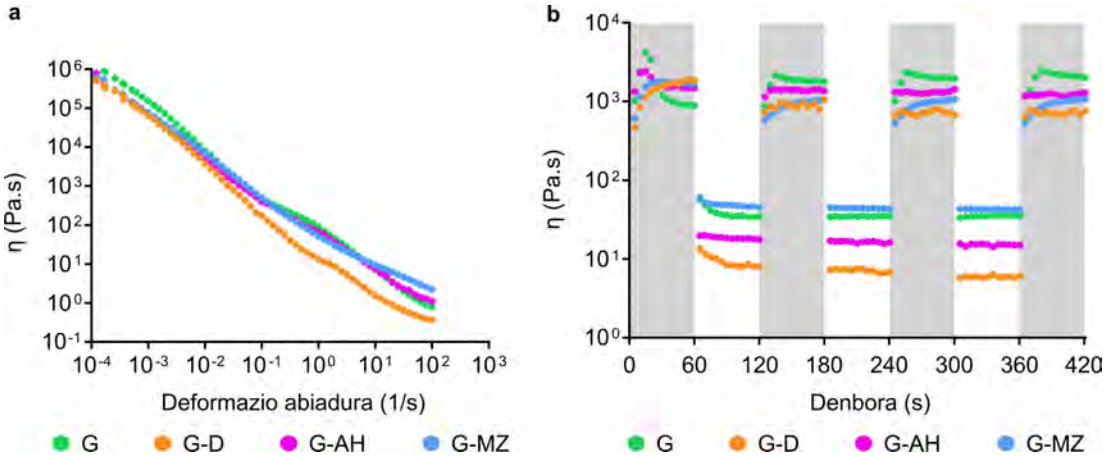

IV.10. IRUDIA: **a**) G, G-D, G-AH eta G-MZ hidrogeletako fluxu-ekorketak. **b**) G, G-D, G-HA eta G-MZ hidrogeletako tartekatutako ebakidura neurketak, lau ziklotan txandakatutako ebakidura-indar baxuan (grisa; 0.1 s^{-1}) eta altuan (zuria; 10 s^{-1}).

Hidrogelek beren propietateak berreskuratzeko zuten gaitasuna tartekatutako ebakidura neurketen bidez ebaluatu genuen. Hidrogel guztien biskositateak behera egin zuen ia bi magnitude-ordenen artean ebakidura altuko pasarteetan (10 s^{-1}), baina hauek erreferentziako biskositate maila 5 segundotan berreskuratu zuten ebakidura-abiadura jaitsi ondoren (0.1 s^{-1}) (IV.10 irudiko **b**). Autosendatze eta argaltze-saiakuntzek hidrogelak orratz baten bidez injektatzeko mekanismoa simulatu zuten. Orratz horretan ebakidura-abiadura handiak erabiliko ziratekeen hidrogela kornea-gainazalean aplikatzeko, beraz emaitza horrek frogatu zuen hidrogel likatsu bat jar zitekeela eta korneako zaurian iraungo zuela, hidrogelean kapsulatutako edukia modu kontrolatuan askatzea erraztuz.

Fluxu- eta ebakidura-ekorketak hidrogelak argi urdinarekin erretikulatu aurretik egin genituen giro-tenperaturan.

Muga elastikoaren neurketak ere giro-tenperaturan eta hidrogela argiz irradiatu aurretik egin genituen. Muga elastiko estatikoaren balioak IV.11 irudiari dagokion grafikoan adierazita daude.

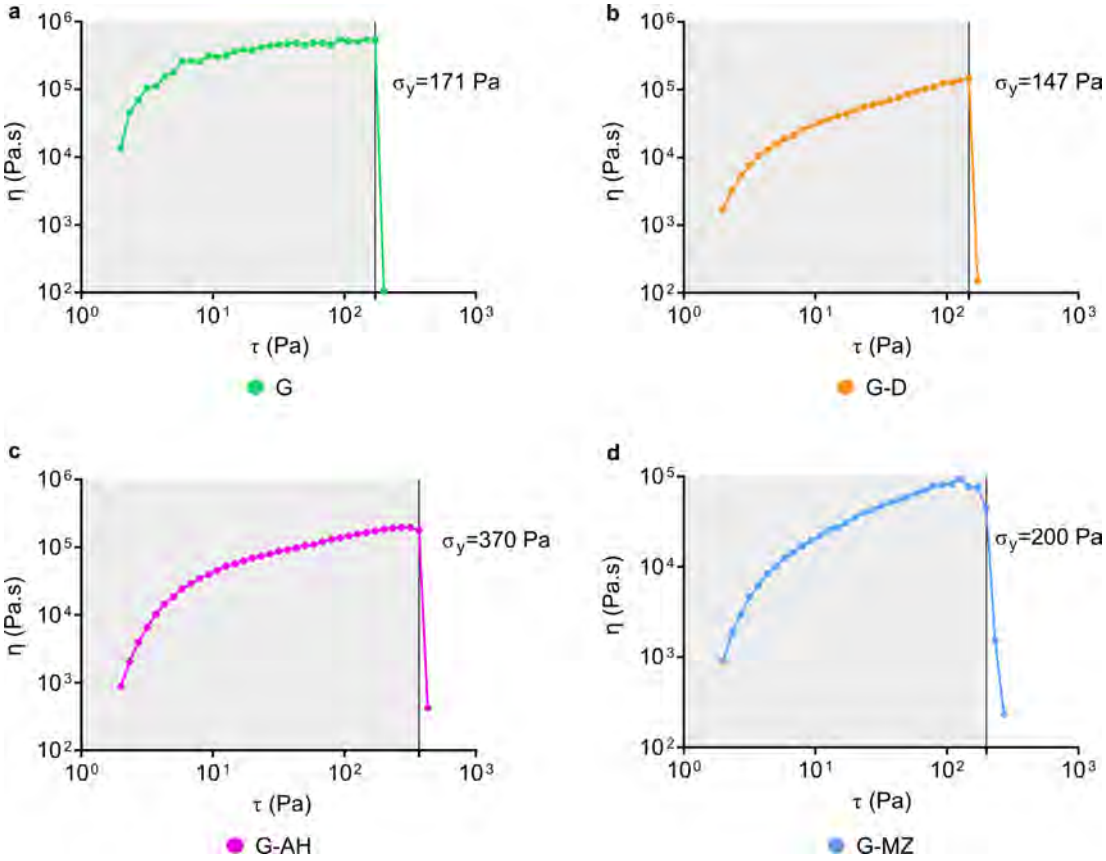

IV.11. IRUDIA: G (**a**), G-D (**b**), G-AH (**c**) eta G-MZ (**d**) hidrogelen muga elastikoaren neurketak. Muga elastiko estatikoaren balioak dagozkien grafikoetan adierazita daude.

Hidrogela jariatzen hasteko beharrezko indarra handiagoa izan zen hidrogelari AH gehitu zitzaionean (IV.11 irudiko **c**), hidrogela xiringaren bidez aplikatzeko tentsio handiagoa beharko zela adieraziz. MZ gehitzeak ere muga elastiko estatikoaren balioa handitu zuen G-rekin alderatuta, hidrogel likatsuagoa sortuz (IV.11 irudiko **d**). G-D-k aldiz, σ_y baliorik txikiena erregistratu zuen (IV.11 irudiko **b**).

2.2. Puzte- eta hedatze-neurketak

Puzte- eta hedatze-saiakuntzak 24 orduz PBS-tan murgildu ondoren hidrogelen bolumen eta azaleraren handipena zehazteko egin genituen. Grafikoki irudikatutako emaitzak, PBS-tan buzti aurretiko hidrogelen hasierako bolumen eta azalerak kontuan hartuz kalkulatu genituen (IV.12 irudia).

Atxikitako bolumenari dagokionez, G-D-k eta G-AH-k erakutsi zuten aldaketarik handiena, hasierako pisuekin alderatuz % 26-ko eta % 39-ko handipena jasan baitzuten hurrenez hurren (IV.12 irudiko **a**). G hidrogelak % 10-eko igoera izan zuen eta G-MZ hidrogelak, berriz, aldaketa txiki bat baino ez (% 0.6). Hala ere, ez genuen alde estatistikoki esanguratsurik erregistratu G-D, G-AH eta G-MZ-k atxikitako bolumenaren eta G bolumenaren artean.

Azaleraren handipenari dagokionez, G hidrogelak % 20-ko igoera jasan zuen hasierako azalerarekiko. G-rekiko aldaketa estatistikoki nabarmenak erregistratu genituen G-D eta G-AH kasuetan, % 85 eta % 100 zabaldu baitziren, hurrenez hurren, hasierako eremuaren ia bikoitza alegia (IV.12 irudiko **b**).

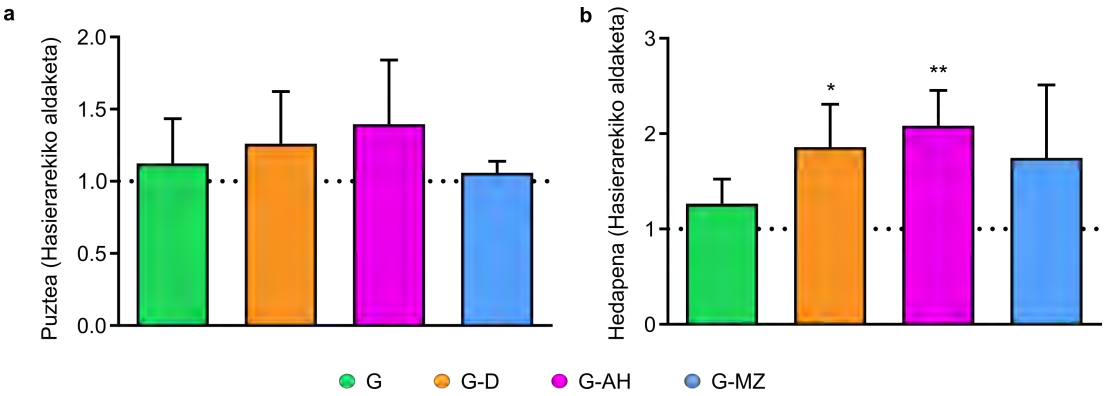

IV.12. IRUDIA: G, G-D, G-AH eta G-MZ hidrogeletan egindako puzte (**a**) eta hedatze (**b**) neurketak, PBS-tan murgildu eta 24 ordura. Emaitzek G hidrogelarekiko aldaketa $\pm$ DE adierazten dute. Alde estatistikoki esanguratsuak $*$ $p < 0{,}05$, $**$ $p < 0{,}01$, $***$ $p < 0{,}001$, $****$ $p < 0{,}0001$ bezala definitu ditugu.

2.3. Transmitantzia eta gardentasuna

Erretikulatutako hidrogelen eta erretikulatu gabeen transmitantzia espektro ikusgaian (400-800 nm) neurtu genuen. Gardentasuna erretikulatutako eta erretikulatu gabeko hidrogel bakoitzaren 500 μl hizki-patroi ezagun baten gainean jarriz ebaluatu genuen.

G eta G-MZ hidrogelek aurkeztu zuten argi transmisio ahalmenik handiena, 500 nm-tik gora % 90 baino gehiagoko balioak erregistratuz. Gardentasunari dagokionez, patroien bistaratze argiena erakutsi zuten hidrogelak izan ziren (IV.13 irudia). Argiaren transmisio-balioen aldakuntzek, hidrogel guztietan beren forma gurutzatuen eta ez-gurutzatuen artean, beherakada bat erakutsi zuten uhin-luzera handitu ahala. Desberdintasun horiek detektaezinak bihurtu ziren G eta G-MZ hidrogeletan 520 nm-tik aurrera (IV.13 irudiko **a,d**).

Erretikulatu eta erretikulatu gabeko G-D hidrogelaren bertsioak bereizi egin ziren 600 nm-tik aurrera (IV.13 irudiko **b**). Nahiz eta G-AH-ren bi bertsioen arteko aldeak nabariak izan espektro ikusgai osoan zehar, ez ziren estatistikoki esanguratsuak izatera iritsi (IV.13 irudiko **c**).

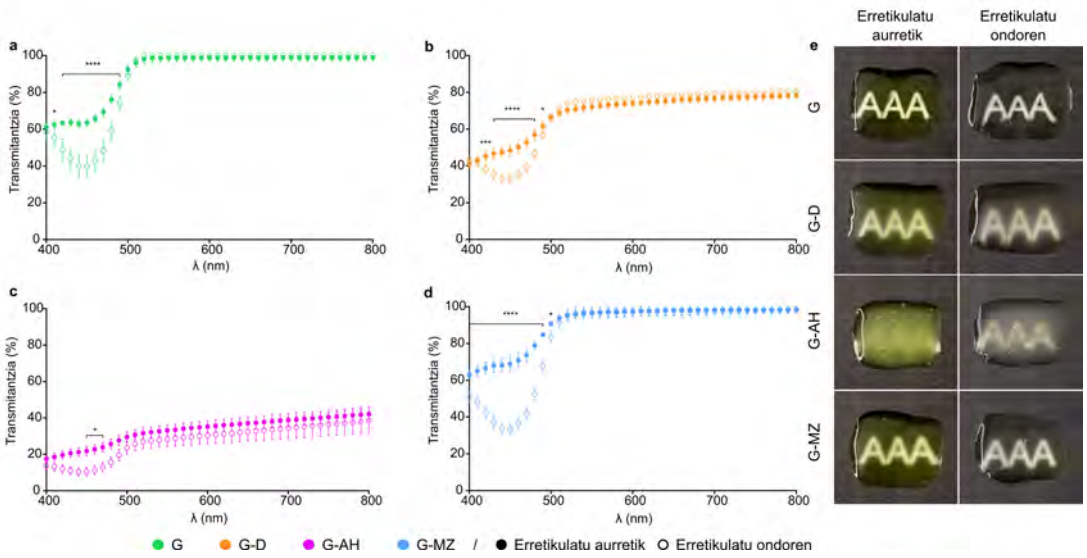

IV.13. IRUDIA: G, G-D, G-AH eta G-MZ hidrogelen transmitantzia eta gardentasun ezberdintasunak, erretikulazioaren aurretik eta ondoren. **a-d**) Grafikoek erretikulatu eta erretikulatu gabeko hidrogelek transmititutako argiaren ehunekoa erakusten dute, 400-800 nm tartean. Datuek transmisioaren batez besteko ehunekoa $\pm$ DE adierazten dute. Ezberdintasun estatistikoki esanguratsuek film bakoitzaren erretikulatutako eta erretikulatu gabeko egoeren arteko aldaketak adierazten dituzte ($*$ p < 0,05, $**$ p < 0,01, $***$ p < 0,001, $****$ p < 0,0001). **e**) Irudiek hidrogel bakoitzaren gardentasun-maila erakusten dute, argi urdinarekin irradiatu aurretik eta ondoren. Irudi guztiak baldintza berberak erabiliz atera genituen.

G-D-rentzako transmisio-baliorik altuena gutxi gorabehera % 80-koa izan zen 600 nm-tik aurrera (IV.13 irudiko **b**). Era berean, halo horixka eta halo zurixka bat ikusi ahal izan genuen erretikulatu eta erretikulatu gabeko hidrogeletan hurrenez hurren (IV.13 irudiko **e**). G-AH-k, argi kantitate txikiena transmititzen zuen hidrogelak, % 40 inguruko transmisio-balio maximoa lortu zuen. Emaitza hau bat zetorren IV.13 irudiko **e** irudietan ikusitako desenfokatze-efektuarekin.

RFP hidrogelari gehitzeak kolore horixka eman zion, baina horrek ez zuen haren gardentasuna arriskuan jarri. Lau grafikoek alde nabarmenak erakutsi zituzten argi urdineko espektroan erriboflabinak xurgatzen duen uhin-luzera maximoan, erretikulazio-lanparak erabilitako uhin-luzeran alegia. Hori, IV.13 irudiko **e** irudian ageriko kolore horixkarik ez izatearekin lotu genuen.

2.4. *In vitro* askapen saiakuntzak

Hidrogelaren lau bertsioetatik 3 konposatu desberdinen askapena bi astetan zehar alderatu genuen. FITC-IgG, FITC-Albumina eta Vigamox konposatuak hidrogeletan kapsulatu genituen, haien askapen-zinetika behatzeko eta hidrogelen errendimendua ezaugarritzeko. Konposatu horiek pisu molekular altuko (150 kDa), ertaineko (66 kDa) eta txikiko (0,44 kDa) konposatuak ziren eta pisu molekular ezberdineko molekulak karakteriza genitzan aukeratu genituen.

FITC-IgG eta FITC-Albuminaren askapen-kantitateak 485-520 nm-ko kitzikapen eta igorpen-uhin-luzerekin egindako fluoreszentzia-neurketen bidez erregistratu genituen. Vigamox-en askapena 290 nm-tan neurtutako absorbantzia balioekin kalkulatu genuen. Konposatu bakoitzaren balioa kurba estandar bat gehituz kalkulatu genuen eta emaitzak irudikatzeko, denbora-puntu bakoitzeko kontzentrazio-balioa aurreko kontzentrazio-neurketari gehitu zitzaion. Esperimentuaren hasieran (t = 0 h), kapsulatutako konposatu bakoitzaren kontzentrazioa % 100-ekoa izan zen, eta ondorengo denbora-puntu bakoitzean irudikatutako ehunekoa balio horren arabera kalkulatu genuen. Lau erreplika aztertu genituen askatutako tratamendu eta konposatu bakoitzeko.

IgG-a pixkanaka askatu zen hidrogel formulazio guztietatik, hamargarren egunetik aurrera honen askapena egonkortu zelarik. G hidrogelak edukiaren erdia askatu zuen azterketaren lehen astearen ondoren (% 49 $\pm$ % 4,4), eta G-D, G-AH eta G-MZ hidrogelek, berriz, % 36 $\pm$ % 1,5, % 41 $\pm$ % 3,9 eta % 37 $\pm$ % 0,9 kargaren ehunekoa, hurrenez hurren (IV.14 irudiko **a**). Estatistikoki ezberdintasun esanguratsuak erregistratu genituen G-D eta G-MZ hidrogelen eta G kontrolaren artean denbora-tarte desberdinetan (IV.1 taula). G-D, G-AH eta G-MZ-ren kasuetan, alde handiak ikusi genituen egun 1 igaro arte, G hidrogelarekin alderatuta. G-AH-ren kasuan, desberdintasun horiek ez ziren azterketaren hirugarren egunetik aurrera hauteman.

Albuminaren askapenari dagokionez, G-AH-k eta G-MZ-k edukiaren erdia askatu zuten hirugarren egunerako. G hidrogelak kargaren erdia askatu zuen laugarren egunean, eta G-D hidrogelak seigarren egunean. IgG-n ez bezala, konposatu honen askapen-zinetikan ez genuen egonkortzerik ikusi, eta hidrogel guztiek, G-D izan ezik, edukiaren % 100 askatu zuten bi asteren buruan (IV.14 irudiko **b**). G-rekin

alderatuta eta denbora-puntu desberdinetan, ezberdintasun estatistikoki nabarmenak ikusi genituen hidrogelaren hiru bertsioen artean (G-D, G-HA eta G-MC) (IV.1 taula).

Vigamox-ek kargaren ia erabateko atxikidura eta gutxieneko askapena erregistratu zituen. Bi aste geroago, askatutako kopurua ez zen % 35 baino handiagoa izan (G, G-D, G-AH eta G-MZ hidrogelentzako % 30,15 $\pm$ % 1,04, % 30,06 $\pm$ % 1,45, % 32,37 $\pm$ % 3,27 eta % 25,93 $\pm$ % 0,61, hurrenez hurren) (IV.14 irudiko **c**). IgG eta Albuminaren askapenarekin alderatuta, gainontzeko hidrogelen G-rekiko desberdintasunak ez ziren estatistikoki esanguratsuak izan (IV.1 taula).

IV.1. TAULA: G, G-D, G-AH eta G-MZ hidrogeletan pilatutako karga bakoitzaren askapen profilen ehunekoen batez bestekoa ± DE. Alde estatistikoki esanguratsuak G-rekiko adierazi ditugu ($*$ p < 0,05, $**$ p < 0,01, $***$ p < 0,001, $****$ p < 0,0001).

	IgG-ren askapena				Albuminaren askapena				Vigamox-en askapena			
Denbora	G	G-D	G-AH	G-MZ	G	G-D	G-AH	G-MZ	G	G-D	G-AH	G-MZ
1h	1,58 ± 0,06	1,02 ± 0,04 ****	1,99 ± 0,08 ***	2,38 ± 0,31 *	4,47 ± 0,32	2,46 ± 0,13 ***	6,42 ± 0,34 ***	6,62 ± 0,62 **	1,37 ± 0,42	1,04 ± 0,31	1,22 ± 0,65	1,2 ± 0,47
2h	2,74 ± 0,12	1,9 ± 0,07 ***	3,32 ± 0,09 ***	4,07 ± 0,56 *	7,72 ± 0,35	4,56 ± 0,32 ****	10,7 ± 0,51 ***	10,5 ± 1,08 *	2,81 ± 0,13	1,98 ± 0,08 ***	2,39 ± 0,4	2,29 ± 0,07 **
4h	4,44 ± 0,21	3,23 ± 0,05 **	5,21 ± 0,17 **	5,99 ± 0,75 *	11,93 ± 0,35	7,21 ± 0,48 ****	14,99 ± 1,04 *	15,12 ± 1,25 *	4,01 ± 0,27	3,1 ± 0,31 *	3,35 ± 0,5	3,05 ± 0,21 **
6h	5,9 ± 0,28	4,54 ± 0,05 **	6,88 ± 0,19 **	7,79 ± 0,86 *	15,64 ± 0,23	9,81 ± 0,77 ***	19,32 ± 1,51 *	19,49 ± 1,36 *	5,07 ± 0,34	4,05 ± 0,37 *	4,28 ± 0,76	3,79 ± 0,38 **
8h	7,12 ± 0,31	5,64 ± 0,03 **	8,28 ± 0,25 **	9,29 ± 0,99 *	18,74 ± 0,19	12,06 ± 0,67 ***	23,03 ± 2,15	23,2 ± 1,47 *	6,3 ± 0,77	4,93 ± 0,61	5,21 ± 0,54	4,82 ± 0,07
12h	8,73 ± 0,37	7,09 ± 0,09 **	10,11 ± 0,32 **	11,07 ± 1,04 *	22,76 ± 0,19	15,42 ± 0,83 ***	27,84 ± 2,81	27,89 ± 1,58 *	7,46 ± 0,64	5,92 ± 0,55 *	5,93 ± 0,79	5,63 ± 0,36 *
1d	12,05 ± 0,41	9,76 ± 0,17 **	14,08 ± 0,21 **	14,89 ± 1,08 *	30,17 ± 0,31	20,9 ± 0,78 ****	36,11 ± 3,33	36,11 ± 1,59 **	9,75 ± 0,57	8,35 ± 0,83	8,55 ± 0,64	5,63 ± 0,32 *
2d	17,66 ± 0,57	13,02 ± 0,43 ****	19,03 ± 0,2 *	18,74 ± 0,79	38,42 ± 0,17	27,33 ± 0,82 ***	45,41 ± 3,66	45,6 ± 0,45 ****	12,13 ± 0,9	11,12 ± 0,86	11,15 ± 1,15	10,45 ± 0,23
3d	25,07 ± 1,28	17,49 ± 0,54 ***	24,01 ± 0,4	22,53 ± 0,92 *	46,57 ± 0,32	33,31 ± 1,01 ***	54,83 ± 3,86 *	53,96 ± 1,05 ***	16,06 ± 1,03	14,54 ± 1,48	15,75 ± 1,74	14,28 ± 0,28
4d	33,98 ± 4,85	22,29 ± 0,69 *	29,68 ± 1	26,44 ± 0,78	53,89 ± 0,44	38,87 ± 1,03 ****	65,59 ± 1,94 **	61,22 ± 1,63 **	20,18 ± 1,94	18,61 ± 1,47	19,47 ± 2,52	17,37 ± 0,02
5d	38,99 ± 4,22	26,31 ± 0,62 *	34,06 ± 2,3	30,13 ± 0,69 *	61,04 ± 0,47	44,49 ± 0,86 ****	73,91 ± 2,65 **	68,15 ± 1,27 **	22,87 ± 1,4	21,11 ± 1,44	22,66 ± 2,75	20,46 ± 0,43
6d	44,5 ± 4,39	31,43 ± 0,37 *	37,68 ± 2,61	33,44 ± 0,92 *	68,76 ± 0,96	50,17 ± 0,73 ****	82,74 ± 2,58 **	75,42 ± 1,03 ***	25 ± 1,45	23,69 ± 1,37	25,46 ± 2,71	22,25 ± 0,25
7d	49,11 ± 4,42	36,12 ± 1,52 *	41,45 ± 3,95	37,03 ± 0,93 *	77,1 ± 1,81	55,42 ± 0,77 ****	90,29 ± 2,73 ***	81,85 ± 1,68 *	27,03 ± 0,96	25,93 ± 1,2	27,99 ± 3,02	23,84 ± 0,16 *
10d	55,78 ± 4,73	46,92 ± 3,56	49,22 ± 4,87	41,65 ± 0,86 *	84,9 ± 1,61	64,12 ± 0,86 ****	99,74 ± 0,52 ***	92,17 ± 1,02 **	28,54 ± 0,9	27,96 ± 1,32	30,27 ± 3,08	24,88 ± 0,36 **
15d	63,93 ± 4,68	56,84 ± 1,77	57,02 ± 6,56	48,93 ± 0,9 *	97,47 ± 1,43	75,02 ± 1,81 ****	100 ± 0	100 ± 0	30,16 ± 1,05	30,07 ± 1,45	32,27 ± 3,28	25,93 ± 0,61 **

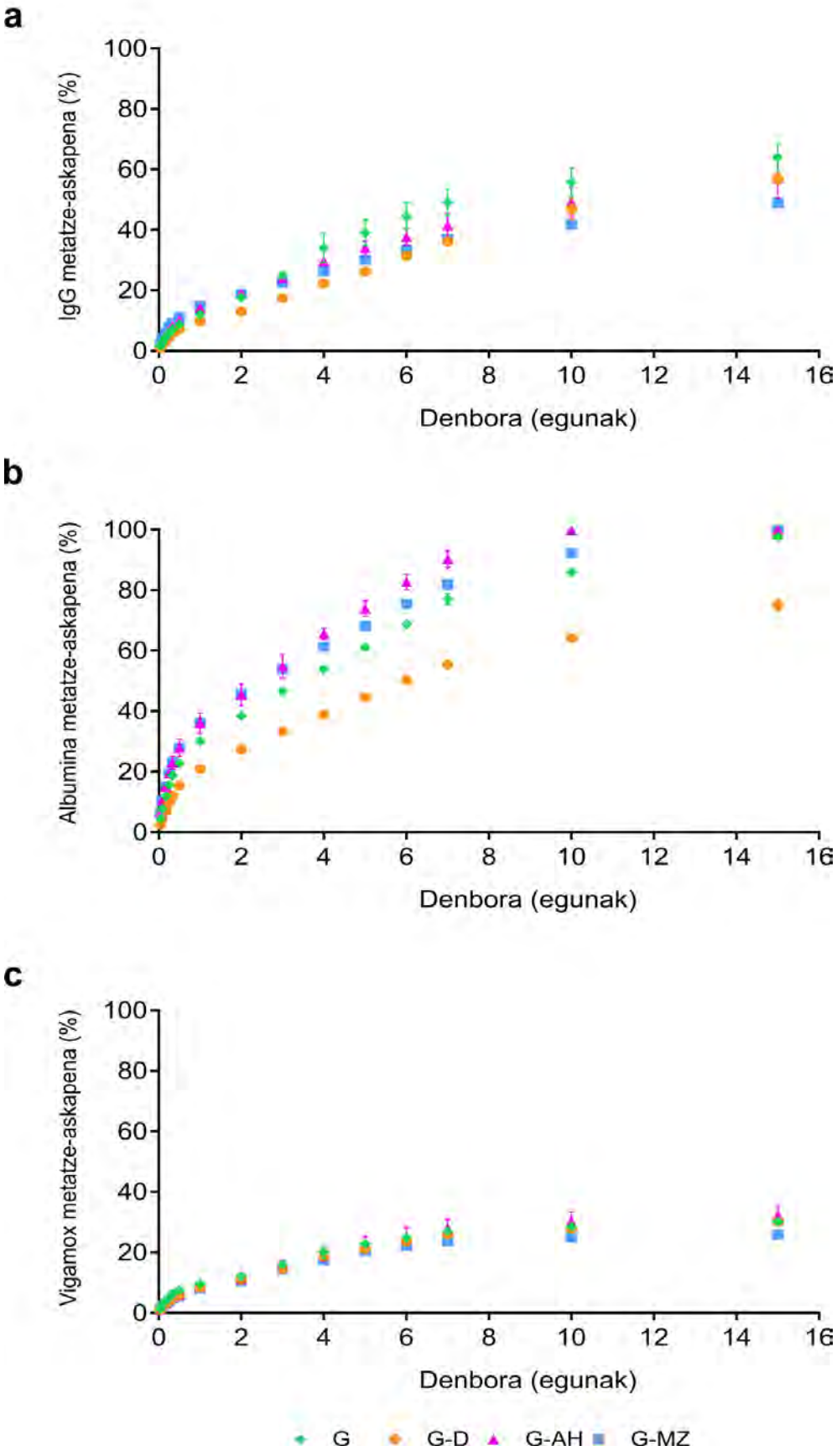

IV.14. IRUDIA: Hidrogeletan pilatutako FITC-IgG (**a**), FITC-Albumina (**b**) eta Vigamox (**c**) konposatuen askapen zinetika. Datuek 15 egunetan askatutako guztizko kopuruaren ehuneko normalizatua adierazten dute.

2.5. Zitobateragarritasunaren ebaluazioa

Hidrogelen zitobateragarritasuna AM-Kaltzeina-EthD1 saiakuntzaren bidez, hidrogelekin ereindako zelulen kopurua zenbatuz eta ziklo zelularra aztertuz ebaluatu genuen. Azterketa egiteko SV-40-rekin hilezkortutako giza korneako zelula epitelialak (KZE) eta NIH-3T3 fibroblastoen zelula-lerro komertziala erabili genituen. Bi zelula-mota horiek zegokien hidrogel motarekin kontaktuan erein genituen. Zelulak erein eta plakara itsatsi arte ez zitzaien hidrogela gehitu. Behin plakari atxikita, kikara bakoitzean jarritako hazkuntza-medioaren % 20-a erretikulatutako hidrogelarekin ordezkatu genuen. Hazkuntzak 72 orduz mantendu genituen.

Ia % 99-ko bideragarritasuna erregistratu genuen bi zelula motekin kasu guztietan, eta ez genuen alde estatistiko nabarmenik ikusi hidrogelekin kontaktuan zeuden hazkuntzen eta kontrolaren artean (IV.15 irudiko **a, c**). Gainera, zenbatutako zelulen kopurua kontrolaren antzekoa izan zen, 72 orduren ondoren milioi bat zelula inguru erregistratu baikenituen gutxi gorabehera kasu guztietan (IV.15 irudiko **b**).

Fluxu-zitometria bidezko ziklo zelularraren analisiari dagokionez, ez genuen kontrol eta tratamenduen artean ezberdintasun esanguratsurik aurkitu. Zelula-zikloaren fase desberdinetako zelulen proportzioa ikertutako zelula motaren arabera aldatu zen. NIH-3T3 fibroblastoen % 66 inguru G0-G1 fasean erregistratu genituen, horrek zelula gehienak zatiketa zelularra jasateko ez zirela aktiboki prestatzen ari adierazi zigun. Aitzitik, beren funtzio zelular normalak (G0) edo ARNm eta proteinak (G1) sintetizatzen ari ziren. Zelulen % 11 inguru sintesi-fasean (S) ikusi genituen, eta % 23-a mitosirako prestatze-fasean edo zelula-zatiketa osoan (G2-M) (IV.15 irudiko **d**).

Sintesian (S), mitosirako prestakuntzan (G2) edo zelula-zatiketan (M) erregistratutako KZE zelulen ehunekoa handiagoa izan zen, 3T3 fibroblastoekin alderatuta. Guztizko zelula kopuruaren % 56-a erregistratu genuen G0-G1 faseetan, % 16-a sintesian (S) eta % 28-a G2-M faseetan (IV.15 irudiko **e**).

Hidrogelen propietate erreologikoak, transmitantzia, gardentasuna, askapen zinetika eta zitobateragarritasuna aztertu ondoren, G hidrogela hautatzea erabaki genuen material gisa. D, AH edo MZ-ren gehikuntzak ez zituen hidrogelaren propietateak nabarmen hobetu, horregatik konposizio sinpleenarekin jarraitzea erabaki genuen.

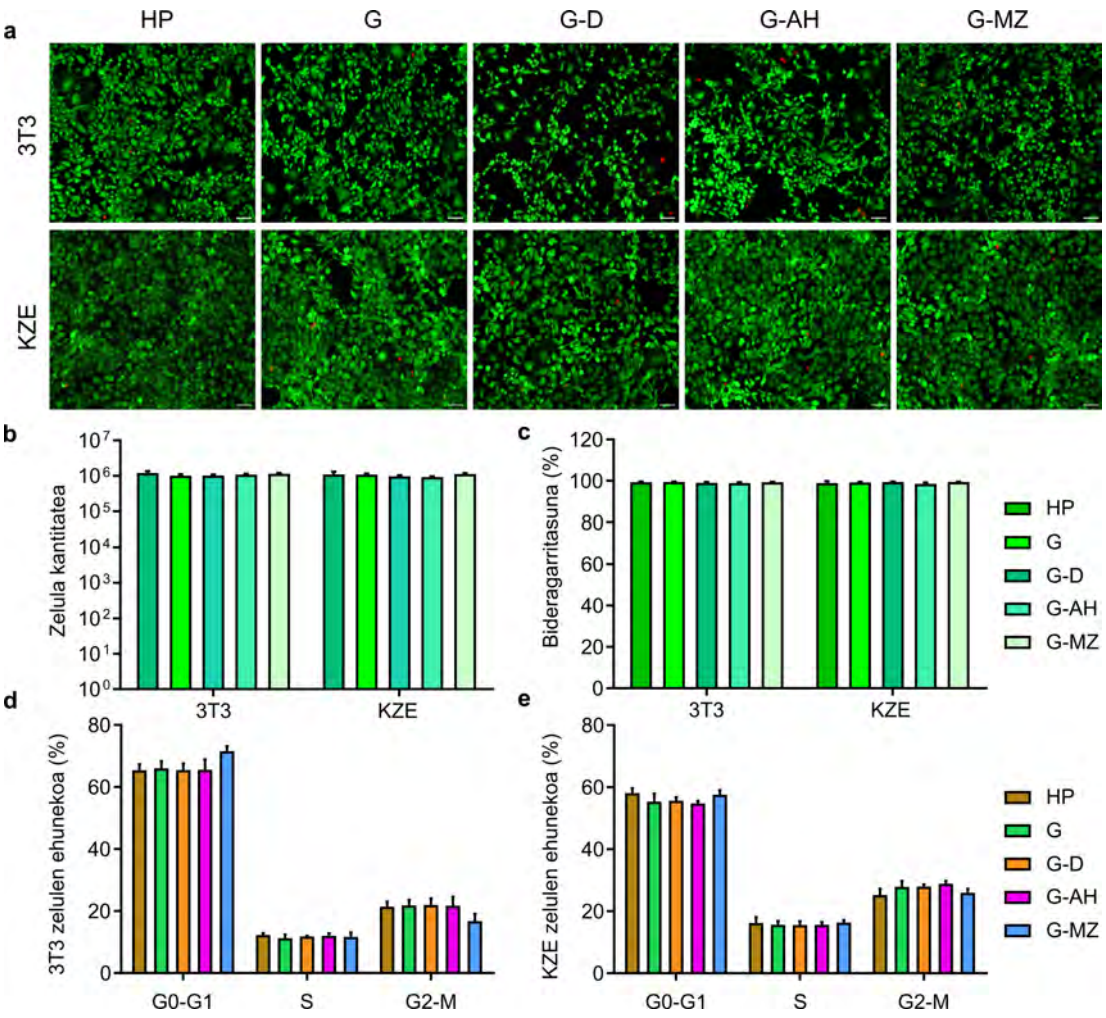

IV.15. IRUDIA: G, G-D, G-AH eta G-MZ hidrogelekin ereindako NIH-3T3 eta KZE zelula-hazkuntzen zitobateragarritasunaren ebaluazioa, hazkuntza-plaka (HP) arrunt batean ereindako zelulekin alderatuta. **a**) AM-Kaltzeina-EthD1 saiakuntzaren NIH-3T3 eta KZE zelula-hazkuntzen irudiak, hidrogel ezberdinen eraginpean. **b**) Zelulen kontaketa 72 orduz kultibatu ondoren. **c**) Talde bakoitzean erregistratutako zelula bideragarrien ehunekoa. **d, e**) Ziklo zelularraren fase bakoitzean erregistratutako NIH-3T3 (**d**) eta KZE (**e**) zelulen ehunekoa.

2.6. Hidrogelean txertatutako korneako zelulen hazkuntza

G hidrogelaren zitobateragarritasuna baieztatzeko, giza korneako zelula estromal primarioak hidrogelaren barruan txertatu eta AM Kaltzeina-EthD1 saiakuntza gauzatu genuen 48 orduren ondoren. Behatutako morfologia ez zetorren bat hazkuntza bidimentsionaletan lortutakoarekin; izan ere, zelula-taldeak hainbat sakoneratan txertatuta zeuden eta ez zuten estroma-zeluletan ohikoa den morfologia luzatu eta ildaskatua erakutsi. IV.16 irudian ikus daitekeen bezala, zelula gehienak AM Kaltzeinarekin tindatu ziren. Zelulen antolaketa desberdina bazen ere, zelula gehienak bizirik zeuden, eta horrek hidrogelaren zitobateragarritasuna berresteko

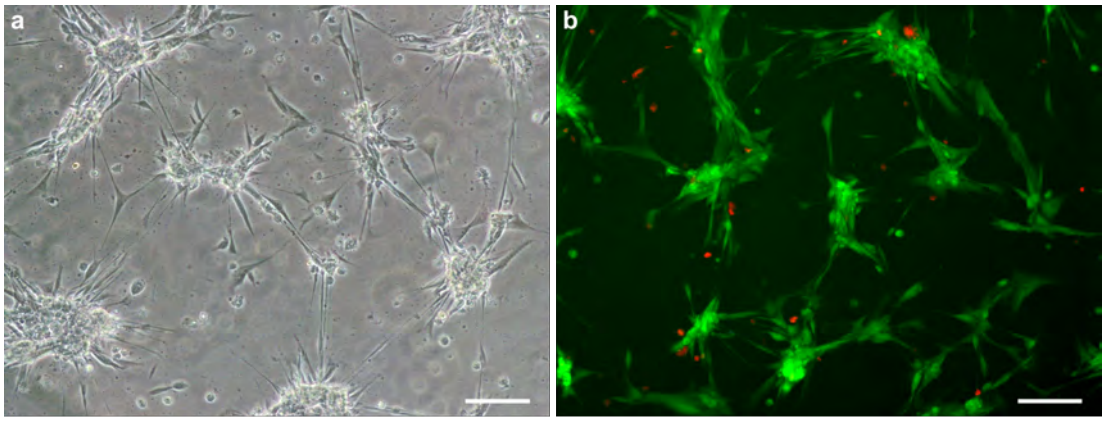

IV.16. IRUDIA: G hidrogelean txertatutako giza estromako zelula primarioen hazkuntzak. **a**) Fase-kontraste mikroskopioaren bitartez, zelulak 48 orduz kultiboan egon ondoren lortutako irudia. **b**) AM Kaltzeina-EthD1 saiakuntzaren bitartez, zelulak 48 orduz kultiboan egon ondoren lortutako irudia. Eskala lerroek 100 μm-ko neurriak adierazten dituzte.

balio izan zigun.

3. Hazkuntza faktoreen kuantifikazioa

Gelatina-RFP hidrogelaren konposizioa hautatu ondoren, hidrogeletik modu kontrolatuan askatuko ziren hainbat konposatu aukeratu genituen. Konposatu horien artean odoletik eratorritako bi produktu, hala nola, serum autologoa (SA) eta hazkuntza faktoreetan aberatsa den plasmatik eratorritako seruma (sPRGF), eta giza mintz amniotikoaren estraktuak (GMAe) gehitu genituen, guzti hauek kornearen orbaintze prozesuan lagunduko zutenak. Hidrogeletan kapsulatu aurretik, konposatu horiek 11 hazkuntza faktoreen edukia kuantifikatuz karakterizatu genituen.

Sei pazienteren 2 odol-eratorrien kuantifikazioaren batez bestekoa eta desbideratze estandarra erregistratu genituen. Odoletik eratorritako SA eta sPRGF paziente bakoitzaren odol-laginetan oinarrituta lortu genituen, hala, produktu bakoitzeko sei lagin hartu genituen guztira. Gainera, SA-ren 6 laginen nahasketa bat eta sPRGF-ren 6 laginen beste nahasketa bat ere kuantifikatu genituen (x-SA, x-PRGF). GMAe-ri dagokionez, 3 mintz desberdinetako urruneko, erdiko eta hurbileko eremuetatik (GMAe-D, GMAe-M, GMAe-P) ateratako laginak kuantifikatu genituen. GMAe-rako, kuantifikazio horien batez bestekoa eta desbideratze estandarra kalkulatu genituen, mintz bakoitzetik ateratako hiru zatietako nahasketarekin batera (x-GMAe).

3.1. Odol-eratorrien kuantifikazioa

Paziente guztietako bi odol-eratorrien artean estatistikoki esanguratsuak ziren ezberdintasunak erregistratu genituen hazkuntza faktore batzuetan, nahiz eta ezberdintasun horiek gizabanako bakoitzaren izatetik etorri (IV.2 taula). HGF-n izan ezik, 4. eta 5. pazienteek ez zuten aldaketa nabarmenik erakutsi SA-ren eta sPRGF-ren artean aztertutako hazkuntza faktoreetako bakar batean ere. 1. eta 6. pazienteek, berriz, ezberdintasun esanguratsuak erakutsi zituzten BDNF, PEDF, SP, EGF eta HGF faktoreetan. Horrez gain, desberdintasunak aurkitu genituen pazienteen lagin indibidualak SA edo sPRGF nahasketekin alderatu genituenean. SA eta sPRGF lagin guztietako nahasketak sortzeak faktoreen kuantifikazioa murriztu zuen paziente guztien datuen batez besteko teorikoarekin (T.x-SA, T.x-sPRGF) alderatuta, desberdintasun hori estatistikoki nabarmena izatera iristeraino zenbait faktoreetan. Nahasketak sortzeko osagarria inaktibatzeko behar diren tenperatura altuek azal dezakete jasandako kuantifikazioaren murrizketa, zeinak eragina izan zuen hazkuntza faktore eta molekula interesgarri batzuen galeran.

3.2. GMAe laginen kuantifikazioa

GMAe aztertzean, aldeak nabarmenagoak izan ziren erdiko eremuaren eta hurbileko eremuaren artean, nahiz eta ezberdintasun horiek banakoen artean ere aldakorrak izan (IV.3 taula).

Faktore guztien beherakada estatistikoki esanguratsua erregistratu genuen paziente beraren mintzaren zati bakoitza taldekatu eta kuantifikatu genuenean.

Hiru mintz emaileen zati guztietatik abiatuta egindako nahasketei dagokienez, aztertutako 11 faktoreetatik 4-k bakarrik erakutsi zituzten ezberdintasun estatistikoki esanguratsuak: PEDF, IL-1β, SP eta EGF. Emaitza horiek iradoki zuten nahasketaren kuantifikazioa konstante mantendu zela gizabanakoen artean (IV.4 taula). Odol-eratorrien kasuan bezala, taldekatutako laginen kuantifikazioak behera egin zuen banakako datuekin alderatuta.

IV.2. TAULA: Hazkuntza-faktoreen kontzentrazioa odol-eratorrien laginetan. Emaitzek kuantifikazioaren batez bestekoa ± DE adierazten dute. Paziente bakoitzaren SA eta sPRGF-en arteko alde estatistikoki esanguratsuak honela definitu ditugu: $*$ p < 0,05, $**$ p < 0,01, $***$ p < 0,001, $****$ p < 0,0001.

HF-k	BDNF (ng/ml)		NGF (pg/ml)		PEDF (ng/ml)		IL-1β (pg/ml)		GDNF (pg/ml)		SP (pg/ml)	
Samples	AS	sPRGF	AS	sPRGF	AS	sPRGF	AS	sPRGF	AS	sPRGF	AS	sPRGF
p1	33,4 ± 0,82	13,93 ± 1,34 ****	0 ± 10,33	0 ± 18,77	1108,58 ± 22,23	720,36 ± 129,56 ***	0,19 ± 0,08	0,12 ± 0,02 *	27,99 ± 2,07	21,28 ± 0,47	1256,52 ± 293,92	436,61 ± 65,02 *
p2	19,45 ± 0,51	8,07 ± 0,43 ****	0	0 ± 4,71	762,69 ± 86,96	547,49 ± 39,82	0,01 ± 0,01	0 ± 0,08	63,79 ± 3,25	58,72 ± 0,87	122,84 ± 5,98	69,26 ± 0,13
p3	30,21 ± 2,28	23,70 ± 1,49 ***	0 ± 2,81	0,42 ± 1,86	1243,59 ± 79,54	1054,26 ± 109,31	0,04 ± 0,02	0,03	84,36 ± 5,59	69,60 ± 4,53	1935,65 ± 265,21	2485,92 ± 178,16
p4	26,96 ± 0,90	26,07 ± 1,85	96,25 ± 17,69	99,86 ± 12,59	914,09 ± 30,83	736,60 ± 113,50	0,09	0,09	264,81 ± 9,83	244,63 ± 11,46	510,16 ± 9,80	765,07 ± 126,64
p5	14,62 ± 0,43	10,51 ± 1,22	0 ± 4,63	0 ± 23,10	841,02 ± 96,50	734,58 ± 33,17	0 ± 0,02	0 ± 0,02	117,56 ± 7,09	92,12 ± 7,97	297,34 ± 28,73	403,11 ± 115,77
p6	18,34 ± 2,71	8,98 ± 1,02 ****	19,34 ± 6,40	0 ± 1,85	1283,91 ± 46,92	614,88 ± 19,62 ****	0 ± 0,01	0 ± 0,02	121,82 ± 9,15	112,73 ± 7,26	3866,38 ± 706,78	695,82 ± 204,19 ****
x	20,46 ± 0,04	12,96 ± 0,51 ****	22,54 ± 12,76	39,78 ± 13,43	863,08 ± 58,46	581,99 ± 5,39 *	0 ± 0,01	0 ± 0,01	266,48 ± 8,85	201,16 ± 10,26 ****	152,25 ± 0,25	154,05 ± 3,29
T,x	23,83 ± 7,18	15,21 ± 7,49	20,57 ± 36,54	20,85 ± 37,79	1025,65 ± 213,28	734,70 ± 177,91	0,06 ± 0,08	0,04 ± 0,05	113,39 ± 78,34	99,85 ± 73,98	1331,48 ± 1372,73	809,30 ± 823,62

HF-k	EGF (pg/ml)		FGF2 (pg/ml)		HGF (pg/ml)		IGF (ng/ml)		KGF (pg/ml)	
Samples	AS	sPRGF	AS	sPRGF	AS	sPRGF	AS	sPRGF	AS	sPRGF
p1	393,27 ± 32,77	200,55 ± 1,19 ****	64,48 ± 33,03	82,55 ± 17,92	201,44 ± 16,36	80,45 ± 3,66 ***	0,21 ± 0,02	0,25 ± 0,02	0,00	0,00
p2	236,43 ± 9,87	85,71 ± 3,58 ****	156,88 ± 13,58	169,67 ± 14,91	296,60 ± 9,44	125,59 ± 10,37 ****	8,33 ± 0,05	8,12 ± 0,30	9,32 ± 1,44	8,67 ± 0,14
p3	300,66 ± 30,65	245,42 ± 15,11 *	160,98 ± 2,64	144,31 ± 20,94	823,61 ± 79,10	253,98 ± 19,17 ****	59,48 ± 3,35	45,42 ± 0,43	15,46 ± 0,04	9,55 ± 1,30
p4	133,76 ± 5,03	128,11 ± 4,31	134,21 ± 0	154,78 ± 16,55	268,66 ± 7,94	161,69 ± 0 **	122,73 ± 0,18	114,66 ± 1,86	85,66 ± 28,48	75,39 ± 0,53
p5	252,17 ± 7,89	229,42 ± 17,93	64,48 ± 33,03	55,50 ± 20,33	307,71 ± 6,27	155,72 ± 11,79 ****	4,59 ± 0,17	3,68 ± 0,18	8,67 ± 0,70	5,97 ± 0,48
p6	326,49 ± 20,11	130,08 ± 0,51 ****	98 ± 14,38	100,90 ± 18,48	370,39 ± 4,63	166,42 ± 0 ****	1,38 ± 0,05	0,97 ± 0,05	7,8 ± 0,33	6,57 ± 0,09
x	200,65 ± 10,67	145,07 ± 4,30 *	138,64 ± 6,27	137,96 ± 18,92	98,26 ± 14,27	100,84 ± 3,55	39,30 ± 21,55	27,58 ± 4,12	56,54 ± 0,95	45,56 ± 1,70
T,x	273,79 ± 85,86	169,88 ± 61,64	113,17 ± 44,52	113,96 ± 32,90	378, 07 ± 216,03	157,31 ± 55,07	32,79 ± 47,19	28,85 ± 43,27	21,15 ± 31,69	17,69 ± 27,14

HF-k: Hazkuntza faktoreak.
BDNF: Garunetik eratorritako faktore neurotrofikoa.
NGF: Nerbio hazkuntza faktorea.
PEDF: Epitelio pigmentariotik eratorritako faktorea.
IL-1β: Interleukina 1β.
GDNF: Glia-zeluletatik eratorritako faktore neurotrofikoa.
SP: P Substantzia.
FGF2: Fibroblastoen hazkuntza faktorea 2.
HGF: Hepatozitoen hazkuntza faktorea.
EGF: Hazkuntza faktore epidermikoa.
IGF: Intsulina antzeko hazkuntza faktorea 1.
KGF: Keratinozitoen hazkuntza faktorea.
p1-p6: 1-6 pazienteak.
x: Odol-eratorri bakoitzetik sortutako nahasketa.
T.x: Nahasketa teorikoa.

IV.3. TAULA: Hazkuntza-faktoreen kontzentrazioa GMAe laginetan. Emaitzek kuantifikazioaren batez bestekoa ± DE adierazten dute. Alde estatistikoki esanguratsuak honela definitu ditugu: ∗, +, † $p < 0,05$, ∗∗, ++, †† $p < 0,01$, ∗∗∗, +++, ††† $p < 0,001$, ∗∗∗∗, ++++, †††† $p < 0,0001$. "∗", "+" eta "†" ikurrek GMAe-D, GMAe-P eta GMAe-Nahasketarekiko aldeak erakusten dituzte, hurrenez hurren.

HF-k	BDNF (pg/ml)				NGF (pg/ml)				PEDF (ng/ml)			
Laginak	D	M	P	x	D	M	P	x	D	M	P	x
p1	48,56 ± 4,71	21,33 ± 0,79 *	39,11 ± 5,50 †	6,33 **	901,33 ± 72,58	882,27 ± 84,43 †††	675,81 ± 137,03 ††	167,18 58,58 ***	33,85 ± 2,08	27,72 ± 3,20 $^{++}$	15,26 ± 0,28 ***†	0,06 ± 0,01 *
p2	8 ± 0,79	9,67 ± 1,57	19,11 ± 2,36	8,56	493,29 ± 71,43	348,10 ± 260,12	580,65 ± 144,18 ††	73,96 ± 45,93 *	36,73 ± 1,34	38,55 ± 0,02 $^{++++}$	12,95 ± 2,14 ****††††	0,17 ± 0,02
p3	39,11 14,93	64,11 ± 22 ††	43 ± 9,43	24,67 ± 0,79	1065,69 ± 33,01	1218,21 ± 45,85 $^{+\dagger\dagger\dagger\dagger}$	831,11 ± 201,99 ††††	148,18 ± 22,62 ****	20,04 ± 1	15,22 ± 1,16 $^{++\dagger\dagger\dagger}$	26,87 ± 1,15	0,28 ± 0,01 *

HF-k	IL-1β (pg/ml)				GDNF (pg/ml)				SP (pg/ml)			
Laginak	D	M	P	x	D	M	P	x	D	M	P	x
p1	1 ± 0,06	0,49 ± 0,02 $^{****+++\dagger\dagger\dagger\dagger}$	0,86 ± 0,03 *††††	0,06 ± 0,01 ****	25,06 ± 0,69	21,77 ± 4,43 $^{++\dagger\dagger\dagger}$	10,92 ± 0,96 ***	8,70 ± 4,10 ****	6,25 ± 0,13	6,83 ± 0,60	6,01 ± 0,12	6,91 ± 1,26
p2	0,30 ± 0,06	0,19 ± 0,04 $^{++++}$	0,81 ± 0,02 ****††††	0,17 ± 0,02 *	0,26 ± 1,97	0,26 ± 1,97 $^{++++}$	15,13 ±0,71 ****††	6,49 ± 0,97	8,84 ± 0,65	7,57 ± 0,52	8,30 ± 0,23	8,14 ± 1,02
p3	0,17 ± 0,01	0,46 ± 0,08 $^{*****+++\dagger\dagger}$	1,12 ± 0,01 ****††††	0,28 ± 0,01	4,77 ± 1,95	8,37 ± 0,24 $^{+}$	16,47 ± 0,71 ***††	7,68 ± 2,66	7,11 ± 0,03	6,04 ± 0,16 $^{++++\dagger\dagger\dagger\dagger}$	14,46 ± 0,08 ****††	11,28 ± 1,56 ***

HF-k	FGF2 (pg/ml)				HGF (pg/ml)			
Laginak	D	M	P	x	D	M	P	x
p1	1986,80 ± 53,75	2988,89 ± 189,24 $^{**+++++\dagger\dagger\dagger\dagger}$	4638,27 ± 499,69 ****††††	421,62 ± 19,02 ****	16526,12 ± 831,18	17002,09 ± 2332,96 $^{++++\dagger\dagger\dagger\dagger}$	26283,42 ± 1351,62 ****††††	2542,30 ± 72,43 ****
p2	1923 ± 31,11	1718,88 ± 170,34 $^{++++\dagger\dagger\dagger}$	6878,22 ± 338,92 ****††††	521,08 ± 12,12 ****	6559,69 ± 27,10	4602,99 ± 0,55 $^{++++\dagger\dagger\dagger}$	28387,46 ± 2254,51 ****††††	862,38 ± 113 ***
p3	1534,62 ± 108,52	2311,04 ± 71,07 $^{**++++\dagger\dagger\dagger\dagger}$	5104,23 ± 67,58 ****††††	521,54 ± 18,60 **	8418,67 ± 579,61	7115,15 ± 610,87 $^{++++\dagger\dagger\dagger}$	31077,24 ± 278,15 ****†††	1176,67 ± 94,72 ***

HF-k	EGF (pg/ml)				IGF (ng/ml)				KGF (pg/ml)			
Laginak	D	M	P	x	D	M	P	x	D	M	P	x
p1	65,38 ± 0,26	118,86 ± 3,41 $^{***++\dagger\dagger}$	82,05 ± 1,65	80,26 ± 2,48	0,29 ± 0,04	0,27 ± 0,02 †	0,28 ± 0,03 †	0,07 ± 0,04 **	1,20 ± 0,17	2,57 ± 1,29 $^{*+++++\dagger\dagger\dagger}$	11,17 ± 0,43 ****††††	N/A
p2	42,47 ± 3,44	24,45 ± 2,16	39,51 ± 2,00	27,81 ± 0,31	0,15 ± 0,01	0,19 ± 0,01	0,27 ± 0,05 †	0,10 ± 0,01	N/A	N/A $^{++++}$	15,13 ± 0,13 ****††††	N/A
p3	289,14 ± 5,65	284,47 ± 20,43 ††††	266,93 ± 17,96 ††	226,27 ± 7,22 ****	0,16 ± 0,10	0,10 ± 0,13 $^{+}$	0,28 ± 0,02	0,12	0,00	N/A $^{++++}$	14,51 ± 0,29 ****††††	0,49 ± 0,10

HF-k: Hazkuntza faktoreak.
BDNF: Garunetik eratorritako faktore neurotrofikoa.
NGF: Nerbio hazkuntza faktorea.
PEDF: Epitelio pigmentariotik eratorritako faktorea.
IL-1β: Interleukina 1β.
GDNF: Glia-zeluletatik eratorritako faktore neurotrofikoa.
SP: P Substantzia.
FGF2: Fibroblastoen hazkuntza faktorea 2.
HGF: Hepatozitoen hazkuntza faktorea.
EGF: Hazkuntza faktore epidermikoa.
IGF: Intsulina antzeko hazkuntza faktorea 1.
KGF: Keratinozitoen hazkuntza faktorea.
p1-p3:1-3 pazienteak.
D: GMA-ren urruneko eremua.
M: GMA-ren erdiko eremua.
P: GMA-ren hurbileko eremua.
x: GMA-ren alde desberdinen nahasketa.

IV.4. TAULA: Hazkuntza-faktoreen kontzentrazioa GMAe-Nahasketako-laginetan. Emaitzek kuantifikazioaren batez bestekoa ± DE adierazten dute. Alde estatistikoki esanguratsuak honela definitu ditugu: $*$, † $p < 0,05$, $**$, †† $p < 0,01$, $***$, ††† $p < 0,001$, $****$, †††† $p < 0,0001$. "$*$" eta "†" ikurrek p1 pazientearekiko eta p3 pazientearekiko aldeak erakusten dituzte, hurrenez hurren.

Laginak	BDNF (pg/ml)	NGF (pg/ml)	PEDF (ng/ml)	IL-1β(pg/ml)	GDNF (pg/ml)	SP (pg/ml)	EGF (pg/ml)	FGF2 (pg/ml)	HGF (pg/ml)	IGF (pg/ml)	KGF (pg/ml)
p1	6,33 ± 0,00	167,18 58,58	24,86 ± 6,14	0,06 ± 0,01	8,70 ± 4,10	6,91 ± 1,26	80,26 ± 2,48	421,62 ± 19,02	2542,30 ± 72,43	0,07 ± 0,04	N/A
p2	8,56 ± 0,00	73,96 ± 45,93	42,74 ± 3,19 ***	0,17 ± 0,02 *	6,49 ± 0,97	8,14 ± 1,02	27,81 ± 0,31 ***	521,08 ± 12,12	862,38 ± 113	0,10 ± 0,01	N/A
p3	24,67 ± 0,79	148,18 ± 22,62	30,23 ± 4,59 $^{++}$	0,28 ± 0,01 $^{***+}$	7,68 ± 2,66	11,28 ± 1,56 $^{***++}$	226,27 ± 7,22 $^{*******+++}$	521,54 ± 18,60	1176,67 ± 94,72	0,12	0,49 ± 0,10

BDNF: Garunetik eratorritako faktore neurotrofikoa.
NGF: Nerbio hazkuntza faktorea.
PEDF: Epitelio pigmentariotik eratorritako faktorea.
IL-1β: Interleukina 1β.
GDNF: Glia-zeluletatik eratorritako faktore neurotrofikoa.
SP: P Substantzia.
FGF2: Fibroblastoen hazkuntza faktorea 2.
HGF: Hepatozitoen hazkuntza faktorea.
EGF: Hazkuntza faktore epidermikoa.
IGF: Intsulina antzeko hazkuntza faktorea 1.
KGF: Keratinozitoen hazkuntza faktorea.
p1-p3:1-3 pazienteak.

4. *In vitro* inflamazio saiakuntza

Funtzionalizatutako hidrogelek hantura murriztu zezaketen zehazteko, *in vitro* probak egin genituen lehendabizi.

4.1. *In vitro* inflamazio ereduaren ezarpena

KZE zelulekin *in vitro* inflamazio eredu bat ezarri genuen lehen urrats gisa, eta horretarako 10 μg/ml LPS eta 100 ng/ml TNFα erabili genituen hantura-eragile bezala. Zelulak agenteen eraginpean mantendu genituen 24 orduz KZE edo DMEM:F12 hazkuntza-medioetan. Saiakuntzan 6 baldintza desberdin gehitu genituen: K-M.KZE, KZE medioan kultibatutako KZE zelulak; K-DMEM, DMEM:F12 medioan kultibatutako KZE zelulak; M.KZE-LPS, KZE medioan eta LPS estimuluarekin kultibatutako KZE zelulak; DMEM-LPS, DMEM:F12 medioan eta LPS estimuluarekin kultibatutako KZE zelulak; M.KZE-TNFα, KZE medioan eta TNFα estimuluarekin kultibatutako KZE zelulak; eta DMEM-TNFα, DMEM:F12 medioan eta TNFα estimuluarekin kultibatutako KZE zelulak. Hantura-estimulurik gabe ereindako KZE zelulak (K-M.KZE) kontrol gisa jarri genituen. Jarraian, IL-6 eta IL-1β markatzaileen adierazpena kuantifikatu genuen, inflamazio-maila zehazteko. Gusβ eta TBP erreferentzia gene gisa erabili genituen.

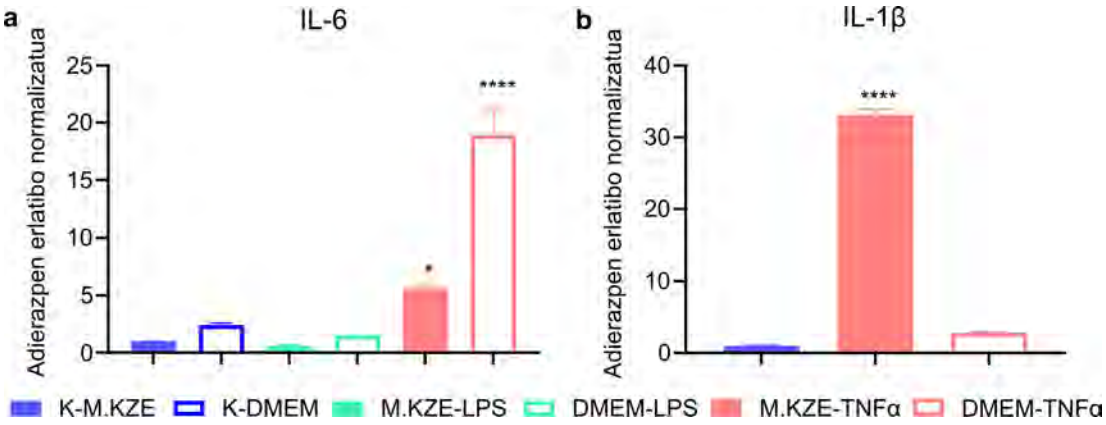

IV.17. IRUDIA: **a**) IL-6 eta **b**) IL-1β geneen adierazpen erlatibo normalizatua ($\Delta\Delta$Cq) KZE hazkuntza inflamatu eta inflamatu gabeetan. KZE medioarekin eta hantura-estimulurik gabe kultibatutako zelulak kontrol gisa erabili genituen (K-M.KZE). Kontrolarekin alderatutako (K-M.KZE) alde estatistikoki esanguratsuak $*$ p < 0,05, $**$ p < 0,01, $***$ p < 0,001, $****$ p < 0,0001 bezala definitu ditugu.

TNFα-rekin ereindako zelulek LPS-rekin ereindakoek baino hantura-geneen adierazpen handiagoa erakutsi zuten bai IL-6 eta IL-1β-rekin (IV.17 irudia). TNFα hantura-estimulu bezala aukeratzeaz gain, KZE hazkuntza-medioa TNFα disolbatzeko hazkuntza-medio gisa aukeratu genuen. Kontrol-laginetan erabilitako hazkuntza-medio estandarra izateaz gain, KZE medioan ereindako eta TNFα-ren eraginpean egondako zelulek alde estatistikoki esanguratsuak erakutsi zituzten IL-1β-ren adierazpenean kontrolarekin eta DMEM:F12 medioan ereindakoekin alderatuta.

4.2. *In vitro* inflamazio saiakuntza

TNFα hantura-estimulu gisa eta KZE hazkuntza-medio bezala finkatu ondoren, hantura-saiakuntza osoa gauzatu genuen. IL-1β-ren adierazpen genikoa funtzionalizatutako hidrogelekin tratatutako KZE hazkuntzen hanturaren lehengoratzea neurtzeko erabili genuen. IL-1β-ren adierazpen normalizatua Gusβ eta TBP erreferentziako geneak erabiliz zehaztu genuen. Emaitzak kontrol laginarekiko (M-M) aztertu genituen.

Lau baldintza probatu genituen funtzionalizatutako hidrogelaren lau bertsio erabiliz, hanturazko estimulurik egon ezean, hidrogelaren beraren eragina aztertzeko (IV.18 irudiko "M-" izeneko laginak). Baldintza esperimentalen kopurua murrizteko, aukera bakarra probatu genuen TNFα-ren estimulurik gabeko hidrogel-bertsio bakoitzerako: hidrogel ez-funtzionalizatua (M-H), antigorputza zuen hidrogela (M-H-Ag), sPRGF odol-eratorri gisa zeukan hidrogela (M-H-sPRGF) eta mintz amniotikoaren zati ezberdinen nahasketa zuen hidrogela (M-H-GMAe (Nahasketa)). Hidrogela funtzionalizatutako edozein formatan erabiltzeak (M-H, M-H-Ag, M-H-sPRGF, M-H-GMAe (Nahasketa)) zeluletan hantura-efektua eragin zuen nahiz eta TNFα-rik ez eduki, funtzionalizatu gabeko hidrogelaren (M-H) kasuan alde esanguratsuak egon zirelarik. Antigorputzaren, sPRGF-ren edo GMAe nahasketaren gehikuntzak eragin hori murriztu zuen kontrolarekin (M-M) alderatuta, desberdintasun estatistiko nabarmenik ez egoteraino.

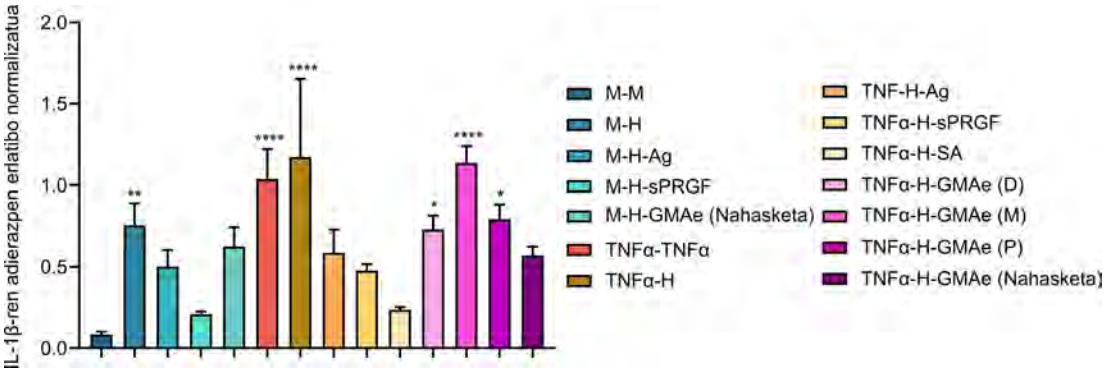

IV.18. IRUDIA: IL-1β genearen adierazpen erlatibo normalizatua ($\Delta\Delta$Cq) hidrogel funtzionalizatuaren bertsio desberdinekin kultibatutako KZE hazkuntzetan. Estatistikoki esanguratsuak diren desberdintasunak KZE medioarekin eta hantura-estimulurik gabe (M-M) kultibatutako zelulekiko adierazi ditugu, $*$ p < 0,05, $**$ p < 0,01, $***$ p < 0,001, $****$ p < 0,0001.

Hantura-maila handiagoak erregistratu genituen 72 orduz H hidrogelaren (TNFα-H) eraginpean egondako zeluletan soilik TNFα-ren eraginpean (TNFα-TNFα) egondako zeluletan baino. Hidrogela bera gehitzeak, lehendik ere hantura-efektua (M-H) erakutsi zuena, zelula-hazkuntzen hantura areagotu zuen. Antigorputzaren (TNFα-H-Ag), odol-eratorrien (TNFα-H-SA eta TNFα-H-sPRGF) edo GMAe nahasketaren (TNFα-H-GMAe (Nahasketa)) gehikuntzak hantura murriztu zuen, eta kontrolarekin alderatuta ez zen alde nabarmenik antzeman. Horrek hantura lehengoratzeko produktuen eraginkortasuna berretsi zuen. Hala ere, mintz amniotikoaren zati bakoitzetik (TNFα-H-GMAe (D), TNFα-H-GMAe (M) edo TNFα-H-GMAe (P)) erauzitako GMAe-rekin funtzionalizatutako hidrogelek ez zuten hanturaren eragin murriztaile hori erakutsi; IL-1β maila estatistikoki esanguratsuak erregistratu baikenituen hiru kasuetan, aldeak nabarmenak izanik GMA-ren erdiko eremutik lortutako GMAe-rekin funtzionalizatutako hidrogelaren kasuan (TNFα-H-GMAe (M)). *In vitro* emaitzek, ondorengo *ex vivo* eta *in vivo* saiakuntzetan erabilitako 4 hidrogel-bertsioak hautatzeko balio izan ziguten. SA aukeratu genuen odol-eratorri gisa, sPRGF-rekin alderatuta eragin murriztaile handiagoa erakutsi baitzuen. GMA-ren hurbileko eremutik lortutako GMAe-ren aukeraketarako irizpide berdina jarraitu genuen.

5. *Ex vivo* saiakuntzak

In vivo esperimentuan erabili beharreko animalia kopurua murrizteko, *ex vivo* saiakuntzak hidrogela aplikatzeko prozesua erreproduzitzeko, emandako dosia eta erretikulazioaren iraupena doitzeko, eta hidrogela zelula epitelialak hazteko substratu gisa egokia zela egiaztatzeko egin genituen. Hainbat erretikulazio-denbora (40 s, 1 min, 1,5 min eta 2 min) eta hidrogel kantitate (30-100 μl) probatu ondoren, argi urdinarekin 2 minutuko erretikulazioa eta 50 μl hidrogel sartzea nahikoa zirela erabaki genuen, zauria estali eta zelula epitelialak ugal zitezen.

Ex vivo hazkuntzak 8 egunez mantendu genituen zelula epitelialek zauria itxi zuten arte. 8 egunetan, zauriaren itxiera zentrokide eta progresiboa ikusi genuen (IV.19 irudia).

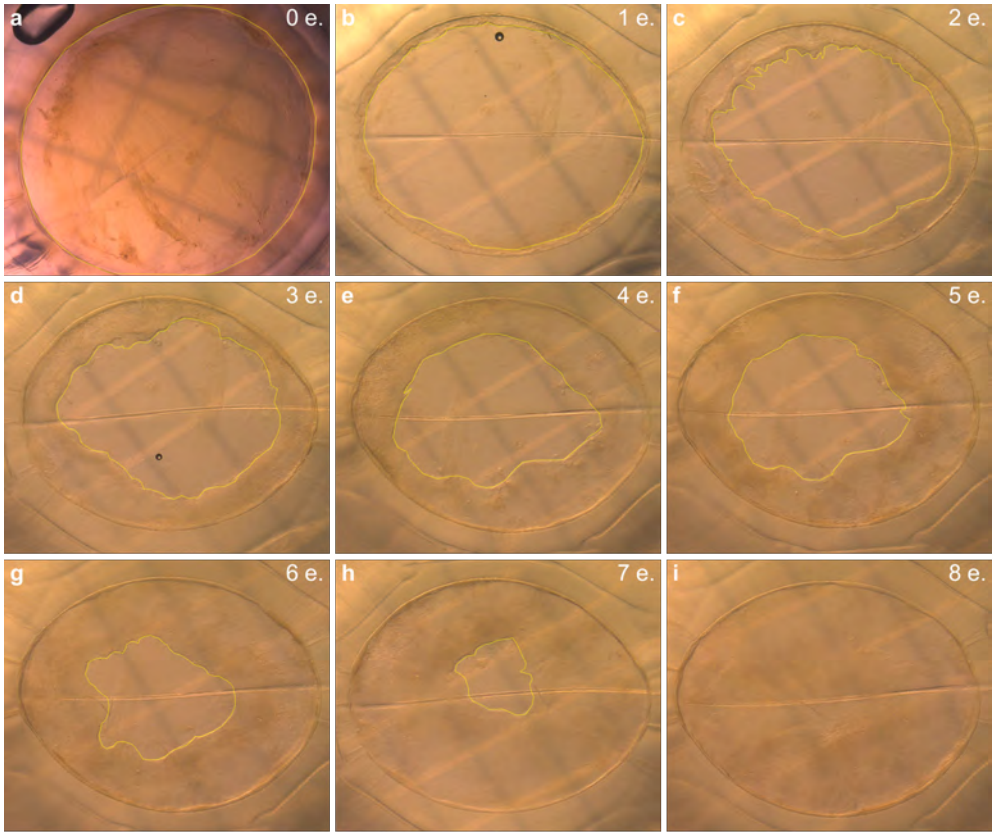

IV.19. IRUDIA: Zauri epitelialaren itxieraren bilakaera *ex vivo* behi-korneako ereduan hidrogelarekin tratatutako 8 eguneko aldian.

Kontrol-taldearekin alderatuta, hidrogelarekin tratatutako hazkuntzak 3 egun gehiago behar izan zituzten ixteko (Kontrol taldeko korneak 5. egunean itxi ziren, hidrogelarekin tratatutakoak aldiz, 8. egunean). Kontrol-taldeko zelula epitelialak aske migratu zuten inolako eragozpenik aurkitu gabe, hidrogelarekin tratatutako hazkuntzak ez bezala. Hidrogelak erabili ziren kasuetan zauriaren itxiera motelagoa izan bazen ere, zelulek epitelio lodiago bat sortu zuten.

Nahiz eta korneak prozesatzean hidrogela noizbehinka galdu, materiala hondatutako eremuari itsatsi eta epitelio sortu berria honen gainean hasten zela frogatu ahal izan genuen (IV.20 irudia).

Behi-begietan egindako saiakuntzak untxi-korneetan errepikatu genituen, zauriaren bilakaeraren eta itxieraren ezaugarri berak dokumentatuz (IV.21 irudia). Bi ereduen arteko ezberdintasun nabarmenena ehunen manipulazioan hauteman genuen: behi-ereduak zauriaren itxiera-prozesua hobeto behatzeko aukera eman zigun, begiaren tamaina handia zela eta, baina ehunen gogortasunaren ondorioz, zaila izan zen zauriak kornea batetik bestera modu zehatzean erreproduzitzea.

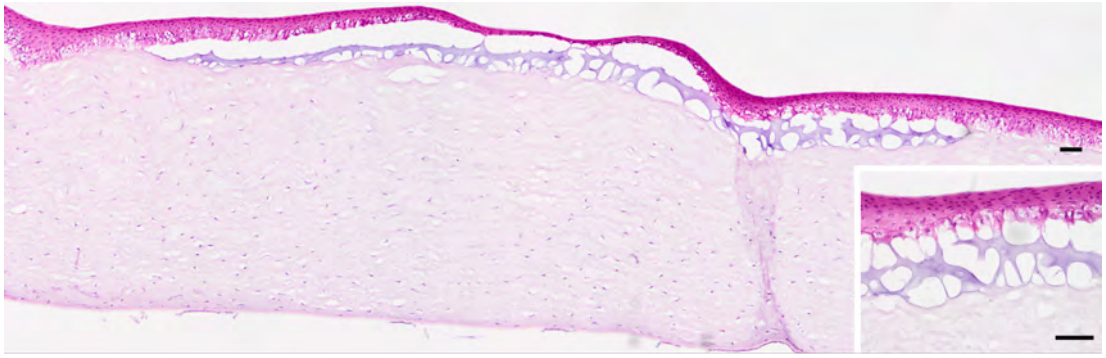

IV.20. IRUDIA: Hematoxilina-Eosina tindaketa *ex vivo* kultibatutako behi-kornearen ereduan. Irudiak H hidrogelarekin tratatu osteko berrepitelizazioa adierazten du. Zauria egin eta 8 egunetara prozesatu genuen kornea. Irudiak 10× eta 40× objektiboekin atera genituen, hurrenez hurren. Eskala lerroek 50 μm-ko neurria adierazten dute. Berrepitelizazio osoa ikusi genuen, baita aplikatutako hidrogelaren mantenua ere. 400× handipenarekin, hidrogelak epitelioarekin eta aurreko estromarekin sortutako atxikimendu puntuak ikus daitezke.

Analisi histologikoak bi ereduen arteko desberdintasun nabarmena erakutsi zuen linboko eremuan. Behien linboko epitelioaren oinarrizko geruzak melanina-kontzentrazio nabarmena zuen, azaleko geruzetara hedatzen zena. Aitzitik, melanina nekez antzeman zitekeen untxien korneako sekzioetan (IV.22 irudia).

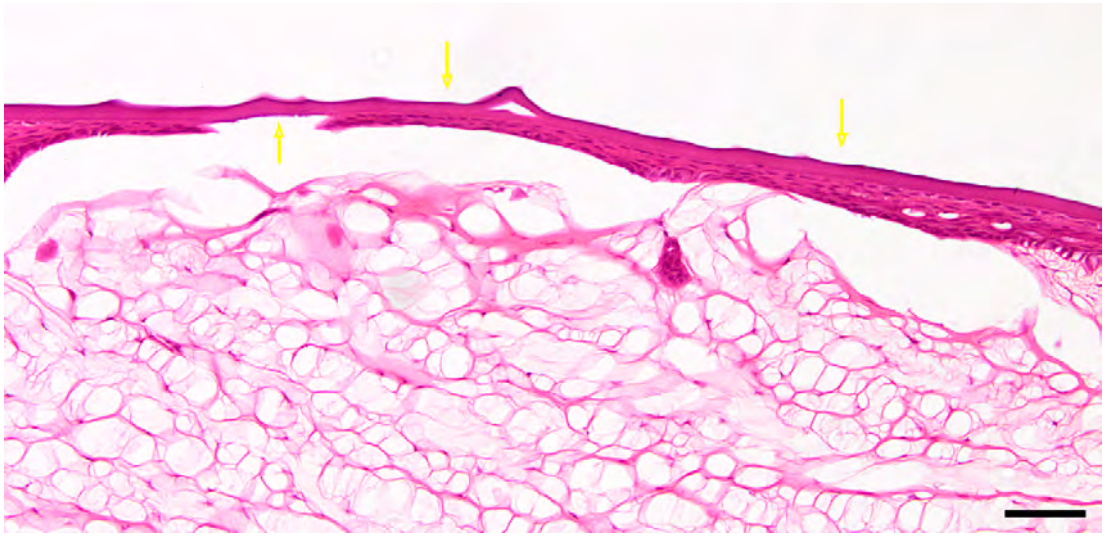

IV.21. IRUDIA: Hematoxilina-Eosina tindaketa *ex vivo* kultibatutako untxi-kornearen ereduan. Irudiak H hidrogelarekin tratatu osteko berrepitelizazioa adierazten du. Zauria egin eta 6 egunetara prozesatu genuen kornea. Irudia 10× objektiboarekin atera genuen eta eskala lerroak 100 μm-ko neurria adierazten du. Berrepitelizazio osoa ikusi genuen, baita aplikatutako hidrogelaren mantenua ere (gezi horiekin adierazita). Aplikatutako hidrogelaren zati bat epitelio berriaren gainetik ikus zitekeen, hidrogelak zauria orbaintzeko prozesuan zehar duen eragin iraunkorra adieraziz.

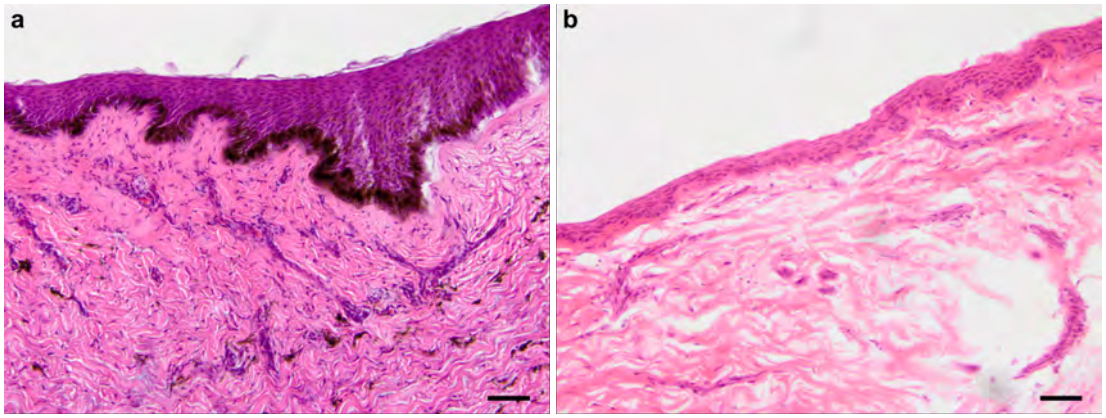

IV.22. IRUDIA: Hematoxilina-Eosina tindaketa *ex vivo* kultibatutako behi- (**a**) eta untxi-kornea (**b**) ereduen linboko eremuan. Behi-kornearen linbo eremuko geruza basalean melanina-kontzentrazioa untxi-kornean baino nabarmenagoa izan zen. Irudiak 20× handipen objektiboarekin atera genituen eta eskala lerroek 50 μm-ko neurriak adierazten dituzte.

6. *Ex vivo* atxikidura proba

Hidrogelaren eta zauriaren arteko itsaspena zunda zilindrikoz hornitutako TA.XT.Plus C gailuan aztertu genuen. Behi-korneak substratu biologiko gisa erabili genituen eta hidrogelaren eta kornea-gainazalaren arteko elkarreragina (F_{max}) eta hidrogela behi-korneatik bereizteko beharrezko lanaren balioak (W_{adh}) kalkulatu

genituen. Proba 3 erreplika biologikorekin eta bakoitzaren 3 erreplika tekniko eginez gauzatu genuen.

IV.23 irudiko tontorraren altuerak hidrogela zuen zunda korneatik bereizteko behar izan zen gehieneko indarra erakusten du (F_{max}). Atxikitze-lana (W_{adh}), distantzia eta indarraren-grafikotik zenbatetsia, zundaren erretiratze-energia osoa adierazten du.

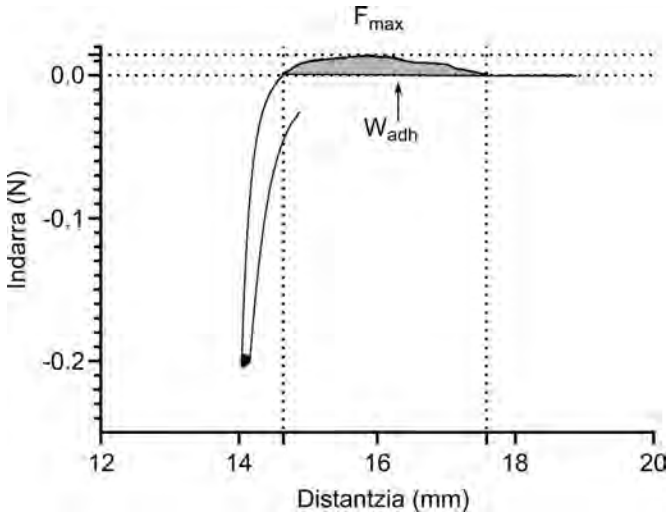

IV.23. IRUDIA: Atxikidura-proban, H hidrogelarentzako indar-desplazamendu kurba bereizgarria. Hidrogela duen zunda korneatik bereizteko behar den gehieneko indarra, F_{max} balioak adierazten du. Grisez itzaldutako eremuak hidrogela eta kornea bereizteko beharrezkoa den atxikitze-lana adierazten du (W_{adh}).

Hidrogelak atxikidura-indar positiboa erakutsi zuen aztertutako hiru lagin biologikoetan, eta horrek hidrogela zauriari atxikitzen zitzaiola berretsi zuen. Atxikitze-lanari dagokionez, erreplika biologikoen artean aldaketa estatistikoki esanguratsuak hauteman genituen, zauriaren eremuetako irregulartasunekin lotuta egon zitezkeenak (IV.24 irudia).

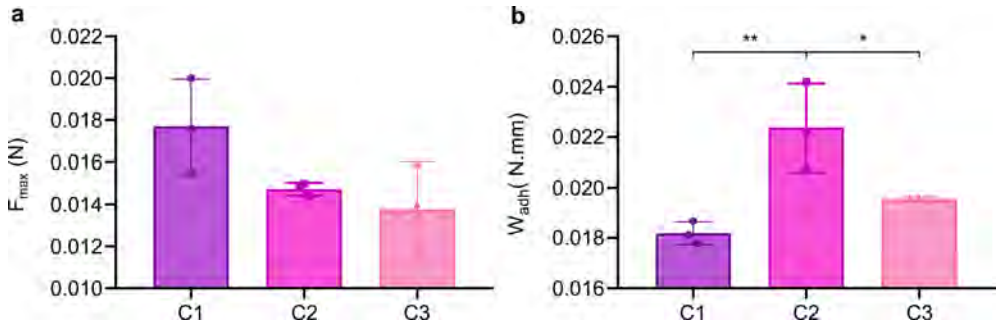

IV.24. IRUDIA: H hidrogelaren propietate itsaskorrak, **a**) gehieneko askatze-indarrari (F_{max}) eta **b**) atxikitze-lanari (W_{adh}) dagokienez. Neurketak 3 erreplika biologikotan egin genituen. Alde estatistikoki esanguratsuak honela definitu ditugu: $*$ $p < 0,05$, $**$ $p < 0,01$, $***$ $p < 0,001$, $****$ $p < 0,0001$.

7. *In vivo* saiakuntza

In vitro eta *ex vivo* emaitzak berresteko, *in vivo* saiakuntza egin genuen untxietan. Korneako ultzerak aurreko estromako keratektomia baten bitartez egin genituen 30 untxietan. Animaliak 5 taldetan banatu genituen ausaz, eta honela tratatu:

- Kontrola: % 0,2 AH-zko malko artifizialak 4 aldiz egunean zauria itxi arte.
- H: 50 μl % 5 gelatinaz eta % 0,01 RFP-z osatutako eta 2 minutuz argi urdinarekin erretikulatutako hidrogela + % 0,2 AH-zko malko artifizialak 4 aldiz egunean zauria itxi arte.
- H-Ag: 50 μl % 5 gelatinaz, % 0,01 RFP-z eta 1 mg/ml Infliximab-ez osatutako eta 2 minutuz argi urdinarekin erretikulatutako hidrogela + % 0,2 AH-zko malko artifizialak 4 aldiz egunean zauria itxi arte.
- H-SA: 50 μl % 10 gelatinaz, % 0,02 RFP-z eta SA-z 1:1 diluzioan osatutako eta 2 minutuz argi urdinarekin erretikulatutako hidrogela + % 0,2 AH-zko malko artifizialak 4 aldiz egunean zauria itxi arte.
- H-GMAe: 50 μl % 10 gelatinaz, % 0,02 RFP-z eta GMAe-z 1:1 diluzioan osatutako eta 2 minutuz argi urdinarekin erretikulatutako hidrogela + % 0.2 AH-zko malko artifizialak 4 aldiz egunean zauria itxi arte.

60 korneak 6 esperimentutan banatu genituen.

7.1. Prozedura esperimentalaren baldintzak doitzeko azterketa pilotua

Hasierako esperimentua (E01) proba pilotu gisa erabili genuen baldintzak doitzeko eta protokoloak ezartzeko. Bi kornea erabili genituen baldintza bakoitzerako (n = 10 kornea taldeko). Zauria sortzearekin batera, kirurgiaren egunean 25 μl % 0,1 benzalkonio kloruro (BAK) instilatu genituen kaltetutako kornea bakoitzean, hantura areagotzeko. Gainera, zauria sortu eta hidrogela aplikatu ondoren, tratatutako korneak ukipen-lenteekin estali genituen. BAK-k eragindako narritadurak eta ultzerak eragindako eragozpenen ondorioz, animaliek etengabe igurtzi zuten kaltetutako eremua. Ondorioz, hamar untxietatik hiruk bakarrik eutsi zioten lenteari kirurgia egin eta bigarren egunera arte, eta hirugarren egunetik aurrera untxi guztiek erretiratua zuten lentea.

7.1.1. Berrepitelizazioa

Berrepitelizazioa azkarragoa izan zen H eta H-SA tratamendu taldeetan, zauriaren eremu irekiaren batez besteko ehunekoa % 1,87 $\pm$ % 2,65 H-z eta % 0,00 $\pm$ % 0,00, hau da, akatsen itxiera osoa, H-SA-z tratatutako korneetarako 5 eguneko epean (IV.25 eta IV.26 irudiak eta IV.5 taula). H-GMAe hidrogelarekin tratatutako korneak itxi ziren ondoren, seigarren egunean zauri-eremu irekiaren batez besteko balioa % 0,89 $\pm$ % 1,26 izanik.

Era berean, H-SA hidrogelak zauri guztien erabateko itxiera erakutsi zuen 5. egunean, ondoren H tratamenduak 6. egunean eta H-GMAe taldeak 7. egunean. Kontrol tratamenduaren eta H-Ag tratamenduaren zaurien erdiak 8. egunean itxi ziren, baina H-Ag taldeko zauri guztiak ez ziren erabat itxi 10. egunerako (IV.26 irudiko **b**).

Kontrol eta H-Ag tratamenduek zauri-itxieraren bilakaera oso antzekoa izan zuten, baina itxiera-tasa ez zen % 0-ra iritsi H-Ag-rako, tratatutako korneetako bat ez zelako erabat berrepitelizatu.

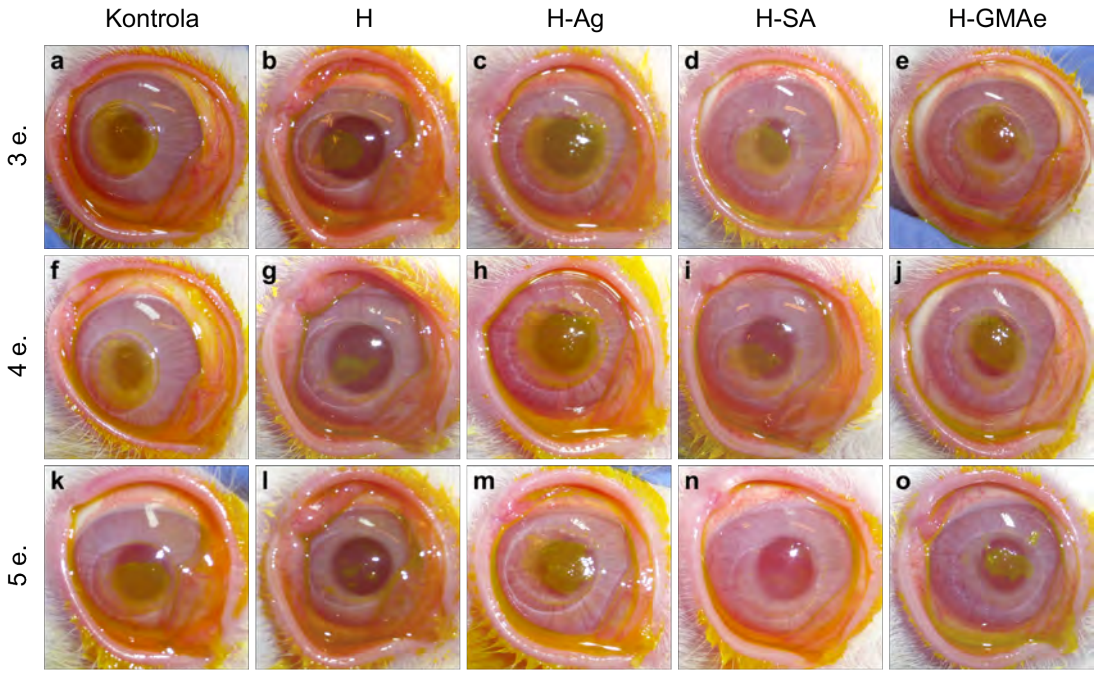

IV.25. IRUDIA: Malko artifizialekin (Kontrola) edo hidrogelaren bertsio desberdinekin (H, H-Ag, H-SA eta H-GMAe) tratatutako proba pilotuko untxi-korneen akats epitelialen *in vivo* bilakaera, 3. egunetik (3 e.) 5. eguneraino (5 e.). Akats epiteliala fluoreszeinarekin tindatuta ebaluatu genuen.

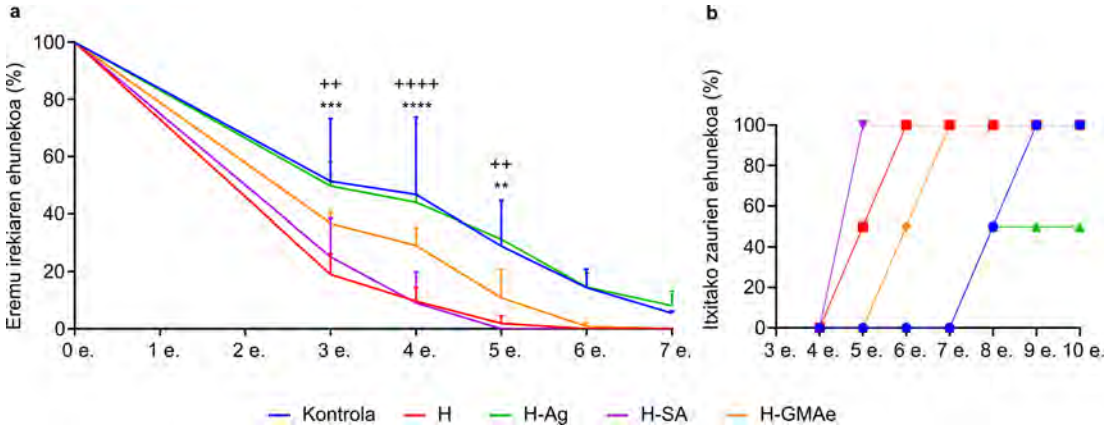

IV.26. IRUDIA: Proba pilotuko untxi-korneetako akats epitelialen *in vivo* bilakaera. **a**) Irekitako zauri epitelialaren eremuaren ehunekoa kirurgiaren egunetik (0 e.) 10. egunera (10 e.). *b*) Itxitako zaurien ehunekoa, 4. egunetik (4 e.) 10. egunera (10 e.). Alde estatistikoki esanguratsuak honela definitu ditugu: $*$, + $p < 0,05$, $**$, ++ $p < 0,01$, $***$, +++ $p < 0,001$, $****$, ++++ $p < 0,0001$. "$*$" eta "+", H eta H-AS hidrogelek kontrol-tratamenduarekiko dituzten desberdintasunak adierazten dituzte.

IV.5. TAULA: Proba pilotuko untxi-korneen berrepitelizazioaren bilakaera, hidrogelekin edo kontrol-tratamenduarekin tratatutako begietan. Emaitzak irekitako zauri-eremuaren ehunekoaren batez besteko $\pm$ DE gisa adierazi ditugu. Alde estatistikoki esanguratsuak honela definitu ditugu: $*$, + $p < 0,05$, $**$, ++ $p < 0,01$, $***$, +++ $p < 0,001$, $****$, ++++ $p < 0,0001$. "$*$" eta "+" ikurrek, kontrol eta H-Ag tratamenduekiko desberdintasun esanguratsuak erakusten dituzte, hurrenez hurren.

	Denbora (egunak)								
Tratamendua	0	3	4	5	6	7	8	9	10
Kontrola	100,00	51,37 ± 21,83	46,80 ± 27,08	28,89 ± 15,79	14,43 ± 6,45	5,45 ± 0,79	0,40 ± 0,57	0,00 ± 0,00	0,00 ± 0,00
H	100,00	18,98 ± 7,11 $^{******+}$	9,64 ± 4,70 $^{*******+}$	1,87 ± 2,65 $^{**++}$	0,00 ± 0,00	0,00 ± 0,00	0,00 ± 0,00	0,00 ± 0,00	0,00 ± 0,00
H-Ag	100,00	49,71 ± 8,54	44,05 ± 2,75	31,30 ± 12,97	14,60 ± 4,87	8,05 ± 5,19	2,98 ± 2,12	1,80 ± 2,55	0,57 ± 0,81
H-SA	100,00	25,12 ± 13,39 $^{***+}$	9,04 ± 10,88 $^{*******+}$	0,00 ± 0,00 $^{*****+}$	0,00 ± 0,00	0,00 ± 0,00	0,00 ± 0,00	0,00 ± 0,00	0,00 ± 0,00
H-GMAe	100,00	36,71 ± 4,02	29,11 ± 6,32	10,81 ± 9,91	0,89 ± 1,26	0,00 ± 0,00	0,00 ± 0,00	0,00 ± 0,00	0,00 ± 0,00

7.1.2. Ebaluazio klinikoa

Sintoma klinikoak Draize eskalaren bidez ebaluatu genituen hirugarren egunetik aurrera. Ondoren, tratamendu bakoitzari Kay eta Kalandraren sailkapenean oinarritutako narritadura-indize bat esleitu genion.

Tratamendu guztiek H hidrogelak izan ezik, narritadura-balioak gutxieneko narritadura-tartean (2,5-15 tartea Kay eta Kalandraren sailkapenaren arabera) izan zituzten kirurgiaren osteko lehen egunetan (2., 3. eta 4. egunak). H tratamendua ia ez zen narritagarria izan (0,6-2,5 tartea Kay eta Kalandraren sailkapenaren arabera) 3. egunetik aurrera. Ebaluazioan zehar, bai kontrol-taldeak bai H-Ag taldeak hasieratik lortu zituzten puntuaziorik altuenak (IV.27 irudia).

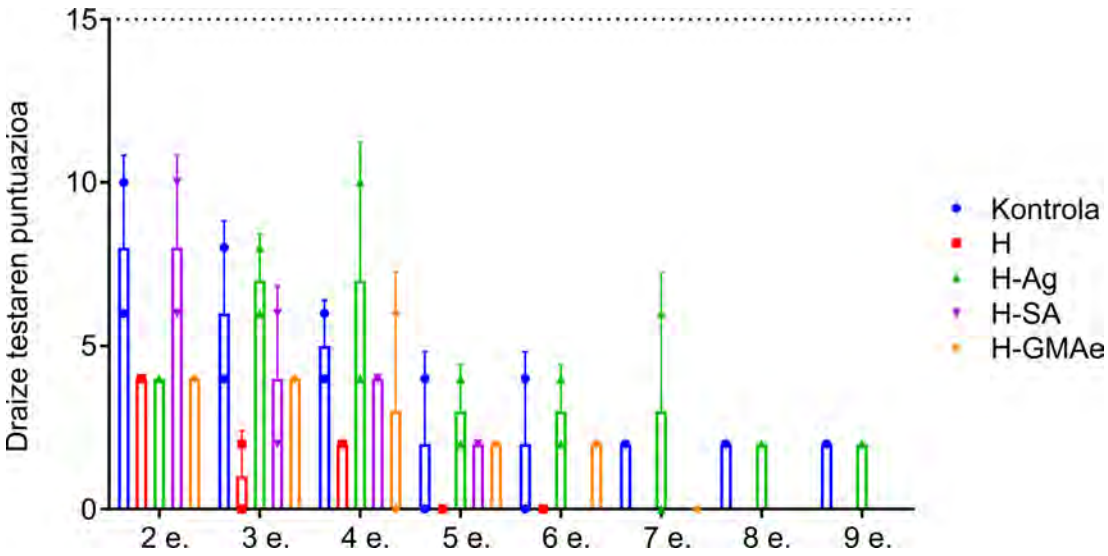

IV.27. IRUDIA: Proba pilotuaren Draize testaren puntuazioa azterketaren 2. egunetik (2 e.) 9. egunera (9 e.). Draize eskalaren Kay eta Kalandraren sailkapenean, 2,5-etik 15-era bitarteko puntuazio-tarteak gutxieneko narritadura tartea adierazten du (y = 15). 15 puntutik gorako edozein balio apur bat narritagarri edo oso narritagarri gisa sailkatuko litzateke. Laginen artean ez genuen alde estatistikoki esanguratsurik ikusi.

7.1.3. Malko-laginetako hantura-zitokinen adierazpenaren ebaluazioa

Proteina edukia eluzio prozesu eta zentrifugazioen bidez atera genuen Schirmer-en tiretan jasotako malkoetatik, eta BCA saiakuntzen bidez kuantifikatu genuen. 50 erreplika biologiko kuantifikatu genituen (10 untxi $\times$ 5 ebaluazio-denbora) lehenengo esperimentu pilotuan, eta hantura-zitokinen adierazpena QAL-CYT-1 Quantibody Rabbit Cytokine Array kitaren bidez (Raybiotech, Norcross, GE, AEB) ebaluatu genuen.

Aztertutako zitokina guztien artean, MIP-1β, MMP-9, NCAM-1 eta IL-8 izan ziren konfiantza-tarte handiena eta detekzio-mugatik gorako datuak erakutsi zituzten molekulak. Lau molekula horiek lesio baten ondoriozko hasierako hantura-erantzunarekin lotuta daude.

IV.28 irudiak lau zitokinen balioak erakusten ditu azterketa-egunaren arabera, tratamendu guztiak multzokatuz. Lau molekulen adierazpenaren gorakada 1. egunean hauteman genuen, lagin bakoitzaren balioak gehiago sakabanatuz (grafikoan adierazitako puntu urdinak). MMP-9 eta IL-8-rentzat, sakabanatze eta gorakada hori 7. egunean ere ikusi genuen. Desberdintasun horiek bat datoz egun horietan tratamendu bakoitzerako erregistratu genituen desberdintasunekin (IV.29 irudia).

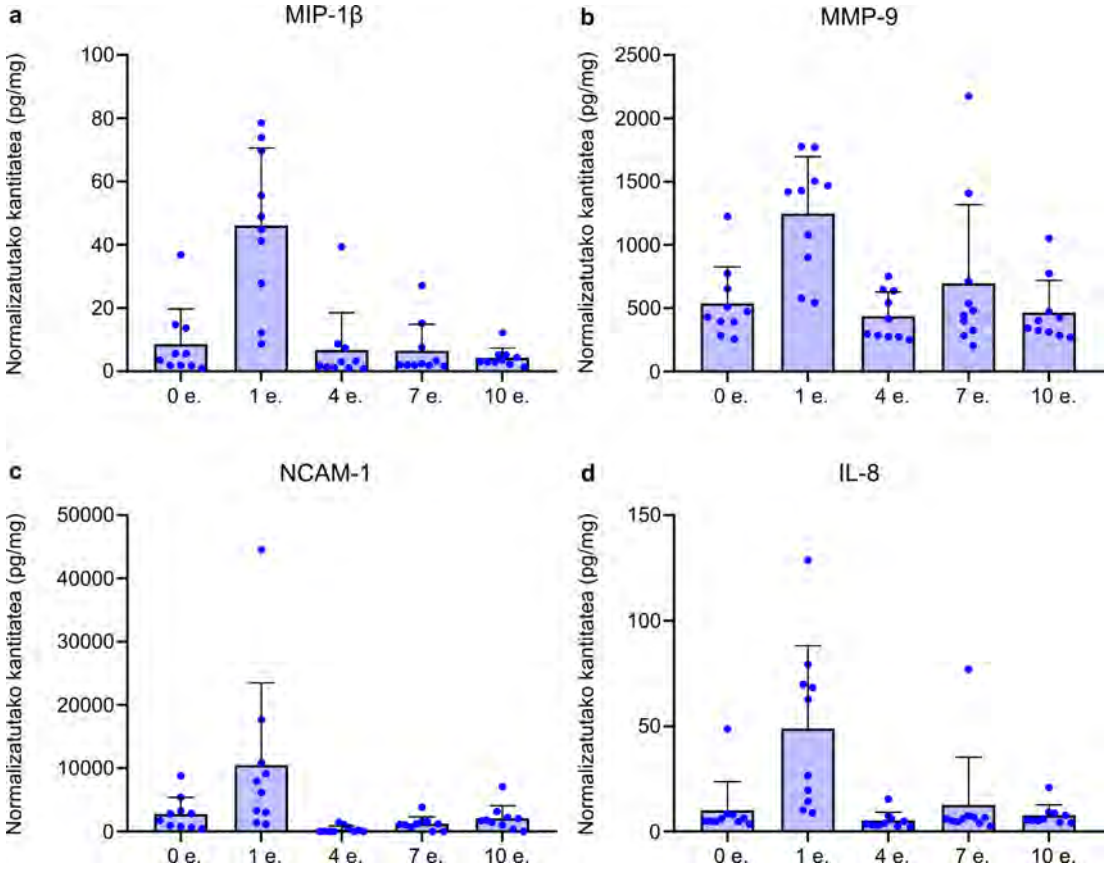

IV.28. IRUDIA: Proba pilotuan bildutako malko-laginetako **a**) MIP-1β, **b**) MMP-9, **c**) NCAM-1 eta **d**) IL-8 zitokinen balio normalizatuak. Grafikak aztertutako egun bakoitzeko zitokina bakoitzaren adierazpena erakusten du, tratamenduak bereizi gabe.

Joera alderagarria ikusi genuen MIP-1β, MMP-9 eta NCAM-1-entzat, ebaluazioaren 1. egunean adierazpen-maila handiagoekin, bai H-SA taldearentzat, bai kontrol-taldearentzat. Emaitzak koherenteak izan ziren 2. egunean Draize proban lortutakoekin, non kontrol-tratamenduak eta H-SA hidrogelak narritadura-puntuazio altuagoak erakutsi zituzten. 3. egunetik aurrera, Draize-ren emaitzak altuagoak izan ziren H-Ag hidrogelarentzat, 7. egunean lortutako MMP-9 gorakadarekin bat eginez (IV.29 irudia).

Zitokinen adierazpena gutxieneko mailara jaitsi zen azterketaren 4. egunetik aurrera. 7. egunean, H-Ag eta H-GMAe taldeetan MMP-9-ren igoera txiki bat erregistratu genuen, eta H-GMAe taldean IL-8-rentzat (IV.29 irudiko **b** eta **d**).

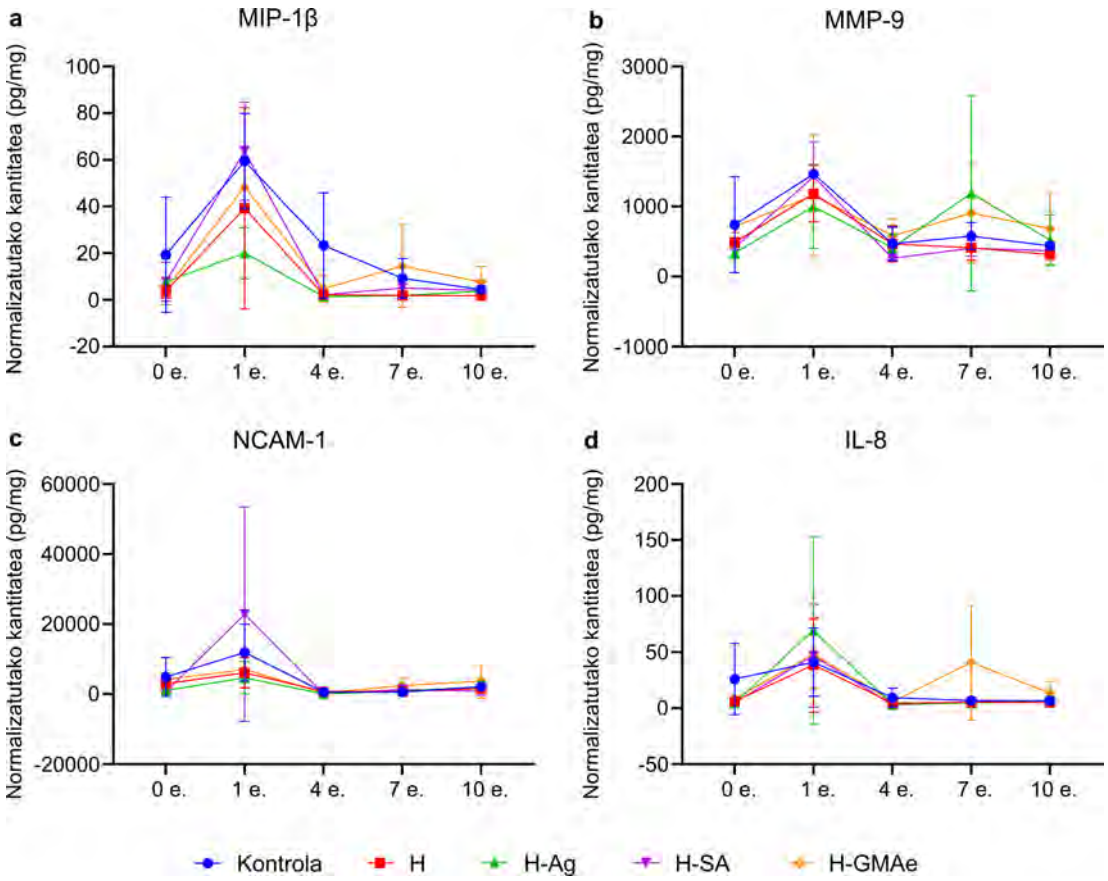

IV.29. IRUDIA: Proba pilotuan bildutako malko-laginetako **a**) MIP-1β, **b**) MMP-9, **c**) NCAM-1 eta **d**) IL-8 zitokinen balio normalizatuak, eguneko eta azterketa-taldeko.

7.2. Korneetako *in vivo* berrepitelizazioa untxietan

Azterketa pilotuaren emaitzak ikusita, ukipen-lenteak tarsorrafiengatik ordeztu genituen ondorengo esperimentuetan. BAK-k eragindako hantura-estimulu erantsia ere ezabatu genuen.

Gainerako bost esperimentu-txandak (E02-E06) tarsorrafia partzialarekin egin genituen, hau ebakuntza ondoko hirugarren egunera arte mantenduz. Beraz, puntu honetatik aurrera aurkeztutako emaitzek E02 eta E06 esperimentuen emaitzak erakusten dituzte. Zauriaren itxieraren bilakaera, tarsorrafiaren ondorioz lehen bi egunetan erregistratu ezin izan genuena, bizkortu egin zen betazalen itxiera kirurgikoa zela-eta (IV.6 taula eta IV.30 irudia). 7. egunaren ondoren irekitako eremuaren batez besteko ehunekoa % 2,70 $\pm$ % 3,81-koa izan zen esperimentu pilotuaren 10 untxientzat eta % 1,51 $\pm$ % 2,60-koa E02-E06 esperimentuetarako.

Zauriaren eremu irekiak nekez gainditzen zuen % 20-ko batez besteko balioa hiru egunen buruan (IV.7 taula eta IV.31 irudiko **a**). Kontrol-taldeak itxiera azkarrena lortu

IV.6. TAULA: Azterketa pilotuaren (E01) eta gainerako 5 esperimentuen (E02-E06) arteko aldeak irekitako zauri-eremuaren batez besteko ± DE ehunekoan esperimentuko egun bakoitzerako. Alde estatistikoki esanguratsuak honela definitu ditugu: $*$ p < 0,05, $**$ p < 0,01, $***$ p < 0,001, $****$ p < 0,0001.

	Denbora (egunak)					
Saiakuntza	0	3	4	5	6	7
E01	100,00	36,38 ± 14,42	27,73 ± 18,08	14,57 ± 14,77	5,98 ± 7,80	2,70 ± 3,81
E02-E06	100,00	18,60 ± 1,26 **	7,90 ± 1,46 **	4,61 ± 1,08	1,66 ± 1,47	1,51 ± 2,60

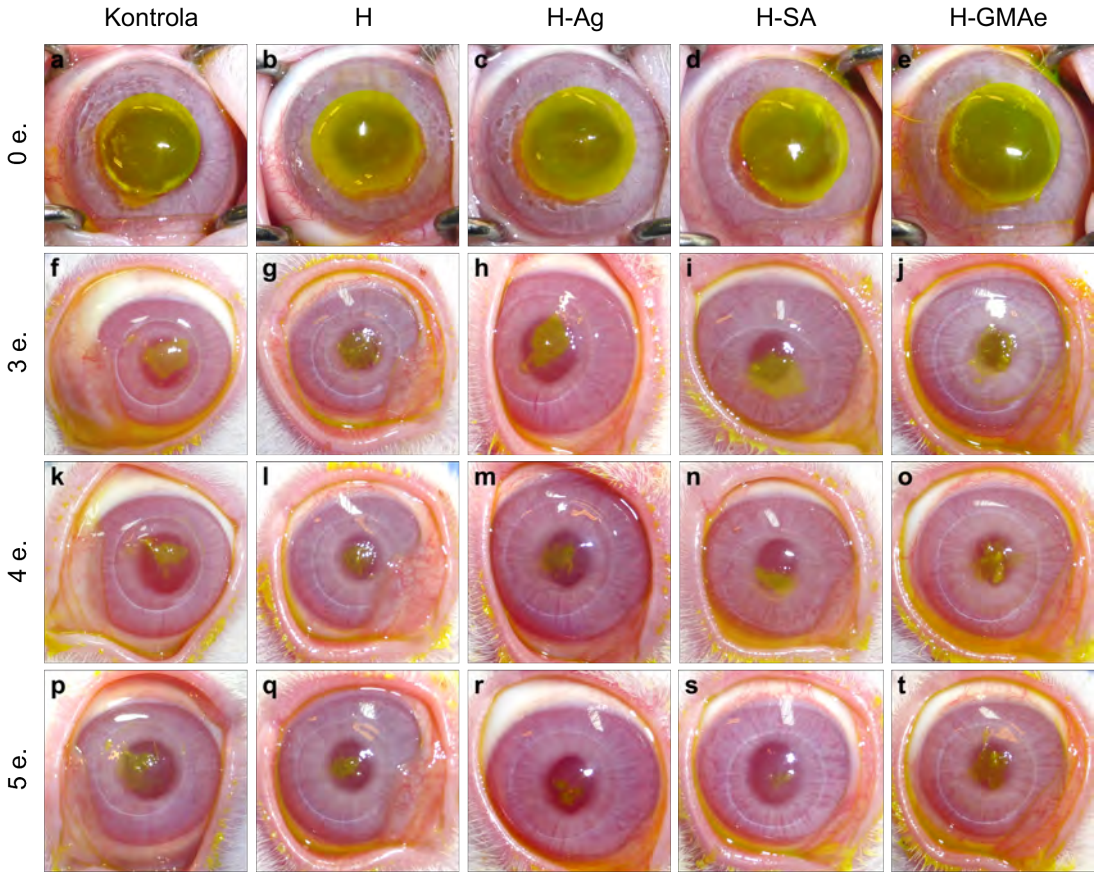

IV.30. IRUDIA: Malko artifizialekin (Kontrola) edo hidrogelaren bertsio desberdinekin (H, H-Ag, H-SA eta H-GMAe) tratatutako untxi-korneetako akats epitelialen *in vivo* bilakaera kirurgiaren egunetik (0 e.) 5. eguneraino (5 e.). Akats epiteliala fluoreszeinarekin tindatuta ebaluatu genuen.

zuen bosgarren egunean (IV.31 irudiko **c**), eta, guztira, kasuen % 60 itxi ziren (IV.31 irudiko **b**). Hala ere, 5. egunetik aurrera zaurien itxieraren eboluzioa moteldu zen, eta 7. egunean zauri-eremua apur bat handitu zela ere iruditu zitzaigun, kornea batzuk erabat itxi gabe egon zitezkeela edo itxi eta berriro ireki zitezkeela iradokiz. Kontrol-korneen % 20 inguru ez ziren itxi (IV.31 irudiko **b**).

Hidrogeletan oinarritutako tratamenduei dagokienez, zaurien itxieraren bilakaera mailakatua eta luzea erregistratu genuen. Zauria azkarrago itxi zen H-SA-ekin tratatutako korneetan, zauri-eremuaren irekiera ehunekoa % 2,7 ± % 3,19 izanik 5. egunean (IV.31 irudiko **c**). Korneen erdiak itxita zeuden 5. egunerako, % 80 6. egunerako eta % 100 7. egunerako (IV.31 irudiko **b**).

IV.7. TAULA: Hidrogel- edo kontrol-tratamenduekin tratatutako untxi-korneen berrepitelizazioaren bilakaera. Emaitzak irekitako zauri-eremuaren ehunekoaren batez besteko ± DE gisa adierazi ditugu. Ez genuen desberdintasun estatistikoki esanguratsurik aurkitu tratamenduen artean une desberdinetan.

	Denbora (egunak)					
Tratamendua	0	3	4	5	6	7
Kontrola	100,00	16,90 ± 12,00	6,06 ± 7,42	4,94 ± 8,14	3,99 ± 11,38	6,11 ± 16,10
H	100,00	18,63 ± 9,67	7,30 ± 8,32	5,10 ± 7,39	1,97 ± 4,12	0,79 ± 2,50
H-Ag	100,00	19,30 ± 15,22	10,05 ± 6,03	4,90 ± 3,44	0,63 ± 1,15	0,00 ± 0,00
H-SA	100,00	20,22 ± 9,64	7,83 ± 6,44	2,71 ± 3,19	0,23 ± 0,49	0,00 ± 0,00
H-GMAe	100,00	17,98 ± 8,67	8,27 ± 6,98	5,37 ± 6,17	1,50 ± 2,45	0,64 ± 2,03

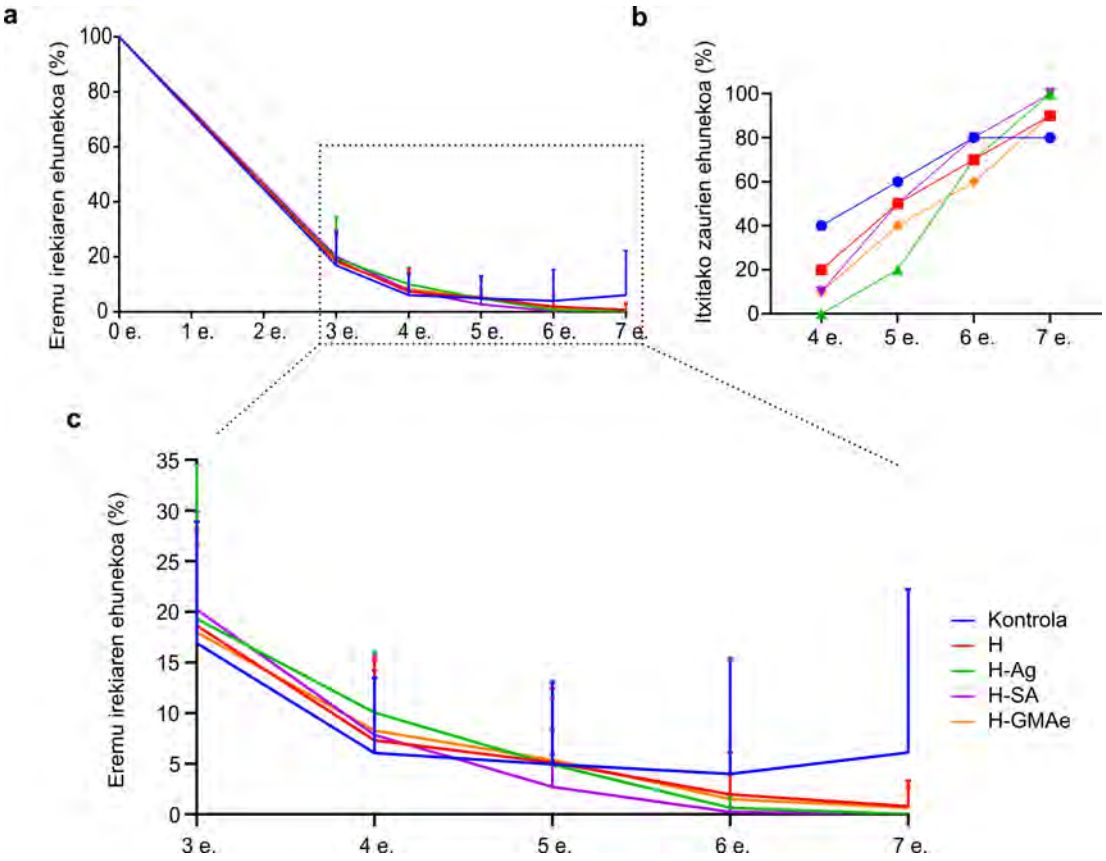

IV.31. IRUDIA: Untxi-korneetako akats epitelialen *in vivo* bilakaera. **a**) Irekitako zauri-eremuaren ehunekoa kirurgiaren egunetik (0 e.) 7. egunera (7 e.). **b**) Itxitako zaurien ehunekoa eguneko, 4. egunetik (4 e.) 7. egunera (7 e.). **c**) Irekitako zauri-eremuaren ehunekoa 3. egunetik (3 e.) 7. egunera (7 e.). Laginen artean ez genuen alde estatistikoki esanguratsurik aurkitu.

H-Ag-rekin tratatutako korneek eremu itxiaren ehuneko txikiena erakutsi zuten 4. egunean, batez beste zauriaren % 10,05 $\pm$ % 6,03 itxiera soilik adieraziz (IV.7 taula). Hala ere, zauri guztiak itxita zeuden 7. egunerako. IV.31 irudiko **b** grafikoak adierazi bezala, H-Ag-rekin tratatutako korneetako zauri gehienak 5. eta 6. egunen artean itxi ziren (itxitako kasuen % 20-tik % 70-era). Talde honetako kornea guztiek, H-SA tratamenduarekin erregistratu genuen bezala, zauriaren itxiera osoa erakutsi zuten 7. egunean.

H eta H-GMAe-rekin tratatutako korneek antzeko joera erakutsi zuten. 5. egunean zauritutako azaleraren ehunekoa, batez beste, % 5,10 $\pm$ % 7,39 eta % 5,37 $\pm$ % 6,17 izan zen, hurrenez hurren (IV.7 taula eta IV.31 irudiko **c**). Aldiz, korneen % 90 itxi ziren 7. egunerako bi kasuetan. Beraz, begien % 10 ez ziren 7 egunetan berrepitelizatu.

Zauria ixtean ez genuen alde nabarmenik ikusi kasu bakar batean ere, ziur asko erreplika biologikoen aldakortasunagatik.

7.3. Ebaluazio klinikoa

Narritadura-zantzu minimoak erregistratu genituen 3. egunean tratamendu guztietarako (IV.32 irudia). Puntuazioak, betazaleko konjuntiben gorritzeagatik, hanturagatik edo, kasu batzuetan, muki-jariaketagatik eman genituen batez ere. 3. egunean ikusitako gorritzea kirurgiarekin lotutako hanturaren eta narritaduraren ondorio izan ziren ziurrenik. Oro har, H-SA bidezko tratamenduak hantura-adierazleetan efektu arintzaile bat erakutsi zuen.

Esperimentu guztien ebaluazio-aldian, kornea-opakutasuna animalia bakarrean baino ez genuen ikusi. Hala ere, kasu atipikotzat hartu eta azterketatik kanpo utzi genuen. Laugarren egunean, kasu guztiek sintomak hobetu zituzten, eta kontrol-taldearen, H eta H-SA-en batez besteko puntuazioek, tratamendu horiek ia narritagarriak ez zirela (0,6-2,5 puntuko tartea Kay eta Kalandraren sailkapenaren arabera) adierazi zuten. H-Ag eta H-GMAe taldeak 5. egunetik aurrera sartu ziren maila honetan.

H-SA tratamendua jasotako korneek emaitza kliniko onenak erakutsi zituzten. 6. egunean edozein suminkortasun-zeinu ia desagertu zen (0,2 $\pm$ 0,63 puntuazioak), eta 7. egunean kornea guztiek 0-ko puntuazioa lortu zuten.

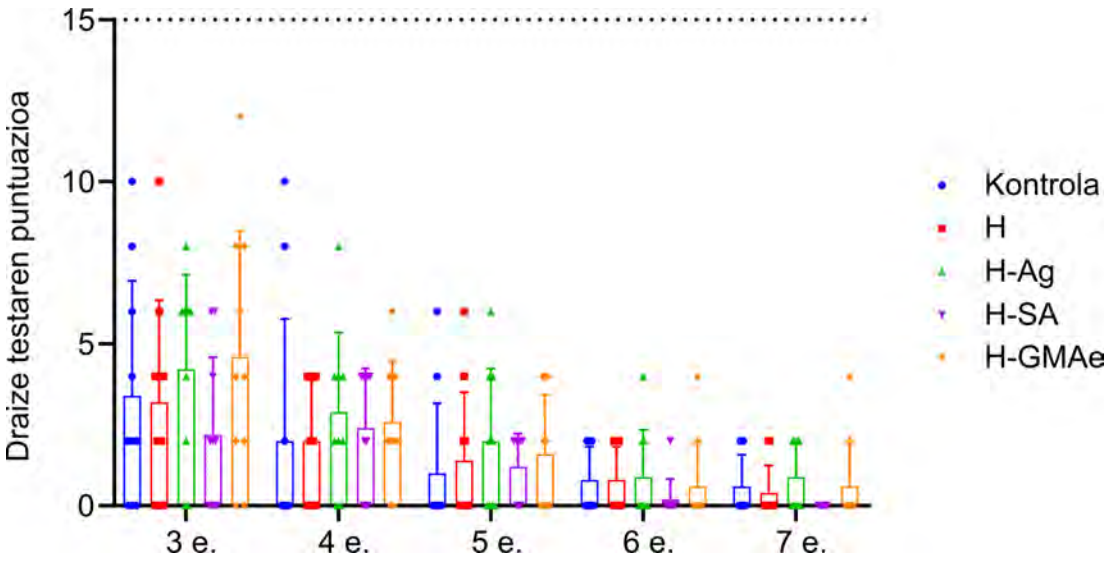

IV.32. IRUDIA: Draize testaren puntuazioa azterketaren 3. egunetik (3 e.) 7. egunera (7 e.). Draize eskalaren Kay eta Kalandraren sailkapenean, 2,5-etik 15-era bitarteko puntuazio-tarteak gutxieneko narritadura tartea adierazten du (y = 15). 15 puntutik gorako edozein balio apur bat narritagarri edo oso narritagarri gisa sailkatuko litzateke. Laginen artean ez genuen alde estatistikoki esanguratsurik hauteman.

Erregistroetako batek ere ez zuen 15 puntuko puntuazioa gainditu, eta, beraz, lortutako balioek ez zuten suminkortasun-egoera arina ere lortu (15,1-25 puntuko tartea Kay eta Kalandraren sailkapenaren arabera).

7.4. Malko-bolumen eta proteina edukiaren kuantifikazioa

E02-E06 esperimentuen Schirmer tiretatik ateratako 200 erreplika biologikoko (10 untxi $\times$ 4 ebaluzio-denbora $\times$ 5 saiakuntza) proteina kantitate osoa, 5 BCA saiakuntzatan kuantifikatu genuen (IV.33 eta IV.34 irudiak).

Proteina edukiak malko-bolumenaren antzeko joera jarraitu zuen kasu gehienetan, baina ez guztietan. Proteina kantitatearen batez besteko balioa malko-bolumenaren balioa baino txikiagoa izan zen 0. egunean H-GMAe tratamendurako eta 4. eta 7. egunetan H-Ag tratamendurako.

Malko-bolumen txikiagoa jaso genuen kirurgia egin eta egun batera hartutako laginetan eta, beraz, kuantifikatutako proteina kantitatea ere murriztu zen (IV.33 eta IV.34 irudiak). Kirurgiak eragindako narritaduragatik eta hanturagatik gertatu zen hori. Kirurgiak eragindako narritadurak eta hanturak malkoa sortzea zail ditzakete, eta horrek lortutako malko-bolumen txikia azal dezake.

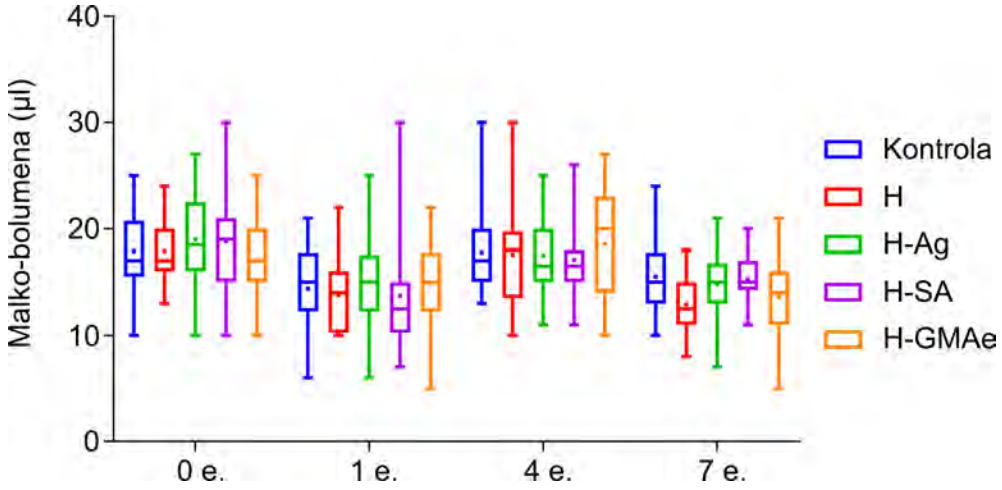

IV.33. IRUDIA: Azterketaren 0., 1., 4. eta 7. egunetan, Schirmer-en tiren bidez bildutako malkoen bolumena tratamendu bakoitzerako. Laginen artean ez genuen alde estatistikoki esanguratsurik aurkitu.

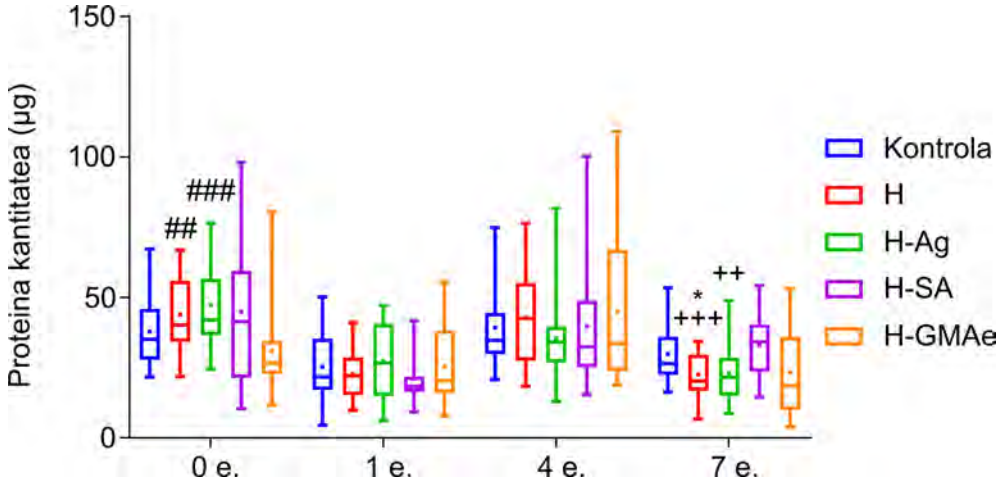

IV.34. IRUDIA: Azterketaren 0., 1., 4. eta 7. egunetan Schirmer-en tiren bidez jasotako malko-laginen eluziotik abiatuta kuantifikatutako proteina kantitatea tratamendu bakoitzerako. Alde estatistikoki esanguratsuak honela definitu ditugu: $*$, +, # $p < 0,05$, $**$, ++, ## $p < 0,01$, $***$, +++, ### $p < 0,001$, $****$, ++++, #### $p < 0,0001$. "$*$", "+" eta "#" ikurrek kontrol, H-SA eta H-GMAe tratamenduekiko desberdintasunak adierazten dituzte, hurrenez hurren.

Ikerketaren laugarren eta zazpigarren egunetan, jasotako malko bolumenak eta neurtutako proteinak ez zuten desbideratze nabarmenik erakutsi.

E02-tik E06-ra arteko esperimentuetan batutako laginen garraio-arazoak zirela-eta, array bidezko hantura-zitokinen adierazpenaren ebaluazioa ezin izan genuen gauzatu.

7.5. Gene-adierazpenaren analisia untxi-korneetako laginetan

Kirurgia egin eta 7 eta 21 egunera lortutako kornea-laginetan hainbat generen adierazpena aztertu genuen (E02, 04 eta 06 esperimentueko korneak 7. eguneko laginak eta E03 eta E05 esperimentuetako korneak 21. eguneko laginak). Hantura (IL-1β), linboko zelula ama/progenitoreak (PAX6, p63), erdiko korneako zelulak (CK3), zelulen proliferazioa (Ki67), atxikidura eta migrazio zelularra (CD44) eta erantzun fibrotikoa (α-SMA) adierazteko markatzaileak erabili genituen.

Ikertutako gene bakoitzaren adierazpen erlatibo normalizatua kalkulatzeko, GAPDH, HPRT1 eta RIG S15 erabili genituen erreferentziazko gene gisa. Kontrol-taldeak kasu bakoitzaren datuak (7. eta 21. egunera) irudikatzeko kontrol bezala balio izan zigun. 21 eguneko analisia egiteko, 2 erreplika biologiko erabili genituen, kasu bakoitzean hiru erreplika tekniko barne. 7 eguneko azterketarako, taldeko 3 erreplika biologiko erabili genituen, lagin bakoitzerako hiru erreplika teknikorekin.

7. eguneko hidrogel-taldeetako IL-1β mailatan ez genuen alde estatistikoki esanguratsurik hauteman kontrol-taldearekin alderatuta (IV.35 irudiko **a**). H taldearen IL-1β-ren adierazpena kontrol-tratemenduaren adierazpenaren antzekoa izan zen, baina erdira jaitsi zen H-Ag-tratamenduarentzat. Hala ere, $\Delta\Delta$Cq-ren balioa 0,5 batez beste handitu zen H-SA eta H-GMAe tratamenduekin. Hantura-markatzailearen desberdintasunak nabarmenak izan ziren 21. eguneko laginetan (IV.35 irudiko **b**). Hidrogeletan oinarritutako tratamendu guztietan, hantura % 50 baino gehiago murriztu zen kontrol-tratamenduarekin alderatuta, H-GMAe-k (batez besteko 0,05 $\Delta\Delta$Cq), H-Ag-k (batez besteko 0,18 $\Delta\Delta$Cq), eta H-k (batez besteko 0,17 $\Delta\Delta$Cq) emaitza nabarmenak erakutsiz. H hidrogel ez-funtzionalizatuaren aplikazioak ere hanturaren murrizpenean eragina zuela erakutsi zuen.

Estatistikoki alde esanguratsuak ikusi genituen α-SMA markatzailearen 7. eta 21. eguneko laginetan (IV.35 irudiko **c, d**). Hidrogel-tratamenduek α-SMA mailak murriztu zituzten kasu guztietan, H-Ag eta H-SA taldeek, markatzaile honen jaitsiera nabarmenena erakutsiz. Gainera, H-k ere α-SMA-ren adierazpena murriztu zuen.

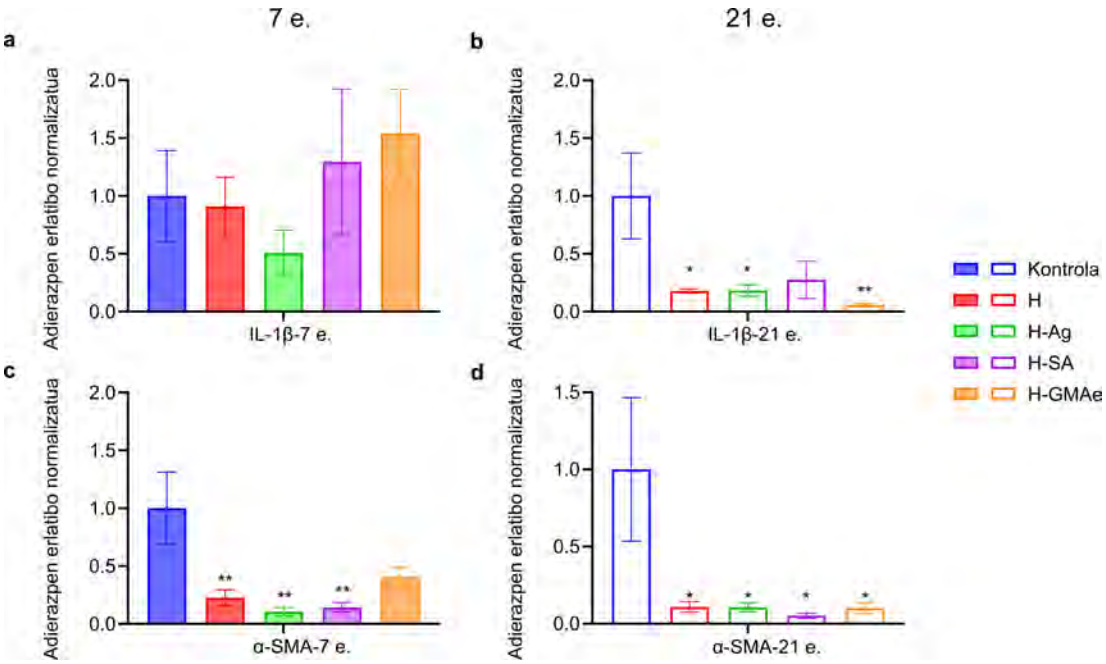

IV.35. IRUDIA: IL-1β eta α-SMA geneen adierazpen erlatibo normalizatua ($\Delta\Delta$Cq) 7 egunez (**a, c**) edo 21 egunez (**b, d**) prozesatutako untxi-korneen laginetan. p $*$ p < 0,05, $**$ p < 0,01, $***$ p < 0,001, $***$ p < 0,0001 balioek denbora-puntu bakoitzeko kontrol-tratamenduarekiko alde estatistikoki esanguratsuak erakusten dituzte.

Linboko zelula ama/progenitoreen (PAX6, p63) eta erdiko korneako zelulen (CK3) markatzaileei dagokienez, ez genuen desberdintasun esanguratsurik ikusi tratamenduetako bakar baten ere ez 7. ez 21. egunean (IV.36 irudia). p63 eta CK3 markatzaileek adierazpen-antzekotasuna erakutsi zituzten 7 eta 21 egunetan: 7 egunetara H-SA eta H-GMAe tratamenduek adierazpen-baliorik altuenak erakutsi zituzten adierazitako bi markatzaileentzat, baina hauen adierazpena murriztu zen H-SA-en kasuan 21 egunetara.

p63-ren adierazpena 7 egunetako laginetan kontuan hartuta, H-SA eta H-GMAe tratamenduek adierazpen-balio handiagoak erakutsi zituzten kontrolarekin alderatuta, eta adierazpena murriztu egin zen H tratamendurako. p63 adierazpena H-Ag tratamendurako kontrolaren antzekoa izan zen. 21 egunen ondoren, H eta H-Ag tratamenduak kontrolaren antzeko balioetan mantendu ziren, baina H-SA adierazpenaren murrizketa eta H-GMAe adierazpenaren igoera erregistratu genituen.

7 egunetara, CK3-ren adierazpena antzekoa izan zen kontrol, H eta H-Ag taldeetan. H-SA eta H-GMAe taldeek kontrol-taldekoek baino adierazpen-maila handiagoak erakutsi zituzten, baina estatistikoki alde esanguratsurik gabe. 21. egunera, gene-adierazpenak behera egin zuen H, H-Ag eta, batez ere, H-SA

tratamenduetan. H-GMAe-ren adierazpenak aldiz, gora egin zuen. Markatzaile honekin ez genuen desberdintasun estatistiko esanguratsurik erregistratu.

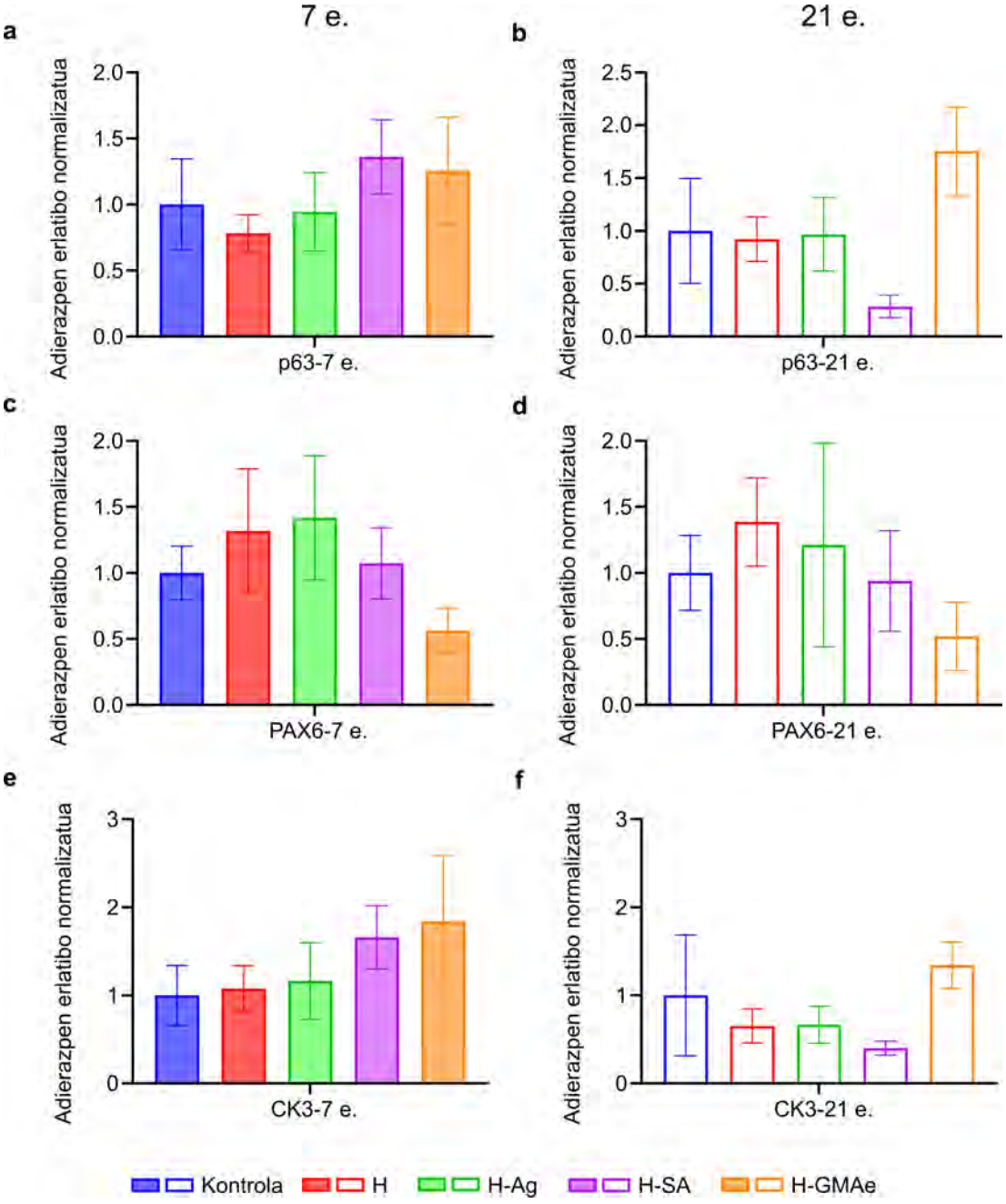

IV.36. IRUDIA: p63, PAX6 eta CK3 geneen adierazpen erlatibo normalizatua ($\Delta\Delta$Cq) 7 egunez (**a, c, e**) edo 21 egunez (**b, d, f**) prozesatutako untxi-korneen laginetan. p $*$ p < 0,05, $**$ p < 0,01, $***$ p < 0,001, $****$ p < 0,0001 balioek denbora-puntu bakoitzeko kontrol-tratamenduarekiko alde estatistikoki esanguratsuak erakusten dituzte.

PAX6-rako, 7 eta 21 egunetan lortutako tratamendu-bilakaerek antzekotasun nabarmena erakutsi zuten (IV.36 irudiko **c, d**): H eta H-Ag taldeak kontrolaren gainetik nabarmendu ziren, H-SA taldea kontrolaren oso antzeko mailetan mantendu zen, eta H-GMAe-ren adierazpena ia erdira murriztu zen kontrolarekin alderatuta.

21. eguneko laginak aztertzean, estatistikoki alde esanguratsuak erregistratu genituen Ki67 proliferazio-markatzailean (IV.37 irudiko **b**). Ki67 adierazpena gutxienez % 70 murriztu zen H, H-Ag, H-SA eta H-GMAe kasuetan kontrolarekin alderatuta, 0,29, 0,18, 0,10 eta 0,08-ko $\Delta\Delta$Cq batez besteko balioak erregistratuz, hurrenez hurren. Esanahi estatistiko esanguratsurik izan ez arren, 7. eguneko laginek 21. eguneko laginen antzeko bilakaera izan zuten (IV.37 irudiko **a**).

Ez genuen estatistikoki alde adierazgarririk ikusi atxikidurarekin eta zelula-migrazioarekin lotutako CD44 markatzailean, ez 7. ez 21. eguneko laginetan (IV.37 irudiko **c, d**), nahiz eta H, H-Ag eta H-SA adierazpen-maila altuagoak erakutsi bi kasuetan.

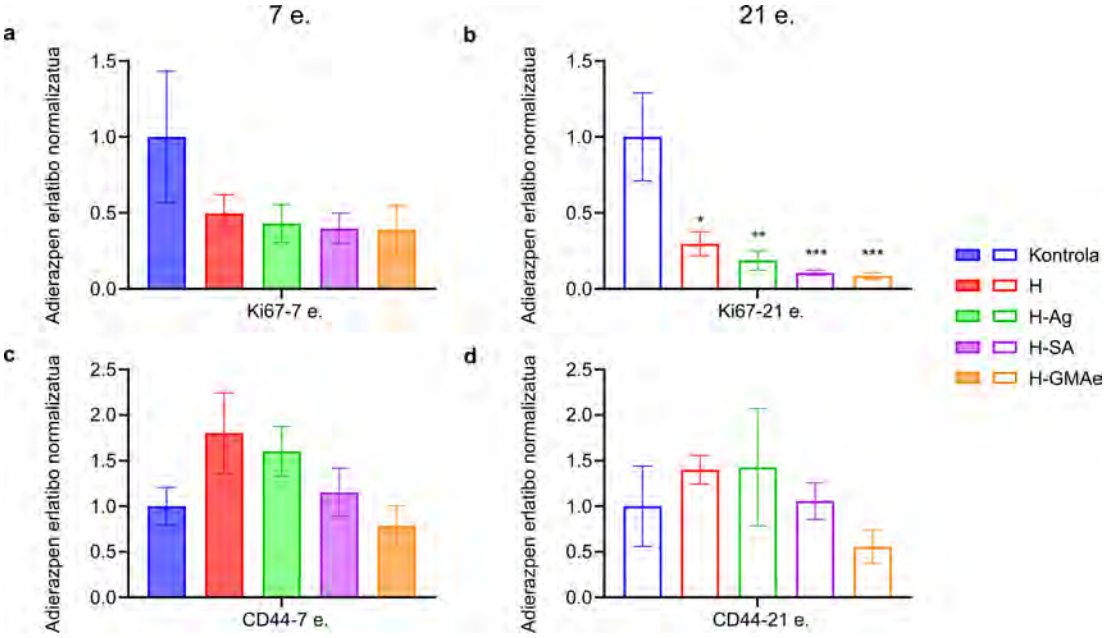

IV.37. IRUDIA: Ki67 eta CD44 geneen adierazpen erlatibo normalizatua ($\Delta\Delta$Cq) 7 egunez (**a, c**) edo 21 egunez (**b, d**) prozesatutako untxi-korneen laginetan. p $*$ p < 0,05, $**$ p < 0,01, $***$ p < 0,001, $****$ p < 0,0001 balioek denbora-puntu bakoitzeko kontrol-tratamenduarekiko alde estatistikoki esanguratsuak erakusten dituzte.

7.6. Analisi histologikoa

7.6.1. Inprimatze zitologiaren bidez lortutako laginen Hematoxilina-PAS tindaketa

Goiko-konjuntibako zelulen laginak inprimatze zitologiaren bidez lortu genituen, kirurgiaren aurretik eta ondoren. Kirurgiaren aurreko unea (0 e.) begi osasuntsuei zegokion; kirurgia egin eta 7 eta 21 egunera lortutako laginak, berriz, animalia bakoitzaren ezkerreko eta eskuineko begietatik lortu genituen, hurrenez hurren. Lagin guztiak esperimentuaren azken egunean jaso genituen, 7 eta 21 eguneko laginak egun berean jasoz, hau da, 7 eguneko lagina ezkerreko begitik hartu genuen eta 21 egunekoa, berriz, animalia bakoitzaren eskuineko begitik. Kirurgiaren aurretik (0 e.) hartutako zitologien emaitzek erakutsi zutenez, PAS tindaketaz markatutako zelula kaliziforme konjuntibalek sekretatutako mukopolisakaridoen kantitate esanguratsua hauteman genuen (IV.38 irudia). Aldiz, tindaketa hau ez zen nabarmendu 7 eta 21. egunetako zitologietan, zelula kaliziformeen murrizpena adieraziz (IV.39 irudia).

Zelulen morfologian desberdintasunak hauteman genituen aztertutako tratamendu-taldeen edo denbora-puntuen artean. 7 eguneko laginak alderatzean, H eta H-GMAe tratamenduek zelula kaliziforme gehiago zituztela ikusi genuen, nahiz eta tindatuta ez egon. Gainera, zelula-zitoplasma erlazioa murriztu egin zen H-SA tratamenduko zeluletan. 21 eguneko zitologietan, zelula kaliziformeak ikusi genituen tratamendu guztietan, baina haien morfologia kontrol-tratamenduko eta H-GMAe-eko korneetan bakarrik egokia izanik. Zelulen morfologia nabarmen aldatu zen H-Ag bidezko tratamenduarekin, 7 eta 21 egunen buruan. Irudi hauek une eta tratamendu bakoitzerako bost laginetako bakoitzaren begi bakarra erakusten dute. Emaitza argigarriak baino ez dituzte adierazten, eta ez dute tratamenduen eraginkortasunari buruzko ondorio eztabaidaezinik adierazi nahi.

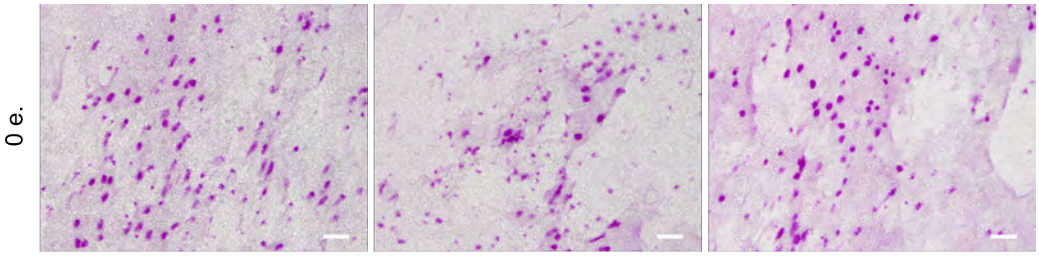

IV.38. IRUDIA: Untxi-begien konjuntibetatik, inprimatze zitologia bidez lortutako *in vivo* laginen Hematoxilina-PAS tindaketa kirurgia egin aurreko unean (0 e.). Irudiak 20× handipen objetiboarekin egin genituen eta eskala lerroek 50 μm-ko neurriak adierazten dituzte.

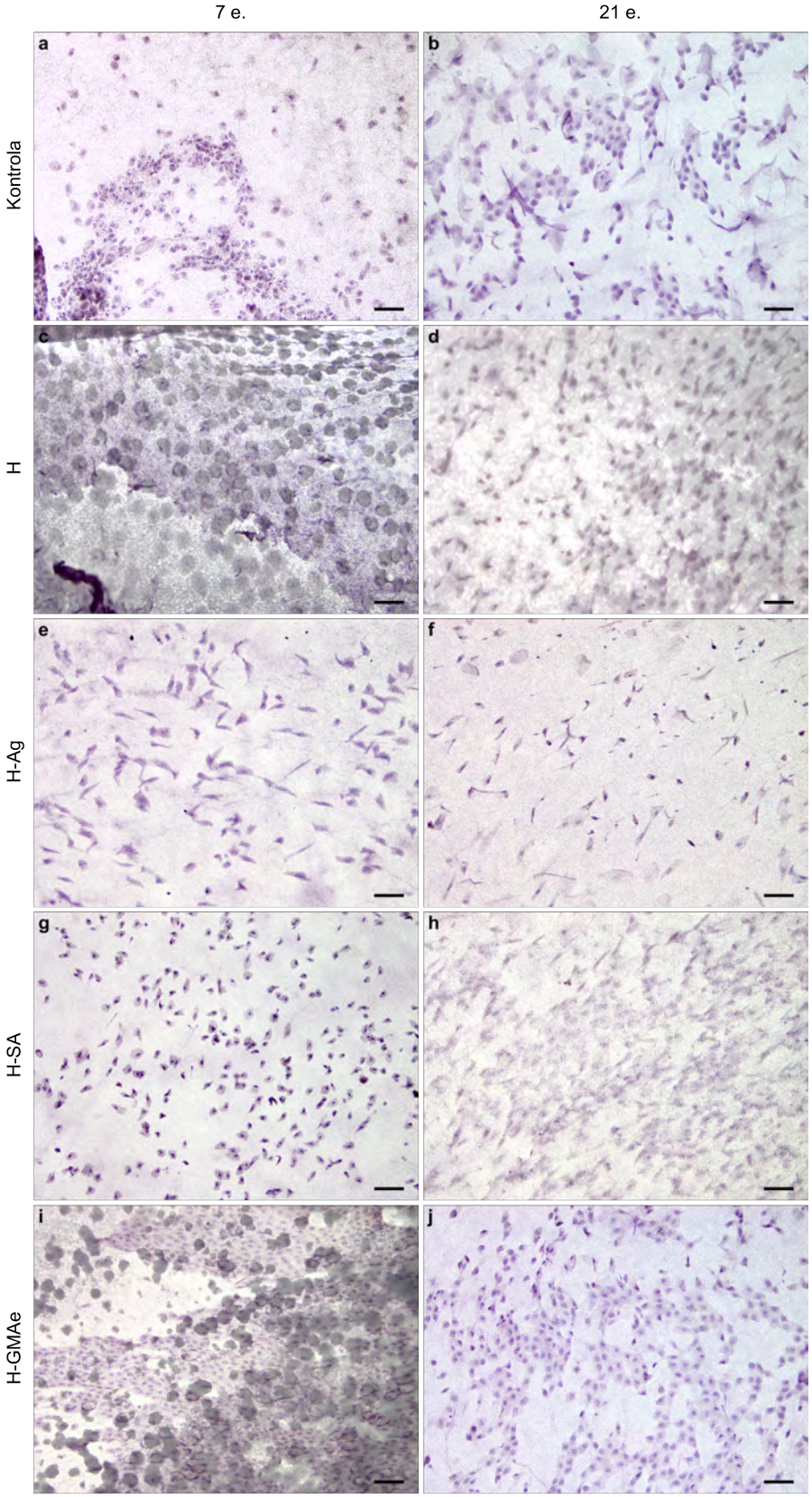

IV.39. IRUDIA: Untxi-begien konjuntibetatik, inprimatze zitologia bidez lortutako *in vivo* laginen Hematoxilina-PAS tindaketa kirurgia osteko 7. (**a-e**) eta 21. egunetan (**f-j**). Untxi-korneak malko artifizialekin (Kontrola) edo H, H-Ag, H-SA edo H-GMAe hidrogelekin tratatu genituen. Irudiak 20× handipen objetiboarekin egin genituen eta eskala lerroek 50 μm-ko neurriak adierazten dituzte.

7.6.2. Untxi-korneetako laginen Hematoxilina-Eosina (H-E) tindaketa

Lagin histologikoetan (IV.40 irudia) zauritutako eremuak ikus zitezkeen, epitelio berriaren hazkuntza kornea guztietan nabarmenduz.

Lagin horien ehuna izoztu eta parafinaren ordez OCT-an txertatuz prozesatu genuen, eta horrek ehun-egitura okerrago kontserbatzea eta interpretazioa zailtzea ekarri zuen, estromaren mailan bereziki.

Hidrogela laginaren prozesamenduan gal zitekeen arren, hidrogelarekin egindako tratamenduetan, hondatutako estromaren eta epitelio berriaren arteko guneek hidrogela ehuna orbaindu bitartean mantendu zela eta ehunari tinko atxiki zitzaiola frogatu zuten. 7 eguneko kontrol-tratamenduan erregistratutako barrunbeak (IV.40 irudiko **a**) epitelioaren eta estromaren arteko atxikimendu-eremu akastunei egotz dakizkieke.

Kontrol-tratamenduaren analisi histologikoak epitelio trinko eta lodi bat erakutsi zuen 7 egunetara, honen azpiko miofibroblastoen infiltrazioarekin (IV.40 irudiko **a**). 21 egunen buruan, miofibroblastoen infiltrazio nabariagoa erregistratu genuen, epitelio edematotsu batekin batera (IV.40 irudiko **b**). Oro har, hidrogela zuten taldeek epitelio trinkoagoa erakutsi zuten kontrol-tratamenduarekin alderatuta.

Hidrogeletan oinarritutako tratamenduei dagokienez, H tratamenduak epitelio lodi berrepitelizatu bat erakutsi zuen 7 egunen buruan, miofibroblastoen infiltrazioarekin, batez ere zauriaren ertzetan (IV.40 irudiko **c**). Hala ere, epitelio finago bat erregistratu genuen 21 egunera beste tratamenduekin alderatuta, miofibroblastoen ageriko presentziarekin (IV.40 irudiko **b**). Epitelioa lodiagoa eta trinkoagoa zirudien H-Ag tratamenduarekin 21 egunera 7 egunera baino. Tratamendu honekin, miofibroblastoen presentzia ez zen hain nabarmena izan ez 7 ez 21 egunetara (IV.40 irudiko **e** eta **f**). IV.40 irudiko **g** -k, H-SA tratamenduaren epitelioa estromatik askatuta zegoela erakutsi zuen, jarritako hidrogela 7 egunetara galdu zela iradokiz. Gainera, zelulaz kanpoko matrize desordenatua ikusi genuen. Aitzitik, miofibroblastoen infiltraziorik gabeko zelulaz kanpoko matrize ordenatu bat erregistratu genuen 21 egunetara (IV.40 irudiko **h**).

H-GMAe bidezko tratamenduari begira, 7 egunetara prozesatutako IV.40 irudiko **i** -k erakutsi zuen epitelioa estromatik askatuta zegoela, ziurrenik lagina prozesatzean hidrogela galdu zelako. 21 egunetara, miofibroblastoen infiltrazioa hauteman genuen, zelulaz kanpoko matrize desordenatuaz gainera (IV.40 irudiko **j**).

Oro har, lagin guztietan ikusi genuen epitelio berriaren hazkuntza eta honen eta estromaren arteko atxikidura, hidrogelei zegozkien barrunbeak utziz hidrogelarekin tratatutako korneetan.

Inprimatze zitologiako laginen kasuan bezala, aurkeztutako emaitzak argigarriak eta deskribatzaileak baino ez dira. Ezin dugu erreplika biologiko guztien batez besteko emaitzarik eman, beste saiakuntza batzuetan bezala. Lagin biologikoak berez dira aldakorrak, eta, beraz, ezin dugu behin betiko ondoriorik edo bereizketarik atera tratamenduen artean emaitza horietan bakarrik oinarrituta.

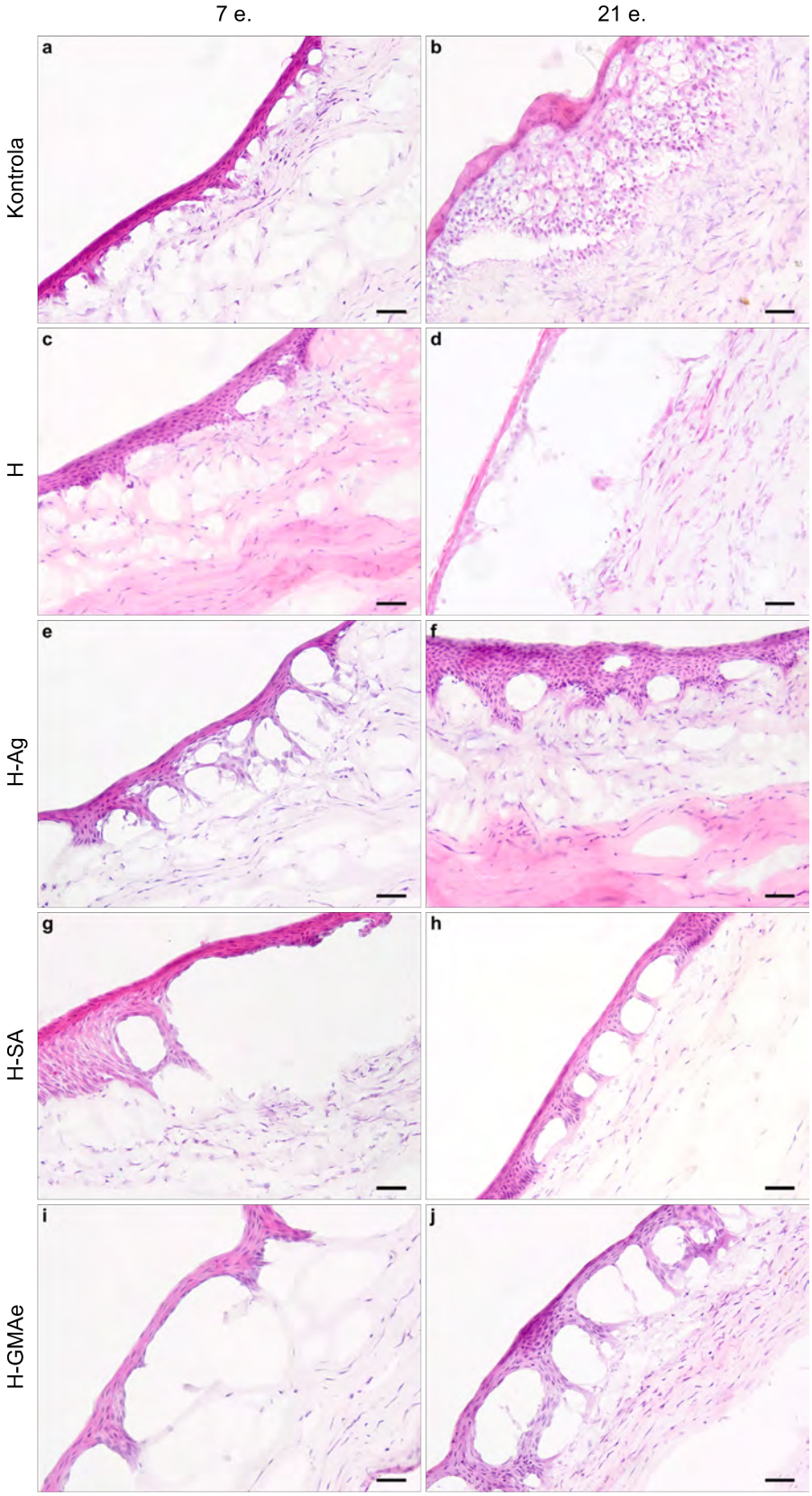

IV.40. IRUDIA: Hematoxilina-Eosina tindaketak *in vivo* saiakuntzatik lortutako berrepitelizatutako untxi-korneen laginetan. Untxi-korneak malko artifizialekin (Kontrola) edo H, H-Ag, H-SA edo H-GMAe hidrogelekin tratatu eta 7 (**a-e**) eta 21 egunetara (**f-j**) prozesatu genituen. Irudiak 20× handipen objektiboarekin atera genituen eta eskala lerroek 50 μm-ko neurriak adierazten dituzte.

7.7. Immunofluoreszentzia analisia untxi-korneetako laginetan

Immunohistokimika kirurgia egin eta 7 eta 21 egunetara lortutako untxien kornea-ehunetan ebaluatu genuen (E02, E04 eta E06 esperimentuetatik 7. eguneko laginak eta E03 eta E05 esperimentuetatik 21. eguneko laginak lortu genituen). Fibrosi-prozesuarekin (α-SMA), berrepitelizazioarekin (CK3, PanCK), linboko aktibazioarekin (CK15), hesi-funtzioarekin (ZO-1), zelula-atxikidurarekin (Int-β4) eta proliferazioarekin (Ki67) lotutako markatzaileak aztertu genituen.

Kornea kaltetzean, keratozito estromalak fibroblasto korneal bihurtzen dira, eta, ondoren, miofibroblasto. Miofibroblastoek muskulu-zelula lauen ezaugarri ultraestrukturalak eta fisiologikoak dituzte, baita mikrofilamentu-sortak edo estres-zuntzak ere. Ezaugarri horiei esker, indar kontraktilak erabil ditzakete eta zelulaz kanpoko matrizearen berrantolaketa zuzendu dezakete lesioa gertatu den lekuan. α-SMA muskulu-zelula lauen eta miofibroblastoen adierazlea da. 7 egunetara prozesatutako korneen tratamendu guztietan α-SMA markaketa ikusi genuen epitelio azpiko estroman. Lagin horietan, α-SMA-z tindatutako eremu txikiak baino ez genituen ikusi, korneako epitelioaren azpian, α-SMA-rentzako negatiboak ziren eremuak txandakatuz. Tindaketaren intentsitatea 21 egunetara handitu zen prozesatutako korneetan. α-SMA eremu positibo handia erregistratu genuen kontrol, H eta H-GMAe taldeen estroma subepitelialean, miofibroblastoen presentzia berretsiz (IV.42 irudiko **f, g, j**). Intentsitate baxuagoarekin hauteman genuen H-Ag-z tratatutako laginean (IV.42 irudiko **h**). Hala ere,IV.42 irudiaren **i** irudian erakutsitako erreplika biologikoan, α-SMA-rentzako tindaketa guztiz negatiboa hauteman genuen H-SA taldearen estroman. Oro har, maila ezberdinetan bada ere, zelulaz kanpoko matrize desordenatu bat eta miofibroblastoak ikusi genituen tratamendu guztietan.

Int-β4-k hemidesmosomen eraketan esku hartzen du, epitelioaren eta azpiko zelulaz kanpoko matrizearen arteko atxikidura-markatzaile gisa jardunez. Proteinak banaketa polarizatua erakusten du korneako eta linboko epitelioko zelula basaletan. Tratamendu guztietan, Int-β4 tindaketaren jarraitutasunik eza hauteman genuen 7 egunetara prozesatutako korneen zauriaren eremuan. Kontrol taldeko korneak Int-β4-ren markaketa irregularra erakutsi zuen; hidrogelarekin tratatutako korneetan, berriz, hutsuneak hauteman genituen zauriaren eremuan. Tindaketa intentsoagoa izan zen kirurgia egin eta 21 egunetara hartutako lagin guztietan, seinale positiboa erakutsiz bai zaurien eremuan zein lesionatu gabeko eremuetan (IV.43 irudia).

PanCK antigorputzak zitokeratina gehienak detektatzen ditu eta, beraz, korneako epitelio osoa zehaztasunez markatzeko gai da. Hala, lesioaren osteko berrepitelizazioaren markatzaile gisa erabili genuen. Kornea guztien epitelio osoan PanCK tindaketa detektatu genuen, bai zauriaren ondoren birsortu berri zen epitelioan (IV.44 irudia), bai zauririk gabeko eremuan (datu hau ez da irudian ageri).

CK3 korneako zitokeratina espezifikoa da, zelula epitelial bereiziekin berariaz lotzen dena. Haren adierazpena ehun esklerokornealaren epitelio osoan ikus daiteke, baina adierazpen-patroia aldatzen da eremuaren arabera. Erdiko korneako epitelioaren lodiera osoan ageri da, linboko epitelioaren azaleko geruzetara mugatzen da eta ez dago konjuntiban. CK3 markaketa erdiko kornea osoan detektatu genuen lagin guztietan, tratamendu-taldea eta erauzketa-denbora alde batera utzita (IV.45 irudia). CK3 tindaketa murriztu egin zen linboko eremuan. CK15 epitelio estratifikatuetan dauden zelula epitelialen zitoeskeletoaren proteina espezifikoa eta linboko zelula amen balizko markatzaileetako bat da. CK15 markaketa linbo esklerokornealetan detektatu genuen, ez ordea erdiko kornean (IV.45 irudia). Kornea periferikotik hurbil, linboaren goiko geruza epitelialetan kokaturiko zelula jakin batzuetan CK3 eta CK15-en tindaketa bateratua hauteman genuen. Kirurgia egin eta 7 egunetara prozesatutako korneetan, CK15-en tindaketa oso antzekoa izan zen talde guztietan (IV.45 irudiko **a-e**). Kirurgia egin eta 21 egunetara ateratako kornea guztietan, CK15-en markaketa intentsoagoa hauteman genuen 7 egunetara ateratako korneekin alderatuta, aktibazioa linbala zegoela adieraziz. CK15-en positibotasuna lagin guztietan ikusi arren, nabarmentzekoa da ebakuntza egin eta 21 egunetara H-Ag, H-SA eta H-GMAe tratamendua jaso zuten begiek linboko epitelio basalean bereizi gabeko CK15 zelula positiboen multzo esanguratsuak erakutsi zituztela (IV.45 irudiko **h, i, j**).

ZO-1 *zonula occludens* proteinen familiako proteina da. Proteina horiek zelula epitelialen eta endotelialen mintz plasmatikoan daude, eta zelulen arteko lotura-konplexuen parte dira, lotura hertsiak edo *zonula occludens* izenekoak. ZO-1-ren funtzio nagusia zelulen arteko substantzien fluxu askea blokeatzen duen hesi iragazgaitz bat ezartzea da. Ondorioz, substantziak zeluletatik selektiboki igarotzen dira. Kornean, ZO-1-ren presentziak azaleko zelula epitelial bereiziak daudela eta kornea-hesiaren efektua ezartzen dela adierazten du, korneako epitelio funtzional batekin bat etorriz. Kornea guztietan ZO-1 markaketa ikusi genuen,

taldea eta erauzketa-denbora edozein izanda ere, epitelioaren azaleko geruzetan batez ere (IV.46 irudia). Zelula positibo proportzio handiagoa ikusi genuen Ki67 markatzailearentzako kirurgiaren osteko 7 egunetara prozesatutako korneetan kirurgia egin eta 21 egunetara prozesatutakoetan baino, jasotako tratamendua gorabehera (IV.46 irudia). Gainera, kontrol-taldean Ki67-rekin tindatutako zelula-kopuru handiagoa detektatu genuen bi uneetan (IV.41 irudia eta IV.46 irudiko **a, f**). Hidrogel bidezko tratamendu-taldeak alderatuz, zelula positiboen ehunekoa handiagoa izan zen H-SA-rekin.

Lagin histologikoen kasuan bezala, atal honetan aurkeztutako emaitzak beste esperimentu batzuen adierazgarri eta osagarri baino ez dira. Esperimentu horietan lagin biologiko guztien batez bestekoa eman daiteke, hala nola qPCR-aren edo Draizeren saiakuntzaren emaitzetan. Aurkeztutako irudiak koherenteak dira beste saiakuntza batzuen emaitzekin, baina baliteke erreplika biologiko guztiak zehatz-mehatz ez irudikatzea, oso aldakorrak direlako.

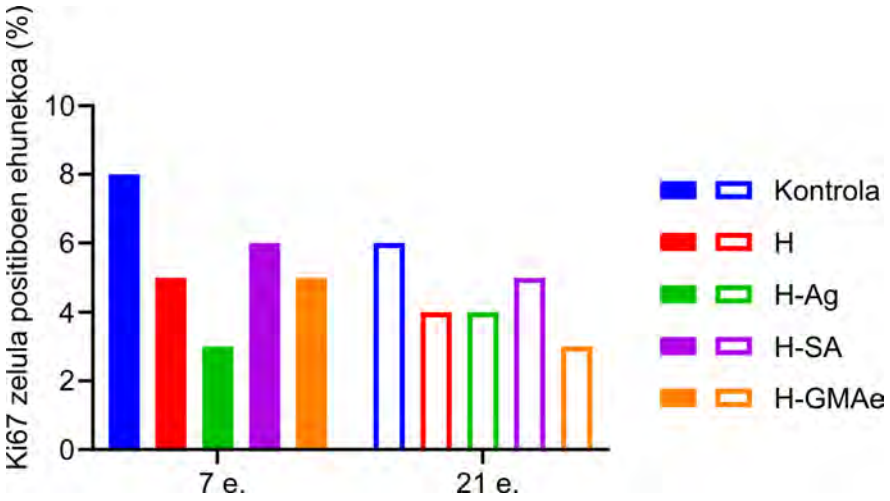

IV.41. IRUDIA: *In vivo* saiakuntzako untxi-korneako laginetan detektatutako Ki67 zelula positiboen ehunekoa. Korneak malko artifizialekin (Kontrola) edo H, H-Ag, H-SA edo H-GMAe hidrogelekin tratatu eta kirurgia egin eta 7 eta 21 egunetara prozesatu genituen.

IV.42. IRUDIA: α-SMA markatzailearen immunofluoreszentzia tindaketa *in vivo* saiakuntzatik lortutako untxi-korneako laginetan. Untxi-korneak malko artifizialekin (Kontrola) edo H, H-Ag, H-SA edo H-GMAe hidrogelekin tratatu eta kirurgia egin eta 7 (**a-e**) eta 21 (**f-j**) egunetara prozesatu genituen. **c** eta **h** irudietako gezi horiek α-SMA tindaketa erreala adierazten dute. Estromaren tindaketa berdea **c** eta **h** irudietan ehunaren beraren autofluoreszentziatik eratorria da batez ere. Irudiak 20$\times$ handipen objektiboarekin egin genituen eta eskala lerroek 100 μm-ko neurriak adierazten dituzte.

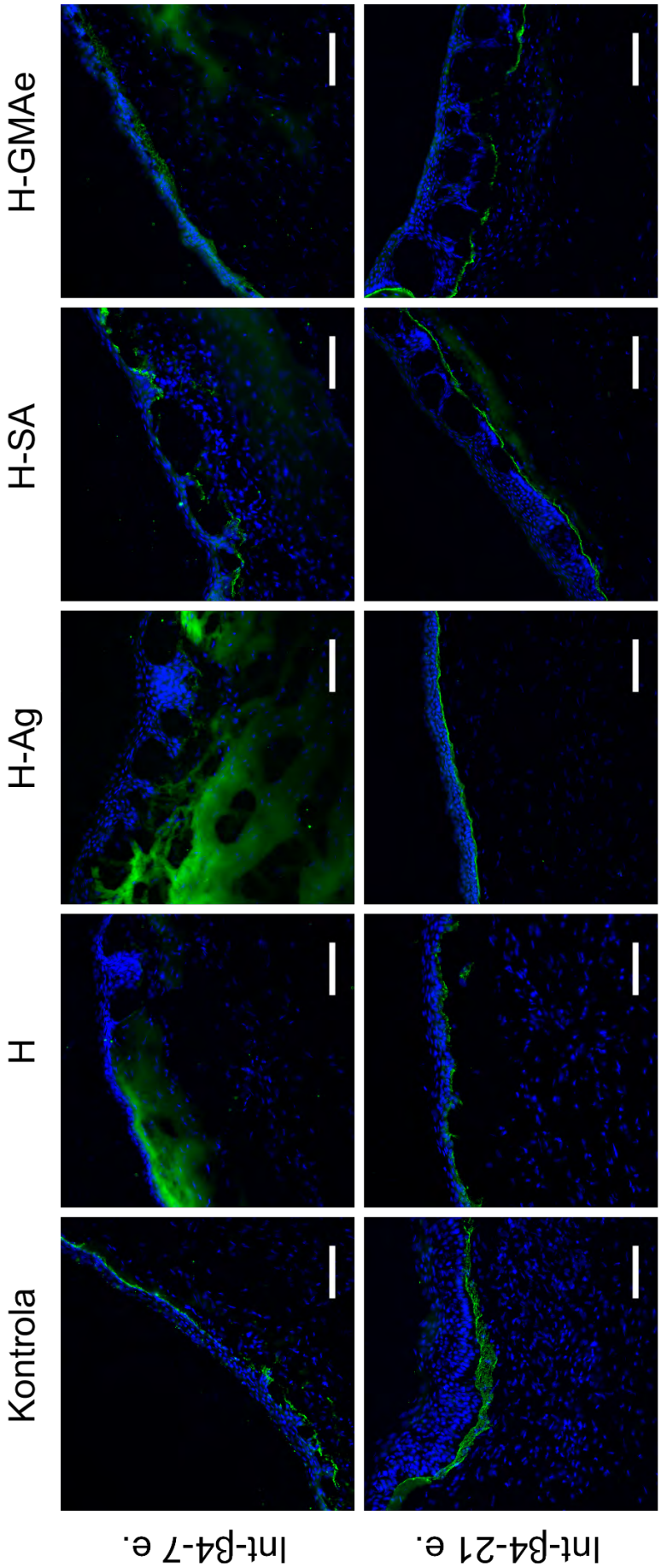

IV.43. IRUDIA: Integrina-$\beta 4$ markatzailearen immunofluoreszentzia tindaketa *in vivo* saiakuntzatik lortutako untxi-korneako laginetan. Untxi-korneak malko artifizialekin (Kontrola) edo H, H-Ag, H-SA edo H-GMAe hidrogelekin tratatu eta kirurgia egin eta 7 (**a-e**) eta 21 (**f-j**) egunetara prozesatu genituen. Irudiak 20× handipen objektiboarekin egin genituen eta eskala lerroek 100 μm-ko neurriak adierazten dituzte.

IV.44. IRUDIA: PanCK markatzailearen immunofluoreszentzia tindaketa *in vivo* saiakuntzatik lortutako untxi-korneako laginetan. Untxi-korneak malko artifizialekin (Kontrola) edo H, H-Ag, H-SA edo H-GMAe hidrogelekin tratatu eta kirurgia egin eta 7 (**a-e**) eta 21 (**f-j**) egunetara prozesatu genituen. Irudiak 20× handipen objektiboarekin egin genituen eta eskala lerroek 100 μm-ko neurriak adierazten dituzte.

IV.45. IRUDIA: CK3 (gorria) eta CK15 (berdea) markatzaileen immunofluoreszentzia tindaketa *in vivo* saiakuntzatik lortutako untxi-korneako laginetan. Untxi-korneak malko artifizialekin (Kontrola) edo H, H-Ag, H-SA edo H-GMAe hidrogelekin tratatu eta kirurgia egin eta 7 (**a-e**) eta 21 (**f-j**) egunetara prozesatu genituen. Irudiak 20× handipen objektiboarekin egin genituen eta eskala lerroek 100 μm-ko neurriak adierazten dituzte.

IV.46. IRUDIA: ZO-1 (gorria) eta Ki67 (berdea) markatzaileen immunofluoreszentzia tindaketa *in vivo* saiakuntzatik lortutako untxi-korneako laginetan. Untxi-korneak malko artifizialekin (Kontrola) edo H, H-Ag, H-SA edo H-GMAe hidrogelekin tratatu eta kirurgia egin eta 7 (**a-e**) eta 21 (**f-j**) egunetara prozesatu genituen. Irudiak 20× handipen objektiboarekin egin genituen eta eskala lerroek 100 μm-ko neurriak adierazten dituzte.

8. Linboko zelula primarioen hazkuntza

Giza korneetatik erauzitako zelulen hazkuntza primarioak, LZAG-a tratatzeko ehun-ingeniaritzako kornea-ordezkoak garatzeko lehen urrats gisa karakterizatu genituen. Linboko zelula amen presentzia egiaztatu genuen, haien kantitatea eta giza ehun esklerokornealeko epitelioan zuten kokapena. Gainera, *in vitro* hazteko eta linboko zelula amen iturri bihurtzeko ahalmena ebaluatu genuen. Analisi immunohistokimikoak eta immunozitokimikoak LEZA/P-en ezaugarriak eta linboko nitxoan dauden zelula-populazioak zehazteko egin genituen.

8.1. ΔNp63α eta melan A markatzaile zelularren adierazpena giza ehun esklerokornealetan

Melan A markatzailea p63 antigorputzarekin konbinatu genuen, giza ehun esklerokornealetako epitelioan bi markatzaileen arteko erlazioa eta kokapena aztertzeko. p63 linboko zelula ama/progenitoreen behin betiko markatzailea ez bada ere, zelula horiek identifikatzeko gehien erabiltzen den markatzaileetako bat da, eta ΔNp63α da linbo eremuko isoforma nagusia.

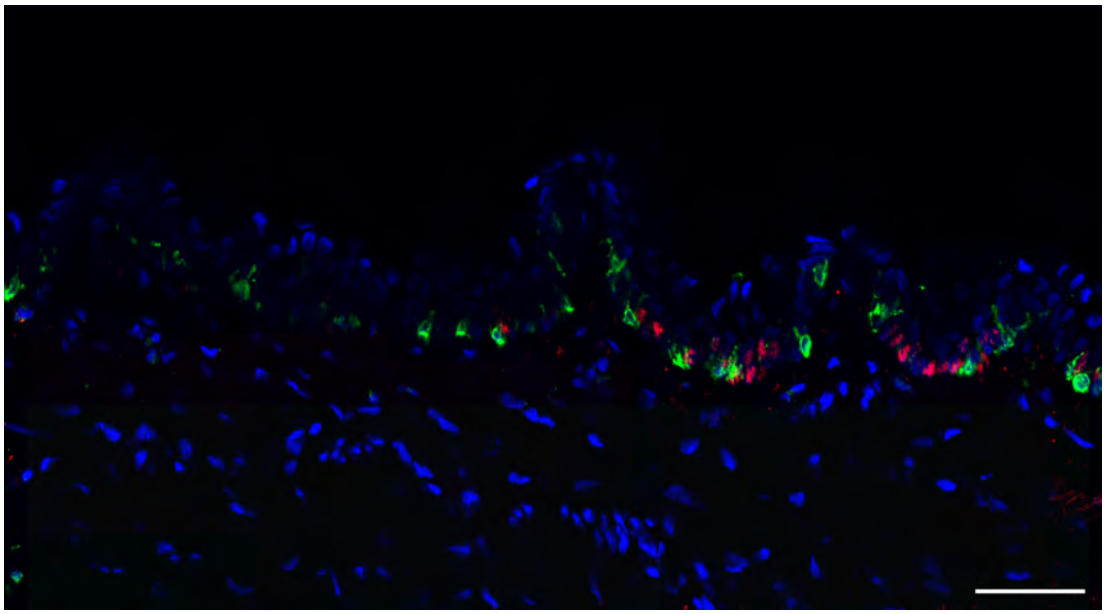

IV.47. IRUDIA: ΔNp63α eta melan A zelula-positiboen adierazpena ehun korneoskleralaren linboko eremuan. Irudia 20× handipen objektiboarekin atera genuen eta eskala lerroak 50 μm-ko neurria adierazten du. Irudiak kripta linbarretan ΔNp63α eta melan A zelula-positiboen kokapen zehatza erakusten du.

Bi markatzaile horiek linboko eremuan ikusi genituen, zehazki linboko kriptetan (IV.47 irudia). Melanozitoak (berdez) ΔNp63α-rentzako positiboak (gorriz) ziren zelula ama/progenitoreen artean ikusi genituen. Melan A-rako zelula positiboek morfologia adarkatua erakutsi zuten.

8.2. Linboko epitelio-zelulen erauzketa eta hazkuntza

Ehun esklerokornealetako zelulak erauzteko tekniken eraginkortasuna eta horien *in vitro* hedapena prozedura immunozitokimiko anitzen bidez ebaluatu genuen. Zelula-markatzaileen adierazpenaren bilakaera hazkuntza-fase desberdinetan neurtu genuen. Korneako linbo-eremutik zuzenean lortutako zelula epitelialak zitospina erabiliz prezipitatu eta hauen zelula-markatzaileak aztertu genituen. CK15, bimentina eta ΔNp63α-entzako positiboak ziren zelulak detektatu genituen zitospin bitartez prezipitatutako zelula epitelialetan (IV.48 irudiko **a, e**). Ondoren, ehun esklerokornealetatik isolatutako linboko zelula epitelialen hazkuntzak mantendu genituen 12 $\pm$ 2 egunez (p0 pasea), eta CK15 markatzailearen tindaketa altua mantendu zela egiaztatu genuen (IV.48 irudiko **b**). Zelulen paseak egin ahala, CK15 proteinaren adierazpenak behera egin zuen. Zitospinetik prezipitatutako zelulen % 40-a bakarrik tindatu ziren CK15-ekin, eta zelulen % 10-a bakarrik 0. paseko zelulen kasuan. CK15 adierazpena erabat desagertu zen zelula-hazkuntzen bigarren pasetik aurrera (IV.48 irudiko **c**). Desberdintasun estatistikoak erregistratu genituen p0 (Zitospin) paseko eta p1, p2 eta p3 paseko zelulen artean CK15 markatzaile zelularrentzat (p = 0,005) eta bimentinarentzat (p = 0,037) (IV.48 irudiko **d**). Bimentinaren adierazpena zitospina erabiliz isolatutako eta zentrifugatutako ehun esklerokornealetatik lortutako zelulen proportzio txiki batean baino ez genuen ikusi (zelulen guztizkoaren % 7 inguru). Gainera, zelula-hazkuntzen 0. pasean, bimentinarentzako positiboak ziren zelulek morfologia adarkatua eta luzanga erakutsi zuten (IV.48 irudiko **b**), zelula horietako batzuk CK15-positiboak zirelarik. Hazkuntzetako 1. paseko zelulek ezaugarri morfologiko aldakorrak erakutsi zituzten, bigarren eta ondorengo paseetan ikusitako bimentina adierazi zuten zelulekin alderatuta (IV.48 irudiko **c**).

2. paseko bimentinarentzako zelula positibo horiek, zelula estromalekin bat zetorren morfologia erakutsi zuten, baina ez zuten zelula epitelialen fenotipoa erakutsi.

Bai ehun esklerokorneal fresko zein kultibatuetatik lortutako zelula epitelialak ΔNp63*α*-ren adierazpena erakutsi zuten. Tindaketaren adierazpenaren bilakaera uniformea izan zen hainbat ehunetatik ateratako zelula-hazkuntza guztietan. ΔNp63*α* zelula distiratsuen kopuruak nabarmen egin zuen behera pase batetik bestera, seinalerik gabeko zelulen kopuruak gora egin zuen bitartean (IV.48 irudiko **e-h**). ΔNp63*α* zelula distiratsuen adierazpena % 20-tik % 6-ra jeitsi zen zuzenean zitospinetik prezipitatutako zelulen eta p0 hazkuntza-pasean hazitako zelulen artean. p0 pasetik aurrera, ΔNp63*α* zelulen proportzioa ez zen % 5-etik igo. Estatistikoki alde esanguratsuak erregsitratu genituen p0 (Zitospin) paseko eta p1, p2 eta p3 paseko ($p = 0,043$) zelulen artean (IV.48 irudiko **h**).

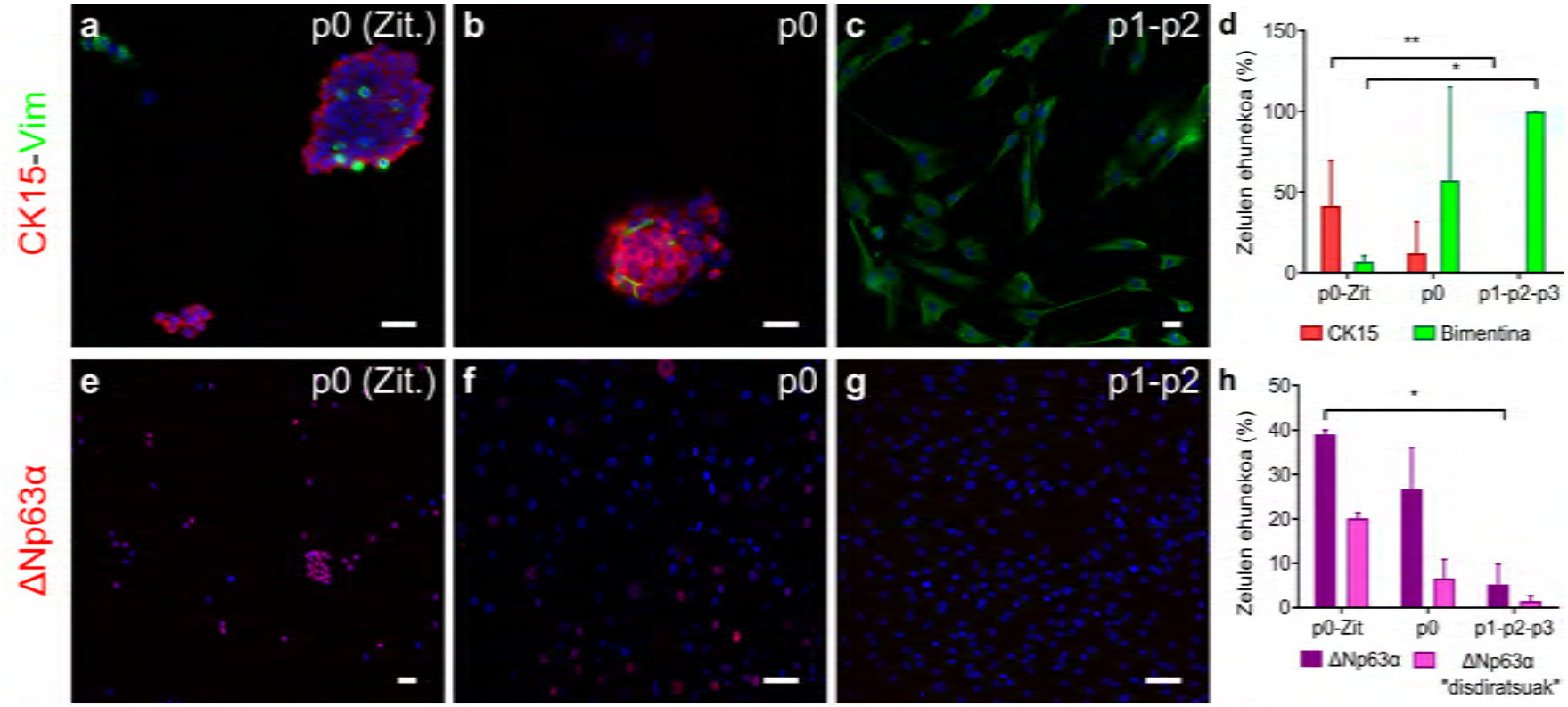

IV.48. IRUDIA: CK15, bimentina eta ΔNp63α markatzaileen adierazpena ehunetik zuzenean isolatutako zelula epitelialetan (**a** eta**e**, p0 pasea, zitospinarekin isolatuta) edo kultibatutako p0 (**b, f**) eta p1-2 (**c, g**) paseetako zeluletan. **a** eta **e** irudiek erakusten dutenez, ehunaren digestioaren ondoren zuzenean erauzitako zelulek CK15 eta ΔNp63α markatzaileen adierazpen altua erakusten dute. Paseetan zehar, desberdintze-markatzaileen murrizketa esponentziala eta bimentinaren markaketaren nagusitzea erregistratu genituen (**b, c, f, g** irudiak). Grafikoek ehun esklerokornealeko CK15-bimentina (**d** grafikoa) eta ΔNp63α (**h** grafikoa) zelula-positiboen ehunekoaren bilakaera adierazten dute. Esanahi estatistikoa honela definitu genuen: $p * p < 0{,}05$, $** p < 0{,}01$, $*** p < 0{,}001$, $**** p < 0{,}0001$. Irudiak 20$\times$ handipen objektiboarekin atera genituen eta eskala lerroek 25 μm-ko neurriak adierazten dituzte.

8.3. Melanozitoen presentzia zelula epitelialen hazkuntzetan

Desberdintasun morfologikoak ikusi genituen bimentinarako positiboak ziren zelula epitelialen eta estromalen hazkuntzen p0 paseetan. Bimentinaz tindaturiko hazkuntza epitelialetako zelulek melanozitoen antzeko fenotipo dendritikoa erakutsi zuten (IV.49 irudiko **a**). Zelula adarkatuak ikusi genituen zelula epitelialen koloniak inguratuz (IV.50 irudiko **a**). Melan A markatzailea (IV.50 irudiko **b, c**) erabiliz, melanozitoak detektatu genituen epitelioko zelula-hazkuntzetan.

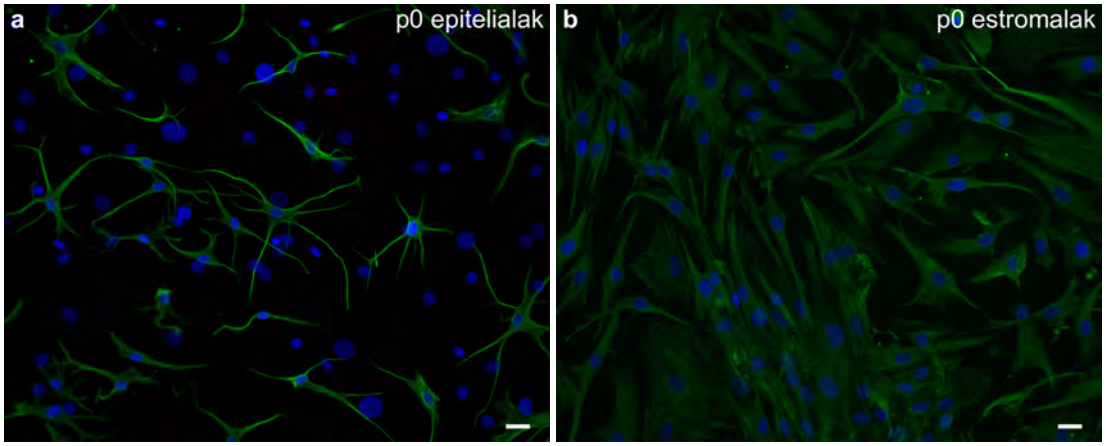

IV.49. IRUDIA: Bimentina markatzailearen adierazpena linboko zelula epitelial (**a**) eta zelula estromalen (**b**) hazkuntzetan. Bi hazkuntzak p0 paseari dagozkie. Bi irudiak 20× handipen objektiboarekin atera genituen eta eskala lerroek 25 μm-ko neurriak adierazten dituzte.

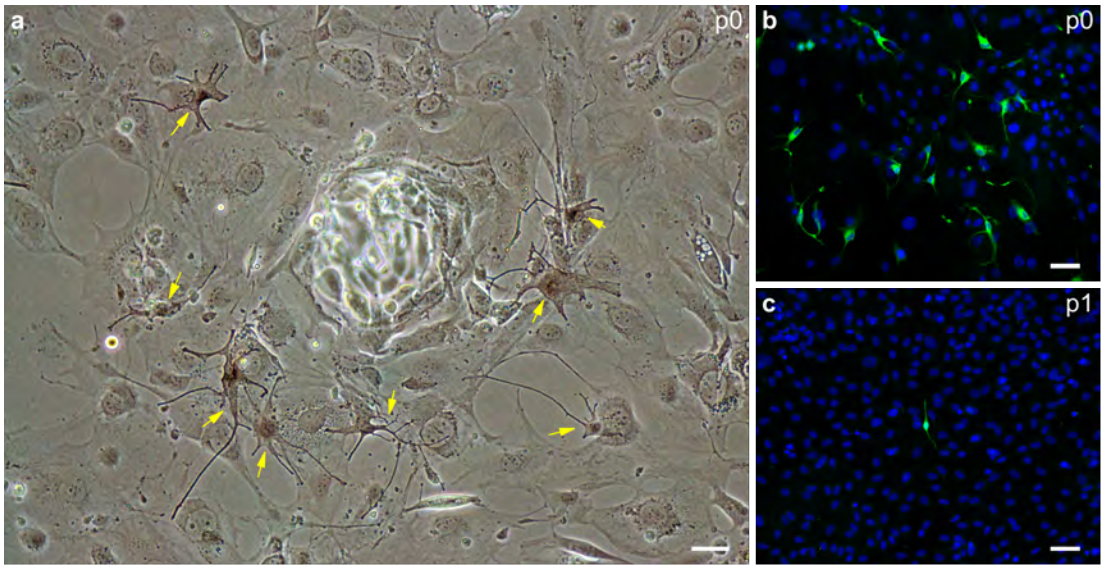

IV.50. IRUDIA: p0 eta p1 paseetako linboko zelula epitelialen hazkuntzak. Ezkerreko irudiak (**a**), inaktibatutako 3T3 zelula-geruza baten gainean ereindako p0 paseko zelula epitelialak erakusten ditu. Gezi horiz markatutako zelulak sortzen ari ziren zelula ama epitelialen kolonia inguratzen zuten melanozitoei dagozkie. **b**) eta **c**) irudiek p0 eta p1 paseetako zelula epitelialetan melan A markatzailearen adierazpena erakusten dute. Irudi guztiak 20× handipen objektiboarekin atera genituen eta eskala lerroek 50 μm-ko neurriak adierazten dituzte.

Aztertutako ehun esklerokornealetako zelulen p0 paseek melan-A adierazpen nabarmena erakutsi zuten. ΔNp63α eta CK15 markatzaileen adierazpen-patroien antzera, melan-A-k jaitsiera esanguratsua erakutsi zuen pase batetik bestera (IV.50 irudia). IV.51 irudiak melan A-rako melanozito positiboen eta CK15-erako zelula positiboen kokapena erakusten du linboko zelula epitelialen kolonia batean. Melan-A melanozito positiboak CK15 zelulen artean ikusi genituen, haien adarrekin CK15 zelula positiboak modu babeslean inguratuz.

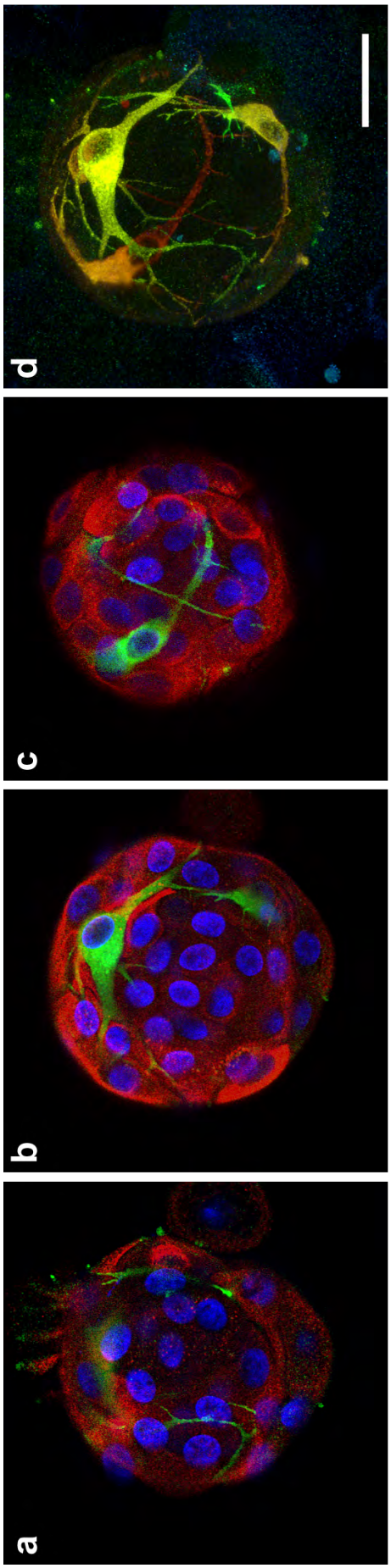

IV.51. IRUDIA: CK15-z markatutako zelula ama/progenitore epitelialez osatutako holokloi baten plano konfokal desberdinak (**a-c**), melanozito Melan A positiboz inguratuta. **d** irudiak koloniako plano guztien muntaia erakusten du. Irudia bereizmen handiko mikroskopio batekin atera genuen 40× handipeneko objektiboarekin. Eskala lerroak 25 μm-ko neurria adierazten du.

V. EZTABAIDA

1. Korneako zauriak orbaintzeko erabil litezkeen biofilmen ebaluazioa

Gaur egun, hainbat material korneako zelulen atxikipena eta bideragarritasuna erraztu dezaketen substratu edo euskarri bezala erabiltzeko hautagai gisa ebaluatzen ari dira [343–345]. Kornea-ehuna imitatu nahi duten materialek, honen funtzio nagusiek ezarritako baldintzak bete behar dituzte. Laburbilduz, jatorrizko ehunaren antzeko propietate optikoak eskaini behar dituzte, biobateragarritasunarekin, biodegradagarritasunarekin eta biointegrazioarekin batera, hazkuntza, ugalketa eta zelulen migrazioa estimulatuz [346].

Hasierako ebaluazio gisa, korneako bioingeniaritza aplikazioetarako hautagai potentzialak izan zitezkeen proteinetan oinarritutako material ezberdinen *in vitro* azterketa egitea erabaki genuen. Film-formatua erabili genuen, *in vitro* saiakuntzetan erraz erabil zitezkeelako.

Kornea begiaren errefrakzio ahalmenaren % 60 baino gehiagoren erantzulea da [347]; beraz, estromako keratozitoen argaltasunaz, morfologiaz eta banaketaz gain, kolageno-zuntzen antolaketa ordenatuak ehun garden bihurtzen du kornea, eta, aldi berean, sakabanatutako argiaren interferentzia suntsitzaileak eragiten ditu, argiaren transmisioa hobetzen dutenak [10]. Kornearen funtsezko funtzio hori dela eta, kornea-aplikazioetarako hautatutako materialen propietate optikoak neurtzea oso garrantzitsua da.

Kimikoki erretikulatutako gelatinazko filmek (GEL-LAK, GEL-AZ) argiaren transmisio handiagoa erakutsi zuten hidratatu ondoren. Gelatinaren amino taldearen eta laktosaren karbonilo taldearen edo azido zitrikoaren karboxilo taldearen arteko erretikulazioak, propietate optikoak hobetzea ekarri zuen, baita egitura trinkoago bat ere, SEM irudiek erakutsi bezala. Proteinen talde polarren eta glizerolaren talde hidroxiloen arteko hidrogeno-loturen bidez erretikulatutako KOL eta SPI filmekin alderatuta, GEL-LAK eta GEL-AZ filmek portaera optiko hobea erakutsi zuten.

Argiaren guztizko transmisioak bi osagai ditu: transmisio zuzena, non argiaren hedapen-norabidea ez den aldatzen, eta sakabanatutako transmisioa, objektuen argitasuna eta lausotasuna zehazten dituena [348]. Sakabanatutako transmisioaren edo dispertsioaren eragina neurtzeko, filmak irudi-patroi batetik distantzia ezagun

batera jarri behar izan genituen, kontaktu-zehaztasun faltsua saihesteko [349, 350]. Hidratatutako gelatinazko filmek gardentasun ona erakutsi zuten, KOL eta SPI-k aldiz, % 60 eta % 80-ko transmitantzia balioak erregistratu arren, ez zuten irudia bereizteko adinako argitasunik eskaini. Horren arrazoia filmen egiturarekin lotu genuen, argia barreiatzea zaildu baitzuen [351]. Argiaren objektu barneko dispertsioak gardentasunaren, zeharrargitasunaren eta opakutasunaren arteko erlazioa azaltzen duen fenomenoa da. Material zeharrargiek argia sakabanatzen dute, eta erabat gardenak direnek berriz, ez. Hala ere, argiaren zati bat sakabanatu eta zati bat transmititzen den kasuetan, sakabanatze-kantitatea txikia bada edo objektua fina bada, objektuaren atzeko irudia argi ikus daiteke nahiz eta hau zeharrargia izan. Material baten gardentasunari hainbat faktorek eragin diezaiokete, hala nola argia xurgatzeak, materialaren mikroegiturak, materialaren lodierak edo bi inguruneen errefrakzio-indizeen arteko aldeak [352]. Film hidratatuen kasuan, haien gardentasunak hobera egin dezake uretan murgiltzean, materialaren eta uraren errefrakzio-indizeen hurbiltasuna dela eta. Errefrakzio-indizeak material bat zeharkatzean argiak duen desbideratzea adierazten du. Bi indizeak hurbil badaude edo bat badatoz, materialak argi gutxi sakabanatu edo islatuko du, zeinak gardentasuna hobetuko duen.

Emaitzen arabera, gardentasuna propietate nagusitzat jo ezkero, gelatina izango litzateke hautagairik onena. Gelatina substantzia moldakorra da, berez kolagenoak baino gardentasun handiagoa duena [345]. GEL-LAK eta GEL-AZ filmek erakutsitako argitasun eta definizio bikainaz gain, GEL-LAK filmek UV izpien aurkako babes gisa jokatuko lukete, gelatinaren eta laktosaren glikazio ez-entzimatikoaren bidez eratutako Maillard-erreakzioaren produktuek eragindako tonu horixkaren ondorioz [353]. Hori oso ezaugarri interesgarria da begi-gainazalerako erabiliko liratekeen materialentzat. Adibidez, ikerketa batek horiz tindatutako lenteek betsareako zelulen babesa eskaintzen zutela frogatu zuen [354].

Kolagenasa bidezko degradazioaren emaitzek argi utzi zuten agente gurutzatzailearen zein biomaterialen degradazio-tasak kontrolatzeko erretikulazio-metodo eta denboraren garrantzia. Fisikoki erretikulatutako KOL eta SPI filmek degradazio azkarra erakutsi zuten, KOL 15 minututan guztiz degradatu zen eta SPI-k 24 ordutan % 60-ko pisu-galera izan zuen (filmaren hasierako pisuaren % 40-a soilik geratu zen). Gainera, gelatinazko filmen degradazio-profilek erreakzio

kimiko motaren eragina erakutsi zuten. 24 orduren ondoren, GEL-LAK filmaren % 50-a mantendu zen gutxi gorabehera, eta GEL-AZ-ren % 40-a baino zertxobait gutxiago. Aipatzekoa da film guztiek hasieran izandako pisu-galera glizerolari egokitu zitzaiola, hau soluzioan disolbatu baitzen. Hasierako pisu-galera horren ondoren, hidrolisiaren ondorioz KOL filma bakarrik degradatu zen pixkanaka.

Kornearen zelulaz kanpoko matrizearen (ZKM) birmoldaketa keratozitoek jariatzen dituzten metaloproteinasek (MMP) arautzen dute. MMP horiek zinkaren mendeko endopeptidasak dira, eta ZKM degradatu eta birmoldatzen dute. MMP-ak mintz motako MMP-etan, kolagenasetan, gelatinasetan, estromelisinetan eta matrilisinetan banatzen dira, substratu kimikoaren eta funtzioaren arabera. Metaloproteinasen inhibitzaileek (TIMP) MMP-en ekintza arautzen dute. Beraz, MMP/TIMP-en arteko desoreka batek kornearen gainazalaren homeostasia aldatzea ekar dezake, eta horrek hainbat patologiatan inplikatuta dauden MMP maila handiagoak dakartza [355].

Adibidez, ingurune hiperosmolar batean, begi lehorraren gaixotasuna simulatuz, korneako zelula epitelial primarioen kontrol-taldea medio hiperosmolar baten eraginpean zeuden zelulekin konparatu zuten eta MMP-1 mailak batez besteko 12,02 ng/ml-tik 88,46 ng/ml-ra handitu ziren [356]. Halaber, MMP maila altuak deskribatu izan dituzte kornea-higadurak dituzten pazienteen epitelioan edo aurreko keratoplastia lamelar sakona behar duten pazienteetan, besteak beste [357, 358]. Tesi honetan erabilitako kolagenasa kantitatea handia izan zen (200 μg/ml) benetako begi-ingurune batean aurkitutako mailekin alderatuta, eta filmak etengabe egon ziren entzimaren eraginpean. Egoera erreal batean, filmen degradazioa gure emaitzetan erregistratutakoa baino denbora luzeagoan gertatuko litzateke. Kornearako sortutako edozein substratuk, ehunen birsorkuntza-prozesuan behar besteko euskarria eman behar du hazkuntza, migrazioa eta zelulen ugalketa sustatzeko, baina, era berean, degradatu egin behar da korneako estroma birmoldatzen den heinean [306, 359]. Hala, filmak kolagenasak degradatu izanak iradoki zuen biodegradagarriak zirela eta beraz ehuna birmoldatzea erraz zezaketela.

Materialen zitotoxikotasunari dagokionez, kolagenozko filmekin erregistratutako % 70-etik beherako bideragarritasun-balioek zelulentzako film egokiak ez zirela adierazi zuten [360]. Hala ere, emaitza desegokiak ez zitzaizkion I motako kolagenoari berez egotzi, kolagenoa beste ikertzaile batzuek lehenago probatutako materiala

baita [361, 362]. Adibidez, Isaacson eta kolaboratzaileek I motako kolageno horren forma metakrilatua erabili zuten alginatoarekin konbinatuta beren euskarrietan, eta korneako keratozitoekin bideragarritasuna % 90-ekoa izan zen 24 ordutan eta % 83-koa 7 egunen ondoren. Zelula horiek konparagarriak izan daitezke gure ikerketan erabilitakoekin [363]. Beraz, horrek materiala prozesatzearen garrantzia, erretikulazio-teknikak eta hainbat osagai gehitzeak zelulen bateragarritasunean izan dezakeen eragina agerian uzten du. Hazkuntza medioa ez genuen azterketa iraun bitartean aldatu, eta horrek 72 orduko esposizioaren ondoren eragina izan zuen tratamendu-talde guztietan estatistikoki esanguratsuak diren aldeak behatzeko. Hala ere, egoera hori ez litzateke ingurune erreal batean agertuko; izan ere, malkoek eta kliskak etengabe berrituko lukete korneako zelulekin kontaktuan dagoen ingurunea [364].

Bi zelula-motek bideragarritasun egokia, atxikimendu eta migrazio ahalmena erakutsi zuten film guztietan. GEL-LAK eta SPI filmetan ereindako zelulek zauria azkarrago itxi zuten.

Euskarri-materialen zurruntasunak zelulen izate eta funtzioa erregulatzen ditu. Ikerketek adierazi dutenez, gainazal lauetan ereindako korneako zelula epitelialek indiferentziazio-potentziala mantentzeko ahalmen handiagoa dute gainazal zurrunetan ereindakoan baino [365]. Gainera, gainazal bigunak onuragarriak dira keratozitoek fenotipoa manten dezaten; izan ere, material zurrunagoek miofibroblasto bihurtzeko probabilitatea handitzen dute, eta horrek, kornea-ehunaren funtzioen hondatze bizkorra dakar [366]. Beraz, hainbat filmetako portaera zelularraren aldaketek gainazalaren ezaugarriak ikertzeko beharra dakarte (adibidez, zimurtasuna, topografia edo kimika), erantzun zelularrei, hala nola atxikimenduari, zelulen ugaltzeari edo migrazioari, eragin diezaieketenak [367].

2. Korneako ultzerak tratatzeko hidrogela

Korneako epitelio-akatsak ohiko zauriak dira. Tratamendu kobentzionalekin sendatu ohi dira, hala nola kontserbatzailerik gabeko malko artifizialekin eta antibiotikoekin eta/edo kortikoesteroide topikoekin, begi-ur edo pomada moduan aplika daitezkeenak. Kasu batzuetan, ordea, ultzerek estromaraino egin dezakete aurrera, edo, kasurik okerrenean, baita begia zulatu ere. Horrek ikusmenean alterazioak eragin ditzake, begi-globoaren osotasuna arriskuan jarriz. Hainbat

aukera terapeutiko daude honi aurre egiteko: kolirio ez-inbaditzaileak, epitelioaren egitura eta funtzio normala berrezartzen saiatuko direnak [94], ukipen-lenteak edo presio-adabakiak [94, 96], edota tratamendu kirurgikoak, hala nola mentuak [114, 115], tarsorrafiak [117–119] edo zelula amen transplanteak [120].

Kasu arinenetan, kolirio ez-inbaditzaileak erabiltzen dira normalean, epitelioaren egitura eta funtzio normalak berrezartzeko; kasu larrienetan, berriz, pazienteei ebakuntza kirurgikoak egiten zaizkie zuzenean, hala nola mentuak edo zelula amen transplanteak.

Tesi honetan aplikazio klinikoetarako bitarteko irtenbide bat proposatu dugu, korneako akatsak aldi baterako bete eta orbaintzea eta birsortzea hobetzen duten molekulak pixkanaka aska ditzakeena, ebakuntza kirurgikorik egin beharrik gabe.

Filmen karakterizazioaren emaitzetan oinarrituta, gelatina aukeratu genuen hidrogelaren sintesirako material nagusi gisa.

Gelatina kolagenoaren hidrolisi azidotik edo alkalinotik dator, eta honen biobateragarritasunagatik, immunogenizitate ezagatik, manipulatzeko erraztasunagatik eta ugaritasunagatik aukeratu genuen, besteak beste. Kolagenoarekin alderatuta, zeina sentiberagoa den pH eta tanpoi aldaketekiko, gelatina material moldagarriagoa, errentagarriagoa eta klinikoak erabiltzeko material gomendagarriagoa da.

% 2 p/bol baino kontzentrazio handiagoetan disolbatzen denean, gelatina 30-35 °C baino gutxiagoko tenperaturetan fisikoki erretikulatutako hidrogelak sortzeko gai da, molekulen konformazioan ausazko egitura kiribil batetik helize hirukoitz batera aldatu delako. Ondorioz, hidrogeno intermolekularreko loturak sortzen dira gelatina kateen frakzio handien artean [368, 369]. Hala ere, sare fisiko hori tenperatura altuagoetan desintegratzen da, eta horrek haren erabilera 37 °C -ko tenperatura fisiologikoetara mugatzen du.

2.1. Hidrogelaren konposizioa eta erretikulazioa mekanismoa

Begi-gainazalaren tenperatura fisiologikoa 34 °C ingurukoa bada ere [370], gelatina erriboflabina fosfatoarekin (RFP) fotopolimerizazio bidez kimikoki erretikulatu genuen hidrogelaren egonkortasuna eta ezaugarri mekanikoak hobetzeko.

RFP saretzaile gisa erabiltzea erabakitzeko, oftalmologiaren arloan duen erabilera zabalean oinarritu ginen.

Kornean, kolageno-zuntzen egitura eta antolaketa ehunaren egonkortasun mekanikoaren erantzuleak dira. Gainera, kolageno-zuntzen saretzeak, hauek kornea kurbatuan irristatzea eragozten dute. Erretikulazio edo saretze-mailak gora edo behera egiten duenean, ehunaren propietate biomekanikoak kaltetu egiten dira, ikusmen-zorroztasuna murriztuz [371]. Adibidez, korneako gaixotasun ektasikoek kornea mehetzea eta puztea eragiten dute. Kalte horrek korneako kolageno zuntzen erretikulazioa murrizten du, eta horrek korneako zurruntasuna murriztea dakar. Keratokonoa gaixotasun ektasiko ohikoenetako bat da, kolageno-molekulen arteko erretikulazio aldaketengatik kornearen zurruntasuna murrizten duena [372].

Kaltetutako estromari aplikatutako erretikulazio prozedura UVA izpien eta fotoabiarazle baten konbinazioan oinarritzen da, kolageno-zuntzexken artean lotura kobalente berriak sortu eta, ondorioz, kornea-zurruntasuna handitzea eragiten duena [373]. UVA-rekin irradiatutako erriboflabina, honen eragin mugatuagatik, tratamendu-denbora laburragatik eta kornea-gardentasuna aldatzen ez duelako erabiltzen hasi ziren [371]. Tratamendu honen lehen saiakuntza klinikoa 2003-an ezagutarazi zen [374], eta teknikak FDA-ren onespena jaso zuen 2016an [375], kolagenoaren saretze puntu berriak sortzeko orain arte onartutako erretikulazio teknika bakarra izanik.

Erriboflabina, B2 bitamina ere deritzona, B bitamina mota bat da, batez ere esnekietan, haragietan, arrainetan, berde ilun koloreko barazkietan, aleetan eta zerealetan aurkitzen dena. Hori koloreko koloratzaile natural gisa dihardu eta egitura kimiko fotosentikorra du, argia xurgatzeko lau tontor erakusten dituena, bat argi urdinaren tarte ikusgarrian (445 nm) eta hiru UV tartean (375, 265, 220 nm) [376].

Erriboflabina II motako fotoabiarazle gisa sailkatzen da, horrek fotopolimerizazioa hasteko elektroi-emaile bat behar duela esan nahi du [218]. Bere konfigurazioak bi osagai ditu: 7,8-dimetil-10-alkilisoaloxazina 3 eraztunez osatutako zatia, bere redox propietateen, fotosentikortasunaren eta UV xurgapenaren arduraduna dena eta flabina nukleoa bezala ere ezagutzen dena; eta lau talde hidroxiloz osatutako ribitol isatsa, modifikaziorako aukera ematen duena [377–379]. Erriboflabinaren jatorrizko egitura aldatzeak fosfato multzo bat sartzea dakar. Hala, flabina mononukleotidoa edo erriboflabina fosfatoa (RFP) flabina nukleoa duen erriboflabinaren gatz sodikoari

dagokio. RFP-k erriboflabinak dituen propietate fotokimiko berberak mantentzen ditu, disolbagarritasun hobea erakutsiz [380].

Erriboflabinaren erretikulazio-mekanismoak honela funtzionatzen du: erriboflabinaren flabina-nukleoak argia xurgatzen du eta bizitza laburreko singlete egoera duen produktu erreaktibo batera kitzikatzen da, ondoren izaera oso erreaktiboa duen triplete egoera batera iristen delarik ($^3RF^*$). Singlete egoerako produktu batzuek beren energia bero edo fluoreszentzia moduan askatzen dute, triplete egoerara iritsi gabe, eta $^3RF^*$-ren zati bat oinarrizko egoera ez kitzikatu batera itzultzen da [380]. Oinarrizko egoera horretara itzuli ez den $^3RF^*$-ren gainerako zatia da erretikulazio-erreakzioa eragiten duena. $^3RF^*$ egoera hirukoitza birradikal iraunkorra da, proteinen aminoazido-kateak oxida ditzakeena [381].

Oxigenoa tartean dagoenean, erriboflabinaren egoera hirukoitzak oxigeno singletea sor dezake ($^1O_2$), eta horrek sare polimerikoaren erretikulazioa eragiten duten oxidazio-erreakzio erradikal eta ez-erradikal gehiago sortzen ditu [382]. Erriboflabinak eragindako erretikulazio-dentsitatea, proteinen aminoazidoen konposizioaren arabera aldatzen da [383].

Korneako zurruntasuna handitzea UVA irradiazioaren ondoren erriboflabina egoera hirukoitzean eszitatzearen emaitza da. Irradiazio horrek $HO^\bullet$, $O_2^{\bullet 2-}$ eta $O_2^{\bullet -}$ oxigeno-espezie erreaktiboak sortzen ditu I motako mekanismoaren kasuan; II motako mekanismoaren kasuan aldiz, oxigeno singletea sortzen du, geroago peroxido eta hidroxilo erradikalak sortuko dituena [384]. Erriboflabinak eragindako erradikal aske edo oxigeno espezie erreaktibo horiek kolageno molekulekin erreakzionatzen dute, kolageno zuntzexketako aminoazidoen arteko lotura kobalenteak sortuz [374, 385, 386].

Erriboflabinaren oxidazioak aminoazidoetan eduki handia duten proteinen erretikulazioa eragiten du, hala nola histidina, lisina, tirosina eta triptofanoa. Gainera, zisteina, metionina, tirosina, triptofanoa eta arginina ere oxida daitezke erriboflabinaren eraginpean. Kolagenoak prolina, hidroxiprolina, hidroxilisina, histidina, tirosina edo treonina ditu, eta I edo II motako oxidazio-mekanismoen bidez oxida daitezke erriboflabina dagoenean [371].

Hala, gelatinazko hidrogelerako erretikulatzaile gisa erriboflabina hautatzean, haren jatorri naturala, toxikotasun eza eta erabilera kliniko zabala hartu genituen

oinarri. Gure helburua ezarritako metodoak eta sistema biologiko erreal bat imitatzea izan zen, kornea kasu, gelatinazko hidrogel-soluzioa erabiliz.

Kolagenoan dauden aminoazido guztiak ere gelatina aurki daitezke, baina metionina, zisteina eta tirosina kantitate gutxi ditu hidrolisian zehar gertatutako degradazioaren ondorioz [159].

Gelatinaren egituran aldaketarik egin nahi ez genuenez, hipotesi hau planteatu genuen: hidrolisiaren ondoren gelatina-molekuletan atxikita dauden eta kolagenoan dauden gainerako aminoazidoek RFP-arekin elkarreragingo dute eta erretikulatu egingo dira erretikulazio- dentsitate nahikoa sortzeko.

Argi-iturri gisa argi urdina erabiltzea erabaki genuen. Erriboflabinak argi-xurgapen tontorrak ditu, bai UV tartean, bai espektro urdinean (445 nm-tako xurgapen tontorra). Oftalmologian, argi urdina fluoreszeinaz bustitako korneako zauriak behatzeko erabiltzen da, eta UVA argia baino aukera seguruagotzat jotzen da. UVA argiak korneako erretikulazioa eragiteko modurik eraginkorrena izaten jarraitzen duen arren, ikerketek argi urdinak gurutzaketa has dezakeela eta ordezko metodo gisa erabil daitekeela erakutsi dute [212, 215, 387].

Argi-iturria 10 cm-tara jarri genuen, 2 minutuz 100 mW/cm^2-ko dosia emanez. Tarte hori *ex vivo* korneetan denbora-tarte ugari ebaluatu ondoren hautatu genuen.

Gainera, hainbat osagai sartzea proposatu genuen, hidrogelari gehitzean erretikulazioan duten eragina eta izan zitzaketen propietate onuragarriak aztertzeko.

Dextranoa eta metilzelulosa oftalmologian duten erabileragatik hautatu genituen.

Dextranoa glukosaren kondentsazioz sortutako polisakaridoa da, bakterio laktikoek sakarosatik sintetizatutakoa. Glukosa molekulak α(1,6) loturen bidez lotzen dira eta kate nagusiaren C-3 posizioan albo kateak izan ditzake. Dextranoak 1000 eta 40000 Da arteko pisu molekularra izan dezake [388].

Oftalmologian, dextranoaren propietate lubrifikatzaileek kolirioetarako osagai erabilgarri bihurtzen dute. Keratokonoaren tratamendurako onartutako lehen prozedurak adibidez, hau da, Dresden erretikulazio epitelialaren protokoloak, % 20-ko (p/bol) dextranoko soluzioa erabiltzen du gehigarri nagusi gisa % 0,1 (p/bol) erriboflabina-5-fosfato soluzio bat sortzeko, [374]. Nahasketa horrek kolirioaren

biskositatea handitu eta soluzio isotoniko bat sortzen du erriboflabina disoluzio hiperosmolar baten bidez [389].

Metilzelulosa (MZ) zelulosatik eratorritako polisakarido hidrodisolbagarria da, ur hotzaren eraginpean hidratatzen dena eta berotzean gel bat eratzen duena. 10-220 kDa arteko pisu molekularretan lor daiteke, eta, oftalmologian, film edo txertoen osagai gisa, kolirioetako agente lodigarri gisa eta injekzioetako agente gelifikatzaile gisa balio dezake [390, 391].

Dextranoa zein MZ erriboflabina-soluzioetan kornearen erretikulazio prozeduretarako erabili izan dira. Ikerketek erriboflabina-dextrano soluzioak modu eraginkorren erretikulatzen duela frogatu badute ere, erriboflabina-MZ metodo gogokoena bihurtu da, korneako lodiera zentrala hobetu [392, 393], hedapen-abiadura handitu [394] eta estroma-gurutzaketa sakonagoak lortzen dituelako [395]. Horrek emaitza klinikoetan eragina izan dezake.

Azido hialuronikoa (AH) talde funtzional asko dituen eta ura erakartzeko gaitasun handia duen polisakarido natural bat da. Giza begietako fisiologiaren osagaia ere bada, horregatik hidrogelari gehitzea erabaki genuen. AH malkoaren osagaia ere bada eta bertan honela funtzionatzen du: begia kliskatzean, bere molekulak lerrokatu egiten dira, AH-k aldi baterako bere biskositatea galtzen du eta emeki-emeki kornearen gainazalean zabaltzen da. Begi-klisken artean, soluzioak biskositatea handitzen du, begi-gainazaleran irauten duen denbora handituz eta hidratazioa eta lubrifikazioa hobetuz [396]. Ezaugarri horiek, zelulen ugaltzean duen eraginarekin eta propietate antiinflamatorio eta antioxidatzaileekin batera, kolirioetarako oso osagai egokia bihurtzen dute [144].

AH-k dextranoak edo MZ-k sortutako antzeko emaitza sortzea espero genuen. Gainera, erriboflabinak eragindako erradikal libreetako batzuk erregulatzea edo neutralizatzea espero genuen [397].

Hidrogelen *in vitro* karakterizaziotik ondorio hauek atera genituen: hidrogela jariatzen hasteko beharrezko tentsioa handitu egin zen hidrogelari AH edo MZ gehitzean. Sakai eta kolabaratzaileek AH-ren efektua azido hialuronikoz eta gelatinaz osatutako hidrogelen garapenean ikusi zuten, non ebakidura-tensio baxuetan hidrogelen biskositatea AH kontzentrazioa handitzearekin batera handitzen zela ikusi zuten. Aitzitik, biskositateak behera egin zuen ebakidura-tentsio handiagoetan,

ebakidura bidezko argaltze-portaera hobetuz [398]. Emaitza hauek kontuan hartuta eta zelulosa eta haren eratorriak lodigarri gisa ere erabiltzen direla jakinda [390, 391, 399], AH-k eta MZ-k hidrogelen portaeran izandako eraginak ez gintuen arritu. Dextranoak ordea, kontrako efektua eragin zuen.

In vitro askapenari dagokionez, dextrano hidrogelak nabarmen moteldu zuen hainbat tamainatako konposatuen askapena. G hidrogelarekin alderatuta AH eta MZ zuten hidrogelen errendimendua antzekoa izan zen, IgG askapena geldotuz eta albumina askapena handituz.

Gardentasun eta transmitantzia neurketen emaitzek hiru osagaietako edozein sartzeak bi parametroak gutxitzen zituela adierazi zuten. Bereziki, hidrogelen atzean kokatutako irudiak opakuagoak eta lausoagoak ziruditen, HA gehitzean batez ere. Silvestrok eta kolaboratzaileek ere kitosano-aposituen gardentasun-mailak AH kontzentrazio desberdinak gehitzean murriztu egiten zirela adierazi zuten, eragina bi materialen arteko agregatu polielektrolitikoen eraketari egotziz [400].

MZ gehitzeak gelatina hidrogelaren antzeko transmitantzia mailak eragin bazituen ere, irudien gardentasuna ez zen hobetu. Gardentasun eta transmitantzia maila handiak bermatzea funtsezkoa da begi-gainazaleko kalteak tratatzeko, eta, beraz, azken hautaketarako aintzat hartutako parametro nagusietako bat da.

Dextranoa, AH edo MZ gehitzeak puzte- eta hedatze-maila handiagoa eragin zuen. AH-ren efektua konposatuaren ura erakartzeko gaitasun handiari egotz dakioke, AH-aren karboxilato taldeak karga negatiboak eragiten ditu, hidrogeno-loturen bidez ur-molekulak erakartzen dituztenak [396, 401]. Dextranoa edo zelulosa eta horren eratorriak ere, ura erakartzen duten konposatuak dira. Adibidez, 70 kDa-ko pisu molekularra duen 1 g dextranok 25 ml ur erakar ditzake [402]. Zelulosak ur-molekulekin hidrogeno-lotura sendoak osatzen dituzten hidroxilo talde ugari ditu, eta horrek ura atxikitzeko ahalmen handia duen material bihurtzen du [403]. Hala ere, baliteke propietate hori onuragarria ez izatea hidrogela zaurian aplikatzeko. Puzte-indizea hidrogelaren egonkortasunaren funtsezko adierazlea da. Koefiziente baxuagoak hidrogela korneari atxiki ahal izatea bermatzen du, estromatik askatzea saihestuz [404]. Azkenik, biobateragarritasunaren eta ziklo zelularraren analisien emaitzek antzekotasunak erakutsi zituzten talde guztien artean.

In vitro esperimentuak egin ondoren, dextranoa, AH edo MZ gehitzeak

hidrogelaren propietateak nabarmen hobetzen ez zituela ondorioztatu genuen. Beraz, hidrogelaren funtsezko gelatina eta RFP osaera mantentzea erabaki genuen. Hala, ondorengo funtzionalizazio, *ex vivo* eta *in vivo* esperimentuak gelatina eta RFP hidrogelarekin bakarrik egin genituen.

2.2. Hidrogelaren funtzionalizazioa

Hidrogela hantura murrizten duten eta birsortze prozesua bizkortzen duten osagaiekin aberastu genuen.

Hidrogela funtzionalizatzeko odol-eratorriak eta giza mintz amniotikoaren estraktuak (GMAe) hautatu genituen hazkuntza-faktoreetan aberatsak diren iturri gisa.

Duela 5 hamarkadatik, odol-eratorrietatik abiatuta prestatutako kolirioak begi-gainazaleko gaixotasunak tratatzeko erabili izan dira [405]. Terapia honen erabilera, odol periferikoan dauden proteinen eta hazkuntza-faktoreen proportzio esanguratsu bat malkoan ere egotetik sortzen da. Aurkikuntza horrek balio terapeutikoa du, begiaren gainazalak malko-unitate funtzionaleko zelulek sortutako faktore trofikoen bidez homeostasia mantentzen baitu [406].

Ikerketa honetan 2 odol-eratorri erabili genituen: serum autologoa (SA) eta hazkuntza-faktoreetan aberatsa den plasmatik eratorritako seruma (sPRGF). AS odol koagulatuaren laginak zentrifugatu ondoren bildutako gainjalkina da, leukozitoek askatutako edukia ere barne hartzen duena. sPRGF-a lortzeko, koagulatu gabeko odola zentrifugatu eta leukozitoen gaineko frakzioa hartzen da lehendabizi. Soluzio hori kaltzio kloruroarekin koagulatzen da ondoren, azkenik sPRGFa lortuz. Kasu honetan, hazkuntza-faktoreak leukozitorik ez dagoenean askatzen dira, kaltzio kloruroarekin koagualatzean alegia. Hala, globulu zurietan dauden zitokina proinflamatorioen eragina saihesten da [407].

SA-zko kolirioak begietako patologiak tratatzeko erabilitako lehen odol-eratorriak izan ziren [106, 408, 409]. Begi-gainazalaren mailan, SA-k lubrifikatzaile gisa jarduteaz gain, kaltetutako epitelioa berreskuratzeko funtsezko substantzia ugari ematen ditu, hala nola A bitamina, hazkuntza epidermikoaren faktorea (EGF), fibronektina eta hainbat zitokina [410]. Era berean, SA kolirioek orbaintze epiteliala errazten dutela eta erretikulazio prozedurekin lotutako ebakuntza osteko mina murrizten dutela frogatu dute [411].

sPRGF-a urte batzuk geroago erabiltzen hasi ziren [110, 412], begi-gainazaleko kalteak tratatzeko metodo terapeutiko gisa duen ahalmena erakutsiz. Begi-gainazalaren birsorkuntzan [413] hantura murriztean [414] eta molekula bakteriostatiko/bakterizidetan [415, 416] inplikatutako faktore-sorta zabala du eta keratozitoen eta fibroblasto konjuntibalen ugaltze eta migrazioan zein estromako miofibroblastoen modulazioan eragina du [417, 418]. sPRGF-k bere eraginkortasuna gaixotasun desberdinetako tratamendu gisa erakutsi du, hala nola, keratitis neurotrofikoan [419], begi lehorrean [420], glaukoma duten pazienteetan emandako begi-gainazaleko gaixotasunetan [421], keratektomia fotoerrefraktiboaren osteko zaurien orbaintzean [422, 423] edota urradura epitelialek eragindako kornea-zaurietan [424, 425].

Giza mintz amniotikoa (GMA) aplikazio oftalmiko askotan erabili izan da, propietate antiinflamatorioak, immunomodulatzaileak, immunogenizitate txikikoak, bakterioen aurkakoak, angiomodulatzaileak, orbaintzearen kontrakoak eta hemobateragarriak dituelako [426–430]. Kornearen birsorkuntzan dituen efektuak EGF-ri, keratinozitoen hazkuntza faktoreari (KGF), hazkuntza faktore endotelial baskularrari (VEGF), fibroblastoen oinarrizko hazkuntza faktoreari (bFGF), hepatozitoen hazkuntza faktoreari (HGF), plaketetatik eratorritako hazkuntza faktoreari (PDGF) eta egiturazko proteina batzuei, hala nola kolagenoa (I, III, VI eta VII motak), laminina, fibronektina, lumikana eta osteoglizina, egotz dakizkieke. GMA erabiltzeak begi-gainazala berrezartzeko eta LZAG-a tratatzeko ahalmena erakutsi du [434], baita EAI-k, erredura kimikoak eta Stevens-Johnsons sindromearen tratamenduan ere [435]. Hainbat zelula mota hazteko eta askatzeko erabili izan da [436, 437], kornea-ehunaren ingeniaritzan zein LZAG kasuetan korneako zelula epitelialen transplantean [434].

Era berean, mintz amniotikoaren estraktuek (MAe) arrakastaz tratatu dituzte begietako lehortasuna eta erredura kimikoak, korneako zelula epitelialen ugaltzea eta desberdintzea hobetu dituzte, zauri epitelialen orbaintzea erraztu dute eta korneako neobaskularizazioa inhibitu dute [432, 438, 439].

Protokolo normalizaturik ez dagoenez, MAe prestatzeko hainbat prozedura garatu dira. Tesi honetan erabilitako metodoa honako hau izan zen: aldez aurretik isolatuta zeuden mintz amniotikoak, antibiotikoen soluzio batekin garbitu genituen lehendabizi. Nitrogeno likidoan murgildu eta eskuz mortero batekin apurtu

genituen ondoren, hauts fin bat lortzeko. Hauts hori, PBS-arekin homogeneizatu eta sonikatu genuen, ingurunean faktore gehiago askatzeko. Zentrifugazioaren ondoren, gainjalkina jaso eta esterilizatu genuen, iragazki batetik pasatuz. Azterketa honetan erabilitako mintzak -80°C-tan gorde genituen estraktuak lortu arte. Beste metodo batzuek lehortu eta birrindutako mintz amniotikoak [113] edo mintz amniotiko deszelularizatutik lortutako estraktuak erabili izan dituzte [440].

2.2.1. Hazkuntza-faktoreen kuantifikazioa

Odol-eratorrietan eta GMAe-tan dauden hazkuntza-faktoreek kornearen birsortze-prozesuan eragina dutela uste da, beraz, horien kuantifikazioak produktu bakoitzaren efektu terapeutiko desberdina azal dezake.

sPRGF-k leukozitorik ez duenez baina plaketen kontzentrazio handiagoa duenez, zitokina proinflamatzailerik ez izatea baina SA-k baino hazkuntza-faktore gehiago izatea espero da [407, 441]. Hala eta guztiz ere, faktore epiteliotrofikoen kontzentrazio handiagoa iradokitzen zuten beste ikerketa batzuek adierazi bezala [442–444], lan honetan aztertutako hazkuntza-faktore gehienen kuantifikazioa handiagoa izan zen AS laginetan sPRGF laginetan baino.

Odol-eratorri desberdinetan hazkuntza-faktoreen kontzentrazioa alderatzea erronka bat izan daiteke, bibliografian aurkitutako emaitzen aldakortasun nabarmena dela eta. Emaitzen aldaketa hori prozesamendu- eta biltegiratze-metodoen arteko desberdintasunei [441, 445] eta SA prestatzeko protokolo estandarrik ez egoteari (zentro kliniko bakoitzak bere erara garatu ohi du) egotz dakieke. Adibidez, gure ikerketa-taldearen argitaratu gabeko datuek adierazten dute odolak koagulatuta irauten duen denbora luzatzean, hazkuntza-faktoreen maila handiagoak lortzen direla. Gainera, tesi honen kuantifikazioaren emaitzek gizabanakoen arteko kontzentrazio desberdintasun nabarmenak erakutsi zituzten. Banakoen arteko aldakortasun horrek, bibliografiarekiko desberdintasunekin batera, zaildu egin zuen odol-eratorrien eraginkortasunaren eta hazkuntza-faktoreen kontzentrazioaren arteko erlazioari buruzko ondorio orokorrak ateratzea.

Gainera, emaileen odol-eratorri bakoitzaren lagin guztien nahasketak sortu eta kuantifikatu genituen, aldez aurretik osagarriaren faktorea inaktibatu ondoren. PEDF, SP eta HGF mailak nabarmen jaitsi ziren lagin guztien batez besteko balio teoriko batekin alderatuta, gainerako faktoreetan inolako murrizketarik ikusi gabe.

Gure kuantifikazio gehienak, beraz, bat etorri ziren Anituak eta kolaboratzaileek esandakoarekin, laginen berotzeak kuantifikatutako proteina-edukian eraginik ez zuela adierazi baitzuten [446, 447]. Hala ere, beste faktore batzuk tenperaturarekiko sentikorrak izan ziren eta inaktibazio termikoaren ondorioz neurri handiagoan edo txikiagoan galdu genituen.

In vitro hantura-probek, SA-rekin funtzionalizatutako hidrogelak, TNFα-z estimulatutako KZE zelulen IL-1β mailak gehiago murrizten zituela erakutsi zuten. Hala, *in vivo* probetarako odol-eratorri gisa SA hautatzearen arrazoiak lortutako hazkuntza-faktoreen kuantifikazio handiagoa eta *in vitro* ebaluazioetan ikusitako hanturaren murrizketa handiagoa izan ziren.

Eremu anatomikoaren arabera amnioa hainbat azpieskualdetan bana daiteke. Amnio plazentarioak plazenta estaltzen du eta islapen amnioak umetokiaren pareta estali eta zaku amniotikoa deritzona osatzen du. Azkenik, zilbor-hesteko amnioak zilbor-hestea estaltzen du. Ikerketa honetarako GMA-ren zatiak islapen amnioetatik lortu genituen. Mintzaren zati hau amnio plazentarioaren ordez erabili genuen, GMA plazentarioak baino potentzial immunomodulatzaile handiagoa duela hauteman delako, amnio plazentarioa proinflamatorioagoa baita [332].

Pazienteen arteko eta GMA-ren eskualde desberdinetatik lortutako estraktuen artean kuantifikazio-aldeak erregistratu genituen. GMA-ren eremu desberdinetatik lortutako estraktuen hazkuntza-faktoreen kuantifikazioari dagokionez, gure aurkikuntzak bat etorri ziren aurreko azterlanekin. Gicquel eta kolaboratzaileek, EGF-ren maila altuen berri eman zuten urruneko eta erdiko eremuetan, eta hori bat dator gure emaitzekin [448] Era berean, KGF, IGF1 edo HGF kontzentrazio handiagoak erregistratu zituzten plazentako mintzean [449–451], islatutako GMA-ren hurbileko eremuan ikusitako mailen gorakadarekin bat etorriz, plazentatik hurbilen dagoen eskualdea baita.

Estraktuen osagai bioaktiboak ere alda daitezke hauek prestatzeko metodoaren arabera. GMAe-ren prestakuntzari buruzko ikerketa batek birrintzeak homogeneizazioak baino % 20 faktore gehiago erauzten zituela frogatu zuen; izan ere, metodo errazagoa izateaz gain, nitrogeno likidoak eragindako kalte zelularrak proteina eta HGF gehiago ateratzea eragin zuen. Era berean, proteasa inhibitzailearen erabilerak eta errepikatutako zentrifugazioak erauzitako HGF kantitatea handitu

zuten. Hala ere, estraktuak -170 °F 6 hilabetez biltegiratzeak HGF eta proteinen maila % 50 murriztea ekarri zuen [452].

Gure kasuan ere mintzen arteko aldakuntza estatistikoki esanguratsua izan zen, neurri handi batean eskuragarri zeuden lagin biologikoen kopuru murritza zela eta. Odol-eratorrien kasuan bezala, paziente bakoitzaren mintzaren eremu desberdinetako estraktuak multzokatu eta kuantifikatu genituen. Kasu horretan, ez zen inaktibazio termikoa beharrezkoa izan. Hala ere, aztertutako hazkuntza-faktore gehienen kuantifikazioan beherakada estatistikoki esanguratsua erregistratu genuen.

FGF2, HGF edo KGF bezalako faktoreek zaurien orbaintze prozesuan zelula epitelialen ugalketan, migrazioan eta homeostasi korneala mantentzean duten eraginagatik [59] eta gure emaitzetan erregistratutako kontzentrazio altuengatik, GMAe-ren hurbileko eremua hautatu genuen *in vivo* esperimentuetarako hidrogelak funtzionalizatzeko. Hala ere, faktore guztien kuantifikazioan, *in vitro* hantura-saiakuntzako IL-1β-ren murrizketan eta bibliografian oinarrituta, hidrogela funtzionalizatzeko urruneko eremua erabiltzea egokiagoa zatekeen.

Hidrogela odol-eratorrien eta GMAe-ren % 50-eko kontzentrazioarekin funtzionalizatu genuen. Erabaki hori gure taldeak aldez aurretik egindako behaketan oinarritu zen: sPRGF-ren % 50-eko kontzentrazioa tanta oftalmikoetan tratamendu arrakastatsua izan zen EAI-ak zituzten pazienteen begi-gainazala birsortzeko [110, 425].

2.2.2. Infliximab: hanturaren aurkako eragilea

Infliximab-a hanturari aurreko egiteko molekula gisa hautatu genuen.

Infliximab-a TNFα-ren aurkako giza/arratoi antigorputz monoklonal kimerikoa da eta mintzeko TNFα edo TNFα-ren forma askeekin bat egiten du honen hartzaileekiko lotura inhibitzeko [453]. Tratamendu honen erabilera sistemikoa ubeitis pediatrikoaren tramenduan [454], artritis erreumatoidea duten pazienteetan kornea-urtzea saihesteko eragile gisa [455] eta ultzeradun keratitis periferikoaren tratamenduan eraginkorra dela ikusi dute [456]. Gainera, gaixotasun autoimmuneen eta korneako ultzeren kasuetan, keratoprotesiko kirurgiaren osteko hantura murrizteko eraginkorra dela ere frogatu dute [457–460].

Era berean, kolirioetan terapia lokal gisa erabiltzea ikertzen ari dira, farmakoa injektatzean ematen den esposizio globala murrizteko. Ikerketek animalia-ereduetan

begi lehorra eta neobaskularizazioa tratatzeko eraginkorrak direla frogatu dute [461, 462], eta gaur egun giza pazienteetan saiakuntza kliniko bat martxan dago kornea-urtzea tratatzeko 10 mg/ml Infliximab kolirioaren tolerantzia eta segurtasuna ebaluatzeko [463].

Hidrogelean 1 mg/ml infliximab dosia sartzea hautatzeko, antigorputz hau kapsulatu zuten aurreko azterlanetan oinarritu ginen [464–466]. Abian den saiakuntza klinikoak Infliximab-en kolirioak erabiltzen ditu, 10 mg/ml-ko kontzentrazioan. Kornearen babes-mekanismoek mugatu egiten dute kanpoko eragileen infiltrazioa, eta horrek nabarmen murrizten du bide topikotik administratutako agenteen bioerabilgarritasuna.

Korneak farmakoaren kantitate txiki bat soilik xurgatzen du, % 5 baino gutxiago. Gainerako kopurua malkoaren, begiaren kliskaren eta drainatze nasolagrimalaren bidez kanporatzen da [467]. Tanta oftalmikoen banagailuek gehiegizko kantitatea ematen dute, begi-azalerak har dezakeen edukiera baino handiagoa, eta, ondorioz, soluzioa alferrik galtzen da. Gainera, malkoen jario eraginkor eta etengabeak eragotzi egiten du tantak kornearekin kontaktuan egotea denbora luzean. Garatutako hidrogelak betegarri gisa jardungo duenez eta zaurian lokalizatuta egongo denez, dosi txikiago bat gaindosia saihesteko egokitzat jo genuen.

3. Funtzionalizatutako hidrogelen aplikazioa eta eragina *in vivo*

Ehunen sendatzearen testuinguruan, ordezkatzea eta birsortzea kontzeptu desberdinak dira. Birsortzeak, hazkuntza berria sustatuz kaltetutako ehunaren jatorrizko egoera guztiz berreskuratzeko aukera ematen du. Ehuna ordezkatzeak, bestalde, kaltetutako eremua jatorrizkoa ez den ehun berri desordenatu batekin ordezteari dagokio; eta gehienetan orbainen sorrera dakar.

Prozesu bikoitz hori ere agerikoa da kornean. Korneako akats epitelial baten osteko lehen faseak zauria egonkortzea dakar; horren bidez, zelula-hondarrak ezabatu, zelulak biribildu eta hemidesmosomak murriztu egiten dira kaltetutako eremuan [468]. Horren ondoren, zelulen migrazioan, ugaltzean eta estromaren ZKM-aren ekoizpenean oinarritutako **ordezkapen** fase bat dator. Fase honetan, mugikortasun zelularra bizkortu egiten da, horrek irekitako eremua azkar estaltzea

ahalbidetzen du. Aldi berean, hesi-efektua berrezartzen da, zelulen azalera handituz. Hasiera batean, ZKM berria sortzea beharrezkoa da zauria ixteko; hala ere, matrize desantolatu hori jariatzeak kornea-ehunaren uzkurtzea eta opakutasuna eragiten du, orbaintze fibrotikoa sortuz [18].

Era berean, LEZA/P-ak aktibatu eta ugaltzen hasten dira. Behin linbotik datozen zelulek akats epiteliala estali dutenean, epitelioko zelula basalak ugaltzen eta bereizten hasten dira geruza zelular epitelialak berrezartzeko [25]. Mintz basal akastuna birsortzeko lamininak ere ekoizten dituzte, zauriaren azpian dauden keratozitoekin lankidetzan [57]. Mintz basala berrezartzea korneako epitelioan dauden zelulen arteko lau loturetako biren eraketarekin batera gertatzen da, GAP loturekin eta desmosomekin alegia. Beste bi loturak, atxikidura loturak eta lotura hertsiak, migratzen ari den epitelioan ikus daitezke [469].

Azkenik, **birsortze** fasea gertatzen da, non ehun berria antolatu eta bereizi egiten den, baldintza egokietan jatorrizko ehunaren ezaugarriak lortu arte [470, 471]. **Ordezkapen** fasean, epitelioak 7 eta 14 egun artean behar izaten ditu konpontzeko, inerbazio epiteliala berrezarri gabe, honek hilabeteak behar izaten baititu [80, 472]. **Birsortze** prozesuan, epitelioak, endotelioak eta keratozitoek zitokinak, kimiokinak eta hainbat hazkuntza-faktore askatzen dituzte, baina prozesu honek 2 urte baino gehiago behar izan ditzake estromaren funtzio eta argitasun egokiak berrezartzeko [473].

Gai honetan arreta jarriz, funtzionalizatutako hidrogela estromaren konponketa azkartu eta ehuna behar bezala birsortzeko helburuarekin garatu genuen. Gure asmoa hidrogelaren aplikazioarekin epitelio berri baten eraketa azkartzea eta kornearen kurbadura mantentzea izan zen, estromaren bisortze egokia sustatzeko.

3.1. *In vivo* prozedura kurgikoaren baldintzen ezarpena

In vivo esperimentuetarako baldintzak hasierako azterketa pilotu baten ondoren ezarri genituen. Hasierako saiakuntzan begiak % 0,2 benzalkonio kloruroarekin (BAK) tratatu genituen, hantura handiagoa eragiteko, eta ukipen-lente babesgarriak erabili genituen malko-jarioa eta hidrogela kentzea saihesteko. Aurreko estromako keratektomiak hantura eragin zuen berezko ondorio gisa. Hala, BAK-a baztertzea erabaki genuen, narritadura eta alferrikako eragozpenak saihesteko. Gainera, ukipen-lenteen erabilerak eragozpen gehiago eragiten zituen kaltetutako begietan

hobekuntzak baino. Lenteen tamaina desegokiak eta untxien begietara gaizki egokitzeak zauria etengabe igurztea eragin zuten eta, ondorioz, untxi guztiek lenteak kenduta zituzten hirugarren egunerako.

Proba horien ondoren, kirurgia osteko neurri gisa tarsorrafia partzial bat egitea erabaki genuen, 3 egunera arte mantenduko genuena. Horrez gain, ez genuen hantura-estimulu gehigarririk sartu.

Tarsorrafia betazalen ertzak aldi baterako jostean datzan teknika kirurgikoa da. Prozedura horrek arrakasta-tasa handiak erakutsi ditu EAI-en tratamenduan. Betazalaren irekidura murrizteak malko-lurrunketaren tasa murrizten du, eta betazalaren immobilizazioak, berriz, orbaintzeko prozesua hobetzen du, begi kliskaren inpaktua murrizten baitu [474].

Tarsorrafia zela eta, ezin izan genituen ebakuntzaren ondorengo lehen eta bigarren egunetan epitelioaren itxieraren eboluzioa erregistratzeko argazkiak atera. Gainera, tarsorrafiak tratamendu guztietan berrepitelizazio azkarra eragin zuen, azterketa pilotuaren emaitzekin alderatuta. Zenbait kasutan, kirugia osteko 4. edo 5. egunean berrepitelizazio osoa eta hanturaren murrizketa erregistratu genuen, Draize eskalaren bidez egindako behaketa klinikoetan oinarrituta. Emaitza horiek beste azterketa batzuek egindako behaketekin bat datoz. Tarsorrafiak akats epitelialak orbaintzeko prozesua azkartzen duela frogatu izan dute klinikoki erabilitako tratamenduekin alderatuta, hala nola mintz amniotikoaren transplantearekin [119]. Gainera, Sjögren sindromea bezalako gaixotasunetan, malko-filma mantendu eta korneako epitelioa orbaintzen laguntzen duela frogatu izan dute [475].

Gure emaitzen aldakuntzari dagokionez, garrantzitsua da kontuan hartzea animalia bizidunen presentziak eragin handia izan duela emaitzetan, gure kontroletik kanpo eta azken emaitzetan eragina izan dezaketen faktoreak daudelako. Efektu biologikoak kontrolatu gabeko aldagaiak sartu eta banakoen arteko desberdintasunak sortzen ditu, tratamendua edozein dela ere. Beraz, tamaina handiko lagin bat eduki beharra dago, desberdintasun estatistikoak benetan esanguratsuak izan eta tratamenduekin lotuta egon daitezen.

3.2. Berrepitelizazioa eta sendatzea

Esperimentuaren hasierako egunetan (3, 4 edo 5), itxitako batez besteko eremu epiteliala handiagoa izan zen kontrol-taldean hidrogelarekin tratatutako taldeetan

baino. Hala ere, kontrol-taldeko begi batzuk ez ziren guztiz itxi, eta, kasu batzuetan, epitelioa berriro ireki zen azterketaren amaieran.

Kontrol-taldeko zelula epitelialek ugaltzeko gaitasun handia erakutsi zuten. Zauriaren bilakaeraz gain, immunofluoreszentzia-analisiak Ki67 zelula positiboen prebalentzia kontrol-tratamenduko korneetan handiagoa zela erakutsi zuen, kirurgia egin eta 7 egunera prozesatutako korneetan batez ere. Gene-adierazpenaren analisiak gainera, kontrolarekin tratatutako korneetan hidrogelarekin tratatutakoetan baino Ki67-ren adierazpen handiagoa berretsi zuen, hidrogelarekin tratatutako taldeetan Ki67 adierazpenaren beherakada estatistikoki esanguratsua erakutsiz 21 eguneko kontrol-tratamenduarekin alderatuta. Untxi osasuntsuetan, hau da, aurreko estromako keratektomia egin aurretik patologiarik gabeko animalietan, aplikatutako tarsorrafiak akatsen itxiera azkartzean eragina izan zuen. Hidrogela bezalako betegarririk ez egoteak kontrol-korneetako zelula epitelialen ugalketa estimulatu eta zauria azkarrago ixtea eragin zezakeela zirudien, ixteko ezinbesteko beharraren ondorioz [476]. Hidrogelarekin tratatutako korneen berrepitelizazioaren hasierako moteltzea hidrogela kornea-akatsean aplikatzeari egotz dakioke. Aplikatu beharreko kantitatea ez bada kontu handiz kontrolatzen eta hidrogel likidoak akatsaren lekutik gainezka eginez gero, hidrogelaren gaineko migrazio epitelialaren moteltzea gerta daiteke [305, 477].

Kontrolarekin tratatutako korneak azkarrago itxi arren, hidrogeletan oinarritutako tratamendu guztiek berrepitelizatzea lortu zuten. Izan ere, berrepitelizazio-kasu guztiak kontuan hartuta, H-SA-k begi guztiak azkarrago ixtea eragin zuen, 5. egunetik aurrera itxiera azkar bereziki nabarmena eraginez. Gainera, H-SA-rekin tratatutako korneek Ki67 adierazpen handiena erakutsi zuten hidrogeletan oinarritutako taldeen artean. Emaitza hori bat dator odol-eratorrien faktoreen presentziak zelula epitelialen ugaltzeko ahalmena areagotu dezakeela erakusten duten ikerketekin [108, 422, 425, 478–480].

H-AS-en ondoren, H-GMAe-k, antzeko zauri-itxieraren bilakaera eta immunohistokimika bidezko Ki67 zelula positiboen zenbaketa handia erakutsi zuen, bereziki 7. egunean prozesatutako laginetan. Mintz amniotikoaren edo honetatik eratorritako produktuen efektu onuragarriak biomolekulei eta hazkuntza-faktoreei egozten zaizkie, hala nola HGF, EGF, TGF edo I, III, IV eta V motako kolagenoari, besteak beste, zeinak zelula epitelialen migrazioa, atxikipena eta desberdintzapena

sustatzen duten. Choi eta kolaboratzaileek MA-ren esekidurak bere propietateei eusten ziela eta *in vitro* hazkuntzetan kontzentrazioa handitu ahala, zelula epitelialen ugalketan eta migrazioan eragina zuela frogatu zuten [481]. % 0,1 MA-ren estraktuek eragindako ugaltze efektua ere korneako epitelioko zeluletan *in vitro* egindako kalte-mekanikoetan frogatu izan dute [438]. Gainera, 0,1-1 mg/ml-ko kontzentrazioetan aplikatutako mintz amniotikoko kolirioek, LEZA/P-en ugaltzea areagotu zuten; ABCG2 zelula amen ustezko markatzailearen adierazpena handitu eta CK3 korneako zelula epitelial desberditzatuen markatzailearen adierazpena gutxitu zutelarik [432]. Era berean, giza zelula epitelial amniotikoetatik eratorritako zelulaz kanpoko besikulen erabilerak modu eraginkorrean hobetu zuen giza korneako zelula epitelial eta estromalen *in vitro* ugalketa eta migrazioa. Besikula horiek zelulaz kanpoko matrizea berrantolatzea eta zelulen ehunarekiko atxikipena sustatu zuten, kontaktu-fokalen seinaleztapen bidea aktibatuz [482].

H-Ag tratamenduak zauriaren bilakaera motelena eta itxitako kasuen kopuru txikiena erakutsi zuen azterketaren 4. egunera (IV.7 taula) eta 5. egunera arte, hurrenez hurren (IV.31 irudiko **b**), baina itxiera-bilakaera progresiboena erakutsi zuen. Aipatzekoa da kornea guztien itxiera osoa H-Ag eta H-SA taldeetan baino ez genuela ikusi.

ARPE (giza betsareako zelula epitelial pigmentarioen lerroa) zelulen Infliximab bidezko tratamenduak ez zuen zelulen ugalketan eraginik izan, Infliximab-ak zelula hauetan eraginik ez zuela iradokiz [483]. Gainera, Infliximab-ak ez zuen gizaki zein saguen hezur-muineko zelula estromal mesenkimalen biziraupenean, fenotipoan, morfologian, ugaltzean, zelula-zikloan eta apoptosian eraginik erakutsi [484]. Infliximab-ak hantura kontrolatzen du, TNFα-ren forma ezberdinekin afinitate handiz lotuz. Antigorputzak hantura kontrolatzen badu, malkoetako zitokinen azterketa pilotuan ikusi zen bezala, eta aipatutako emaitzak kontuan hartzen baditugu, korneak gainerako prozesuak gauza ditzake berez, hala nola, berrepitelizazioa, ugalketa edo migrazio zelularra. Hori izan liteke H-Ag tratamenduaren zauri-itxieraren emaitzak H-SA edo H-GMAe tratamenduekin lortutakoen antzekoak izateko arrazoietako bat.

Neurri handiago edo txikiagoan eta tratamendua edozein izanda ere, epitelioaren hiperplasia ikusi genuen kornea batzuetako eremu berrepitelizatuetan.

Epitelioak birmoldatzeko gaitasun handia du, eta bere helburuetako bat ikusmen-zorroztasunean eragina duten kurbadura-irregulartasunak txikiagotzea

da. Birmoldaketa mota honetan inplikatutako mekanismoak eztabaidagai izaten jarraitzen duten arren, epitelioa estroma-ehuna galtzen den eremuetan loditzen da, kornea zentralean emandako kurbadura aldaketa konpentsatzeko [485]. Garatutako hidrogelak zauriaren betegarri gisa funtzionatu zuten, kurbadura aldaketa hori konpentsatuz eta epitelioak bete beharreko eremua finagoa izatea eraginez. Horrek kirurgia egin eta 21 egunera prozesatutako kontrol-korneako laginetan epitelio lodiago bat ikustea azalduko luke.

Denborak aurrera egin ahala eta estroma birmoldatu heinean, hiperplasiarik gabeko epitelio bat ikustea esperoko genuke, zeinak ehunaren erabateko birsorkuntza baieztatuko lukeen. Hala ere, prozesu honek gure azterketaren 21 egunak baino denbora gehiago beharko luke.

Linboko zelula ama/progenitoreak identifikatzeko erabili ohi diren markatzaileek (PAX6 eta p63) ez zuten denbora eta tratamendu desberdinetan kontrol-taldearekiko alde estatistikoki esanguratsurik erakutsi adierazpen genikoaren analisian. RNA-ren erauzketa ehun esklerokorneal osoa erabiliz egin genuen, epitelioa, estroma eta endotelioa zituena. Markatzaile horiek linboko epitelioko zelula basalen geruzan dauden zelula espezifikoekin lotuta daudenez, beharbada kornea osoko zelulen kopuruak eragina izan zuen emaitzetan. Linboko epitelioa berariaz hautatu izan balitz, aldeak nabarmenagoak izan zitezkeen. Hala ere, CK15-en adierazpenak, linboko epitelioaren geruza basalean soilik dauden epitelioko zelula progenitoreen markatzaileak [37], tratamendu-taldeen arteko desberdintasunak erakutsi zituen analisi immunohistokimikoetan. Gure ikerketak zelula horien existentzia egiaztatu zuen aztertutako kornea guztien linbo esklerokornealetan. Gainera, CK15 adierazpen maila handiagoa ikusi genuen kirurgia egin eta 21 egunera prozesatutako H-Ag, H-SA eta H-GMAe-rekin tratatutako korneetan. Emaitza horrek tratamendu horiek epitelioaren eremu kaltetutik haratago eragina zutela iradoki zuen.

H-SA eta H-GMAe hidrogeletan CK15 adierazpen handiagoa SA eta GMAe-en hazkuntza-faktoreen ekarpenagatik azal daiteke. Gure ikerketa taldeak aldez aurretik adierazi zuen linboko zelula ama/progenitoreen potentziala mantentzeko s-PRGF-ren eraginkortasuna [425]. Plaketetan aberatsa den plasma erabiltzean ere antzeko emaitzak aurkitu zituzten giza muskulutik eratorritako zelula progenitoreen [486] eta beste zelula ama/progenitore mesenkimalen ama izatearen mantenuan [487]. MA-ari dagokionez, MA-ren transplantearen eta MA-ko estraktuekin egindako

kolirioaren erabilera konbinatuak zelula amen hazkuntzan eta korneako epitelioaren desberdintzapenean eragin sinergikoa izan zuen. Linboko transplantearekin batera MA-ko estraktuekin egindako kolirioaren erabilerak, kornearen gardentasuna hobetzea eta baskularizazioa eta konjuntibalizazioa gutxitzea eragin zuen. Hala, erdiko kornean p63 eta ABCG2 zelula positiboen adierazpenak zelula horiek zelula amak zirela baieztatu zuen [433]. Bitxia bada ere, Lai eta Luok MA eta argi ultramorearekin erretikulatutako erriboflabinarekin kultibatutako zelulek ama izatea modulatzeko gai zirela frogatu zuten. MA-zko euskarri fotoretikulatuek ABCG2 adierazpena sustatzen zutela ikusi zuten LEZA/P-etan, eta frogatu zuten erriboflabina kontzentrazioak eragina zuela hauen ama izatearen adierazpenean [488].

CK15 zelula positiboak begiaren eremu periferikora ere hedatzen dira, eta erantzun orokor bat sortzen dute akats epitelialari aurre egiteko. Zelula horiek banatu, bereizi eta kornean zentripetoki gorantz mugitzen diren heinean, gero eta CK3 adierazpen handiagoa erakusten dute [33, 35]. Hau kornea guztietan berretsi genuen, tratamendua edozein izanda ere. Gainera, analisi immunohistokimikoen bitartez PanCK markatzailearen adierazpena zaurian, kaltetu gabeko eremuan eta linboko eremuan hauteman genuen.

Era berean, korneako epitelioaren goiko aldean dauden zelula epitelialek ZO-1 adierazten dute, lotura hertsiekin lotutako proteina. Ebakuntza egin eta 7 eta 21 egunetara, proteina honen antzeko adierazpena ikusi genuen tratamendu-talde guztietan, kaltetutako korneen berrepitelizazio egokia eta kornea-epitelio heldu eta funtzional baten garapena baieztatuz. Aipatzekoa da korneako epitelioaren hesi-funtzioaren ezarpen azkarra (ZO-1 zelula positiboak) kaltea konpontzeko hasierako faseetan. Beraz, kornea-hesiaren funtzioa ezartzea funtsezkoa da kornearen birsortzea sustatzeko [480, 489, 490].

3.3. Atxikidura

CD44 mintzeko glikoproteina eta HA-ren funtsezko hartzailea da, zelulen ugalketa estimulatu eta zelulen zitoeskeletoan alterazioak eragiten dituena [491]. CD44 adierazpena kaltetu gabeko kornearen geruza epitelial basaletan ikus daiteke nagusiki, eta areagotu egiten da lesio baten ondoren [492]. AH-rekin tratatutako korneako zelula epitelialetan, CD44-ren adierazpenaren gorakada ikusi izan dute, zeinak migrazioa handitzea eta hanturazko proteinen mailak murriztea dakarren

[493]. Halaber, CD44-ren sintesiak korneako zaurien orbaintzearen migrazio-fasean eragina duela ere adierazi dute [494].

Aztertutako bi denbora-puntuetan CD44 genearen adierazpenak hidrogelarekin egindako tratamendu gehienetan kontrolarekiko gorakada txiki bat erakutsi bazuen ere, ez genituen alde estatistikoki esanguratsuak erregistratu. % 0,2 HA tantak instilatu genituen hidrogelarekin tratatutako korneetan eta kontrol-taldean. Horrek talde guztien arteko desberdintasun eza azal dezake.

Integrina β4 proteinak epitelioaren eta matrizearen arteko hemidesmosoma motako loturetan parte hartu eta ehun iraunkor bat sortzen laguntzen du [495]. Integrina β4-ren adierazpenak jarraitasunik eza erakutsi zuen zauriaren eremuan 7 egunetara prozesatutako talde guztietan. Kontrol-korneak Int-β4-z markatutako gune irregularra erakutsi zuen; hidrogelarekin tratatutako korneetako zaurietan, berriz, adierazpenik gabeko guneak ikusi genituen. Hala ere, 21 egunetara prozesatutako lagin guztien Int-β4-ren adierazpena altuagoa izan zen, lotura epitelial sendoagoak adieraziz eta epitelio berriaren eta honen azpiko zelulaz kanpoko matrizearen arteko atxikidura berretsiz.

Integrinek korneako zelula epitelialak kolageno, fibronektina, laminina edo bitronektinari atxikitzeko berebiziko garrantzia dute [496]. Adibidez, fibronektina proteina itsasgarri gisa jarduten duen glikoproteina bat da, atxikimenduarekin, askapenarekin eta zelulen migrazioarekin lotutako hainbat prozesu biologikotan funtsezko eginkizuna betetzen duena [497].

Kornea-zaurien birsortze prozesuan, fibronektina zelula epitelialen atxikimendua eta migrazioa errazteko matrize gisa dihardu. Fibronektina-tanta oftalmikoak kalte epitelialaren ondoren erabili izan dituzte gaixotasun alergikoen, epitelio akats iraunkorren edo zenbait distrofia kornealen kasu larrietan, kirurgiaren ondoren berrepitelizazio azkarra eta osoa lortzeko [498, 499]. Fibronektinatik eratorritako PHSRN peptidoaren tanta oftalmikoen eraginkortasun klinikoa eta erantzun azkarra EAI-ak tratatzeko frogatu dute, akats epitelialen tamaina 3 egunetan nabarmen murriztuz [500].

Era berean, Nap-FFPHSRN hidrogelak, Nap-F sekuentziak eta fibronektinatik eratorritako PHSRN peptidoa zituen hidrogelak alegia, untxien korneako berrepitelizazioa errazten zuela frogatu zuten *in vivo*, berrezarpen morfologiko eta

arkitektoniko oso batekin [501]. Fibronektina odol-eratorrietan eta mintz amniotikoan aurki daiteke. Gure taldeak odol-eratorri desberdinen fibronektina kantitatearen berri eman izan du aldez aurretik, haien arteko alde estatistiko esanguratsurik gabe [479]. Mintz amniotikoaren zelulaz kanpoko matrizeak kolagenoak, lamininak, fibronektina, elastina, proteoglikanoak eta glikoproteinak ere baditu, baita migrazioa eta zelula-atxikipena sustatzen duten hazkuntza-faktoreak ere [502]. Litekeena da SA eta GMAe bidez funtzionalizatutako hidrogeletan dagoen fibronektinak zelula epitelialen migrazioa suspertu eta berrepitelizazioan lagundu izana, batez ere itxieraren lehen egunetan. Hipotesi hau, lehen aipatutako zauriaren itxieraren bilakaerak balioztatzen du.

Ideia hori kontuan hartuta, beharbada hidrogelaren konposizioari fibronektina edo mintz basalaren beste osagai batzuk gehitzeak zelula epitelialen atxikipena hobetuko luke.

3.4. Fibrosia

α-SMA aktibatutako miofibroblastoen markatzailea da eta bere adierazpenak korneako estroman fibrosiaren aktibazioa adierazten du. Korneako estromaren orbaintze prozesuan, korneako fibroblastoen infiltrazioa eta hauen ondorengoko miofibroblastoetarako transformazioa ikus daiteke [503]. Beraz, keratozitoen aktibazioa eta miofibroblastoetan bereiztea funtsezko prozesu fisiologikoak dira kornea-kaltea konpontzeko.

Keratozitoak gandor neuraletik eratorritako zelulak dira eta zelulaz kanpoko matrizearen osagaiak ekoiztuz eta birmoldatuz, hala nola kolagenoak, proteoglikanoak eta kristalinak, kornearen gardentasuna mantentzeko ardura dute. Kolageno xaflen artean kokatzen diren zelula txikiak dira, elkarrekin konektatu eta estroma osoan sare bat osatzen dutenak [504]. Keratozitoek keratokana adierazten dute, baita 1 eta 3 aldehido deshidrogenasa (ALDH1A1 eta ALDH3A1), CD34, lumikan eta bimentina ere [12, 504]. Akats baten ondoren, keratozitoak aktibatu eta fibroblasto bihurtzen dira, zauriaren lekura migratu eta estroma konpontzen hasteko. Fibroblastoek keratokana eta CD34 markatzaileak adierazteari uzten diote, morfologia dendritikoa galtzen dute eta bimentinaren adierazpena handitzen dute. Hala ere, oraindik ez dute α-SMA eta desmina adierazten [505]. ZKM zelulaz kanpoko matrizearen osagaiak eta metaloproteinasak jariatuz birmoldatzen dute, eta mintz basal epitelialaren eta hantura-erantzunaren birsorkuntza modulatzen

dute. Lesioa larria denean, TGFβ bezalako hazkuntza-faktoreek nabarmen egiten dute gora estroman, eta horrek fibroblastoak miofibroblasto bihurtzen ditu [506]. Hazkuntza-faktore horiek batez ere epiteliotik eta malkoetatik datoz [79]. Miofibroblastoek α-SMA, bimentina y desmina adierazpena dute ezaugarri, baita funtzio kontraktila ere [79]. Zelulaz kanpoko matrizearen osagaiak kantitate handietan eta modu nahasian sintetizatzen dituzte, eta horrek kornea-opakutasuna eta orbainak sortzea eragiten du. Ez dago argi zer gertatzen den zelula horiekin ehunen birsorkuntzaren ondoren, baina hazkuntza-faktoreen fluxua murriztean apoptosi bitartez desagerrarazten direla uste da. Izan ere, TGFβ seinaleztapenak miofibroblastoen biziraupena sustatzen du [506]. *In vitro* azterketek miofibroblastoak inaktiba daitezkeela eta fibroblastoen antzeko fenotipo batera itzul daitezkeela frogatu dute. Hala ere, fenomeno hau oraindik ez da *in vivo* frogatu [505].

Azterketa honetan, erantzun miofibroblastikoa erregistratu dugu bai kontrol-korneetan bai hidrogelarekin tratatutakoetan, lesio estromal baten ondoren espero bezala. Hala ere, hidrogelarekin tratatutako korneek α-SMA adierazpen baxuagoa erakutsi zuten.

Hasierako erantzun fibrotikoa funtsezkoa bada ere, miofibroblastoek sekretatutako zelulaz kanpoko matrizeak askotan estroma-opakutasuna eragin dezake. Ehun hau gardena izan beharko litzateke, hori dela eta, keratozitoek matrizea berriro xurgatu behar dute ondoren, gardentasun normala berrezartzeko eta opakutasuna saihesteko.

Gene-adierazpenaren emaitzek hidrogelarekin egindako tratamenduen α-SMA mailak kontrolarekiko nabarmen jaitsi zirela frogatu zuten, bai kirurgia egin eta 7 egunetara, bai 21 egunetara. 7. eguneko laginak kontuan izanik, H-Ag eta H-SA-rekin tratatutako korneek kontrolarekiko α-SMA murrizketa handiena erakutsi zuten, efektu hori 21 egunez mantenduz. Gure ikerketa taldearen aurreko emaitzek jada adierazi zuten diluitu gabeko sPRGF kolirioek, α-SMA positibotasuna murrizten zutela, opakutasun eta orbaintze txikiagoa erakutsiz kirurgia egin eta 30 egunetara [425].

Nabarmentzekoa da 7. egunean prozesatuko laginetan funtzionalizatu gabeko hidrogelaren (H) erabilerak eragin murriztaile handiagoa izan zuela GMAe-rekin funtzionalizatutako hidrogelarekin baino. Hala ere, 21 egunen ondoren, α-SMA mailak konparagarriak izaten jarraitu zuten hidrogel tratamendu guztien artean,

hidrogelarekin tratatutako kornea guztietan fibrosia murriztu egin zela adieraziz. Hala, emaitzek funtzionalizatu gabeko hidrogela aplikatzeak ere, ez aplikatzea baino eragin antifibrotiko hobea eragiten zuela frogatu zuten.

Gelatina gehitzeak ehunaren erantzun fibrotikoan eragina izan dezake. Chen eta kolaboratzaileen arabera, GelMA-n kerazitoak txertatzeak hauen miofibroblastoetarako desberdintzapena eta ondoriozko erantzun fibrotikoa saihestu zuen. Arratoietako korneetan kirurgia egin eta hiru hilabetera ere, ez zuten erantzun fibrotikorik hauteman, eta kornea osasuntsu baten antzeko lodiera eta errefrakzio-ahalmenak erregistratu zituzten [507]. Gelatina sartzeari eta gainazalaren zurruntasunari dagokienez, Ibáñez eta kolaboratzaileek gelatina aplikatzearen eta gainazalaren zurruntasunaren arteko korrelazioa erakutsi zuten. GelMA hidrogelen zurruntasuna handitzeak miofibroblasto dermikoen aktibazioan eta fibrosiarekin lotutako gene eta proteinen adierazpenean (α-SMA) eragina zuela adierazi zuten [508]. Honetan oinarrituta, garatutako hidrogelek zurruntasun egokia zutela pentsa genezake, fibroblastoen indar kontraktilak murriztu eta erantzun fibrotiko handia ekidin zitzaketenak. Hala ere, hau lortutako emaitzetan oinarritutako hipotesi bat besterik ez da.

Immunofluoreszentziari dagokionez, α-SMA adierazpena erregistratu genuen bai estroman bai epitelioan. Aurretik egindako azterketek, kristalinoko zelula epitelialen α-SMA adierazpena, trantsizio epitelio-mesenkimalaren markatzailetzat hartu izan dute [509]. Gainera, TGF-β, SA-n edo GMAe-n dagoen hazkuntza-faktoreetako bat, trantsizio epitelio-mesenkimala kaltetutako kristalinoan sustatzen duela frogatu izan dute [510, 511]. Epitelioaren goiko aldeko α-SMA-ren adierazpena sagu eta untxiekin egindako azterlanetan ere dokumentatu izan dute [512, 513]. Hala ere, adierazpen horren zergatia ezezaguna da oraindik.

Epitelioko α-SMA positibotasunerako azalpen posible bat, trantsizio epitelio-mesenkimala jasaten duten zelulak, eta, beraz, α-SMA adierazten dutenak, zauria ixteko eta aurreko epitelio basaletik bereizteko migratzen dutenak izan daitezkeela izan liteke. Adierazpena eremu basalean edo apikalean kokatzea epitelioaren estratifikazio-abiaduraren araberakoa izan daiteke. Era berean, 21 egunen buruan adierazpen epitelialik ez izatearen arrazoia, aurretik α-SMA-rentzako positiboak ziren zelulak askatu izana izan daiteke.

Kornea-orbainentzako tratamendua eraginkorragoa da lesioaren ondorengo

lehen faseetan aplikatzen denean. Hantura eta fibrosia murrizteko tratamendu mediko nagusiak kortikosteroide topikoak dira. Prednisolona, dexametasona edo fluorometolona bezalako eragileak esparru klinikoan erabili ohi dira. Hala ere, hanturaren aurkako ahalmen eta kornean barneratzeko gaitasun desberdina dute [514, 515]. Ukipen-lente bereziek kasu arinenen ondorioak tratatu ahal dituzte [516], baina orbaina opakua eta sakona denean, ikusmen-galera eragiteraino, beharrezkoa da kornea aloinjertoa edo transplantea [517]. Kornearen opazifikazioa lehen asteetan mugatzeak kirurgia inbaditzailea, epe luzerako medikazioa eta jarraipen zehatza saihesten lagun dezake.

Chameettachal eta kolaboratzaileen lanak aurrerapen berriak lortu ditu, izan ere, keratozitoak transdiferentziaziorik jasan gabe kultibatzeko mikrogiro egokia sustatzen duen soluzioa erakutsi baitu. Frogatu dutenez, giza korneatik eratorritako zelulaz kanpoko matrizeko hidrogela eta behi-korneako hidrogel xenogenikoa erabiltzeak, orbaintzea eta kornea-opazifikazioa saihesten ditu, eta estromaren ohiko birsorkuntza erraztu [518, 519].

Gainera, hidrogeletan oinarritutako opakutasunaren murrizketari buruzko bi azterlan egin berri dira. Zelula ama mesenkimalez kargatutako gellam gomatik eratorritako hidrogelak, α-SMA bezalako fibrosi-markatzaileak kodetzen dituen ARNm adierazpena murriztea lortu du untxien estroman. Hidrogelak ere zelula ama mesenkimalen askapen motela frogatu du akats estromalean, opakutasun estromala saihestuz [520]. Halaber, giza zelula ama epitelial amniotikoetatik eratorritako keratozito estromalekin kargatutako gelMA hidrogelak kornea-ehunaren egitura eta mikrogiroa leheneratzeko lortu du. Proteoglikanoak jariatzeari esker, gardentasuna sustatu, hantura inhibitu eta fibrosia % 75 murriztea lortu du [521].

qPCR eta analisi immunohistokimikoen emaitzen arabera, tratamendu bakar batek ere ez zuen guztizko propietate antifibrotikorik frogatu. Fibrosia sortzeko potentziala desberdina izan zen tratamenduen artean, eta animaliaren beraren eragina ere izan zuen. Hala ere, hidrogela erabiltzeak eragin positiboa izan zuen fibrosiaren murrizketan.

α-SMA adierazpena hidrogel-tratamenduekin behera egiten zuenez, ondoriozta daiteke produktu horiek oso erakargarriak direla kornea-akatsei aurre egiteko.

3.5. Begiaren narritadura eta hantura

Hantura-zitokinen adierazpena azterketa pilotuan ateratako malkoetako proteina edukia erabiliz neurtu genuen. Balio fidagarrienak aurkeztu zituzten zitokinak hasierako hantura-erantzunari lotutakoak izan ziren.

Makrofagoen 1β proteina inflamatorioa (MIP-1β) makrofagoek eta monozitoek endotoxina bakterianoei edo IL-1β bezalako zitokina proinflamatorioei erantzunez sortutako faktorea da. Giza granulozitoak aktibatzen ditu (neutrofiloak, eosinofiloak eta basofiloak) eta neutrofiloek eragindako hantura akutuarekin lotzen da [522]. MMP-9-ak ZKM-ko proteinak degradatu eta ehunen birmoldaketa erregulatzeko zitokinak aktibatzen ditu. Neutrofiloek eta makrofagoek sortzen dute batez ere eta ehun eta gaixotasunetako hantura erregulatzen du [523]. IL-8-a lesio baten ondoren batez ere makrofagoek askatzen duten hanturarekin lotutako proteina da. Neutrofiloak eta beste zelula immunitario batzuk infekzioaren lekura erakartzeko funtsezkoa da [524]. Azkenik, NCAM-1 zelula dendritikoetan eta zelula ama neural edo mesenkimaletan ez ezik, T eta B linfozitoen eta NK zelulen azpimultzoetan ere adierazten da. Garunarekin lotutako hainbat prozesu biologikotan inplikatzeaz gain, beste funtzio biologiko batzuetan ere esku hartzen du, hala nola atxikipenean, migrazioan, ugaltzean edo zelulen desberdintzapenean [525].

Kirurgiaren ondorengoko egunean, kontrol zein H-SA taldeek MIP-1β, MMP-9 eta NCAM-1 adierazpen-baliorik altuenak erakutsi zituzten. Bi tratamenduen balioak gutxitu egin ziren laugarren egunean, kontrolarekin tratatutako korneetan MIP-1β zitokina izan ezik, horietan gutxitze progresiboagoa erregistratu baikenuen. Kirurgiaren ondorengoko 1. egunean, H-Ag-rekin tratatutako korneek MIP-1β, MMP-9 eta NCAM-1 adierazpen-baliorik baxuenak erakutsi zituzten, antigorputzaren hanturaren aurkako eragina erakutsiz.

Azterketaren 4. egunera arteko zitokinen adierazpenaren emaitzak Draize eskalaren bidez erregistratutako narritadura-balioekin bat zetozen. Kontrol eta H-SA taldeek puntuaziorik altuenak erakutsi zituzten azterketaren 2. egunean. Hala ere, 4. egunetik aurrera, zitokinen adierazpenaren emaitzak fidagarriagoak izan ziren Draizeren puntuazioak baino, arrayen teknologiak hantura txikiko testuinguru batean ere sentsibilitate altua erakutsi baitzuen.

Proba pilotuak izandako banako kopuru txikiaren ondorioz (n = 2 tratamendu

bakoitzerako), animalia bakoitzaren izaera indibidualak talde bakoitzak erregistratutako desbideratze handietan eragina izan zuen. Emaitzek tratamenduen gutxi gorabeherako joera erakutsi ziguten. Zoritxarrez, ezin izan genuen E02-E06 azterketetako laginen hantura ebaluatu, eta beraz, pilotuan erregistratutako joeraren baliozkotasuna berrestu.

E02-E06 esperimentuei dagokienez, Draizeren eskalako puntuazioek H-SA narritadura gutxien eragin zuen tratamendua izan zela adierazi zuten. H-Ag-k eta H-GMAe-k puntuazio altuagoak izan zituzten 3., 4. eta 5. egunetan, baina ia ez genuen narritadura seinalerik hauteman 6. egunetik aurrera.

H-Ag tratamenduak Draize eskalaren araberako narritadura-puntuazio handiagoak erakutsi bazituen ere, hidrogela antigorputzarekin funtzionalizatzea hantura murrizteko aukerarik onena izan zen, IL-1β-ren adierazpen genikoaren emaitzek erakutsi zuten bezala. Tratamendu honek kirurgiatik 7 egunetara hantura murriztu zuen, nahiz eta kontrolarekiko aldea estatistikoki esanguratsua ez izan. Hala ere, 21 egunen buruan alde esanguratsuak erregistratu genituen. Infliximab-en administrazio topikoaren bidez IL-1β mailen murrizpena begi gainazaleko orbaintze prozesuan frogatu izan dute aurretik [526]. Hala, kaltetutako korneetan Infliximab-a modu eraginkor eta seguruan sartzen zela egiaztatu zuten. Gainera, Infliximab-en instilazioa fornixeko fibrosi murrizketarekin eta konjuntibako hantura-zelulen infiltrazioa gutxitzearekin erlazionatu zuten. Ikerketak infliximab bidezko TNFα-ren blokeo topikoak hantura eta horren korneako, konjuntibako eta betazaletako kalteak murrizten zituela frogatu zuten. Guzti hau *in vivo* zein *ex vivo* esperimentuekin baieztatu zuten: alde batetik, kornearen gardentasunaren hobekuntzarekin, eta bestetik betazaletako CD45 hantura-zelulen infiltrazioaren eta hantura-zitokinen adierazpenaren murrizketarekin.

qPCR-aren emaitzen bidez, hanturaren murrizketarik nabarmenena 21 egunen ondoren H-GMAe tratamenduarekin ikusi genuen. H-GMAe-ren onurak GMAe-k dituen hazkuntza-faktore askorekin lotzen dira, kornea birsortzen laguntzen baitute. Hanturari dagokionez, GMAe-ren erabilerak zitokina proinflamatorioen ekoizpena murrizten du, TNFα eta IL-6 esaterako, baita antigenoak aurkezten dituzten zelula markatzaileen adierazpena ere, hala nola CD80, CD86 eta erantzun immunitarioak arautzen dituen 2. motako histokonpatibilitate-konplexu nagusiaren antigenoa. Gainera, hanturaren aurkako zitokinen mailen igoera eragiten du, hala nola IL-10

zitokinarena, eta horrek hantura murriztea eta infekzio-arriskua txikiagotzea dakar. Era berean, TGF-1 eta TGF-2-ren murrizketak fibrosia murrizten du. Hala, mekanismo guzti horiek batera zaurien sendatze eta birsortzea sustatzeko lankidetzan dihardute [113].

GMA-aren eta honen eratorrien propietate eta onurak sakon aztertu dira. IL-1ra (giza interleuzina-1 hartzailearen antagonista) eta IL-10, kornea-hantura ezabatzeko gai diren faktoreak, giza zelula epitelial amniotikoen hazkuntzetatik eratorritako medioetan identifikatu dituzte [527]. *In vitro* esperimentuek GMA substratu gisa erabiltzeak, lipopolisakaridoak eragindako IL-1α eta IL-1β gehitzea eragotz dezakeela frogatu dute [528]. Gainera, GMAe-z osatutako kolirioak, begi bakarreko LZAG kasuetan korneako epitelioaren orbaintzea sustatzeko eta konjuntibalizazioa eta baskularizazioa murrizteko eraginkorrak direla frogatu izan dute [433]. Horrez gain, GMA-ren osagai den HC-HA/PTX3-k (kate astuneko hialuronanpentraxina 3) hantura, angiogenesia eta orbaintzea eraginkortasunez prebenitzen dituela baieztatu dute, lehen aipatutako hazkuntza-faktoreez gain [529].

Aurkikuntza guzti horiek bat datoz kirurgia egin eta 21 egunera prozesatutako korneetan lortutako emaitzekin. Nabarmentzekoa da H-Ag eta H-GMAe-rekin tratatutako korneek, IL-1β-ren murrizketa handiena eskaini zuten bi hidrogelek hain zuzen, Draize eskala erabiliz egindako eguneroko ebaluazio klinikoan hantura-sintoma handienak erakutsi zituztela kirurgiaren ondorengo lehen egunetan, erredura eta gorritzea barne.

H-SA tratamenduari dagokionez, IL-1β-ren adierazpena handiagoa izan zen kirurgia egin eta 7 egunera kontrol tratamenduan baino. IL-1β-ren adierazpena H-SA-rekin tratatutako untxietan 21 egunetara prozesatutako laginen kontrolarekiko murriztu zen arren, aldeak ez ziren estatistikoki esanguratsuak izan. Hala ere, untxietan H-AS emateak Draize probaren puntuazioak murriztea eta gorritze eta erredura maila baxuagoak izatea eragin zuen, H-Ag eta H-GMAe tratamenduekin alderatuta.

SA-k kornea sendatzeko eta begi-gainazaleko gaixotasunak tratatzeko onurak izan ditzakeela erakutsi du, hala nola begi lehorraren gaixotasuna. Begi lehorra (BL) malko-geruzaren eta begi-gainazaleko faktore anitzek eragiten duten gaixotasuna da, non hantura gaixotasunaren mekanismo nagusia den. Malko-geruzaren lubrifikazio eta homeostasi eskasak ikusmen-alterazioak, narritadura, gorputz

arrotzaren sentsazioa, argiarekiko sentikortasuna eta azkura eragiten ditu, besteak beste [530]. BL larrirako, SA-z egindako kolirioak eta plaketetatik eratorritako kolirioak gomendatzen dituzte, malko artifizialen ordezko tratamendu gisa. Izan ere, odoletik eratorritako kolirioek lubrifikazioa emateaz gain, faktore gehigarriak ere badituzte, begi-gainazala hobetu eta zaurien orbaintzea erraztu dezaketenak. Aurreko ikerketek frogatu dute % 20 SA soluzioa eraginkorra eta klinikoki oso erabilia dela BL larriaren tratamenduan [412, 531–533], bai eta plaketetatik eratorritako kolirioa, hobekuntza esanguratsuak edo BL-ren desagerpena eragin dezakeela erakutsi baitu [534–536].

Hala ere, odol-eratorrien potentzial terapeutikoa malko naturalekin duten antzekotasunari egotz dakiokeenez, funtsezkoa da kontuan hartzea tratatutako pazientearen osasun orokorrak serumaren osaeran eragina izan dezakeela.

Serumaren konposizioa odolarenaren araberakoa da, beraz organismoaren momentuko osasun-egoerak osagaietan eragin dezake. Adbibidez, VEGF eta IL-6 mailak artritis erreumatoidea duten pazienteetan handiagoak direla frogatu dute [537], eta Sjögren sindromea duten pazienteen serumean zitokina proinflamatorioen maila altuak daudela, hala nola TNFα, IL-1β, IL-6 edo IL-8 [538, 539].

Beraz, argi dago serumean dauden faktoreen kantitatea eta kalitatea desberdinak direla, eta horrek eragina du, azken batean, odol-eratorrien eraginkortasunean eta tolerantzian. *In vivo* esperimenturako serumak kirurgiak eta tratamenduak egin aurretik atera genituen, eta, beraz, untxi osasuntsuen serumak zirela asumitu genuen.

3.6. Tratamenduen *in vivo* erantzun orokorra

Hidrogelekin tratatutako korneen artean, H-SA tratamenduak epitelioaren itxiera azkarragoa eragin zuen hidrogelen gainontzeko tratamenduekin alderatuta. Hau analisi immunohistokimikoan ikusitako Ki67-positibo zelula kopuru handiagoak berretsi zuen. Gainera, CK15 adierazpen altuko zelula multzoak ere ikusi genituen. Fibrosia eta hantura murrizteaz gain, qPCRan IL-1β eta α-SMA bitartez erregistratu zuten bezala, Draize eskalaren bidezko behaketa klinikoek suminkortasun-seinale minimoak erakutsi zituzten.

GMAe bidez funtzionalizatutako hidrogelek H-SA-en antzeko eragina izatea espero genuen. Hantura eta fibrosi erantzuna konparagarria izan bazen ere,

epitelioaren itxiera motelagoa izan zen eta *in vivo* narritadura-seinale handiagoak ikusi genituen.

Azkenik, H-Ag hidrogelak bere funtzio antiinflamatorio eta antifibrotikoa frogatu zuen, qPCR erregistroetan IL-1β eta α-SMA mailak murriztean. Zaurien itxieraren bilakaera motelagoa izan zen, eta hori immunohistokimika bidez Ki67 zelula positibo gutxiago erregistratzearekin berretsi genuen. H-AS-rekin batera, tratatutako kornea guztiek zauriak itxi zituzten. *In vivo* narritadura eta hanturari dagokienez, H-Ag-k suminkortasun seinale handienak sortzen zituela ikusi genuen. Hala ere, balioak gutxieneko narritadura edo ia suminkortasunik gabeko mailaren barruan kokatu ziren uneoro.

Oro har, hidrogela funtzionalizatuta edo funtzionalizatu gabe sartzeak zauriaren orbaintzea hobetu zuen. Hidrogelekin tratatutako korneek hantura eta erantzun fibrotikoa murriztu, qPCR bidez IL-1β eta α-SMA-ren jaitsierak erakutsi bezala, eta kasu guztietan berrepitelizazioa lortu zuten.

4. Linboko zelula primarioen karakterizazioa

LZAG-a tratatzeko linboko ordezko baten garapena ere gure helburuetako bat izan da. Hori lortzeko, bi ikerketa-eremu nagusi identifikatu ditugu: Ordezko horren sintesia eta hauetan sartuko diren zelula-hazkuntzen optimizazioa.

Ehun-ingeniaritza bidez sortutako ordezko edo euskarriek ZKM-ren konposizioa, egitura eta propietateak imitatzen dituen inguru bat erreproduzitu behar dute *in vivo*, zelulei seinale biologiko eta fisiko-kimikoak eskaintzeaz gainera. ZKM-a hiru dimentsiotako egitura bigun, erresistente eta elastikoa da eta ehunen eta organoen egitura eusten eta mantentzen du. Polisakaridoen nahasketa batek eta proteina mota ezberdinek osatzen dute, hala nola kolagenoak, elastinak eta fibronektinak. Funtsezko funtzioak betetzen ditu garraioan, zelulen arteko komunikazioan, mekanotransdukzioan eta hazkuntza-faktoreen seinaleztapenean, zelula hartzaileekiko elkarreraginen, hazkuntza-faktoreen eta seinaleztapeneko beste molekula batzuen arteko loturen bidez.

Linboko ordezkoaren garapena tesi honetatik kanpo geratu da. Hala ere, giza korneetatik erauzitako zelula primarioen karakterizazioa landu dugu. Hala, analisi

immunohistokimikoak eta immunozitokimikoak egin ditugu LEZA/P-en ezaugarriak eta linboko nitxoan dauden zelulen populazio ezberdinak zehazteko.

LEZA/P-ak linboko nitxoan bizi dira eta korneako homeostasi epiteliala mantentzen dute. Zelula amen linboko nitxoak ZKM-ren konposizio berezia, linboko baskulatura eta LEZA/P-en izatea arautzen duten linboko nitxoaren inguruko zelulak ditu ezaugarri. Linboko nitxoaren inguruko zelula hauek, mantentzeko eta bereizteko funtsezko seinale molekularrak ematen dizkiete LEZA/P-ei [24, 540–542].

Zelula primarioen hazkuntzei dagokionez, CK15 markaketa positiboa ikusi genuen zitospinetik zuzenean isolatutako zelula epitelialetan, baita zenbait zelula bimentina-positibo ere. Ehunen digestio bidez erauzitako zelula CK15-positiboen ehuneko altuak (% 40 inguru) eta estromako zelulen hazkuntzetan markatzaile horren adierazpenik ezak, zelulak isolatzeko erabilitako metodoa balioetsi zuten, populazio epitelial eta estromal nahiko garbiak lortu baikenituen. CK15 zitokeratinaren adierazpena paseetan zehar murriztu zen bitartean, bimentinaren adierazpena handitu zen, eta zelula bimentina-positiboek zelula estromal bereizien antzeko morfologia erakutsi zuten. Horrek, hazkuntza zelularrak zelula ama epitelialak kontserbatzeari lehentasuna eman ezean, zelula estromalak azkar ugaldu daitezkeela eta epitelialak gainditu ditzaketela iradokitzen du.

Zitokeratinez gain, p63 transkripzio-faktorea korneako laginetan zelula amak daudela ziurtatzeko ere erabiltzen da. Zehazki, ΔNp63α isoforma linboko nitxoan kokatutako zelula amen markatzaile positibo gisa identifikatu dute [543].

Ehun esklerokornealetatik erauzitako zelula epitelialek ΔNp63α tindaketa positiboa erakutsi zuten. Hala ere, ΔNp63α mailen jaitsiera nabarmena erregistratu genuen pase batetik bestera. Giza linboko explanteen hazkuntzetan p63-aren murrizketa ere deskribatu izan dute. Joseph eta kolaboratzaileek 1-3 astez mantendutako zelulen hazkuntzetan p63 zelula positiboen murrizketa ematen zela adierazi zuten. Ikerketa horrek, p63-a linboko zelula amen eta zelula anplifikatzaile iragankorren markatzailea izan zitekeela iradoki zuen. Hala, p63-ren murrizketa hori zelulak konfluentziara iritsi osteko proliferazioaren jaitsierarekin lotuta dagoela ondorioztatu zuten [544].

Gainera, Rama eta kolaboratzaileek terapia zelularrak arrakasta izan dezan p63 zelula distiratsu gutxieneko bat behar dela frogatu zutenetik, ΔNp63α markatzailea

zelulan amak identifikatzeko ustezko markatzaile gisa erabili izan da linboko biopsien hazkuntza zelularretan [545]. Holoclar zelula ametan oinarritutako tratamendua da, eta LZAG moderatua edo larria duten paziente helduen korneako epitelioa birsortzeko erabiltzen da [56]. Tratamendua 1-2 mm^2 biopsia baten bidez pazientearen linbo osasuntsutik zelulak ateratzean datza. Biopsia hori *ex vivo* kultibatu egiten da ondoren transplantatzeko. Zelulak kultibatzearen helburua hasierako biopsiako ahalik eta zelula ama gehien berreskuratzea da eta ΔNp63α zelula amen ustezko markatzailea erabiltzen da hauek identifikatzeko.

Ez genuen CK15 zelula positiborik ikusi zelula estromalen hazkuntzetan. Hazkuntza hauetako markatzaile nagusia bimentina izan zen. Hazkuntza hauetan zelula guztiak norabide berean lerrokatuta ikusi genituen, korneako estroman edukiko luketen antolamendua imitatuz [12].

Melan A markatzaileari dagokionez, egindako behaketek melanozitoen eta linboko zelula ama epitelialen arteko erlazio espezifikoa iradoki zuten. Fenotipo zelular adarkatua zuten Melan A zelula positiboak detektatu genituen kripta linbarretan, eratzen ari ziren kolonia epitelialen inguruko melanozitoekin bat zetorrena. Gainera, ΔNp63α, CK15 eta Melan A markatzaileen adierazpenaren aldi bereko murrizketa erregistratu genuen pase batetik bestera.

Dziasko eta kolaboratzaileen arabera, melanozitoek eta linboko zelula amek harreman estua mantentzen dute nitxoan [26, 546], non melanozitoek bereizi gabeko zelulak babesteko funtzioa duten [24, 547]. Bi markatzaileen murrizketa paraleloa bat dator melanozitoek zelulen ama izate hori mantentzeko duten ustezko funtzioarekin. Gainera, korneako zelula epitelialen hazkuntzetan hautemandako bimentinaren adierazpen faltarekin lotuta egon daiteke, Polisettik eta kolaboratzaileek, melanozitoen hazkuntzek Melan A zein bimentina adierazten zutela frogatu baitzuten [548]. Gainera, epitelioan behatutako zelula adarkatuak ere Langerhansen zelulekin lotuta egon daitezke, melanozitoak bezala, linboaren geruza basalean baitaude eta bimentina adierazten baitute [549–552].

Linboko zelulak nitxotik isolatzea erronka bat bada ere, zelula horiek LEZA/P-en xedea *in vitro* zein *in vivo* erabakitzeko gaitasuna dute [547, 553–555]. Beraz, LEZA/P-en eta linboko melanozitoen arteko lotura estuak aukera ematen du haien aplikazioa *in vitro* ikertzeko eta LEZA/P-en ama izatea mantentzen duten hazkuntza-baldintzak hobetzeko. Ikuspegi horri esker, hazkuntza zelula ama

gehiagorekin aberastu daiteke, eta, hala, haien eraginkortasuna handitu begien birsorkuntzako terapia aurreratuetan edo ehun-ingeniaritzako produktuetan.

Linboko melanozitoen eta linboko zelula epitelialen hazkuntza bateratuak edo 3T3 fibroblastoen ordez melanozito hauek hazkuntza-geruza gisa erabiltzeak, LEZA/P-en zelula amen fenotipoa eta klonak osatzeko gaitasuna mantentzen dituela frogatu dute [556]. Melanozitoek profil immunogeniko baxua eta ezaugarri antiangiogenikoak dituztenez, egokiak dira LZAG duten pazienteentzako zelula amen terapiak hobetzeko. Horrek saguetatik eratorritako 3T3 fibroblastoen erabilera ezabatzen du, molekula xenogenikoen bidezko kutsadura, immunitate-errefusa eta espezieen arteko birus-transmisioa dela-eta, arazo etikoak eta segurtasunekoak sortzen baitituzte.

Gainera, ehun-ingeniaritza bidez sortutako korneako euskarri epitelialetan, linboko melanozitoek LEZA/P-ak ugaltzea eta mantentzea errazten dutela erakutsi dute [547, 548, 557]. Halaber, bi zelula mota horiek fibrinazko hidrogeletan batera kultibatzeak geruza anitzeko eraikuntza epitelialak 10 egunetan sortzean eragiten dutela frogatu dute [548].

Ikerketa guzti horiek, begiaren gainazala berrezartzeko ordezkoen sintesian linboko melanozitoak sartzeak, LEZA/P-en ama izatea mantentzen eta tratamenduaren eraginkortasuna hobetzen lagun dezaketela iradokitzen dute. Beraz, funtsezkoa da LEZA/P-ekin duten elkarreragina hobeto ulertzea, LZAG-a tratatzeko terapia zelularrak edo ehun-ingeniaritzako ordezkoak garatzeko duten ahalmenaz baliatzeko.

VI. ONDORIOAK

1. Proteinetan oinarritutako lau biofilmen karakterizazioak, fabrikazio-metodoaren eta erretikulazio motaren arabera, material hauek zelulen hazkuntzarako zitobateragarriak izan daitezkeela edo ez iradokitzen du. Fisikoki konprimatutako eta erretikulatutako KOL eta SPI filmen eta kimikoki erretikulatutako GEL filmen artean, gelatina da hidrogelak garatzeko hautagairik egokiena. Gainera, proba enpirikoek, RFP-k gelatinaren beraren talde funtzionalekin erreakziona dezakeela adierazten dute.

2. Gelatina-RFP hidrogelak antzeko biobateragarritasun zelularra eta propietate erreologikoak mantetzen ditu dextranoa, azido hialuronikoa edo metilzelulosa bezalako osagaiak gehitzen zaizkionean ere. Hala ere, osagai horiek gehitzeak ezaugarri optikoak murriztu eta hidrogelaren puztea areagotzen du, hidrogela korneako zauriari atxikitzea eta egokitzea zailduz. Beraz, gelatina-RFP hidrogela konposizio sinpleena eta funtzionalena dela esan daiteke.

3. Infliximab edo guk prestatutako odol-eratorriekin funtzionalizatutako gelatina-RFP hidrogelak, TNFα bidez estimulatutako zelula hazkuntzen hantura modu eraginkorrean murrizten du. Hantura-egoeretan eraginkorra izateak *in vitro* hazitako inflamatu gabeko zeluletan sortzen den hantura intrintsekoa indargabetzen du.

4. Gelatina-RFP hidrogela *ex vivo* eta *in vivo* egindako korneako zauriei atxikitzen zaie, hidrogelaren gaineko hazkuntza epiteliala sustatuz. Hidrogela erabiltzeak, funtzionalizatu gabe egonda ere, zauria orbaintzeko erantzun orokorra hobetzen du *in vivo*. Horren erakusle dira hantura murriztea, berrepitelizazioa sustatzea eta erantzun fibrotikoa gutxitzea. Ezin dugu hidrogel bakarra tratamendu optimo gisa hautatu, baina SA-rekin funtzionalizatutako hidrogelak berrepitelizaziorik azkarrena, narritadura sintoma kliniko txikiagoak eta fibrosi-maila txikiena erakutsi ditu 21 egunera. Hala ere, H-Ag eta H-GMAe-k hanturaren murrizketa handiagoa erakutsi dute.

5. Korneako birsorkuntzarako beharrezkoa den linboko nitxoa mantentzeari dagokionez, zelula amen eta melanozitoen markatzaileak aldi berean gutxitzeak LEZA/P-en hazkuntza primarioen eta linboko nitxoko melanozitoen arteko lotura estua iradokitzen du. Haien elkarreragina ulertzeak, LZAG-aren tratamenduan transplantea egin aurretik LEZA/P-en funtzioa eta fenotipoa zaintzen dituzten hazkuntza-baldintza berriak garatzen lagun dezake.

EAI-en tratamenduen eta korneako ultzeren beharrari erantzunez, gelatinatik eta RFP-tik abiatuta garatutako eta odol-eratorriekin, GMAe-rekin edo hanturaren aurkako antigorputz batekin funtzionalizatutako hidrogelak, berrepitelizazioa erraztu eta birsortze mekanismoak sustatzen dituen tratamendua dela erakutsi du, fibrosia murriztuz, hantura-maila kontrolatuz eta begiaren osasuna lehengoratuz. Tratamendua klinikan aplikatzeko erraza dela frogatu dugu, beharrezko interbentzioen kopurua hidrogela lehen bisitan bakarrik aplikatzera eta antibiotikoa epitelioa itxi arte aplikatzera murriztuz.

Era berean, LEZA/P-en hazkuntza primarioen karakterizazioak eta linbo esklerokornealean dauden beste zelula batzuekin (melanozitoekin, esaterako) duten erlazioak ulertzeak bide bat ireki dute etorkizuneko kornea-ordezkoetarako beharrezkoak diren hazkuntza-baldintzak optimizatzeko. Ordezko horiek LEZA/P-en hazkuntza sustatzeko eta gaur egun LZAG-a tratatzeko erabiltzen diren emaileen transplanteei alternatiba bat eskaintzeko sortuko dira.

REFERENCES

1. Gipson, I. K. The ocular surface: The challenge to enable and protect vision. The Friedenwald lecture. *Investigative Ophthalmology and Visual Science* **48** (10 2007).
2. Adler, F. H. Adler's Physiology of the Eye. *RA Moses (St. Louis: The CV Mosby Company 1981)* (2011).
3. Viitaja, T., Moilanen, J., Svedström, K. J., Ekholm, F. S. & Paananen, R. O. Tear Film Lipid Layer Structure: Self-Assembly of O-Acyl-ω-hydroxy Fatty Acids and Wax Esters into Evaporation-Resistant Monolayers. *Nano Letters* **21** (18 2021).
4. Aldeen, S. & AlRyalat, S. *Eye Yield* (2021).
5. Forrester, J. V., Dick, A. D., McMenamin, P. G., Roberts, F. & Pearlman, E. *Anatomy of the eye and orbit* 2016.
6. Eghrari, A. O., Riazuddin, S. A. & Gottsch, J. D. Overview of the Cornea: Structure, Function, and Development. *Progress in Molecular Biology and Translational Science* **134** (2015).
7. Del Monte, D. W. & Kim, T. Anatomy and physiology of the cornea. *Journal of Cataract and Refractive Surgery* **37** (3 2011).
8. Sridhar, M. S. Anatomy of cornea and ocular surface. *Indian Journal of Ophthalmology* **66** (2 2018).
9. Ljubimov, A. V. *et al.* Human corneal basement membrane heterogeneity: Topographical differences in the expression of type IV collagen and laminin isoforms. *Laboratory Investigation* **72** (4 1995).
10. Dawson, D. G., Ubels, J. L. & Edelhauser, H. F. *Cornea and Sclera* 2011.
11. Wilson, S. E. Bowman's layer in the cornea - structure and function and regeneration. *Experimental Eye Research* **195** (2020).
12. Espana, E. M. & Birk, D. E. Composition, structure and function of the corneal stroma. *Experimental Eye Research* **198** (2020).

13. Ruberti, J. W. & Zieske, J. D. Prelude to corneal tissue engineering - Gaining control of collagen organization. *Progress in Retinal and Eye Research* **27** (5 2008).
14. Komai, Y. & Ushiki, T. The three-dimensional organization of collagen fibrils in the human cornea and sclera. *Investigative Ophthalmology and Visual Science* **32** (8 1991).
15. Funderburgh, J. L., Mann, M. M. & Funderburgh, M. L. Keratocyte phenotype mediates proteoglycan structure: A role for fibroblasts in corneal fibrosis. *Journal of Biological Chemistry* **278** (46 2003).
16. Zhivov, A., Stave, J., Vollmar, B. & Guthoff, R. In vivo confocal microscopic evaluation of Langerhans cell density and distribution in the normal human corneal epithelium. *Graefe's Archive for Clinical and Experimental Ophthalmology* **243** (10 2005).
17. Mousa, H. M., Saban, D. R. & Pérez, V. L. The cornea IV immunology, infection, neovascularization, and surgery chapter 1: Corneal immunology. *Experimental Eye Research* **205** (2021).
18. Kamil, S. & Mohan, R. R. Corneal stromal wound healing: Major regulators and therapeutic targets. *Ocular Surface* **19** (2021).
19. Medeiros, C. S. & Santhiago, M. R. Corneal nerves anatomy, function, injury and regeneration. *Experimental Eye Research* **200** (2020).
20. Dua, H., Faraj, L., Said, D., Gray, T. & Lowe, J. Human corneal anatomy redefined: A novel pre-descemet's layer (Dua's Layer). *Ophthalmology* **120** (9 2013).
21. Massoudi, D., Malecaze, F. & Galiacy, S. D. Collagens and proteoglycans of the cornea: importance in transparency and visual disorders. *Cell and Tissue Research* **363** (2 2016).
22. De Oliveira, R. C. & Wilson, S. E. Descemet's membrane development, structure, function and regeneration. *Experimental Eye Research* **197** (2020).
23. Davanger, M. & Evensen, A. Role of the pericorneal papillary structure in renewal of corneal epithelium. *Nature* **229** (5286 1971).
24. Polisetti, N., Zenkel, M., Menzel-Severing, J., Kruse, F. E. & Schlötzer-Schrehardt, U. Cell Adhesion Molecules and Stem Cell-Niche-Interactions in the Limbal Stem Cell Niche. *Stem Cells* **34** (1 2016).

25. Yazdanpanah, G., Jabbehdari, S. & Djalilian, A. R. Limbal and corneal epithelial homeostasis. *Current Opinion in Ophthalmology* **28** (4 2017).
26. Dziasko, M. A. & Daniels, J. T. Anatomical Features and Cell-Cell Interactions in the Human Limbal Epithelial Stem Cell Niche. *Ocular Surface* **14** (3 2016).
27. González, S., Oh, D., Baclagon, E. R., Zheng, J. J. & Deng, S. X. Wnt signaling is required for the maintenance of human limbal stem/progenitor cells in vitro. *Investigative Ophthalmology and Visual Science* **60** (1 2019).
28. González, S., Uhm, H. & Deng, S. X. Notch Inhibition Prevents Differentiation of Human Limbal Stem/Progenitor Cells in vitro. *Scientific Reports* **9** (1 2019).
29. González, S., Halabi, M., Ju, D., Tsai, M. & Deng, S. X. Role of Jagged1-mediated Notch Signaling Activation in the Differentiation and Stratification of the Human Limbal Epithelium. *Cells* **9** (9 2020).
30. Kolios, G. & Moodley, Y. Introduction to stem cells and regenerative medicine. *Respiration* **85** (1 2013).
31. Hertsenberg, A. J. & Funderburgh, J. L. Stem Cells in the Cornea. *Progress in Molecular Biology and Translational Science* **134** (2015).
32. Pellegrini, G. *et al.* Location and clonal analysis of stem cells and their differentiated progeny in the human ocular surface. *Journal of Cell Biology* **145** (4 1999).
33. Secker, G. A. & Daniels, J. T. Limbal epithelial stem cells of the cornea. *StemBook* (2009).
34. Bonnet, C. *et al.* Human limbal epithelial stem cell regulation, bioengineering and function. *Progress in Retinal and Eye Research* **85** (2021).
35. Schlötzer-Schrehardt, U. & Kruse, F. E. Identification and characterization of limbal stem cells. *Experimental Eye Research* **81** (3 2005).
36. Watanabe, K. *et al.* Human limbal epithelium contains side population cells expressing the ATP-binding cassette transporter ABCG2. *FEBS Letters* **565** (1-3 2004).
37. Yoshida, S. *et al.* Cytokeratin 15 can be used to identify the limbal phenotype in normal and diseased ocular surfaces. *Investigative Ophthalmology and Visual Science* **47** (11 2006).
38. Hayashi, R. *et al.* N-Cadherin Is Expressed by Putative Stem/Progenitor Cells and Melanocytes in the Human Limbal Epithelial Stem Cell Niche. *Stem Cells* **25** (2 2007).

39. Merjava, S., Neuwirth, A., Tanzerova, M. & Jirsova, K. The spectrum of cytokeratins expressed in the adult human cornea, limbus and perilimbal conjunctiva. *Histology and Histopathology* **26** (3 2011).
40. Ksander, B. R. *et al.* ABCB5 is a limbal stem cell gene required for corneal development and repair. *Nature* **511** (7509 2014).
41. Kawasaki, S., Tanioka, H., Yamasaki, K., Connon, C. J. & Kinoshita, S. Expression and tissue distribution of p63 isoforms in human ocular surface epithelia. *Experimental Eye Research* **82** (2 2006).
42. Pellegrini, G. *et al.* p63 identifies keratinocyte stem cells. *Proceedings of the National Academy of Sciences of the United States of America* **98** (6 2001).
43. Truong, T. T., Huynh, K., Nakatsu, M. N. & Deng, S. X. SSEA4 Is a Potential Negative Marker for the Enrichment of Human Corneal Epithelial Stem/Progenitor Cells. *Investigative Ophthalmology and Visual Science* **52** (9 2011).
44. Yang, K., Jiang, Z., Wang, D., Lian, X. & Yang, T. Corneal epithelial-like transdifferentiation of hair follicle stem cells is mediated by pax6 and β-catenin/Lef-1. *Cell Biology International* **33** (8 2009).
45. Yang, Y. & Mlodzik, M. Wnt-Frizzled/Planar Cell Polarity Signaling: Cellular Orientation by Facing the Wind (Wnt). *Annual Review of Cell and Developmental Biology* **31** (2015).
46. Pellegrini, G., Rama, P., Mavilio, F. & De Luca, M. Epithelial stem cells in corneal regeneration and epidermal gene therapy. *Journal of Pathology* **217** (2 2009).
47. Majo, F., Rochat, A., Nicolas, M., Jaoudé, G. A. & Barrandon, Y. Oligopotent stem cells are distributed throughout the mammalian ocular surface. *Nature* **456** (7219 2008).
48. Thoft, R. A. & Friend, J. The X, Y, Z hypothesis of corneal epithelial maintenance. *Investigative Ophthalmology and Visual Science* **24** (10 1983).
49. Hanna, C. & O'brien, J. E. Cell Production and Migration in the Epithelial Layer of the Cornea. *Archives of Ophthalmology* **64** (4 1960).
50. Sharma, A. & Coles, W. H. Kinetics of corneal epithelial maintenance and graft loss: A population balance model. *Investigative Ophthalmology and Visual Science* **30** (9 1989).
51. Vazirani, J. *et al.* Limbal Stem Cell Deficiency—Demography and Underlying Causes. *American Journal of Ophthalmology* **188** (2018).

52. Deng, S. X. *et al.* Global consensus on definition, classification, diagnosis, and staging of limbal stem cell deficiency. *Cornea* **38** (3 2019).
53. Deng, S. X. *et al.* Global Consensus on the Management of Limbal Stem Cell Deficiency. *Cornea* **39** (10 2020).
54. Singh, V., Tiwari, A., Kethiri, A. R. & Sangwan, V. S. Current perspectives of limbal-derived stem cells and its application in ocular surface regeneration and limbal stem cell transplantation. *Stem Cells Translational Medicine* **10** (8 2021).
55. Calonge, M. *et al.* Goals and challenges of stem cell-based therapy for corneal blindness due to limbal deficiency. *Pharmaceutics* **13** (9 2021).
56. European Medicine Agency. *Summary of the European public assessment report (EPAR) for Holoclar* Feb. 2015.
57. Wilson, S. E., Marino, G. K., Torricelli, A. A. & Medeiros, C. S. Injury and defective regeneration of the epithelial basement membrane in corneal fibrosis: A paradigm for fibrosis in other organs? *Matrix Biology* **64** (2017).
58. Lu, L., Reinach, P. S. & Winston, W. Y. Corneal epithelial wound healing. *Experimental Biology and Medicine* **226** (7 2001).
59. Ljubimov, A. V. & Saghizadeh, M. Progress in Retinal and Eye Research Progress in corneal wound healing. *Progress in Retinal and Eye Research* **49** (2015).
60. Müller, L. J., Marfurt, C. F., Kruse, F. & Tervo, T. M. Corneal nerves: Structure, contents and function. *Experimental Eye Research* **76** (5 2003).
61. Reid, T. W., Murphy, C. J., Iwahashi, C. K., Foster, B. A. & Mannis, M. J. Stimulation of epithelial cell growth by the neuropeptide substance P. *Journal of Cellular Biochemistry* **52** (4 1993).
62. Garcia-Hirschfeld, J., Lopez-Briones, L. G. & Belmonte, C. Neurotrophic influences on corneal epithelial cells. *Experimental Eye Research* **59** (5 1994).
63. Lambiase, A., Bonini, S., Aloe, L., Rama, P. & Bonini, S. Anti-inflammatory and healing properties of nerve growth factor in immune corneal ulcers with stromal melting. *Archives of Ophthalmology* **118** (10 2000).
64. Medeiros, C. S., Marino, G. K., Santhiago, M. R. & Wilson, S. E. The corneal basement membranes and stromal fibrosis. *Investigative Ophthalmology and Visual Science* **59** (10 2018).
65. Torricelli, A. A., Santhanam, A., Wu, J., Singh, V. & Wilson, S. E. The corneal fibrosis response to epithelial-Stromal injury. *Experimental Eye Research* **142** (2016).

66. Santhanam, A., Marino, G. K., Torricelli, A. A. & Wilson, S. E. EBM regeneration and changes in EBM component mRNA expression in stromal cells after corneal injury. *Molecular Vision* **23** (2017).

67. Mohan, R. R. *et al.* Apoptosis, necrosis, proliferation, and myofibroblast generation in the stroma following LASIK and PRK. *Experimental Eye Research* **76** (1 2003).

68. He, J. & Bazan, H. E. Synergistic effect of platelet-activating factor and tumor necrosis factor-α on corneal myofibroblast apoptosis. *Investigative Ophthalmology and Visual Science* **47** (3 2006).

69. Fine, B. S. & Yannof, M. *Ocular Histology. A Text and Atlas* Second edition, 196–247 (Harper & Row, 1979).

70. Bukowiecki, A., Hos, D., Cursiefen, C. & Eming, S. A. Wound-healing studies in cornea and skin: Parallels, differences and opportunities. *International Journal of Molecular Sciences* **18** (6 2017).

71. Li, Z., Burns, A. R., Han, L., Rumbaut, R. E. & Smith, C. W. IL-17 and VEGF are necessary for efficient corneal nerve regeneration. *American Journal of Pathology* **178** (3 2011).

72. Roshandel, D. *et al.* Current and emerging therapies for corneal neovascularization. *Ocular Surface* **16** (4 2018).

73. Liu, Q., Smith, C. W., Zhang, W., Burns, A. R. & Li, Z. NK cells modulate the inflammatory response to corneal epithelial abrasion and thereby support wound healing. *American Journal of Pathology* **181** (2 2012).

74. Jester, J. V. & Ho-Chang, J. Modulation of cultured corneal keratocyte phenotype by growth factors/cytokines control in vitro contractility and extracellular matrix contraction. *Experimental Eye Research* **77** (5 2003).

75. Garana, R. M. *et al.* Radial keratotomy: II. Role of the myofibroblast in corneal wound contraction. *Investigative Ophthalmology and Visual Science* **33** (12 1992).

76. Jester, J. V., Petroll, W. M., Barry, P. A. & Cavanagh, H. D. Expression of α-smooth muscle (α-SM) actin during corneal stromal wound healing. *Investigative Ophthalmology and Visual Science* **36** (5 1995).

77. Pietraszkiewicz, A. *et al.* Desmin deficiency is not sufficient to prevent corneal fibrosis. *Experimental Eye Research* **180** (2019).

78. Chen, Y., Thompson, D. C., Koppaka, V., Jester, J. V. & Vasiliou, V. Ocular aldehyde dehydrogenases: Protection against ultraviolet damage and

maintenance of transparency for vision. *Progress in Retinal and Eye Research* **33** (1 2013).

79. Wilson, S. E. Corneal myofibroblasts and fibrosis. *Experimental Eye Research* **201** (2020).
80. Wilson, S. E. Corneal wound healing. *Experimental Eye Research* **197,** 108089 (2020).
81. Sumioka, T. *et al.* Inhibitory effect of blocking TGF-β/Smad signal on injury-induced fibrosis of corneal endothelium. *Molecular Vision* **14** (2008).
82. Lee, J. G., Ko, M. H. K. & Kay, E. D. P. Endothelial mesenchymal transformation mediated by IL-1β-induced FGF-2 in corneal endothelial cells. *Experimental Eye Research* **95** (1 2012).
83. Miyamoto, T., Sumioka, T. & Saika, S. Endothelial mesenchymal transition: a therapeutic target in retrocorneal membrane. *Cornea* **29 Suppl 1** (2010).
84. Al-Saleh, G. S. & Alfawaz, A. M. Management of traumatic corneal abrasion by a sample of practicing ophthalmologists in Saudi Arabia. *Saudi Journal of Ophthalmology* **32** (2 2018).
85. Vaidyanathan, U. *et al.* Persistent Corneal Epithelial Defects: A Review Article. *Medical Hypothesis, Discovery, and Innovation in Ophthalmology* **8** (3 2019).
86. Wilson, S. E., Medeiros, C. S. & Santhiago, M. R. Pathophysiology of corneal scarring in persistent epithelial defects after PRK and other corneal injuries. *Journal of Refractive Surgery* **34** (1 2018).
87. Moon, H. S., Li, L., Yoon, H. J., Ji, Y. S. & Yoon, K. C. Effect of epidermal growth factor ointment on persistent epithelial defects of the cornea. *BMC Ophthalmology* **20** (1 2020).
88. Lange, A. P., Moloney, G., Sheldon, C. A., Sasaki, S. & Holland, S. P. Bilateral corneal ulceration caused by vitamin A deficiency in eosinophilic gastroenteropathy. *Case Reports in Ophthalmology* **2** (3 2011).
89. Wirostko, B., Rafii, M. J., Sullivan, D. A., Morelli, J. & Ding, J. Novel Therapy to Treat Corneal Epithelial Defects: A Hypothesis with Growth Hormone. *Ocular Surface* **13** (3 2015).
90. Ziaei, M., Greene, C. & Green, C. R. Wound healing in the eye: Therapeutic prospects. *Advanced Drug Delivery Reviews* **126** (2018).

91. Gire, A., Mathews, P., Cui, D. & Akpek, E. K. Long-term Corneal Complications in Patients with Primary Sjögren's Syndrome. *Investigative Ophthalmology & Visual Science* **61,** 339–339 (2020).
92. Vajpayee, R. B. *et al.* Evaluation of umbilical cord serum therapy for persistent corneal epithelial defects. *British Journal of Ophthalmology* **87** (11 2003).
93. Berman, M., Manseau, E., Law, M. & Aiken, D. Ulceration is correlated with degradation of fibrin and fibronectin at the corneal surface. *Investigative Ophthalmology and Visual Science* **24** (10 1983).
94. Katzman, L. R. & Jeng, B. H. Management strategies for persistent epithelial defects of the cornea. *Saudi Journal of Ophthalmology* **28** (3 2014).
95. Blackmore, S. J. The use of contact lenses in the treatment of persistent epithelial defects. *Contact Lens and Anterior Eye* **33** (5 2010).
96. Jacobs, D. S. *et al.* CLEAR – Medical use of contact lenses. *Contact Lens and Anterior Eye* **44** (2 2021).
97. Pastor, J. C. & Calonge, M. Epidermal growth factor and corneal wound healing: A multicenter study. *Cornea* **11** (4 1992).
98. Lambiase, A., Rama, P., Bonini, S., Caprioglio, G. & Aloe, L. Topical Treatment with Nerve Growth Factor for Corneal Neurotrophic Ulcers. *New England Journal of Medicine* **338.** PMID: 9554857, 1174–1180 (1998).
99. Pflugfelder, S. C. *et al.* Topical Recombinant Human Nerve Growth Factor (Cenegermin) for Neurotrophic Keratopathy: A Multicenter Randomized Vehicle-Controlled Pivotal Trial. *Ophthalmology* **127** (1 2020).
100. Yamada, N. *et al.* Open clinical study of eye-drops containing tetrapeptides derived from substance P and insulin-like growth factor-1 for treatment of persistent corneal epithelial defects associated with neurotrophic keratopathy. *British Journal of Ophthalmology* **92** (7 2008).
101. Cai, J. Q. *et al.* Toxicology study of long-term administration of rhKGF-2 eye drops on rabbit corneas. *Regulatory Toxicology and Pharmacology* **103** (2019).
102. Ergen, S. K., Subasi, S., Rencber, S. F., Duruksu, G. & Yazir, Y. Evaluation of clinical and histological effects of KGF-2 and NGF on corneal wound healing in an experimental alkali burn rabbit model. *Experimental Eye Research* **223** (2022).
103. Jeng, B. H. *et al.* Exploratory Phase II Multicenter, Open-Label, Clinical Trial of ST266, a Novel Secretome for Treatment of Persistent Corneal Epithelial Defects. *Translational Vision Science and Technology* **11** (1 2022).

104. Diaz-Valle, D. *et al.* Topical insulin for refractory persistent corneal epithelial defects. *European Journal of Ophthalmology* **31** (5 2021).

105. Diaz-Valle, D. *et al.* Comparison of the efficacy of topical insulin with autologous serum eye drops in persistent epithelial defects of the cornea. *Acta Ophthalmologica* **100** (4 2022).

106. Tsubota, K., Goto, E., Shimmura, S. & Shimazaki, J. Treatment of persistent corneal epithelial defect by autologous serum application. *Ophthalmology* **106** (10 1999).

107. Noble, B. A. *et al.* Comparison of autologous serum eye drops with conventional therapy in a randomised controlled crossover trial for ocular surface disease. *British Journal of Ophthalmology* **88** (5 2004).

108. Liu, L. *et al.* Corneal epitheliotrophic capacity of three different blood-derived preparations. *Investigative Ophthalmology and Visual Science* **47** (6 2006).

109. Jeng, B. H. & Dupps, W. J. Autologous serum 50% eyedrops in the treatment of persistent corneal epithelial defects. *Cornea* **28** (10 2009).

110. López-Plandolit, S., Morales, M. C., Freire, V., Etxebarría, J. & Durán, J. A. Plasma rich in growth factors as a therapeutic agent for persistent corneal epithelial defects. *Cornea* **29** (8 2010).

111. Shen, E. P. *et al.* Comparison of corneal epitheliotrophic capacity among different human blood-derived preparations. *Cornea* **30** (2 2011).

112. Soni, N. G. & Jeng, B. H. Blood-derived topical therapy for ocular surface diseases. *British Journal of Ophthalmology* **100** (1 2016).

113. Murri, M. S. *et al.* Amniotic membrane extract and eye drops: A review of literature and clinical application. *Clinical Ophthalmology* **12** (2018).

114. Mimouni, M. *et al.* Sutureless dehydrated amniotic membrane for persistent epithelial defects. *European Journal of Ophthalmology* **32** (2 2022).

115. Konomi, K., Satake, Y., Shimmura, S., Tsubota, K. & Shimazaki, J. Long-term results of amniotic membrane transplantation for partial limbal deficiency. *Cornea* **32** (8 2013).

116. Seitz, B., Das, S., Sauer, R., Mena, D. & Hofmann-Rummelt, C. Amniotic membrane transplantation for persistent corneal epithelial defects in eyes after penetrating keratoplasty. *Eye* **23** (4 2009).

117. Mimouni, M. *et al.* Tape Splint Tarsorrhaphy for Persistent Corneal Epithelial Defects. *American Journal of Ophthalmology* **237** (2022).

118. Ackerman, I., Gorski, M., Steiner, A., Udell, I. J. & Winokur, J. The effectiveness of tarsorrhaphy in healing persistent epithelial defects in cases of office based sutureless amniotic membrane treatment failure. *Investigative Ophthalmology & Visual Science* **58,** 2641–2641 (2017).
119. Dhillon, H., Bahadur, H. & Raj, A. A comparative study of tarsorrhaphy and amniotic membrane transplantation in the healing of persistent corneal epithelial defects. *Indian Journal of Ophthalmology* **68** (1 2020).
120. Alfonso, E. C. Treatment of severe ocular-surface disorders with corneal epithelial stem cell transplantation. *Archives of Ophthalmology* **118** (1 2000).
121. Daar, A. S. & Greenwood, H. L. A proposed definition of regenerative medicine. *Journal of Tissue Engineering and Regenerative Medicine* **1** (3 2007).
122. Armstrong, J. P. *et al.* A blueprint for translational regenerative medicine. *Science Translational Medicine* **12** (572 2020).
123. Williams, D. F. On the nature of biomaterials. *Biomaterials* **30** (30 2009).
124. Lanza, R., Langer, R. & Vacanti, J. *Principles of Tissue Engineering* (2020).
125. Zhang, H. & Neau, S. H. In vitro degradation of chitosan by a commercial enzyme preparation: Effect of molecular weight and degree of deacetylation. *Biomaterials* **22** (12 2001).
126. Huang, Y., Onyeri, S., Siewe, M., Moshfeghian, A. & Madihally, S. V. In vitro characterization of chitosan-gelatin scaffolds for tissue engineering. *Biomaterials* **26** (36 2005).
127. Ozcelik, B. *et al.* Ultrathin chitosan-poly(ethylene glycol) hydrogel films for corneal tissue engineering. *Acta Biomaterialia* **9** (5 2013).
128. Liu, T. Y., Chen, S. Y., Lin, Y. L. & Liu, D. M. Synthesis and characterization of amphiphatic carboxymethyl-hexanoyl chitosan hydrogel: Water-retention ability and drug encapsulation. *Langmuir* **22** (23 2006).
129. Tang, Q. *et al.* Thermosensitive chitosan-based hydrogels releasing stromal cell derived factor-1 alpha recruit MSC for corneal epithelium regeneration. *Acta Biomaterialia* **61** (2017).
130. Fallacara, A., Baldini, E., Manfredini, S. & Vertuani, S. Hyaluronic acid in the third millennium. *Polymers* **10** (7 2018).
131. Stern, R. Hyaluronan catabolism: A new metabolic pathway. *European Journal of Cell Biology* **83** (7 2004).

132. Kendall, F. E., Heidelberger, M. & Dawson, M. H. A Serologically inactive polysaccharide elaborated by mucoid strains of group A hemolytic streptococcus. *Journal of Biological Chemistry* **118** (1 1937).

133. Ding, Y. W., Wang, Z. Y., Ren, Z. W., Zhang, X. W. & Wei, D. X. Advances in modified hyaluronic acid-based hydrogels for skin wound healing. *Biomaterials Science* **10** (13 2022).

134. Gatta, A. L. *et al.* Hyaluronan-based hydrogels as dermal fillers: The biophysical properties that translate into a "volumetric" effect. *PLoS ONE* **14** (6 2019).

135. Kim, J. H. *et al.* Comparative Evaluation of the Effectiveness of Novel Hyaluronic Acid-Polynucleotide Complex Dermal Filler. *Scientific Reports* **10** (1 2020).

136. Koivusalo, L. *et al.* Tissue adhesive hyaluronic acid hydrogels for sutureless stem cell delivery and regeneration of corneal epithelium and stroma. *Biomaterials* **225** (2019).

137. Bermejo-Velasco, D. *et al.* First Aldol Cross-Linked Hyaluronic Acid Hydrogel: Fast and Hydrolytically Stable Hydrogel with Tissue Adhesive Properties. *ACS Applied Materials and Interfaces* **11** (41 2019).

138. Chatterjee, S. *et al.* Influence of pH-responsive compounds synthesized from chitosan and hyaluronic acid on dual-responsive (pH/temperature) hydrogel drug delivery systems of Cortex Moutan. *International Journal of Biological Macromolecules* **168** (2021).

139. Huang, D., Chen, Y. S., Xu, Q., Hanes, J. & Rupenthal, I. D. Effects of enzymatic degradation on dynamic mechanical properties of the vitreous and intravitreal nanoparticle mobility. *European Journal of Pharmaceutical Sciences* **118** (2018).

140. Su, X. *et al.* Recent Progress in Using Biomaterials as Vitreous Substitutes. *Biomacromolecules* **16** (10 2015).

141. Thakur, S. S., Shenoy, S. K., Suk, J. S., Hanes, J. S. & Rupenthal, I. D. Validation of hyaluronic acid-agar-based hydrogels as vitreous humor mimetics for in vitro drug and particle migration evaluations. *European Journal of Pharmaceutics and Biopharmaceutics* **148** (2020).

142. Fernandes-Cunha, G. M. *et al.* Supramolecular host-guest hyaluronic acid hydrogels enhance corneal wound healing through dynamic spatiotemporal effects. *Ocular Surface* **23** (2022).

143. Williams, D. L., Wirostko, B. M., Gum, G. & Mann, B. K. Topical cross-linked HA-based hydrogel accelerates closure of corneal epithelial defects and repair of stromal ulceration in companion animals. *Investigative Ophthalmology and Visual Science* **58** (11 2017).

144. Kim, D. J. *et al.* Development of a novel hyaluronic acid membrane for the treatment of ocular surface diseases. *Scientific Reports* **11** (1 2021).

145. Hsiao, M. Y. *et al.* Drug-loaded hyaluronic acid hydrogel as a sustained-release regimen with dual effects in early intervention of tendinopathy. *Scientific Reports* **9** (1 2019).

146. Nikjoo, D., Van der Zwaan, I., Brülls, M., Tehler, U. & Frenning, G. Hyaluronic acid hydrogels for controlled pulmonary drug delivery—a particle engineering approach. *Pharmaceutics* **13** (11 2021).

147. Trombino, S., Servidio, C., Curcio, F. & Cassano, R. *Strategies for hyaluronic acid-based hydrogel design in drug delivery* 2019.

148. Lee, K. Y. & Mooney, D. J. Alginate: Properties and biomedical applications. *Progress in Polymer Science (Oxford)* **37** (1 2012).

149. Kostenko, A., Swioklo, S. & Connon, C. J. Alginate in corneal tissue engineering. *Biomedical Materials (Bristol)* **17** (2 2022).

150. Ahearne, M., Fernández-Pérez, J., Masterton, S., Madden, P. W. & Bhattacharjee, P. Designing Scaffolds for Corneal Regeneration. *Advanced Functional Materials* **30** (44 2020).

151. Dinescu, S. *et al. Collagen-Based Hydrogels and Their Applications for Tissue Engineering and Regenerative Medicine* 2019.

152. Yamauchi, M., Taga, Y., Hattori, S., Shiiba, M. & Terajima, M. *Analysis of collagen and elastin cross-links* 2018.

153. Davison-Kotler, E., Marshall, W. S. & García-Gareta, E. Sources of collagen for biomaterials in skin wound healing. *Bioengineering* **6** (3 2019).

154. Sklenářová, R., Akla, N., Latorre, M. J., Ulrichová, J. & Franková, J. Collagen as a Biomaterial for Skin and Corneal Wound Healing. *Journal of Functional Biomaterials* **13** (4 2022).

155. Hattrem, M. N., Molnes, S., Haug, I. J. & Draget, K. I. Interfacial and rheological properties of gelatin based solid emulsions prepared with acid or alkali pretreated gelatins. *Food Hydrocolloids* **43** (2015).

156. Rashid, T. U. *et al. Gelatin-Based Hydrogels* 2019.

157. Karim, A. A. & Bhat, R. Fish gelatin: properties, challenges, and prospects as an alternative to mammalian gelatins. *Food Hydrocolloids* **23** (3 2009).

158. Mariod, A. A. *et al.* Preparation and Characterisation of Gelatins from Two Sudanese Edible Insects. *Journal of Food Science and Engineering* **1** (2011).

159. Nhari, R. M. H. R., Man, Y. C., Ismail, A. & Anuar, N. Chemical and functional properties of bovine and porcine skin gelatin. *International Food Research Journal* **817** (2011).

160. Djagny, K. B., Wang, Z. & Xu, S. Gelatin: A valuable protein for food and pharmaceutical industries: Review. *Critical Reviews in Food Science and Nutrition* **41** (6 2001).

161. Kretlow, J. D., Klouda, L. & Mikos, A. G. Injectable matrices and scaffolds for drug delivery in tissue engineering. *Advanced Drug Delivery Reviews* **59** (4-5 2007).

162. Park, H., Temenoff, J. S., Holland, T. A., Tabata, Y. & Mikos, A. G. Delivery of TGF-β1 and chondrocytes via injectable, biodegradable hydrogels for cartilage tissue engineering applications. *Biomaterials* **26** (34 2005).

163. Zheng, H. & Zuo, B. Functional silk fibroin hydrogels: preparation, properties and applications. *Journal of Materials Chemistry B* **9** (5 2021).

164. Kim, S. H. *et al.* 3D bioprinted silk fibroin hydrogels for tissue engineering. *Nature Protocols* **16** (12 2021).

165. Zhao, Y., Zhu, Z. S., Guan, J. & Wu, S. J. Processing, mechanical properties and bio-applications of silk fibroin-based high-strength hydrogels. *Acta Biomaterialia* **125** (2021).

166. Brovold, M. *et al. Naturally-Derived Biomaterials for Tissue Engineering Applications* 2018.

167. Zhang, X. *et al.* Decellularized extracellular matrix scaffolds: Recent trends and emerging strategies in tissue engineering. *Bioactive Materials* **10** (2022).

168. Jelodari, S. & Sadroddiny, E. *Decellularization of Small Intestinal Submucosa* 2021.

169. Patel, B. *et al.* Decellularized dermis extracellular matrix alloderm mechanically strengthens biological engineered tunica adventitia-based blood vessels. *Scientific Reports* **11** (1 2021).

170. Anderson, A. E. *et al.* An immunologically active, adipose-derived extracellular matrix biomaterial for soft tissue reconstruction: concept to clinical trial. *npj Regenerative Medicine* **7** (1 2022).

171. Wan, L. *et al.* Human heart valve-derived scaffold improves cardiac repair in a murine model of myocardial infarction. *Scientific Reports* **7** (2017).

172. Harris, G. M., Raitman, I. & Schwarzbauer, J. E. *Cell-derived decellularized extracellular matrices* 2018.

173. Satyam, A., Tsokos, M. G., Tresback, J. S., Zeugolis, D. I. & Tsokos, G. C. Cell-Derived Extracellular Matrix-Rich Biomimetic Substrate Supports Podocyte Proliferation, Differentiation, and Maintenance of Native Phenotype. *Advanced Functional Materials* **30** (44 2020).

174. Liu, X. *et al.* Culturing on decellularized extracellular matrix enhances antioxidant properties of human umbilical cord-derived mesenchymal stem cells. *Materials Science and Engineering C* **61** (2016).

175. Tang, G. *et al.* Advances of Naturally Derived and Synthetic Hydrogels for Intervertebral Disk Regeneration. *Frontiers in Bioengineering and Biotechnology* **8** (2020).

176. Correa, S. *et al.* Translational Applications of Hydrogels. *Chemical Reviews* **121** (18 2021).

177. Wichterle, O. & Lím, D. Hydrophilic Gels for Biological Use. *Nature* **185** (4706 1960).

178. Huebsch, N. & Mooney, D. J. Inspiration and application in the evolution of biomaterials. *Nature* **462** (7272 2009).

179. Cao, H., Duan, L., Zhang, Y., Cao, J. & Zhang, K. Current hydrogel advances in physicochemical and biological response-driven biomedical application diversity. *Signal Transduction and Targeted Therapy* **6** (1 2021).

180. Bashir, S. *et al.* Fundamental concepts of hydrogels: Synthesis, properties, and their applications. *Polymers* **12** (11 2020).

181. Shaibani, P. M., Etayash, H., Naicker, S., Kaur, K. & Thundat, T. Metabolic Study of Cancer Cells Using a pH Sensitive Hydrogel Nanofiber Light Addressable Potentiometric Sensor. *ACS Sensors* **2** (1 2017).

182. Farrukh, A., Páez, J. I. & Del Campo, A. 4D Biomaterials for Light-Guided Angiogenesis. *Advanced Functional Materials* **29** (6 2019).

183. Liu, Y. & Hsu, S. H. Synthesis and biomedical applications of self-healing hydrogels. *Frontiers in Chemistry* **6** (SEP 2018).

184. Yang, Y., Ren, Y., Song, W., Yu, B. & Liu, H. Rational design in functional hydrogels towards biotherapeutics. *Materials and Design* **223** (2022).

185. Nguyen, N. *et al.* Engineering an integrated electroactive dressing to accelerate wound healing and monitor noninvasively progress of healing. *Nano Energy* **99** (2022).

186. Liang, Y., Qiao, L., Qiao, B. & Guo, B. Conductive hydrogels for tissue repair. *Chemical Science* **14** (12 2023).

187. Maitra, J. & Shukla, V. K. Cross-linking in Hydrogels - A Review. *American Journal of Polymer Science* **4** (2 2014).

188. Lu, L. *et al.* The Formation Mechanism of Hydrogels. *Current Stem Cell Research & Therapy* **13** (7 2017).

189. Bae, Y. H., Huh, K. M., Kim, Y. & Park, K. H. Biodegradable amphiphilic multiblock copolymers and their implications for biomedical applications. *Journal of Controlled Release* **64** (1-3 2000).

190. Hunt, J. N. *et al.* Tunable, high modulus hydrogels driven by ionic coacervation. *Advanced Materials* **23** (20 2011).

191. Rao, P. *et al.* Tough Hydrogels with Fast, Strong, and Reversible Underwater Adhesion Based on a Multiscale Design. *Advanced Materials* **30** (32 2018).

192. Gao, Z., Duan, L., Yang, Y., Hu, W. & Gao, G. Mussel-inspired tough hydrogels with self-repairing and tissue adhesion. *Applied Surface Science* **427** (2018).

193. Li, Y. *et al.* Multifunctional Hydrogels Prepared by Dual Ion Cross-Linking for Chronic Wound Healing. *ACS Applied Materials and Interfaces* **9** (19 2017).

194. Dong, H., Snyder, J. F., Williams, K. S. & Andzelm, J. W. Cation-induced hydrogels of cellulose nanofibrils with tunable moduli. *Biomacromolecules* **14** (9 2013).

195. Wahid, F., Wang, H. S., Zhong, C. & Chu, L. Q. Facile fabrication of moldable antibacterial carboxymethyl chitosan supramolecular hydrogels cross-linked by metal ions complexation. *Carbohydrate Polymers* **165** (2017).

196. Leong, J. Y. *et al.* Advances in fabricating spherical alginate hydrogels with controlled particle designs by ionotropic gelation as encapsulation systems. *Particuology* **24** (2016).

197. Rezvanian, M., Ahmad, N., Amin, M. C. I. M. & Ng, S. F. Optimization, characterization, and in vitro assessment of alginate-pectin ionic cross-linked hydrogel film for wound dressing applications. *International Journal of Biological Macromolecules* **97** (2017).

198. Shariatinia, Z. & Jalali, A. M. Chitosan-based hydrogels: Preparation, properties and applications. *International Journal of Biological Macromolecules* **115** (2018).

199. Jiang, X. *et al.* Preparation and characterization of poly(vinyl alcohol)/sodium alginate hydrogel with high toughness and electric conductivity. *Carbohydrate Polymers* **186** (2018).

200. Zhang, Y. *et al.* Preparation and properties of polyacrylamide/polyvinyl alcohol physical double network hydrogel. *RSC Advances* **6** (113 2016).

201. Berger, J., Reist, M., Mayer, J. M., Felt, O. & Gurny, R. Structure and interactions in chitosan hydrogels formed by complexation or aggregation for biomedical applications. *European Journal of Pharmaceutics and Biopharmaceutics* **57** (1 2004).

202. Sung, J. H. *et al.* Gel characterisation and *in vivo* evaluation of minocycline-loaded wound dressing with enhanced wound healing using polyvinyl alcohol and chitosan. *International Journal of Pharmaceutics* **392** (1-2 2010).

203. Li, X. *et al.* Integrated Functional High-Strength Hydrogels with Metal-Coordination Complexes and H-Bonding Dual Physically Cross-linked Networks. *Macromolecular Rapid Communications* **39** (23 2018).

204. Shi, F. K., Zhong, M., Zhang, L. Q., Liu, X. Y. & Xie, X. M. Robust and self-healable nanocomposite physical hydrogel facilitated by the synergy of ternary crosslinking points in a single network. *Journal of Materials Chemistry B* **4** (37 2016).

205. Chang, C. & Zhang, L. Cellulose-based hydrogels: Present status and application prospects. *Carbohydrate Polymers* **84** (1 2011).

206. Şolpan, D., Torun, M. & Güven, O. The usability of (sodium alginate/acrylamide) semi-interpenetrating polymer networks on removal of some textile dyes. *Journal of Applied Polymer Science* **108** (6 2008).

207. Sun, J. & Tan, H. Alginate-based biomaterials for regenerative medicine applications. *Materials* **6** (4 2013).

208. Chen, Y. *Hydrogels based on natural polymers* (2019).

209. Hu, W., Wang, Z., Xiao, Y., Zhang, S. & Wang, J. Advances in crosslinking strategies of biomedical hydrogels. *Biomaterials Science* **7** (3 2019).

210. Van Dijk-Wotthuis, W. N. *et al.* Synthesis, Characterization, and Polymerization of Glycidyl Methacrylate Derivatized Dextran. *Macromolecules* **28** (18 1995).

211. Williams, C. G., Malik, A. N., Kim, T. K., Manson, P. N. & Elisseeff, J. H. Variable cytocompatibility of six cell lines with photoinitiators used for polymerizing hydrogels and cell encapsulation. *Biomaterials* **26** (11 2005).

212. Lee, H. J., Fernandes-Cunha, G. M. & Myung, D. In situ-forming hyaluronic acid hydrogel through visible light-induced thiol-ene reaction. *Reactive and Functional Polymers* **131** (2018).

213. Park, Y. D., Tirelli, N. & Hubbell, J. A. Photopolymerized hyaluronic acid-based hydrogels and interpenetrating networks. *Biomaterials* **24** (6 2003).

214. Jeon, O., Powell, C., Solorio, L. D., Krebs, M. D. & Alsberg, E. Affinity-based growth factor delivery using biodegradable, photocrosslinked heparin-alginate hydrogels. *Journal of Controlled Release* **154** (3 2011).

215. Fernandes-Cunha, G. M. *et al.* Immobilization of Growth Factors to Collagen Surfaces Using Pulsed Visible Light. *Biomacromolecules* **18** (10 2017).

216. Kushibiki, T. *et al.* Photocrosslinked gelatin hydrogel improves wound healing and skin flap survival by the sustained release of basic fibroblast growth factor. *Scientific Reports* **11** (1 2021).

217. Yao, H., Wang, J. & Mi, S. Photo processing for biomedical hydrogels design and functionality: A review. *Polymers* **10** (1 2018).

218. Zaborniak, I. & Chmielarz, P. Riboflavin-mediated radical polymerization – Outlook for eco-friendly synthesis of functional materials. *European Polymer Journal* **142** (2021).

219. Urbánek, P. *et al.* Controlled Drug Delivery Device for Cornea Treatment and Novel Method for Its Testing. *Pharmaceuticals* **16** (4 2023).

220. McHale, M. K., Setton, L. A. & Chilkoti, A. *Synthesis and in vitro evaluation of enzymatically cross-linked elastin-like polypeptide gels for cartilaginous tissue repair* in. **11** (2005).

221. Kobayashi, S., Uyama, H. & Kimura, S. Enzymatic polymerization. *Chemical Reviews* **101** (12 2001).

222. Jin, R. *et al.* Injectable chitosan-based hydrogels for cartilage tissue engineering. *Biomaterials* **30** (13 2009).

223. Jin, R. *et al.* Chondrogenesis in injectable enzymatically crosslinked heparin/dextran hydrogels. *Journal of Controlled Release* **152** (1 2011).

224. Kolb, H. C., Finn, M. G. & Sharpless, K. B. Click Chemistry: Diverse Chemical Function from a Few Good Reactions. *Angewandte Chemie International Edition* **40** (11 2001).

225. Rizwan, M., Baker, A. E. & Shoichet, M. S. Designing Hydrogels for 3D Cell Culture Using Dynamic Covalent Crosslinking. *Advanced Healthcare Materials* **10** (12 2021).

226. Deng, C. C., Brooks, W. L., Abboud, K. A. & Sumerlin, B. S. Boronic acid-based hydrogels undergo self-healing at neutral and acidic pH. *ACS Macro Letters* **4** (2 2015).

227. Smithmyer, M. E. *et al.* Self-Healing Boronic Acid-Based Hydrogels for 3D Co-cultures. *ACS Macro Letters* **7** (9 2018).

228. Gain, P. *et al.* Global survey of corneal transplantation and eye banking. *JAMA Ophthalmology* **134** (2 2016).

229. Yang, J. *et al.* Cell sheet engineering: Recreating tissues without biodegradable scaffolds. *Biomaterials* **26** (33 2005).

230. Li, M., Ma, J. U., Gao, Y. & Yang, L. E. Cell sheet technology: a promising strategy in regenerative medicine. *Cytotherapy* **21** (1 2019).

231. Venugopal, B., Mohan, S., Kumary, T. V. & Kumar, P. R. A. Peripheral Blood As a Source of Stem Cells for Regenerative Medicine: Emphasis Towards Corneal Epithelial Reconstruction—An In Vitro Study. *Tissue Engineering and Regenerative Medicine* **17** (4 2020).

232. Park, I. S. *et al.* Corneal Repair with Adhesive Cell Sheets of Fetal Cartilage-Derived Stem Cells. *Tissue Engineering and Regenerative Medicine* **18** (1 2021).

233. Navas, A. *et al.* Anti-Inflammatory and Anti-Fibrotic Effects of Human Amniotic Membrane Mesenchymal Stem Cells and Their Potential in Corneal Repair. *Stem Cells Translational Medicine* **7** (12 2018).

234. Sumide, T. *et al.* Functional human corneal endothelial cell sheets harvested from temperature-responsive culture surfaces. *The FASEB Journal* **20** (2 2006).

235. Khalili, M. *et al.* Corneal endothelial cell sheet bioengineering from neural crest cell-derived adipose stem cells on novel thermo-responsive elastin-mimetic dendrimers decorated with RGD. *Chemical Engineering Journal* **429** (2022).

236. Mohammadpour, M. *et al.* Comparison of Lotrafilcon B and Balafilcon A silicone hydrogel bandage contact lenses in reducing pain and discomfort

after photorefractive keratectomy: A contralateral eye study. *Contact Lens and Anterior Eye* **38** (3 2015).

237. Gil-Cazorla, R., Teus, M. A., Hernández-Verdejo, J. L., De Benito-Llopis, L. & García-González, M. *Comparative study of two silicone hydrogel contact lenses used as bandage contact lenses after LASEK* in. **85** (2008).
238. Peral, A. *et al.* Contact lenses as drug delivery system for glaucoma: A review. *Applied Sciences (Switzerland)* **10** (15 2020).
239. Filipe, H. P. *et al.* Contact lenses as drug controlled release systems: A narrative review. *Revista Brasileira de Oftalmologia* **75** (3 2016).
240. Hsu, K. H., Gause, S. & Chauhan, A. Review of ophthalmic drug delivery by contact lenses. *Journal of Drug Delivery Science and Technology* **24** (2 2014).
241. Gallagher, A. G. *et al.* A Novel Peptide Hydrogel for an Antimicrobial Bandage Contact Lens. *Advanced Healthcare Materials* **5** (16 2016).
242. Morgan, P. B., Efron, N. & Woods, C. A. Determinants of the frequency of contact lens wear. *Eye and Contact Lens* **39** (3 2013).
243. Efron, N., Morgan, P. B. & Woods, C. A. International survey of rigid contact lens fitting. *Optometry and Vision Science* **90** (2 2013).
244. Grentzelos, M. A. *et al.* Efficacy of 2 types of silicone hydrogel bandage contact lenses after photorefractive keratectomy. *Journal of Cataract and Refractive Surgery* **35** (12 2009).
245. Chou, B. *Contact Lens Spectrum - The Evolution of Silicone Hydrogel Lenses* 2008.
246. Holland, S., Morck, D. & Schultz, C. Treatment of corneal defects with delayed re-epithelization with a medical device/drug delivery system for epidermal growth factor. *Clinical and Experimental Ophthalmology* **40** (7 2012).
247. Li, C. C. & Chauhan, A. Ocular transport model for ophthalmic delivery of timolol through p-HEMA contact lenses. *Journal of Drug Delivery Science and Technology* **17** (1 2007).
248. Hsu, K. H., Carbia, B. E., Plummer, C. & Chauhan, A. Dual drug delivery from vitamin e loaded contact lenses for glaucoma therapy. *European Journal of Pharmaceutics and Biopharmaceutics* **94** (2015).
249. Hsu, K. H. *et al.* Release of betaine and dexpanthenol from vitamin E modified silicone-hydrogel contact lenses. *Current Eye Research* **40** (3 2015).

250. Peng, C. C., Kim, J. & Chauhan, A. Extended delivery of hydrophilic drugs from silicone-hydrogel contact lenses containing Vitamin E diffusion barriers. *Biomaterials* **31** (14 2010).

251. Jung, H. J., Abou-Jaoude, M., Carbia, B. E., Plummer, C. & Chauhan, A. Glaucoma therapy by extended release of timolol from nanoparticle loaded silicone-hydrogel contact lenses. *Journal of Controlled Release* **165** (1 2013).

252. García-Millán, E., Koprivnik, S. & Otero-Espinar, F. J. Drug loading optimization and extended drug delivery of corticoids from pHEMA based soft contact lenses hydrogels via chemical and microstructural modifications. *International Journal of Pharmaceutics* **487** (1-2 2015).

253. Behl, G., Iqbal, J., O'Reilly, N. J., McLoughlin, P. & Fitzhenry, L. Synthesis and Characterization of Poly(2-hydroxyethylmethacrylate) Contact Lenses Containing Chitosan Nanoparticles as an Ocular Delivery System for Dexamethasone Sodium Phosphate. *Pharmaceutical Research* **33** (7 2016).

254. Jung, H. J. & Chauhan, A. Temperature sensitive contact lenses for triggered ophthalmic drug delivery. *Biomaterials* **33** (7 2012).

255. Souto, E. B., Doktorovova, S., Gonzalez-Mira, E., Egea, M. A. & Garcia, M. L. Feasibility of lipid nanoparticles for ocular delivery of anti-inflammatory drugs. *Current Eye Research* **35** (7 2010).

256. Danion, A., Brochu, H., Martin, Y. & Vermette, P. Fabrication and characterization of contact lenses bearing surface-immobilized layers of intact liposomes. *Journal of Biomedical Materials Research - Part A* **82** (1 2007).

257. Hiratani, H., Fujiwara, A., Tamiya, Y., Mizutani, Y. & Alvarez-Lorenzo, C. Ocular release of timolol from molecularly imprinted soft contact lenses. *Biomaterials* **26** (11 2005).

258. Tieppo, A. *et al.* Sustained in vivo release from imprinted therapeutic contact lenses. *Journal of Controlled Release* **157** (3 2012).

259. White, C. J., McBride, M. K., Pate, K. M., Tieppo, A. & Byrne, M. E. Extended release of high molecular weight hydroxypropyl methylcellulose from molecularly imprinted, extended wear silicone hydrogel contact lenses. *Biomaterials* **32** (24 2011).

260. Bengani, L. C. & Chauhan, A. Extended delivery of an anionic drug by contact lens loaded with a cationic surfactant. *Biomaterials* **34** (11 2013).

261. Ciolino, J. B. *et al.* A drug-eluting contact lens. *Investigative Ophthalmology and Visual Science* **50** (7 2009).

262. Carvalho, I. M. *et al.* Sustained drug release by contact lenses for glaucoma treatment - A review. *Journal of Controlled Release* **202** (2015).

263. Choi, S. W. & Kim, J. Therapeutic contact lenses with polymeric vehicles for ocular drug delivery: A review. *Materials* **11** (7 2018).

264. Jahanafrooz, Z., Bakhshandeh, B., Abdollahi, S. B. & Seyedjafari, E. Human amniotic membrane as a multifunctional biomaterial: recent advances and applications. *Journal of Biomaterials Applications* **37** (8 2023).

265. Elkhenany, H. *et al.* Applications of the amniotic membrane in tissue engineering and regeneration: the hundred-year challenge. *Stem Cell Research and Therapy* **13** (1 2022).

266. Sheha, H., Liang, L., Li, J. & Tseng, S. C. Sutureless amniotic membrane transplantation for severe bacterial keratitis. *Cornea* **28** (10 2009).

267. Kheirkhah, A. *et al.* Temporary sutureless amniotic membrane patch for acute alkaline burns. *Archives of Ophthalmology* **126** (8 2008).

268. Kheirkhah, A., Casas, V., Raju, V. K. & Tseng, S. C. Sutureless Amniotic Membrane Transplantation for Partial Limbal Stem Cell Deficiency. *American Journal of Ophthalmology* **145** (5 2008).

269. Pachigolla, G. *et al.* Evaluation of the role of prokera in the management of ocular surface and orbital disorders. *Eye and Contact Lens* **35** (4 2009).

270. Yelchuri, M. L. *et al.* In vitro evaluation of the drug reservoir function of human amniotic membrane using moxifloxacin as a model drug. *Cornea* **36** (5 2017).

271. Cai, M., Zhang, J., Guan, L. & Zhao, M. Novel implantable composite biomaterial by fibrin glue and amniotic membrane for ocular surface reconstruction. *Journal of Materials Science: Materials in Medicine* **26** (3 2015).

272. Zhou, Z. *et al.* Nanofiber-reinforced decellularized amniotic membrane improves limbal stem cell transplantation in a rabbit model of corneal epithelial defect. *Acta Biomaterialia* **97** (2019).

273. Guo, Q. *et al.* Modulation of keratocyte phenotype by collagen fibril nanoarchitecture in membranes for corneal repair. *Biomaterials* **34** (37 2013).

274. Ambrose, W. M. I. *et al.* Collagen vitrigel membranes for the in vitro reconstruction of separate corneal epithelial, stromal, and endothelial cell

layers. *Journal of Biomedical Materials Research - Part B Applied Biomaterials* **90 B** (2 2009).

275. Chae, J. J. *et al.* Regeneration of corneal epithelium utilizing a collagen vitrigel membrane in rabbit models for corneal stromal wound and limbal stem cell deficiency. *Acta Ophthalmologica* **93** (1 2015).
276. Vauthier, C., Dubernet, C., Fattal, E., Pinto-Alphandary, H. & Couvreur, P. Poly(alkylcyanoacrylates) as biodegradable materials for biomedical applications. *Advanced Drug Delivery Reviews* **55** (4 2003).
277. Trivedi, D., McCalla, M., Squires, Z. & Parulekar, M. Use of cyanoacrylate glue for temporary tarsorrhaphy in children. *Ophthalmic Plastic and Reconstructive Surgery* **30** (1 2014).
278. Singh, R. B. *et al.* Efficacy of cyanoacrylate tissue adhesive in the management of corneal thinning and perforation due to microbial keratitis. *Ocular Surface* **18** (4 2020).
279. Al-Shahwan, S., Al-Torbak, A. A., Al-Jadaan, I., Omran, M. & Edward, D. P. Long-term follow up of surgical repair of late bleb leaks after glaucoma filtering surgery. *Journal of Glaucoma* **15** (5 2006).
280. Haslinda, A. R., Azhany, Y., Noor-Khairul, R., Zunaina, E. & Liza-Sharmini, A. T. Cyanoacrylate tissue glue for wound repair in early posttrabeculectomy conjunctival bleb leak: A case series. *International Medical Case Reports Journal* **8** (2015).
281. Trujillo-de Santiago, G. *et al.* Ocular adhesives: Design, chemistry, crosslinking mechanisms, and applications. *Biomaterials* **197** (2019).
282. Potvin, R. & Makari, S. Cataract surgery and methods of wound closure: A review. *Clinical Ophthalmology* **9** (2015).
283. Masket, S. *et al.* Hydrogel sealant versus sutures to prevent fluid egress after cataract surgery. *Journal of Cataract and Refractive Surgery* **40** (12 2014).
284. Uy, H. S. & Kenyon, K. R. Surgical outcomes after application of a liquid adhesive ocular bandage to clear corneal incisions during cataract surgery. *Journal of Cataract and Refractive Surgery* **39** (11 2013).
285. Sykakis, E. *et al.* Study of fluid ingress through clear corneal incisions following phacoemulsification with or without the use of a hydrogel ocular bandage: a prospective comparative randomised study. *Acta ophthalmologica* **92** (8 2014).

286. Park, H. C., Champakalakshmi, R., Panengad, P. P., Raghunath, M. & Mehta, J. S. Tissue adhesives in ocular surgery. *Expert Review of Ophthalmology* **6** (6 2011).

287. Baxter, R., Hastings, N., a. Law & Glass, E. J. FDA Summary of the Safety and Effectiveness Data ReSure® Sealant. *Animal Genetics* **39** (5 2013).

288. Somani, S. N., Moshirfar, M., Shmunes, K. M. & Ronquillo, Y. C. Comparison and application of commercially available fibrin sealants in ophthalmology. *Ocular Surface* **18** (3 2020).

289. Sharma, A. *et al.* Fibrin glue versus N-butyl-2-cyanoacrylate in corneal perforations. *Ophthalmology* **110** (2 2003).

290. Srinivasan, S. *et al.* Fibrin glue versus sutures for attaching the conjunctival autograft in pterygium surgery: A prospective observer masked clinical trial. *British Journal of Ophthalmology* **93** (2 2009).

291. Kheirkhah, A. *et al.* Amniotic Membrane Transplantation with Fibrin Glue for Conjunctivochalasis. *American Journal of Ophthalmology* **144** (2 2007).

292. Kaufman, H. E., Insler, M. S., Elzembely, H. A. I. & Kaufman, S. C. Human Fibrin Tissue Adhesive for Sutureless Lamellar Keratoplasty and Scleral Patch Adhesion: A Pilot Study. *Ophthalmology* **110** (11 2003).

293. Han, B., Schwab, I. R., Madsen, T. K. & Isseroff, R. R. A fibrin-based bioengineered ocular surface with human corneal epithelial stem cells. *Cornea* **21** (5 2002).

294. Sonmez, B. & Ümit Beden. Fibrin glue-assisted sutureless limbal stem cell transplantation surgery for the treatment of severe ocular chemical injury. *Cornea* **30** (3 2011).

295. Zhao, X. *et al.* Natural polymer-derived photocurable bioadhesive hydrogels for sutureless keratoplasty. *Bioactive Materials* **8** (2022).

296. Liu, W. *et al.* Recombinant human collagen for tissue engineered corneal substitutes. *Biomaterials* **29** (9 2008).

297. Kong, B. *et al.* Recombinant human collagen hydrogels with hierarchically ordered microstructures for corneal stroma regeneration. *Chemical Engineering Journal* **428** (2022).

298. McTiernan, C. D. *et al.* LiQD Cornea: Pro-regeneration collagen mimetics as patches and alternatives to corneal transplantation. *Science Advances* **6** (25 2020).

299. Chen, F., Le, P., Fernandes-Cunha, G. M., Heilshorn, S. C. & Myung, D. Bio-orthogonally crosslinked hyaluronate-collagen hydrogel for suture-free corneal defect repair. *Biomaterials* **255** (2020).

300. Fernandes-Cunha, G. M. *et al.* In situ-forming collagen hydrogel crosslinked via multi-functional PEG as a matrix therapy for corneal defects. *Scientific Reports* **10** (1 2020).

301. Chen, F., Le, P., Lai, K., Fernandes-Cunha, G. M. & Myung, D. Simultaneous Interpenetrating Polymer Network of Collagen and Hyaluronic Acid as an in Situ-Forming Corneal Defect Filler. *Chemistry of Materials* **32** (12 2020).

302. Logan, C. M. *et al.* In Situ-forming Collagen Hydrogels Crosslinked by Multifunctional Polyethylene Glycol as a Matrix Therapy for Corneal Defects: 2-Month Follow-up in Vivo. *Cornea* **42** (1 2023).

303. Patra, H. K. *et al.* Rational Nanotoolbox with Theranostic Potential for Medicated Pro-Regenerative Corneal Implants. *Advanced Functional Materials* **29** (38 2019).

304. Zhao, X., Song, W., Chen, Y., Liu, S. & Ren, L. Collagen-based materials combined with microRNA for repairing cornea wounds and inhibiting scar formation. *Biomaterials Science* **7** (1 2019).

305. Na, K. S. *et al.* Effect of mesenchymal stromal cells encapsulated within polyethylene glycol-collagen hydrogels formed in situ on alkali-burned corneas in an ex vivo organ culture model. *Cytotherapy* **23** (6 2021).

306. Sani, E. S. *et al.* Sutureless repair of corneal injuries using naturally derived bioadhesive hydrogels. *Science Advances* **5** (3 2019).

307. Sharifi, S. *et al.* Tuning gelatin-based hydrogel towards bioadhesive ocular tissue engineering applications. *Bioactive Materials* **6** (11 2021).

308. Li, M. *et al.* A "T.E.S.T." hydrogel bioadhesive assisted by corneal cross-linking for in situ sutureless corneal repair. *Bioactive Materials* **25** (2023).

309. Uyanlklar, M., Günal, G., Tevlek, A., Hosseinian, P. & Aydin, H. M. Hybrid Cornea: Cell Laden Hydrogel Incorporated Decellularized Matrix. *ACS Biomaterials Science and Engineering* **6** (1 2020).

310. Seow, W. Y., Kandasamy, K., Peh, G. S., Mehta, J. S. & Sun, W. Ultrathin, Strong, and Cell-Adhesive Agarose-Based Membranes Engineered as Substrates for Corneal Endothelial Cells. *ACS Biomaterials Science and Engineering* **5** (8 2019).

311. Bektas, C. K. & Hasirci, V. Mimicking corneal stroma using keratocyte-loaded photopolymerizable methacrylated gelatin hydrogels. *Journal of Tissue Engineering and Regenerative Medicine* **12** (4 2018).

312. Chatterjee, A. *et al.* Designing and enhancing the antifungal activity of corneal specific cell penetrating peptide using gelatin hydrogel delivery system. *International Journal of Nanomedicine* **14** (2019).

313. Park, S. K. *et al.* Hyaluronic acid hydrogels crosslinked via blue light-induced thiol-ene reaction for the treatment of rat corneal alkali burn. *Regenerative Therapy* **20** (2022).

314. Fiorica, C., Palumbo, F. S., Pitarresi, G., Bongiovì, F. & Giammona, G. Hyaluronic acid and beta cyclodextrins films for the release of corneal epithelial cells and dexamethasone. *Carbohydrate Polymers* **166** (2017).

315. Feng, L. *et al.* Thermo-Gelling Dendronized Chitosans as Biomimetic Scaffolds for Corneal Tissue Engineering. *ACS Applied Materials and Interfaces* **13** (41 2021).

316. Tsai, C. Y. *et al.* Thermosensitive chitosan-based hydrogels for sustained release of ferulic acid on corneal wound healing. *Carbohydrate Polymers* **135** (2016).

317. Chen, X. *et al.* Chitosan-based thermosensitive hydrogel as a promising ocular drug delivery system: Preparation, characterization, and in vivo evaluation. *Journal of Biomaterials Applications* **27** (4 2012).

318. Tang, Q. *et al.* Exosomes-loaded thermosensitive hydrogels for corneal epithelium and stroma regeneration. *Biomaterials* **280** (2022).

319. Yazdanpanah, G. *et al.* Fabrication, Rheological, and Compositional Characterization of Thermoresponsive Hydrogel from Cornea. *Tissue Engineering - Part C: Methods* **27** (5 2021).

320. Zhou, Q. *et al.* Hydrogels derived from acellular porcine corneal stroma enhance corneal wound healing. *Acta Biomaterialia* **134** (2021).

321. Yazdanpanah, G. *et al.* In-situ porcine corneal matrix hydrogel as ocular surface bandage. *Ocular Surface* **21** (2021).

322. Wang, F. *et al.* Decellularized porcine cornea-derived hydrogels for the regeneration of epithelium and stroma in focal corneal defects. *Ocular Surface* **18** (4 2020).

323. Zieske, J. D. *et al.* Basement membrane assembly and differentiation of cultured corneal cells: Importance of culture environment and endothelial cell interaction. *Experimental Cell Research* **214** (2 1994).

324. Griffith, M. *et al.* Functional human corneal equivalents constructed from cell lines. *Science* **286** (5447 1999).

325. Hutcheon, A. E., Zieske, J. D. & Guo, X. 3D in vitro model for human corneal endothelial cell maturation. *Experimental Eye Research* **184** (2019).

326. McKay, T. B., Karamichos, D., Zieske, J. D., Hutcheon, A. E. & Guo, X. Corneal epithelial–stromal fibroblast constructs to study cell–cell communication in vitro. *Bioengineering* **6** (4 2019).

327. Wang, S. *et al.* In vitro 3D corneal tissue model with epithelium, stroma, and innervation. *Biomaterials* **112** (2017).

328. Rico-Sánchez, L. *et al.* Successful development and clinical translation of a novel anterior lamellar artificial cornea. *Journal of Tissue Engineering and Regenerative Medicine* **13** (12 2019).

329. De la Cruz-Cardona, J. *et al.* Transparency in a fibrin and fibrin-agarose corneal stroma substitute generated by tissue engineering. *Cornea* **30** (12 2011).

330. Ionescu, A. M. *et al.* Investigating a novel nanostructured fibrin-agarose biomaterial for human cornea tissue engineering: Rheological properties. *Journal of the Mechanical Behavior of Biomedical Materials* **4** (8 2011).

331. González-Andrades, M. *et al.* A study protocol for a multicentre randomised clinical trial evaluating the safety and feasibility of a bioengineered human allogeneic nanostructured anterior cornea in patients with advanced corneal trophic ulcers refractory to conventional treatment. *BMJ Open* **7** (9 2017).

332. Weidinger, A., Poženel, L., Wolbank, S. & Banerjee, A. Sub-Regional Differences of the Human Amniotic Membrane and Their Potential Impact on Tissue Regeneration Application. *Frontiers in Bioengineering and Biotechnology* **8** (2021).

333. Shah, K. & Maghsoudlou, P. Enzyme-linked immunosorbent assay (ELISA): the basics. *British Journal of Hospital Medicine* **77.** PMID: 27388394, C98–C101. eprint: `https://doi.org/10.12968/hmed.2016.77.7.C98` (2016).

334. Ehrich, M. & Sharova, L. In Vitro Methods for Detecting Cytotoxicity. *Current Protocols in Toxicology* **3** (1 2000).

335. Garbison, K. E., Heinz, B. A., Lajiness, M. E., Weidner, J. R. & Sittampalam, G. S. Assay Guidance Manual. *Eli Lilly & Company and the National Center for Advancing Translational Sciences* (2004).

336. Haugland, R. P. Handbook of fluorescent probes and research chemicals. *Molecular Probes, Eugene* **8** (1996).

337. Wilhelmus, K. R. The Draize eye test. *Survey of ophthalmology* **45** (6 2001).

338. Kay, J. & Calandra, J. Interpretation of eye irritation tests. *Journal of the Society of Cosmetic Chemists* **13,** 281–289 (1962).

339. Smith, P. *et al.* Measurement of protein using bicinchoninic acid. *Analytical Biochemistry* **150,** 76–85 (1985).

340. Pfaffl, M. W. A new mathematical model for relative quantification in real-time RT–PCR. *Nucleic Acids Research* **29** (9 2001).

341. Vandesompele, J. *et al.* Accurate normalization of real-time quantitative RT-PCR data by geometric averaging of multiple internal control genes. *Genome Biology* **3** (7 2002).

342. Livak, K. J. & Schmittgen, T. D. Analysis of relative gene expression data using real-time quantitative PCR and the 2-ΔΔCT method. *Methods* **25** (4 2001).

343. Hancox, Z. *et al.* The progress in corneal translational medicine. *Biomaterials Science* **8** (23 2020).

344. Palchesko, R. N., Carrasquilla, S. D. & Feinberg, A. W. Natural Biomaterials for Corneal Tissue Engineering, Repair, and Regeneration. *Advanced Healthcare Materials* **7** (16 2018).

345. Chen, Z. *et al.* Biomaterials for corneal bioengineering. *Biomedical Materials (Bristol)* **13** (3 2018).

346. Griffith, M. *et al.* Biosynthetic alternatives for corneal transplant surgery. *Expert Review of Ophthalmology* **15** (3 2020).

347. Land, M. F. & Fernald, R. D. The evolution of eyes. *Annual Review of Neuroscience* **15** (1992).

348. Höpe, A. *Diffuse Reflectance and Transmittance* 2014.

349. Motoyoshi, I. Highlight-shading relationship as a cue for the perception of translucent and transparent materials. *Journal of vision* **10** (9 2010).

350. Marlow, P. J., Kim, J. & Anderson, B. L. Perception and misperception of surface opacity. *Proceedings of the National Academy of Sciences of the United States of America* **114** (52 2017).

351. Salameh, C. *et al.* Origin of transparency in scattering biomimetic collagen materials. *Proceedings of the National Academy of Sciences of the United States of America* **117** (22 2020).

352. Gigilashvili, D., Thomas, J. B., Hardeberg, J. Y. & Pedersen, M. Translucency perception: A review. *Journal of Vision* **21** (8 2021).

353. Etxabide, A., Uranga, J., Guerrero, P. & de la Caba, K. Improvement of barrier properties of fish gelatin films promoted bygelatin glycation with lactose at high temperatures. *LWT* **63** (1 2015).

354. Tanito, M., Kaidzu, S. & Anderson, R. E. Protective effects of soft acrylic yellow filter against blue light-induced retinal damage in rats. *Experimental Eye Research* **83** (6 2006).

355. García-López, C. *et al.* The role of matrix metalloproteinases in infectious corneal ulcers. *Survey of Ophthalmology* **68** (5 2023).

356. Li, D. Q., Chen, Z., Song, X. J., Luo, L. & Pflugfelder, S. C. Stimulation of matrix metalloproteinases by hyperosmolarity via a JNK pathway in human corneal epithelial cells. *Investigative Ophthalmology and Visual Science* **45** (12 2004).

357. Jadczyk-Sorek, K., Garczorz, W., Bubała-Stachowicz, B., Francuz, T. & Mrukwa-Kominek, E. Increased Matrix Metalloproteinase-2 and Matrix Metalloproteinase-3 Concentrations in Corneal Epithelium of Patients with Recurrent Corneal Erosions. *Journal of Ophthalmology* **2022** (2022).

358. Wolf, M. *et al.* Overexpression of mmps in corneas requiring penetrating and deep anterior lamellar keratoplasty. *Investigative Ophthalmology and Visual Science* **60** (5 2019).

359. Martins, J. P. *et al. Chapter 4 - 3D printing: prospects and challenges* 2018.

360. International Organization for Standardization, I. ISO 10993-5 Biological evaluation of medical devices - Part 5: Tests for cytotoxicity: in vitro methods. *International Standard ISO* **3 Ed** (2009).

361. Liu, Y., Ren, L. & Wang, Y. A novel collagen film with micro-rough surface structure for corneal epithelial repair fabricated by freeze drying technique. *Applied Surface Science* **301** (2014).

362. Li, W. *et al.* Fabrication and characterization of chitosan-collagen crosslinked membranes for corneal tissue engineering. *Journal of Biomaterials Science, Polymer Edition* **25** (17 2014).

363. Isaacson, A., Swioklo, S. & Connon, C. J. 3D bioprinting of a corneal stroma equivalent. *Experimental Eye Research* **173** (2018).

364. Dartt, D. A. & Willcox, M. D. Complexity of the tear film: Importance in homeostasis and dysfunction during disease. *Experimental Eye Research* **117** (2013).

365. Gouveia, R. M. *et al.* Assessment of corneal substrate biomechanics and its effect on epithelial stem cell maintenance and differentiation. *Nature Communications* **10** (1 2019).

366. Chen, J., Backman, L. J., Zhang, W., Ling, C. & Danielson, P. Regulation of Keratocyte Phenotype and Cell Behavior by Substrate Stiffness. *ACS Biomaterials Science and Engineering* **6** (9 2020).

367. Bhattacharjee, P., Cavanagh, B. L. & Ahearne, M. Effect of substrate topography on the regulation of human corneal stromal cells. *Colloids and Surfaces B: Biointerfaces* **190** (2020).

368. Bode, F., Da Silva, M. A., Drake, A. F., Ross-Murphy, S. B. & Dreiss, C. A. Enzymatically cross-linked tilapia gelatin hydrogels: Physical, chemical, and hybrid networks. *Biomacromolecules* **12** (10 2011).

369. Xing, Q. *et al.* Increasing mechanical strength of gelatin hydrogels by divalent metal ion removal. *Scientific Reports* **4** (2014).

370. Tan, L., Cai, Z. Q. & Lai, N. S. Accuracy and sensitivity of the dynamic ocular thermography and inter-subjects ocular surface temperature (OST) in Chinese young adults. *Contact Lens and Anterior Eye* **32** (2 2009).

371. Raiskup, F. & Spoerl, E. Corneal crosslinking with riboflavin and ultraviolet A. I. principles. *Ocular Surface* **11** (2 2013).

372. Andreassen, T. T., Simonsen, A. H. & Oxlund, H. Biomechanical properties of keratoconus and normal corneas. *Experimental Eye Research* **31** (4 1980).

373. Tomkins, O. Collagen cross-linking: Strengthening the unstable cornea. *Clinical Ophthalmology* (2008).

374. Wollensak, G., Spoerl, E. & Seiler, T. Riboflavin/ultraviolet-A-induced collagen crosslinking for the treatment of keratoconus. *American Journal of Ophthalmology* **135** (5 2003).

375. Belin, M. W. *et al.* Corneal cross-linking: Current USA status report from the cornea society. *Cornea* **37** (10 2018).

376. Ghosh, S. & Puranik, M. Deep ultraviolet initiated excited state dynamics of riboflavin and flavin mononucleotide. *Journal of Raman Spectroscopy* **49** (10 2018).

377. Beztsinna, N., Solé, M., Taib, N. & Bestel, I. Bioengineered riboflavin in nanotechnology. *Biomaterials* **80** (2016).

378. Northrop-Clewes, C. A. & Thurnham, D. I. The discovery and characterization of riboflavin. *Annals of Nutrition and Metabolism* **61** (3 2012).

379. Rostas, A. *et al.* Long-Lived Hydrated FMN Radicals: EPR Characterization and Implications for Catalytic Variability in Flavoproteins. *Journal of the American Chemical Society* **140** (48 2018).

380. Lee, Y. B., Lim, S., Lee, Y., Park, C. H. & Lee, H. J. Green Chemistry for Crosslinking Biopolymers: Recent Advances in Riboflavin-Mediated Photochemistry. *Materials* **16** (3 2023).

381. Cardoso, D. R., Franco, D. W., Olsen, K., Andersen, M. L. & Skibsted, L. H. Reactivity of bovine whey proteins, peptides, and amino acids toward triplet riboflavin as studied by laser flash photolysis. *Journal of Agricultural and Food Chemistry* **52** (21 2004).

382. Davies, M. J. Singlet oxygen-mediated damage to proteins and its consequences. *Biochemical and Biophysical Research Communications* **305** (3 2003).

383. Redmond, R. W. & Kochevar, I. E. Medical Applications of Rose Bengal- and Riboflavin-Photosensitized Protein Crosslinking. *Photochemistry and Photobiology* **95** (5 2019).

384. Ionita, G. & Matei, I. *Application of Riboflavin Photochemical Properties in Hydrogel Synthesis* 2020.

385. Zhang, Y., Conrad, A. H. & Conrad, G. W. Effects of ultraviolet-A and riboflavin on the interaction of collagen and proteoglycans during corneal cross-linking. *Journal of Biological Chemistry* **286** (15 2011).

386. Tirella, A., Liberto, T. & Ahluwalia, A. Riboflavin and collagen: New crosslinking methods to tailor the stiffness of hydrogels. *Materials Letters* **74** (2012).

387. Schuldt, C. *et al.* Dose-dependent collagen cross-linking of rabbit scleral tissue by blue light and riboflavin treatment probed by dynamic shear rheology. *Acta Ophthalmologica* **93** (5 2015).

388. Song, E. H., Shang, J. & Ratner, D. M. *9.08 - Polysaccharides* 2012.

389. Mark, T., Ngounou, F., Tamon, J., Marx-Gross, S. & Preussner, P. R. Modulatory effect of different riboflavin compositions on the central corneal thickness of African keratoconus corneas during collagen crosslinking. *Middle East African Journal of Ophthalmology* **21** (1 2014).

390. Brady, J, Dürig, T, Lee, P. I. & Li, J. X. in (2017).

391. Tundisi, L. L., Mostaço, G. B., Carricondo, P. C. & Petri, D. F. Hydroxypropyl methylcellulose: Physicochemical properties and ocular drug delivery formulations. *European Journal of Pharmaceutical Sciences* **159** (2021).

392. Oltulu, R. *et al.* Intraoperative corneal thickness monitoring during corneal collagen cross-linking with isotonic riboflavin solution with and without dextran. *Cornea* **33** (11 2014).

393. Zaheer, N., Khan, W. A., Khan, S. & Khan, M. A. M. Comparison of Changes in Central Corneal Thickness during Corneal Collagen Cross-Linking, Using Isotonic Riboflavin Solutions with and Without Dextran, in the Treatment of Progressive Keratoconus. *Cornea* **37** (3 2018).

394. Rapuano, P. B., Mathews, P. M., Florakis, G. J., Trokel, S. L. & Suh, L. H. Corneal collagen crosslinking in patients treated with dextran versus isotonic hydroxypropyl methylcellulose (HPMC) riboflavin solution: a retrospective analysis. *Eye and Vision* **5** (1 2018).

395. Thorsrud, A., Hagem, A. M., Sandvik, G. F. & Drolsum, L. Superior outcome of corneal collagen cross-linking using riboflavin with methylcellulose than riboflavin with dextran as the main supplement. *Acta Ophthalmologica* **97** (4 2019).

396. Fallacara, A. *et al.* Novel artificial tears containing cross-linked hyaluronic acid: An in vitro re-epithelialization study. *Molecules* **22** (12 2017).

397. Constantin, M. M. *et al.* Model systems for evidencing the mediator role of riboflavin in the uva cross-linking treatment of keratoconus. *Molecules* **27** (1 2022).

398. Sakai, S., Ohi, H. & Taya, M. Gelatin/hyaluronic acid content in hydrogels obtained through blue light-induced gelation affects hydrogel properties and adipose stem cell behaviors. *Biomolecules* **9** (8 2019).

399. Gupta, B., Mishra, V., Gharat, S., Momin, M. & Omri, A. Cellulosic polymers for enhancing drug bioavailability in ocular drug delivery systems. *Pharmaceuticals* **14** (11 2021).

400. Silvestro, I. *et al.* Hyaluronic acid reduces bacterial fouling and promotes fibroblasts' adhesion onto chitosan 2D-wound dressings. *International Journal of Molecular Sciences* **21** (6 2020).

401. Dovedytis, M., Liu, Z. J. & Bartlett, S. Hyaluronic acid and its biomedical applications: A review. *Engineered Regeneration* **1** (2020).

402. Narayan, R., Arcovito, A., Dahiya, D. & Nigam, P. S. Dextran of Diverse Molecular-Configurations Used as a Blood-Plasma Substitute, Drug-Delivery Vehicle and Food Additive Biosynthesized by Leuconostoc, Lactobacillus and Weissella (2023).

403. Seddiqi, H. *et al.* Cellulose and its derivatives: towards biomedical applications. *Cellulose* **28** (4 2021).

404. Shen, X. *et al.* Dual-crosslinked regenerative hydrogel for sutureless long-term repair of corneal defect. *Bioactive Materials* **20** (2023).

405. Fox, R. I., Chan, R., Michelson, J. B., Belmont, J. B. & Michelson, P. E. Beneficial Effect of Artificial Tears Made with Autologous Serum in Patients with Keratoconjunctivitis Sicca. *Arthritis & Rheumatism* **27** (4 1984).

406. Soifer, M. *et al.* A multicenter report of the use of plasma rich in growth factors (PRGF) for the treatment of patients with ocular surface diseases in North America: PRGF Treatment Outcomes in Patients with Ocular Surface Diseases. *Ocular Surface* **25** (2022).

407. Anitua, E. *et al.* Autologous serum and plasma rich in growth factors in ophthalmology: Preclinical and clinical studies. *Acta Ophthalmologica* **93** (8 2015).

408. Tsubota, K. *et al.* Treatment of dry eye by autologous serum application in Sjogren's syndrome. *British Journal of Ophthalmology* **83** (4 1999).

409. Geerling, G., MacLennan, S. & Hartwig, D. Autologous serum eye drops for ocular surface disorders. *British Journal of Ophthalmology* **88** (11 2004).

410. Lee, J. H., Kim, M. J., Ha, S. W. & Kim, H. K. Autologous Platelet-rich Plasma Eye Drops in the Treatment of Recurrent Corneal Erosions. *Korean journal of ophthalmology : KJO* **30** (2 2016).

411. Kirgiz, A. *et al.* The Use of Autologous Serum Eye Drops after Epithelium-off Corneal Collagen Crosslinking. *Optometry and Vision Science* **97** (4 2020).

412. López-Plandolit, S., Morales, M. C., Freire, V., Grau, A. E. & Durán, J. A. Efficacy of plasma rich in growth factors for the treatment of dry eye. *Cornea* **30** (12 2011).

413. Anitua, E. *et al.* Infiltration of plasma rich in growth factors enhances in vivo angiogenesis and improves reperfusion and tissue remodeling after severe hind limb ischemia. *Journal of Controlled Release* **202** (2015).

414. Bendinelli, P. *et al.* Molecular basis of anti-inflammatory action of platelet-rich plasma on human chondrocytes: Mechanisms of NF-κB inhibition via HGF. *Journal of Cellular Physiology* **225** (3 2010).

415. Drago, L. *et al.* Plasma components and platelet activation are essential for the antimicrobial properties of autologous platelet-rich plasma: An in vitrostudy. *PLoS ONE* **9** (9 2014).

416. Anitua, E. *et al.* Antibacterial effect of plasma rich in growth factors (PRGF-Endoret) against Staphylococcus aureus and Staphylococcus epidermidis strains. *Clinical and Experimental Dermatology* **37** (6 2012).

417. Anitua, E. *et al.* Plasma rich in growth factors (PRGF-Endoret) stimulates proliferation and migration of primary keratocytes and conjunctival fibroblasts and inhibits and reverts TGF-β1-induced myodifferentiation. *Investigative Ophthalmology and Visual Science* **52** (9 2011).

418. Ibares-Frías, L. *et al.* Potential Effect of Plasma Rich in Growth Factors-Endoret in Stromal Wound Healing in Additive Surgery. *Ophthalmic Research* **63** (2 2020).

419. Sánchez-Ávila, R. M. *et al.* Treatment of patients with neurotrophic keratitis stages 2 and 3 with plasma rich in growth factors (PRGF-Endoret) eye-drops. *International Ophthalmology* **38** (3 2018).

420. Sánchez-Ávila, R. M. *et al.* Plasma rich in growth factors for the treatment of dry eye after LASIK surgery. *Ophthalmic Research* **60** (2 2018).

421. Sánchez-Ávila, R. M. *et al.* Plasma rich in growth factors eye drops to treat secondary ocular surface disorders in patients with glaucoma. *International Medical Case Reports Journal* **11** (2018).

422. Anitua, E., Muruzabal, F., Alcalde, I., Merayo-Lloves, J. & Orive, G. Plasma rich in growth factors (PRGF-Endoret) stimulates corneal wound healing and reduces haze formation after PRK surgery. *Experimental Eye Research* **115** (2013).

423. Sánchez-Ávila, R. M. *et al.* Plasma rich in growth factors versus Mitomycin C in photorefractive keratectomy. *Medicine (United States)* **100** (3 2021).

424. Freire, V. *et al.* Corneal wound healing promoted by 3 blood derivatives: An in vitro and in vivo comparative study. *Cornea* **33** (6 2014).

425. Etxebarria, J. *et al.* Serum from plasma rich in growth factors regenerates rabbit corneas by promoting cell proliferation, migration, differentiation, adhesion and limbal stemness. *Acta Ophthalmologica* **95** (8 2017).

426. Kakavand, M., Yazdanpanah, G., Ahmadiani, A. & Niknejad, H. Blood compatibility of human amniotic membrane compared with heparin-coated ePTFE for vascular tissue engineering. *Journal of Tissue Engineering and Regenerative Medicine* **11** (6 2017).

427. Garfias, Y., Zaga-Clavellina, V., Vadillo-Ortega, F., Osorio, M. & Jiménez-Martínez, M. C. Amniotic membrane is an immunosuppressor of peripheral blood mononuclear cells. *Immunological Investigations* **40** (2 2011).

428. Kubo, M., Sonoda, Y., Muramatsu, R. & Usui, M. Immunogenicity of human amniotic membrane in experimental xenotransplantation. *Investigative Ophthalmology and Visual Science* **42** (7 2001).

429. Yazdanpanah, G., Paeini-Vayghan, G., Asadi, S. & Niknejad, H. The effects of cryopreservation on angiogenesis modulation activity of human amniotic membrane. *Cryobiology* **71** (3 2015).

430. Niknejad, H., Yazdanpanah, G. & Ahmadiani, A. Induction of apoptosis, stimulation of cell-cycle arrest and inhibition of angiogenesis make human amnion-derived cells promising sources for cell therapy of cancer. *Cell and Tissue Research* **363** (3 2016).

431. Ogawa, Y. *et al.* Heavy Chain-Hyaluronan/Pentraxin 3 from Amniotic Membrane Suppresses Inflammation and Scarring in Murine Lacrimal Gland and Conjunctiva of Chronic Graft-versus-Host Disease. *Scientific Reports* **7** (2017).

432. Asl, N. S. *et al.* Amniotic membrane extract eye drop promotes limbal stem cell proliferation and corneal epithelium healing. *Cell Journal* **20** (4 2019).

433. Baradaran-Rafii, A. *et al.* The role of amniotic membrane extract eye drop (AMEED) in in vivo cultivation of limbal stem cells. *Ocular Surface* **16** (1 2018).

434. Le, Q. & Deng, S. X. The application of human amniotic membrane in the surgical management of limbal stem cell deficiency. *Ocular Surface* **17** (2 2019).

435. Suri, K. *et al.* Sutureless amniotic membrane ProKera for ocular surface disorders: Short-term results. *Eye and Contact Lens* **39** (5 2013).

436. Tan, S. L. *et al.* Human amnion as a novel cell delivery vehicle for chondrogenic mesenchymal stem cells. *Cell and Tissue Banking* **12** (1 2011).

437. Qi, X., Wang, J., Sun, D., Zhou, Q. & Xie, L. Postoperative changes in amniotic membrane as a carrier for allogeneic cultured limbal epithelial transplantation. *American Journal of Ophthalmology* **158** (6 2014).

438. Dudok, D. V. *et al.* Effects of amniotic membrane extract on primary human corneal epithelial and limbal cells. *Clinical and Experimental Ophthalmology* **43** (5 2015).

439. Jiang, A. *et al.* In Vivo and In Vitro Inhibitory Effect of Amniotic Extraction on Neovascularization. *Cornea* **25** (Supplement 1 2006).

440. Shakouri-Motlagh, A., O'Connor, A. J., Kalionis, B. & Heath, D. E. Improved ex vivo expansion of mesenchymal stem cells on solubilized acellular fetal membranes. *Journal of Biomedical Materials Research - Part A* **107** (1 2019).

441. Kang, M.-J., Lee, J. H., Hwang, J. & Chung, S.-H. Efficacy and safety of platelet-rich plasma and autologous-serum eye drops for dry eye in primary Sjögren's syndrome: a randomized trial. *Scientific Reports* **13,** 19279 (1 2023).

442. Wróbel-Dudzińska, D. *et al.* The Comparison between the Composition of 100% Autologous Serum and 100% Platelet-Rich Plasma Eye Drops and Their Impact on the Treatment Effectiveness of Dry Eye Disease in Primary Sjogren Syndrome. *Journal of Clinical Medicine* **12** (9 2023).

443. Anitua, E. *et al.* Plasma rich in growth factors (PRGF) eye drops stimulates scarless regeneration compared to autologous serum in the ocular surface stromal fibroblasts. *Experimental Eye Research* **135** (2015).

444. Kim, K. M., Shin, Y. T. & Kim, H. K. Effect of autologous platelet-rich plasma on persistent corneal epithelial defect after infectious keratitis. *Japanese Journal of Ophthalmology* **56** (6 2012).

445. Metheetrairut, C. *et al.* Comparison of epitheliotrophic factors in platelet-rich plasma versus autologous serum and their treatment efficacy in dry eye disease. *Scientific Reports* **12** (1 2022).

446. Anitua, E., De la Fuente, M., Muruzabal, F. & Merayo-Lloves, J. Development and optimization of a personalized fibrin membrane derived from the plasma rich in growth factors technology. *Experimental Eye Research* **203** (2021).

447. Anitua, E., De la Fuente, M., Merayo-Lloves, J. & Muruzabal, F. Optimization of a Plasma Rich in Growth Factors Membrane for the Treatment of Inflammatory Ocular Diseases. *Bioengineering* **9** (10 2022).

448. Gicquel, J. J. *et al.* Epidermal growth factor variations in amniotic membrane used for ex vivo tissue constructs. *Tissue Engineering - Part A* **15** (8 2009).

449. Yu, M. H. *et al.* Region-specific gene expression profiling: Novel evidence for biological heterogeneity of the human amnion. *Biology of Reproduction* **79** (5 2008).

450. Litwiniuk, M., Radowicka, M., Krejner, A., Śladowska, A. & Grzela, T. Amount and distribution of selected biologically active factors in amniotic membrane

depends on the part of amnion and mode of childbirth. Can we predict properties of amnion dressing? A proof-of-concept study. *Central European Journal of Immunology* **43** (1 2018).

451. Banerjee, A. *et al.* Oxygen tension strongly influences metabolic parameters and the release of interleukin-6 of human amniotic mesenchymal stromal cells in vitro. *Stem Cells International* **2018** (2018).
452. Mahbod, M. *et al.* Amniotic Membrane Extract Preparation: What is the Best Method? *Journal of Ophthalmic and Vision Research* **9** (3 2014).
453. Cordero-Coma, M. & Sobrin, L. Antietumor necrosis factor-α therapy in uveitis. *Survey of Ophthalmology* **60** (6 2015).
454. Simonini, G., Druce, K., Cimaz, R., Macfarlane, G. J. & Jones, G. T. Current evidence of anti-tumor necrosis factor α treatment efficacy in childhood chronic uveitis: A systematic review and meta-analysis approach of individual drugs. *Arthritis Care and Research* **66** (7 2014).
455. Antao, S. F., Ayoub, T., Tahir, H. & Parmar, D. N. Stabilization of Bilateral Progressive Rheumatoid Corneal Melt with Infliximab. *Case Reports in Ophthalmological Medicine* **2012** (2012).
456. Benchérifa, S., Amine, B., Binoune, I. E., Rostom, S. & Bahiri, R. Two cases of perforated corneal ulcers complicating rheumatoid arthritis treated successfully by biological therapy. *BMC Rheumatology* **4** (1 2020).
457. Robert, M. C. *et al.* Infliximab after Boston Keratoprosthesis in Stevens–Johnson Syndrome: An Update. *Ocular Immunology and Inflammation* **25** (3 2017).
458. Thomas, J. W. & Pflugfelder, S. C. Therapy of progressive rheumatoid arthritis-associated corneal ulceration with infliximab. *Cornea* **24** (6 2005).
459. Odorcic, S., Keystone, E. C. & Ma, J. J. Infliximab for the treatment of refractory progressive sterile peripheral ulcerative keratitis associated with late corneal perforation: 3-year follow-up. *Cornea* **28** (1 2009).
460. Pham, M., Chow, C. C., Badawi, D. & Tu, E. Y. Use of infliximab in the treatment of peripheral ulcerative keratitis in Crohn disease. *American Journal of Ophthalmology* **152** (2 2011).
461. Li, Z., Choi, W., Oh, H. J. & Yoon, K. C. Effectiveness of topical infliximab in a mouse model of experimental dry eye. *Cornea* **31** (11 SUPPL.1 2012).
462. Kim, J. W. & Chung, S. K. The effect of topical infliximab on corneal neovascularization in rabbits. *Cornea* **32** (2 2013).

463. Claude, R. M. *Topical Infliximab for Sterile Corneal Melt* Dec. 2022.

464. Chen, W. *et al.* Intraarticular injection of infliximab-loaded thermosensitive hydrogel alleviates pain and protects cartilage in rheumatoid arthritis. *Journal of Pain Research* **13** (2020).

465. Bon, I., Cano-Sarabia, M., De la Ossa, N., Bartolí, R. & Lorenzo-Zúñiga, V. Development and Characterization of a New Endoscopic Drug-Eluting Platform With Proven Efficacy in Acute and Chronic Experimental Colitis. *Frontiers in Medicine* **7** (2020).

466. Steven, M. *et al.* Delivery of therapeutic infliximab from nanostructured porous silicon. *Frontiers in Bioengineering and Biotechnology* **4** (2016).

467. Moiseev, R. V., Morrison, P. W., Steele, F. & Khutoryanskiy, V. V. Penetration enhancers in ocular drug delivery. *Pharmaceutics* **11** (7 2019).

468. Liu, C. Y. & Kao, W. W. Y. Corneal Epithelial Wound Healing. *Progress in Molecular Biology and Translational Science* **134,** 61–71 (Jan. 2015).

469. Suzuki, K., Tanaka, T., Enoki, M. & Nishida, T. Coordinated reassembly of the basement membrane and junctional proteins during corneal epithelial wound healing. *Investigative Ophthalmology and Visual Science* **41** (9 2000).

470. Klenkler, B. & Sheardown, H. Growth factors in the anterior segment: Role in tissue maintenance, wound healing and ocular pathology. *Experimental Eye Research* **79** (5 2004).

471. Eraslan, M. & Toker, E. Mechanisms of corneal wound healing and its modulation following refractive surgery. *Marmara Medical Journal* **22** (2 2009).

472. Medeiros, C. S. *et al.* The impact of photorefractive keratectomy and Mitomycin C on corneal nerves and their regeneration. *Journal of Refractive Surgery* **34** (12 2018).

473. Fini, M. E. & Stramer, B. M. How the cornea heals: Cornea-specific repair mechanisms affecting surgical outcomes. *Cornea* **24** (8 SUPPL. 2005).

474. Maharjan, S. S., Pant, A. R., Joshi, P., Shrestha, P. & Sharma, R. Outcomes of Fungal Corneal Ulcer with Impending Perforation after Temporary Suture Tarsorrhaphy. *Nepalese Journal of Ophthalmology* **14** (1 2022).

475. Bamrolia, N. R., Arora, R. & Yadava, U. Unusual presentation of a case of Sjogren's syndrome with neurological and ocular manifestation. *Contact Lens and Anterior Eye* **35** (2 2012).

476. Zhang, W. *et al.* Healing Ability of Central Corneal Epithelium in Rabbit Ocular Surface Injury Models. *Translational Vision Science and Technology* **11** (6 2022).

477. Chun, Y. H. *et al.* In vivo biocompatibility evaluation of in situ-forming polyethylene glycol-collagen hydrogels in corneal defects. *Scientific Reports* **11** (1 2021).

478. Akyol-Salman, I. Effects of autologous serum eye drops on corneal wound healing after superficial keratectomy in rabbits. *Cornea* **25** (10 2006).

479. Freire, V., Andollo, N., Etxebarria, J., Durán, J. A. & Morales, M. C. In vitro effects of three blood derivatives on human corneal epithelial cells. *Investigative Ophthalmology and Visual Science* **53** (9 2012).

480. Suárez-Barrio, C. *et al.* Hyaluronic acid combined with serum rich in growth factors in corneal epithelial defects. *International Journal of Molecular Sciences* **20** (7 2019).

481. Choi, J. A. *et al.* Effects of amniotic membrane suspension in human corneal wound healing in vitro. *Molecular vision* **15** (2009).

482. Hu, S. *et al.* Human amniotic epithelial cell-derived extracellular vesicles provide an extracellular matrix-based microenvironment for corneal injury repair. *Journal of Tissue Engineering* **13** (2022).

483. Uchida, M. *et al.* Safety of Infliximab for the Eye Under Human T-Cell Leukemia Virus Type 1 Infectious Conditions in vitro. *Frontiers in Microbiology* **10** (2019).

484. Duijvestein, M. *et al.* Mesenchymal stromal cell function is not affected by drugs used in the treatment of inflammatory bowel disease. *Cytotherapy* **13** (9 2011).

485. Hwang, E. S., Schallhorn, J. M. & Randleman, J. B. Utility of regional epithelial thickness measurements in corneal evaluations. *Survey of Ophthalmology* **65** (2 2020).

486. Li, H. *et al.* Platelet-Rich Plasma Promotes the Proliferation of Human Muscle Derived Progenitor Cells and Maintains Their Stemness. *PLoS ONE* **8** (6 2013).

487. Andia, I. & Abate, M. Platelet-rich plasma in the treatment of skeletal muscle injuries. *Expert Opinion on Biological Therapy* **15** (7 2015).

488. Lai, J. Y. & Luo, L. J. Effect of riboflavin concentration on the development of photo-crosslinked amniotic membranes for cultivation of limbal epithelial cells. *RSC Advances* **5** (5 2015).

489. Movahedan, A. *et al.* Loss of Notch1 Disrupts the Barrier Repair in the Corneal Epithelium. *PLoS ONE* **8** (7 2013).

490. An, S. *et al.* Wound-Healing Effects of Mesenchymal Stromal Cell Secretome in the Cornea and the Role of Exosomes. *Pharmaceutics* **15** (5 2023).

491. Knudson, W. & Peterson, R. S. *The Hyaluronan Receptor: CD44* 2004.

492. Zhu, S. N. Expression of adhesion molecule CD44 on human corneas. *British Journal of Ophthalmology* **81** (1 1997).

493. Zhong, J. *et al.* Hyaluronate acid-dependent protection and enhanced corneal wound healing against oxidative damage in corneal epithelial cells. *Journal of Ophthalmology* **2016** (2016).

494. Gomes, J. A., Amankwah, R., Powell-Richards, A. & Dua, H. S. Sodium hyaluronate (hyaluronic acid) promotes migration of human corneal epithelial cells in vitro. *British Journal of Ophthalmology* **88** (6 2004).

495. Lauweryns, B., den Oord, J. J. V., Volpes, R., Foets, B. & Missotten, L. Distribution of very late activation integrins in the human cornea: An immunohistochemical study using monoclonal antibodies. *Investigative Ophthalmology and Visual Science* **32** (7 1991).

496. Stepp, M. A. Corneal integrins and their functions. *Experimental Eye Research* **83,** 3–15 (1 July 2006).

497. Nishida, T., Inui, M. & Nomizu, M. Peptide therapies for ocular surface disturbances based on fibronectin–integrin interactions. *Progress in Retinal and Eye Research* **47,** 38–63 (July 2015).

498. Fukuda, K., Yamada, N. & Nishida, T. Case report of restoration of the corneal epithelium in a patient with atopic keratoconjunctivitis resulting in amelioration of ocular allergic inflammation. *Allergology International* **59** (3 2010).

499. Morita, Y. *et al.* New mode of treatment for lattice corneal dystrophy type I: Corneal epithelial debridement and fibronectin eye drops. *Japanese Journal of Ophthalmology* **56** (1 2012).

500. Yamada, N. *et al.* Open clinical study of eye drops containing the fibronectin-derived peptide PHSRN for treatment of persistent corneal epithelial defects. *Cornea* **31** (12 2012).

501. Hu, Y. *et al.* Highly stable fibronectin-mimetic-peptide-based supramolecular hydrogel to accelerate corneal wound healing. *Acta Biomaterialia* **159,** 128–139 (Mar. 2023).

502. Hu, Z. *et al.* Biological importance of human amniotic membrane in tissue engineering and regenerative medicine. *Materials Today Bio* **22** (2023).

503. Wilson, S. E. Corneal myofibroblast biology and pathobiology: Generation, persistence, and transparency. *Experimental Eye Research* **99** (1 2012).

504. Yam, G. H., Riau, A. K., Funderburgh, M. L., Mehta, J. S. & Jhanji, V. Keratocyte biology. *Experimental Eye Research* **196** (2020).

505. Wilson, S. E. The corneal fibroblast: The Dr. Jekyll underappreciated overseer of the responses to stromal injury. *Ocular Surface* **29** (2023).

506. Acosta, A. C. *et al.* Keratocyte-Derived Myofibroblasts: Functional Differences With Their Fibroblast Precursors. *Investigative Ophthalmology and Visual Science* **64** (13 2023).

507. Chen, Y. *et al.* Effects of Gelatin Methacrylate Hydrogel on Corneal Repair and Regeneration in Rats. *Translational Vision Science and Technology* **10** (14 2021).

508. Ibañez, R. I. *et al.* 3d-printed gelatin methacrylate scaffolds with controlled architecture and stiffness modulate the fibroblast phenotype towards dermal regeneration. *Polymers* **13** (15 2021).

509. Saika, S. *et al.* Loss of osteopontin perturbs the epithelial-mesenchymal transition in an injured mouse lens epithelium. *Laboratory Investigation* **87** (2 2007).

510. Zheng, D. *et al.* Downregulation of transforming growth factor-β type II receptor prohibit epithelial-to-mesenchymal transition in lens epithelium. *Molecular Vision* **18** (2012).

511. Guo, R. *et al.* TGF-β2 induces epithelial-mesenchymal transition in cultured human lens epithelial cells through activation of the PI3K/Akt/mTOR signaling pathway. *Molecular Medicine Reports* **13** (2 2016).

512. Li, Y. *et al.* Effects of different sutures on fibrosis and wound healing in a rabbit model of corneal wounds. *Experimental and Therapeutic Medicine* **12** (5 2016).

513. Yu, B. *et al.* LRG1 facilitates corneal fibrotic response by inducing neutrophil chemotaxis via Stat3 signaling in alkali-burned mouse corneas. *American Journal of Physiology - Cell Physiology* **321** (3 2021).

514. Kwok, S. S. *et al.* Systematic Review on Therapeutic Strategies to Minimize Corneal Stromal Scarring after Injury. *Eye and Contact Lens* **45** (6 2019).

515. Gaballa, S. A. *et al.* Corticosteroids in ophthalmology: drug delivery innovations, pharmacology, clinical applications, and future perspectives. *Drug Delivery and Translational Research* **11** (3 2021).

516. Aung, Y. Y. & McLeod, A. Contact lens management of irregular corneas after traumatic aphakia: A pediatric case series. *Contact Lens and Anterior Eye* **38** (5 2015).

517. Maharana, P. *et al.* Component corneal surgery: An update. *Indian Journal of Ophthalmology* **65** (8 2017).

518. Chameettachal, S. *et al.* Prevention of Corneal Myofibroblastic Differentiation in Vitro Using a Biomimetic ECM Hydrogel for Corneal Tissue Regeneration. *ACS Applied Bio Materials* **4** (1 2021).

519. Chameettachal, S. *et al.* Human cornea-derived extracellular matrix hydrogel for prevention of post-traumatic corneal scarring: A translational approach. *Acta Biomaterialia* **171** (2023).

520. Liu, Y. & Hong, J. MSC-Laden In Situ–Forming Hydrogel for Preventing Corneal Stromal Opacity. *Cornea* (2024).

521. Huang, J. *et al.* Biomimetic Corneal Stroma for Scarless Corneal Wound Healing via Structural Restoration and Microenvironment Modulation. *Advanced Healthcare Materials* **13** (5 2024).

522. Menten, P., Wuyts, A. & Damme, J. V. Macrophage inflammatory protein-1. *Cytokine and Growth Factor Reviews* **13** (6 2002).

523. Wang, Y. *et al.* The role of matrix metalloproteinase 9 in fibrosis diseases and its molecular mechanisms. *Biomedicine & Pharmacotherapy* **171,** 116116 (Feb. 2024).

524. Qazi, B. S., Tang, K. & Qazi, A. Recent Advances in Underlying Pathologies Provide Insight into Interleukin-8 Expression-Mediated Inflammation and Angiogenesis. *International Journal of Inflammation* **2011** (2011).

525. Guan, G. *et al.* Upregulation of Neural Cell Adhesion Molecule 1 (NCAM1) by hsa-miR-141-3p Suppresses Ameloblastoma Cell Migration. *Medical Science Monitor* **26** (2020).

526. Ferrari, G., Bignami, F., Giacomini, C., Franchini, S. & Rama, P. Safety and efficacy of topical infliximab in a mouse model of ocular surface scarring. *Investigative Ophthalmology and Visual Science* **54** (3 2013).

527. Kamiya, K. *et al.* Topical application of culture supernatant from human amniotic epithelial cells suppresses inflammatory reactions in cornea. *Experimental Eye Research* **80** (5 2005).

528. Solomon, A *et al.* Suppression of interleukin 1α and interleukin 1β in human limbal epithelial cells cultured on the amniotic membrane stromal matrix. *The British journal of ophthalmology* **85,** 444–9 (4 Apr. 2001).

529. Tseng, S. C. HC-HA/PTX3 purified from amniotic membrane as novel regenerative matrix: Insight into relationship between inflammation and regeneration. *Investigative Ophthalmology and Visual Science* **57** (5 2016).

530. Wei, Y. & Asbell, P. A. The core mechanism of dry eye disease is inflammation. *Eye and Contact Lens* **40** (4 2014).

531. Celebi, A. R. C., Ulusoy, C. & Mirza, G. E. The efficacy of autologous serum eye drops for severe dry eye syndrome: A randomized double-blind crossover study. *Graefe's Archive for Clinical and Experimental Ophthalmology* **252** (4 2014).

532. Ali, T. K. *et al.* Use of Autologous Serum Tears for the Treatment of Ocular Surface Disease From Patients With Systemic Autoimmune Diseases. *American Journal of Ophthalmology* **189** (2018).

533. Shtein, R. M. *et al.* Autologous Serum-Based Eye Drops for Treatment of Ocular Surface Disease: A Report by the American Academy of Ophthalmology. *Ophthalmology* **127** (1 2020).

534. Alio, J. L., Colecha, J. R., Pastor, S., Rodríguez, A. & Artola, A. Symptomatic dry eye treatment with autologous platelet-rich plasma. *Ophthalmic Research* **39** (3 2007).

535. Alio, J. L., Rodríguez, A. E., Ferreira-Oliveira, R., Wróbel-Dudzińska, D. & Abdelghany, A. A. Treatment of Dry Eye Disease with Autologous Platelet-Rich Plasma: A Prospective, Interventional, Non-Randomized Study. *Ophthalmology and Therapy* **6** (2 2017).

536. García-Conca, V. *et al.* Efficacy and safety of treatment of hyposecretory dry eye with platelet-rich plasma. *Acta Ophthalmologica* **97** (2 2019).

537. Oranskiy, S. P., Yeliseyeva, L. N., Tsanaeva, A. V. & Zaytseva, N. V. Body composition and serum levels of adiponectin, vascular endothelial growth factor, and interleukin-6 in patients with rheumatoid arthritis. *Croatian Medical Journal* **53** (4 2012).

538. Hwang, J. *et al.* Comparison of clinical efficacies of autologous serum eye drops in patients with primary and secondary sjögren syndrome. *Cornea* **33** (7 2014).

539. Chen, Y. *et al.* High circulating level of interleukin-18 in patients with primary Sjögren's syndrome is associated with disease activity. *Modern Rheumatology* **26** (1 2016).

540. Shortt, A. J. *et al.* Characterization of the Limbal Epithelial Stem Cell Niche: Novel Imaging Techniques Permit In Vivo Observation and Targeted Biopsy of Limbal Epithelial Stem Cells. *Stem Cells* **25** (6 2007).

541. Ordoñez, P. & Girolamo, N. D. Concise review: Limbal epithelial stem cells: Role of the niche microenvironment. *Stem Cells* **30** (2 2012).

542. Mei, H., González, S. & Deng, S. Extracellular Matrix is an Important Component of Limbal Stem Cell Niche. *Journal of Functional Biomaterials* **3** (4 2012).

543. Di Iorio, E. *et al.* Isoforms of ΔNp63 and the migration of ocular limbal cells in human corneal regeneration. *Proceedings of the National Academy of Sciences of the United States of America* **102** (27 2005).

544. Joseph, A., Powell-Richards, A. O., Shanmuganathan, V. A. & Dua, H. S. Epithelial cell characteristics of cultured human limbal explants. *British Journal of Ophthalmology* **88** (3 2004).

545. Rama, P. *et al.* Limbal Stem-Cell Therapy and Long-Term Corneal Regeneration. *New England Journal of Medicine* **363** (2 2010).

546. Dziasko, M. A. *et al.* Localisation of epithelial cells capable of holoclone formation in vitro and direct interaction with stromal cells in the native human limbal crypt. *PLoS ONE* **9** (4 2014).

547. Dziasko, M. A., Tuft, S. J. & Daniels, J. T. Limbal melanocytes support limbal epithelial stem cells in 2D and 3D microenvironments. *Experimental Eye Research* **138** (2015).

548. Polisetti, N. *et al.* Laminin-511-E8 promotes efficient in vitro expansion of human limbal melanocytes. *Scientific Reports* **10** (1 2020).

549. Waal, R. M. D., Semeijn, J. T., Cornelissen, I. M. & Ramaekers, F. C. Epidermal Langerhans cells contain intermediate-sized filaments of the vimentin type: An immunocytologic study. *Journal of Investigative Dermatology* **82** (6 1984).

550. Higa, K., Shimmura, S., Miyashita, H., Shimazaki, J. & Tsubota, K. Melanocytes in the corneal limbus interact with K19-positive basal epithelial cells. *Experimental Eye Research* **81** (2 2005).

551. Si, S. P., Tsou, H. C., Lee, X. & Peacocke, M. Cultured human melanocytes express the intermediate filament vimentin. *Journal of Investigative Dermatology* **101** (3 1993).

552. Vantrappen, L., Geboes, K., Missotten, L., Maudgal, P. C. & Desmet, V. Lymphocytes and Langerhans cells in the normal human cornea. *Investigative Ophthalmology and Visual Science* **26** (2 1985).

553. Nakatsu, M. N., González, S., Mei, H. & Deng, S. X. Human limbal mesenchymal cells support the growth of human corneal epithelial stem/progenitor cells. *Investigative ophthalmology & visual science* **55** (10 2014).

554. Li, G. *et al.* Human limbal niche cells are a powerful regenerative source for the prevention of limbal stem cell deficiency in a rabbit model. *Scientific Reports* **8** (1 2018).

555. Polisetti, N. *et al.* Melanocytes as emerging key players in niche regulation of limbal epithelial stem cells. *Ocular Surface* **22** (2021).

556. Polisetti, N., Sharaf, L., Schlötzer-Schrehardt, U., Schlunck, G. & Reinhard, T. Efficient Isolation and Functional Characterization of Niche Cells from Human Corneal Limbus. *International Journal of Molecular Sciences* **23** (5 2022).

557. Polisetti, N. *et al.* A decellularized human limbal scaffold for limbal stem cell niche reconstruction. *International Journal of Molecular Sciences* **22** (18 2021).

PUBLISHED ARTICLES

International Journal of
Molecular Sciences

MDPI

Article

Cytocompatibility and Suitability of Protein-Based Biomaterials as Potential Candidates for Corneal Tissue Engineering

Cristina Romo-Valera [1], Pedro Guerrero [2,3], Jon Arluzea [1], Jaime Etxebarria [1,4], Koro de la Caba [2,3] and Noelia Andollo [1,4,*,†]

1 Department of Cell Biology and Histology, School of Medicine and Nursing, University of the Basque Country (UPV/ EHU), Barrio Sarriena S/N, 48940 Leioa, Spain; cristinaromo1@gmail.com (C.R.-V.); jon.arluzea@ehu.eus (J.A.); JAIME.ECHEVARRIAECENARRO@osakidetza.eus (J.E.)
2 BIOMAT Research Group, Escuela de Ingeniería de Gipuzkoa, University of the Basque Country (UPV/EHU), Plaza de Europa 1, 20018 Donostia-San Sebastián, Spain; pedromanuel.guerrero@ehu.es (P.G.); koro.delacaba@ehu.es (K.d.l.C.)
3 BCMaterials, Basque Center for Materials, Applications and Nanostructures, UPV/EHU Science Park, 48940 Leioa, Spain
4 Department of Ophthalmology, BioCruces Bizkaia Health Research Institute, University Hospital of Cruces, Begiker, Plaza de Cruces S/N, 48903 Barakaldo, Spain
* Correspondence: noelia.andollo@ehu.eus; Tel.: +34-94-601-3295
† N.A. belongs to the Spanish Society for Cell Biology (SEBC).

check for updates

Citation: Romo-Valera, C.; Guerrero, P.; Arluzea, J.; Etxebarria, J.; de la Caba, K.; Andollo, N. Cytocompatibility and Suitability of Protein-Based Biomaterials as Potential Candidates for Corneal Tissue Engineering. *Int. J. Mol. Sci.* **2021**, *22*, 3648. https://doi.org/10.3390/ijms22073648

Academic Editor: Antonino Mazzaglia

Received: 26 February 2021
Accepted: 30 March 2021
Published: 31 March 2021

Abstract: The vision impairments suffered by millions of people worldwide and the shortage of corneal donors show the need of substitutes that mimic native tissue to promote cell growth and subsequent tissue regeneration. The current study focused on the in vitro assessment of protein-based biomaterials that could be a potential source for corneal scaffolds. Collagen, soy protein isolate (SPI), and gelatin films cross-linked with lactose or citric acid were prepared and physicochemical, transmittance, and degradation measurements were carried out. In vitro cytotoxicity, cell adhesion, and migration studies were performed with human corneal epithelial (HCE) cells and 3T3 fibroblasts for the films' cytocompatibility assessment. Transmittance values met the cornea's needs, and the degradation profile revealed a progressive biomaterials' decomposition in enzymatic and hydrolytic assays. Cell viability at 72 h was above 70% when exposed to SPI and gelatin films. Live/dead assays and scanning electron microscopy (SEM) analysis demonstrated the adhesion of both cell types to the films, with a similar arrangement to that observed in controls. Besides, both cell lines were able to proliferate and migrate over the films. Without ruling out any material, the appropriate optical and biological properties shown by lactose-crosslinked gelatin film highlight its potential for corneal bioengineering.

Keywords: corneal scaffolds; collagen; gelatin; SPI; cross-linking; cytocompatibility; optical properties; biodegradability

1. Introduction

When a large injury or trauma is suffered, the damage caused to the tissues exceeds in some cases their healing capacity, making transplantation necessary to help them restore their function. However, the great imbalance between the demand and available donors and the possible complications related to graft rejection has led to the seeking of alternative solutions. It is in this search for new tissue substitutes where the market and the potential of biomaterials has gotten involved, which is estimated to be close to $150 billion by 2021 [1].

The tissue engineering field is one of the areas in which the applicability of biomaterials could lead to valuable clinical outcomes, where they aim to mimic the structure of native components and extracellular matrix (ECM) to promote cell growth and subsequent tissue regeneration. Protein-based materials are some of the available alternatives.

Collagen is one of the most interesting proteins derived from a tissue source, as it is the most abundant protein in the ECM [2]. In this study, collagen was extracted from porcine skin. By virtue of its various advantages as being biodegradable, biocompatible, highly adaptable, or easily available, the use of collagen and collagen-derived materials has recently been widely increased in tissue engineering applications.

Gelatin is a natural protein derived from partially denatured collagen obtainable from the skin, bone, or connective tissue of all animal species [3]. Its biocompatibility, film formation capacity, and biodegradability are some of the characteristics that make it a suitable alternative for use as implantable biomaterials for regenerative medicine [4–7]. Likewise, the presence of arginine-glycine-aspartic (RGD) sequences in this polymer facilitate cellular uptake, the functional groups of the amino acid residues allow the structural modification of this material, and its ability to absorb large volumes of water facilitate hydrogels' formation. Besides, depending on the cross-linking agent used to improve its mechanical behavior, the stability and strength of the resulting structure differ, leading to a material with unique properties. In this work, gelatin was cross-linked with lactose through a non-enzymatic glycation known as Maillard reaction [8] or with citric acid, a tricarboxylic acid that forms amide bonds through the nucleophilic reaction between the amino groups of gelatin and the carboxyl groups of the acid [9].

Plant-derived proteins have also been studied. Soy protein, for example, has shown promising characteristics for its application in the biomedical field. In particular, soy protein isolate (SPI), obtained from soy flour [10], can be physically and chemically modified or combined with other polymers, mainly through its amino and hydroxyl groups [11]. Furthermore, the anti-inflammatory and antioxidant effects offered by its high amount of isoflavones provide properties to promote wound healing [12].

Within this field of tissue engineering, the development of tissue analogues for corneal tissue has become the focus of many current investigations. Naturally-derived materials (e.g., collagen, gelatin, silk fibroin, decellularized corneas, chitosan, hyaluronic acid, etc.), synthetic polymers (e.g., polyethylene glycol-based materials, poly glycolic acid (PGA), acrylate-based polymers, etc.), or composite materials have been proposed for corneal bioengineering approaches with various degree of success [13]. Overall, materials of natural origin tend to be highly biocompatible and can be integrated with no adverse effects; however, they can sometimes increase the chances of rejection by the host tissue or show insufficient mechanical properties. Synthetic materials give the chance to adapt the mechanical and chemical needs to each therapeutic case, but their toxicity evaluation is important because the compounds released when they are degraded can induce adverse reactions that could harm body tissues. Lastly, composite materials aim to combine the advantages of both natural and synthetic materials, such as maintaining biocompatibility while improving strength and controlling degradation rate.

Collagen and its derivatives combined with other materials or crosslinking agents have been the materials of choice of many studies. For instance, Isaacson et al., used sodium alginate and methacrylated type I collagen to prepare bioinks, including corneal keratocytes for developing corneal stromal equivalents. The 3D printed and encapsulated cells demonstrated viability values of 83% seven days post printing [14]. Jumelle et al., used their own patent named GelCORE, consisting of an in situ photo-polymerizable gelatin methacryloyl (GelMA), for healing corneal defects. They incorporated HGF in the developed hydrogel to promote the healing of corneal wounds and tested it in ex vivo models of pig corneal defects [15].

Alternatively, Wang et al. opted for silk fibroin for the development of a corneal model including stroma, epithelium, and innervation. This material allowed them to adjust its mechanical properties and to mold it into transparent films or sponges that could support the growth of neurons and the formation of neuronal connections [16].

The use of composites has also been reported. McTiernan et al. combined collagen-like peptides with polyethylene glycol and mixed with fibrinogen to create an adhesive hydrogel to treat corneal ulcers [17]. Similarly, Rico-Sánchez et al. developed a fibrin–

0.1% agarose scaffold containing corneal epithelial cells and human allogeneic stromal keratocytes to mimic the human native anterior cornea. This construct is currently under phase 1/2 clinical trial [18].

Therefore, designing natural or biosynthetic alternatives to human donor corneas has recently gained more attention as it could become a very useful tissue substitute source for overcoming the shortage of supplies, the increasing length of waiting lists and donors' waiting times, and the rejection limitations related to cadaveric grafts.

One of the strategies to deal with the challenge of mimicking the complex nature of the cornea in terms of mechanical, optical, and biological properties is to focus on the development of scaffolds for the cells of the epithelial, stromal, and endothelial layers. Within this context, the objective of this study was to evaluate the optical adequacy and the cytocompatibility of different natural materials (collagen, soy protein, and gelatin) for their use as corneal scaffolds. To do so, proliferation, adhesion, and migration processes were analyzed in vitro with both epithelial and stromal cells.

2. Results

2.1. Physicochemical and Morphological Analyses

Fourier transform infrared spectroscopy (FTIR) spectra of all films are shown in Figure 1. The broad band observed in the 3500–3000 cm^{-1} range is attributable to free and bound O–H and N–H groups (amide A), and the absorption peak at 2931 cm^{-1} is attributable to CH_2 asymmetrical stretching (Figure 1a) [19]. The main absorption bands of proteins are related to C=O stretching at 1635 cm^{-1} (amide I), N–H bending at 1545 cm^{-1} (amide II), and C–N stretching and N–H bending (amide III) at 1241 cm^{-1} (Figure 1b) [20]. Regarding the bands corresponding to the plasticizer, absorption bands of glycerol were located in the region from 800 cm^{-1} up to 1155 cm^{-1}, where the absorption band at 1051 cm^{-1} is related to the stretching of C–O bond [20]. Concerning the crosslinkers used in this study, the bands associated with lactose were located between 1180 and 953 cm^{-1} [21], while that related to the carboxylic groups of citric acid appeared at 1743 cm^{-1} [22]. When citric acid reacted with gelatin, the band at 1743 cm^{-1} disappeared, and the gelatin band at 1545 cm^{-1} shifted to 1585 cm^{-1} due to the crosslinking reaction.

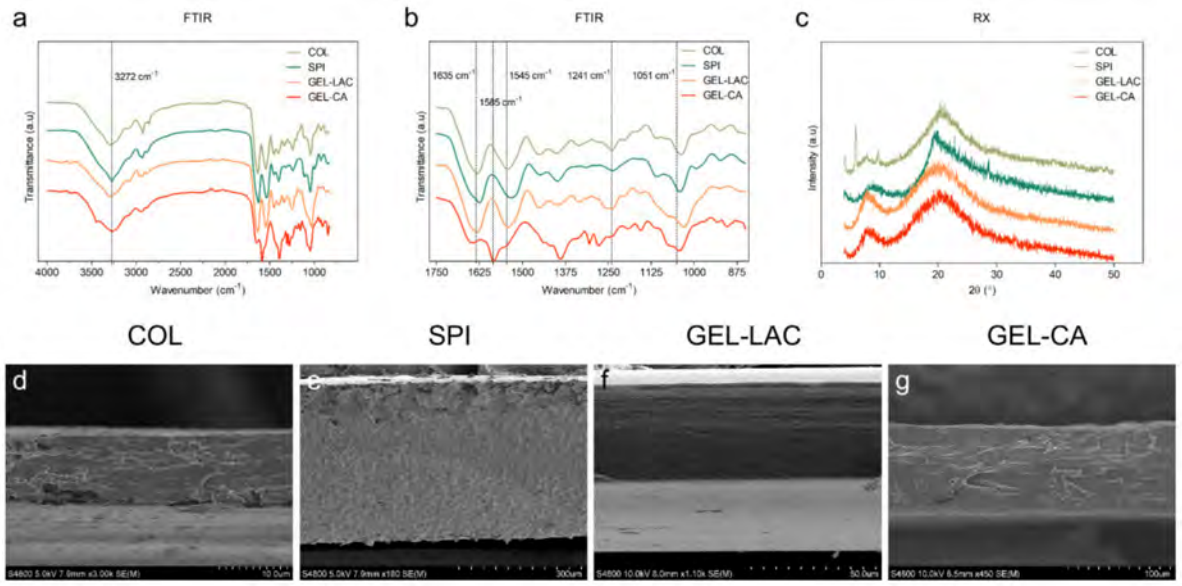

Figure 1. FTIR spectra of films (**a**) from 4000 to 850 cm^{-1} and (**b**) from 1750 to 850 cm^{-1}. (**c**) XRD patterns of films. (**d**–**g**) SEM image sections of films obtained with (**d**) 3000×, (**e**) 180×, (**f**) 1100×, and (**g**) 450× magnification. COL, collagen; SPI, soy protein isolate; GEL-LAC, lactose-cross-linked gelatin; GEL-CA, citric acid-cross-linked gelatin.

In order to investigate the film structure and relate it to the physicochemical properties measured, XRD and SEM analyses were carried out. As can be seen in Figure 1c, collagen (COL) films exhibited a XRD pattern characteristic of partially crystalline materials, with a small peak around 2 θ = 7°, indicating an intermolecular lateral packing distance between the molecular collagen chains and a broad diffuse peak at about 2 θ = 20° due to the diffuse scattering of collagen fibers, representing the amorphous structure of the films. The diffraction patterns of SPI films exhibited a dominant amorphous halo, with a broad band with a maximum at 2 θ = 20°, characteristic of SPI, which has 7S and 11S amorphous globulins as main components [23]. Lactose-cross-linked gelatin (GEL-LAC) films displayed two diffraction peaks: the peak at 21°, related to the crystallinity of gelatin; and the peak at 7.4°, corresponding to the residual triple helix from native collagen. In the same manner, citric acid-cross-linked gelatin (GEL-CA) films exhibited the characteristic peak of gelatin at about 21° and a distinctive diffraction peak corresponding to the triple-helix at a 2 θ value at around 8°. Regarding the film cross-section (Figure 1d–g), all films showed a compact and homogeneous morphology. COL films exhibited a dense fibrillar morphology, in accordance with the lateral packaging of collagen chains observed by XRD analysis. This fibrous morphology became less obvious for gelatin films due to the decrease of the triple helix content.

2.2. Light Transmittance and Transparency

COL (Figure 2a) and SPI (Figure 2b) films showed the lowest transmittance values, the dried films being more translucent than the hydrated ones. The differences in light transmission values between the dried and hydrated SPI films decreased as the wavelengths increased, and the differences were no longer statistically significant from 620 nm on. However, the dried collagen film transmitted around 30% more light than the hydrated sample across the entire visible spectrum. In both dried and hydrated SPI films as well as in dried COL films, around 60–80% of light was transmitted in almost all the wavelengths of the visible spectrum. However, the photographs showed blurred patterns, meaning that these films were translucent and allowed the passage of light but did not allow objects placed at a certain distance to be focused clearly (Figure 2e,f,i,j).

Gelatin films transmitted a higher amount of light once hydrated. Light transmission hardly varied in dried or hydrated GEL-LAC films (Figure 2c), and this was the film that transmitted the highest amount of light. The transmission decreased to a low value of 3% in the UVA region. This may indicate a beneficial protective property against this type of radiation. The transmission of light remained low in the wavelengths near the UVA region but increased exponentially as it moved toward yellow (570–580 nm), orange (580–620 nm), or reddish (620–780 nm) regions. The cross-linking procedure used in this film produced a yellowish hue compared with the rest of films, but this did not influence its almost total transparency. The photographed patterns were clear and readable (Figure 2g,k). The greatest light transmission improvement when the film was hydrated was registered for GEL-CA films. Their transparency increased around 20% throughout the visible spectrum, transmitting more than 80% of the incident light from 500 nm on (Figure 2d). This improvement was consistent with the change in transparency since the pattern was clearly recognizable when the film was hydrated (Figure 2h,l).

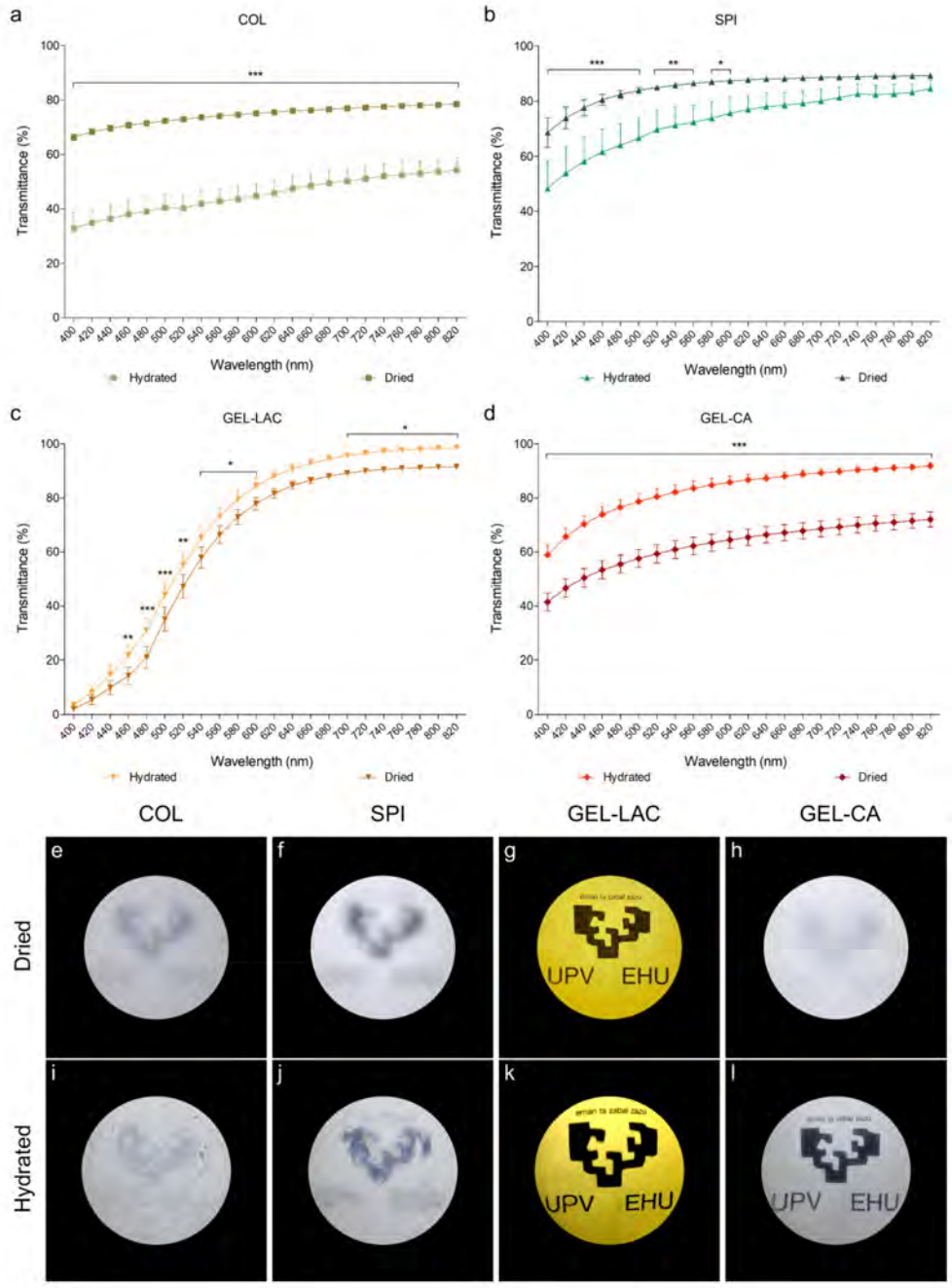

Figure 2. Light transmittance and transparency differences of dried and hydrated films. (**a**–**d**) Graphs show the percentage of light transmitted by each film in the visible spectrum. Data are represented as transmittance percentage mean ± SD. Statistically significant differences show differences of dried with respect to hydrated conditions of each film (* $p < 0.05$, ** $p < 0.01$, *** $p < 0.001$; $n = 9$). (**e**–**l**) Figures show the transparency degree of each film placed at 12 cm from a specific pattern for dried (**e**–**h**) and hydrated (**i**–**l**) films. All the images were taken of the same pattern and with the same conditions.

2.3. Degradability

The in vitro degradation profile revealed the behavior of films when exposed to collagenase A enzyme, PBS, or deionized water. Complete degradation of COL films was observed after 15 min immersed in enzymatic solution, probably because it was only

physically cross-linked. This complete degradation was translated as very significant statistical differences compared with the control (degradation profile in MilliQ water, Figure 3a). Similar degradation pattern was registered for PBS and MilliQ water solutions, but statistically significant differences were recorded at different time points ($p < 0.001$ at 15 min, 4 h, and 24 h; $p < 0.01$ at 1 h; and $p < 0.05$ at 2 h). Greater weight loss was caused by deionized water than by PBS.

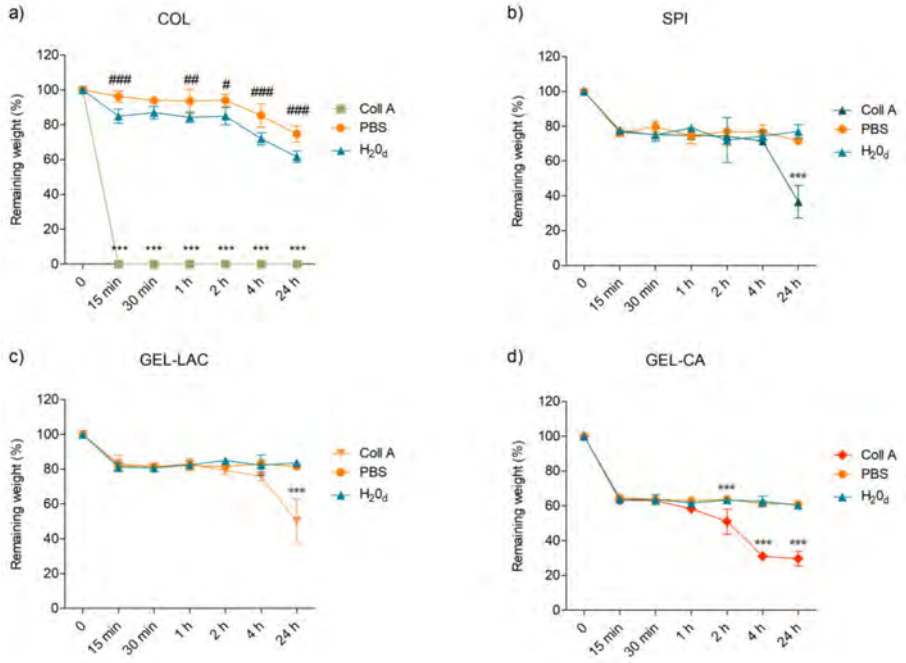

Figure 3. In vitro degradation of the films immersed in 200 ug/mL collagenase A solution or PBS alone at 37 °C over time. Films immersed in distilled water at 37 °C were used as control. **(a)** represents the degradation profiles of COL films; **(b)** the degradation profiles of SPI films; **(c)** the degradation profiles of GEL-LAC films and **(d)** the degradation profiles of GEL-CA films. Data are reported as means ± SD, and statistically significant differences of films in collagenase A (*) and PBS (#) are reported with respect to those in distilled water. * $p < 0.05$, ** $p < 0.01$, *** $p < 0.001$; # $p < 0.05$, ## $p < 0.01$, ### $p < 0.001$; $n = 3$.

A similar degradation trend was registered for SPI, GEL-LAC, and GEL-CA films (Figure 3b–d). A rapid weight decrease was recorded after 15 min in the presence of collagenase A, PBS, or MilliQ water. The remaining weight of SPI and GEL-LAC films after this time point was maintained around 70% and 80% in the subsequent time steps, and significant differences in relation to control were only recorded after 24 h of enzymatic degradation, when weight percentages decreased up to 40% and 50%, respectively. Regarding GEL-CA films, their weight was reduced up to 60% after being exposed to the three solutions during 15 min, and this weight percentage remained stable until 2 h. The effect of collagenase A became statistically significant in relation to hydrolytic degradation caused by MilliQ water and PBS from 2 h on, when only 30% of the initial weight remained. Unlike COL films, no significant differences between the weight loss caused by the control and PBS solution were observed in the rest of the films. GEL-LAC films suffered the lowest weight decrease in the presence of the enzyme, followed by SPI, GEL-CA, and COL films. The degradation differences between gelatin films highlighted the importance of the cross-linking agent used.

2.4. Cell Proliferation and Viability Results

Cell proliferation was studied at 0, 24, 48, and 72 h in 3T3 fibroblasts and human corneal epithelial (HCE) cells seeded in direct contact with the films. Wells with fresh medium and without the biomaterials were used as positive controls. Results showed a

time-dependent proliferation pattern in all the wells seeded with 3T3 cells and conditioned with the studied films but with significant differences for wells conditioned with collagen films (Figure 4). Although viability values close to 70% were recorded at 24 h compared with the control, the exposure of the cells to this film in the subsequent time points produced a mild to moderate cytotoxic effect. Statistically very significant differences were registered between the control group and COL films-conditioned cell culture at 48 and 72 h, when an average metabolic activity of 40% and 50%, respectively, were recorded. Viability values recorded for 3T3 cultures in contact with SPI, GEL-LAC, and GEL-CA films were higher than 70% at all the time points. The viability compared with the control at 72 h was 82, 89, and 73% for SPI, GEL-LAC, and GEL-CA films, respectively.

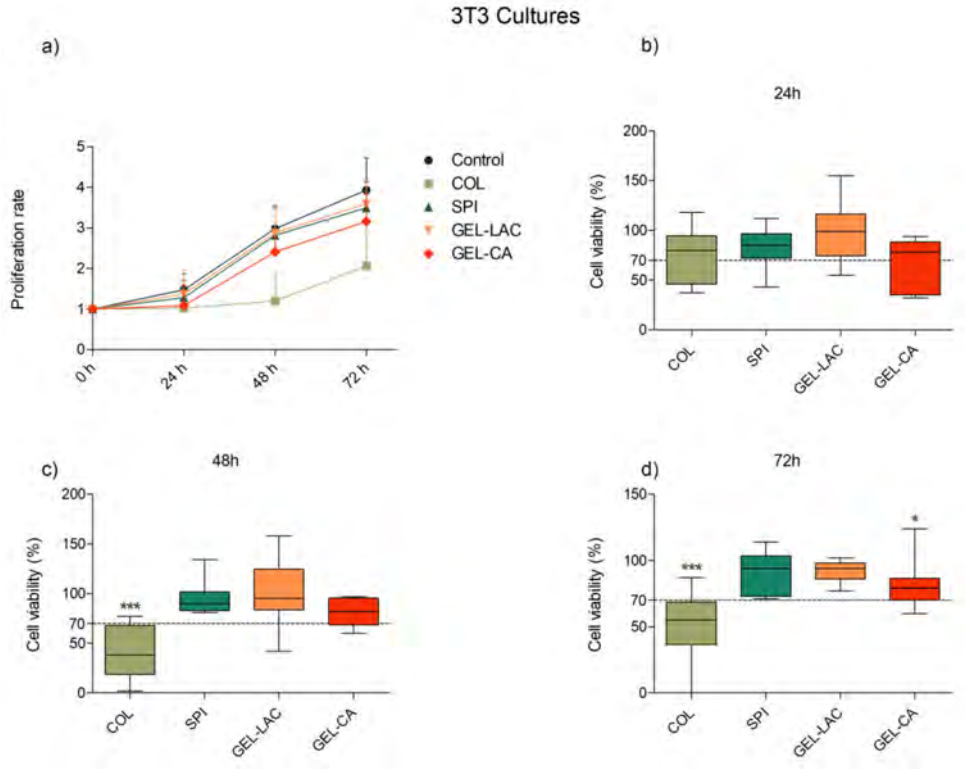

Figure 4. Effects of film composition on the (**a**) proliferation and (**b**–**d**) viability of 3T3 cells. Cells seeded in p96-well plates were exposed to each film for 24, 48, and 72 h. Cells seeded on wells without any biomaterial were used as controls. Proliferation results are represented as proliferation rate mean ± SD of viable cells compared with viable cells at t = 0 h. Viability results are expressed as percentages of viable cells in relation to control wells (100% viability). The lines drawn inside each box represent the medians of viability values of each film. Statistically significant differences showed differences with respect to control (* $p < 0.05$, ** $p < 0.01$, *** $p < 0.001$; $n = 9$).

Results concerning HCE cultures also showed a time-dependent proliferation pattern in all cases (Figure 5). Better proliferative pattern and higher viability values were recorded in the HCE-containing wells conditioned with COL films compared with 3T3 cultures. Except for 72 h, when 60% of viability was registered, the viability was much higher than 70% at 24 and 48 h. Even so, the values recorded for COL films were the lowest compared with the other films. The viability recorded for SPI, GEL-LAC, and GEL-CA was well above 70% in all cases.

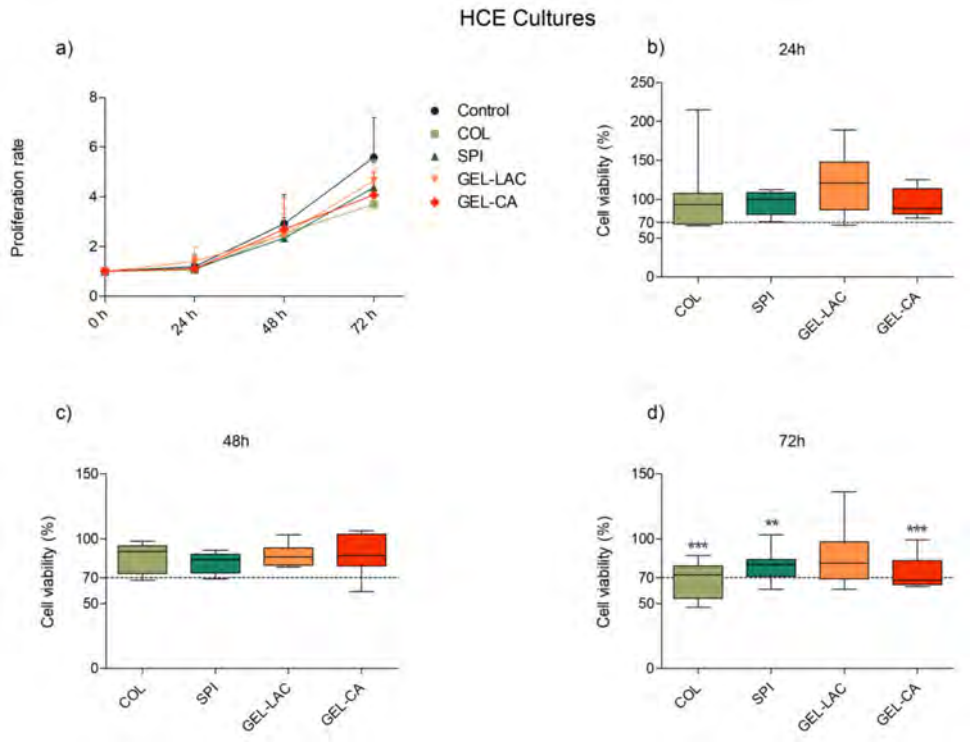

Figure 5. Effects of film composition on the (**a**) proliferation and (**b**–**d**) viability of human corneal epithelial (HCE) cells. Cells seeded in p96-well plates were exposed to each film for 24, 48, and 72 h. Cells seeded on wells without any biomaterial were used as controls. Proliferation results are represented as proliferation rate mean ± SD of viable cells compared with viable cells at t = 0 h. Viability results are expressed as percentages of viable cells in relation to control wells (100% viability). The lines drawn inside each box represent the medians of viability values of each film. Statistically significant differences showed differences with respect to control (* $p < 0.05$, ** $p < 0.01$, *** $p < 0.001$; $n = 9$).

2.5. Cell Adhesion

Cell adhesion and film cyto-compatibility were studied by cell culture observations through the phase contrast microscope, performing the Calcein AM/Ethidium homodimer-1 live/dead assay (EthD1) at different time points (24, 48, and 72 h) and through scanning electron microcopy (SEM) images. The 3T3 cells seeded on SPI, GEL-LAC, and GEL-CA films showed similar cell morphology to the control treatment. They presented the typical bi- and multipolar branched morphology of fibroblasts (Figure 6a–d). Regarding the disposition over the films, a flat and elongated monolayer configuration similar to the control was observed in SPI and GEL-LAC films. However, the cells were arranged in patches in GEL-CA films rather than in a monolayer. Regarding the live/dead Calcein AM-EthD1 assay, very few dead cells were observed above the films; around 1–5% of the cells adhered to the films were stained with EthD-1 (Figure 6e–h). These values were maintained until 72 h. The images taken through SEM showed a very flat and stretched arrangement of these cells over the films. At high magnification, nonsignificant morphological differences were observed among the different samples (Figure 6i–l).

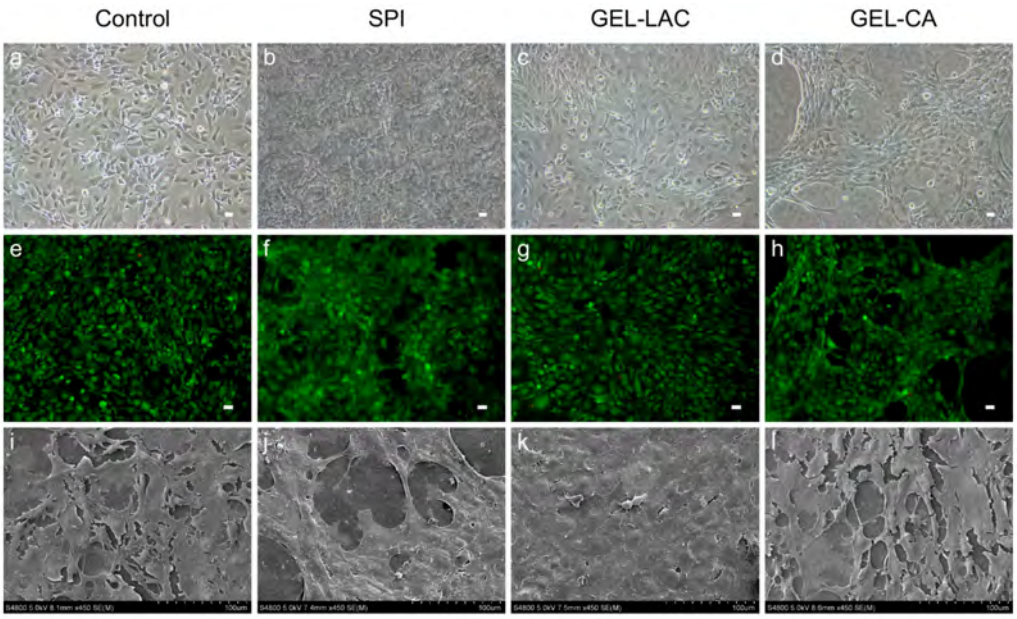

Figure 6. Culture of 3T3 cells above the films. (**a**–**d**) Contrast phase microscopic images of 3T3 cells on tissue culture well plate (control) and the films after 24 h of cell seeding; (**e**–**h**) representative Calcein AM/Ethidium homodimer-1 live/dead (CA-EthD1) assay images and (**i**–**l**) SEM images. (**a**–**h**) Images taken with 10× magnification; scale bars correspond to 25 µm. (**i**–**l**) Images taken with 450× magnification.

Considering HCE cells, morphological differences were recorded between the cells seeded on different films (Figure 7a–d). The typical cobblestone-like structure of the corneal epithelial cells observed in the control was also recorded in the cell culture on the GEL-LAC film. However, the cells seeded on SPI and GEL-CA films showed a more stretched and rounded cell shape. Similarly, the polygonal outline of cells registered with the control and GEL-LAC films was not so evident. As with 3T3 cells, very few dead cells were observed above the films on live/dead Calcein AM-EthD1 assays performed at 24, 48, and 72 h (Figure 7e–h). The morphological differences of HCE cultures observed by means of phase contrast microscopy were also evident with Calcein AM staining. These cells showed greater cell volume and did not appear as flat as 3T3 fibroblasts through SEM observations. Differences between the control wells and the cells seeded on the different films were neither observed (Figure 7i–l). A stratified arrangement of the cells could be visualized in all conditions.

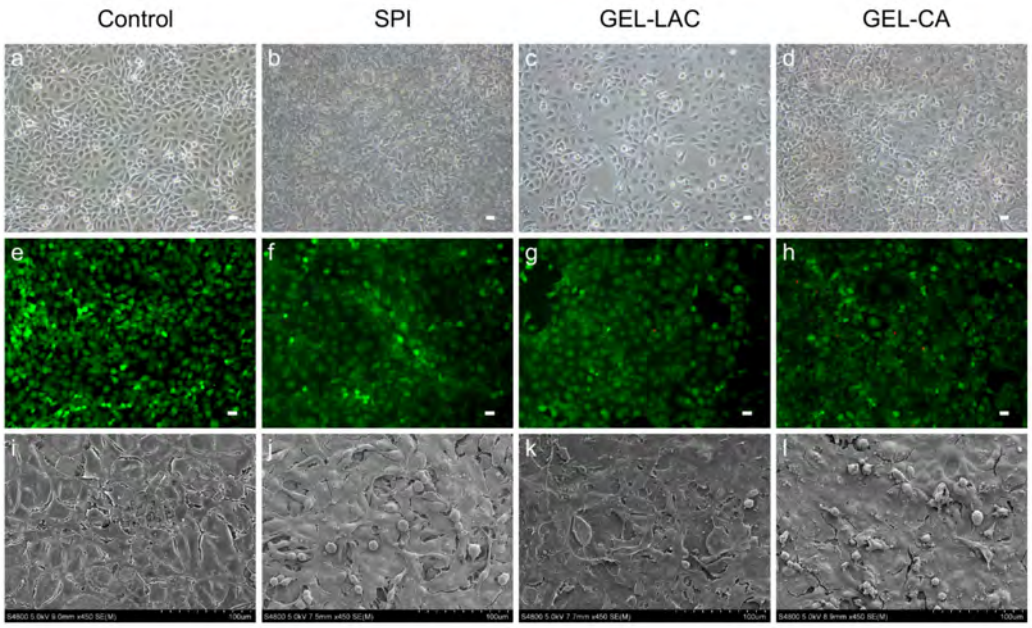

Figure 7. Culture of HCE cells above the films. (**a**–**d**) Contrast phase microscopic images of HCE cells on tissue culture well plate (control) and the films after 24 h of cell seeding; (**e**–**h**) representative CA-EthD1 assay images and (**i**–**l**) SEM images. (**a**–**h**) Images taken with 10× magnification; scale bars correspond to 25 µm. (**i**–**l**) Images taken with 450× magnification.

With respect to both type of cells, cell cultures were clearly observed in GEL-LAC films in the phase contrast microscope. However, it was not possible to focus the cells on the same plane within the same image's quadrant in SPI and GEL-CA films in some cases due to the films' surface irregularities. Finally, it was not possible to cultivate any cell type in collagen films; the cells did not adhere to the film so they died and were removed with PBS washes.

2.6. Cell Migration

The ability of both cell types to migrate over the films was assessed creating a cell-free gap and recording the time of the gaps' closure at 0, 24, 48, and 72 h. Technical replicates made with each film type showed the ability of both cell types to migrate over biomaterials. The gaps were closed faster with 3T3 cells than with HCE cells. In both cases, the cells seeded on GEL-CA were the ones that took a longer time for gaps to close; however, all the culture ended up covering the cell-free area by 72 h (Figure 8). As with adhesion assays, it was not possible to cultivate any cell type in COL films.

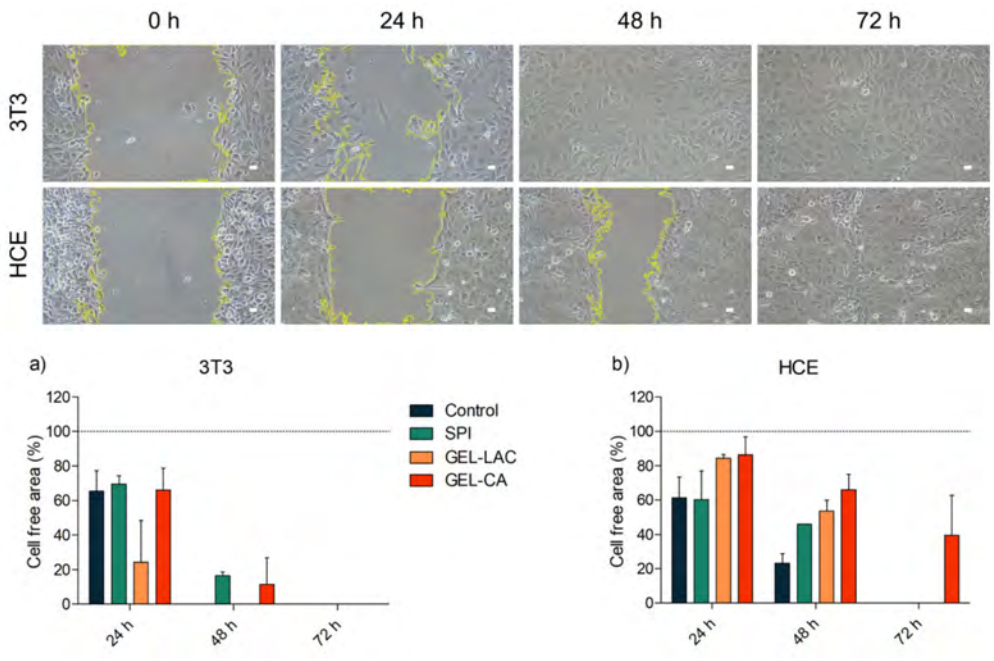

Figure 8. Migration assay of HCE and 3T3 cell seeded above GEL-LAC after 24, 48, and 72 h. Images taken with 10× magnification; scale bars correspond to 25 µm. Data in (**a**) and (**b**) represent the evolution of the gap closure by 3T3 (**a**) and HCE (**b**) cells in each film.

3. Discussion

Numerous materials are currently being assessed as potential candidates to serve as corneal scaffolds or cell support platforms on which cells can adhere and live [13,24,25]. These materials that aim to mimic the native cornea should fulfill the requirements established by the main corneal functions: they should be biocompatible and biodegradable, provide optical properties similar to those of the native tissue, and have the ability to biointegrate by stimulating the growth, proliferation, and migration of the tissue cells [26]. The current study focused on the in vitro assessment of protein-based biomaterials that could serve as alternative materials for creating corneal scaffolds. This assessment is an essential first step in the design of new materials that could interact with native tissues.

The ability to transmit most of the incident light is one of the essential functions of the cornea. The cornea is responsible for more than 60% of the total refractive power of the eye [27], and this function is strongly linked to its characteristic transparency. In addition to the thinness, morphology, and distribution of the keratocytes in the stroma, the ordered arrangement of collagen fibrils make the cornea a transparent tissue and, in turn, produce destructive interference from scattered light that improves the transmission of light [28]. The artificially generated corneal scaffold substitutes should transmit such an amount of light and resemble the natural structure as closely as possible. That is why the measurement of the optical properties of selected materials is of such importance.

The analysis carried out in this study revealed that the transmittance of the films increased with the increasing wavelength. COL and SPI films transmitted less visible light when hydrated, unlike GEL-LAC and GEL-CA films, in which the hydrated films were the ones that showed the highest amount of light transmission. This indicated that the cross-linking reaction affected the structure and optical properties of the films, as shown by FTIR results.

Concerning COL and SPI films, physical cross-linking by hydrogen bonding between polar groups of proteins and hydroxyl groups of glycerol occurred; however, chemical cross-linking occurred between the amino group of gelatin and the carbonyl group of

lactose and the carboxyl group of citric acid. This chemical reaction led to a more compact structure, as shown by SEM images, and to better optical properties.

The total transmittance of light is given by two components: direct transmittance, where the direction of light propagation does not change, and by diffuse transmittance, which is the component that determines the haze and clarity of the objects [29]. To see the effect of diffuse transmission or scattering and to avoid the deceptive contact clarity [30,31], patterns were placed at a distance from the matrices to be tested. It was an observational measure that did not provide quantitative data but was valuable for recording differences between materials. Considering the hydrated state of any material that would be placed on the ocular surface, the transparency acquired by gelatin films was very favorable. By contrast, considering the eye's essential function of objects' recognition and focusing, COL and SPI films should be modified to provide better transparency and less blurring since they transmitted between 60% and 80% of the incident light, but they were not translucent enough to recognize patterns clearly. This lack of clarity had to do with the partial structural order of the films that inhibited light scattering [32].

Thus, if transparency would be the major concern, gelatin films would be selected as the best candidates. Gelatin is a versatile material that in itself offers greater transparency than collagen [25]. The gelatin-based gel polymerizable by free radicals in the presence of a type 2 initiator Eosin Y, triethanolamine (TEA), and N-vinylcaprolactam (VC), developed by Shirzaei Sani et al., showed adequate transparency up to 14 days after being applied in rabbit eyes [33]. In the same manner, the gelatin films crosslinked with lactose and citric acid developed in this study demonstrated good clarity and shape definition. Besides, GEL-LAC films specifically could add new beneficial characteristics since the yellowish hue given by the Maillard reaction products, generated after the non-enzymatic glycation of gelatin and lactose [34], provided the benefit of protection against UV radiation. This is a very interesting feature for materials that would be used for the ocular surface. For instance, yellow-tinted lenses have been found to provide a protective function against retinal cell damage [35,36].

Regarding degradation, a suitable material for the cornea should withstand the progressive degradation mechanisms of enzymes in the eye for long enough for the host tissue to regenerate and integrate with the local healthy tissue. The effect of cross-linking was clearly seen since the physical cross-linking occurred in COL and SPI films made them degrade faster than chemically cross-linked gelatin films. In particular, the degradation pattern of collagen decreased exponentially; it was degraded in only 15 min and did not offer resistance to the action of collagenase in vitro. Considering SPI films, soy protein was not degraded by collagenase; it remained stable up to 4 h and then degraded up to 40% after 24 h.

The type of chemical reaction also had influence on gelatin films. After 24 h, around 50% of GEL-LAC remained; in contrast, slightly less than 40% of GEL-CA film was preserved. These results highlight the importance of the cross-linking agent, method, and time to tune the degradation rates of the films. It should not be forgotten that the developed scaffolds or films should provide a suitable substrate and support for cells to grow, migrate, and proliferate during the tissue regeneration process, but these scaffolds should be degraded at the same time that the new corneal stromal ingrowth happens [33,37].

Regarding the cytotoxicity of materials, one of the essential requirements for the biomaterials is the verification of being biologically safe and non-toxic. Within this aim, tests provided by the ISO10993 guidelines for biomedical device evaluation, which are based on the direct or indirect exposure of the material to cell cultures and the comparison of its effects with respect to a control group, can be used [38]. If the effect of the tested material produces a harmful response compared with the limits established with the control, the material is considered unsuitable for use. In this context, the MTT (3-(4,5-dimethylthiazol-2-yl)-2,5-diphenyltetrazolium bromide) tests carried out demonstrated the cellular biocompatibility of SPI and gelatin films with both cell types. On the contrary, the viability values lower than 70% that were registered with collagen films prevented

them from being considered a non-harmful material for cells. However, the unsatisfactory results were not attributed to the collagen type I itself. The collagen used in this study was a material that has already been used by other researchers [39,40]. For instance, Isaacson et al., used methacrylated type I collagen mixed with alginate in their constructs and showed viability values of 90% at 24 h and 83% at 7 days with corneal keratocytes, cells that could be equivalent to the fibroblasts used in our study [14]. This underlines the importance of material processing, type of crosslinking, or the addition of components that can completely change the achievable cellular compatibility.

Although statistically significant differences were recorded at 72 h of exposure compared with control wells, it should be taken into account that culture media did not change during this period of time. This condition would not happen in a real environment, where tears and eye blinking would constantly renew the medium exposed to corneal cells [41].

Both cell types of the study were able to be adhered and remained viable over the films. Additionally, the scratch assays revealed that both cell types were able to migrate over the films and that the cell density acquired in the wound area over time was similar to that of the control, especially cells cultured on GEL-LAC and SPI films healed first. Good cell migration and proliferation on gelatin-based materials was also recorded by Shirzaei Sani et al., where it was even higher than in the control [33].

It has been proven that the stiffness of the support material is one of the factors that regulates the behavior and fate of cells. It has been demonstrated that corneal epithelial cells seeded on smooth surfaces more likely retain their undifferentiation potential [42] and that soft surfaces are also interesting for keratocytes to maintain their phenotype since stiffer materials accelerate the transformation to myofibroblasts and, therefore, contribute to an early deterioration of corneal tissue functions [43]. Thus, the differences in cell behavior on the different films suggested the convenience of a study of the surface characteristics of the films, such as roughness, topography, or chemistry, which could influence cell responses in the way they adhere, proliferate, and migrate over the materials [44].

4. Materials and Methods

4.1. Materials

Porcine collagen was supplied by Tenerias Omega (Navarre, Spain). The treatments of porcine skin to obtain native collagen were carried out according to the method of Andonegi et al. [45]. Soy protein isolate (SPI), PROFAM 974, with 90% protein on a dry basis, was supplied by ADM Protein Specialties Division (Amsterdam, Netherlands). A commercial fish gelatin, with the quality standard for edible gelatin (1999/724/CE), was also employed. Glycerol, used as plasticizer, and lactose and citric acid, used as cross-linking agents, were obtained from Panreac (Barcelona, Spain). Finally, agar was extracted from *Gelidium sesquipedale*.

4.2. Preparation of Films

Collagen films were prepared by mixing collagen, glycerol (20 wt %, based on dry collagen), and 0.05 M acetic acid (1:1 collagen/acetic acid ratio). The resulting pastes were stored in a plastic bag for 24 h at room temperature for the dough hydration. The dough was placed between two aluminum plates, put into a Specac press, previously heated up to 90 °C, and then pressed at 0.5 MPa for 1 min to obtain the collagen films, designated as COL.

SPI films were prepared by mixing SPI and glycerol (40 wt % based on dry SPI) for 5 min in order to obtain a good blend. These blends were placed between two aluminum sheets using a caver laboratory press (Specac, Barcelona, Spain), previously heated at 120 °C, and pressed at 4 MPa for 2 min to obtain the SPI films, designated as SPI.

Gelatin films with lactose were prepared by dissolving gelatin and lactose (20 wt % based on dry gelatin) in distilled water for 30 min at 80 °C under continuous stirring to obtain a good blend. After that, 10 wt % glycerol (on gelatin dry basis) was added to the solution, maintained at 80 °C for other 30 min under stirring. Solution pH was adjusted to

10 with NaOH (0.1 M). Finally, solutions were poured into Petri dishes and left drying 48 h at room temperature to obtain films. Additionally, films were heated at 105 °C for 24 h to obtain the lactose-cross-linked gelatin films, designated as GEL-LAC.

Gelatin films with citric acid were prepared by mixing gelatin, citric acid (20 wt % on dry gelatin basis), and agar (10 wt % on dry gelatin basis) in distilled water. Solutions were heated at 80 °C for 30 min and stirred. Then, 20 wt % glycerol (on dry gelatin basis) was added, and solution pH was adjusted to pH 10 with NaOH (0.1 M). The heating procedure was repeated, and finally, solutions were poured into Petri dishes and allowed to cool for 48 h at room temperature to obtain citric acid-cross-linked films, designated as GEL-CA.

Film thickness was measured to the nearest 0.080 mm with a handheld QuantuMike digimatic micrometer (Elgoibar, Spain). Three measurements at different positions were taken from seven specimens for each composition. The calculated average thickness was 0.040–0.050 mm.

4.3. Fourier Transform Infrared (FTIR) Spectroscopy

Attenuated total reflectance Fourier transform infrared (ATR-FTIR) spectroscopy was used to identify the characteristic functional groups of the films. Measurements were performed with a Nicolet Nexus FTIR spectrometer equipped with a MKII Golden Gate accessory (Specac) with a diamond crystal as ATR element at a nominal incidence angle of 45° with a ZnSe lens. Measurements were recorded in the 4000–850 cm^{-1} region using 32 scans at a resolution of 4 cm^{-1}.

4.4. X-ray Diffraction (XRD)

XRD was performed with a diffraction unit PANalytical Xpert PRO (PANalytical, Madrid Spain), operating at 40 kV and 40 mA. The radiation was generated from a Cu-Kα (λ = 1.5418 Å) source, and the diffraction data were collected from 2 θ values from 2 to 90°, where θ was the angle of incidence of the X-ray beam on the sample.

4.5. Scanning Electron Microscopy (SEM)

Morphology of the film cross-section was visualized using a Hitachi S-4800 field emission scanning electron microscope (Hitachi High-Technologies Corporation, Madrid, Spain). The samples were mounted on a metal stub with a double-sided adhesive tape. Finally, they were coated under vacuum with gold (JFC-1100) in an argon atmosphere prior to observation. All samples were examined using an accelerating voltage of 15 kV.

SEM visualization of cell cultures was also performed. Samples were fixed using 2% glutaraldehyde in 0.1 M Sorensen buffer with pH 7.4 at 4 °C overnight and then rinsed in Sorensen 0.1 M for three times during 10 min. Samples were dehydrated in increasing concentrations of 30, 50, 70, 90, and 96% ethanol for 30 min each. Two washes of absolute ethanol during 30 min were applied as the last ethanol dehydration step. Dehydrated samples were then immersed into hexamethyldisilazane (HMDS) for 30 min twice and were left in a desiccator to air-dry at room temperature. Once dried, samples were mounted into SEM sample stubs with a double-sided sticky tape. Finally, they were sputtered with gold in argon atmosphere for SEM visualization.

4.6. Dialysis and Sterilization

Films were dialyzed by soaking in deionized MilliQ water during 24 h under constant stirring. This step was performed before film sterilization as a first step to remove possible dirt. Once cleaned, they were introduced in the Biolink cross-linker (Vilber Lourmat BLX-254, Collégien, France) for UV sterilization. Samples were located 14.5 cm from the UV light source of 80 W, placed in the internal chamber's surface of 858 cm^2, and irradiated for 20 min by each side. The sterilization process was carried out placing the films in the culture plate to be used for subsequent experiments.

4.7. Light Transmittance

Light transmission of each film in the visible spectrum (400–800 nm) was evaluated by placing 3 mm diameter disks of each material in a p96-well plate and measuring its absorption in ELx800 Microplate Reader (BioTek® Instruments, Winooski, VT, USA). Light absorption was measured with dried and hydrated films. Wells were filled with PBS to measure light absorption of hydrated films, and empty wells filled with PBS were used as control. Empty wells were used as baseline reference for absorption values of dried films. Measured absorbance values were transformed to transmittance percentages with the following Equation (1):

$$\%T = 10^{(2-\text{Absorbance})} \quad (1)$$

Apart from light transmittance, the transparency of the films was qualitatively measured by analyzing specific photographic patterns placed at a distance of 12 cm from the films.

4.8. Biodegradability Assay

Degradation tests were performed to determine weight loss of each film subjected to hydrolytic and enzymatic degradation. To measure the in vitro enzymatic degradation, initially weighed (W_o) square fractions of dried samples (6 mm × 6 mm) were immersed in a 200 μg/mL collagenase A solution (Sigma, St. Louis, MO, USA) in PBS for different time points (15 min, 30 min, 1 h, 2 h, 4 h, and 24 h) and incubated at 37 °C. At each time point, samples were removed, lyophilized, and weighed (Wt). The in vitro hydrolytic degradation was equally assessed, but samples were incubated in PBS with no enzyme instead. Films soaked in MilliQ water were used as controls. The percentage of degradation was calculated considering the weight loss over time using the following Equation (2):

$$\text{Remaining weight } (\%) = \frac{W_t}{W_0} \times 100 \quad (2)$$

All the measurements were performed in triplicates per time point and sample type. Mean values ± SD of the remaining weight percentages were plotted versus time.

4.9. Cell Lines

SV-40 immortalized human corneal epithelial (HCE) cells and NIH/3T3 fibroblasts were used for cytocompatibility evaluation. NIH/3T3 fibroblasts were cultured in Dulbecco's modified Eagle's medium (DMEM): Ham's F12 mix (Lonza, Verviers, Belgium) with 10% (v/v) fetal bovine serum (FBS; Lonza), 2.5 mM L-glutamine (Lonza), and 50 U-mg/mL penicillin–streptomycin (Lonza) at 37 °C and 5% CO_2. HCE cells were maintained under the same conditions as NIH/3T3 cells with the addition of 0.5% (v/v) DMSO (Sigma), 50 μg/mL insulin (Sigma), 10 ng/mL EGF (Sigma), and 0.1 μg/mL cholera toxin (Gentaur Molecular Products, Brussels, Belgium) to the culture medium.

4.10. Cell Proliferation and Viability Assay

Cells were seeded in flat bottom 96-well culture plates to perform MTT (3-(4,5-dimethylthiazol-2-yl)-2,5-diphenyltetrazolium bromide) assay. Once attached, cells were starved for 16 h with a solution of DMEM:F12 and 1% of bovine serum albumin (BSA) (Sigma) to synchronize cell cycles. Subsequently, the starving medium was replaced by the corresponding culture or treatment medium according to each assay. Time 0 was set at this step. Cells were seeded in triplicates, and positive controls and treatment blanks were included. Treatment wells were prepared by incubating film sections with the corresponding cell culture media to expose cells directly to the biomaterial tested. Metabolic activity of cells was assessed at times 0, 24, 48, and 72 h. After the corresponding incubation period, the cultures were washed with PBS 1×, and 100 μL of 0.5 mg/mL MTT reagent (Sigma) dissolved in DMEM:F12 was added per well for 3 h at 37 °C and 5% CO_2. The MTT-containing medium was carefully removed, and 100 μL of DMSO was added per

well to dissolve the formazan crystals. Optical densities were determined at 570 nm on a EL × 800 microplate reader (BioTek® Instruments), and absorbance values in treatment and control wells were compared.

4.11. Live/Dead Cytotoxicity Assay

The number of alive/dead cells was determined after 24, 48, and 72 h from cells seeding on the films tested using LIVE/DEAD® Viability/Cytotoxicity Assay Kit (Thermo Fisher Scientific, Waltham, MA, USA). A portion of 2 µM of Calcein-AM and 4 µM of EthD-1 was diluted in PBS 1× to prepare the assay's solution. Culture media was aspirated and a PBS 1× wash was performed on the cells before incubating them for 40 min with the dyes' solution at room temperature and dark environment. Enough volume of the test solution was added to cover the cells completely. Following incubation, cells were imaged by the fluorescence microscope (Olympus IX71, Olympus, Tokyo, Japan). The test was performed in triplicates, and films without cells seeded on them were included as blanks.

4.12. Migration

The migration of HCE and 3T3 cells was studied using two-well culture-inserts (Ibidi, Gräfelfing, Germany) placed above the films. The silicone inserts consisted of two reservoirs for cell culture separated by a defined cell-free gap. Cells were seeded in each reservoir and were left overnight until they attached and formed a monolayer above the films. The defined cell-free gap left by the removal of the insert was registered as the maximum distance between both cell fronts at time 0. Cell migration was then quantified by phase contrast images taken at 24, 48, and 72 h.

4.13. Statistical Analysis

Non-parametric Kruskal–Wallis test followed by Dunn's post hoc test was used for transparency analysis. Degradation and MTT values were subjected to two-way analysis of variance (ANOVA) in which Bonferroni's test was used for multiple comparisons. Statistical differences were set at $p < 0.05$ level, and all the measurements were performed in triplicates. GraphPad Prism 5 software (San Diego, CA, USA) was used for all statistical calculations.

5. Conclusions

The in vitro biological assessment performed has shown that three of the four types of films under study present promising properties as materials for the development of artificial corneal implants, corneal scaffolds, or cell support films. The unsatisfactory results obtained with collagen films were attributed more to the pretreatment of collagen fibers than to the material itself. Although showing adequate biological properties, SPI films would not be the most suitable alternative for implantation in the cornea due to the lack of optical brightness and pattern definition. However, they could serve for the development of scaffolds for the peripheral cornea or other tissues of the body, or even for the central cornea if they were modified to obtain adequate transparency. In sum, gelatin films were found to be the most suitable films to serve as scaffold for corneal tissue substitutes, especially those cross-linked with lactose since they have shown good optical and biological properties. Although this is a first in vitro evaluation, these promising results encourage further study of their potential for corneal tissue engineering.

Author Contributions: Conceptualization, N.A., J.E., P.G., and K.d.l.C.; methodology, C.R.-V. and P.G.; formal analysis, C.R.-V. and P.G.; investigation, C.R.-V. and P.G.; resources, N.A., J.A., and K.d.l.C.; data curation, C.R.-V. and P.G.; writing—original draft preparation, C.R.-V. and P.G.; writing—review and editing, N.A., J.A., J.E., and K.d.l.C.; supervision, N.A., J.A., and K.d.l.C.; project administration, N.A. and K.d.l.C.; funding acquisition, N.A., J.A., and K.d.l.C. All authors have read and agreed to the published version of the manuscript.

Funding: This research study was supported by grants from the Department of Heath of the Basque Government (RIS3, 2019222049), the University of the Basque Country UPV/EHU-Instituto Clinico Quirurgico de Oftalmologia ICQO (US19/18), and MCI/AEI/FEDER, UE (grant number RTI2018-

097100-B-C22). C.R.-V. was supported by a fellowship from the University of the Basque Country UPV/EHU.

Institutional Review Board Statement: Not applicable.

Informed Consent Statement: Not applicable.

Data Availability Statement: Not applicable.

Acknowledgments: The authors thank SGIker (UPV/EHU/ERDF, EU) for technical and human support.

Conflicts of Interest: The authors declare no conflict of interest. The funders had no role in the design of the study; in the collection, analyses, or interpretation of data; in the writing of the manuscript, or in the decision to publish the results.

References

1. Chawla, K. (Ed.) *Biomaterials for Tissue Engineering*; Methods in Molecular Biology; Springer: New York, NY, USA, 2018; Volume 1758, ISBN 978-1-4939-7739-0.
2. Cen, L.; Liu, W.; Cui, L.; Zhang, W.; Cao, Y. Collagen Tissue Engineering: Development of Novel Biomaterials and Applications. *Pediatr. Res.* **2008**, *63*, 492–496. [CrossRef] [PubMed]
3. Kariduraganavar, M.Y.; Kittur, A.A.; Kamble, R.R. Chapter 1—Polymer Synthesis and Processing. In *Natural and Synthetic Biomedical Polymers*; Kumbar, S.G., Laurencin, C.T., Deng, M., Eds.; Elsevier: Oxford, UK, 2014; ISBN 978-0-12-396983-5.
4. Bello, A.B.; Kim, D.; Kim, D.; Park, H.; Lee, S.-H. Engineering and Functionalization of Gelatin Biomaterials: From Cell Culture to Medical Applications. *Tissue Eng. Part B Rev.* **2020**, *26*, 164–180. [CrossRef] [PubMed]
5. Catoira, M.C.; Fusaro, L.; Di Francesco, D.; Ramella, M.; Boccafoschi, F. Overview of natural hydrogels for regenerative medicine applications. *J. Mater. Sci. Mater. Med.* **2019**, *30*, 115. [CrossRef] [PubMed]
6. Subhan, F.; Hussain, Z.; Tauseef, I.; Shehzad, A.; Wahid, F. A review on recent advances and applications of fish collagen. *Crit. Rev. Food Sci. Nutr.* **2020**, 1–11. [CrossRef] [PubMed]
7. Manikandan, A.; Raja, S.T.K.; Thiruselvi, T.; Gnanamani, A. Engineered fish scale gelatin: An alternative and suitable biomaterial for tissue engineering. *J. Bioact. Compat. Polym.* **2018**, *33*, 332–346. [CrossRef]
8. Etxabide, A.; Ribeiro, R.D.C.; Guerrero, P.; Ferreira, A.M.; Stafford, G.P.; Dalgarno, K.; de la Caba, K.; Gentile, P. Lactose-crosslinked fish gelatin-based porous scaffolds embedded with tetrahydrocurcumin for cartilage regeneration. *Int. J. Biol. Macromol.* **2018**, *117*, 199–208. [CrossRef]
9. Najafpour, G.D. CHAPTER 12—Production of Citric Acid. In *Biochemical Engineering and Biotechnology*; Najafpour, G.D., Ed.; Elsevier: Amsterdam, The Netherlands, 2007; ISBN 978-0-444-52845-2.
10. Al Loman, A.; Islam, S.M.M.; Li, Q.; Ju, L.-K. Soybean bio-refinery platform: Enzymatic process for production of soy protein concentrate, soy protein isolate and fermentable sugar syrup. *Bioprocess Biosyst. Eng.* **2016**, *39*, 1501–1514. [CrossRef]
11. Tansaz, S.; Boccaccini, A.R. Biomedical applications of soy protein: A brief overview. *J. Biomed. Mater. Res. Part A* **2016**, *104*, 553–569. [CrossRef]
12. Santin, M.; Morris, C.; Standen, G.; Nicolais, L.; Ambrosio, L. A New Class of Bioactive and Biodegradable Soybean-Based Bone Fillers. *Biomacromolecules* **2007**, *8*, 2706–2711. [CrossRef] [PubMed]
13. Hancox, Z.; Heidari Keshel, S.; Yousaf, S.; Saeinasab, M.; Shahbazi, M.-A.; Sefat, F. The progress in corneal translational medicine. *Biomater. Sci.* **2020**, *8*, 6469–6504. [CrossRef]
14. Isaacson, A.; Swioklo, S.; Connon, C.J. 3D bioprinting of a corneal stroma equivalent. *Exp. Eye Res.* **2018**, *173*, 188–193. [CrossRef] [PubMed]
15. Jumelle, C.; Sani, E.S.; Taketani, Y.; Yung, A.; Gantin, F.; Chauhan, S.K.; Annabi, N.; Dana, R. Growth factor-eluting hydrogels for management of corneal defects. *Mater. Sci. Eng. C* **2021**, *120*, 111790. [CrossRef] [PubMed]
16. Rico-Sánchez, L.; Garzón, I.; González-Andrades, M.; Ruíz-García, A.; Punzano, M.; Lizana-Moreno, A.; Muñoz-Ávila, J.I.; Sánchez-Quevedo, M.D.C.; Martínez-Atienza, J.; Lopez-Navas, L.; et al. Successful development and clinical translation of a novel anterior lamellar artificial cornea. *J. Tissue Eng. Regen. Med.* **2019**, *13*, 2142–2154. [CrossRef]
17. Wang, S.; Ghezzi, C.E.; Gomes, R.; Pollard, R.E.; Funderburgh, J.L.; Kaplan, D.L. In vitro 3D corneal tissue model with epithelium, stroma, and innervation. *Biomaterials* **2017**, *112*, 1–9. [CrossRef] [PubMed]
18. McTiernan, C.D.; Simpson, F.C.; Haagdorens, M.; Samarawickrama, C.; Hunter, D.; Buznyk, O.; Fagerholm, P.; Ljunggren, M.K.; Lewis, P.; Pintelon, I.; et al. LiQD Cornea: Pro-regeneration collagen mimetics as patches and alternatives to corneal transplantation. *Sci. Adv.* **2020**, *6*. [CrossRef]
19. Garrido, T.; Etxabide, A.; de la Caba, K.; Guerrero, P. Versatile soy protein films and hydrogels by the incorporation of β-chitin from squid pens (Loligo sp.). *Green Chem.* **2017**, *19*, 5923–5931. [CrossRef]
20. Andonegi, M.; Las Heras, K.; Santos-Vizcaíno, E.; Igartua, M.; Hernandez, R.M.; de la Caba, K.; Guerrero, P. Structure-properties relationship of chitosan/collagen films with potential for biomedical applications. *Carbohydr. Polym.* **2020**, *237*, 116159. [CrossRef]

21. Etxabide, A.; Coma, V.; Guerrero, P.; Gardrat, C.; de la Caba, K. Effect of cross-linking in surface properties and antioxidant activity of gelatin films incorporated with a curcumin derivative. *Food Hydrocoll.* **2017**, *66*, 168–175. [CrossRef]
22. Uranga, J.; Leceta, I.; Etxabide, A.; Guerrero, P.; de la Caba, K. Cross-linking of fish gelatins to develop sustainable films with enhanced properties. *Eur. Polym. J.* **2016**, *78*, 82–90. [CrossRef]
23. Guerrero, P.; Garrido, T.; Garcia-Orue, I.; Santos-Vizcaino, E.; Igartua, M.; Hernandez, R.M.; de la Caba, K. Characterization of Bio-Inspired Electro-Conductive Soy Protein Films. *Polymers* **2021**, *13*, 416. [CrossRef]
24. Palchesko, R.N.; Carrasquilla, S.D.; Feinberg, A.W. Natural Biomaterials for Corneal Tissue Engineering, Repair, and Regeneration. *Adv. Healthc. Mater.* **2018**, *7*, 1701434. [CrossRef] [PubMed]
25. Chen, Z.; You, J.; Liu, X.; Cooper, S.; Hodge, C.; Sutton, G.; Crook, J.M.; Wallace, G.G. Biomaterials for corneal bioengineering. *Biomed. Mater.* **2018**, *13*, 032002. [CrossRef] [PubMed]
26. Griffith, M.; Poudel, B.K.; Malhotra, K.; Akla, N.; González-Andrades, M.; Courtman, D.; Hu, V.; Alarcon, E.I. Biosynthetic alternatives for corneal transplant surgery. *Expert Rev. Ophthalmol.* **2020**, *15*, 129–143. [CrossRef]
27. Land, M.F.; Fernald, R.D. The Evolution of Eyes. *Annu. Rev. Neurosci.* **1992**, *15*, 1–29. [CrossRef] [PubMed]
28. Dawson, D.; Ubels, J.L.; Edelhauser, H. Cornea and Sclera. In *Adler's Physiology of the Eye*; Saunders: Edinburgh, Scotland, 2011; pp. 71–130. ISBN 9780323057141.
29. Höpe, A. Chapter 6—Diffuse Reflectance and Transmittance. In *Spectrophotometry*; Germer, T.A., Zwinkels, J.C., Tsai, B.K., Eds.; Experimental Methods in the Physical Sciences; Academic Press: Cambridge, MA, USA, 2014; Volume 46, pp. 179–219.
30. Motoyoshi, I. Highlight–shading relationship as a cue for the perception of translucent and transparent materials. *J. Vis.* **2010**, *10*, 6. [CrossRef] [PubMed]
31. Marlow, P.J.; Kim, J.; Anderson, B.L. Perception and misperception of surface opacity. *Proc. Natl. Acad. Sci. USA* **2017**, *114*, 13840–13845. [CrossRef] [PubMed]
32. Salameh, C.; Salviat, F.; Bessot, E.; Lama, M.; Chassot, J.-M.; Moulongui, E.; Wang, Y.; Robin, M.; Bardouil, A.; Selmane, M.; et al. Origin of transparency in scattering biomimetic collagen materials. *Proc. Natl. Acad. Sci. USA* **2020**, *117*, 11947–11953. [CrossRef]
33. Shirzaei Sani, E.; Kheirkhah, A.; Rana, D.; Sun, Z.; Foulsham, W.; Sheikhi, A.; Khademhosseini, A.; Dana, R.; Annabi, N. Sutureless repair of corneal injuries using naturally derived bioadhesive hydrogels. *Sci. Adv.* **2019**, *5*, eaav1281. [CrossRef]
34. Etxabide, A.; Uranga, J.; Guerrero, P.; de la Caba, K. Improvement of barrier properties of fish gelatin films promoted by gelatin glycation with lactose at high temperatures. *LWT-Food Sci. Technol.* **2015**, *63*, 315–321. [CrossRef]
35. Tanito, M.; Kaidzu, S.; Anderson, R.E. Protective effects of soft acrylic yellow filter against blue light-induced retinal damage in rats. *Exp. Eye Res.* **2006**, *83*, 1493–1504. [CrossRef]
36. Tanito, M.; Okuno, T.; Ishiba, Y.; Ohira, A. Estimation for Protective Effects of Clear and Yellow-Tinted Intraocular Lenses Against Sunlight-Induced Retinal Damage. *Investig. Ophthalmol. Vis. Sci.* **2010**, *51*, 5738.
37. Martins, J.P.; Ferreira, M.P.A.; Ezazi, N.Z.; Hirvonen, J.T.; Santos, H.A.; Thrivikraman, G.; França, C.M.; Athirasala, A.; Tahayeri, A.; Bertassoni, L.E. Chapter 4—3D printing: Prospects and challenges. In *Nanotechnologies in Preventive and Regenerative Medicine*; Uskoković, V., Uskoković, D.P., Eds.; Micro and Nano Technologies; Elsevier: Amsterdam, The Netherlands, 2018; ISBN 978-0-323-48063-5.
38. International Organization for Standardization. *Biological Evaluation of Medical Devices—Part 5: Tests for In Vitro Cytotoxicity*; (ISO Standard No. 10993-5); International Organization for Standardization: Geneva, Switzerland, 2009.
39. Liu, Y.; Ren, L.; Wang, Y. A novel collagen film with micro-rough surface structure for corneal epithelial repair fabricated by freeze drying technique. *Appl. Surf. Sci.* **2014**, *301*, 396–400. [CrossRef]
40. Li, W.; Long, Y.; Liu, Y.; Long, K.; Liu, S.; Wang, Z.; Wang, Y.; Ren, L. Fabrication and characterization of chitosan-collagen crosslinked membranes for corneal tissue engineering. *J. Biomater. Sci. Polym. Ed.* **2014**, *25*, 1962–1972. [CrossRef] [PubMed]
41. Dartt, D.A.; Willcox, M.D.P. Complexity of the tear film: Importance in homeostasis and dysfunction during disease. *Exp. Eye Res.* **2013**, *117*, 1–3. [CrossRef] [PubMed]
42. Gouveia, R.M.; Lepert, G.; Gupta, S.; Mohan, R.R.; Paterson, C.; Connon, C.J. Assessment of corneal substrate biomechanics and its effect on epithelial stem cell maintenance and differentiation. *Nat. Commun.* **2019**, *10*, 1496. [CrossRef] [PubMed]
43. Chen, J.; Backman, L.J.; Zhang, W.; Ling, C.; Danielson, P. Regulation of Keratocyte Phenotype and Cell Behavior by Substrate Stiffness. *ACS Biomater. Sci. Eng.* **2020**, *6*, 5162–5171. [CrossRef] [PubMed]
44. Bhattacharjee, P.; Cavanagh, B.L.; Ahearne, M. Effect of substrate topography on the regulation of human corneal stromal cells. *Colloids Surf. B Biointerfaces* **2020**, *190*, 110971. [CrossRef]
45. Andonegi, M.; de la Caba, K.; Guerrero, P. Effect of citric acid on collagen sheets processed by compression. *Food Hydrocoll.* **2020**, *100*, 105427. [CrossRef]

Experimental Eye Research 211 (2021) 108720

Contents lists available at ScienceDirect

Experimental Eye Research

journal homepage: www.elsevier.com/locate/yexer

Characterisation of corneas following different time and storage methods for their use as a source of stem-like limbal epithelial cells

Cristina Romo-Valera [a], Miguel Pérez-Garrastachu [a], Raquel Hernáez-Moya [a], Maddalen Rodriguez-Astigarraga [a], Paula Romano-Ruiz [a], Jaime Etxebarria [a,b,c], Jon Arluzea [a], Noelia Andollo [a,c,*]

[a] Department of Cell Biology and Histology, School of Medicine and Nursing, University of the Basque Country, Sarriena, S/N, 48940, Leioa, Spain
[b] Department of Ophthalmology, University Hospital of Cruces, Cruces Plaza S/N, 48903, Barakaldo, Spain
[c] BioCruces Bizkaia Health Research Institute, Begiker, Cruces Plaza S/N, 48903, Barakaldo, Spain

ARTICLE INFO

Keywords:
Corneoscleral tissues
Sclerocorneal rims
Limbal epithelial stem cells (LESCs)
Limbal stem cell deficiency (LSCD)
Corneal storage
Corneal shortage/availability
Corneal cell cultures
Melanocytes

ABSTRACT

The transplantation of expansions of limbal epithelial stem cells (LESC) remains one of the most efficient therapies for the treatment of limbal stem cell deficiency (LSCD) to date. However, the available donor corneas are scarce, and the corneas conserved for long time, under hypothermic conditions (after 7 days) or in culture (more than 28 days), are usually discarded due to poor viability of the endothelial cells. To establish an objective criterion for the utilisation or discarding of corneas as a source of LESC, we characterized, by immunohistochemistry analysis, donor corneas conserved in different conditions and for different periods of time. We also studied the potency of LESCs isolated from these corneas and maintained in culture up to 3 cell passages. We hoped that the study of markers of LESCs present in both the corneoscleral histological sections and the cell cultures would show the adequacy of the methods used for cell isolation and how fit the LESC enrichment of the obtained cell populations to be expanded was. Thus, the expressions of markers of the cells residing in the human limbal and corneal epithelium (cytokeratin CK15 and CK12, vimentin, Collagen VII, p63α, ABCG2, Ki67, Integrin β4, ZO1, and melan A) were analysed in sections of corneoscleral tissues conserved in hypothermic conditions for 2–9 days with post-mortem time (pmt) < 8 h or for 1 day with pmt > 16 h, and in sclerocorneal rims maintained in an organ culture medium for 29 days. Cell populations isolated from donor corneoscleral tissues were also assessed based on these markers to verify the adequacy of isolation methods and the potential of expanding LESCs from these tissues. Positivity for several putative stem cell markers such as CK15 and p63α was detected in all corneoscleral tissues, although a decrease was recorded in the ones conserved for longer times. The barrier function and the ability to adhere to the extracellular matrix were maintained in all the analysed tissues. In limbal epithelial cell cultures, a simultaneous decrease in the melan A melanocyte marker and the putative stem cell markers was detected, suggesting a close relationship between the melanocytes and the limbal stem cells of the niche. Holoclones stained with putative stem cell markers were obtained from long-term, hypothermic, stored sclerocorneal rims. The results showed that the remaining sclerocorneal rims after corneal transplantation, which were conserved under hypothermic conditions for up to 7 days and would have been discarded at a first glance, still maintained their potential as a source of LESC cultures.

1. Introduction

Corneal blindness is estimated to affect 23 million people worldwide. However, due to the shortage of corneal donors, only 1 out of 70 needs can be covered (Oliva et al., 2012; Gain et al., 2016). A population of limbal epithelial stem cells (LESCs) is responsible for the maintenance of a healthy corneal epithelium throughout life by constantly supplying daughter cells, which migrate centripetally towards the central cornea to replace lost cells and differentiate as they progress from the basal to superficial epithelial layers (Thoft and Friend, 1983). LESCs reside in the

* Corresponding author. Department of Cell Biology and Histology, School of Medicine and Nursing, University of the Basque Country, BioCruces Health Research Institute, B° Sarriena, s/n, 48940, Leioa, Spain.
E-mail address: noelia.andollo@ehu.eus (N. Andollo).

https://doi.org/10.1016/j.exer.2021.108720
Received 29 January 2021; Received in revised form 21 July 2021; Accepted 5 August 2021
Available online 11 August 2021

basal layer of the epithelium within the corneal limbus—the vascularised and highly innervated border between the central cornea and conjunctiva. More specifically, the limbal crypts—the downward invaginations of the limbal epithelium into the limbal stroma between the palisades of Vogt—have been proposed as the LESC niche (Shortt et al., 2007; Dziasko et al., 2014; Bonnet et al., 2021). During LESC failure, the conjunctiva can invade the cornea, causing chronic inflammation, corneal opacity, vascularisation and severe discomfort, which can lead to blindness.

Current treatments for LESC deficiency rely upon transplantation of allogenic or autologous limbal cultures. Cultured LESC delivery is one of several examples of a successful adult stem cell therapy used in patients, which achieves permanent restoration of damaged tissues in 76% of cases (Baylis et al., 2011). The number of stem cells present in a limbal biopsy is in the order of hundreds and this number increases during the primary culture due to the amplification of the original stem cell population. This amplification is actually the basis for the grafts' clinical success (Rama et al., 2010; Pellegrini et al., 2011). In this context, the use of growth-arrested mouse embryonic fibroblasts (3T3-J2) as feeder cells is considered the gold-standard method for *in vitro* amplification (Barrandon et al., 2012), but the use of other support cells for LESC expansion and enrichment has also been reported. For example, human amniotic membranes (HAM) have been used as culture substrates to enhance limbal epithelial sheet growth and stemness (Lee et al., 2018; Sharma et al., 2018). González et al. demonstrated the efficiency of bone marrow stromal cell (BMSC) feeder layers for the expansion of LESC population in 3D cultures (González et al., 2016). Human limbal melanocyte feeders showed successful results in the maintenance of epithelial stem cells characteristics and suggested an active involvement in the niche's preservation (Dziasko et al., 2015).

However, several factors during extraction and conservation of the corneal tissue prior to any amplification step can influence the viability and capability of LESCs to proliferate *in vitro*, such as death-to-preservation time of the corneas, storage procedure and even the age of the donor patient (Notara et al., 2013). Considering this, the aim of this study was to assess the suitability of corneas conserved in different conditions and for different periods of time in terms of the quantity of LESCs. To achieve this, the expressions of putative stem cell markers CK15 (Yoshida et al., 2006), ΔNp63α (Pellegrini et al., 2011), ABCG2 (De Paiva et al., 2005; Schlötzer-Schrehardt and Kruse, 2005) and vimentin (Brookes et al., 2003), of differentiated epithelial cell markers CK12 and CK3 (Chaloin-Dufau et al., 1990), and of the cell proliferation marker Ki67 (Joyce et al., 1996) were evaluated. In addition, the adequacy of cell isolation methods, the evolution of the mentioned markers along cell culture passages and the presence of melanocytes were assessed.

2. Materials and methods

2.1. Classification of the study corneas by time and conditions of conservation

Human corneoscleral tissues and data from 40 to 81 year-old donors included in this study were provided by the following eye banks: the Basque Biobank www.biobancovasco.org; the Blood and Tissue Bank, Government of Catalonia; the Navarra Blood and Tissue Bank, Navarrabiomed Biobank, Navarra Health Department; and the Biobank A Coruña of SERGAS. The corneoscleral tissues were processed following standard operating procedures under the tenets of the Declaration of Helsinki with appropriate approval of the Ethical and Scientific Committees (CEISH/342/2015/ANDOLLO VICTORIANO). Information about donor tissues and their use in this study are determined in Table 1. Considering the storage method, two types of samples were obtained:

- Donor corneoscleral tissues (including the cornea and the sclerocorneal rim), preserved in hypothermic conditions. They were maintained at 4 °C in the corneal conservation medium Eusol-C (Alchimia, Ponte San Nicolò, Italy) or Optisol-GS solution (Bausch and Lomb, Alcobendas, Madrid, Spain). Likewise, two types of donor corneoscleral tissue samples were distinguished: i) Corneoscleral tissues extracted from donors less than 8 h after death (post-mortem time (pmt) < 8 h) and kept in the conservation medium for 2–9 days; ii) Corneoscleral tissues maintained in the conservation medium for only one day but extracted 16–22 h after donors' death (pmt > 16 h). The type of corneoscleral tissue sample is an important point to consider since the death-to-preservation time could affect the viability of the different corneal cell populations.
- Cultured sclerocorneal rims (after using corneal button for clinical purposes) preserved at 31 °C for 10 and 29 days in Tissue C organ culture medium (Alchimia), a medium for organ culture. The death-to-preservation time was less than 8 h (pmt < 8 h) in these samples.

We used 15 human tissue samples in all. For tissue section analysis, 11 samples were used: 8 fresh corneoscleral tissues conserved in hypothermic conditions for 2–9 days (pmt < 8 h); 2 fresh corneoscleral tissues conserved in hypothermic conditions for 1 day (pmt > 16 h); and 1 sclerocorneal rim maintained in Tissue C organ culture medium for 29 days. For cell cultures, 4 samples were used: 1 fresh corneoscleral tissue conserved in hypothermic conditions for 3 days, 1 for 5 days, 1 for 7 days and 1 sclerocorneal rim maintained in Tissue C organ culture medium for 10 days.

Fig. 1 shows a schematic representation of the procedure followed and the storage condition of each sample.

Table 1
Donor tissue information and use of each tissue in this study.

Sample Number	Age (years)	Sex	Post morten time (h)	Conservation method	Conservation time (days)	Use
1	61	Male	16	HC	1	Tissue sections
2	62	Female	22	HC	1	Tissue sections
3	N.A	N.A	<8	HC	2	Tissue sections
4	N.A	N.A	<8	HC	3	Tissue sections
5	N.A	N.A	<8	HC	4	Tissue sections
6	N.A	N.A	<8	HC	5	Tissue sections
7	N.A	N.A	<8	HC	6	Tissue sections
8	N.A	N.A	<8	HC	7	Tissue sections
9	N.A	N.A	<8	HC	8	Tissue sections
10	N.A	N.A	<8	HC	9	Tissue sections
11	N.A	N.A	<8	Cultured	29	Tissue sections
12	64	Female	3	HC	5	Cell isolation
14	66	Female	3	HC	3	Cell isolation
15	N.A	N.A	<8	HC	7	Cell isolation
16	56	Female	<8	Cultured	10	Cell isolation

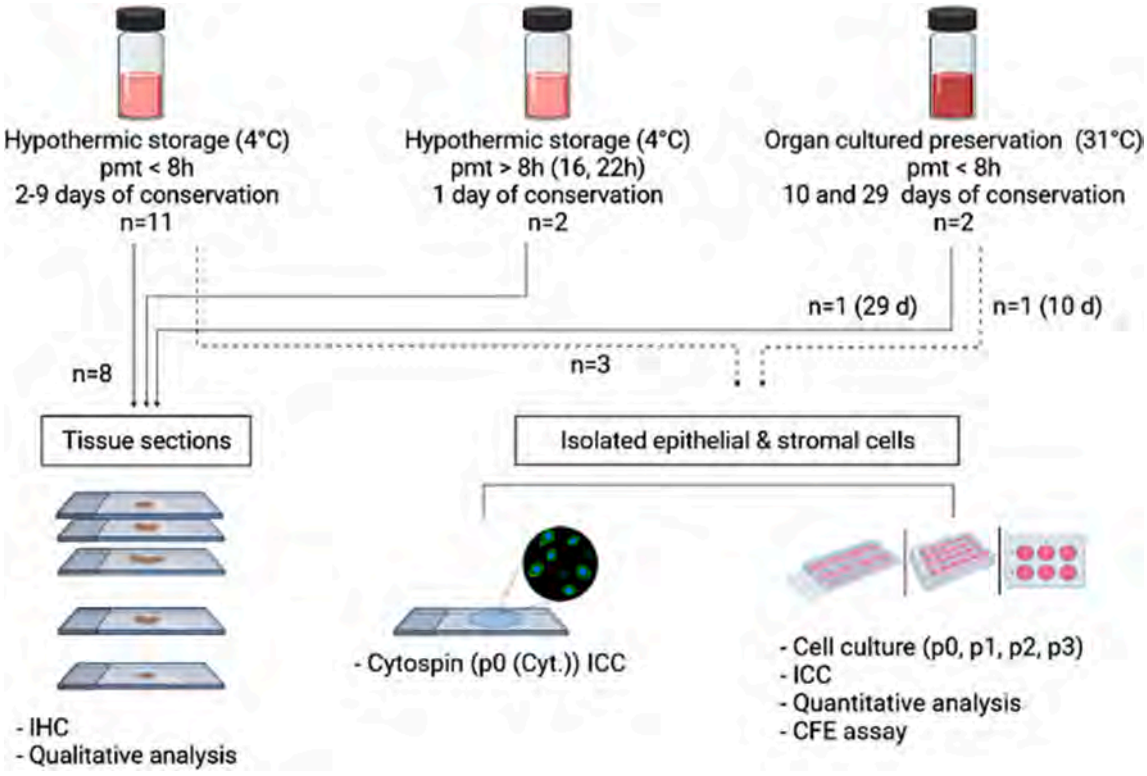

Fig. 1. Schematic representation of the experimental design showing the storage condition and the procedure followed with each of the corneoscleral samples.

2.2. Dissection of donor corneoscleral tissues and sclerocorneal rims

Donor tissues were immersed in Hank's solution containing HEPES (20 mM, Sigma, St. Louis, MO, USA), 1% Penicillin-Streptomycin (Lonza, Verviers, Belgium) and 1.25 μg/ml Amphotericin B (Sigma) to wash off the remaining traces of the preservation medium. Once cleaned, the tissues were dissected under a dissection microscope (Stemi 508, Zeiss; Axiocam ERc 5s) to remove the iris, endothelium, Tenon's capsule and conjunctiva. For corneoscleral tissues, the corneal button was separated from the sclerocorneal rim by an 8.5 mm punch and discarded.

Subsequently, samples intended for histological sections were cut and included in OCT (Optimal Cutting Temperature) compound (TissueTek®, Sakura Finetek, NL) blocks with the desired orientation to obtain transversal sections of the tissues. The blocks were kept at −80 °C.

2.3. Tissue digestion and cell isolation

Samples for cell culture were enzymatically digested. Dispase II (Hoffmann-La Roche; Basel, Switzerland), at a concentration of 2.4 U/ml, in a DMEM:F12 (Lonza) medium supplemented with 5% fetal bovine serum (FBS; Lonza) was used for 2 h at 37 °C to separate the epithelium from the stroma. Supernatants containing suspended isolated cells and cell clusters from the limbal epithelium were collected, centrifuged at 200 g for 10 min and suspended in the corresponding solution to perform the following assays.

The remaining stromal tissue, after digestion with dispase, was introduced in a mixture of 4 mg/ml Collagenase A (Hoffmann-La Roche) and 0.01% Hyaluronidase (Sigma) at 37 °C overnight for the extraction of stromal cells. The supernatant obtained from this digestion was centrifuged at 200 g for 10 min and suspended in the corresponding solution to perform the following assays.

2.4. Cell culture

For the *in vitro* propagation of limbal epithelial cells collected after digestion with dispase, cells were suspended in a SHEM5 hormonal medium—containing DMEM:F12 (Lonza), 5% fetal bovine serum (FBS; Lonza), 1% Penicillin-streptomycin (Lonza), 1% N_2 supplement (Thermo Fisher Scientific; Waltham, Massachusetts, USA), 0.5 μg/ml Hydrocortisone (Sigma), 0.5% DMSO (Sigma), 8.4 ng/ml Cholera toxin (Gentaur Molecular Products, Brussels, Belgium) and 2 ng/ml EGF (Sigma)—and seeded at a density of 25000 cells/cm^2 in 24 well plates previously coated with poly-L-lysine. They were detached with 0.25% trypsin-EDTA (Sigma) when confluence was reached and reseeded in new 24 well plates.

The stromal cells extracted from the cornea after digestion with collagenase and hyaluronidase were suspended in a stromal cell medium (DMEM:F12, 10% FBS, 2.5 mM Glutamine and 1% Penicillin-streptomycin) and seeded in 6 well plates (5000 cells/cm^2). They were detached with 0.25% trypsin-EDTA when confluence was reached and reseeded in new 6 well plates.

For all cell cultures, cell media were changed every 2–3 days.

For immunocytochemical staining of cultured epithelial and stromal cells, 20000 cells/well were seeded on chambered coverslips with 8 wells for cell culture (Ibidi; Gräfelfing, Germany). The coverslips were previously coated with a poly-L-lysine solution diluted with deionised water (1:10) to facilitate cell adhesion.

For their clonal growth, the limbal epithelial cells were seeded at a density of 300 cells/cm^2 on growth-arrested 3T3 mouse fibroblasts. These cells were inactivated using 7 μg/ml Mitomycin C (Sigma) for 2.5 h at 37 °C and seeded at a density of 30000 cells/cm^2 in 6 well plates. A SHEM5 hormonal medium was used for clonal cultures.

2.5. Colony-forming efficiency (CFE) assay

To perform colony-forming efficiency (CFE) assays, plates used for clonal growth were fixed with 4% paraformaldehyde (PFA) on the 14th

day of growth. Then, the 3T3 monolayer was mechanically removed by pipetting over the cell layer surface several times, and the remaining colonies were stained with Crystal Violet for 10 min at room temperature (RT).

2.6. Immunocytochemistry and immunohistochemistry

To perform the immunocytochemical analysis of cells directly isolated from sclerocorneal rims, part of the cells obtained from tissue digestion, both epithelial and stromal cells, were washed in PBS 1X (Sigma) and fixed in 2% paraformaldehyde for 20 min. Once fixed, they were washed in PBS 1X, centrifuged for 7 min at 300 g and suspended in PBS-BSA (1%) (Sigma). The cell solution was then spun at 1300 rpm for 8 min using a Cytospin (Cytospin 4 Centrifuge; Thermo Scientific) and precipitated over slides coated with poly-L-lysine (Sigma). One hundred microlitres (100 μl) of cell suspension with a density of around 20000 cells were added per cytofunnel.

Immunocytochemistry was assessed in slides containing cells directly isolated from tissues and in 8-well chambered coverslips (Ibidi) containing the cultured limbal cells fixed in 2% paraformaldehyde in PBS for 20 min at room temperature. Fixed samples were then permeabilised for 10 min with 0.1% Triton TX-100 in PBS (PBT) and blocked for an hour with a blocking solution containing 5% BSA and 10% FBS in PBT to reduce non-specific interactions that could result in background and false-positive staining. Samples were treated with the corresponding solution of primary antibodies (Table 2) overnight at 4 °C, washed with PBT 3 times for 10 min each and stained with secondary antibodies for 2 h at room temperature in darkness. Finally, the samples were counterstained with DAPI (Sigma), diluted 1:1000 in PBS, or with 4 mg/ml Hoechst 33342 (Invitrogen, Thermo Fisher Scientific), diluted 1:1000 in PBS, at room temperature for 15 min and washed two times with PBS for 5 min each. The cells seeded on 8-well chambered coverslips (Ibidi) were maintained in PBS and the slides of directly isolated cells were mounted onto microscope slides with Fluoromount-G® mounting media (SouthernBiotech; Birmingham, England).

The same immunostaining procedure was used for tissue sections but 4% paraformaldehyde in PBS was used for the fixation step instead. All images were taken on the fluorescence microscope Apotome.2 (Zeiss; Oberkochen, Germany).

Fluorescence images of tissue sections were divided into three regions—conjunctiva, limbus and peripheral cornea—to perform a semi-quantitative analysis of the expressions of CK15, vimentin, ΔNp63α and Ki67 markers. Fluorescence ratios of the stained sections were calculated by dividing the mean fluorescence intensity by the area of the region of interest. These ratios allowed having comparable fluorescence values between the samples studied. Three sections were analysed to semi-quantitatively determine the expressions of the markers. For nuclear markers, the number of positive nuclei was counted. For cultured cells, the number of positive cells for the markers of interest and their corresponding mean intensities were automatically determined. The fluorescence analysis of both tissue sections and cell culture was performed using ImageJ software (developed by Wayne Rasband at the Research Services Branch, National Institute of Mental Health, Bethesda, MD).

Table 2
List of primary antibodies and dilutions used in the study.

Antibody	Dilution	Secondary Antibody	Commercial product
Cytokeratin 3	1:100	Goat anti-mouse IgG1	Millipore CBL218
Cytokeratin 12	1:50	Goat anti-rabbit IgG	Abcam ab185627
Cytokeratin 15	1:400	Goat anti-mouse IgG2a	Santa Cruz sc-47697
Vimentin	1:1000	Goat anti-rabbit IgG	Abcam ab16700
Collagen VII	1:400	Goat anti-mouse IgG1	Millipore MAB1345
p63α[a]	1:800	Goat anti-rabbit IgG	Cell signaling Tech. #13109
Ki67	1:400	Goat anti-mouse IgG1	Millipore MAB4190
ZO-1	1:20	Donkey anti-goat IgG	Abcam ab190085
Integrin β4	1:50	Goat anti-mouse IgG1	Abcam ab29042
Melan A	1:200	Goat anti-rabbit IgG	Abcam ab51061

[a] Since the predominant p63 in the limbus is ΔNp63, it is presumed that positive cells express ΔNp63.

2.7. Statistical analysis

Quantification results were subjected to the Kruskal–Wallis test in which the Dunn test was used for multiple comparisons. Statistical differences were set at the $p < 0.05$ level. IBM SPSS Statistics 24 (IBM, Armonk, NY, USA) software was used for this analysis.

3. Results

3.1. Histological appearance of the tissue sections

The integrity of the corneoscleral tissues between 1 and 5 days of conservation showed healthy appearance and well-conserved morphology of the epithelium, irrespective of the death-to-exeresis time being higher or lower than 8 h.

Corneoscleral tissues that had been conserved for 6 days or more showed signs of deterioration such as loss of most superficial layers of the epithelium and oedema. These signs were evident in the corneoscleral tissues on the 8th to 9th day of conservation, where a single layer of epithelial cells or even total loss of the epithelium was observed in small areas.

Cultured rims were more affected by the passage of time and showed unstructured and oedematous epithelia. Furthermore, the staining pattern of the studied proteins was not precise and appeared intermingled between the peripheral cornea and the limbus.

3.2. Analysis of corneal markers in tissue sections

Considering the integrity, death-to-exeresis time and preservation characteristics of the corneoscleral tissues, the results of the expressions of cell markers were classified into 5 groups. The first 3 groups showed the information related to fresh corneoscleral tissues (obtained less than 8 h after the donor's death (pmt < 8 h)) conserved in hypothermic conditions for different conservation periods (2–5, 6 to 7, and 8–9 days of conservation, Fig. 2). The fourth group represented the corneoscleral tissues conserved for 1 day but extracted more than 16 h post-mortem (Fig. 3 left column). The remaining group included the results pertinent to cultivated sclerocorneal rims (Fig. 3 right column).

3.2.1. CK12–CK15 cell marker expressions

The results obtained showed the expected staining patterns of both cytokeratins in all fresh corneoscleral tissues despite the different days of conservation. The expression of CK12 was limited to the suprabasal areas throughout the peripheral corneal epithelium. Its specificity decreased in tissue sections obtained from corneoscleral samples conserved for a longer time. The fluorescence pattern of CK15 was limited to the basal areas of the limbal and conjunctival epithelium (a–c of Fig. 2 and a–b of Fig. 3).

In order to observe the possible differences in CK15 staining between groups, a quantitative study of the CK15-stained area in analysed corneoscleral rim sections was performed. The staining pattern was quantified in the conjunctiva, limbus and peripheral cornea. The results showed a decreasing CK15 staining trend in the limbal area as the conservation time of the corneoscleral tissues increased from 2 to 8 days. However, its expression increased in the tissue at 9 days of conservation (Fig. 4). The corneoscleral rims conserved for 1 day (pmt > 16 h) and the ones cultured for 29 days were not included in the statistical analysis due to alterations in the markers' expressions.

Similar fluorescence ratios were quantified in all tissue samples for the conjunctiva and peripheral cornea.

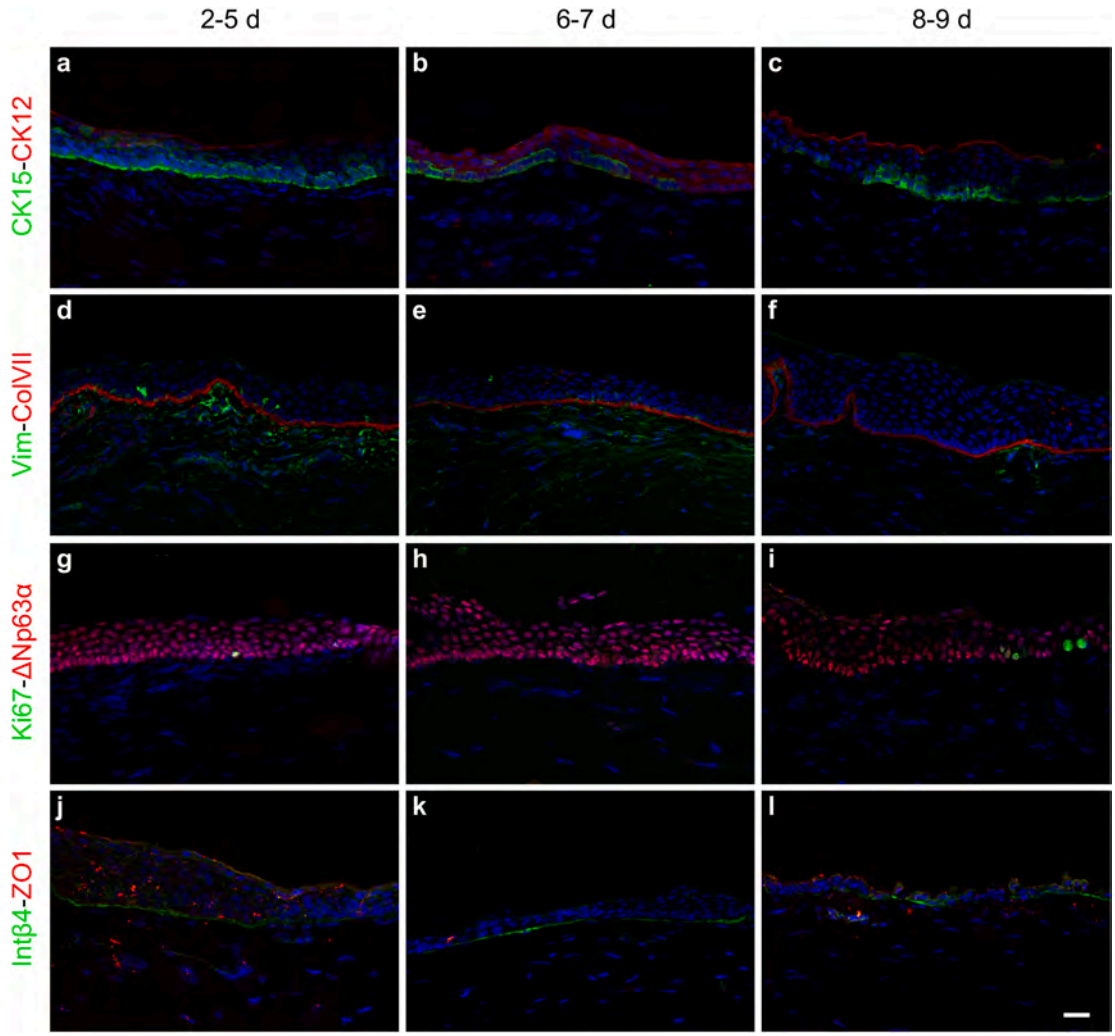

Fig. 2. Expressions of different markers in the limbal area of corneoscleral tissues stored in hypothermic conditions for 2–9 days (pmt < 8 h). The samples used during the study were classified in 3 groups (2–5, 6–7 and 8–9 days) represented in one column each. After 6 or 7 days, the expression of the putative stem cell markers (CK15, Vim, ΔNp63α) diminished. Differentiation (CK12), adhesion (ZO-1, integrin β4, Collagen VII), and proliferation (Ki67) markers were maintained in all groups.Vimentin labelling was notably lost in the tissues of more than 5 days of conservation. All the images were taken with 20 x magnification objective (scale bar corresponds to 25 μm).

3.2.2. Vimentin–collagen VII cell marker expressions

Because vimentin is a marker of fibroblastic cells, vimentin-positive staining was observed for stromal keratocytes in all analysed tissue sections. Concerning the epithelium, a positive staining pattern of vimentin in the sections conserved for 2–5 days was observed in the basal area of the limbal and conjunctival epithelium (d of Fig. 2). However, a significant loss of specific staining in the basal area of the limbus was registered in the tissues conserved for 6–7 days (e of Fig. 2). This loss was even more noticeable in the corneoscleral rims conserved for 8–9 days (f of Fig. 2), in which the staining became completely negative for all the cells of the basal limbal epithelium. For corneoscleral rims conserved for 1 day with pmt >16 h, positive labelling was detected in specific cells of the limbus (c of Fig. 3). Finally, complete absence of expression in the epithelium of cultivated sclerocorneal rims was observed. The only vimentin-positive cells of this last group were located in the conjunctiva (d of Fig. 3).

The expression of collagen VII was similar and homogeneous for the entire epithelial extent in all the samples, clearly delimiting the junction between the epithelium and the stroma (d–f of Fig. 2 and c–d of Fig. 3).

The specific staining of vimentin in the peripheral corneal epithelium was quantitatively analysed in the corneoscleral rims conserved for 3–5 days. The positive staining pattern was displaced towards the limit of the limbus with the peripheral cornea as tissue preservation days increased (Fig. 5). Thus, an increasing trend of vimentin expression in the peripheral cornea and a decreasing trend in the limbus were registered over time. The expression registered in the conjunctiva was variable and did not follow any clear pattern.

Vimentin was also combined with CK15 and CK3 to observe possible colocalisation of these markers. The results for vimentin and CK15 showed colocalisation in specific areas of the sclerocorneal transition epithelium. However, CK3 and vimentin were not registered together; the expression of CK3 was limited to the superficial areas of the limbal and conjunctival epithelia whereas vimentin stained the basal cells of both epithelia (Fig. 6).

3.2.3. Vimentin–melan A cell marker expressions

After the identification of vimentin positive cells in the corneal epithelium of the corneoscleral tissues conserved for 3–5 days, the melanocyte marker melan A was combined with this protein to observe possible colocalisations. The staining pattern of melan A was limited to a few cells located in the limbal crypts (Fig. 7). Vimentin and melan A colocalised in some cells, but not all vimentin-positive cells were classified as melanocytes. The cells that expressed any of these markers exhibited a ramified morphology.

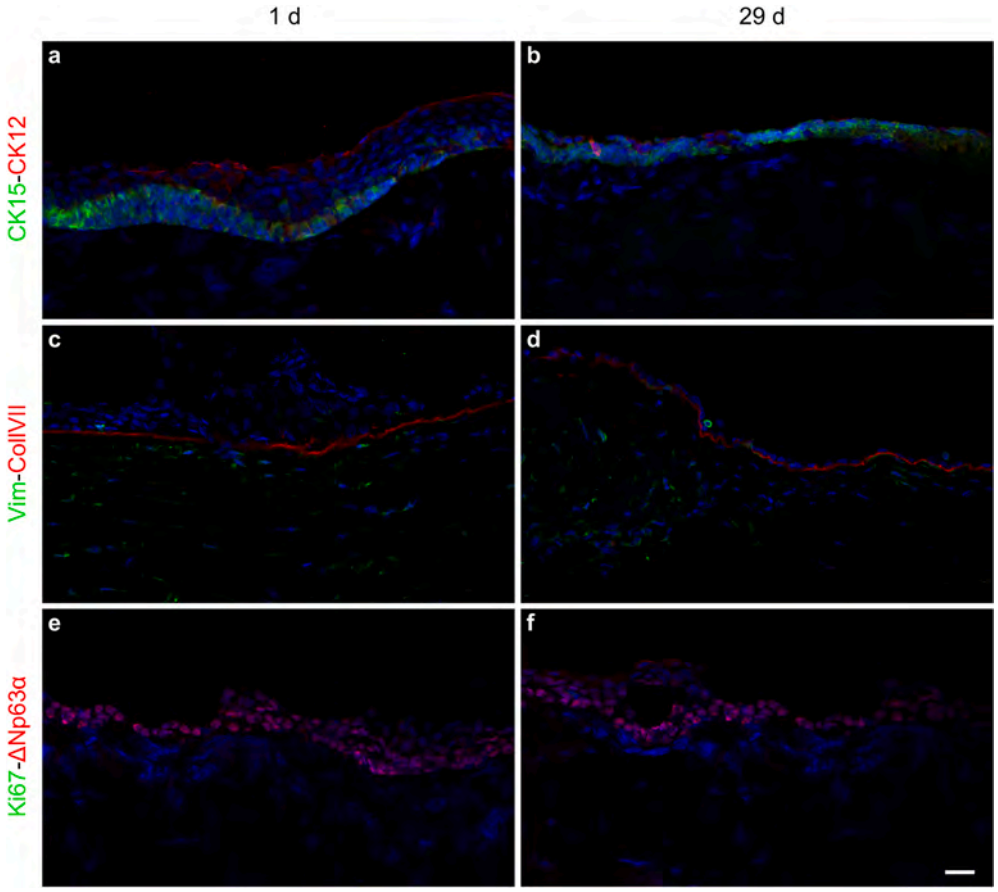

Fig. 3. Expressions of different markers in the limbal area of the corneoscleral tissue stored in hypothermic conditions for only 1 day with pmt >16 h, and in the culture medium for 29 days. Both conditions showed similar expression patterns of non-differentiation markers (CK15, Vim and ΔNp63α),but the expressions decreased in the cultured tissue. Moreover, the corneoscleral sample cultured for 29 days showed great tissue deterioration. All the images were taken with a 20 x magnification objective (scale bar corresponds to 25 μm).

3.2.4. *ΔNp63α–Ki67 cell marker expressions*

The staining pattern of ΔNp63α was almost identical in all corneoscleral rim sections. The limbal or conjunctival basal area of the epithelium contained the most intensely marked cells; even so, cells in the suprabasal areas as well as in the peripheral cornea were slightly labelled too (g–i of Fig. 2 and e–f of Fig. 3).

Besides quantifying the number of ΔNp63α-positive cells, the percentage of "bright" ΔNp63α cells was specifically recorded, as they were supposed to be the ones with higher stemness potential. The results showed that all the corneoscleral rims expressed ΔNp63α regardless of their preservation time. The presence of ΔNp63α "bright" cells corresponded mainly to the limbus and conjunctiva (Fig. 4).

Cells with high mitotic activity, that is Ki67-positive cells, were observed in all the groups (g–i of Fig. 2) except for the corneoscleral tissues conserved for 1 day with pmt >16 h and the ones cultured for 29 days (e–f of Fig. 3). The number of Ki67-positive cells was also determined in each tissue section of the samples conserved for 2–9 days. The presence of Ki67-positive cells was registered in all these tissue samples, especially in the limbal area of corneoscleral tissues preserved for a few days, but it was not possible to determine any clear trend (Fig. 4).

3.2.5. *Integrin β4–ZO-1 cell marker expressions*

The results of the corneoscleral rims conserved for 1 day with pmt >16 h and the ones cultured for 29 days were omitted for integrin β4 and ZO-1 markers due to their deteriorated state.

A homogeneous staining pattern of integrin β4 was observed in the basal area along the epithelium of the tissues conserved 2–5 days (j of Fig. 2), whereas ZO-1 was localized in the epithelial surface. However, the integrin β4 expression became discontinuous and extended across the whole epithelial thickness over time (tissues conserved for 6–7 days) (k of Fig. 2), so that it appeared interlaced with ZO-1 in the corneoscleral tissues conserved for 8–9 days (i of Fig. 2).

3.3. *Isolation and culture of limbal epithelial cells*

The suitability of the methodologies used for the isolation of cells from corneoscleral tissues conserved in hypothermic or culture conditions, as well as for the *in vitro* cell expansion of the isolated cells, was evaluated by a series of immunocytochemical procedures. The evolution of the expressions of the cell markers was evaluated for the different culture passages.

Epithelial cells directly isolated from the corneal limbal region were precipitated using a Cytospin, and the cell markers were analysed. CK15-, vimentin- and ΔNp63α-positive cells were observed in directly precipitated epithelial cells (Fig. 8, a, f). When limbal epithelial cells isolated from corneoscleral tissues were cultured for 12 ± 2 days (p0 passage), they maintained high staining for the CK15 marker (b of Fig. 8). However, the expression of this protein decreased as the cells were subcultured: from 40% of cells stained with CK15 in the cells precipitated from the Cytospin, to 10% of cells stained with CK15 in cultured passage 0, to total absence of its expression at the second passage of cultures (c of Fig. 8). Statistical differences were observed between p0 (Cytospin) and p1, p2 and p3 of cultured cells for CK15 ($p = 0.005$) and vimentin ($p = 0.037$) cell markers (e of Fig. 8). On the contrary, the expression of the vimentin cell marker in cells isolated from corneoscleral tissues and centrifuged with the Cytospin was limited to a few cells (around 7% of the total cells). In p0 passage cultures, vimentin-positive cells showed an elongated and branched morphology (b of Fig. 8), with some of them enclosing CK15-positive cells. These positive cells observed in epithelial cultures at early passages presented a different morphology from the cells marked with vimentin in epithelial cultures of second and later passages (c, d of Fig. 8). The latter cells

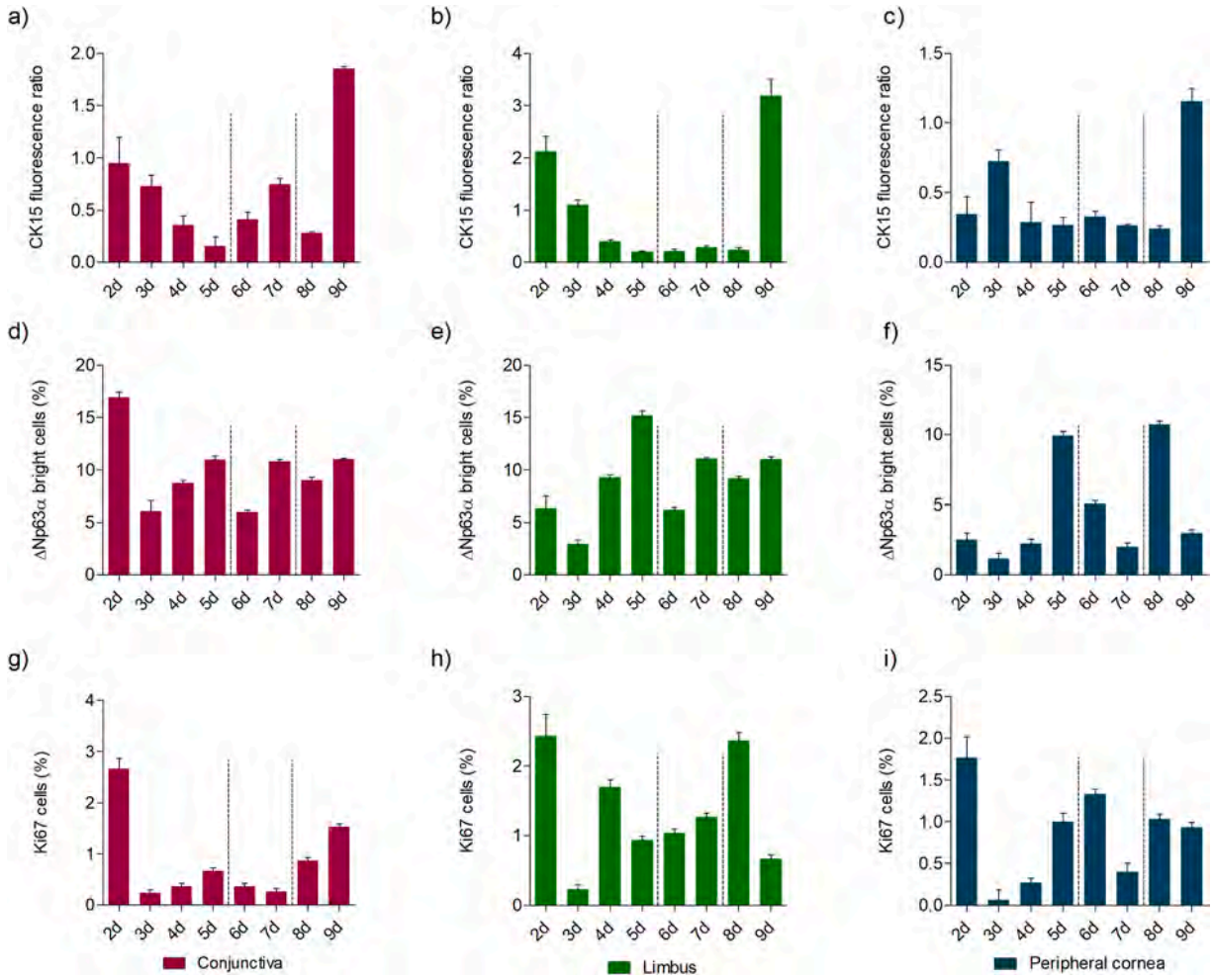

Fig. 4. Quantification of fluorescence staining of CK15 (a–c) and the percentage of ΔNp63α- "bright" (d–f) and Ki67-positive cells in the corneoscleral tissues (g–i). The specific expression of CK15 was observed in the limbal region of all samples. As time of conservation increased, the expression reduced and the distribution of CK15 became more unspecific. At short storage time (up to 5 days), ΔNp63α "bright" cells were more abundant in the limbal region than in the peripheral cornea. All corneoscleral tissues presented Ki67-positive cells but with no clear trend.

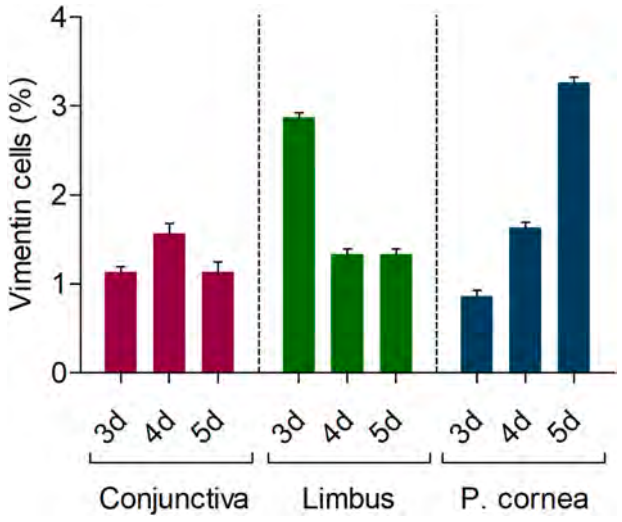

Fig. 5. Quantification of vimentin fluorescence marker in the three corneoscleral regions for the samples conserved for 3–5 days. The graphs show the displacement of vimentin staining from the limbal region to the peripheral cornea as conservation time increases.

showed a morphology consistent with the differentiated stromal cells but not with the epithelial cell phenotype.

Epithelial cells obtained just after tissue digestion from both fresh and cultured corneoscleral tissues showed ΔNp63α-positive staining. The evolution of the staining pattern was the same in cells from all tissues: the number of bright cells decreased drastically from one passage to another while the number of cells with no or insignificant signal increased (f, g, h and i of Fig. 8). The staining pattern decreased from 20% to 6% of counted bright cells from the passage of cells directly precipitated from the Cytospin to the p0 culture. From the p0 passage onwards, the number of ΔNp63α-positive cells did not exceed 5%. Statistical differences between p0 (Cytospin) and p1, p2 and p3 of cultured cells were recorded ($p = 0.043$) (j of Fig. 8).

3.4. Isolation and culture of limbal stromal cells

Directly isolated or cultured stromal cell populations were very pure and the double CK15 –vimentin staining revealed a lack of CK15 expression and a predominance of the vimentin marker. In addition, the cells were specifically aligned throughout the passages (Fig. 9).

3.5. Presence of melanocytes in the epithelial cell culture

Morphological differences were observed in vimentin-positive cells observed in epithelial and stromal cell cultures of p0 passage. The cells

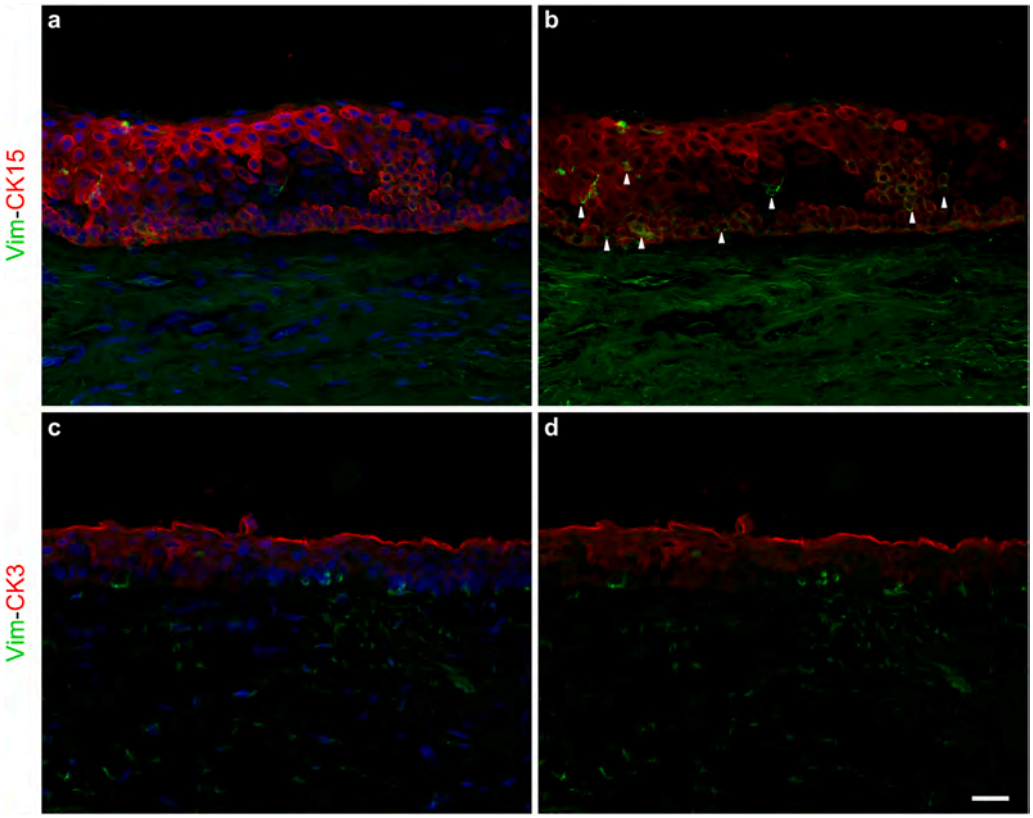

Fig. 6. Colocalisation of vimentin with CK3 and CK15 (differentiation and non-differentiation markers, respectively). Images on the left (a and c) show vimentin, CK15 or CK3 and DAPI nuclear staining. Images on the right (b and d) are the same as those on the left without the nuclear staining. No overlap between vimentin and CK3 was observed whereas some vimentin-positive cells colocalised with CK15-positive cells at the limbal epithelium (cells marked with white arrowheads). All the images were taken with a 20 x magnification objective (scale bar corresponds to 25 μm).

stained with vimentin in the epithelial culture showed a dendritic phenotype similar to that of melanocytes, whose positivity to vimentin was already registered in histological sections (Fig. 10). This cell phenotype was observed in limbal epithelial cell cultures seeded above the 3T3 cell feeder layer. These ramified cells were especially observed around forming colonies of epithelial cells (Fig. 11).

The presence of melanocytes was also registered using the melan A marker in epithelial cultures. Positive melan A staining was registered especially in p0 passages of cultured cells from the analysed corneoscleral tissues. Following the same trend as the undifferentiation markers ΔNp63α and CK15, melan A staining decreased considerably throughout all passages (Fig. 11).

3.6. Presence of limbal putative stem cell markers in cell colonies formed in the epithelial cell culture of a sclerocorneal rim conserved for 7 days

The presence of limbal stem cell markers was also assessed in epithelial cultures of a sclerocorneal rim conserved for 7 days in hypothermic conditions. Isolated cells in the culture expressed CK15 and ABCG2 undifferentiation markers after several culture passages (Fig. 12). Furthermore, isolated cells seeded at clonal dilution were able to grow, forming holoclone-like colonies, which demonstrated the presence in the culture of cells with self-renewing capability.

4. Discussion

Because of the shortage of donor corneas for both research and stem cell therapy purposes, it was important to investigate how the storage time and conditions (culture media and temperature) and conservation procedures of corneoscleral tissues affect their quality in terms of the quantity of limbal stem cells. These cells are essential for the treatment of limbal stem cell deficiency, a disease caused by the lack of stem cells in the limbus or damage to the limbal niche, resulting in partial or complete loss of the corneal regenerative ability (Le et al., 2018).

The way the corneas are handled and preserved may play an important role in successful *ex vivo* limbal cell transplant. The two main methods of corneoscleral tissue storage prior to corneal transplantation are organ culture, in which corneas are stored at 31 °C in a medium for organ culture of donor corneas (Pels and Rijneveld, 2009), and hypothermic storage in commercially available media such as Optisol-GS or Eusol-C, in which corneas are stored at 2–8 °C (Kanavi et al., 2015).

Raeder et al. showed that the layered structure of corneal epithelial cells was better preserved and the number of dead cells reduced when the cells are kept at 23 °C in organ culture conditions rather than in Optisol-GS at 5 °C (Raeder et al., 2007). Kim et al. examined how time variables were related to *in vitro* limbal epithelial growth from corneas stored at 4 °C in Optisol-GS or an organ culture medium (Kim et al., 2004). They found that "fresher" tissues with low death-to-enucleation and low death-to-storage times were more likely to produce successful culture growth. The aim of the present study was to verify the presence or lack of limbal stem cells, their amount and exact location in the epithelium of sclerocorneal rims preserved in hypothermic conditions or organ culture media, and their potential to grow in culture and become a source of stem-like limbal epithelial cells for limbal cell transplantation. Several fluorescence non-differentiation markers as well as colony-forming efficiency assays were used for such purposes.

CK15 is a basal type I cytokeratin, a specific epithelial cell cytoskeletal protein present in stratified epithelia. It is part of the intermediate filaments and has been proposed as a potential putative marker of limbal stem cells (Yoshida et al., 2006). The expression pattern of this cytokeratin in corneoscleral tissues preserved for 2–5 days was very clear and delimited the beginning of the transition from the peripheral cornea to the sclerocorneal limbus. The fluorescence ratio recorded for this marker decreased progressively as the preservation time of fresh corneoscleral tissues increased from 2 to 8 days. However, its expression was lost in cultured tissues preserved for 29 days and in fresh tissues preserved for more than 7 days, evolving towards a less specific expression intermingled with CK12 staining. The noticeable increase in

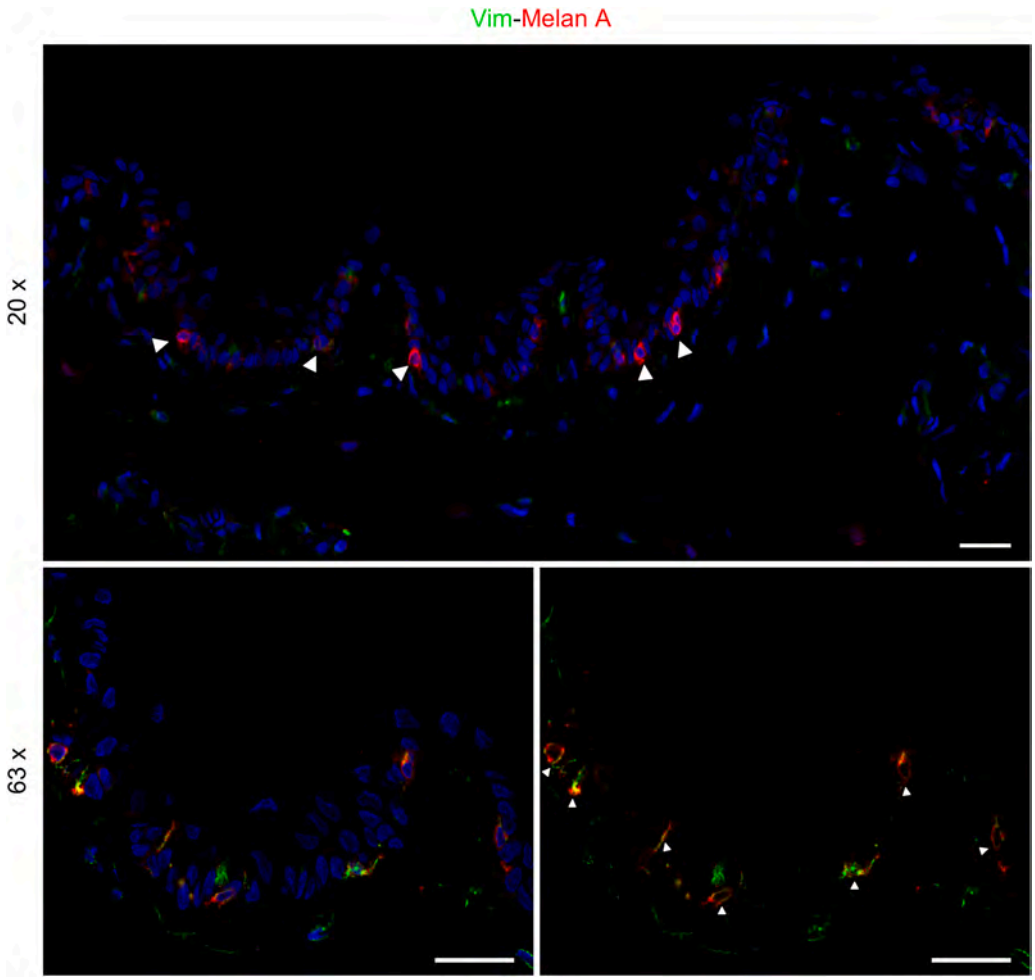

Fig. 7. Expressions of vimentin- and melan A-positive cells in a histological section of the limbal area of a corneoscleral tissue conserved for 3 days. The image above was taken with a 20 x magnification objective (scale bar corresponds to 25 μm) and shows the specific localization of melan A-positive cells (cells marked with white arrowheads) in the limbal crypts. The images below were taken with 63 x magnification objective (scale bars correspond to 25 μm). Both images correspond to the same tissue section with or without the nuclear staining with Hoechst 33342. Vimentin colocalised with melan A-positive cells (cells marked with white arrowheads) but not all vimentin-positive cells in the epithelium stained for melan A.

CK15 fluorescence ratios registered in three areas (conjunctiva, limbus and peripheral cornea) in the tissues preserved for 9 days and in the cultured sample was the result of the detachment of the epithelial cells and the progressive deterioration of the epithelium. In general, the morphological alterations recorded in long-stored donor tissue sections were alike to those already described: sloughing and loss of the superficial layers of the epithelium (Greenbaum et al., 2004). This damage caused the altered quantification of CK15 marker.

CK12 and CK3 are documented as cornea-specific cytokeratins specifically related to differentiated epithelial cells. Their expression can be observed throughout the whole corneal epithelium, although their pattern of expression varies among areas. They are present across the whole epithelial thickness in the central cornea; their pattern is limited to the superficial layers of the epithelium in the limbus, and they are absent in the conjunctiva (Merjava et al., 2011). In our study, CK12 staining was recorded throughout the suprabasal areas of the peripheral corneal epithelium. The loss of specificity of this marker was also detected as the conservation time of the corneoscleral tissues increased. Considering that CK12 forms a dimer with CK3 and that both are considered specific corneal epithelial cell markers, these results are in line with the ones reported by Joseph et al. who observed a decrease in CK3 staining as the duration of donor corneal samples in culture increased (Joseph et al., 2004).

The presence of vimentin in the corneoscleral epithelium was also assessed. Vimentin is a cytoskeletal protein classified under type III intermediate filament family. It is considered a specific marker of cells with mesenchymal origin such as keratocytes. Nonetheless, the expression of this protein has also been linked with a specific cell population in the limbal niche (Schlötzer-Schrehardt and Kruse, 2005). Vimentin staining of specific basal epithelial cells of the limbus and conjunctiva strikingly disappeared in the corneoscleral tissues conserved for 7 days or more, narrowing down the quantification of its expression in only the samples conserved for 3–5 days, which were the ones that showed the most remarkable staining. As conservation time of the tissue samples increased, a simultaneous decrease and increase in the vimentin expression in the limbus and the peripheral cornea, respectively, were registered. These results could be related to the highly motile vimentin-positive cells reported by Castro-Muñozledo et al., who suggested that some vimentin-positive cells located in the limbal epithelium could be early differentiated and highly motile epithelial progenitors that migrate from the limbal zone towards the peripheral and central cornea (Castro-Muñozledo et al., 2017).

Vimentin was combined with the differentiation marker CK3, the non-differentiation protein CK15 and the melanocytic marker melan A to analyse possible colocalisations. On the one hand, the individual cells stained with vimentin in the limbal epithelium were consistent with the undifferentiated cell phenotype. Lauweryns et al. already indicated the expression of vimentin in corneal epithelial cells with stemness characteristics, as they identified a subpopulation of transitional cells co-expressing CK19 and vimentin (Lauweryns et al., 1993). On the other hand, the colocalisation of some vimentin cells with melan A marker indicated that some of the vimentin-positive cells of the epithelium corresponded to melanocytes (Polisetti et al., 2020a, b).

Another putative marker used for limbal stem cells staining was ΔNp63α, the predominant isoform of the transcription factor p63 in the corneoscleral limbus. ΔNp63α is expressed in the basal cells of stratified

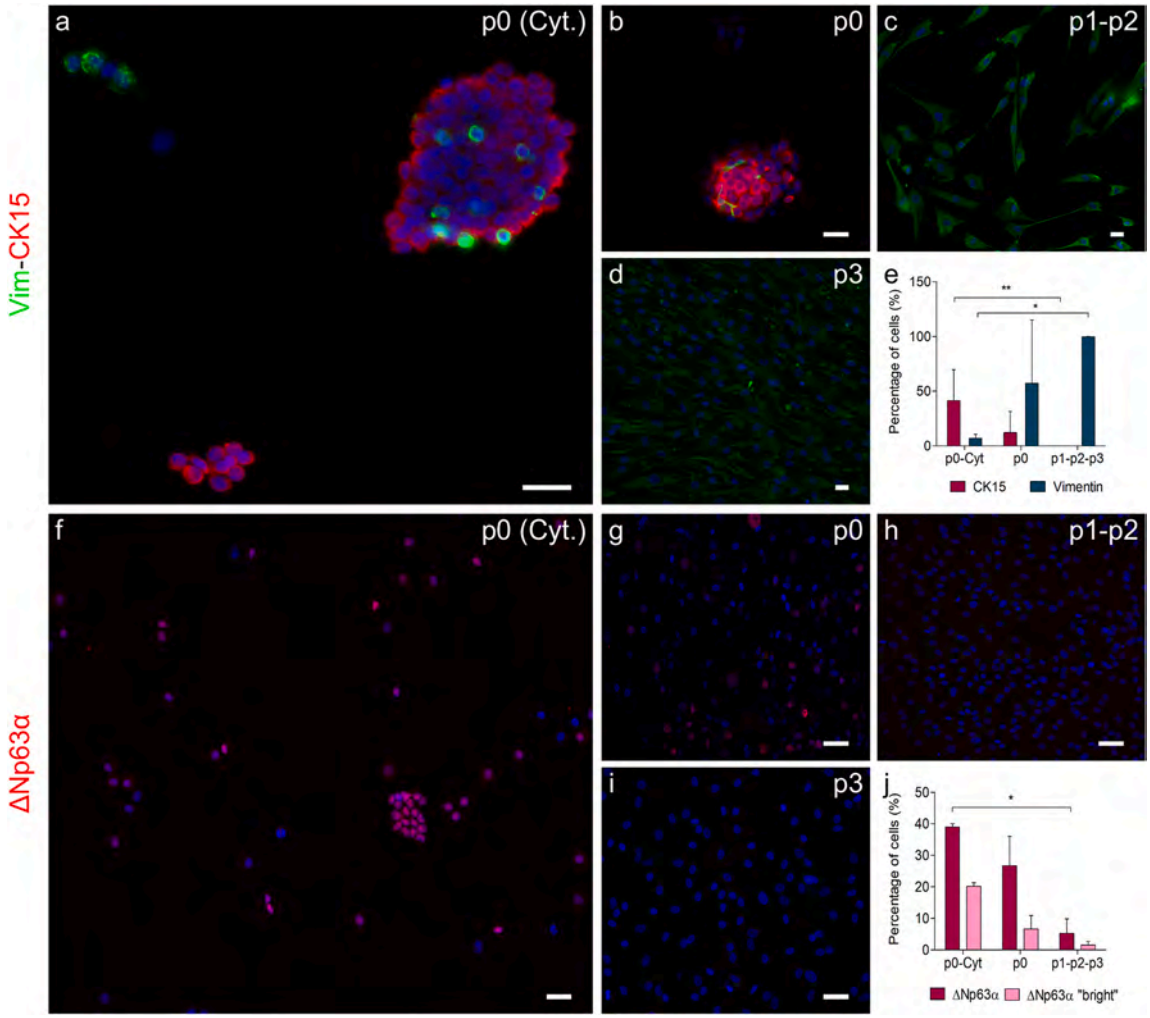

Fig. 8. Expressions of CK15, vimentin and ΔNp63α markers in limbal epithelial cell directly isolated after tissue enzymatic digestion (a and f, p0 Cytospin) or cultured during several cell passages p0 (b, g), p1, p2 (c, h) and p3 (d, i). The images a and f show that the cells extracted directly after tissue digestion highly expressed the putative non-differentiation markers CK15 and ΔNp63α. An exponential decrease in the undifferentiation markers and a predominant vimentin staining were registered throughout the passages (images b, c and d). The graphs show on the one hand the evolution of the percentage of CK15- and vimentin-positive cells (graph e) and on the other hand the expression of ΔNp63α bright cells from several corneoscleral tissues throughout the passages (graph j). Statistical differences were recorded between p0 (Cytospin) and p1, p2 and p3 of cultured epithelial cells for the three markers. All the images were taken with a 20 x magnification objective (scale bars correspond to 25 μm).

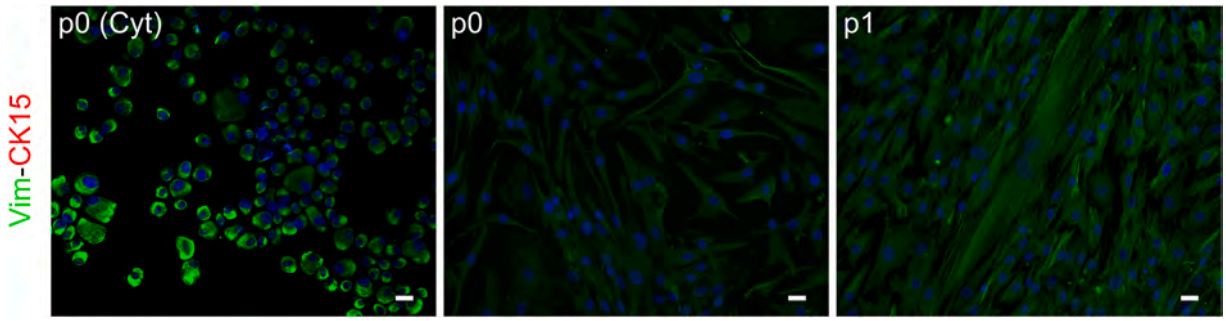

Fig. 9. Expressions of vimentin and CK15 markers in limbal stromal cells directly isolated after tissue digestion (p0 Cytospin) and p0 and p1 of cultured stromal cells. Cell cultures were characterised by complete absence of the CK15 epithelial marker. As the passage of the cell culture increased, the cell orientation and morphology tended to change. All the images were taken with a 20 x magnification objective (scale bars correspond to 25 μm).

epithelia and is highly related to limbal stem cells (Kawasaki et al., 2006). It is expressed as nuclear staining especially in the cells of the basal region of the limbal epithelium, but it can also be observed in more suprabasal areas of both the corneal and conjunctival epithelium (Melino et al., 2015). Our results indicated that the conservation time of the corneoscleral tissues was not the most critical factor affecting the abundance of ΔNp63α-positive cells, especially ΔNp63α "bright" cells, whose expression corresponds to potentially undifferentiated

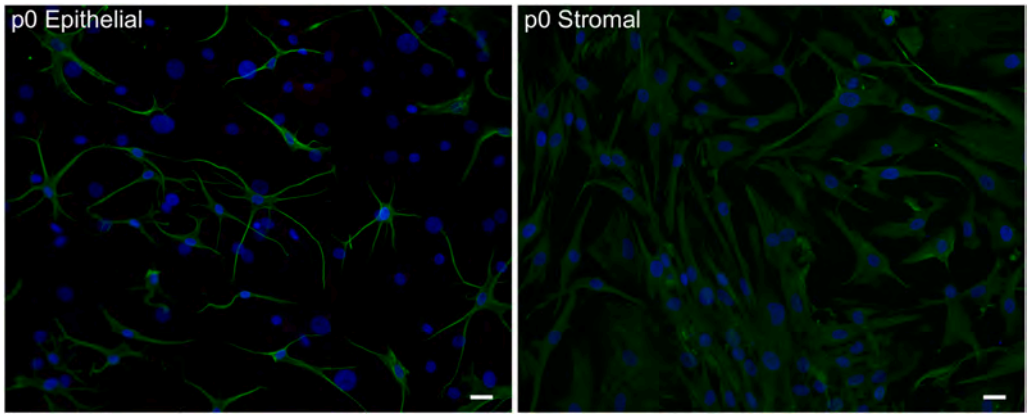

Fig. 10. Expression of the vimentin marker in limbal epithelial (a) and stromal (b) cell cultures. Both cultures corresponded to p0 passage. Both images were taken with a 20 x magnification objective (scale bars correspond to 25 μm).

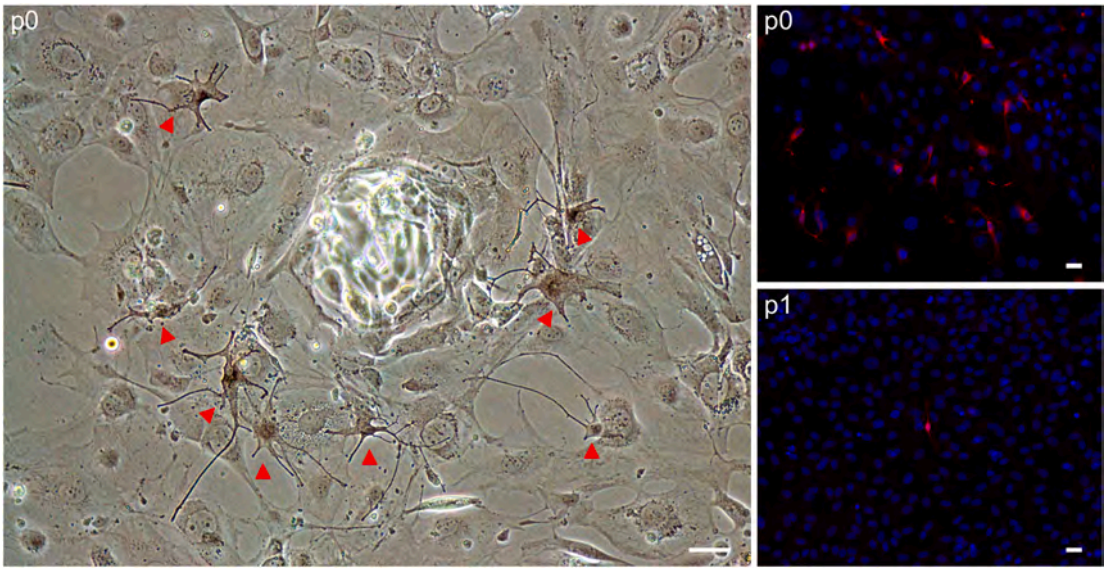

Fig. 11. Limbal epithelial cell culture of passage p0 and passage p1. The image on the left shows epithelial cells of passages p0 and seeded above a feeder layer of 3T3 cells. Cells marked with red arrowheads correspond to the melanocytes that enclosed the forming epithelial stem cell colony. The image was taken with a 20 x magnification objective (scale bar corresponds to 25 μm). The images on the right show the expression of the melan A marker in epithelial cells of passages p0 and p1. Both images were taken with a 20 x magnification objective (scale bars correspond to 25 μm). (For interpretation of the references to colour in this figure legend, the reader is referred to the Web version of this article.)

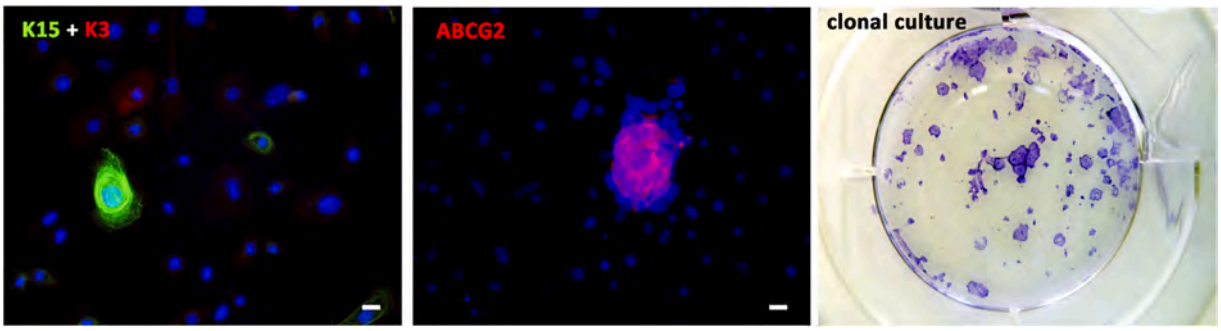

Fig. 12. Expressions of CK15 and ABCG2 undifferentiation markers in the second passage of the limbal epithelial cell culture (first and second images) and clonal culture of epithelial cells stained with violet crystal (third image). First and second images were taken with a 20 x magnification objective (scale bars correspond to 25 μm). Clonal cultures demonstrated cell growth into holoclone-like colonies. Images reproduced from Hernáez-Moya et al. (2015), with permission of the authors. (For interpretation of the references to colour in this figure legend, the reader is referred to the Web version of this article.)

stem/progenitor cells (Rama et al., 2010). Its staining was registered in all the corneal tissues, prevailing in the basal area of the limbal epithelium.

The expression pattern of integrin β4 and ZO-1 adhesion proteins was also assessed to complete the analysis of tissue sections. Integrin β4 is involved in the formation of hemidesmosomes, therefore it constitutes an adhesion marker between the epithelium and the underlying extracellular matrix. This protein shows a polarized distribution in the basal cells of the limbal and corneal epithelium (Schlötzer-Schrehardt and Kruse, 2005). ZO-1 is a protein involved in the formation of tight junctions between cells and it is found mainly in the apical area of the epithelia. It is also implicated in the barrier effect of the corneal epithelium (Sugrue and Zieske, 1997). Both markers were seen along the whole corneoscleral epithelium. Integrin β4 staining was limited to the basal area (basement membrane) and ZO-1 was present in the superficial epithelium (tight junctions). The staining pattern got blurred in the corneoscleral tissues preserved for longer times for both markers, but their expression was maintained even in the most deteriorated epithelia. This confirmed that the barrier function and the ability to adhere to the extracellular matrix were maintained in all the analysed tissues.

Regarding cell cultures, the patterns observed in the corneoscleral tissue sections were similarly maintained in isolated cell populations in their passage 0. CK15-positive labelling of the epithelial cells directly precipitated from the Cytospin was consistent with the areas marked with this protein in the histological sections. Some vimentin-positive cells were also observed in directly isolated cells, as observed in the limbal area of the corneoscleral sections. The high percentage of CK15-positive cells (around 40%) extracted by tissue digestion and the lack of expression of this marker in stromal cell cultures verified the adequacy of the cell isolation methods, which generated quite pure epithelial and stromal populations. Whilst the expression of CK15 cytokeratin decreased throughout the passages, vimentin staining increased, with the vimentin-positive cells showing a morphology that resembled the differentiated stromal cell phenotype. This means that a small number of stromal cells can rapidly proliferate and overcome epithelial cultures if the cell culture does not favour the preservation of epithelial stem cells. Epithelial cells obtained just after tissue digestion from both fresh and cultured corneoscleral tissues showed ΔNp63α-positive staining irrespective of their conservation or culture time. This is consistent with ΔNp63α staining observed in tissue sections preserved for different time periods. However, the decrease in ΔNp63α levels was especially registered throughout all cell passages. The gradual decrease in p63 throughout the culture time was already reported in human limbal explant cultures. Joseph et al. registered a decrease in the number of p63-positive cells maintained for 1–3 weeks in culture. This result, together with their observation of p63 staining in the limbus and central cornea, suggested that p63 is a marker for both stem cells and transient amplifying cells. They concluded that the decrease in the positivity of this marker was related to the decline in the proliferative capacity of the cells after reaching confluence (Joseph et al., 2004). This loss of cells with high fluorescence intensity in *in vitro* cultures but not in corneal sections suggested that certain characteristics of stemness could be adequately maintained in both storage conditions before tissue digestion and that the loss of expression of markers had more to do with the *in vitro* cell culture.

Concerning the isolated stromal population, no CK15-positive staining was observed in directly isolated or cultivated stromal cells, and the vimentin marker was by far the predominant marker observed in these cultures. The specific orientation of these cells in culture was noticeable. Almost all the cells were oriented in the same sense and direction, as if they wanted to simulate their organized disposition in the corneal stroma (Espana and Birk, 2020).

Regarding the relationship between melanocytes and limbal epithelial stem cells, a very specific relationship of both cell types was suggested, based on the following highly significant observations: positive staining of melan A cells was detected in the limbal crypts; the ramified cell phenotype congruent with melanocytes was observed around forming limbal epithelial colonies in cell cultures; and the concurrent decrease throughout the culture passages of ΔNp63α-, CK15- and melan A-positive cells was registered. As suggested by Dziasko et al. a close relationship exists between the melanocytes and the limbal stem cells of the niche (Dziasko et al., 2014, Dziasko and Daniels, 2016), where the former seem to play a protective role in these potentially undifferentiated cells (Dziasko et al., 2015; Polisetti et al., 2016). This close relationship between stem cells and melanocytes and the putative role of melanocytes in preserving stemness are consistent with the simultaneous decrease in both markers. Besides, this could be related to the loss of vimentin expression in the corneal epithelium of the tissues conserved for longer times, as the colocalisations of vimentin and melan A in epithelial cultures of early passages confirmed that some vimentin-positive cells of the epithelium corresponded to melanocytes. The colocalisation of vimentin and melan A markers has already been reported. Polisseti et al. showed relatively pure cultures of melanocytes that stained positive for melan A and vimentin (Polisetti et al., 2020a). Besides, they were able to distinguish different cell types that express vimentin, since they observed positive vimentin staining colocalised with melan A corresponding to melanocytes in the basal epithelial layer of the sclerocorneal limbus, but the vimentin-positive stromal cells of the subepithelial layers lacked expression of the melanocytic marker (Polisetti et al., 2020b).

Even so, not all vimentin-positive cells stained for melan A. Apart from the possibility of being highly motile stem progenitors, the ramified cells observed in the epithelium could also be related to Langerhans cells. Like melanocytes, Langerhans cells are known to reside in the limbal basal layer and both stain positive for vimentin (De Waal et al., 1984; Higa et al., 2005; Si et al., 1993; Vantrappen et al., 1985).

Finally, because of the shortage of available corneal tissues, we considered it of interest to investigate the potential of expanding LESCs from long-term hypothermically stored sclerocorneal rims. We successfully obtained epithelial cultures containing holoclone-like cell colonies positive for the non-differentiation marker ABCG2. The potential of limbal primary cultures to grow in holoclones, instead of meroclones and paraclones, has been considered a means of quality control (Pellegrini et al., 2011), because holoclone-forming cells have all the hallmarks of stem cells, such as self-renewing capability and large proliferative potential.

The conclusions drawn from the study were mostly derived from the observations of the expressions of undifferentiated and differentiated cell markers in fluorescence images. Depending on the conservation time, increasing or decreasing expression patterns of the markers consistent with the deterioration of tissue samples were observed.

The low number of corneas available was translated into a low number of replicates for each study group, which was one of the biggest limitations to performing a detailed quantitative analysis. The shortage of donors and the high demand for corneas complicated the acquisition of tissues for this study.

Samples were classified considering the storage method, and the days of preservation and the pmt, which indicated the time that had elapsed since the death of the donor to the preservation of the tissue.. Two groups were considered based on the pmt: samples with pmt <8 h and samples with pmt >16 h. However, there is no generally established consensus on how to classify samples, and some authors lean towards not establishing such limits and being guided by the fulfilment of certain quality criteria such as donor age, storage time in organ culture, epithelial integrity, and opacity or clarity for the use of corneal grafts (Armitage et al., 2014; Sugar et al., 2009). No conclusions are drawn about the effects of donor age on graft quality because of the low number of samples available for this study. Advanced age has been related to a greater loss of endothelial cells that could compromise the success of transplants (Cruz et al., 2017). However, the Cornea Donor Study reported a similar survival rate of corneas for over a 5-year follow-up period after transplantation from donors aged 66–75 years old and

younger donors (Gal et al., 2008). Notara et al. studied the impact of the age of donor samples on the structural and phenotypic characteristics of the limbal niche. They did not observe differences in the expression of markers with respect to the age of the donors, which indicated that the cells maintained their stemness potential. However, their results indicated a significant decrease in the proliferative capacity of limbal epithelial cells from older donors, especially donors aged over 60 years (Notara et al., 2013). As long as this shortage of corneal tissues continues, it may not be prudent to set any age limit since establishing a maximum donor age could reduce the percentage of discarded corneas even more.

In summary, we have demonstrated that although a decrease in the pattern of several non-differentiation markers was recorded in the histological sections of long-preserved corneoscleral tissues, positivity for the putative stem cell markers was detected in all tissue samples, including in the corneoscleral tissue conserved in hypothermic conditions that exceeded the short desirable post-mortem time for tissue extraction. We have shown that the remaining limbal rims after corneal transplantation, which had been conserved in hypothermic conditions for as long as 7 days and should normally have been ignored, can be a valuable source of LESC cultures for research and even for stem cell therapy.

We hope that this study would in some way reduce the discard rate of tissues and thus increase the available donor pool, since disposable grafts could be used for the isolation of stem cells that could be expanded *in vitro*.

In addition, the results related to vimentin labelling suggested the need for a more exhaustive study to determine which cell type corresponds to the positivity of this marker in the corneal limbal epithelium, which would help to clarify the specific cells residing in the limbus and their interactions with the limbal stem/progenitor cells. The understanding of their behaviour could help to develop new culture conditions that would preserve the phenotype and function of the limbal stem/progenitor cells, before their use for treatment of limbal stem cell diseases.

Funding

This research study has been funded by grants from the Department of Heath of the Basque Government (RIS3, 2019222049) and the University of the Basque Country UPV/EHU-Instituto Clinico Quirurgico de Oftalmologia ICQO (US19/18). C. R–V. has received fellowship support from the University of the Basque Country UPV/EHU.

Declaration of competing interest

No sponsor or funding organisation had any role in the design or conduct of this research. None of the authors had any conflict of interest.

Acknowledgements

The authors thank the Biobank A Coruña of SERGAS, the Navarra Blood and Tissue Bank, Navarrabiomed Biobank from Navarra Health Department, the Blood and Tissue Bank from the Government of Catalonia, and the Basque Biobank (www.biobancovasco.org) for having provided them with the biological samples and/or clinical data necessary for the development of this research.

The authors thank SGIker (UPV/EHU/ERDF, EU) for their technical and human support with imaging and microscopy. They also gratefully acknowledge the technical support and assistance provided by Maria Jesus Fernandez-Martín and Cristina Tobillas.

References

Armitage, W.J., Jones, M.N.A., Zambrano, I., Carley, F., Tole, D.M., 2014. The suitability of corneas stored by organ culture for penetrating keratoplasty and influence of donor and recipient factors on 5-year graft survival. Invest. Ophthalmol. Vis. Sci. 55, 784–791. https://doi.org/10.1167/iovs.13-13386.

Barrandon, Y., Grasset, N., Zaffalon, A., Gorostidi, F., Claudinot, S., Lathion Droz-Georget, S., Nanba, D., Rochat, A., 2012. Capturing epidermal stemness for regenerative medicine. Semin. Cell Dev. Biol. 23, 937–944. https://doi.org/10.1016/j.semcdb.2012.09.011.

Baylis, O., Figueiredo, F., Henein, C., Lako, M., Ahmad, S., 2011. 13 years of cultured limbal epithelial cell therapy: a review of the outcomes. J. Cell. Biochem. 112, 993–1002. https://doi.org/10.1002/jcb.23028.

Bonnet, C., González, S., Roberts, J.S., Robertson, S.Y.T., Ruiz, M., Zheng, J., Deng, S.X., 2021. Human limbal epithelial stem cell regulation, bioengineering and function. Prog. Retin. Eye Res. 100956. https://doi.org/10.1016/j.preteyeres.2021.100956.

Brookes, N.H., Loh, I.P., Clover, G.M., Poole, C.A., Sherwin, T., 2003. Involvement of corneal nerves in the progression of keratoconus. Exp. Eye Res. 77, 515–524. https://doi.org/10.1016/S0014-4835(03)00148-9.

Castro-Muñozledo, F., Meza-Aguilar, D.G., Domínguez-Castillo, R., Hernández-Zequinely, V., Sánchez-Guzmán, E., 2017. Vimentin as a marker of early differentiating, highly motile corneal epithelial cells. J. Cell. Physiol. 232, 818–830. https://doi.org/10.1002/jcp.25487.

Chaloin-Dufau, C., Dhouailly, D., Sun, T.T., 1990. Appearance of the keratin pair K3/K12 during embryonic and adult corneal epithelial differentiation in the chick and in the rabbit. Cell Differ. Dev. 32, 97–108. https://doi.org/10.1016/0922-3371(90)90103-4.

Cruz, G.K.P., Azevedo, I.C. de, Carvalho, D.P., Vitor, A.F., Santos, V.E.P., Ferreira Júnior, M.A., 2017. Clinical and epidemiological aspects of cornea transplant patients of a reference hospital. Rev. Lat. Am. Enfermagem 25, e2897. https://doi.org/10.1590/1518-8345.1537.2897 e2897.

De Paiva, C.S., Chen, Z., Corrales, R.M., Pflugfelder, S.C., Li, D.Q., 2005. ABCG2 transporter identifies a population of clonogenic human limbal epithelial cells. Stem Cell. 23, 63–73. https://doi.org/10.1634/stemcells.2004-0093.

De Waal, R.M.W., Semeijn, J.T., Cornelissen, I.M.H., Ramaekers, F.C.S., 1984. Epidermal Langerhans cells contain intermediate-sized filaments of the vimentin type: an immunocytologic study. J. Invest. Dermatol. 82, 602–604. https://doi.org/10.1111/1523-1747.ep12523577.

Dziasko, M.A., Armer, H.E., Levis, H.J., Shortt, A.J., Tuft, S., Daniels, J.T., 2014. Localisation of epithelial cells capable of holoclone formation *in vitro* and direct interaction with stromal cells in the native human limbal crypt. PloS One 9, 1–9. https://doi.org/10.1371/journal.pone.0094283.

Dziasko, M.A., Tuft, S.J., Daniels, J.T., 2015. Limbal melanocytes support limbal epithelial stem cells in 2D and 3D microenvironments. Exp. Eye Res. 138, 70–79. https://doi.org/10.1016/j.exer.2015.06.026.

Dziasko, M.A., Daniels, J.T., 2016. Anatomical features and cell-cell interactions in the human limbal epithelial stem cell niche. Ocul. Surf. 14, 322–330. https://doi.org/10.1016/j.jtos.2016.04.002.

Espana, E.M., Birk, D.E., 2020. Composition, structure and function of the corneal stroma. Exp. Eye Res. 198, 108137. https://doi.org/10.1016/j.exer.2020.108137.

Gain, P., Jullienne, R., H, e Z., Aldossary, M., Acquart, S., Cognasse, F., Thuret, G., 2016. Global survey of corneal transplantation and eye banking. JAMA Ophthalmol 134, 167–173. http://doi:10.1001/jamaophthalmol.2015.4776.

Gal, R.L., Dontchev, M., Beck, R.W., Cornea Donor Study Investigator Group, 2008. The effect of donor age on corneal transplantation outcome: results of the cornea donor study. Ophthalmology 115, 620–626. https://doi.org/10.1016/j.ophtha.2008.01.003 e6.

González, S., Mei, H., Nakatsu, M.N., Baclagon, E.R., Deng, S.X., 2016. A 3D culture system enhances the ability of human bone marrow stromal cells to support the growth of limbal stem/progenitor cells. Stem Cell Res. 16, 358–364. https://doi.org/10.1016/j.scr.2016.02.018.

Greenbaum, A., Hasany, S.M., Rootman, D., 2004. Optisol vs Dexsol as storage media for preservation of human corneal epithelium. Eye 18, 519–524. https://doi.org/10.1038/sj.eye.6700693.

Hernáez-Moya, R., Etxebarria, J., Asumendi, A., Boyano, M.D., Andollo, N., 2015. Corneal rims following hypothermic storage for seven days can serve as a potential source of stem-like limbal epithelial cells. Updates on Histology 9–13.

Higa, K., Shimmura, S., Miyashita, H., Shimazaki, J., Tsubota, K., 2005. Melanocytes in the corneal limbus interact with K19-positive basal epithelial cells. Exp. Eye Res. 81, 218–223. https://doi.org/10.1016/j.exer.2005.01.023.

Joseph, A., Powell-Richards, A.O.R., Shanmuganathan, V.A., Dua, H.S., 2004. Epithelial cell characteristics of cultured human limbal explants. Br. J. Ophthalmol. 88, 393–398. https://doi.org/10.1136/bjo.2003.018481.

Joyce, N.C., Meklir, B., Joyce, S.J., Zieske, J.D., 1996. Cell cycle protein expression and proliferative status in human corneal cells. Invest. Ophthalmol. Vis. Sci. 37, 645–655.

Kanavi, M.R., Javadi, M.A., Chamani, T., Fahim, P., Javadi, F., 2015. Comparing quantitative and qualitative indices of the donated corneas maintained in Optisol-GS with those kept in Eusol-C. Cell Tissue Bank. 16, 243–247. https://doi.org/10.1007/s10561-014-9466-5.

Kawasaki, S., Tanioka, H., Yamasaki, K., Connon, C.J., Kinoshita, S., 2006. Expression and tissue distribution of p63 isoforms in human ocular surface epithelia. Exp. Eye Res. 82, 293–299. https://doi.org/10.1016/j.exer.2005.07.001.

Kim, H.S., Song, X.J., De Paiva, C.S., Chen, Z., Pflugfelder, S.C., Li, D.Q., 2004. Phenotypic characterization of human corneal epithelial cells expanded ex vivo from limbal explant and single cell cultures. Exp. Eye Res. 79, 41–49. https://doi.org/10.1016/j.exer.2004.02.015.

Lauweryns, B., van den Oord, J.J., De Vos, R., Missotten, L., 1993. A new epithelial cell type in the human cornea. Invest. Ophthalmol. Vis. Sci. 34, 1983–1990.

Lee, H.J., Nam, S.M., Choi, S.K., Seo, K.Y., Kim, H.O., Chung, S.H., 2018. Comparative study of substrate free and amniotic membrane scaffolds for cultivation of limbal epithelial sheet. Sci. Rep. 8, 14628. https://doi.org/10.1038/s41598-018-32914-0.

Le, Q., Xu, J., Deng, S.X., 2018. The diagnosis of limbal stem cell deficiency. Ocul. Surf. 16, 58–69. https://doi.org/10.1016/j.jtos.2017.11.002.

Melino, G., Memmi, E.M., Pelicci, P.G., Bernassola, F., 2015. Maintaining epithelial stemness with p63. Sci. Signal. 8, Re9. https://doi.org/10.1126/scisignal.aaa1033.

Merjava, S., Neuwirth, A., Tanzerova, M., Jirsova, K., 2011. The spectrum of cytokeratins expressed in the adult human cornea, limbus and perilimbal conjunctiva. Histol. Histopathol. 26, 323–331. https://doi.org/10.14670/HH-26.323.

Notara, M., Shortt, A.J., O'Callaghan, A.R., Daniels, J.T., 2013. The impact of age on the physical and cellular properties of the human limbal stem cell niche. Age (Dordr). 35, 289–300. https://doi.org/10.1007/s11357-011-9359-5.

Oliva, M.S., Schottman, T., Gulati, M., 2012. Turning the tide of corneal blindness. Indian J. Ophthalmol. 60, 423–427. https://doi.org/10.4103/0301-4738.100540.

Pellegrini, G., Rama, P., De Luca, M., 2011. Vision from the right stem. Trends Mol. Med. 17, 1–7. https://doi.org/10.1016/j.molmed.2010.10.003.

Pels, E., Rijneveld, W.J., 2009. Organ culture preservation for corneal tissue. In: Developments in Ophthalmology, pp. 31–46. https://doi.org/10.1159/000223837.

Polisetti, N., Zenkel, M., Menzel-Severing, J., Kruse, F.E., Schlötzer-Schrehardt, U., 2016. Cell adhesion molecules and stem cell-niche-interactions in the limbal stem cell niche. Stem Cell. 34, 203–219. https://doi.org/10.1002/stem.2191.

Polisetti, N., Gießl, A., Li, S., Sorokin, L., Kruse, F.E., Schlötzer-Schrehardt, U., 2020a. Laminin-511-E8 promotes efficient in vitro expansion of human limbal melanocytes. Sci. Rep. 10, 11074. https://doi.org/10.1038/s41598-020-68120-0.

Polisetti, N., Schlötzer-Schrehardt, U., Reinhard, T., Schlunck, G., 2020b. Isolation and enrichment of melanocytes from human corneal limbus using CD117 (c-Kit) as selection marker. Sci. Rep. 10, 17588. https://doi.org/10.1038/s41598-020-748691.

Raeder, S., Utheim, T.P., Utheim, Ø.A., et al., 2007. Effects of organ culture and optisol-GS storage on structural integrity, phenotypes, and apoptosis in cultured corneal epithelium. Invest. Ophthalmol. Vis. Sci. 48, 5484–5493. https://doi.org/10.1167/iovs.07-0494.

Rama, P., Matuska, S., Paganoni, G., Spinelli, A., De Luca, M., Pellegrini, G., 2010. Limbal stem-cell therapy and long-term corneal regeneration. N. Engl. J. Med. 363, 147–155. https://doi.org/10.1056/NEJMoa0905955.

Schlötzer-Schrehardt, U., Kruse, F.E., 2005. Identification and characterization of limbal stem cells. Exp. Eye Res. 81, 247–264. https://doi.org/10.1016/j.exer.2005.02.016.

Sharma, N., Mohanty, S., Jhanji, V., Vajpayee, R.B., 2018. Amniotic membrane transplantation with or without autologous cultivated limbal stem cell transplantation for the management of partial limbal stem cell deficiency. Clin. Ophthalmol. 12, 2103–2106. https://doi.org/10.2147/OPTH.S181035.

Shortt, A.J., Secker, G.A., Munro, P.M., Khaw, P.T., Tuft, S.J., Daniels, J.T., 2007. Characterization of the limbal epithelial stem cell niche: novel imaging techniques permit in vivo observation and targeted biopsy of limbal epithelial stem cells. Stem Cell. 25, 1402–1409. https://doi.org/10.1634/stemcells.2006-0580.

Si, S.P., Tsou, H.C., Lee, X., Peacocke, M., 1993. Cultured human melanocytes express the intermediate filament vimentin. J. Invest. Dermatol. 101, 383–386. https://doi.org/10.1111/1523-1747.ep12365595.

Sugar, J., Montoya, M., Dontchev, M., Tanner, J.P., Beck, R., Gal, R., Gallagher, S., Gaster, R., Heck, E., Holland, E.J., Kollman, C., Malling, J., Mannis, M.J., Woody, J., Group, G.C.D.S.I., 2009. Donor risk factors for graft failure in the cornea donor study. Cornea 28, 981–985. https://doi.org/10.1097/ICO.0b013e3181a0a3e6.

Sugrue, S.P., Zieske, J.D., 1997. ZO1 in corneal epithelium: association to the zonula occludens and adherens junctions. Exp. Eye Res. 64, 11–20. https://doi.org/10.1006/exer.1996.0175.

Thoft, R., Friend, J., 1983. The X, Y, Z hypothesis of corneal epithelial maintenance. Invest. Ophthalmol. Vis. Sci. 10, 1442–1443.

Vantrappen, L., Geboes, K., Missotten, L., Maudgal, P.C., Desmet, V., 1985. Lymphocytes and Langerhans cells in the normal human cornea. Invest. Ophthalmol. Vis. Sci. 26, 220–225.

Yoshida, S., Shimmura, S., Kawakita, T., Miyashita, H., Den, S., Shimazaki, J., Tsubota, K., 2006. Cytokeratin 15 can be used to identify the limbal phenotype in normal and diseased ocular surfaces. Investig. Ophthalmol. Vis. Sci. 47, 4780–4786. https://doi.org/10.1167/iovs.06-0574.